



Helmholtz-Zentrum für Ozeanforschung Kiel

RV SONNE Fahrtbericht / Cruise Report S0264

**SONNE-EMPEROR: The Plio/Pleistocene to Holocene
development of the pelagic North Pacific from
surface to depth – assessing its role for the global
carbon budget and Earth's climate**

Suva (Fiji) – Yokohama (Japan)
30.6. – 24.8.2018



Berichte aus dem GEOMAR
Helmholtz-Zentrum für Ozeanforschung Kiel

Nr. 46 (N. Ser.)

November 2018



Helmholtz-Zentrum für Ozeanforschung Kiel

RV SONNE Fahrtbericht / Cruise Report SO264

**SONNE-EMPEROR: The Plio/Pleistocene to Holocene
development of the pelagic North Pacific from
surface to depth – assessing its role for the global
carbon budget and Earth's climate**

Suva (Fiji) – Yokohama (Japan)
30.6. – 24.8.2018



Berichte aus dem GEOMAR
Helmholtz-Zentrum für Ozeanforschung Kiel

Nr. 46 (N. Ser.)

November 2018

Das GEOMAR Helmholtz-Zentrum für Ozeanforschung Kiel
ist Mitglied der Helmholtz-Gemeinschaft
Deutscher Forschungszentren e.V.

The GEOMAR Helmholtz Centre for Ocean Research Kiel
is a member of the Helmholtz Association of
German Research Centres

Herausgeber / Editor:
Dirk Nürnberg

GEOMAR Report
ISSN Nr. 2193-8113, DOI 10.3289/GEOMAR_REP_NS_46_2018

Helmholtz-Zentrum für Ozeanforschung Kiel / Helmholtz Centre for Ocean Research Kiel
GEOMAR
Dienstgebäude Westufer / West Shore Building
Düsternbrooker Weg 20
D-24105 Kiel
Germany

Helmholtz-Zentrum für Ozeanforschung Kiel / Helmholtz Centre for Ocean Research Kiel
GEOMAR
Dienstgebäude Ostufer / East Shore Building
Wischhofstr. 1-3
D-24148 Kiel
Germany

Tel.: +49 431 600-0
Fax: +49 431 600-2805
www.geomar.de

Table of content / Inhaltsverzeichnis

1. Cruise summary (in german and english)	1
2. Participants	4
2.1 Principal investigators	4
2.2 Shipboard scientific party	4
2.3 Participating institutions	4
2.3 Ship's crew	5
3. Narrative of the cruise (in german and english)	6
4. Aims of the Cruise / Zielsetzung der Forschungsfahrt	12
5. Work details and first results	14
5.1 Weather conditions during cruise SO264	14
5.2 Physical oceanography	16
5.2.1 Background and objectives: The N Pacific oceanography	16
5.2.2 Methods	18
5.2.3 Preliminary results	19
5.3 Water column sampling for microfossil-based proxy calibrations	22
5.3.1 Background and objectives: Plankton and water sampling	22
5.3.2 Multinet / plankton-net and underway pumping	23
Zooplankton filtering by underway pumping from ship's seawater intake	23
Multinet / plankton net sampling	24
Suspended organic matter	24
Preliminary results: Living plankton	25
5.3.3 Water sampling by CTD / rosette	27
Carbonate chemistry: Seawater and MUC sampling	27
Stable isotopes, nutrients and radiocarbon	27
Nutrients: Sampling and filtration of water samples for nutrient analyses	28
Trace element measurements: Seawater and MUC sampling	28
Neodymium	28
5.3.4 Underway pumping: Water samples and microplastic samples	29
Microplastics	29
Water sampling and carbonate chemistry, trace elements, stable isotopes	29
5.4 Hydroacoustics	31
5.4.1 Background	31
5.4.2 Bathymetry	31
Acquisition and Processing	31
Coverage and description	33
5.4.3 Marine sediment echosounding	35
5.5 Sediment core logging	37
5.5.1 GEOTEK Multi Sensor Core Logger	37
Magnetic volume susceptibility	37
Electric resistivity logging	37
Line scan imaging – Color Scanning	38
5.5.2 Sediment core MINOLTA light reflectance scanning	39
5.6 Marine geology and paleoceanography of the pelagic N Pacific	40
5.6.1 Background and objectives	40
5.6.2 Surface sediment sampling	41
5.6.2 Sediment coring and core description	43
Sediment core recovery	43
Sediment core handling	45
Visual core description	47
Tephra Sampling	48
5.6.3 Preliminary results of marine geology	49
Main Lithologies	49
5.6.4 Working Area 1: Kimmei to Ninigi seamounts	52
PARASOUND studies at Working Area 1	53
Surface sediment lithology	54
Downcore sediment records	54

5.6.5 Working Area 2: Yomei to Suiko seamounts	58
PARASOUND studies at Working Area 2	60
Surface sediment lithology	60
Downcore sediment records	61
Potential core correlation of Suiko Seamount sediments	64
5.6.6 Working Area 3: Jimmu to Minnetonka seamounts	65
PARASOUND studies at Working Area 3	66
Surface sediment lithology	67
Downcore sediment records from Jimmu Seamount	68
Downcore sediment records from Minnetonka Seamount	70
5.6.7 Working Area 4: Tenji to South of Detroit seamounts	73
PARASOUND studies at Working Area 4	74
Surface sediment lithology	75
Downcore sediment records	75
5.6.8 Working Area 5: Detroit Seamount	79
PARASOUND studies at Working Area 5	80
Surface sediment lithology	81
Downcore sediment records	81
5.7 Tephra layers in sediment cores from the Emperor Seamount Cha in	84
5.8 Sediment / pore-water geochemistry and microbiology	90
6. Acknowledgements /Danksagung (in german and english)	97
7. References	98
8. Appendices	
Appendix 3	Weekly Report
Appendix 4	SO264 Station list
Appendix 5.2-1	Bottle summary and station plots
Appendix 5.2-2	Instrument configuration and calibration report sheet from SBE 911 onboard RV SONNE during cruise SO264
Appendix Table 5.3-1	Plankton net stations, sampling intervals and sample destinations during RV Sonne cruise SO264
Appendix Table 5.3-2	Start and end of plankton filter (PF) samples for foraminiferal and pteropod analyses (sieve mesh size >63 µm)
Appendix Table 5.3-3	Data from the Thermosalinograph during plankton filter (PF) sampling
Appendix Table 5.3-4	Water samples taken from CTD rosette
Appendix Table 5.3-5	Locations, timing, and flow volumes of microplastic samples
Appendix Table 5.3-6	Locations, timing, and flow volumes of biomarker filters collected from the surface ocean along the cruise track of SO264
Appendix Table 5.3-7	Locations and timing of surface water collection of samples for DIC, pH, alkalinity, trace elements, $\delta^{18}\text{O}$, and $\delta^{13}\text{C}$ measurements
Appendix Figure 5.3-1	PF sample tracks for foraminifers and pteropods analyses
Appendix Figure 5.3-2	Locations of all filter samples collected for suspended particles from the seawater intake (membrane pump).
Appendix Figure 5.3-3	Locations of microplastic samples along the SO264 cruise track
Appendix Figure 5.3-4	Locations of surface water samples for DIC, pH, alkalinity, trace elements, $\delta^{18}\text{O}$, and $\delta^{13}\text{C}$ measurements
Appendix 5.4	PARASOUND profiles
Appendix 5.5	Core logging
Appendix 5.6-1	Lithology logs
Appendix 5.6-2	Sediment core photography

1. Zusammenfassung

(Dirk Nürnberg)

Der Nord (N) Pazifik zieht aufgrund seiner vorrangigen Rolle bei der Gestaltung des Erdklimas zunehmend Aufmerksamkeit auf sich. Die FS SONNE-EMPEROR-Expedition SO264, die auf die Emperor Seamount Chain im N Pazifik zielte, konzentrierte sich auf wissenschaftliche Fragestellungen, die paläozeanographische, paläoklimatische, chemisch-ozeanographische und meeresbiologische Untersuchungen in einem integrierten Ansatz verknüpfen, um das dynamische und dreidimensionale prozessorientierte Verständnis der Rolle des komplexen N Pazifiks für die Regulierung des Gasaustausches zwischen Ozean und Atmosphäre auf prä- anthropogenen Zeitskalen voranzutreiben. Die FS SONNE Reise SO264 fand im Rahmen des vom BMBF finanzierten Verbundprojektes „SONNE-EMPEROR: Die Plio/Pleistozäne bis Holozäne Entwicklung des pelagischen Nordpazifiks von der Oberfläche bis zum Meeresboden – Abschätzung seiner Rolle für die globale Kohlenstoffbilanz und das Erdklima“ statt, da von GEOMAR (Kiel) und AWI (Bremerhaven) koordiniert wird.

Die Reise begann am 30. Juni 2018 in Suva (Fidschi) und endete am 24. August 2018 in Yokohama (Fidschi). Bereits am 29. Juni 2018 waren Wissenschaftler von GEOMAR, 5 nationalen und 6 internationalen Organisationen und Universitäten an Bord gegangen. Insgesamt nahmen Wissenschaftler/innen aus elf Nationen teil. Die 54-tägige Expedition, die bis jetzt aufgrund des langen Transits von Fidschi zum eigentlichen Arbeitsbereich der Emperor Seamount Chain die längste Expedition von FS SONNE war, stellte Schiff und Crew vor besondere Herausforderungen.

In einem bislang einzigartigen Ansatz konnten wir nahe beieinander liegende, qualitativ hochwertige Sedimentkerne entlang eines N-S-orientierten Transektes entlang der Emperor Seamount Chain im nördlichen Pazifik (~170°E) gewinnen und somit die subtropischen bis subarktischen Klimazonen von ~30°N bis ~50°N abdecken. Das Kerntransekt kreuzte die wichtigsten ozeanographischen und klimatischen Muster, darunter die Kuroshio-Extension, die Kuroshio Bifurcation Front, die subarktische Grenze und die subarktische Front. Die Tiefseeablagerungen sind wichtige Klimaarchive, die genaue Aussagen z.B. über Änderungen der physikalischen Eigenschaften des Ozeans, der Stratifizierung der Wassersäule und der Tiefenventilation in der Vergangenheit zulassen.

Das marine-geologische Programm umfasste 54 Multicorer-, 40 Schwerelot, 20 Kolbenlot, 5 Kastenlot, 55 Multicorer- und 3 Großkastengreifer-Einsätze. Basierend auf einem Kerngewinn von ~640 m lieferten, wird unser vorwiegend (isotopen) geochemischer Ansatz Aufschluss über die langfristige ozeanographische und klimatische Entwicklung des pelagischen N Pazifiks erlauben. Die große Anzahl von Proxy-Daten wird uns ermöglichen, ein umfassendes Verständnis der interdynamischen Entwicklung von Oberflächen-, Zwischen- und Tiefenwassermassen zu gewinnen und Hinweise auf Gasaustauschprozesse zwischen Atmosphäre und Ozean, die Entwicklung der Kryosphäre, sowie die interhemisphärische interozeanische Kopplung zu erlangen.

Die Gewinnung hochwertiger Sedimentkerne wurde durch intensive bathymetrische Kartierungen und sedimentechographische Profilierung erleichtert. Insgesamt haben wir 178.970 km² Meeresboden kartiert, was der Hälfte der Fläche Deutschlands entspricht.

Ein intensives Beprobungsprogramm für Plankton, Wasser und Oberflächensedimente zwischen 7°N und 50°N diente der Bewertung, Kalibrierung und Validierung paläozeanographischer Proxy-Parameter. Während der SO264 Reise wurden 18 CTD /Wasserkranzschöpfer und 43 Multinetz-Einsätze durchgeführt. Zusätzlich erfolgte die kontinuierliche Probenahme von Oberflächenwasser per Bordpumpe von unterhalb des Schiffes. Die physikalischen und chemischen Eigenschaften des Meerwassers wurden bis zu einer Wassertiefe von max. 5700 m über den gesamten Nordpazifik gemessen.

Plankton mit einem Schwerpunkt auf Foraminiferen und Pteropoden wurde alle zwei bis drei Tage aus verschiedenen Tiefen der Wassersäule entnommen. Das Verständnis der Ökologie dieser Mikroorganismen ist wichtig, da sie Signalträger für (isotopische) geochemische Informationen sind, die für die Rekonstruktionen von Ozeanvariablen relevant sind. Die Meerwasseranalysen konzentrieren sich auf verschiedene Isotopensysteme, Spurenmetallkonzentrationen und Mikroplastik. Über ihre Arbeit an Bord des RV SONNE berichteten die Wissenschaftler/innen regelmäßig mit Fotos, Texten und Videos auf www.oceanblogs.org, www.bmbf.de und www.youtube.com und in Wochenberichten (Appendix 1)



Wissenschaftliche Crew der SO264-Reise / Scientific crew of cruise SO264.

Summary

(Dirk Nürnberg)

The North (N) Pacific increasingly attracts attention due to its prime role in shaping the Earth's climate. The RV SONNE-EMPEROR cruise SO264 aiming at the Emperor Seamount Chain in the N Pacific focussed on scientific questions closely linking paleoceanographic, paleoclimatic, chemical-oceanographic, and marine biological studies in an integrated approach to advance the dynamic and three-dimensional process-oriented understanding of the complex N Pacific's role for regulating ocean-atmosphere greenhouse gas exchanges prior to anthropogenic timescales. RV SONNE cruise SO264 took place in the framework of the BMBF-funded joint project "SONNE-EMPEROR: The Plio/Pleistocene to Holocene development of the pelagic North Pacific from surface to depth – assessing its role for the global carbon budget and Earth's climate" coordinated by GEOMAR (Kiel) and AWI (Bremerhaven).

The cruise started on June 30, 2018 at Suva (Fiji) and ended on August 24, 2018 at Yokohama (Fiji). Thirtyeight scientists from GEOMAR, 5 national and 6 international organizations and universities already boarded on 29 June, 2018. In total, people from 11 nations participated. The 54-day expedition, which has been the longest expedition of FS SONNE so far mainly due to the long transit from Fiji to the actual working area of the Emperor Seamount Chain, posed particular challenges to the ship and crew.

In a so far unique approach, we recovered closely-spaced high-quality sediment records from a broad meridional transect along the Emperor Seamount Chain in the N Pacific (~170°E), spanning subtropical to subarctic ocean climate regimes from ~30°N to ~50°N. The core transect crossed major oceanographic and climatic patterns, comprising the Kuroshio Extension, the Kuroshio Bifurcation Front, the Subarctic Boundary, and the Subarctic Front. The deep-sea deposits are important climate archives, which will allow exact statements on e.g. changes in ocean physical properties, stratification of the water column and deep ocean ventilation in the past.

The marine-geological program comprised 54 multicorer, 40 gravity corer, 20 piston corer, 5 box corer, 55 multicorer and 3 giant box corer deployments. Based on sediment cores retrieved from ~1100 m to ~5700 m water depths providing ~640 m of core recovery, our predominantly (isotope)geochemical proxy approach will shed light on the long-term Plio/Pleistocene oceanographic and climatic development of the pelagic N Pacific. The large suite of proxy data will allow us to yield a comprehensive understanding of the interdynamic development of surface, subsurface, and deep water masses, and will provide clues on atmosphere-ocean exchange processes, the evolution of the cryosphere, interhemispheric coupling, and inter-ocean exchange.

The retrieval of high-quality sediment cores was facilitated by intense bathymetric mapping and sediment-echosounder profiling. In total, we mapped 178.970 km² ocean floor, which is half the area of Germany.

An intense plankton, water and sediment surface sampling program between 7°N and 50°N served to evaluate, calibrate and validate paleoceanographic proxy parameters. During SO264, we ran 18 CTD/rosettes and 43 multinetts, and performed continuous surface water sampling from below the ship. The physical and chemical properties of seawater were measured down to water depths of max. 5700 m across the entire North Pacific. Plankton with a focus on foraminifera and pteropoda was sampled from different depths of the water column every two to three days. The understanding of the ecology of these microorganisms is important as they are signal carriers for unique (isotopic) geochemical information relevant to ocean reconstructions. Seawater analyses will concentrate on different isotope systems, trace metal concentrations, and microplastic.

The scientists regularly reported on their work aboard RV SONNE with photos, texts and videos at www.oceanblogs.org, www.bmbf.de, and www.youtube.com and in weekly reports (Appendix 1).

Appendix 1. Weekly Reports.

2. Participants

2.1 Principal Investigators SO264 SONNE-EMPEROR

Prof. Dr. Dirk Nürnberg, GEOMAR Kiel

Prof. Dr. Ralf Tiedemann, AWI Bremerhaven

2.2 Shipboard Scientific Party

	Name / Name	Tätigkeit / Task	Institut / Institute
1.	Nürnberg, Dirk	Fahrtleiter / <i>Chief Scientist</i>	GEOMAR
2.	Abell, Jordan Tyler	Ph.D. student / Geochemistry	LDEO
3.	Arévalo G., Marcelo C.	Technician / Geology	Serv. Exped.
4.	Brück, Liane P.	Technician / Paleomagnetism	MARUM
5.	Bubenshchikova, Natalia	Scientist / Tephrostratigraphy	IO RAS
6.	Chao, Weng Si	Ph.D. student / Paleoceanogr.	AWI
7.	Dong, Zhi	Scientist / Geochemistry	FIO
8.	Evers, Florian	Technician / Geology	GEOMAR
9.	Fessler, Sebastian C.	Technician / Geology.	GEOMAR
10.	Hars, Martina	Technician / Geology.	GEOMAR
11.	Höfken, Adrian F.	Student / Paleomagn.	MARUM
12.	Jacobi, Lara	Ph.D. student / Paleoceanogr.	GEOMAR
13.	Jentzen, Anna	Scientist / Microplankton	MPI
14.	Karas, Cyrus	Scientist / Paleoceanography	Univ. Santiago
15.	Keul, Nina	Scientist / Microplankton	IFG/Univ. Kiel
16.	Kreps, Gastón	Scientist / Phys. Oceanogr.	CADIC-CONICET
17.	Langemann, Linda	Student. / Sedimentology	AWI
18.	Lembke-Jene, Lester	Scientist / Coordinator	AWI
19.	Liu, Jianxing	Scientist / Paleomag.	FIO
20.	Liu, Ling	Ph.D. student / Micropaleontol.	AWI
21.	Max, Lars W.	Scientist / Hydroacoustics	AWI
22.	Mellon, Stefanie A.	Scientist / Geochemistry	Univ. Dalhousie
23.	Meier, Karl	Student / Sedimentology	GEOMAR
24.	Niemann, Steffen	Student / Geology	FH Kiel
25.	Over, Laura	Student / Bathymetry	AWI
26.	Pape, Christian	Student / Sedimentology	GEOMAR
27.	Ronge, Thomas A.	Scientist / Paleoceanography	AWI
28.	Ruggieri, Nicoletta	Scientist / Org. Geochemistry	AWI
29.	Schnakenberg, Annika	Ph.D. student / Geochemistry	AWI
30.	Schumacher, Valea	Technician / Microplankton	AWI
31.	Stoerling, Tjoerdis	Student / Sedimentology	GEOMAR
32.	Steffen, Melanie U.	Scientist / Bathymetry	AWI
33.	Volz, Jessica	Ph.D. student / Geochemistry	AWI
34.	Wang, Kunshan	Scientist / Mineralogy	FIO
35.	Wu, Yonghua	Scientist / Biostratigraphy	FIO
36.	Yu, Yang	Ph.D. student / Geochemistry	GEOMAR
37.	Zorzi, Coralie D.	Ph.D. student / Biostratigraphy	GEOTOP
38.	Zou, Jianjun	Scientist / Geochemistry	FIO

2.2 Participating Institutions

AWI Alfred-Wegener-Institut – Helmholtz Zentrum für Polar und Meeresforschung; Bremerhaven, Germany

CADIC-CONICET Servicio de Información Ambiental y Geográfica; Ushuaia, Argentine

FH Kiel University of Applied Sciences Kiel, Germany

FIO	The First Institute of Oceanography; Qingdao, China
GEOMAR	Helmholtz Centre for Ocean Research Kiel, Germany
GEOTOP	Département des Sciences de la Terre et de l'Atmosphère, Université du Québec à Montreal, Canada
IFG/CAU	Institute for Geosciences – Christian-Albrechts-University Kiel, Germany
IO RAS	P.P. Shirshov Institute of Oceanology, Moscow, Russia
LDEO	Lamont-Doherty Earth Observatory; Palisades, NY, USA
MARUM	University Bremen; Germany
MPI	Max Planck Institute for Chemistry; Mainz, Germany
Serv. Exp.	Servicio de Apoyo a Expediciones Científicas y Exploración, Punta Arenas, Chile
Univ. Dalhousie	Dept. Oceanography, Dalhousie University, Halifax, Canada
Univ. Santiago	Universidad Mayor, Escuela Geología, Santiago, Chile

2.3 Ship's crew

	Name / Name	Tätigkeit / Task	Institut / Institute
1.	Meyer, Oliver	Captain	
2.	Aden, Nils	Chief Mate, Nautical Officer	
3.	Göbel, Jens	2 nd Mate, Nautical Officer	
4.	Büchele, Ulrich	2 nd Mate, Nautical Officer	
5.	Walther, Anke	Medical doctor	
6.	Hermesmeyer, Dieter	Chief Engineer	
7.	Horsel, Roman	2 nd Engineer	
8.	Stegmann, Tim	2 nd Engineer	
9.	Leppin, Jörg	Electronics engineer	
10.	Pregler, Hermann	Electronics technician	
11.	Tardeck, Frederic	System operator	
12.	Meinecke, Stefan	System operator	
13.	Schmidt, Hendrik	Electrician	
14.	Ulbricht, Martin	Electrician	
15.	Bolik, Torsten	Fitter	
16.	Blaurock, André	Motorman	
17.	Yaylagül, Deniz	Motorman	
18.	Werning, Tom	Motorman	
19.	Bierstedt, Torsten	Boatswain	
20.	Ernst, Arnold	Mechanic	
21.	Vogel, Dennis	Mechanic	
22.	Fricke, Ingo	Mechanic	
23.	Eidam, Oliver	Mechanic	
24.	Freitag, Patrick	Mechanic	
25.	Papke, René	Mechanic	
26.	Siefken, Tobias	Mechanic	
27.	Garnitz, André	1 st cook	
28.	Streifling, Stefan	Assistant Cook	
29.	Vogt, Alexander	1 st Steward	
30.	Manuel, Christopherson	Steward	
31.	Steep, Maik	Steward	
32.	Kroeger, Sven	Steward	

3. Verlauf der Forschungsfahrt SO264

(Dirk Nürnberg)

Ausgangspunkt der SO264-Reise war die Hafenstadt Suva an der Südostküste der größten Insel Fidschis, Viti Levu. Am 29. Juni 2018, 8:00 Uhr, wurden die 38 Teilnehmer vom Schiffsagenten aus dem Hotel zur FS SONNE gebracht, die bereits mit den acht vorausgeschickten Containern beladen war. Der Tag im Hafen wurde für weitere Schiffsvorbereitungen genutzt. Alle Arbeiten wurden pünktlich abgeschlossen, so dass FS SONNE am 30. Juni 2018 um 9:30 Uhr den Hafen bei frischen Winden (8 Bft) verlassen konnte. Der 3000 Seemeilen lange, rund 12-tägige Transit zum Arbeitsgebiet der Emperor Seamount Chain wurde notwendig, um das Schiff aus den tropischen Regionen in die nachfolgenden Arbeitsgebiete im Nordpazifik zu bringen (Abb. 3-1, 3-2). Die ersten Tage bis zum 2. Juli 2018 wurden bei tropischen Wassertemperaturen von 28°C und Lufttemperaturen von 26°C zur Einrichtung der Labore, zur Koordination der Probenahme und zum Beginn des Fahrtberichtes verwendet. Jeden zweiten Tag wurden wissenschaftliche Treffen für die gesamte Gruppe zur gegenseitigen Information und Koordination abgehalten. Die Gruppenleiter trafen sich jeden Tag, um die täglich zu erledigenden Arbeiten zu besprechen. Wir nutzten den langen Transit in den Norden von den Tropen bis zu den subarktischen Klimazonen als einzigartige Gelegenheit, um "en passant" Wasserproben für Nährstoff- und Isotopenmessungen sowie Netzfänge und Wasserfiltration für Mikroplankton und suspendiertes organische Material durchzuführen. Ein Sturm aus südöstlicher Richtung wehte uns in Richtung der ersten Wasserstation bei ~11°S 179°E. Bei Ankunft am 2. Juli 2018 am frühen Morgen um 6:00 Uhr wurde die Station aufgrund von starkem Wind und Wellen aufgegeben. Am Nachmittag des 2. Juli 2018 verbesserte sich das Wetter und der Transit setzte sich fort durch den West Pacific Warmpool, eine weite Ozeanregion, die durch extrem hohe Wassertemperaturen von bis zu 29.5°C gekennzeichnet ist (wobei die Lufttemperaturen um 1-2°C kühler blieben). Am 3. Juli 2018 um 5 Uhr morgens erreichten wir die nächste "Wasserstation" bei ~7°S 179°50'E. In den folgenden Tagen wurden vier weitere Wasserstationen zwischen 2°N und 10°N ausgeführt, mit denen wir das äquatoriale Stromsystem querten. Routinemässig begann nach einem auf ~100 m abgesenkten Multinetz-Fang der Einsatz der CTD/Wasserkransschöpfer-Einheit, mit der die Eigenschaften der Wassermassen gemessen und Wasserproben bis in große Wassertiefen gewonnen wurden. Ein nachfolgendes Multinetz dokumentierte dann die tieferen Vorkommen des Planktons bis in 600 bis 800 m Wassertiefe. Ein Höhepunkt der ersten Woche auf See war die Äquatorüberquerung am 4. Juli 2018 bei einer einzigartigen Position von 0° und einer Länge von 180°.

Am Ende der ersten Woche (8. Juli 2018) erreichten wir die im Uhrzeigersinn drehende subtropische Gyre. Da es sich um eine nährstoffarme, oligotrophe Meeresregion handelt, haben wir die Abstände zwischen den Wasserstationen deutlich vergrößert. Erstmals bei einer Position von 10°03.4'N 178°26.9'E, etwa 400 Seemeilen von den nächsten Siedlungen entfernt, und dann kontinuierlich innerhalb der Subtropischen Gyre sowie im Bereich des Kuroshio-Stroms bis ~30°N dokumentierten wir Sichtungen von treibendem Müll. Die subtropische Gyre, oft als "Great Pacific Garbage Patch" bezeichnet, trägt diesen Namen wegen des hohen Anteils an driftendem Müll wohl zu Recht.

Zu Beginn der Woche vom 9. bis 15. Juli 2018 setzten wir unser "Transpacific Water Sampling Program" bei 18°N, 27°N und 33°N fort. Bei ~32°N verließen wir den Einfluss der subtropischen Gyre und traten in den Kuroshio-Strom ein, einem der größten Stromsysteme der Welt. Mit einem Transportvolumen von ~45 Millionen Kubikmetern Wasser pro Sekunde transportiert der Kuroshio tropische Wärme nach Norden, trifft auf den nach Süden fließenden Oyashio-Strom vor Japan und wird nach Osten in den Nordpazifik abgelenkt.

Am Freitag, den 13. Juli 2018, begannen die geologischen Arbeiten östlich des Kimmei-Vulkans im südöstlichen Gebiet der Emperor Seamount Chain. Die Emperor-Vulkane erheben sich mehrere 1000 m über der 5-6 km tiefen Tiefseeebene. Die Sedimentbeprobung der (südlichen) Vulkane war im Allgemeinen schwierig, da ihre Flanken sehr steil sind und die südlichen Plateaus weitgehend sedimentfrei sind. Durch gezielte und langsam gefahrene bathymetrische und Sediment-Echosound-Profilierungen konnten jedoch kleine Sedimenttaschen und -becken gefunden werden. Auf dem Vulkan östlich von Kimmei führte eine Kernstation in ~2700 m zu unserem ersten Sedimentkern von ~10 m Länge mit karbonatreichen Sedimenten und prominenten vulkanischen Aschelagen.

Der Vulkan Koko (36°N 171°E) im Nordwesten wurde am 14. und 15. Juli 2018 untersucht und beprobt. Vier Stationen auf 1100-4000 m Wassertiefe wurden angefahren. Die Entdeckung eines stark verwitterten flachmarinen Lagunen-sediments verweist auf die Subsidenzgeschichte dieser etwa 50 Millionen Jahre alten Vulkanstruktur.

Im Zeitraum vom 16. bis 22. Juli 2018 verließ RV SONNE nach und nach den Einfluss des Kuroshio-Stromsystems bei ~37°N und erreichte den Bereich der gegen den Uhrzeigersinn drehenden westlichen Subarktischen Gyre. Die Wasser- und Lufttemperaturen sanken signifikant auf 11° C bzw. 13°C. Ab dem 19. Juli 2018 wurde der N Pazifik neblig und dunstig, während der Wind allgemein schwach blieb. Die Woche war geprägt von einem intensiven geologischen Programm mit 33 Einsätzen, bei dem mehrere Vulkane der Emperor Seamount Chain zwischen 37°N und 44°N untersucht wurden: Ojin, Nintoku und Yomei. Sedimentkerne wurden sowohl aus den flachsten Regionen bei 1100-1300 m Wassertiefe als auch von den Vulkanflanken bis zu einer Wassertiefe von ~5700 m gewonnen. Meeresbodenbeobachtungen mit dem TV-MUC zeigten, dass die noch karbonatreichen Sedimente in flachen bis mittleren Wassertiefen häufig durch Strömungen abgetragen bzw. stark verfestigt werden. In flacheren Wassertiefen von weniger als 2500 m konnten wir schöne Kerngewinne von bis zu 19 m erreichen.

Am Sonntag, den 22. Juli 2018, begann am Fuße des Suiko Seamount (~44°50'N 170°E) ein intensives Probenahmeprogramm der Wassersäule auf 4400 m Wassertiefe. Die ozeanische Deckschicht wurde mit dem mehrfach schließenden Multinetz beprobt. Der Vulkan Suiko liegt in der Nähe der subarktischen Front, die als 4°C-Isotherme in 100 m Wassertiefe definiert ist und die ungefähre Grenze zwischen den windgetriebenen, gegenläufig zirkulierenden subtropischen und subarktischen Wirbelsystemen darstellt.

In der Woche vom 23. bis 29. Juli führten wir mit 19 Geräteeinsätzen zehn Geo-Stationen auf dem Suiko Seamount durch. Mit durchschnittlich 80% Kerngewinn und Längen von bis zu 19 m haben wir fast 120 m Sedimentkerne an Deck gebracht. Die Sedimentkerne wurden aus Wassertiefen von 1800-3200 m gewonnen. Die unterschiedlichen Sedimentsequenzen korrelieren sehr gut im Arbeitsbereich. Prominente Tephralagen bieten zusätzliche Möglichkeiten für überregionale Korrelationen und Ansätze für die Altersdatierung. Am Samstag, dem 28. Juli 2018, bei 45°N und 170°E zelebrierten wir das „Bergfest“.

In der ersten Wochenhälfte vom 30. Juli bis 5. August 2018 stand der Vulkan Jimmu bei 46°N im Mittelpunkt unserer Aktivitäten: Vier Stationen in Wassertiefen von ~1900-3200 m wurden durchgeführt. Es wurde festgestellt, dass aufgrund der niedrigeren Sedimentationsraten die kurzen Kerne von den Vulkangipfeln mehr "Zeit" enthalten und einen tieferen Einblick in die geologische Vergangenheit ermöglichen als die längeren Sedimentkerne von den tieferen Hängen. Die typischen Fazies ändern sich von karbonatischen Schlämmen zu terrigenen Ablagerungen, die durch prominente Tephralagen unterbrochen werden. Diese ermöglichen Kernkorrelationen über große Gebiete. Unser Arbeitsfortschritt verlangsamte sich am Donnerstag, dem 2. August 2018,

als sich ein heftiger SW-Sturm mit bis zu 22 m/s Windgeschwindigkeit (9 Bft) und Wellenhöhen von ~6 m entwickelte. Von Freitag bis Samstag (3.-4. August 2018) wurden die Stationsarbeiten eingestellt und wir nutzten die Schiffszeit, um den Vulkan Minnetonka bei 47°N 169°E zu kartieren.

In der Woche vom 6. bis 12. August 2018 wurden die erfolgreichen Arbeiten am Minnetonka Vulkan abgeschlossen. Zehn Geo-Stationen in Wassertiefen von 2100-4000 m und teilweise schwierigem "Gelände" brachten Kerngewinne von fast 110 m. Die sehr variablen Sedimentsequenzen wurden zum ersten Mal durch das Auftreten von Biogenopal-(Diatomeen)-Schlämmen charakterisiert, die sich deutlich von den weiter südlich vorkommenden karbonatreichen Sedimenttypen unterscheiden. Diese Kieselalgen-Lagen sind typisch für den nördlichen Nordpazifik und aus dem nördlichen Beringmeer oder dem Ochotskischen Meer bekannt.

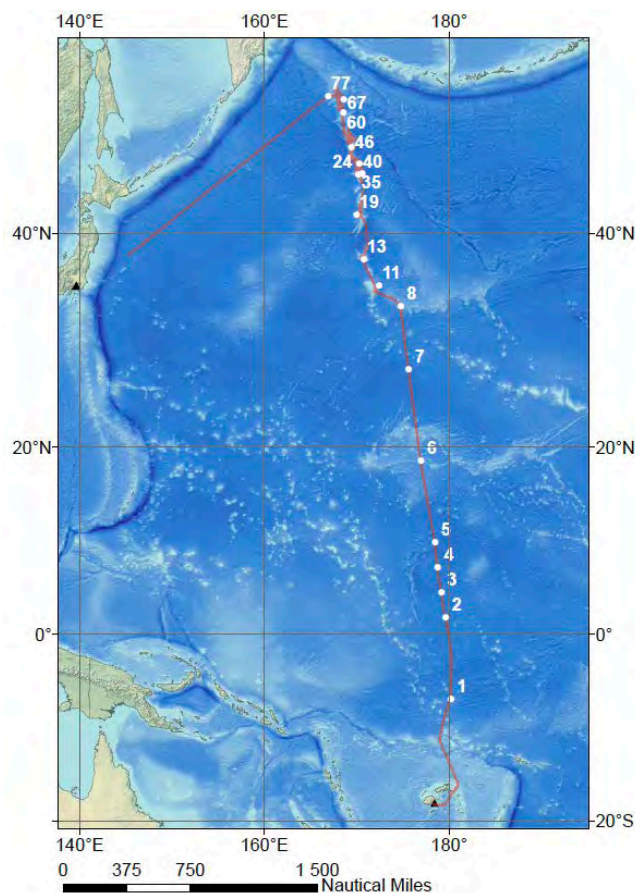


Abbildung 3-1. Bathymetrische Karte des N Pazifiks mit eingezeichneten WATER/PLANKTON Beprobungsstationen.

Figure 3-1. Bathymetric chart of the North Pacific showing WATER/PLANKTON stations.

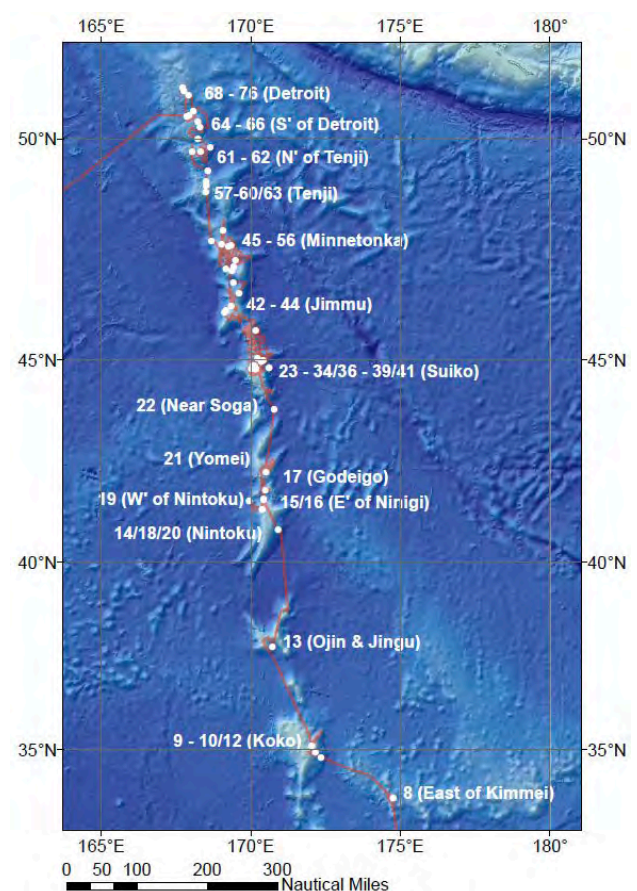


Abbildung 3-2. Bathymetrische Karte mit eingezeichneten GEO-Stationen.

Figure 3-2. Bathymetric chart showing GEO-stations.

Am Mittwoch, dem 8. August 2018, fand der Transit zum Tenji Seamount statt. Tenji überrascht mit mächtigen ungestörten Sedimentsequenzen auch auf den flachen Plateaubereichen. Mit nur wenigen Einsätzen konnten wir ~80 m Sedimentkerne aus Wassertiefen von 2300 bis 5200 m gewinnen. Eine 24-Stunden-Multinetz-Station bei ~49°20'N 168°30'E fand am Donnerstag und Freitag (9. bis 10. August 2018) statt. Die Biologen führten eine große Anzahl von Planktonnetz-Einsätzen bis zu einer Wassertiefe von 800 m durch, um ein detailliertes Bild der Diversität und Aktivität des Planktons zu

erhalten. Nach wochenlangem dichten und kalten Nebel, der für die Sommersaison im Nordpazifik typisch ist, war dieses Wochenende (11. bis 12. August 2018) wieder sonnig und warm. Die letzten Arbeitstage vor der Abreise nach Yokohama (13.-17. August 2018) konzentrierten sich auf den nördlichsten Vulkan der Emperor Seamount-Kette, Detroit Seamount. Bis auf ein paar Seemeilen haben wir uns der 200-Meilen-Zonen von Russland und den USA genähert. Die nördlichste Station befand sich bei 51°N und 167°E. Unsere Aufgabe bestand vor allem darin, längere Kerne an bereits bekannten Standorten zu gewinnen.

Wir erreichten am 23. August 2018 den Hafen von Yokohama. Die Ausschiffung der wissenschaftlichen Crew erfolgte am 30. August 2018. Die gesamte Strecke, die während der SO264-Reise abgefahren wurde, beträgt 8430 sm. Die bathymetrische Kartierung umfasste ~78,017 km² während des Transits von Suva in das Untersuchungsgebiet, ~55,960 km² auf der Emperor Seamount Chain und ~44,993 km² während des Rücktransits von der letzten Station bis zum Beginn der japanischen EEZ. Insgesamt haben wir 178,970 km² kartiert. Während SO264 führten wir 183 Geräteeinsätze an 77 Stationen durch. Wir hatten 18 CTD/Wasserkranzschöpfer- und 43 Multinetz-Einsätze. Das geologische Programm umfasste 54 Multicorer-Einsätze (MUC), 40 Schwerelote (GC), 20 Kolbenlote (PC), 5 Kastenlote (Kasten, KAL) und 3 Grosskastengreifer (GKG). Wir hatten ca. 640 m Sedimentkerngewinn (außer MUC, Pilotkerne und GKG).

Narrative of Cruise SO264

(Dirk Nürnberg)

Starting point of the SO264 trip was the port city Suva on the south-eastern coast of the largest island of Fiji, Viti Levu. On June 29, 2018, 8:00 a.m., the 38 participants were brought by the ship's agent from the hotel to RV SONNE, which was already loaded with the eight containers sent ahead. The day in port was used for further ship-side preparations. All work was completed on time, so that RV SONNE left port on June 30, 2018 at 9:30 a.m. and set off with fresh winds (8 Bft). The 3000 nautical miles-long, ~12-day-long transit to the working area along the Emperor Seamount Chain became necessary to transfer the ship from the tropical regions to the subsequent working areas in the N Pacific (Fig. 3-1, 3-2). The first days until July 2, 2018 at tropical water temperatures of 28°C and air temperatures of 26°C, were used to set up the laboratories, to work out the sampling procedures and to start with the cruise report. Every second day, science meetings for the entire group were held for mutual information and coordination. The group leaders met daily to discuss the work to be done every day. We used the long northbound transit from the tropics to subarctic climatic zones as a unique opportunity to carry out "en passant" water sampling for nutrient and isotope measurements, as well as net catches and water filtration for microplankton and suspended organic matter.

A storm from SE directions blew us towards the first water station at ~11°S 179°E. On arrival on July 2, 2018 early in the morning at 6:00, the station was abandoned due to heavy wind and waves. By the afternoon of July 2, 2018, weather improved and transit continued through the West Pacific Warm Pool, a wide ocean region characterized by extremely high water temperatures of up to 29.5°C (whereby the air temperatures remain 1-2°C cooler). In the morning at 5:00 on July 3, 2018 we reached the next "water station" at ~7°S 179°50'E. In the following days, four more water stations between 2°N and 10°N were carried out, with which we crossed the equatorial current system. Starting routinely with a multinet that has been lowered to ~100 m, the deployment of the CTD/rosette unit followed providing water mass properties and water samples down to large depths. A subsequent multinet documented the deeper occurrences of the plankton down to 600-800 m. A highlight of the first week at sea was the crossing of the equator on July 4, 2018 at an unique geographical latitude of 0° and a longitude of 180°.

At the end of the 1st week (July 8, 2018) we reached the clockwise circulating Subtropical Gyre. As this is a nutrient-poor, oligotrophic ocean region, we significantly increased the distances between water stations. For the first time on 10°03.4'N 178°26.9'E, about 400 nautical miles from the nearest human settlements, and then continuously within the Subtropical Gyre and in the area of the Kuroshio Current up to ~30°N, we documented sightings of drifting garbage. The Subtropical Gyre, often termed as "Great Pacific Garbage Patch", rightly bears this name due to its high portion of floating waste.

At the beginning of the week from July 9 to 15, 2018, we continued our "Transpacific Water Sampling Program" at 18°N, 27°N and 33°N. At ~32°N we left the influence of the Subtropical Gyre and entered the Kuroshio Current, one of the world largest current systems. With a transport volume of ~45 million cubic meters of water per second, the Kuroshio transports tropical heat northwards, meets the southward flowing Oyashio Current off Japan and is deflected eastward into the N Pacific.

On Friday, July 13, 2018, marine geological work started east of the Kimmei Volcano in the SE area of the Emperor Seamount Chain. The Emperor volcanoes rise several 1000 m above the 5-6 km deep sea plain. Sediment sampling of the (southern) volcanoes was commonly difficult, as their flanks are very steep and the southern plateaus are mostly free of sediment. However, targeted and slow bathymetric and sediment echosound profiling allowed to detect small sediment pockets and basins. On the volcano E of Kimmei, a core station in ~2700 m resulted in our first sediment core of ~10 m length with carbonate-rich sediments and prominent volcanic ash layers.

The volcano Koko (36°N 171°E) in the NW was sampled on July 14-15, 2018. Four stations at 1100-4000 m were approached. The discovery of a strongly altered shallow marine lagoonal sediments refers to the subsidence history of this approximately 50 million year old volcanic structure.

During July 16-22, 2018, RV SONNE left the influence of the Kuroshio Current at ~37°N and entered the area of the counterclockwise circulating W Subarctic Gyre. The water and air temperatures dropped significantly to 11°C and 13°C, respectively. From July 19, 2018 the N Pacific became foggy and hazy, while winds remained commonly weak. The week was marked by an intensive geological program with 33 deployments during which several volcanoes of the Emperor Seamount Chain were mapped and sampled between 37°N and 44°N: Ojin, Nintoku and Yomei. Cores were retrieved from both the shallowest regions at 1100-1300 m water depth, and from the seamount flanks down to water depths of ~5700 m. Seafloor observations with the TV-MUC showed that the still carbonate-rich sediments in shallow to medium water depths are frequently eroded or strongly solidified by currents. From below ~2500 m water depth, we registered nice core recoveries of up to 19 m.

On Sunday, July 22, 2018 at the base of Suiko Seamount (~44°50'N 170°E), an intensive sampling program of the water column down to 4400 m commenced. The oceanic surface layer was sampled with the multiple closing net. The Suiko volcano is located close to the Subarctic Front, which is defined as a 4°C isotherm in 100 m water depth and represents the approximate boundary between the wind-driven, counter-rotating Subtropical and Subarctic gyre systems.

In the week from July 23 to 29, we performed ten geo-stations on Suiko Seamount with 19 deployments. With core recoveries averaging 80% and lengths of up to 19 m, we have brought almost 120 m of sediment core length on deck. Sediment cores were extracted from water depths of 1800-3200 m. The varied sediment sequences correlate very well within the working area. Prominent volcanic ash layers offer additional possibilities for supra-regional correlation and approaches for age dating. On Saturday, July 28, 2018 at 45°N and 170°E, we had the midterm celebration.

During the first half of the week from July 30 to August 5, 2018, the volcano Jimmu at 46°N was the focus of our activities: Four stations at water depths of ~1900-3200 m. It was found that due to the lower sedimentation rates, the short cores from the volcano summit contain more "time" and allow a deeper look into the geological past than the longer sediment cores from the deeper slopes. The typical facies changes from carbonate oozes to terrigenous deposits, interrupted by prominent volcanic ash layers, will allow for core correlations across large areas. Our work progress slowed down on Thursday, August 2, 2018, as a violent SW storm developed with up to 22 m/s wind speeds (9 Bft.) and wave heights of ~6 m. On Friday to Saturday (August 3-4, 2018) the station work was abandoned and we used the ship time to map the Minnetonka volcano at 47°N 169°E. During the week from August 6-12, 2018, the successful work on Minnetonka was completed. Ten geo-stations in water depths of 2100-4000 m and partly difficult "terrain" brought core recoveries of almost 110 m. The very variable sediment sequences were characterized for the first time by the occurrence of siliceous diatom oozes, which differ clearly from the carbonate-rich sediment types occurring further south. These diatomaceous oozes are typical of the northern N Pacific and known from the northern Bering Sea or the Sea of Okhotsk.

On Wednesday, August 8, 2018 the transit to Tenji Seamount took place. Tenji surprises with mighty undisturbed sediment sequences also on the shallow plateau areas. With only a few deployments, we recovered ~80 m cores from water depths of 2300- 5200 m. A 24-hour multinet station at ~49°20'N 168°30'E took place on Thursday and Friday (August 9-10, 2018). The biologists carried out a large number of plankton net catches down to water depths of 800 m to obtain a detailed picture of plankton diversity and activity. After weeks of thick and cold fog typical for the N Pacific summer season, this weekend (August 11-12, 2018) was sunny and warm again. The last working days before leaving for Yokohama (August 13-17, 2018) concentrated on the northernmost volcano of the Emperor Seamount Chain, Detroit Seamount. Except for a few nautical miles we worked our way up to the 200 mile zones of Russia and the USA. The northernmost station was at 51°N and 167°E. Our task was primarily to develop longer cores at already known site locations.

We entered the port of Yokohama on August 23, 2018. Disembarkment of the scientific crew was on August 30, 2018. The entire route passed during SO264 was 8430 nm. Bathymetric mapping covered ~78.017 km² during the transit from Suva to the study area, ~55.960 km² on the Emperor Seamount Chain, and ~44.993 km² during the back transit from the last station to the beginning of the Japanese EEZ. In total, we mapped 178.970 km². During SO264 we carried out 183 deployments at 77 stations. We ran 18 CTD/rosettes and 43 multinetts. The geological program comprised 54 multicorer (MUC) deployments, 40 gravity corers (GC), 20 piston corers (PC), 5 box corers (Kasten, KAL) corers, and 3 giant box corers (GKG). We retrieved ca. 640 m of sediment cores (except MUC, pilot cores, and GKG).

Appendix 3. Weekly Reports.

4. Aims of the cruise

(Dirk Nürnberg, Ralf Tiedemann, Lester Lembke-Jene)

The North (N) Pacific increasingly attracts attention due to its prime role in shaping the Earth's climate. The RV SONNE-EMPEROR cruise SO264 took place in the framework of the BMBF-funded joint project "SONNE-EMPEROR: The Plio/Pleistocene to Holocene development of the pelagic North Pacific from surface to depth – assessing its role for the global carbon budget and Earth's climate", jointly managed by paleoceanographers from GEOMAR (Kiel) and AWI (Bremerhaven). The project aiming at the Emperor Seamount Chain in the N Pacific will focus on scientific questions closely linking paleoceanographic, paleoclimatic, chemical-oceanographic, and marine biological studies in an integrated approach to advance the process-oriented understanding of the complex N Pacific's role for regulating ocean-atmosphere greenhouse gas exchanges prior to anthropogenic timescales. In a so far unique approach, the RV SONNE cruise SO264 managed to recover high-quality sediment records from a broad meridional transect along the Emperor Seamount Chain in the N Pacific, spanning subtropical to subarctic ocean climate regimes from ~30°N to ~50°N (Fig. 4-1). This transect will serve as a new paleoceanographic North - South reference transect in the N Pacific. Our approach for the first time progresses beyond previous studies of single isolated sites in this region, as we will systematically compile and study data timeseries to improve our dynamic and three-dimensional understanding of the long-term evolution of physical and chemical conditions of the N Pacific, the climate modes and their linkage to regional N Pacific and large-scale climate and ocean circulation variability.

An integral part of SONNE-EMPEROR will be the development of climate proxy timeseries from the so far largely unexplored offshore, pelagic N Pacific ocean areas with new, quantitative paleoceanographic and paleoclimatological methods. As such records will be rather unaffected by land-near processes – although being of lesser temporal resolution - they will be more reliable for ocean climate model assessment. Based on sediment cores retrieved during SO264 from upper bathyal to mid-abyssal depths, our predominantly (isotope)geochemical proxy approach will shed light on the long-term Plio/Pleistocene to short-term Holocene oceanographic and climatic development of the pelagic N Pacific. The large suite of proxy data will allow us to yield a comprehensive understanding of the interdynamic development of surface, subsurface, and deep water masses, and will provide clues on atmosphere-ocean exchange processes, the long-term evolution of climate modes and of the cryosphere, interhemispheric coupling, and inter-ocean exchange.

Previous studies have shown that sediment cores from the Emperor Seamount Chain have high quality with respect to paleoceanographic studies. While sedimentation rates are often low, sufficient higher-accumulation areas exist to even resolve millennial-scale patterns (e.g., Keigwin et al., 1998; Gebhardt et al., 2008; Jaccard und Galbraith, 2013). By using state-of-the-art hydroacoustic techniques and carrying out detailed mapping (KONGSBERG EM122, ATLAS-Parasound), we were able to find sediment deposits on bathymetric highs showing calcite-bearing, undisturbed sediments. At greater depths, sedimentation rates are commonly low, allowing us to go further back in time, with a particular focus on the last few million of years. Seismic information from previous activities (DSDP, ODP, WEPAMA, INOPEX) provided valuable information for planned hydroacoustic surveying and selection of core locations.

The abovementioned research goals will be pursued by merging conventional and innovative, mainly (isotope)geochemical proxies reflecting physical properties of water masses, (sea surface, subsurface, and intermediate water temperature and salinity, thermocline change, ocean stratification), chemical composition of seawater, terrigenous flux and eolian dust supply, marine productivity, and related nutrient utilization, mode,

intermediate, and deep water ventilation, formation, and circulation changes. These proxies have been partly established and widely used by the applicants within other research projects. Our experience with such a multi-proxy approach will allow us to successfully carry out the envisioned studies. Proxies will be measured in both bulk sediments from cores retrieved, and in biogenic signal carriers (e.g. foraminifers, diatoms, organic tissue).

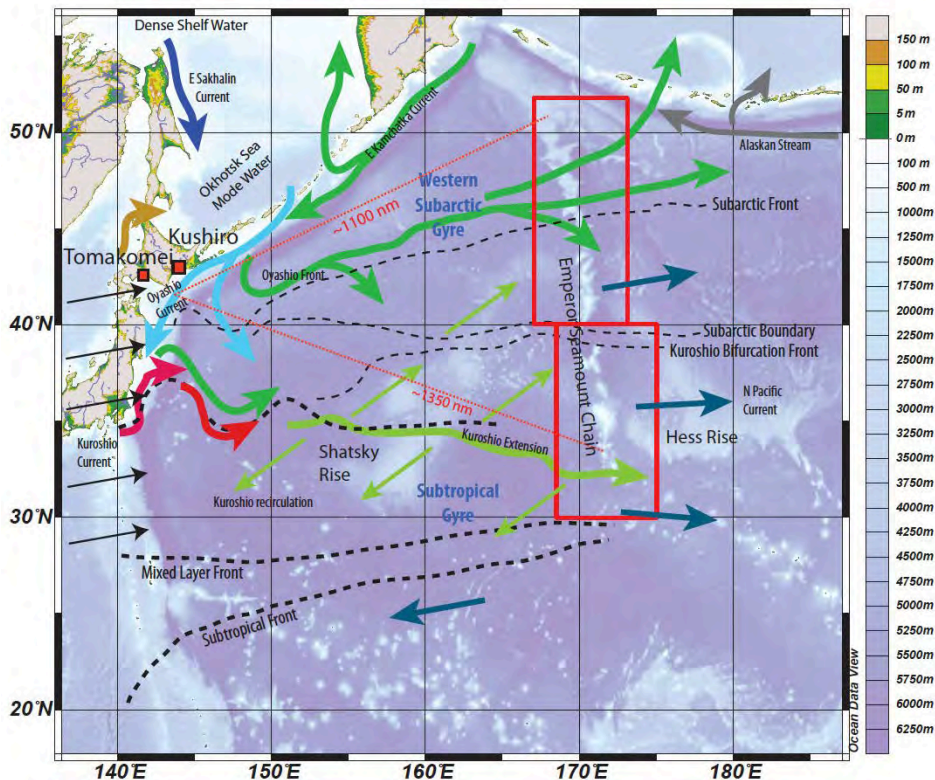


Figure 4-1. Bathymetric chart of the N Pacific showing the SO264 study area. Major features of N Pacific oceanographic and atmospheric patterns are outlined: The N Pacific is characterized by large, seasonally varying circulation patterns, the N Pacific subpolar and the subtropical gyres. The N Pacific subtropical gyre consists of the western boundary current system of the Kuroshio Current (light green), the eastward directed N Pacific Current at the northern part of the Subtropical Gyre (blue), the California Current heading southward (not shown),

and the North Equatorial Current, which flows westward on the south side of the gyre (not shown). North of it at ~40°N and separated by the Subarctic Front, the N Pacific Subpolar Gyre is adjoined, having the eastward directed N Pacific Current in common with the Subtropical Gyre. At the eastern boundary, the California and Alaska currents (dark gray) flow north and westward, changing over into the southward-bound Oyashio (light blue) and E Kamtchatka currents (green). The Subarctic Front is a sharp demarcation between gyres, being present all across the N Pacific and separating upwelled nutrient-rich and productive surface waters to the north from mainly downwelled nutrient-poor surface waters to the south (shaded areas). Black arrows at left margin mark Westerly Wind storm tracks in the N Pacific.

The paleoceanographic approach is strongly supported by proxy calibration, evaluation, and validating studies, which comprised intense seawater and plankton sampling activities during SO264 between 7°S and 50°N. Along the transect, zooplankton was sampled at surface and within the water column, with a main focus on calcifying species (foraminifera and pteropods) and siliceous plankton (radiolarians and diatoms). Water samples were taken at similar depths, to allow for a calibration between ocean parameters and the geochemical signal in the shells. The analytical focus is on trace elements, stable isotopes (carbon, oxygen, silica), carbonate chemistry, neodymium and silicate. Furthermore, suspended organic matter and microplastics was sampled from the water column.

Detailed information on the **scientific backgrounds** and the **research objectives** of the different working groups is given in the beginning of the specific chapters of the cruise report. The **station list** of cruise SO264 is given in Appendix 4.

Appendix 4. SO264 Station list.

5. Work details and first results

5.1 Weather conditions during cruise SO264

(Dirk Nürnberg)

Weather conditions during cruise SO264 were mostly excellent and allowed continuous working on RV SONNE. Station work had to be abandoned just for a couple of hours during SO264. Most of the time, winds were blowing from southeasterly directions, with predominant wind directions from ESE or S (15-20%) (Fig. 5.1-1). Wind speeds of more than 15 m/s (~7 Bft) from southeasterly directions were relatively seldom (<3%). Moderate winds speeds of 5-10 m/s (~4-5 Bft) dominated. Northwestern winds were commonly rare (<5%), and according wind speeds moderate (max. 20 m/s).

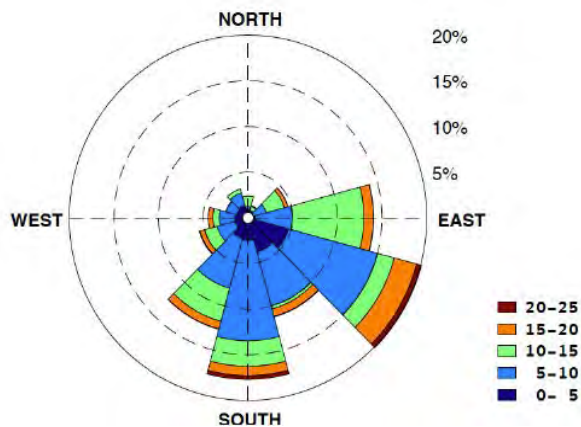


Fig. 5.1-1. Wind direction and speed (m/s) during SO264 from June 26 to Aug. 14, 2018.

Air and seasurface temperatures were continuously monitored by RV SONNE sensors, from the day of disembarkment at Suva (Fiji, ~18°S) on June 26, 2018 to the end of the station work on August 14, 2018 at ~50°N (Detroit Seamount) (Fig. 5.1-2). The dataset series thus cover a latitudinal range from ~68°. In the tropical W Pacific, air temperatures (~27°C) are commonly cooler by ~2°C than the seasurface temperatures (~29°C), a pattern, which is common to the West Pacific Warmpool area up to ~23°N. Slightly north of the equator and restricted to the area of the Equatorial Current system, air temperatures drop to 25°C, while seasurface temperatures remain high and unchanged. North of ~23°N towards the northern boundary of the Subtropical Gyre (the Kuroshio

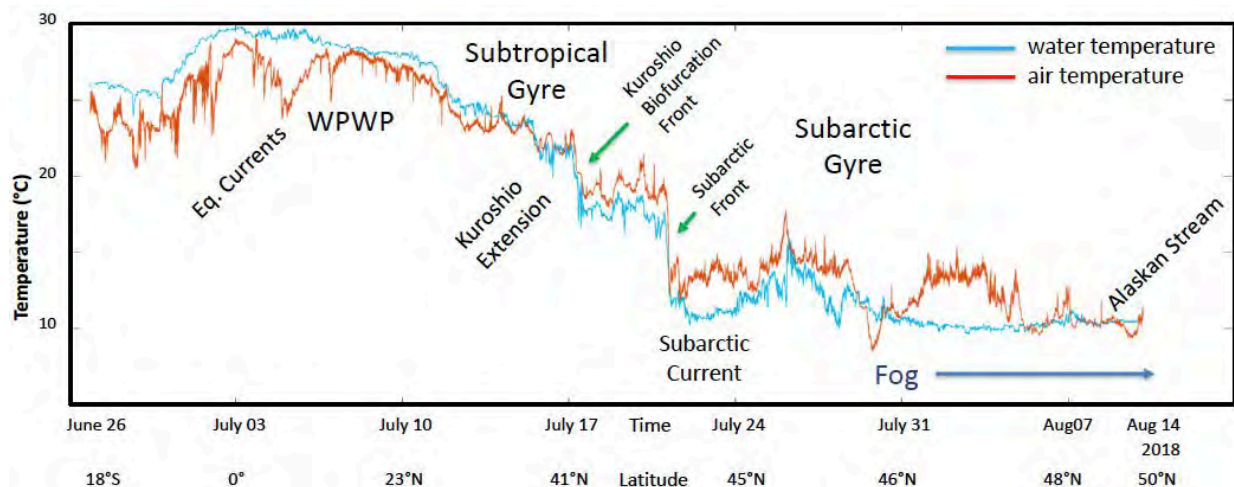


Fig. 5.1-2. Seasurface (blue) and air (red) temperature (°C) during SO264, plotted versus latitude (~18°S to ~50°N) respectively time (June 26 to Aug. 14, 2018).

Bifurcation Front or Subarctic Boundary), seasurface and air temperatures converge and cool down to ~23-24°C.

A significant drop of seasurface and air temperatures to ~17°C and 19°C, respectively, takes place north of ~41°N. From here to the end of our data profile at ~50°N, air temperatures commonly stay considerably higher than the seasurface temperatures. An even more dramatic temperature decline of ~5°C is observed at the Subarctic Front. North of it within the Subarctic Gyre, air temperatures broadly remain at ~13-14°C, while seasurface temperatures are cooler at ~10-12°C and tend to decline further north.

5.2 PHYSICAL OCEANOGRAPHY

(Gastón Kreps)

5.2.1 Background and Objectives: The N Pacific Ocean oceanography

The objective of the physical oceanography studies during cruise SO264 was the determination of the water mass characteristics on a meridional transect (10°S to 52°N) at ~170-178°E along the Emperor Seamount Chain in the western N Pacific (Fig. 5.2-1). These data provide the basic oceanographic data for (1) the extensive water sampling program that was carried out during the cruise, and for (2) working groups focussing on plankton research and proxy calibration studies to assess and compare proxy-based empirical relationships to actual water column data from the same spot location as the respective sampling sites.

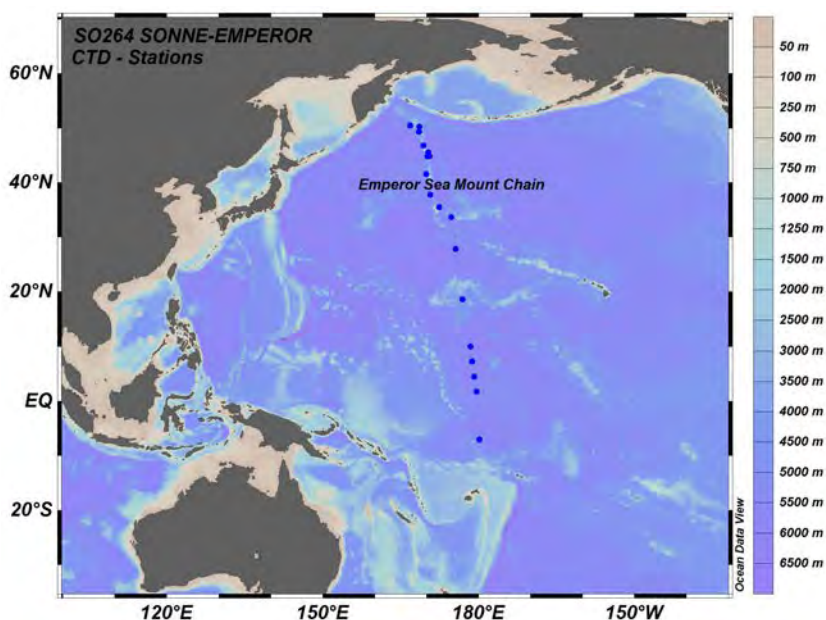


Figure 5.2-1. CTD stations location. 18 CTD stations were done during the SO264 cruise.

The western N Pacific Ocean is a cross road and major pathway, where different water masses converge or traverse from mid-latitude and high-latitude on their way to the ocean basins and adjacent marginal seas (Table 5.2-1). One prominent feature of the lower-latitude western N Pacific Ocean is the 'West Pacific Warm Pool', the world's warmest open ocean surface water spanning the northern and southern tropical western N Pacific Ocean. This warm pool modulates global and regional climate systems, including the El Niño-Southern Oscillation (ENSO) and the Asian and Australian monsoon systems. Another main feature is the world's largest system of Western Boundary Currents (WBC), which consists of the northeastward flowing Kuroshio Current and the southward-flowing Oyashio Current in the Northern Hemisphere, and the East Australian Current in the South. Two equator-ward low-latitude WBCs complete this system, the Mindanao Current in the N Pacific, and the Gulf of Papua Current/New Guinea Coastal Current system in the South. These two features are closely linked; a recharge or discharge of the warm pool triggers a response of the WBCs and in turn, the variability of the WBCs modulates the evolution of the warm pool (Hu et al. 2015).

The wind forcing for the N Pacific consists of the Westerlies at latitudes north of $\sim 30^\circ\text{N}$, and the Trades to the south. Within the Trade Wind area, the Intertropical Convergence Zone (ITCZ) occurs, centered at 10°N . The dominant pattern of atmospheric circulation north of $\sim 30^\circ\text{N}$ is associated with the Aleutian Low. The mean winds create Ekman divergence north of $\sim 40^\circ\text{N}$, Ekman convergence between $\sim 15^\circ\text{N}$ and 40°N , and Ekman divergence between $\sim 5^\circ\text{N}$ and 15°N . These patterns drive Sverdrup transport, which is northward-oriented in Ekman divergence regions and southward-directed in Ekman convergence regions. Because the return flow for this interior ocean transport must be in WBCs, this produces a cyclonic circulation in the north (the Subpolar Gyre), anticyclonic circulation at mid-latitudes (the Subtropical Gyre), and a meridionally narrow cyclonic circulation centered at $\sim 10^\circ\text{N}$. The WBCs associated with these three gyres are: the East Kamchatka Current/Oyashio, the Kuroshio, and the Mindanao currents.

The Emperor Sea Mount Chain is located in the western N Pacific Ocean. From a physical point of view, the Emperor Seamount Chain represents a large-amplitude perforated barrier, the peaks and ridges of which extend upward into the region of strong horizontal temperature and salinity gradients. As a consequence, the impinging flow reaches the bottom topography and is modified by it (Charney and Flier, 1981). In the vicinity of the southern Emperor Seamounts, the impinging flow is the Kuroshio Extension, which is a ~ 100 km wide meandering baroclinic jet with strong vertical and horizontal velocity shear (Kawai, 1972). In the northern part of the Emperor Seamounts, the flow is a weakly baroclinic eastward drift.

Table 5.2-1. Main water masses present in western N Pacific.

Water masses	Abbreviation	Salinity	Density
Antarctic Intermediate Water	AAIW	34.4 – 34.6	27.1 – 27.3
Lower Circumpolar Deep Water	LCDW	34.6 – 34.7	
North Pacific Intermediate Water	NPIW	34.0 – 34.3	26.7 – 27.4
North Pacific Tropical Water	NPTW	<32.25	23.0 – 25.0
South Pacific Tropical Water	SPTW	>32.5	23.5 – 25.0
North Pacific Subtropical Mode Water	STMW	34.6 – 34.8	25.0 – 25.6
Upper Circumpolar Deep Water	UCDW		27.5 – 28.0
Western North Pacific Central Water	WNPCW	33.5 – 34.5	25.2 – 26.4
Western South Pacific Central Water	WSPCW	34.8 – 35.5	26.2 – 26.6
Pacific Sub Arctic Intermediate Water	PSIW	33.8 – 34.3	
Pacific Subarctic Upper Water	PSUW	32.6 – 33.6	

The Emperor Seamount Chain is characterized by three main fronts. These are, from north to south, the Polar Front, which occurs at the southern boundary of the subsurface temperature minimum (Uda, 1963), the Subarctic Front, which occurs at the southern edge of the low-salinity subarctic water mass (Roden, 1977), and the Kuroshio Front, which is located at the northern boundary of the Kuroshio Extension current (Kawai, 1972). The intensity of these fronts varies with geographical position and season.

5.2.2 Methods

The physical-oceanographic working group concentrated its activities along a transect from 7°S to 51°N along ~170°E in the N Pacific. The main working area is the N-S trending submarine chain of volcanos, the Emperor Seamount Chain. Our studies accompany and provide basis oceanographic data for working groups involved in plankton and proxy assessment research. The main instrument used is the RV SONNE owned CTD (conductivity, temperature, depth) sensor attached to a water sampler rosette consisting of 24 non-metallic Niskin bottles of 10 liters each (Fig. 5.2-2). At each station (Appendix Table 5.2-1), the unit was lowered to depth, and raised again while taking water samples. The main instrumentation used is the SeaBird 911+ CTD, with two temperature and conductivity, two oxygen, a fluorescence and turbidity sensors, and a Photosynthetically Active Radiation (PAR) sensor (provides highly sensitive data on light irradiance through the water column). The altimeter sensor attached to the rosette monitors the distance to the seafloor. The Seabird CTD is installed horizontally in the lower part of the rosette (Fig. 5.2-2). With this configuration and location of the sensors close to uncontaminated clean seawater, we minimize turbulent sea wakes, especially during the downcast run. The GPS position of the CTD at any time during the profile is provided by means of NMEA. The raw CTD data were processed with the SeaBird Data processing software according to SeaBird recommendations. In the Appendix Table 5.2-2, the configuration report and calibration sheets are provided.



Figure 5.2-2. SeaBird 911+ CTD from RV SONNE installed horizontally and rosette with 24 bottles of 10 liters. Photography by S. Niemann.

The routine protocol for the deployment of the CTD/Rosette includes several steps: First, the device is lowered to 10 m water depth in order to check whether pump and sensors are working properly. Second, the device is raised to the surface, and subsequently lowered to depth, the first 200 m at 0.5 m/s and then at 0.7 m/s. The upcast is done at 1

m/s with stops at pre-defined water depths to release and fill the Niskin bottles. The communication between CTD lab and the winch operator is done via radio control. When the CTD/rosette is back on board, the sampling of seawater starts (see Chapter 5.3). After each deployment, the minimum maintenance and the proper care of the sensors are necessary to guarantee data quality. It is recommended to rinse all sensors with a solution of detergent (Triton-x) and deionized water, applied by 60 ml syringes fitted with Tygon tubing. The syringes attached to the sensor intakes between the casts allow to bath the temperature and conductivity sensors (but not the oxygen sensor) to keep the sensors clean. Rinsing the bottle-release mechanism (pylon or carousel) with warm freshwater after each cast can help to prevent salt accumulation and thus bottle misfires. After processing the CTD-data with the software SBE Data Process, all datasets of each station were plotted in Ocean Data View (ODV; Schlitzer, 2014) to illustrate different water masses. The bathymetry used in ODV is based on GEBCO-2014-6x6minutes (GEBCO 2008). Data sheets that include station number, GPS data, date time (UTC), the bottle summary and the CTDO diagram are given for each station in the Appendix Table 5.2-1.

5.2.3 Preliminary results

The temperature vs. salinity (T-S) diagram is shown in Fig. 5.2-3. The T-S diagram is a common tool in Oceanography to identify water masses. Both, T and S are conservative properties, as they are modified only by the interaction with the atmosphere and by mixing with other waters, and not by biological or chemical activities. These properties allow to identify water masses along the SO264 transect.

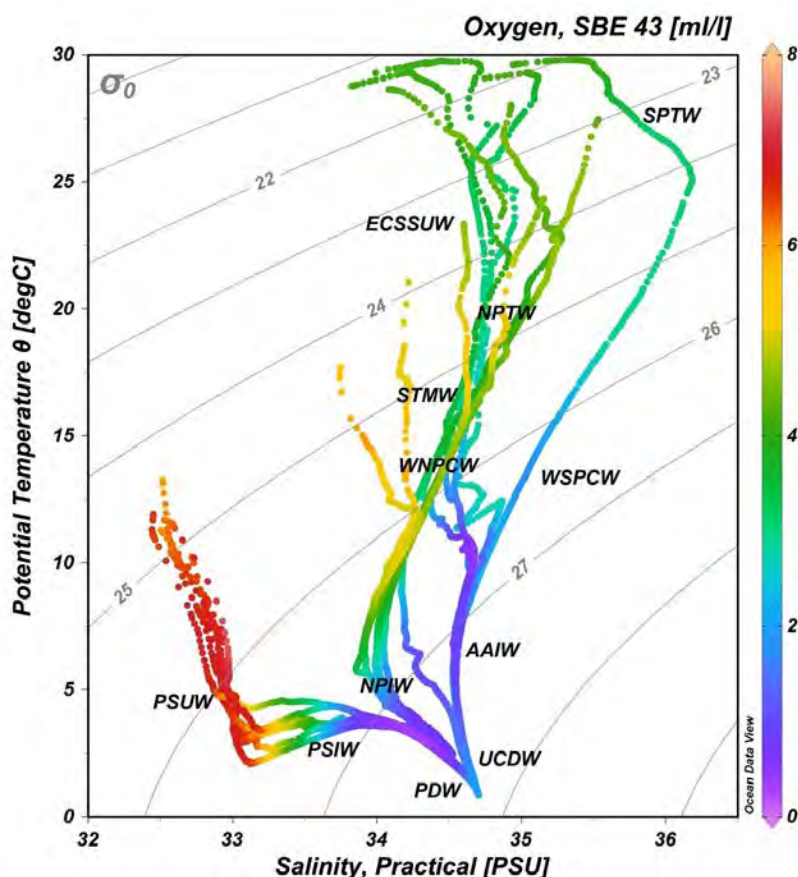


Figure 5.2-3. Temperature vs. salinity. Water mass identification and isopycnals in light grey. Oxygen as 3rd variable colored according to the right hand side color bar. Data taken from Ocean Data View (Schlitzer, 2016).

In Fig. 5.2-3, the intermediate waters in the intermediate salinity minimum layer are the North Pacific Intermediate Water (NPIW), the Antarctic Intermediate Water (AAIW) and the Pacific Subarctic Intermediate Water (PSIW). The NPIW is formed in the mixed water region (waters from the Oyashio, Kuroshio currents and the Tsugaru Warm Current influence the mixed water region) and extends into the Subtropical Gyre (Sverdrup et al., 1942; Talley, 1993). The AAIW forms at the ocean surface in the Antarctic Convergence Zone (commonly termed Antarctic Polar Frontal Zone), and extends into the tropical N Pacific. A vertical change of dissolved oxygen is common at any latitude and reaches maxima in Subarctic waters. It is high in the surface layer, decreases down to minimum values at intermediate layers, and increases to the sea bottom as shown in Fig. 5.2-3.

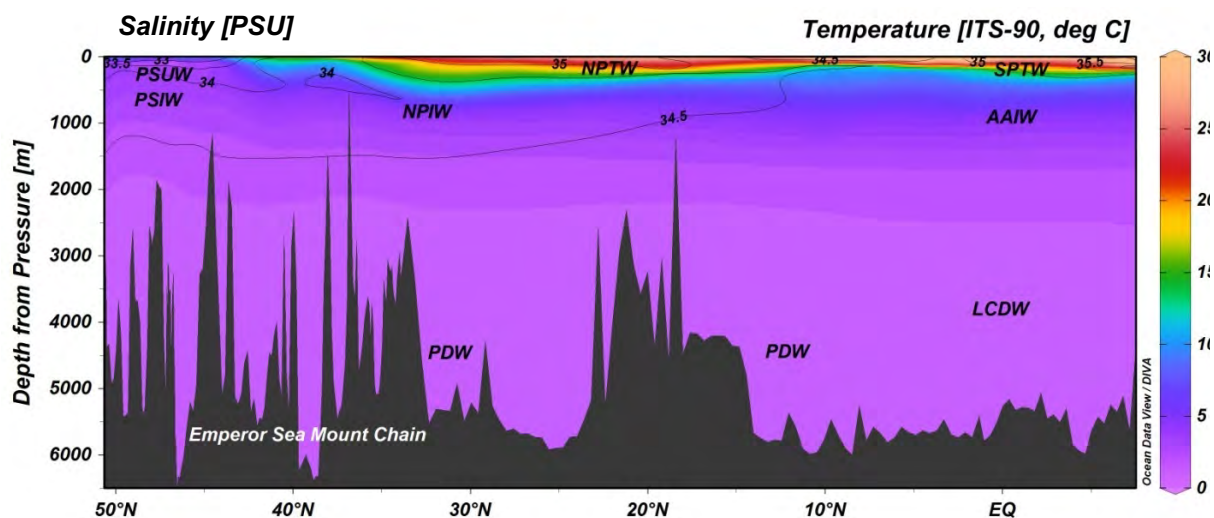


Figure 5.2-4. Section with all CTD stations. Temperature is colored according to the right side color bar (DIVA settings ODV). Isohaline are overlain as black contour lines with numbers. Data taken from SO264 CTDs. Diagram made with Ocean Data View (ODV; Schlitzer, 2014).

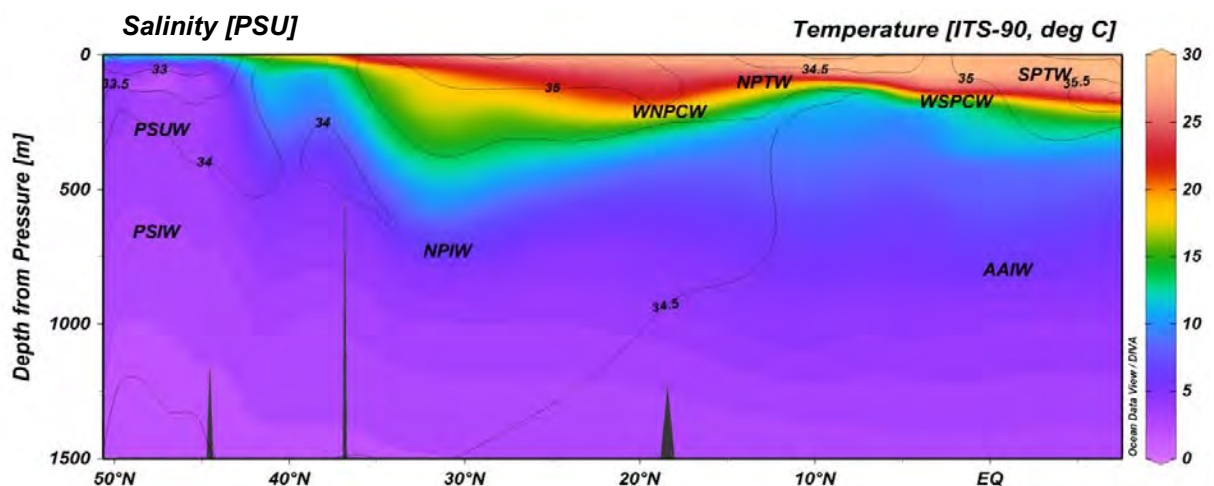


Figure 5.2-5. Section with all CTD stations down to 1500 meters water depth. Temperature is colored according to the right side color bar (DIVA settings ODV). Isohaline are overlain as black contour lines with numbers. Data taken from SO264 CTDs. Diagram made with Ocean Data View (ODV; Schlitzer, 2014).

The sections plot based on all CTD casts accomplished during cruise SO264 are shown in Figs. 5.2-4 and 5.2-5, presented for different depth scales. The different water masses were included into the section plots, based on their identified signatures in the T-S diagram (Fig. 5.2-3). The intermediate water masses, AAIW, NPIW and PSIW were clearly identified, showing well-defined differences in their properties and location during cruise SO264. Water temperature is maximum near the sea surface between 4°S and 2°S, being above 30°C, and is almost uniform above 28°C in a thin surface layer south of ~25°N (Fig. 5.2-5). Salinity in the Subarctic region is <34.0 practical salinity units (psu) in a surface layer of ~400 m. North of 41°N, salinity ranges at 33.5 psu at water depths shallower than 150 m. Water south of 40°N has a subsurface salinity minimum of <34.1 psu. The water at the salinity minimum is defined as NPIW. South of 12°N, a less obvious salinity minimum below 34.55 psu exists at a water depth of ~800 m, which is AAIW from the S Pacific.

Appendix Table 5.2-1

Bottle summary and station plots.

Appendix Table 5.2-2

Instrument configuration and calibration report sheet from SBE 911 onboard RV SONNE during cruise SO264.

5.3 Water column sampling for microfossil-based proxy calibrations

(N. Keul, A. Jentzen, L. Liu, S. Mellon, V. Schuhmacher, Y. Yu, L. Lembke-Jene)

5.3.1 Background and objectives: Plankton and water sampling

An intense water column sampling program has been carried out between 7°S and 50°N, aiming at evaluating, calibrating and validating paleoceanographic proxy parameters. Zooplankton was sampled in both, the surface (along the transect) and within the water column (using multineets), with a main focus on calcifying species: foraminifera and pteropods, as well as on siliceous plankton (radiolarians and diatoms). Water samples were taken at similar depths, to allow for a calibration between water parameters and the geochemical signal in the shells. Here the focus was mainly on trace elements, stable isotopes (carbon, oxygen, silica), carbonate chemistry and silicate. Furthermore, suspended organic matter and microplastics was sampled in the surface.

Targeted calcareous plankton: Planktic foraminifers and pteropods

Planktic foraminifers are unicellular organisms, which dwell in the upper ocean. The calcitic tests of the planktic foraminifers have a high preservation potential in the sediment and are therefore an important signal-carrier for paleo-reconstructions. The species distribution patterns provide information about seawater temperature and trophic conditions (Schiebel and Hemleben, 2017, and references therein). The elemental and stable isotopic compositions of the foraminiferal calcite are important proxies to reconstruct past ocean temperature or salinity variability. Pteropods are marine planktic gastropods that are found globally in the ocean. They consist of two orders: the *Gymnosomata* (naked pteropods) and *Thecosomata* (shelled pteropods), which are separated by their morphology, behavior, and position in the marine food web. Compared to other mesozooplankton, pteropods have high ingestions rates, consuming up to 20% of the daily primary productivity in the Southern Ocean (Hunt et al., 2008). Pteropods themselves are an important prey for predators such as salmon, birds, herring and larger zooplankton. They are also contributing to the downward flux of inorganic and organic carbon through the ballasting effects of their fecal pellets and mucous nets, daily migrations and mass mortality events, burying the shells at the seafloor. Pteropod shells consist of aragonite, making them more susceptible to ocean acidification than other shelled marine plankton such as foraminifers and coccolithophores with calcareous shells. Globally, pteropod shells account for at least 12% of the total carbonate flux (Berner and Honjo, 1982). Despite their ecological and biogeochemical importance, essential details about pteropod global biomass distribution are not well resolved, especially in the central Pacific Ocean (Fig. 5.3-1). Another gap in knowledge constitutes the trace elemental and stable isotopic composition of pteropods: only very few studies have addressed their composition.

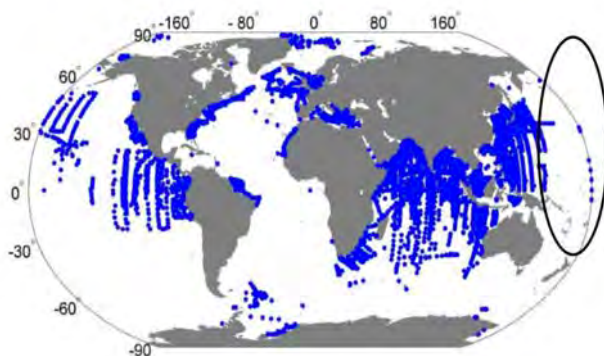


Figure 5.3-1. Map showing global pteropod biomass data, the black circle indicates the area of this study. After Bednaršek et al. (2012).

To understand the ecology, the elemental and stable isotopic composition of both, foraminifers and pteropods, we addressed the following primary research objectives:

- Description of the distribution of pteropod/foraminifer biomass in the central Pacific Ocean in the upper 800 m of the water column.
- Assessing the fractionation of trace elements and stable isotopes between pteropod/foraminiferal shells and the surrounding water masses.

A secondary objective constitutes the phylogenetic analyses of marine planktic gastropods: pteropods and heteropods. These studies will be carried out by the group of K. Peijneburg (Naturalis, Leiden, The Netherlands) on material from the surface net tows (preserved in pure ethanol).

Siliceous plankton: Radiolaria/diatoms

Siliceous sediments are covering large parts of the seafloor in the Northwest Pacific and are mainly composed of diatoms, radiolarian and silicoflagellates. These microfossils, especially diatoms, have been used already successfully in paleoceanographic studies, for instance for the reconstruction of paleo-temperatures using the ratio of warm to cold water diatom species (Kanaya and Koizumi, 1966). We here plan to study the isotopic fractionation between the shells of the siliceous plankton and the surrounding water, with a specific focus on oxygen and silica isotopes. Results will be compared with samples from surface sediments collected during the SO264 expedition. In order to reach the required sample size for isotopic measurements, vertical net hauls were performed at the same location for 28 hours (in the Tenji Seamount area, Station SO264-60, 49°18.451'N 168°33.429'E). An investigatory net haul was performed at this station, to determine at which depth radiolarian were mostly present (700-500-250-160-40-0 m sampling interval). Afterwards, a total of 10 net hauls was performed, with 5 nets opened during each net haul (slacking with 0.5 m/s and hoisting with 0.3 m/s). Four of these nets were cast between 700 and 300 m to sample deep living radiolarian species, where the last net was dedicated to sample the surface waters (0-50 m). Samples were studied under the microscope (smear slide): subarctic species dominated the siliceous plankton community. Samples were pooled according to sampling depth and frozen at -20°C until further processing at the AWI.

5.3.2 Multinet / plankton-net and underway pumping

Zooplankton filtering by underway pumping from ship's seawater intake

Living planktic organisms (foraminifers and pteropods) were collected in the near-surface water during the cruise (transit and stations, ~11°S-40°N). The surface water was taken from the ship's seawater intake (membrane pump) from 2.1-3.9 m water depth and filtered with a sieve of 63 µm mesh size. The sieve was secured inside a PVC tube of 40 cm in length and 10 cm in diameter to collect the zooplankton safely (Fig. 5.3-2). To calculate the abundance of the zooplankton, the filtered water volume was measured with a flow meter attached between the seawater-tap and the filter system. A total of 68 samples were obtained and a total of 91 m³ were filtered (ca. 1.5 m³ seawater per sample, Appendix Table 5.3-2 and Appendix Fig. 5.3-1). The samples were picked wet with a glas pipette after collection, or preserved in filtered seawater and ethanol (50:50), and stored at 4°C. During the cruise surface sea temperature, salinity and chlorophyll concentrations were recorded by the thermosalinograph (Appendix Table 5.3-3).



Figure 5.3-2. Left: Seawater sampled from below the ship with the ship's pump was filtered through a sieve with 63 μm mesh size (GEOMAR). Right: Multiple Closing Net (Hydrobios Kiel) for plankton sampling.

Multinet / plankton-net sampling

During the SO264 cruise, plankton was collected vertically using a multiple closing plankton net (Hydrobios Kiel, nominal mouth area of 0.25 m²) with five nets (100 μm mesh size for calcareous plankton and 55 μm mesh size for siliceous plankton), allowing stratified vertical sampling of five depth intervals (Fig. 3-1). A total of 42 stations were sampled from ~7°S-50°N (Appendix Table 5.3-1). For foraminiferal and pteropod analyses two tows were cast at each station: A shallow plankton net tow between 100 m and the surface (standardized intervals 100-80-60-40-20-0 m) and a deep tow between 700 or 800 m water depth and the surface. The sampling intervals of the deep net tow were chosen according to the water mass distribution at the sampling site and the deep chlorophyll maximum. For instance, at station SO264-11-3 (Koko Seamount, 33°N 33.4'S 172°E 23.2'E), the intervals were 0-40 m (upper mixed layer), 40-160 m (deep chlorophyll maximum), 160-350 m (above NPIW), 350-500 m (upper NPIW), 500-800 m (lower NPIW). All stations and depth intervals are listed in Appendix Table 5.3-1. Slacking and hoisting was carried out at 0.5 m/s. After each haul the net bags were washed with sea water and the net cups were rinsed with filtered sea water. The residue of the net cups containing the plankton >100 μm was immediately observed under the microscope and then diluted with filtered seawater and ethanol (50:50) (pure ethanol in the case for samples for K. Peijnenburg, see below) and stored at 4°C (-20°C for K. Peijnenburg). Calcifying plankton will be sorted and counted from sampling bottles after return to the home laboratory (MPIC and IFG/Univ. Kiel). At all multinet stations a CTD carrying a fluorescence probe to record the fluorescence in the water column (a measure of the chlorophyll concentration) was also performed at the same location (see Chapter 5.3.3).

Suspended organic matter

Suspended particles from the sea surface were sampled during transit, surveys, and "clean ship" water stations (Appendix Table 5.3-6). Dependent on particle concentrations, ~100-600 liters of seawater were filtered through pre-combusted GFF filters (diameter 142 mm, mesh size 0.7 μm). The filters were placed in a Millipore PVC filter holder (Fig. 5.3-3) that was connected to the ship's seawater intake membrane pump. The filters were folded in half, wrapped in pre-combusted aluminum foil, and stored immediately in a freezer at -20°C. Water samples were collected from the filtrate at the beginning and end of each filtering sample. One 60 mL and one 8 oz bottle were

collected at the start for $\delta^{18}\text{O}$ and salinity, respectively, followed by one 60 mL bottle for $\delta^{18}\text{O}$ at the end.

A total of 60 samples were collected along the cruise track (Appendix Fig. 5.3-2). Filters will be analyzed for organic biomarkers including alkenone concentration, alkenone unsaturation ($U^{K_{37}}$ index), and delta-deuterium.

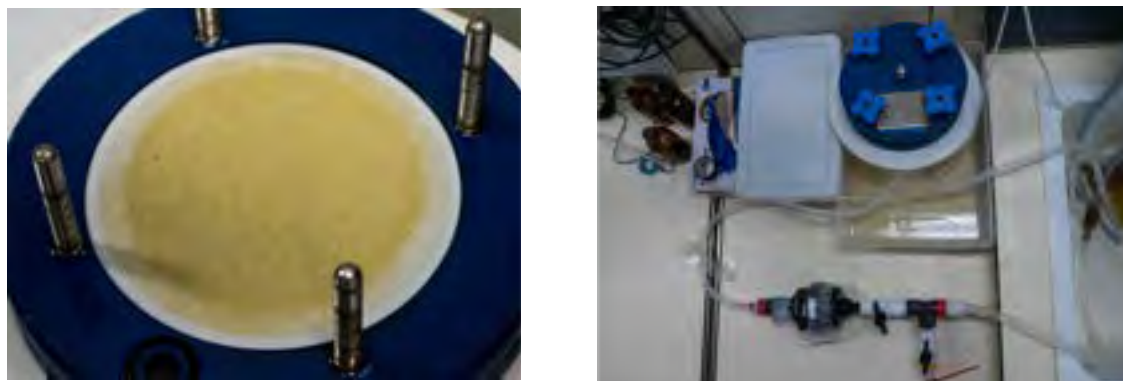


Figure 5.3-3. GFF filter containing suspended particles from the surface ocean (left) and the entire filtration system (right).

Preliminary results: Living plankton

The first stations on our transit to the working area were in the tropical/subtropical waters between $\sim 7^\circ\text{S}$ and $\sim 33^\circ\text{N}$, characterized by high SST, SSS and low chlorophyll concentrations in the surface water (Fig. 5.3-4). At the first station typical tropical to subtropical planktic foraminifers such as *Globigerinoides ruber*, *Globigerinoides sacculifer*, *Globigerinoides conglobatus* and *Globigerinita glutinata* were found alive in the upper water column. At the station close to the NECC we found mainly *Globigerinoides sacculifer* indicating the warm ($\sim 29^\circ\text{C}$) and oligotrophic conditions in the mixed layer (Jentzen et al., 2018). Few empty tests were abundant in the subsurface below 80 m water depth (Fig. 5.3-5A). In these two stations, pteropod abundance was intermediate. Tropical and subtropical species were present, such as *Diacria* sp., *Creseis* sp., as well as heteropods (*Atlanta* sp.). Further north, at $4^\circ\text{--}7^\circ\text{N}$, living planktic calcifiers had a low abundance and the station was mainly characterized by a high abundance of copepods. At 18°N , the southern edge of the north Pacific Gyre, N-fixing cyanobacteria were present (*Trichomonas* sp.) indicating oligotrophic conditions. Here, we also found the rare abundant planktic foraminifer *Candeina nitida* and many pteropods as well as many juvenile heteropods (*Atlanta* sp.). In the deeper nets (>80 m water depth) at the same station we found deep dwellers such as *Globorotalia tumida*. In the oligotrophic north Pacific Gyre ($\sim 27^\circ\text{N}$) high abundances of living planktic foraminifers such as *Globigerinoides sacculifer*, *Globigerinoides ruber*, *Globigerinoides conglobatus* were found in the upper 100 m water depth; in the deeper net we collected *Orbulina universa*, and small specimens of *Globorotalia truncatulinoides*.

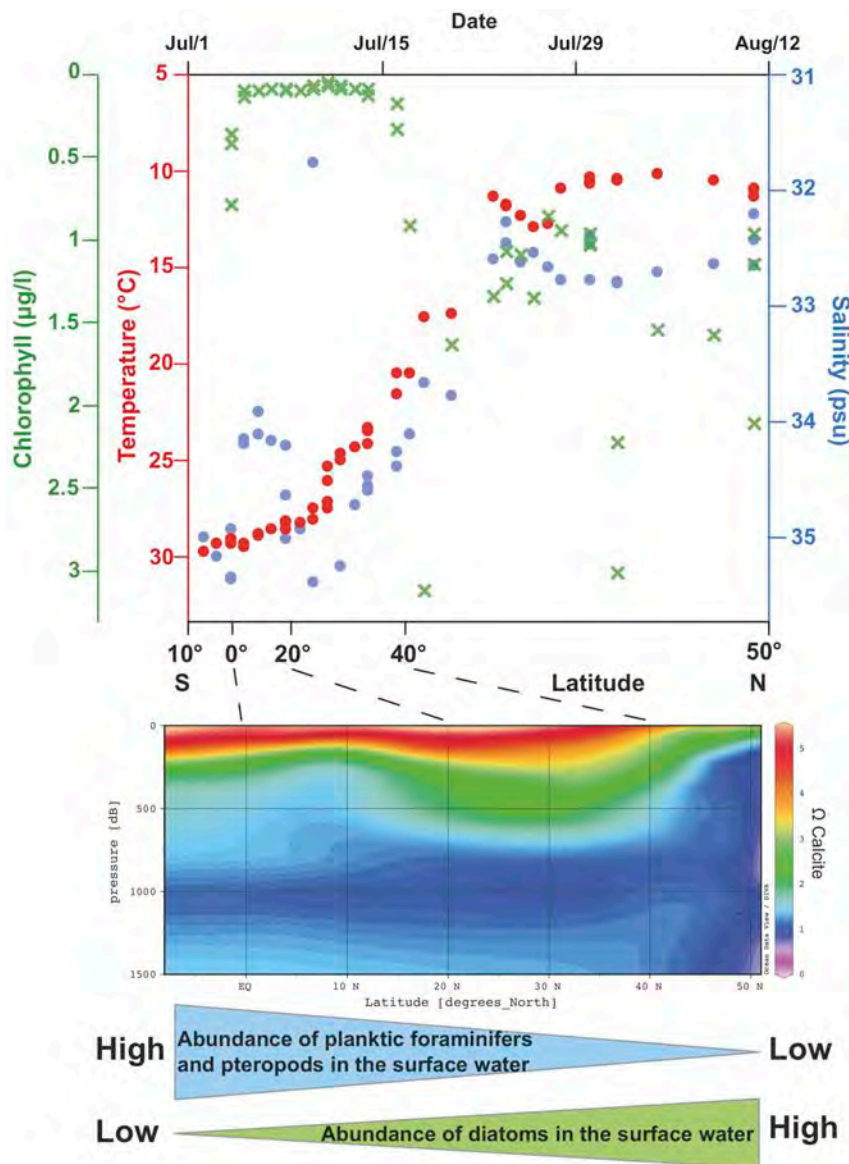


Figure 5.3-4. Upper panel: Average temperature, salinity and chlorophyll concentrations of the sea surface waters measured by the ship's thermosalinograph between the beginning and the end of each filter sample (PF) from PF1 to PF57 between ~10°S and ~50°N (Appendix Table 5.3.3). Middle panel: Ω calcite depth profile along the transit and working area (~10°S-50°N). Ω calcite was calculated from the measured pH and alkalinity of the sampled seawater. Lower panel: Sketch of the abundance of foraminifers, pteropods and diatoms in the PF samples estimated from visual

At the following stations, pteropods were highly abundant: station 8 (33°N), station 11 (35°N) and station 13 (37°N) (mainly small ones), where interestingly only few living planktic foraminifers were found. At ~40°N we observed a change in the plankton composition: diatoms (mainly *Coscinodiscus sp.*) were present in very high abundances (Fig. 5.3-4), as indicated by the high Chlorophyll concentrations in Fig. 5.3-4. Additionally, we found a high abundance of the foraminifer *Neogloboquadrina dutertrei* between 60 and 100 m water depth reflecting most likely the high food availability (Jentzen et al., 2018 and references therein). At the stations further north, abundances of calcifying plankton remained low and higher abundances of the planktic foraminifers *Globigerina bulloides* and *Neogloboquadrina pachyderma* indicate the changing conditions of the water masses. The region north of 40°N is also characterized by lower calcium carbonate saturation (Fig. 5.4-4), probably explaining at least in part the low abundances of calcifiers. Additional factors could be caused by the high diatom abundance (Fig. 5.3-5B), usually coinciding with low foraminiferal abundance. Notably,

this change from a regime dominated by calcifying plankton to diatoms is also reflected in the sediment cores, where a change from calcareous ooze to siliceous ooze occurred at $\sim 45^{\circ}\text{N}$.

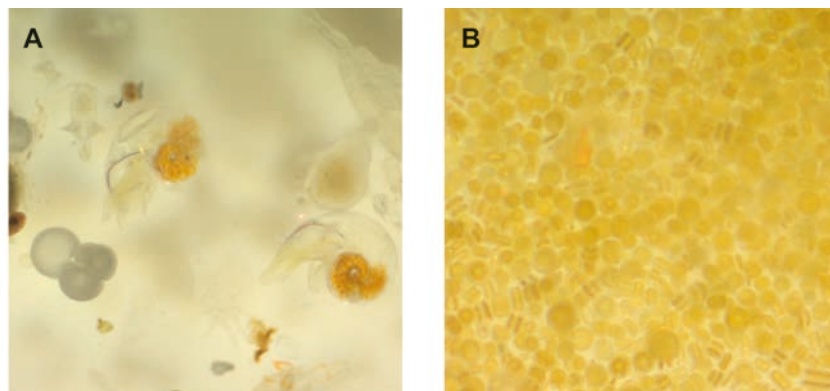


Figure 5.3-5. Pictures from the microscope. A: Pteropods and foraminifers of MSN station 6 (18°N) (Appendix Table 5.3.1). B: Diatoms of PF sample number 49 (46°N) (Appendix Table 5.3.2).

5.3.3 Water sampling by CTD / rosette

Water samples from the CTD (see Chapter 5.2) were taken at all CTD stations (see Appendix Table 5.3-4) to measure the following parameters (listed in the order of sampling):

Carbonate chemistry (pH, total alkalinity, dissolved inorganic carbon), light stable carbon and oxygen-isotopes, trace elements, radiocarbon (not at all stations), Neodymium / Nd-isotopes (not at all stations), Silicate / Si isotopes, microplastic.

Carbonate chemistry: Seawater and MUC sampling

Selected MUC depths of the CTD cast were chosen to take dissolved inorganic carbon (DIC) samples and measure total alkalinity (TA) and pH. After retrieval of the CTD on board, sample vials for carbonate chemistry samples were filled first. Vials containing seawater for pH and TA analysis were stored at 4°C until measurement on board. pH was measured within 120 minutes and TA was measured as soon as samples obtained room temperature. A two-point NBS calibrated glass electrode (Schott Instruments, Mainz, Germany) interfaced to a WTW pH meter was used to measure pH potentiometrically. TA was determined by potentiometric titrations using a TitroLine alpha plus autosampler (Schott Instruments, Mainz, Germany) and calculated from linear Gran plots. DIC samples were filtered ($0.2\ \mu\text{m}$) and stored at 4°C until measurement at the Alfred-Wegener-Institute in Bremerhaven. They will be measured photometrically with a QuaAatro autoanalyzer (Seal Analytical, Mequon, USA) with an average precision of $10\ \mu\text{mol/kg-sw}$. Measured pH and TA values were used to calculate the complete carbonate system using the CO2SYS software adapted to Excel by Pierrot et al. (2006).

Stable isotopes, nutrients and radiocarbon

Samples for isotope and nutrient analyses were taken according to standard protocols immediately after the CTD rosette was retrieved aboard RV SONNE. Clean glass bottles with screw lids were flushed three times with sea water from the Niskin bottles, before fully filling the bottles bubble-free in overflow without air reservoir. From each sampled

bottle depth (cf. Appendix Table 5.2-1 and Appendix Table 5.3-4 for bottle depths) we took the following standard series of samples: (1) one 100 ml glas bottle for oxygen isotope ($\delta^{18}\text{O}$) analysis, (2) one 50 ml glas bottle for stable carbon isotope ($\delta^{13}\text{C}$) analysis of Dissolved Inorganic Carbon ($\delta^{13}\text{C}_{\text{DIC}}$) and DIC concentrations, and (3) one 50 ml wide-necked PE plastic bottle with screw caps for phosphate and nitrate concentrations. All 50 mL samples for $\delta^{13}\text{C}_{\text{DIC}}$ were fixed with 200 μL of saturated HgCl_2 solution under a fume hood to stop biological activity. All glas bottles with screw caps were sealed airtight after sampling with a heated stearin/beeswax mixture to inhibit gas leakage during long-term storage. Samples were thereafter stored refrigerated in the cold rooms at $+4^\circ\text{C}$ (stable isotopes) or deep-frozen at -20°C (nutrients). Sampling for radiocarbon (^{14}C) was similar to $\delta^{18}\text{O}$ sampling, except that sample size was enlarged to 1 L.

Nutrients: Sampling and filtration of water samples for nutrient analysis

For the analysis of sea water nutrients (silicate, $\delta^{30}\text{Si}$ isotopes), water samples of a large volume (8-10L) were taken at various CTD stations and water depths (Appendix Table 5.3-4). The seawater was directly taken from the 10 L Niskin bottle of the CTD rosette by gravity flow into a PE-cubitainer (rinsed with 10% HCl and Milli-Q® water prior to usage). For further analysis, the samples were filtered via a Polycarbonate Track-Etched Membrane filter (pore size 0.4 μm). Prior to each sample filtration, the device and attached filters were rinsed with filtered seawater (Cellulose Nitrate filter, pore size 3.0 μm) from the ship's seawater membrane pump. For rinsing purposes, fresh seawater was filtered nearby each CTD station. After filtration (30-45 minutes per sample), the sample was refilled into the seawater rinsed cubitainer and stored at 4°C at dark conditions. The filters of each sample (4 filters in total / one for each funnel of the filtration plant) were wrapped into aluminium foil and frozen at -20°C . These filters will be used for determination of micro-plastic particles within the water column.

Additionally to the CTD rosette sampling profile during the transit, we carried out one water station with a combined Multinet- (mesh size 40 μm for radiolarians) and Multicorer- (surface sediment) sampling. The Multinet sampling depths were set accordingly to the CTD data. The combination of different sampling tools will allow the data combination and comparison of nutrient water stratification and nutrient consumption of recent and fossile radiolarian species.

Trace element measurements: Seawater and MUC sampling

Seawater samples were taken using AcroPak 500 filter cartridges (0.8/0.2 μm pore size) and those from the MUC/gravity corer using 0.2 μm filter syringes. All samples (Appendix Table 5.3-4). were filled into pre-conditioned bottles (250 mL HDPE for CTD samples, 50 mL plastic vials for MUC samples; pre-conditioned for trace elemental analysis). For transport, trace element samples were packed in two plastic bags and stored at room temperature. After return to the laboratory at Kiel University, elemental concentrations will be determined *via* ICP-OES (Inductively Coupled Plasma Optical Emission Spectrometry).

Neodymium

The oceanic residence time of Nd, though not well established, is known to be of the order of the ocean mixing time. The dissolved Nd isotope composition of seawater is

widely used as water mass tracer in different ocean basins. Although the isotopic distribution of Nd has been examined in great detail, only a limited number of dissolved Nd isotope data is available from the North Pacific. In the modern ocean, North Pacific Deep Water (NPDW, $\epsilon\text{Nd} = -4$ to -6) and North Atlantic Deep Water (NADW, $\epsilon\text{Nd} = -13.5$) represent the two major deep water ϵNd endmembers, which is a consequence of weathering inputs from young volcanic rocks in the North Pacific and older cratonic rocks in the North Atlantic. The north Pacific is the area of major NPDW formation, thus making it a key area for better understanding present and past deep ocean circulation. During the SO264 expedition, we collected 7 vertical seawater profiles along a latitudinal transect between 7°S and 40°N at approximately 178°E longitude. All samples were collected from 10L standard Niskin bottles mounted on a CTD/rosette (Appendix Table 5.3-4). Approximately 20L of seawater per sample were filtered directly from the Niskin bottles into pre-cleaned collapsible 20L LDPE containers for Nd isotopes and [Nd] measurements using AcroPak 500 filter cartridges (0.8/0.2 μm pore size). Each filter was dedicated to a specific depth range and was used for that depth range at each station. The AcroPak 500 Filter cartridges were pre-cleaned and rinsed with MilliQ water, followed by flushing with seawater prior to first use. Following filtration, the water samples were acidified with quartz-distilled hydrochloric acid (HCl) to a target pH of ~ 2 for precise laboratory-based measurements.

5.3.4 Underway pumping: Water samples and microplastic samples

Microplastics

In the framework of a pilot study, surface water samples were collected for the identification of microplastic concentrations along the ship's SO264 route. Samples were collected from the ship's seawater intake (membrane pump) and put through a 63 μm sieve. Material left on the sieve was transferred to a 50 mL bottle using ethanol, and stored at 4°C . Timing of collection, latitude and longitude, and flow volumes of each sample are presented in Appendix Table 5.3.5. Locations are displayed in Appendix Fig. 5.3-3.

Water sampling for carbonate chemistry, trace elements, and stable isotopes

Surface water samples were collected for the measurement of DIC, pH, alkalinity, trace elements concentrations, and $\delta^{18}\text{O}$ and $\delta^{13}\text{C}$ ratios (analogous to samples taken from the rosette) along the ship's SO264 route. Samples were collected from the ship's seawater intake (membrane pump). Timing of collection, latitude and longitude, and flow volumes of each sample are given in Appendix Table 5.3-7. Locations are displayed in Appendix Figure 5.3-4.

Appendix Table 5.3-1. Plankton net stations, sampling intervals and sample destinations during RV Sonne cruise SO264.

Appendix Table 5.3-2 Start and end of plankton filter (PF) samples for foraminiferal and pteropod analyses (sieve mesh size $>63\ \mu\text{m}$) during RV Sonne cruise SO264. * samples for diatom analyses (sieve mesh size $>40\ \mu\text{m}$). ** no end time/seawater volume due to overflow during pumping.

Appendix Table 5.3-3. Data from the Thermosalinograph during plankton filter (PF) sampling (see Appendix Table 5.2.1).

Appendix Table 5.3-4. Water samples taken from CTD rosette.

Appendix Table 5.3-5. Locations, timing, and flow volumes of microplastic samples.

Appendix Table 5.3-6. Locations, timing, and flow volumes of biomarker filters collected from the surface ocean along the cruise track of SO264.

Appendix Table 5.3-7. Locations and timing of surface water collection of samples for DIC, pH, alkalinity, trace elements, $\delta^{18}\text{O}$, and $\delta^{13}\text{C}$ measurements. All samples were collected from the ships seawater intake (membrane pump).

Appendix Figure 5.3-1. PF sample tracks for foraminifers and pteropods analyses (c.f. Appendix Table 5.3-1).

Appendix Figure 5.3-2. Locations of all filter samples collected for suspended particles from the seawater intake (membrane pump) during cruise SO264.

Appendix Figure 5.3-3. Locations of Microplastic samples along SO264 cruise route.

Appendix Figure 5.3-4. Locations of surface water samples for DIC, pH, alkalinity, trace elements, $\delta^{18}\text{O}$, and $\delta^{13}\text{C}$ measurements.

5.4 Hydroacoustics

(Melanie Steffen, Laura Over, Frederic Tardeck, Lars Max, Dirk Nürnberg)

5.4.1 Background

By using *state-of-the-art* hydroacoustic techniques and carrying out detailed mapping (KONGSBERG EM122, ATLAS-Parasound), we were able to find sediment basins (pockets) at bathymetric highs showing sediment deposition of mostly calcite-bearing, undisturbed sediments. Seismic information from previous activities (DSDP, ODP, WEPAMA, INOPEX) in addition provided valuable information for hydroacoustic surveying and selection of core locations.

5.4.2 Bathymetry

Acquisition and Processing

The bathymetric data on cruise SO264 were acquired mainly by using the EM122 and in one part the EM710 echosounder by Kongsberg Maritime. Due to the fact that this cruise took place mainly in deep water, the EM122 was preferred. The EM122 is supposed to measure water depth in a range of 20 m to 11.000 m using an average frequency of 12 kHz (ranging between 10.5 kHz and 13.5 kHz). The ping rate depends on the water depth (max. 5 Hz). In reality at a water depth of ~500 m, the high-frequent EM710 had to be applied, because the EM122 yielded erroneous measurements. This was the case at the summit of Koko Seamount, which with a depth of ~297 m was the shallowest area studied. The EM710 is using a frequency range of 70–100 kHz with 800 soundings per ping. The individual beam width is $0.5^\circ \times 1^\circ$ in a bunch of 256 beams per swath. It operates to a maximum depth of 2000 m.

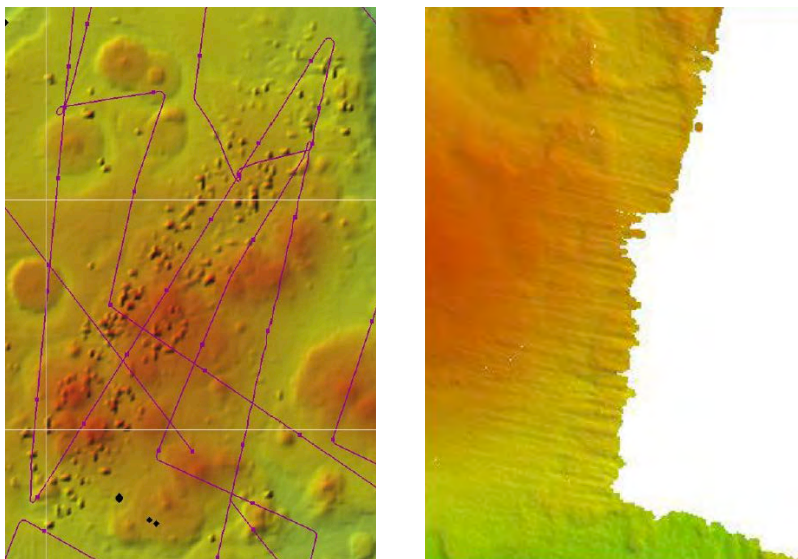


Figure 5.4-1. Systematic errors (left: pancake-shape topographic highs; right: parallel lineaments) in bathymetric data processing were mainly due to bad weather conditions or strong currents.

The EM122 echosounder is able to generate 432 to 864 soundings per ping in the 'Dual Swath' mode. Within that, the arrays consist of 288 beams per swath with an individual beam width of $0.5^\circ \times 1^\circ$. The opening angle can be set manually to a maximum of 150 degrees, which is useful to cover a large area, but at less resolution. The system is connected to a motion sensor (INS), which gives information about the ships movement (heave, pitch and roll), a GPS receiver (DGPS: SeaPath 320+ with FUGRO SeaStar as correction receiver) for the orientation of the data and to a C-Keel-Sonde (Valeport SVPlus), which is mounted in the hydrographic funnel of the vessel and provides continuous information about the sound velocity characteristics of the water.

The EM122 / EM710 echosounder system is paired with the acquisition software SIS (Seafloor Information System). It enables the user to choose between various views of the data and adjust some settings, for example the ping mode, swath angle, and the spacing of the soundings, which is chosen to be equidistant in this cruise. In SIS, the operator feeds in the sound velocity profile (SVP), which was measured by a CTD rosette and the C-Keel-Sonde. The SVP aids the EM 122 to measure the correct depth. Depending on the water's physical properties, the sound velocity changes.

Because of time constraints, a coarser mapping resolution was chosen during transits between working areas. Accordingly, the ship steamed with ~12 kts and the EM122 was operated with an opening angle of 80°, later with use of more current SVPs, these angles were adjusted to 120-140°. The survey lines for transit were defined by the shortest way to the working area and outside the Exclusive Economic Zones (EEZ) of several states, while in the planned working areas points of interest were mapped with higher resolution, and as a process of observing and defining new survey areas/ profile tracks at the same time. On profiles, the speed was reduced to 6 kts to attain a higher accuracy and higher resolution. The opening angle was kept wide open to retain a decent coverage. This is important in order to survey areas of interest for geological sampling with sufficient details.



Figure 5.4-2. Bathymetry and Parasound laboratory onboard RV SONNE.

The resulting data of the SIS is stored in the Kongsberg RAW data (*.all), which can be used in several postprocessing software packages. Caris HIPS and SIPS was used to check the data and reject outliers. On this cruise these mainly occur due to systematic errors, bad weather conditions with high sea states or currents in the deeper water layers (Fig. 5.4-1). The water masses within these currents might have differing physical properties, which lead to different sound propagations. Another challenge that appeared during the transit was the International Date Line, which the SIS software could not handle by itself. As a result, two options can be used to override the software manually. First, one can stop logging and then re-start the system. Alternatively, a new survey line by clicking on 'Line Count' can be manually started. We decided for the first method. The post-processing was done in multiple steps using the Swath, Navigation and Subset Editor. After processing the data, we used the GeoTiff (*.tif) format for exporting the data for subsequent map-making purposes in the Geo-Information System (GIS) software QGIS. In the SO264 GIS Project GEBCO data were used as base map, we defined working areas and seamounts in ASCII files, and underway stations as well as cruise

track way points were defined as separate vector layers, which were kept updated continuously during the cruise (Fig. 5.4-2).

Coverage and description

The mapping started after leaving the EEZ of Fiji and ended before entering Japan's EEZ. The mapped area can be described as long track across the Pacific in northward direction. It has an overall length of ~8500 nm and a mapped area of ~178.970 km² (Tab. 5.4-1). Despite the strict time constraints, we were able to map entire areas on some selected seamounts (Fig. 3-1). The depth of the stations varied between 1100 m as minimum and 5800 m as maximum depth. The working area is characterized by a chain of seamounts, which is identifiable from GEBCO and the EM122 data.

Table 5.4-1. Calculation of bathymetrically mapped area during SO264 in km².

Area	km2
Transit (Fiji (EEZ) – Emperor Seamounts)	78.017
Emperor Seamounts (working area)	55.960
Transit (Emperor Seamounts – Japan (EEZ))	44.993
	178.970

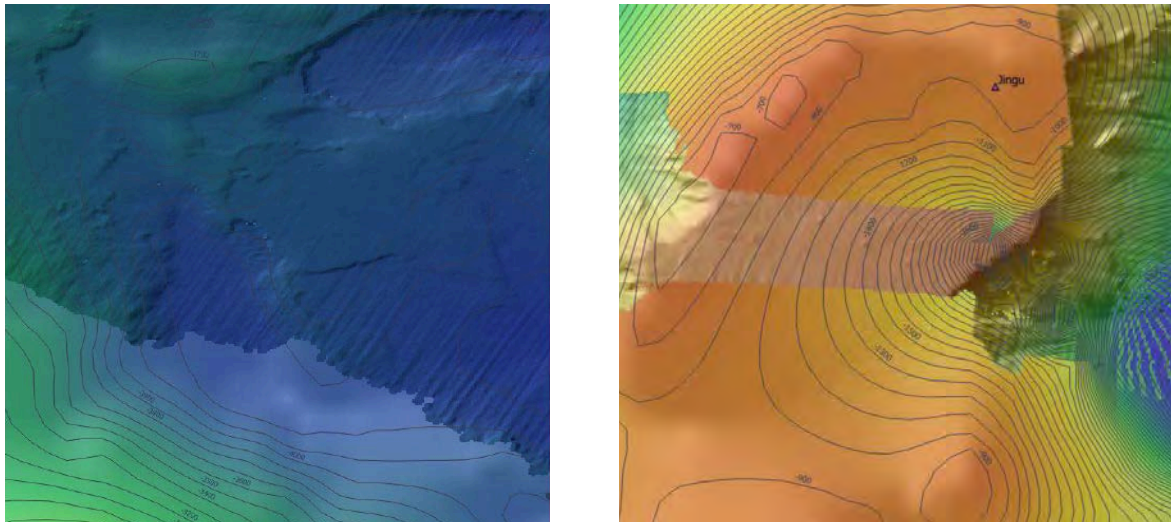


Figure 5.4-3. Comparison of SO264 multibeam EM122 bathymetric mapping to previous GEBCO results. Left: Upper part shows seafloor mapped with the EM122, below the previously existing low-resolution GEBCO bathymetry. Right: North of Ojin Seamount, the GEBCO bathymetric data reveal a trough, while the shaded high-resolution bathymetry from the EM122 echosounder shows a plateau.

Due to a ping rate varying from 0.11 to 0.04 Hz, the grid size varies between ~600 m to ~800 m. Still, the bathymetry of the echosounder is much more precise than the GEBCO data, which in this area are based on satellite altimetry and contain numerous artefacts (Fig. 5.4-3). The latter could be often rectified through our surveys. For example north of Ojin Seamount (Fig. 5.4-3), the GEBCO data shows a trough, while the shaded bathymetry from the echosounder exhibits a plateau. The artefacts mostly were troughs that are comparably small in diameter and appear to be rather deep (several 1000 m). Every now and then they were found right next to the seamount. They might result in wrong computing of the satellite data.

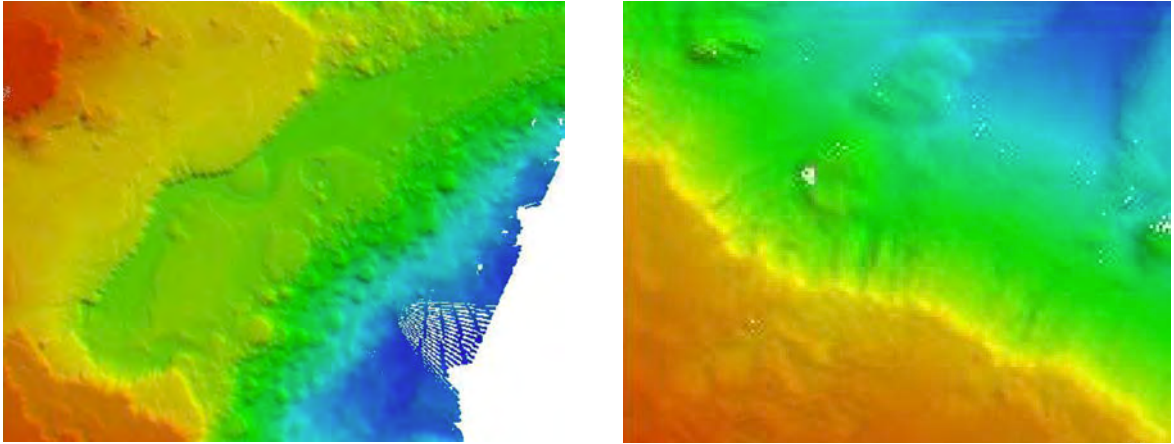


Figure 5.4-4. Examples of volcanic seamount slopes. Left: The gentle slopes on the leeward side of Suiko Seamount provide high sediment accumulation. Right: The steep slopes of Minnetonka Seamount were shaped by deep currents and exhibit basement rock.

For geological sampling, soft slopes are promising to find sediments to be sampled (Fig. 5.4-4). This is supposed to be the leeward side of the seamount, because at the luv side sediments were most probably washed away by currents. These sides turned out to be fairly steep (Fig. 5.4-4) and exhibit hard basement rock.

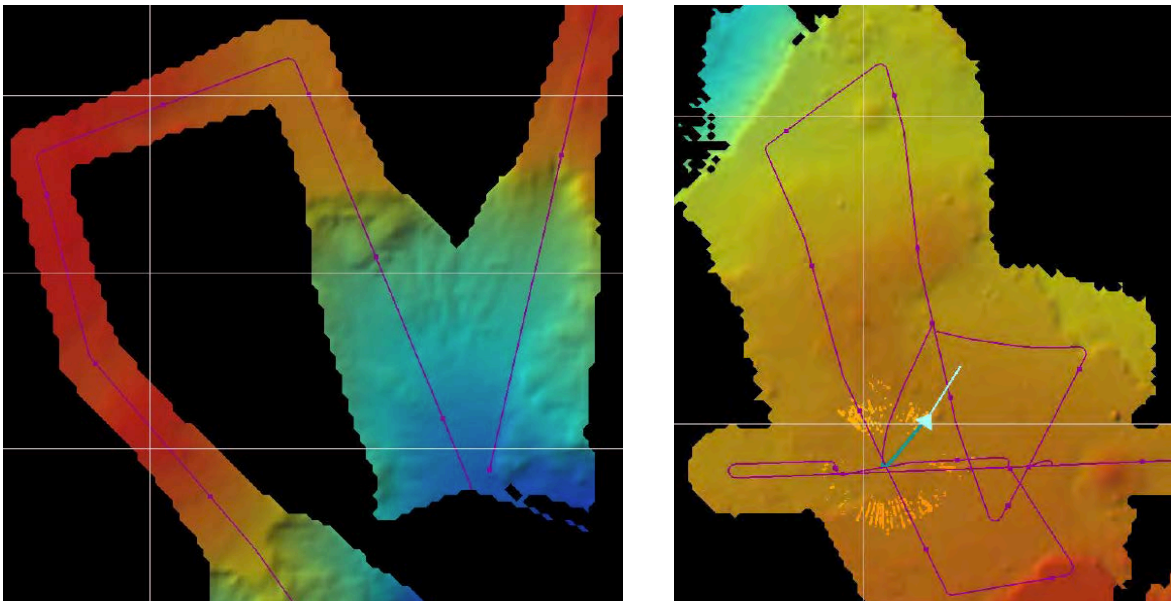


Figure 5.4-5. Left: Most seamounts were mapped focussing solely on their flanks as summits were barren of sediment. Right: North of $\sim 45^{\circ}\text{N}$, however, seamounts were mapped in high detail and to full extent, as sediment cover was more expanded.

The seamounts to the south like Koko Seamount were mapped focussing on the flanks by sailing one track across with a ship speed of 6 kts (Fig. 5.4-5), while the seamounts to the north of $\sim 45^{\circ}$ latitude were mostly mapped to full extent like Suiko Seamount (Fig. 5.4-6). Depending on the seamount's size, the intense mapping took two days and one

night each, at a ship speed of 6–8 kts. It was done preferably, when it was not possible to deploy devices due to the weather conditions and technical problems.

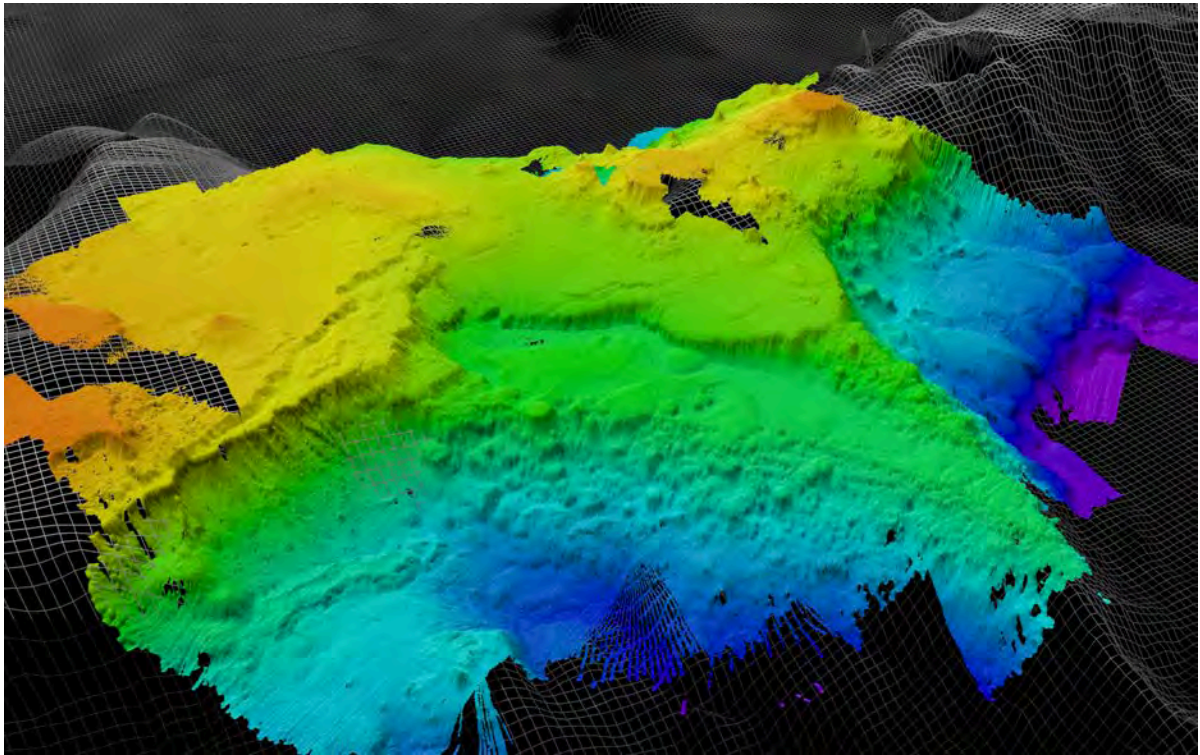


Figure 5.4-6. 3-D imagery of the Suiko Seamount (~44°50'N ~170°10'E) based on EM122 echosounder (Kongsberg Maritime) bathymetric mapping (colored). The background bathymetric grid represents previously existing low-resolution GEBCO bathymetry.

5.4.3 Marine sediment echosounding

(Lars Max)

The ATLAS PARASOUND P70 sub-bottom profiler consists of a low-frequency sediment echosounder and a high-frequency narrow-beam sounder to determine the water depth. Basically, it applies the parametric effect that produces additional frequencies through nonlinear acoustic interaction of finite amplitude waves. If two sound waves of similar frequencies (18 kHz and e.g. 22 kHz) are emitted simultaneously, a signal of the difference frequency (e.g. 4 kHz) is generated for sufficiently high primary amplitudes. The new component is travelling within the emission cone of the original high frequency waves, which are limited to a very narrow angle of only 4.5° for the equipment used. The resulting footprint size of 7% of the water depth is much smaller compared to conventional systems and both vertical and lateral resolution is significantly improved, making the PARASOUND an ideal tool for sediment profiling (Fig. 5.4-7).

The PARASOUND sub-bottom profiler is permanently installed on RV SONNE. The hull-mounted transducer array consists of 128 elements covering an area of 1 m². Up to 70 kW of electric power are necessary to run the system due to the low degree of efficiency of the parametric effect. The PARASOUND system allows digital data acquisition and visualization with software from ATLAS Hydrographic. ATLAS Parastore is used for buffering, transfer and storage as well as the visualization of the digital seismograms at very high repetition rates. ATLAS Hydromap Control allows user-defined modifications of the system (e.g. transmission sequence, pulse rate or pulse interval) and further supports the operator in running the system properly.

PARASOUND Profiles for each coring station is provided in Appendix 5.4.

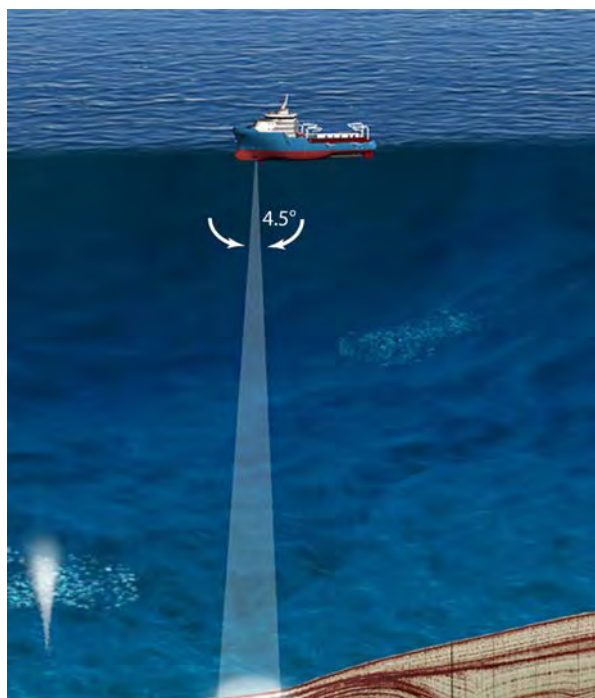


Figure 5.4-7. With its 4.5° beam width the PARASOUND P70 sub-bottom profiler allows detailed investigations of even small-scale bottom structures at the seafloor. It is applicable in parallel to seismic or bathymetric survey campaigns and provides full ocean depth range and >200 m sediment penetration (source: Teledyne Atlas Hydrographic).

Appendix 5.4 PARASOUND profiles.

5.5 Sediment core logging

(Arian Höfken, Liane Brück, Sebastian Fessler, Jianxing Liu, Dirk Nürnberg)

During RV SONNE cruise SO264, routine, onboard logging of geophysical properties and line scan imaging of acquired piston (PC), gravity (GC) and kasten core (BC) sediments were performed. The geophysical properties measurements were applied mainly to split and occasionally to entire/unopened sediment core segments. Line scan imaging was carried out on split cores only. The measurements comprised:

- magnetic volume susceptibility κ ,
- electric resistivity R_s (which acts as a measure for porosity)
- line scan imaging (used to determine wavelength specific reflectance values and core photography)

Two separate *GEOTEK* Multi Sensor Core Logger (one for line scan imaging and one for the geophysical properties measurements) were used (Fig. 5.5-1). Both systems provide high resolution information with standard spacing of 2 cm for electric resistivity and magnetic volume susceptibility and 100 μm for line scan imaging. These systems use stepper motors to push sediment core segments of 100 cm length through a series of sensors. The position in the sediment core is automatically detected by the system and measurements are controlled *via* the systems computer terminal.

5.5.1 GEOTEK Multi Sensor Core Logger

Magnetic volume susceptibility

The magnetic volume susceptibility κ is the dimensionless ratio of a materials magnetization and the strength of the magnetizing field: $\kappa = B \cdot (\mu_0 \cdot \mu_r \cdot H)^{-1}$ with B being the magnetic induction, μ_0 and μ_r being the absolute and the relative permeabilities and H being the magnetizing field.

The susceptibility of marine sediments may vary in the range of $-15 \cdot 10^{-6}$ (this may be the case for sediments that are almost entirely composed of diamagnetic minerals such as carbonates and silicates) up to $10.000 \cdot 10^{-6}$, which may be the case if basaltic debris is included that is rich in (titano-) magnetite. In most cases, however, the varying content of ferrimagnetic minerals is the main contributor to the sediments susceptibility. Higher susceptibility values are therefore an indication for increased concentrations of such lithogenic or authigenic components. This property may be used to characterize and correlate sediment cores material with material from other cores.

For the purpose of measuring magnetic volume susceptibility, the core logger is equipped with a *BARTINGTON* M.S.2 susceptibility meter and a 14 cm loop sensor. The sensor characteristic and the given core diameters lead to the measurements being averaged over 8 cm core length. As a result abrupt changes of the susceptibility appear smoothed in the acquired data and thin layers may not be resolved in the logs at all. This effect would also result in kinks in the logs close to the sections ends. For this reason spacer of 21.5 cm length, which allow to correct the data for this effect, were inserted in between each measured segment of the sediment core. These spacers are also used to determine the susceptometer drift. During the post-processing, all the logged void material (also including the segments end caps and foam inserts) are removed from the logs such that a continuous composite core log is obtained.

Electric resistivity logging

The sediment cores electric resistivity R_s is measured with an active non-contact sensor that uses high-frequency magnetic fields that result in the induction of electric eddy currents within the sediment core material. These eddy currents result in a secondary

magnetic field that is recorded by the sensor. The eddy currents in the sediment and the resulting secondary fields are proportional to the sediments resistivity.

Based on the conductivity the sediments porosity can be estimated using Archie's law: $R_s/R_w = k \cdot \phi^{-m}$ with R_s being the sediment resistivity, R_w being the pore water resistivity and ϕ being the porosity. For sea water saturated sediments that are basically composed of clay minerals the constants k and m were chosen to be 1.3 and 1.45 respectively.

The sensor characteristic causes the measurements to be averaged over 12 cm core length. Equally to the susceptibility measurements this effect and the instrument drift are corrected after the logging with the aid of the spacers and a model of the sensor characteristic. All data related to void material is then removed from the logs and a continuous composite resistivity log is obtained. Calibration of the electric resistivity sensor was performed daily with salt water filled liner segments of 30 cm length.

Line scan Imaging – color scanning

The reflectance is the ratio between the intensity of the light reflected by an object and the intensity of the incident light. This ratio is commonly expressed by values of 0 (no reflectance at all) to 255 (100% of the incident light is reflected) for each of three color bands (600-700 nm for red light, 500-600 nm for green light and 400-500 nm for blue light). The main factors influencing the wavelength dependent reflectance of marine sediments are the overall chemical and mineralogical composition, the redox state of trace constituents such as iron and manganese bearing minerals and the content of organic components. Logs of the wavelength dependent reflectance therefore provide a high resolution tool for preliminary estimations of such sediment specific properties. With the given high spatial resolution of this method, true color sediment core photographs alongside with wavelength specific reflectance logs can be achieved.

For this purpose, the second *GEOTEK* multi sensor core logger is equipped with a line imaging camera module. Inside the camera module three individual CCD detectors (with 3*1024 pixel resolution each) are equipped with dichroic filters for the three different color bands. These CCD sensors detect the light reflected by the sediment cores surface, which is illuminated by two white fluorescent tubes. In order to obtain maximum image quality the freshly cut archive half of the sediment core was carefully leveled prior to the measurement. The axial resolution was set to 850 pixels per row. The along core resolution is 1 row of pixels for every 100 μm of core depth. In order to prevent image saturation the aperture was adjusted to the brightest section of the sediment cores. These settings were maintained constant throughout the scanning of the complete core. Black-white calibration was performed daily with a white tile and the closed camera lens cap. Directly before and after each measured core the CCD sensor was also calibrated with a color test chart to avoid sensor drift errors.

A *MATLAB* based post processing software is used to remove drift errors, to cut away the liner end caps and foam inserts, and to join all scanned sections to form a continuous composite core image as well as a color enhanced composite image.

5.5.2 Sediment core MINOLTA light reflectance scanning

(Sebastian Fessler, Jiangxing Liu, Dirk Nürnberg)

The hand-held MINOLTA spectrophotometer (type CM-600d) was applied to continuously color-scan sediment surfaces from open core segments by measuring the light reflectance (Fig. 5.5-2). Before measurement, the sediment surface was covered by clean and clear plastic wrap. Then, the spectrophotometer was directly placed on the sediment surface. Measurements were taken at 1 cm-intervals. With this technique, the spectrum of the reflected light is measured by a multi-segment light sensor. The spectral reflection is measured at a 20 nm pitch for wavelengths of 400 to 700 nm. The variation in the illumination from the CM-600d pulsed xenon arc lamp is automatically compensated by a double-beam feedback system.

In order to avoid any variation in color measurements due to the environmental (temperature, humidity, background light) and instrumental variations, the CM-600d-device was color-calibrated at the beginning of the measurement of each core-segment. The spectrophotometer was calibrated for black colors using “zero-calibration” as well as for white color reflections. The spectrographic data were finally processed by the program Minolta SpectaMagic v.2.3.

The reflection data and the standard color-values X, Y, Z are automatically calculated by SpectaMagic v.2.3, and are displayed in the Y, L*, a* and b* CIELAB color coordinates. The Y and L*-values represent brightness and can be directly correlated to gray value measurements, while Y represents the lightness on a linear scale and L* on a non-linear scale. The a*-values indicate the relationship between green and magenta and the b*-value reflects blue/yellow colors. The color scans of each core are displayed in Appendix 5.5.

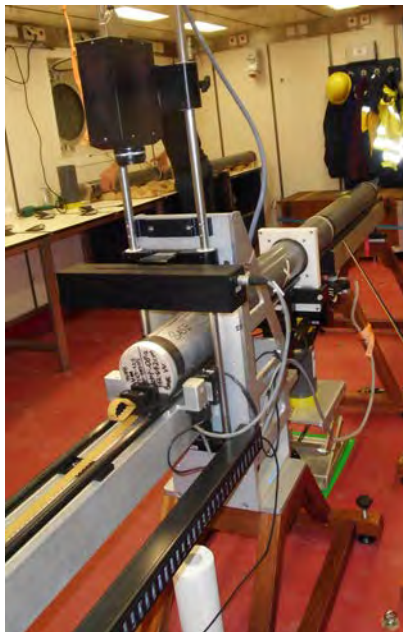


Figure 5.5-1. The geophysical properties measurements with the GEOTEK Multi Sensor Core Logger were applied mainly to split and occasionally to entire/unopened sediment core segments.

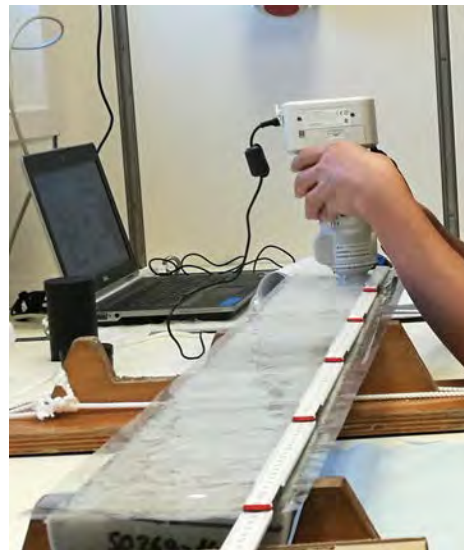


Figure 5.5-2. Sediment surfaces from open core segments were color-scanned at 1 cm-intervals with the MINOLTA spectrophotometer (type CM-600d).

5.6 Marine geology and paleoceanography of the pelagic N Pacific

5.6.1 Background and objectives

(Dirk Nürnberg, Lester Lembke-Jene)

The BMBF joint project SONNE-EMPEROR, in which framework cruise SO264 took place, attempts to establish a new paleoceanographic North - South reference transect along the Emperor Seamount Chain in the N Pacific. The sediment core transect accomplished during SO264 crossed major oceanographic and climatic patterns, comprising the Kuroshio Extension, the Kuroshio Bifurcation Front, the Subarctic Boundary, and the Subarctic Front. SO264 gathered a suite of closely-spaced high-quality sediment cores from the so far largely unexplored offshore, pelagic N Pacific ocean areas (Figs. 3-1, 3-2, 4-1). With the newly acquired sample sets, we are able to address exciting and highly debated hypotheses on the role of the N Pacific across the following themes:

Development of Subarctic N Pacific Surface Stratification: Effects on CO₂ Balance

We intend to assess latitudinal and temporal changes in biogenic export production, and the limits and efficiency of nutrient utilization, which largely determine to a large extent the strength of the “biological carbon pump”. We aim to resolve the mechanisms driving changes in water mass structure and biological productivity and their timing, and to address the vertical variability in nutrient distribution and consumption by multi-proxy studies on centennial to orbital timescales.

Development of the N Pacific Subtropical and Subarctic Gyres

We intend to reconstruct the subtropical to subarctic N Pacific upper ocean thermocline and pycnocline on Plio/Pleistocene to Holocene timescales, and the response to global and regional changes in climate and oceanography. We will decipher the interaction between the subarctic and subtropical gyres, and the variations and work modes of the Kuroshio and Alaska current systems, and their effect on sea ice and iceberg dynamics.

Role of the Pacific Meridional Overturning Circulation in the Climate System

It is still unknown whether the dense surface water masses in the N Pacific penetrated to the intermediate or the deep-water level during the past and how regionally variable such processes were. We now are able to address these issues with the newly recovered sediment cores from <2000 to ~5000 m water depth, and to decipher the regional/vertical temporal variability of deep and intermediate water ventilation and overturning modes.

Subsurface Inter-Oceanic Teleconnections in the Pacific – the Ocean Tunnel

The mode, in which the subsurface water mass exchange between subtropical and tropical ocean areas takes place, is a matter of debate. In particular, the oceanographic details of such flow and the pathways of flow, likewise termed as „ocean tunnel“, need to be determined. We are positive that we may relate the pronounced long-term Plio-/Pleistocene changes in N Pacific subsurface temperature, salinity, and thermocline depth to the equatorial W Pacific area.

Fertilising the Pelagic N Pacific – Atmospheric vs. Oceanic Micronutrient Sources

Transport of critically needed iron to the pelagic N Pacific by atmospheric dust is regarded as principal mechanism to relieve the upper ocean of micro-nutrient limitation during glacial times. The simulation of Last Glacial Maximum dust deposition and dust sources for the N Pacific region changed the views on the role of eolian dust for ocean fertilization

during cool climates. A systematic study on the temporal / spatial variability of eolian dust contribution to the N Pacific variability in response to changes in atmospheric circulation (Westwind Drift) and sea ice distribution, and its effect on marine productivity will be made possible through our newly recovered N-S-oriented core transect.

5.6.2 Surface sediment sampling

(Weng Si Chao, Lara Jacobi)

During SO264, surface and near-surface sediments of up to 40 cm core length were sampled with a Multicorer (MUC) equipped with a camera system (TV-MUC), and/or a giant box corer (GKG). The MUC is commonly equipped with 12 sampling tubes with an inner diameter of 10 cm and a tube length of 60 cm. During SO264, the telemetry of the TV-camera system was mounted and occupied three tube slots, therefore the MUC was commonly mounted with 9 tubes per deployment. It was successfully deployed at 51 stations (Fig. 3-2, Appendix 4). In most cases undisturbed surface sediments and overlying bottom water were recovered (Fig. 5.6-1).

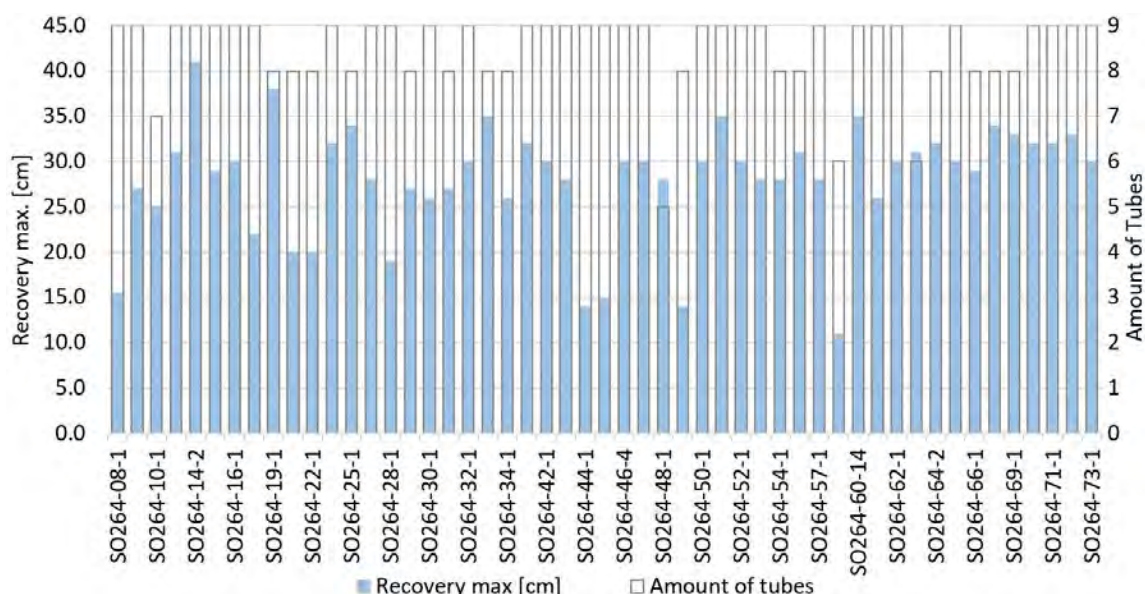


Figure 5.6-1. Maximum sediment recovery in cm (blue) and number of sediment-filled tubes (white) for each TV-MUC deployment during SO264. TV-MUCs were successfully run at 51 stations (Appendix 4).

The TV-MUC was lowered with an average speed of 1 m/s to about a few meter above seafloor where it was stopped for a few minutes to observe the sediment surface with the camera system (Fig. 5.6-2). The deep-sea color TV camera system from “ISITEC” consists of a camera (Marshall HD-SDI), two lamps (DEEPSEA Power & Lights, SeaLite Sphere 5150) and a control unit. The power supply for the system is provided by a Coax cable with LWL (>600 V). The video has a resolution of 1080i and was recorded with 60 transmissions. The final penetration into the seafloor sediments continued with a speed of 0.5 m/s until the cable tension monitored bottom contact. The multicorer was left on the seafloor for a few seconds before being pulled out of the sediment with a speed of 0.5 m/s and subsequently heaved with 1 m/s.

Table 5.6-1. Scheme showing sampling strategy and distribution of MUC tubes among scientific disciplines.

Tubes (label with capital letter)	Sampling
SEDimentology	1 cm sediment slices packed in pre-weighted Whirlpack bags
BENthos I	1 cm sediment slices from the upper 10 cm of the tube stored into Kautex bottles and mixed with Rose Bengal; remaining 1 cm slices packed in Whirlpack bags
PLAnkton	1 cm sediment slices packed in Whirlpack bags
BIOMarker	1 cm sediment slices sampled into brown glass vials covered by aluminum foil
FIO (First Institute of Oceanography, SOA, China)	1 cm sediment slices packed in Whirlpack bags
MICropaleontology	1 cm sediment slices packed in Whirlpack bags
ARChive / PORewater*	1 cm sediment slices packed in Whirlpack bags
	Subsample every 2 cm from upper 10 cm then move to every 10 cm, and all the remaining 1 cm slices in Whirlpack bags
BENthos II	1 cm sediment slices from the upper 10 cm of the tube stored into Kautex bottles and mixed with Rose Bengal; remaining 1 cm slices packed in Whirlpack bags
MICropaleontology II / PORewater II	1 cm sediment slices packed in Whirlpack bags

* Pore water samples were subsampled from the archive / micropaleontology tubes only when samples were required; otherwise both tubes were sampled as described above.

Right after retrieval, bottom water samples were taken from 2 (BENthos) tubes for stable isotope analysis ($\delta^{18}\text{O}$ and $\delta^{13}\text{C}$), nutrient concentration, pH, dissolved inorganic carbon (DIC), trace elements and alkalinity (TA). Subsequently, the plastic tubes were taken out of the MUC and brought into the laboratory, where they were distributed among scientific disciplines (Table 5.6-1). The sediments of each tube were sliced one-by-one centimeter, packed as listed in Table 5.6-1, and stored at 4°C (Fig. 5.6-3).

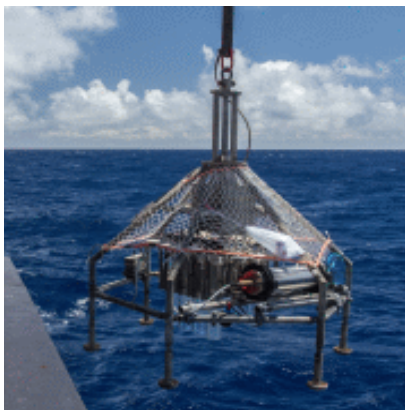


Figure 5.6-2. Image of the TV-MUC deployed during cruise SO264. The telemetry mounted belongs to RV SONNE.



Figure 5.6-3. Sampling of MUC-tubes. The sediment pile (~10 cm in diameter) is sliced one-by-one centimeter.



Figure 5.6-4. Image of the GEOMAR Giant Box Corer (GKG) deployed during cruise SO264.

The GKG was deployed at 3 stations and recovers a sediment volume of 50*50*60 cm (Fig. 5.6-4, Appendix 4). For organic geochemical, micropaleontological and sedimentological studies, the uppermost first centimeter of surface sediment was collected in 4 Kautex bottles. The entire sediment pile was sampled using 3 PVC-liners with 12.5 cm in diameter. Moreover, a U-channel was taken for paleomagnetic studies.

5.6.2 Sediment coring and core description

(Thomas Ronge)

Sediment core recovery

During expedition SO264, long sediment records were retrieved, deploying 40 gravity corers that varied in length between 5 and 20 m, 20 piston corers with a pipe length between 10 and 20 m and 5 kasten corers with a device length of 5.75 m (Appendix 4). The coring system was deployed (Fig. 5.6-5) via RV SONNE's cradle using cable #2 with a diameter of 180 mm.

The main sediment coring device applied during SO264 was the GEOMAR piston corer (PC) of the *Fa. Marinetechnik Kawohl*, which can be run as both piston corer and gravity corer. Equipped with a split piston, the maximum length of the piston corer pipe aboard RV SONNE is 20 m (in 5 m increments; Fig. 5.6-6). The pipe diameter is 12.5 cm. The barrel's weight is ca. 2.8 t. The piston corer was lowered and heaved at a deep-sea winch speed of 1.2 m/s. A 1 m-long pilot (trigger) core is attached to the piston corer by steel via a release mechanism. Upon contact with the seafloor, the pilot core triggers the release of the main device, which then free-falls into the sediment and allows much deeper penetration into the sediments than the gravity corer. To allow for a deep penetration, the piston corer was left at the seafloor for about 30 seconds, then hieaved with 0.3 m/s until it was pulled from the sediments. Hieving activates the split piston, which produces an underpressure within the steel pipe and allows for better core recovery. Penetration into and release from the sediments were monitored through the cable tension. The piston corer can be easily modified into a gravity corer, by removing piston, piston cable, release mechanisms and pilot core. It is deployed like the piston corer using the ship's cradle. Parallel deployments of both piston and gravity corers at the same station revealed that the sediment pile within the gravity core is significantly compressed during the coring process, and core recovery is consistently lower than for a piston corer.



Figure 5.6-5. RV SONNE's cradle system ('Kernabsatzgestell') to deploy sediment corers of max. 20 m length.

For *ad hoc* deployments in order to gain a quick impression on the sediment consistency, we used a simple gravity corer, which consists of a 2.3 t weight and a 5 m steel pipe. We here did not make use of the ship's cradle. The gravity corer was lowered to depth at a speed of 1.2 m/s, while it was accelerated to max. 1.5 m/s for the lowermost 100 m before reaching the seafloor. The device remained in the sediments for ~30 seconds to allow for penetration until it was heaved with a speed of 0.3 m/s out of the seafloor and with 1.2 m/s back to the ship's working deck.

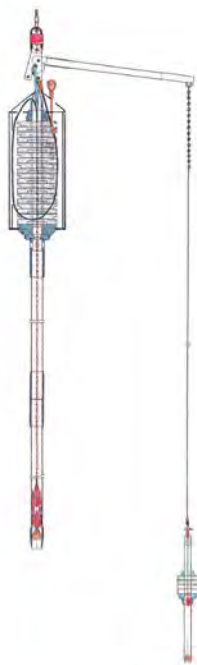


Figure 5.6-6. Schematic view of the Fa. Kawohl *Marinetechnik* split piston corer (PC) used during SO264. This device was also deployed as gravity corer.



Figure 5.6-7. Deployment of the 5.75 m kasten corer (BC).

The largest-in-diameter coring device deployed during SO264 was a 5.75 m kasten corer (BC) (Fig. 5.6-7). The kasten corer's rectangular shape has a footprint of 30*30 cm and is attached to a 2.8 t weight barrel. Due to its large diameter, the BC has a four-times higher sediment recovery compared to the PC. Upon recovery, one of the two angle sections of the BC were removed (Fig. 5.6-8) to allow access to the sediments. Prior to sampling, the outermost sediments layers were removed, which might have been disturbed by the coring process. To sample the recovered BC-sediments, 5 rows rectangular plastic boxes (98*15*7 cm) and U-channels (for paleomagnetic studies) were pushed into the sediments (Fig. 5.6-8).

Core statistics are given in Fig. 5.6-9 and Fig. 5.6-10. The lengths of the sediment cores recovered by the gravity corer ranged from 1.95 m to 19.32 m with on average 10.75 m. The average core recovery was 66.9%. The piston corer deployments gained core recoveries of 0.7 m to 18.55 m with on average 13.7 m, which is 70.1% m core recovery. In total, the core recovery was at ~70%, with an overall sediment core recovery of ~640 m (Appendix 4).



Figure 5.6-8. Sampling of the 5.75 m kasten corer (BC).

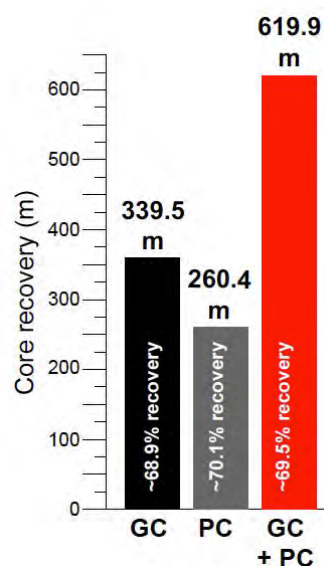


Figure 5.6-9. Total SO264 sediment core recovery in (m) and (%). GC = gravity corer; PC = piston corer.

Sediment core handling

After being placed on deck, the core catcher of the coring devices were removed, with its sediment material being stored in plastic bags. The 5 m-PVC-liner sections were pulled out of the steel pipes. The numbered sections were brought into the laboratory and cut into 1 m round sections. Labeling of the 1-m PVC-sections is according to the following scheme that was also used for the storage (D-tube) containers and their caps (Fig. 5.6-11):

- Cruise number; station number; number of device at station (e.g. SO264-07-2)
- Label for gear (e.g. PC)
- Label A for archive half; label W for working half
- Arrow, pointing to the bottom of the section
- Depth interval (in cm)
- Label Top/Base

Routinely, the 1 m-core sections were split lengthwise into a working (W) and an archive (A) half (Fig. 5.6-12). The archive halves were routinely scanned for magnetic susceptibility and resistivity (Chapter 5.5) using a GEOTEK logging tool. Line scans were conducted after the sediment surfaces were cleaned and flattened. Subsequently, color reflectance and color spectrum measurements were accomplished using a Minolta spectrophotometer. The working halves were described visually (see below), and samples (~3 cc) designated for measurements of the physical sediment properties were taken each 10 cm. As a last step, all core sections were wrapped in transparency foil, placed into D-tubes or vacuum bags, sealed and stored in reefer-containers at ~4°C.

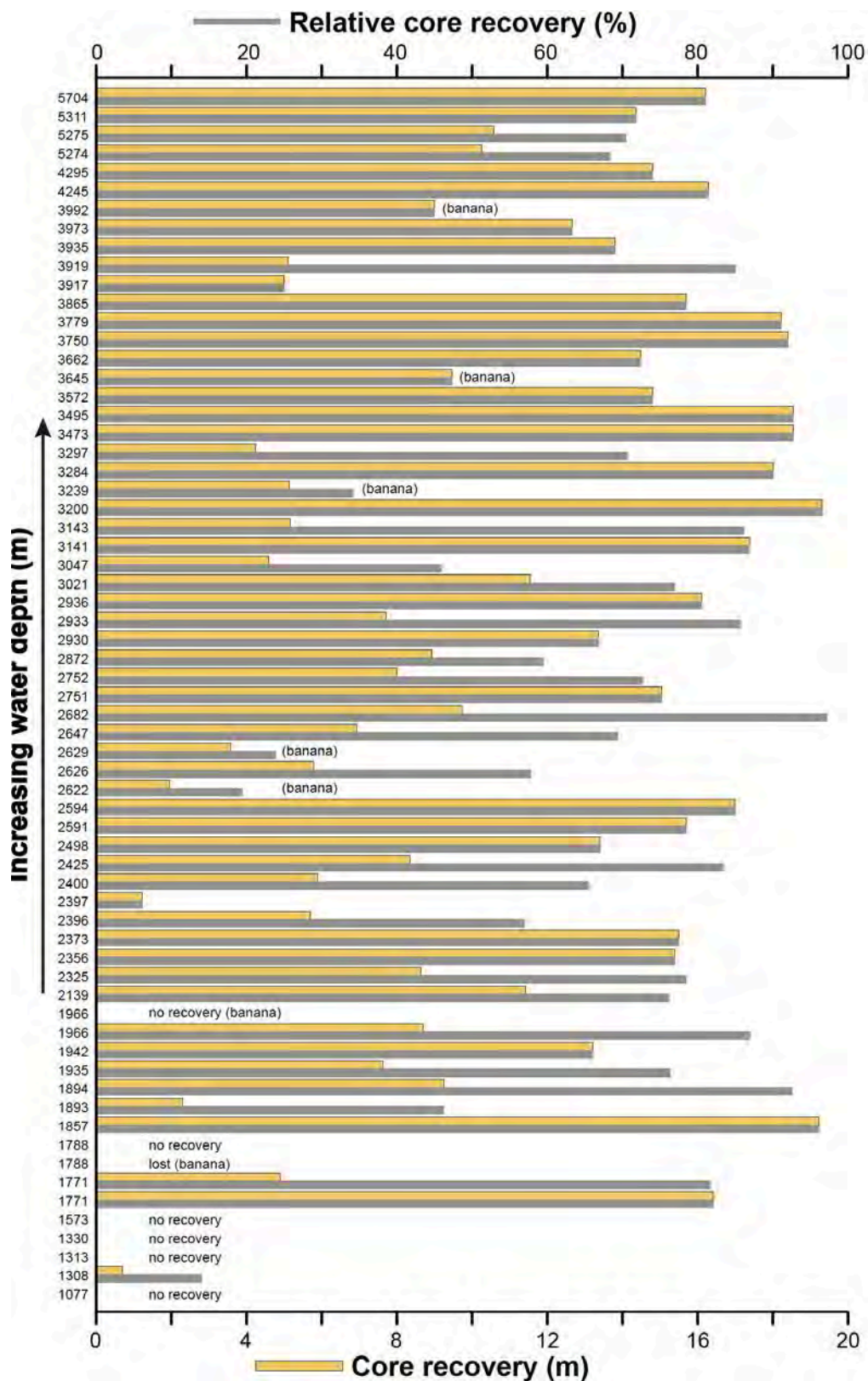


Figure 5.6-10. SO264 sediment core recovery versus water depth (m). Upper scale and gray: Relative core recovery in (%). Lower scale and orange: Absolute core recovery in (m). Banana = bent corer.

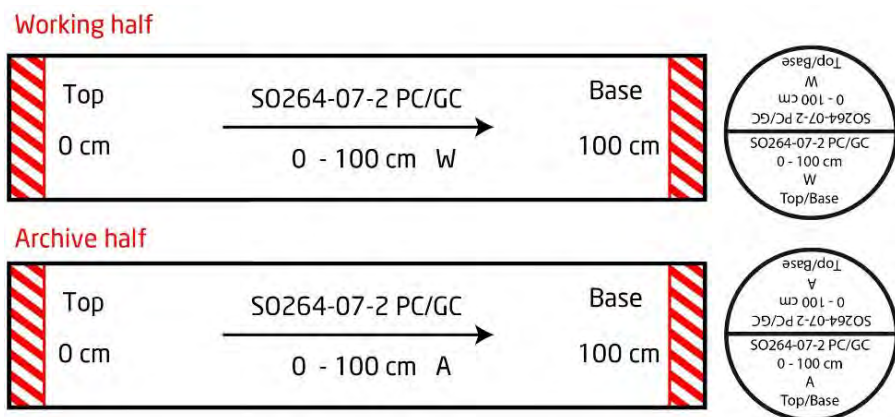


Figure 5.6-11. Labeling scheme for liners, D-tubes and liner caps. Red bars indicate the area, which is reserved for caps and tapes.

Visual core description

The sediment core descriptions, termed lithologs (Appendix 5.6-1), contain sediment textures/structures that were observed during the visual inspection of each core section, but also comprise data that were generated by shipboard core logging. Based on the standard IODP classification scheme and following the lithological classification of Mazzullo et al. (1998), we used the APPLECORE software package with a custom-made lithological file to digitize all visual core descriptions. We used a principal name and additional minor or major modifiers to describe the composition, texture and features of the sediments. The principal name identifies the degree of consolidation (induration) as well as the granular sediment class. Further characteristics like macro and microfossils, ichnofossils, dropstones, shell fragments, tephra layers, laminae, pyrite or iron sulfides etc. were additionally reported in the core descriptions. Appendix 5.6-2 provides the sediment core photography.

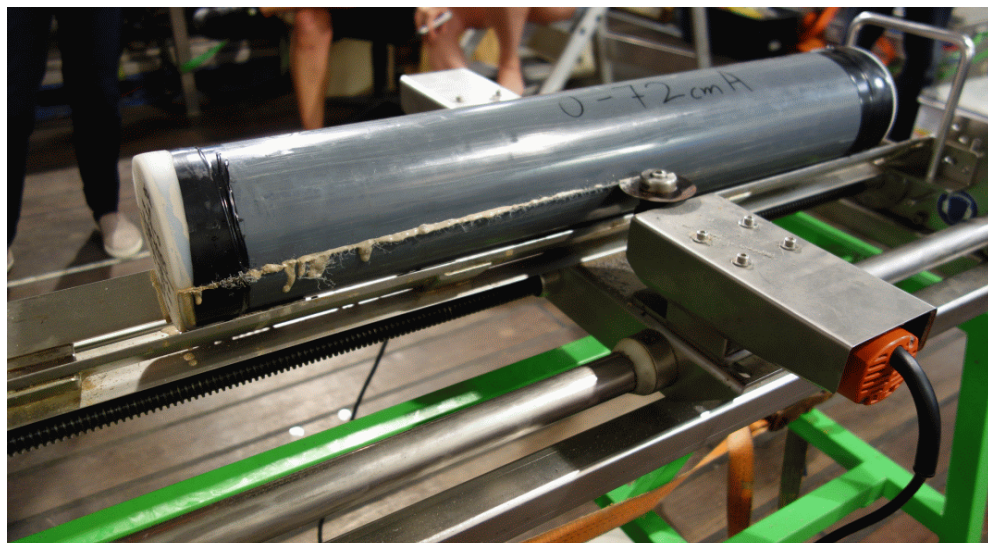


Figure 5.6-12. Splitting of a core segment in working and archive halves, using the Fa. Marinetechnik Kawohl vibration saw tool.

Tephra sampling

We defined volcanic ashes with thicknesses of >0.5 cm as distinct tephra layers and those with less thickness as tephra lenses. In a sediment core, if found, the tephra layers and tephra lenses were labeled with an Area Code (e.g. Ojin), and subsequently numbered (Chapter 5.7). The locations of tephra layers are indicated in the lithological core descriptions (Lithologs) as 'top / bottom core depths' for tephra layers and 'bottom core depth' for tephra lenses. The visual description of the volcanic ashes included information on color, sedimentary structures, components, bioturbation etc.. The distinct tephra layers were sampled for subsequent Electron Microprobe analysis (EMPA) and Laser-Ablation Inductively Coupled Mass Spectrometry (LA-ICP-MS) analysis at GEOMAR. The tephra layers were also sampled for smear slide analysis. Selected prominent tephra layers were studied in more detail using smear slides under the polarization microscope on board. The list of the tephra and smear slide samples can be found in Chapter 5.7.

5.6.3 Preliminary results of marine geology

Main lithologies

(Thomas Ronge, Dirk Nürnberg)

An extensive sediment coring program was carried out along the Emperor Seamount Chain. The coring stations from ~1700 m to ~5800 m water depth cover the major North Pacific water masses from the North Pacific Intermediate Water (NPIW; at least for glacial times) down to the Pacific Deep Water (PDW). The dominant lithologies of the Emperor Seamount Chain working area can be subdivided into three facies types, which laterally and temporally follow each other: the **'southern (and presumably oldest) calcareous ooze facies'** is replaced by the **'mid-transect siliciclastic-carbonaceous facies'**, which then is gradually substituted by the youngest and northernmost **'northern siliciclastic-siliceous facies'** (Fig. 5.6-13; Appendices 5.6-1, 5.6-2).

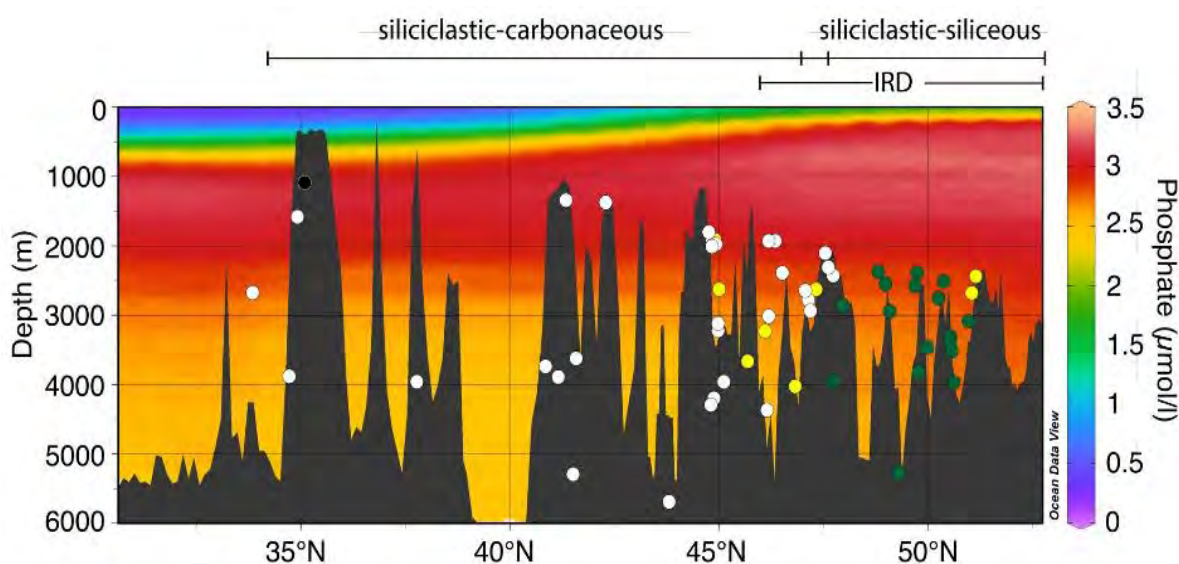


Figure 5.6-13. North-south oriented transect along the SO264 working area of the Emperor Seamount Chain. White dots – predominantly siliciclastic-carbonaceous sediments; green dots – predominantly siliciclastic-siliceous (opaline) sediments; yellow dots – bent sediment cores ('bananas') with successful sediment recovery; black dot – no sediment retrieved. IRD – ice rafted debris. Colored shading of background indicates phosphate concentrations in seawater from the World Ocean Atlas 09 (Garcia et al., 2009). Section has been done with ODV 4 (Schlitzer, 2014).

From the start of our core transect at ~33°N up to core location SO264-26-2 south of Suiko Seamount at ~44°46'N, monotonous silty light-gray to light brown calcareous oozes are the dominant sediments, which generally yield less foraminifera than the preceding and succeeding intervals. Intercalated by several greenish layers (often significantly compacted) of diagenetically altered sediments, the sediment stiffness of these oozes is increasing toward the base, changing from more water-rich soft oozes to highly compacted very dry sections with a significant increase in shear-strength. The calcareous ooze facies of the southern Emperor Seamount Chain is marked by very low MS values being two orders of magnitude lower than in the overlying intervals.

This **'southern calcareous ooze facies'** is overlain by the **'mid-transect siliciclastic-carbonaceous facies'** between ~33°N and 47°N, the sediment thickness of which gets thicker to the north. This facies, which in the uppermost intervals is characterized by brown foraminifera bearing sands, silty sands and silty clays (attributed to the post-glacial or even the Holocene), is prominently developed at Suiko Seamount (e.g., SO264-26-2, ~44°46'N).

The sediments below this sandy facies are best documented in records SO264-28-2 (~44°51'N) and SO264-29-1 (44°52'N) (Fig. 5.6-14), both of which were retrieved from a water depth of ~1990 m from the top of Suiko Seamount at ~44°N 170°E. Sedimentation is dominated by a prominent cyclic facies pattern of light grayish to light brownish foraminifera-bearing silty to silt-bearing calcareous oozes that are intercalated by darker layers of more siliciclastic calcareous sands and silts, hence representing the transition zone between the **'southern calcareous ooze facies'** and the **'mid-transect siliciclastic-carbonaceous facies'**.

At 47°N on Minnetonka Seamount, we noted a transient zone from the **'mid-transect siliciclastic-carbonaceous'** to the **'northern siliciclastic-siliceous'** environment (Fig. 5.6-14), most likely as a result of a depth change of the carbonate compensation depth (CCD). In this transient zone, mid-depth sediment records above ~2500 m water depth still belong to the **'mid-transect siliciclastic-carbonaceous'** (calcareous) environment, while deeper records (e.g. SO264-55-1, ~47°N, 2963 mbsl) show a noticeable increase in siliceous diatom oozes and diatomaceous clays typical for the **'northern siliciclastic-siliceous'** facies. We also noted an increase in the amount of Ice Rafted Debris (IRD), i.e. pebbles and boulders or smaller-scaled layers of terrigenous sands. Record SO264-55-1 still yields some calcareous foraminifera-bearing clays, while the more northerly records (e.g. SO264-60-12, ~49°N) lack any calcareous clays and oozes, and predominantly consist of dark olive-gray siliciclastic clay, which is repeatedly intercalated with greenish-brown to yellowish-brown diatom oozes.

Both, the **'mid-transect siliciclastic-carbonaceous'** facies as well as the **'northern siliciclastic-siliceous'** facies (north of 47°N) are marked by relatively high, but overall variable magnetic susceptibility (MS) values. The more siliciclastic, darker intervals are associated to higher MS values, while the calcareous and diatom oozes exhibit low MS values. In this respect, a distinct pattern of four subsequent MS peaks first observed at Suiko Seamount (SO264-28-2, 44°51'N) can be used for core correlation and traced northward up to core location SO264-60-12 (~49°N) close to Detroit Seamount (Fig. 5.6-14). In combination with the tephrastatigraphy established (see Chapter 5.7), most of the SO264 sediment cores can be internally correlated, reflecting the high quality of the sediment cores recovered.

From Suiko Seamount (SO264-28-2, 44°51'N) southward, the prominent transition from the **'southern calcareous ooze facies'** to the **'mid-transect siliciclastic-carbonaceous facies'** as prominently revealed in the sharp increase in MS-values is not only an excellent marker to correlate sediment cores between ~33°N and ~45°N, but also highlights a significant change in the depositional environment (Fig. 5.6-14). On a still preliminary basis, we relate the monotonous calcareous oozes to the late Pliocene to Early Pleistocene Epoch, dominated by 41.000-year cycles. Instead, the overlying sequences of very light coccolith-dominated oozes to darker, more foraminifera-dominated silts and sands presumably represent glacial/interglacial cycles associated to the

100,000-year world of the Late Pleistocene. If correct, this interpretation would imply that most of the SO264 cores yield important information on the climatic processes across the Mid Pleistocene Transition.

In Fig. 5.6-14, we show how exemplary sediment records from the entire transect might be correlated to each other. This tentative correlation implies that the relatively young siliceous records showing high sedimentation rates presumably cover the last few glacial interglacial cycles, while large parts of these younger intervals are missing in the southernmost records. Notably, we were not able to find any suitable mid-depth sediments (between 1500 and 3500 m water depth) between $\sim 35^\circ\text{N}$ and $\sim 45^\circ\text{N}$. This sediment-barren interval might result from both the low surface productivity and strong erosive currents observed at intermediate depths (also causing the very old core tops discussed above).

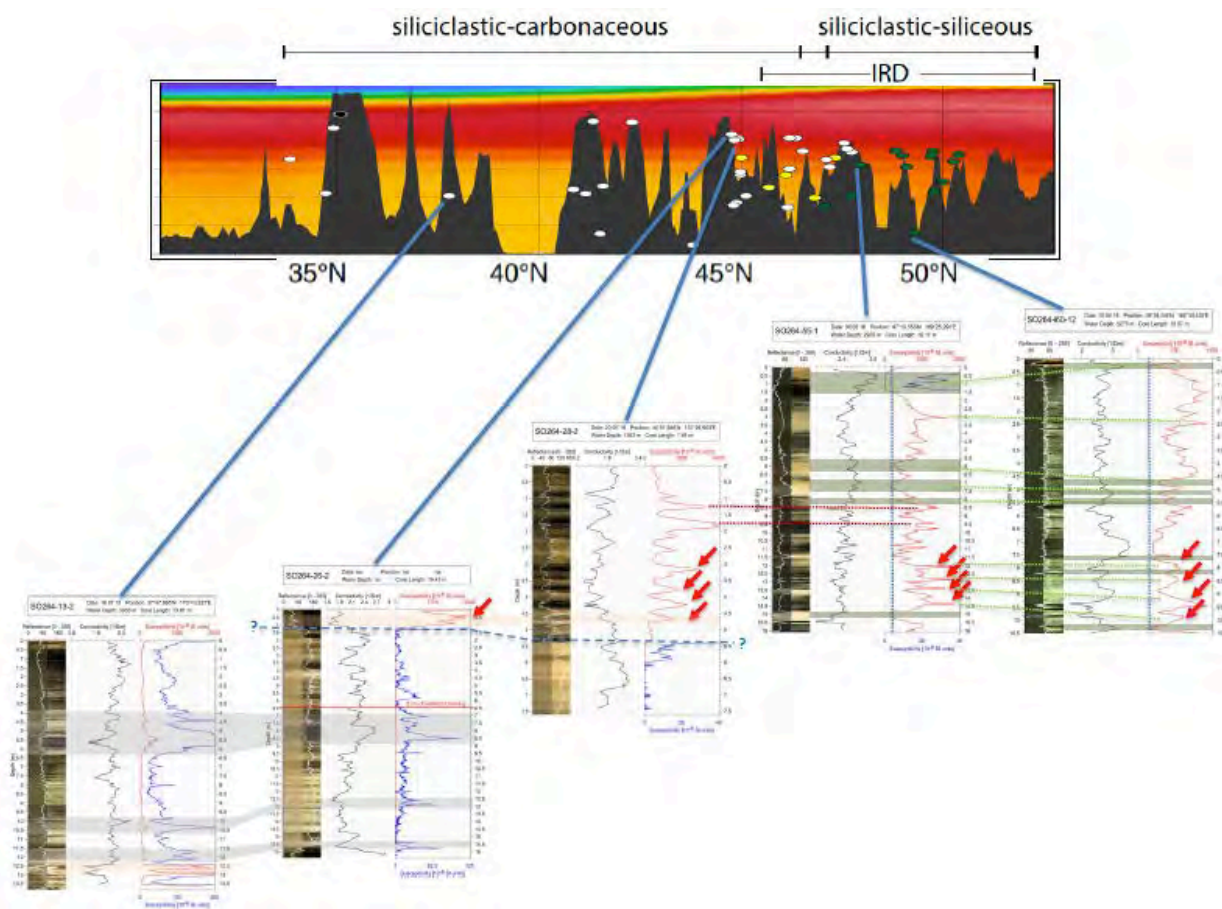


Figure 5.6-14. Tentative core correlation across the Emperor Seamount Chain based on magnetic susceptibility records: The oldest and southernmost calcareous ooze facies (blue records, lowest MS values) is overlain (dashed blue line) by the mid-transect siliciclastic-carbonaceous facies revealing a typical pattern in MS, which can be traced northward (red arrows, red dotted lines). Further north at $\sim 47^\circ\text{N}$, this carbonaceous facies is gradually substituted by the northern siliciclastic-siliceous facies (dashed green shading indicates siliceous ooze).

5.6.4 Working Area 1: Kimmei to Ninigi seamounts (33°-42°N 170°-175°E)

(Lara Jacobi, Nicoletta Ruggieri, Dirk Nürnberg)

The area between the Kimmei and Ninigi seamounts extends from ~33°N to ~41.5°N (Fig. 5.6-15) and includes 6 Seamounts: Kimmei, Koko, Ojin, Jingu, Nintoku and Ninigi. Within this area 4 gravity cores (GC) and 4 piston cores (PC) were recovered from a large range of water depths between ~1300 and 5300 m (Tables 5.6-2, 5.6-3). Additionally, surface sediments were collected with the TV-MUC at 9 stations. The sampling stations, the gear types and the length of the coring devices were chosen based on sediment acoustic profiles with the PARASOUND echo-sounding system.

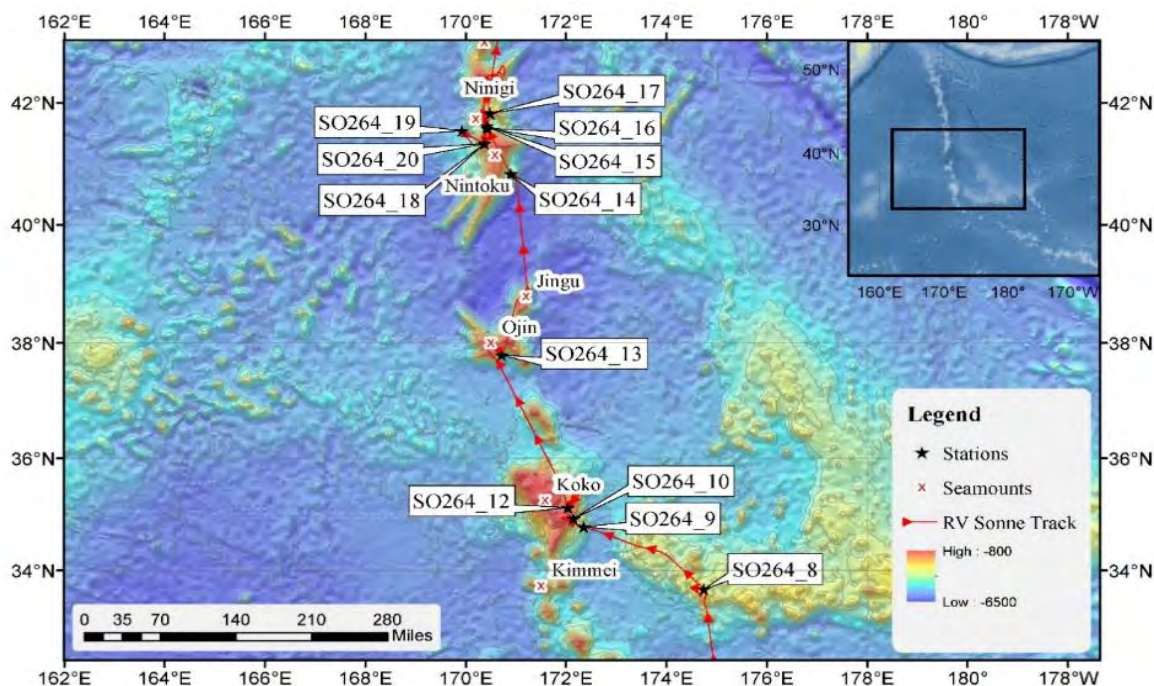


Figure 5.6-15. Bathymetric map showing core and surface sample locations in the Kimmei to Ninigi Seamount area. Red line marks the SO264 cruise track.

Table 5.6-2. Multicorer (MUC and TV-MUC) deployments from the Kimmei to Ninigi Seamount area and sediment recoveries.

Station Nr.	Area/Seamount	Gear	Latitude at depth (deg/min)	Longitude at depth (deg/min)	Water depth (m)	Max Recovery (cm)
SO264-8-1	east of Kimmei	TV-MUC	33°39,618'N	174°45,037'E	2680	15.5
SO264-9-1	Koko	TV-MUC	34°46,980'N	172°20,986'E	3866	27
SO264-10-1	Koko	TV-MUC	34°55,551'N	172°08,745'E	1599	25
SO264-13-1	Ojin & Jingu	TV-MUC	37°47,862'N	170°43,219'E	3933	31
SO264-14-2	Nintoku	MUC	40°50,040'N	170°54,192'E	3739	41
SO264-15-1	east of Ninigi	TV-MUC	41°36,914'N	170°25,343'E	3668	29
SO264-16-1	east of Ninigi	TV-MUC	41°34,991'N	170°25,751'E	3570	30
SO264-18-1	Nintoku	TV-MUC	41°20,057'N	170°22,438'E	1313	22
SO264-19-1	west of Nintoku	MUC	41°32,781'N	169°55,732'E	5304	38

Table 5.6-3. Piston corer (PC) and gravity corer (GC) deployments from the Kimmei to Ninigi Seamount area and sediment recoveries.

Station Nr.	Area/Seamount	Gear	Latitude at depth (deg/min)	Longitude at depth (deg/min)	Water depth (m)	Recovery (m)	Recovery [%]
SO264-8-2	Kimmei	GC10	33°39,616'N	174°45,044'E	2682	9.72	97
SO264-9-2	Koko	PC20	34°46,977'N	172°20,987'E	3865	15.70	79
SO264-10-2	Koko	GC10	34°55,752'N	172°08,752'E	1573	0	0
SO264-12-2	Koko	GC5	35°07,250'N	172°02,191'E	1077	0	0
SO264-13-2	Ojin & Jingu	PC20	37°47,865'N	170°43,327'E	3935	13.81	69
SO264-14-1	Nintoku	GC20	40°50,034'N	170°54,201'E	3750	18.41	92
SO264-15-2	east of Ninigi	GC20	41°36,917'N	170°25,340'E	3662	14.48	72
SO264-16-2	east of Ninigi	PC20	41°34,914'N	170°25,783'E	3572	14.80	74
SO264-18-2	Nintoku	GC5	41°20,042'N	170°22,441'E	1313	0	0
SO264-19-2	west of Nintoku	GC20	41°32,784'N	169°55,738'E	5311	14.37	72
SO264-20-1	Nintoku	PC5	41°20,025'N	170°22,742'E	1308	0.70	14

PARASOUND studies at Working Area 1

Fig. 5.6-16 shows a typical PARASOUND profile from the Kimmei to Nintoku seamount area. In general, volcanic plateaus characterize the top of seamounts in this part of the working area, which are largely barren of sediment deposits. Most sediment cores were recovered on flanks and deeper slopes of the seamounts (>260– 5300 m water depth) that mainly consist of siliciclastic-carbonaceous sediments. PARASOUND images for each coring station are given in the Appendix 5.4.

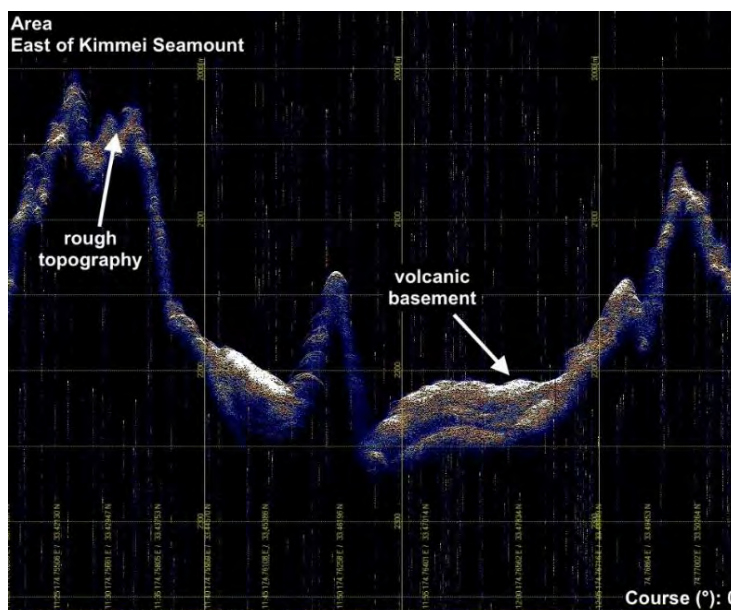


Figure 5.6-16. PARASOUND profile from the summit area of the East of Kimmei Seamount. White arrows provide a first geological interpretation. The shallower parts of the studied seamounts are often characterized by volcanic outcrops and are mostly barren of sediments.

Surface sediment lithology

Along the Kimmei to Ninigi seamounts transect, a trend towards lower foraminifera abundances and finer-grained surface sediments with increasing water depth is apparent. Sediments from the shallowest stations SO264-10-1 and SO264-18-1 (water depth of 1599 m and 1313 m, respectively) are characterized as foraminiferal-bearing fine to medium sands. Surface sediments from deeper stations consist of foraminiferal-bearing clayey silt.

At station SO264-14-2 from Nintoku Seamount (3739 m water depth), surface sediments consist of brownish silty mud and contain few foraminifera. This facies is similar to that found much deeper at a water depth of 5304 m (station SO264-19-1) except that calcitic foraminifera are no longer present. Video clips provided additional important information about the seafloor (Fig. 5.6-17) such as the presence of wave ripples pointing to strong and continuous bottom currents (SO264-12-1; SO264-18-1). Strong currents prevent sedimentation at all at station SO264-17-1 and leave a plain basaltic ocean floor. At stations SO264-8-1 and SO264-9-1, black, cm-sized pebbles of presumably volcanic origin are abundantly lying on the seafloor and point to downslope transport. The seafloor below ~3500 m water depth is strongly bioturbated and shows rich benthic life.

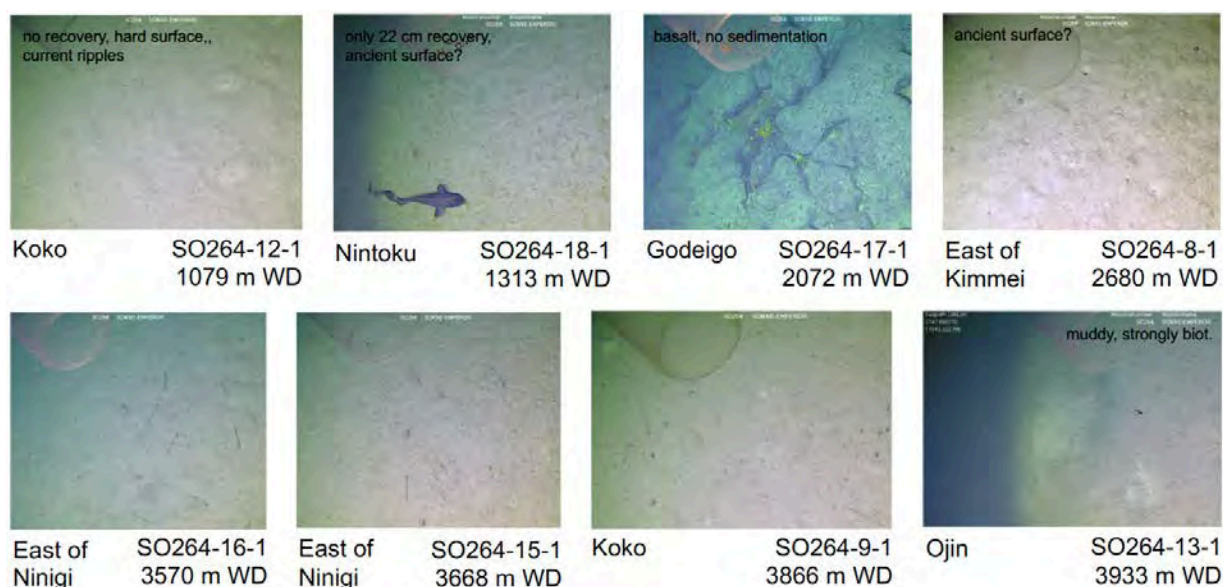


Figure 5.6-17. Seafloor sediments in the Kimmei to Ninigi seamount area, view from shallow (~1079 m, top left) to deep (3933 m, base right) water depths. Current ripples, hard sediment surfaces, and basalt surfaces point to intense erosion/no sedimentation due to strong bottom currents between ~1100 m and ~2100 m water depth. Below ~3500 m water depth, active benthic life leaving burrows and circular spurs point to the intense bioturbation of sediments. Black cm-sized basaltic pebbles point to downslope transport. Images taken by TV-MUC from a few meters above seafloor.

Down-core sediment records

The dominant lithology of the area between the seamounts Kimmei and Ninigi consist of gray to light brown silty calcareous ooze, in large parts foraminifera-bearing. These oozes are sometimes interbedded with diagenetically altered greenish layers and belong to the **southernmost calcareous ooze facies** described in Chapter 5.6.3. In cores SO264-13-

2, 15-2, 16-2, and 19-2, several tephra layers could be identified, which are mostly bioturbated and have uneven contacts (c.f. Chapter 5.7). Detailed core descriptions and core photography can be found in Appendices 5.6-1 and 5.6-2.

Within the eastern area of Kimmei Seamount (Fig. 5.6-15), our southernmost gravity core SO264-8-2 with 9.72 m core length was retrieved from 2682 m water depth. The lithology can basically be divided into three units. The lowermost interval below 3.8 m consists of silty calcareous oozes, with rather high magnetic susceptibility values. It includes several tephra layers. The overlying interval between 3.8-0.8 m core depth changes towards light brownish foraminiferal-bearing calcareous oozes. With very low magnetic susceptibilities it appears typical for the **southernmost calcareous ooze facies**. The uppermost sediments <0.80 m core depth are characterized by the presence of brownish foraminiferal-bearing sandy calcareous ooze intercalated with silty calcareous ooze, but are still low in magnetic susceptibility and most likely belong to the **southernmost calcareous ooze facies**.

In the Koko Seamount area (Fig. 5.6-15), piston core SO264-9-2 with a recovery of 15.7 m was taken from 3865 m water depth. The core mainly consists of brownish foraminiferal-bearing silty calcareous ooze. Between 4.5 m and 1.5 m core depth, the silty ooze changes into brownish foraminiferal-bearing calcareous ooze. The uppermost part is rich in calcareous microfossils, mainly foraminifers, while the lowermost part of the core below 12 m contains several greenish-black volcanic ash layers. Magnetic susceptibility values are relatively low. Gravity cores SO264-10-2 and SO264-12-2 from 1573 and 1077 m water depth, respectively, were empty.

The 13.81 m long piston core SO264-13-2 was recovered from 3935 m water depth at Ojin Seamount (Fig. 5.6-15). This sediment record is mainly composed of grayish foraminiferal-bearing silty calcareous ooze and is rich in calcareous microfossils, mainly planktonic foraminifers. This record includes several turbidites and greenish-black tephra layers. Magnetic susceptibility records are rather low and range below $200 \cdot 10^{-6}$ SI units. Prominent magnetic susceptibility peaks appear below ~12.5 m core depth, which may be correlated to core SO264-8-2 from east of Kimmei (Fig. 5.6-17).

At Nintoku Seamount (Fig. 5.6-15), two gravity cores were recovered from 3750 m and 1308 m water depth at stations SO264-14-1 and SO264-20-1, respectively. Core SO264-14-2 has a total length of 18.41 m and mainly consists of silty ooze, which varies in color (light gray, in some parts greenish), and is generally low in magnetic susceptibility (Fig. 5.6-16). In the uppermost 1.4 m, the sediment becomes darker gray, less carbonaceous, and shows clearly higher magnetic susceptibilities. Foraminifera are abundant in the upper 4 m and between 14 and 17 m core depth. Some lamination in mm and cm-scale of diagenetically altered layers is visible. Core SO264-20-1 is only 0.7 m long and consists of dark sand at 0.7-0.35 cm, showing black terrigenous grains, extremely high magnetic susceptibility values, and low numbers in calcitic foraminifera. The uppermost, increasingly carbonaceous core section <0.35 m core depth is rich in foraminifera, while magnetic susceptibility values come close to zero.

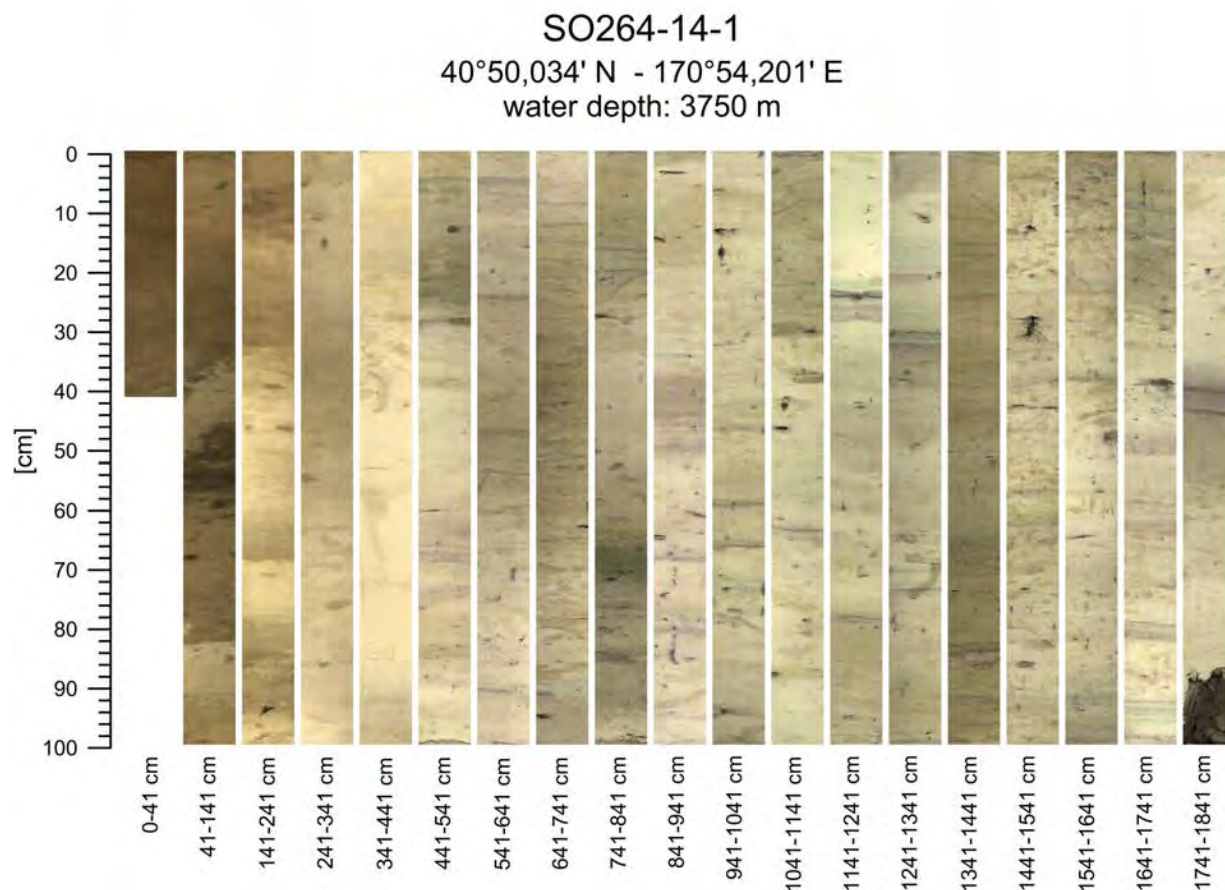


Figure 5.6-16. Core SO264-14-1 from Nintoku Seamount (3750 m water depth) mainly consists of silty calcareous ooze, which varies in color (light gray, in some parts greenish), and is generally low in magnetic susceptibility. The core exemplarily shows the prominent transition between this older 'southern calcareous ooze facies' and the 'mid-transect siliciclastic-carbonaceous facies' in the uppermost 1.4 m (darker gray foraminiferal coarser sand/silt, high magnetic susceptibilities).

West of Nintoku Seamount (Fig. 5.6-15) the gravity core SO26-19-2 showing 14.37 m core recovery was retrieved from 5311 m water depth. It contains a few tephra layers and is composed of light to dark gray silt. Calcareous foraminifera are not longer preserved due to the core location below the carbonate compensation depth (CCD). This core shows higher susceptibility values than all other records from the Nintoku Seamount area.

Further north (~41°N) at Ninigi Seamount (Fig. 5.6-15), gravity core SO264-15-2 (14.18 m core length) and piston core SO264-16-2 (14.80 m core length) were recovered from 3662 m and 3572 m water depth, respectively. Both records consist of foraminifera-bearing silty calcareous oozes and contain some thin tephra layers. A change between darker and lighter gray core sections, also reflected in the magnetic susceptibility records, is prominent in both cores, allowing to correlate them easily.

Due to the inconsistent lithologies, the correlation of the sediment records from Working Area 1 using only shipboard logging data still remains a challenge. A tentative attempt is made in Fig. 5.6-17. This attempt implies that the shallowest (2700-1300 m water depth) sediment cores SO264-8-2 (east of Kimmei) and -20-2 (Nintoku) preferentially cover the

oldest sediments on the Emperor Seamount Chain, below the defined '**southern calcareous ooze facies**', while the overlying younger sediment sequences most likely have been eroded (or not even deposited) by bottom currents. Instead, the deeper cores SO264-13-2 (Ojin) and -14-1 (Nintoku) from >3500 m water depth (partly entirely) preserve the younger sequences of the southern calcareous ooze facies, and even reach into the overlying '**mid-transect siliciclastic-carbonaceous facies**'.

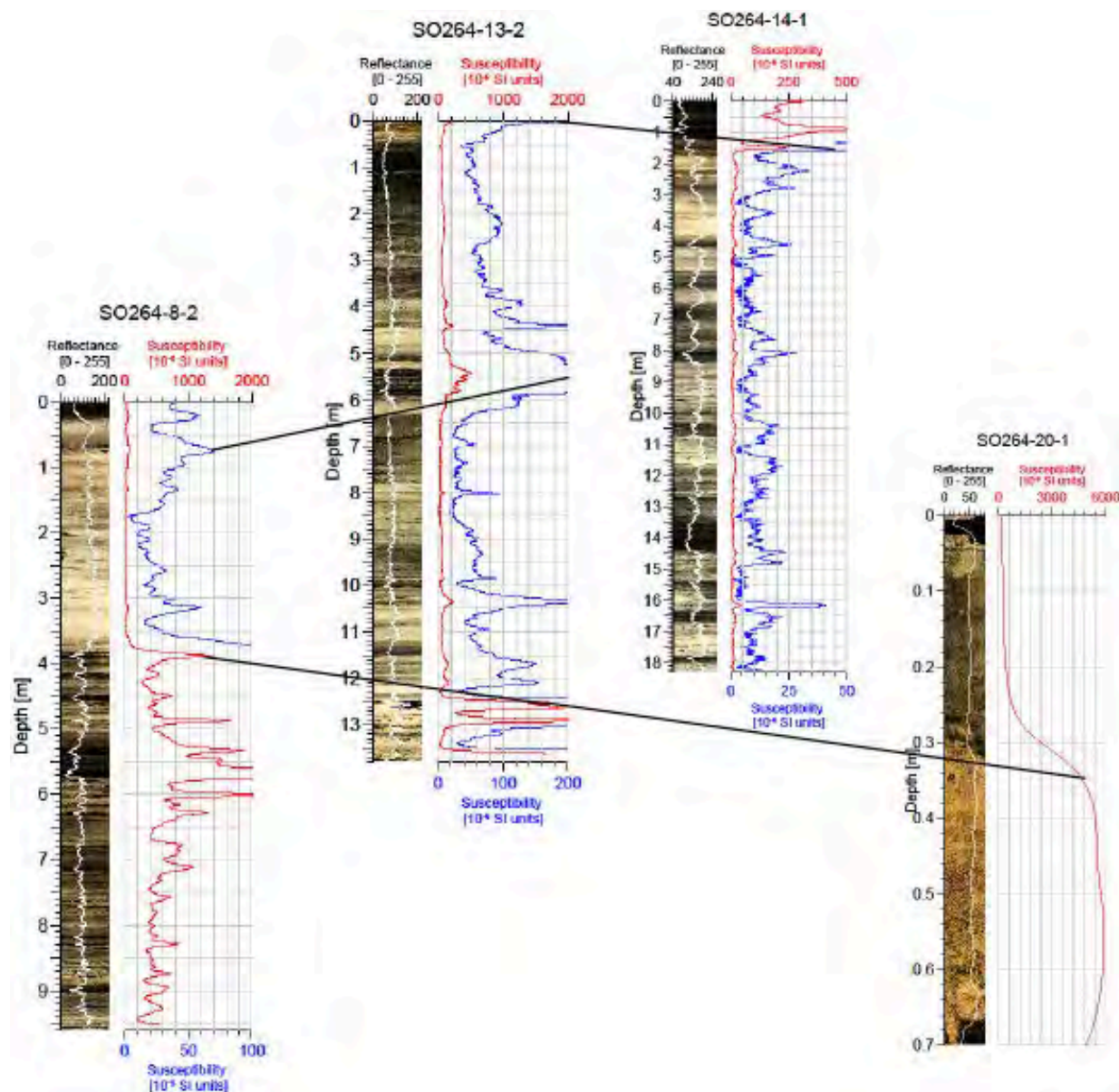


Figure 5.6-17. Tentative correlation of magnetic susceptibility records from selected cores from Kimmei (SO264-8-2: 2682 m water depth), Ojin (SO264-13-2: 3935 m water depth), and Nintoku (SO264-14-1: 3750 m water depth; SO264-20-1: 1308 m water depth) seamounts from south (left) to north (right). All cores show the 'southern calcareous ooze facies', underlain by an even older sediment sequence preserved in cores SO264-8-2 and SO264-20-1. The prominent transition to the 'mid-transect siliciclastic-carbonaceous facies' is only visible in core SO264-14-1.

5.6.5 Working Area 2: Yomei to Suiko seamounts (42°-46°N 163°30'-171°E)

(Weng-si Chao, Jordan Abell, Dirk Nürnberg)

Yomei Seamount and Suiko Seamount, located between ~42°N-43°N, ~170°E-171°E and ~44°N-46°N, ~169°E-170°E, respectively (Fig. 5.6-18), constitute the middle portion of the Emperor Seamount Chain. The sediment coring for these two seamounts consists of 1 piston corer (PC), 11 gravity corers (GC), and 2 kastenlot corers (BC), which resulted in the successful recovery of 170.7 m of sediment (Tables 5.6-4 and 5.6-5). In addition, the surface sediment was sampled by 13 multicorers (MUCs), with 3 accompanied by a TV camera system (TV-MUC), and by 2 box corers (GKG). The maximum recovery of the TV-MUC/MUC was 35 cm, while the maximum recovery reached 49 cm for the GKG.

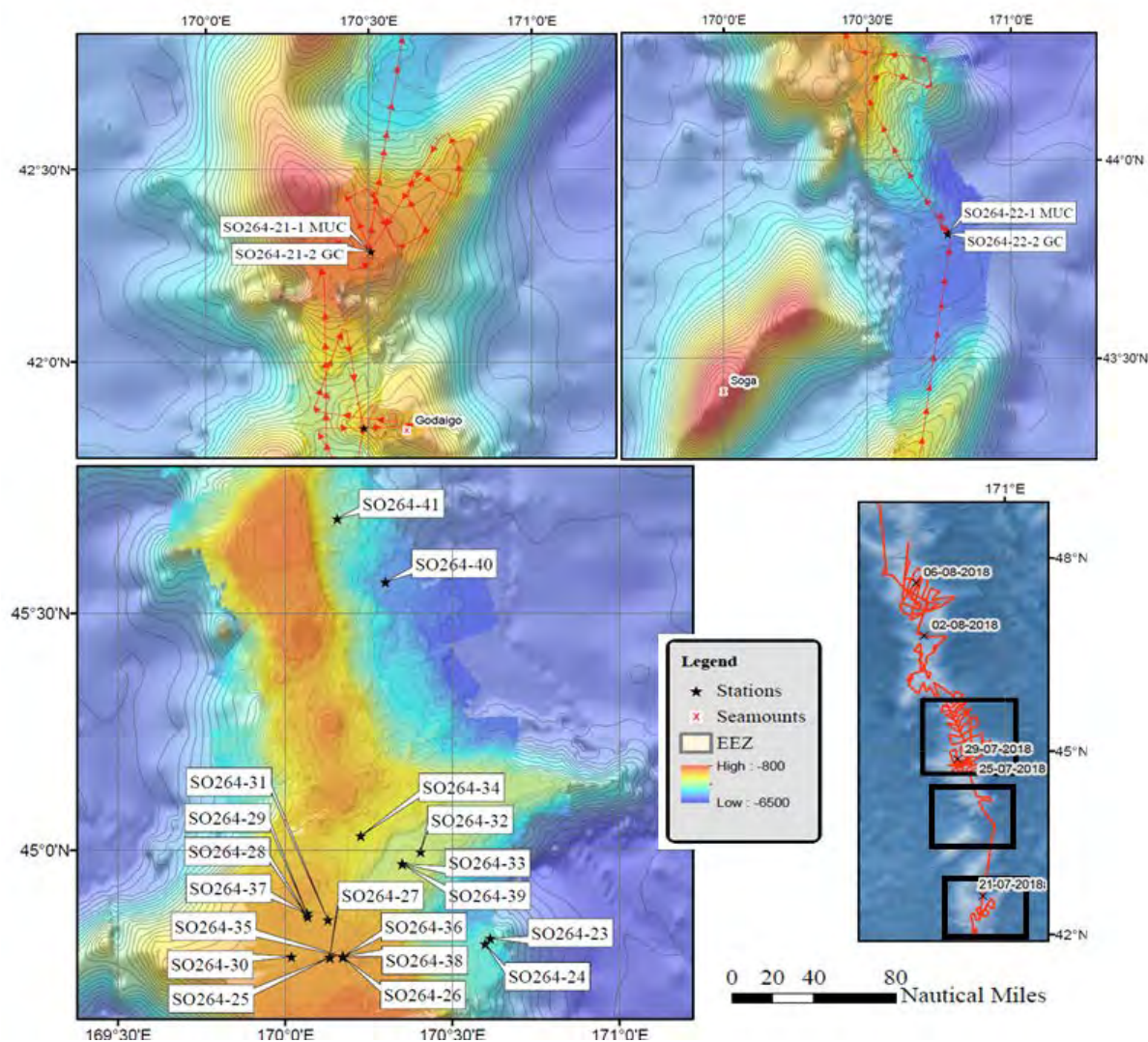


Figure 5.6-18. Bathymetry maps of geology stations overview from Yomei to Suiko Seamounts. Upper left: Yomei Seamount area near Godaigo Seamount. Upper right: Area near Soga Seamount in between Yomei and Suiko. Lower left: Suiko Seamount. Lower right: Overview chart. Black rectangles from south to north indicate Yomei Seamount, Soga Seamount, and Suiko Seamount. Red line marks the SO264 cruise track.

The coring devices and gear length were chosen based on the sediment acoustic profiles (Fig. 5.6-19) collected via the PARASOUND echo-sounding system (see Chapter 3.2.4). For the seamounts of Yomei and Suiko, the PARASOUND profiles displayed very promising sediment sequences.

Table 5.6-4. Multicorer (MUC and TV-MUC) and giant box corer (GKG) deployments and recoveries retrieved from the Yomei to Suiko Seamount area.

Station Nr.	Area/Seamount	Gear	Latitude at depth (deg/min)	Longitude at depth (deg/min)	Water depth (m)	Max Recovery (cm)
SO264-21-1	Yomei	TV-MUC	42°17,222'N	170°30,344'E	1329	20
SO264-22-1	near Soga	MUC	43°48,890'N	170°46,845'E	5709	20
SO264-23-1	Suiko	TV-MUC	44°48,831'N	170°36,785'E	4248	32
SO264-25-1	Suiko	TV-MUC	44°46,345'N	170°07,974'E	1818	34
SO264-26-1	Suiko	MUC	44°46,405'N	170°10,318'E	1772	28
SO264-28-1	Suiko	MUC	44°51,547'N	170°03,997'E	1935	19
SO264-29-2	Suiko	MUC	44°52,026'N	170°03,842'E	1965	27
SO264-30-1	Suiko	MUC	44°46,467'N	170°01,090'E	1857	26
SO264-31-2	Suiko	MUC	44°51,159'N	170°07,659'E	1941	27
SO264-32-1	Suiko	MUC	44°54,773'N	170°24,285'E	3203	30
SO264-33-1	Suiko	MUC	44°58,286'N	170°21,023'E	3140	35
SO264-34-1	Suiko	MUC	45°01,850'N	170°13,549'E	2622	26
SO264-38-1	Suiko	GKG	44°46,430'N	170°10,349'E	1771	41
SO264-39-3	Suiko	GKG	44°58,286'N	170°21,022'E	3142	49
SO264-41-1	Suiko	MUC	45°41,947'N	170°09,298'E	3645	32

Table 5.6-5. Piston corer (PC), gravity corer(GC) and kastenlot corer (BC) deployments and recoveries retrieved from the Yomei to Suiko Seamount area.

Station Nr.	Area/Seamount	Gear	Latitude at depth (deg/min)	Longitude at depth (deg/min)	Water depth (m)	Recovery (m)	Recovery [%]
SO264-21-2	Yomei	GC5	42°17,225'N	170°30,344'E	1329.5	0	0
SO264-22-2	near Soga	GC20	43°48,889'N	170°46,854'E	5704	16.21	81.05
SO264-23-2	Suiko	PC20	44°48,835'N	170°36,781'E	4245	16.29	81.45
SO264-24-3	Suiko	GC20	44°48,066'N	170°35,862'E	4295	14.80	74
SO264-25-2	Suiko	PC20	44°46,341'N	170°07,987'E	1788	0	0
SO264-26-2	Suiko	GC20	44°46,412'N	170°10,327'E	1771	16.43	82
SO264-27-1	Suiko	GC20	44°46,333'N	170°07,986'E	1788	0	0
SO264-28-2	Suiko	GC10	44°51,547'N	170°03,997'E	1935	7.64	76
SO264-29-1	Suiko	GC10	44°52,027'N	170°03,837'E	1966	8.70	87
SO264-30-2	Suiko	GC20	44°46,467'N	170°01,088'E	1857	19.23	96
SO264-31-1	Suiko	GC20	44°51,164'N	170°07,699'E	1942	13.21	66
SO264-32-2	Suiko	GC20	44°59,777'N	170°24,285'E	3200	19.32	97
SO264-33-2	Suiko	GC20	44°58,286'N	170°21,019'E	3141	17.38	87
SO264-34-2	Suiko	GC10	45°01,851'N	170°13,548'E	2622	1.95	20
SO264-36-1	Suiko	BC6	44°46,409'N	170°10,319'E	1771	4.90	82
SO264-37-1	Suiko	BC6	44°52,027'N	170°03,836'E	1966	0	0
SO264-39-1	Suiko	BC6	44°58,283'N	170°21,053'E	3143	5.17	86
SO264-41-2	Suiko	GC20	45°41,947'N	170°09,305'E	3645	9.47	47

PARASOUND studies at Working Area 2

Working Area 2 is subdivided into the smaller Yomei Seamount (southern seamount) and larger Suiko Seamount (northern seamount) that differed substantially in sediment depositional conditions. PARASOUND profiles from Yomei Seamount indicate that most parts of this seamount are barren of sediment deposits. Hence, we were not able to recover sediments from this seamount. However, several suitable core sites were found near ridges or in small-scale depressions on Suiko Seamount. Here, isolated, well-stratified sediment deposits were discovered that varied between several meters and >100m in sediment thickness (Fig. 5.6-19). PARASOUND images for each coring station are given in the Appendix 5.4.

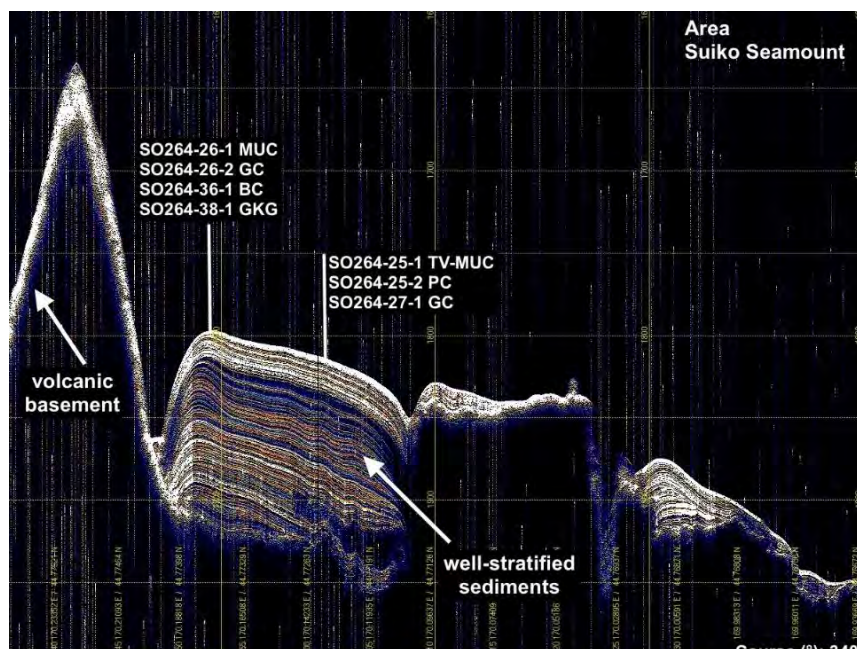


Figure 5.6-19. PARASOUND profile with coring sites and preliminary sedimentological interpretation (white arrows) from Suiko Seamount. Several excellent sediment cores were recovered from huge, isolated sediment deposits (>100m) that are typical for the Suiko Seamount area.

Surface sediment lithology

Video observations accomplished with the three TV-MUC deployments at Yomei Seamount (near Soga) and Suiko Seamount (Fig. 5.6-20) indicate that the seafloor surface varies from wave ripple dominated settings (indicating a relatively strong bottom current environment as already observed in Working Area 1) covered by regular abundances of black (volcanic) pebbles, to a strongly bioturbated, irregular soft/muddy surface. Surface sediments in these areas are commonly dominated by foraminiferal sands, but shift to silty oozes in the northern areas of Suiko Seamount. At great depth on the eastern part of Suiko Seamount (SO264-23-1, 4245 m water depth), sediments change to fine brownish-red (carbonate-free) muds with silt-sized black volcanic particles.

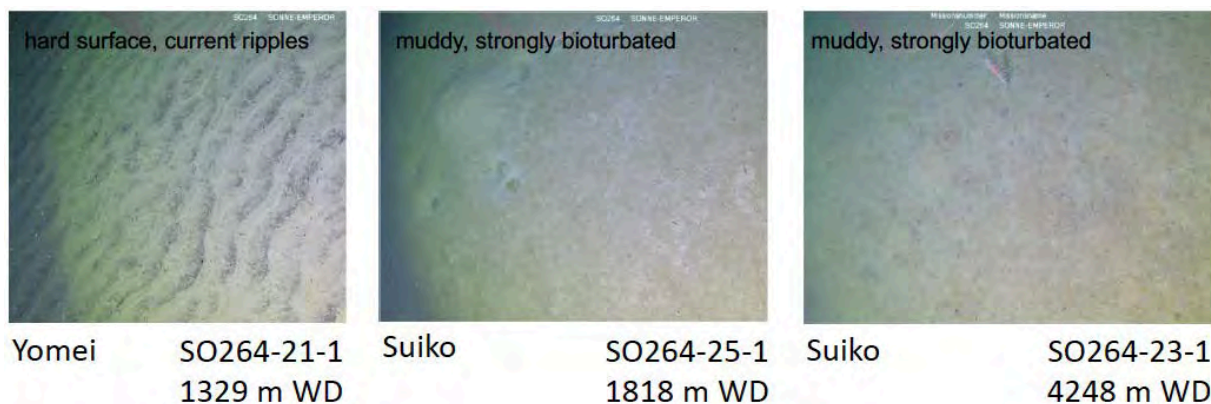


Figure 5.6-20. Seafloor sediments in the Yomei and Suiko seamount area, view from shallow (~1329 m, left) to deep (4248 m, right) water depths. Current ripples and hard sediment surfaces, point to intense erosion/no sedimentation due to strong bottom currents at ~1300 m water depth. Below, active benthic life leaving burrows and circular spurs point to the intense bioturbation of sediments. Images taken by TV-MUC from a few meters above seafloor.

Down-core sediment records

Deep-sea sedimentary facies north of Yomei Seamount (near Soga)

The gravity core SO264-22-2 is located near Soga Seamount, north of Yomei Seamount, and was recovered from a water depth of ~5700m. The sediment facies of this 16.21 m long core is typical for the deep-sea area and consists of light to medium gray silty oozes with dark gray laminated layers distributed throughout. Sediments are void of calcitic foraminifera, which is likely a result of calcium carbonate dissolution at great water depths.

Sedimentary facies at Suiko Seamount

Several sediment cores from Suiko Seamount were retrieved from ~1900 m to ~4300 m water depth, hence spanning the entire depth range of the seamount. The high quality of the sedimentary records is underlined by the fact that they can be correlated based on magnetic susceptibility data, distinct tephra layers, and major lithologies.

Shallow water depth cores SO264-26-2, 28-2, 29-1, 30-2, 31-1: The gravity cores from ~1900m water depth at Suiko Seamount commonly display lightly grayish silty/clayey calcareous oozes at the basal part of the cores (equivalent to the 'southernmost calcareous ooze facies'), while a transition to grayish brown foraminifera bearing sands, silty sands, and silty clays is observed in the upper part (equivalent to the 'mid-transect siliciclastic-carbonaceous facies') (Fig. 5.6-21). Foraminifera are abundant throughout all cores. Most notably, at least four distinct tephra layers are identified from most of the cores (c.f. Chapter 5.7). Some black angular basaltic pebbles are observed, occurring mainly within the foraminifera-bearing silty/sandy facies. It remains questionable whether they are due to ice-rafting or downslope transport. The observed facies changes can also be distinguished from the magnetic susceptibility records, with values changing from ~0 to $\sim 4000 \times 10^{-6}$ SI units, the high values of which might indicate higher terrigenous input. The distinctive magnetic susceptibility patterns of cores SO264-28-2 and 29-1 (Fig. 5.6-22) are easy to correlate with all the prominent peaks being present in both. This also provides potential for these two cores to act as possible reference cores for the core-

correlation across the entire Emperor Seamount Chain. Although the coring sites are nearby and retrieved from rather similar water depths, the sedimentary facies correlation between cores reveals sedimentation rates are variable. This offset is most likely due to regionally varying depositional processes, yet interpretation cannot be drawn until independent age models are established.

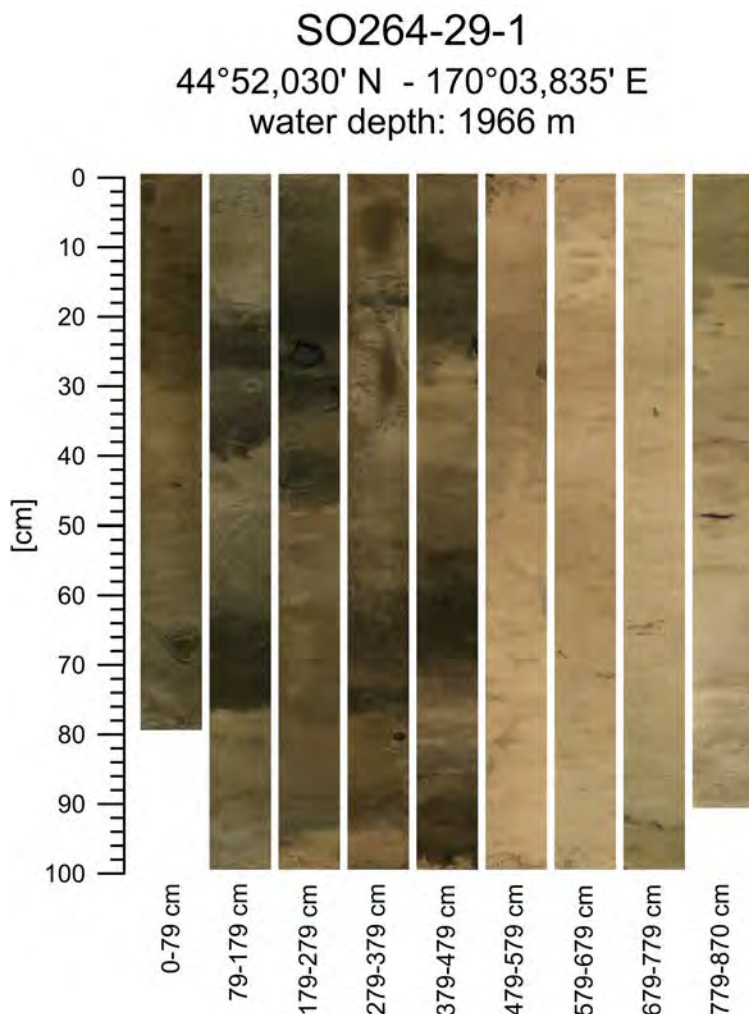


Figure 5.6-21. Core SO264-29-1 from Suiko Seamount displays grayish silty/clayey calcareous oozes at the basal part of the core (equivalent to the 'southernmost calcareous ooze facies'), with the rapid transition to grayish brown foraminifera bearing sands, silty sands, and silty clays in the upper part (equivalent to the 'mid-transect siliciclastic-carbonaceous facies') (c.f. Appendix 5.6-2).

Mid-water depth cores – SO264-32-2, 33-2, 41-2: These three gravity cores were retrieved between ~3100m to ~3600m water depth and are located to the northeast and north of Suiko Seamount. In spite of the rather similar water depth, they show varying sedimentary facies. The gravity cores SO264-32-2 and 33-2 are similar in location and water depth, which leads to a relatively similar lithology, and have resembling core recoveries. The lower part of the sediment record is dominated by whitish gray to light gray calcareous ooze, followed by a pattern of gray sandy ooze to grayish brown foraminifera bearing silty sand that is intercalated by light brown calcareous silty ooze towards the upper portion of the cores (equivalent to the facies change between the 'southernmost calcareous ooze facies' to the 'mid-transect siliciclastic-carbonaceous facies'). Strong bioturbation occurred through the whole record except the most basal

section. Notably, the magnetic susceptibility records show an huge ~9 m offset between these two cores, which might indicate a big difference in regional sedimentation rates. At the far north of Suiko Seamount, the gravity core SO264-41-2 was retrieved from 3645m water depth. The most lower part of the core is mainly composed of white to very light brownish calcareous coccolithophorid oozes with sparse bioturbation, which is marked as close to 0 in the magnetic susceptibility record. A transition sequence follows and is intercalated by dark brownish silty clay with higher bioturbation intensity, while the uppermost portion of the core is dominated by bioturbated brownish silty clay, but is regularly interrupted by mid to light brownish foraminifera-bearing calcareous silt. The top is composed of a thin brown foraminifera-bearing silty sand. The core is basically similar in lithology to cores SO264-32-2 and 33-2 and shows good calcite preservation down to large water depths in the North Pacific.

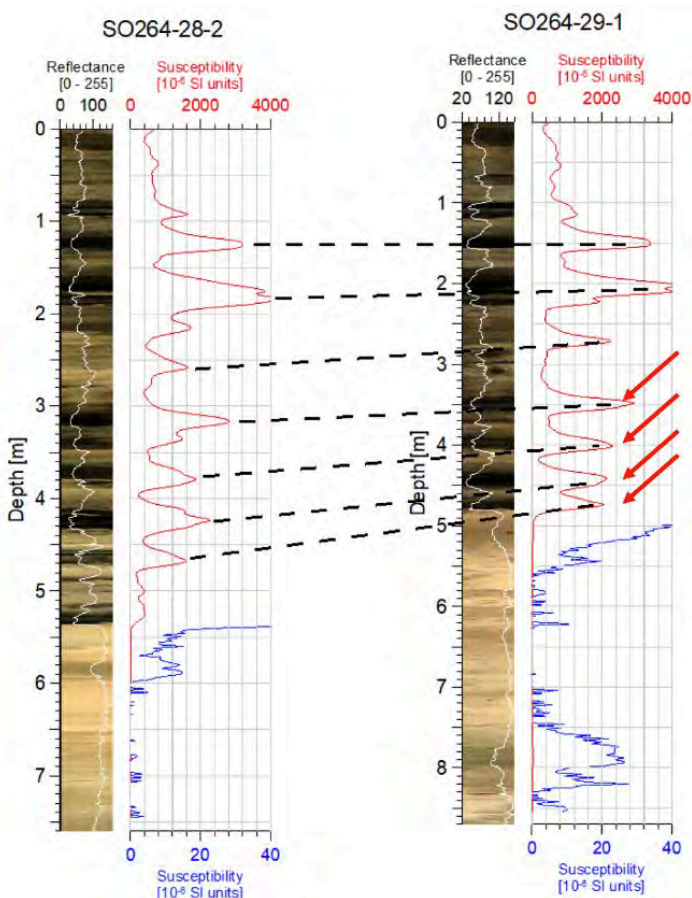


Figure 5.6-21. Gravity cores SO264-28-2 (1935 m water depth) and SO264-29-1 (1966 m water depth) from Suiko Seamount clearly show that the sedimentary facies changes match with the magnetic susceptibility data, and that the magnetic susceptibility peaks can be easily correlated among cores. Most prominent and useful for core correlation are 4 peaks in magnetic susceptibility (red arrows) right above the transition zone between the 'southernmost calcareous ooze facies' and the 'mid-transect siliciclastic-carbonaceous facies'.

Deep-water depth cores – SO264-23-2, 24-3: The gravity cores from the very deep-water depth sites are recovered from ~4200m (core 24-3 not opened yet). No foraminifera were found as a result of calcium carbonate dissolution due to likely reaching the carbonate compensation depth (CCD). The sediment record is entirely composed of reddish brown clay intercalated with darker brownish layers and light brown silty clay, with extremely high bioturbation intensity across most of the sequence. However, at the very bottom of the cores light to dark gray clay is interrupted by green (likely diagenetic) layers, with sparse bioturbation. This bottom sequence is also recorded as close to 0 in magnetic

susceptibility record, and most likely reflects the transition zone between the 'southernmost calcareous ooze facies' and the 'mid-transect siliciclastic-carbonaceous facies'.

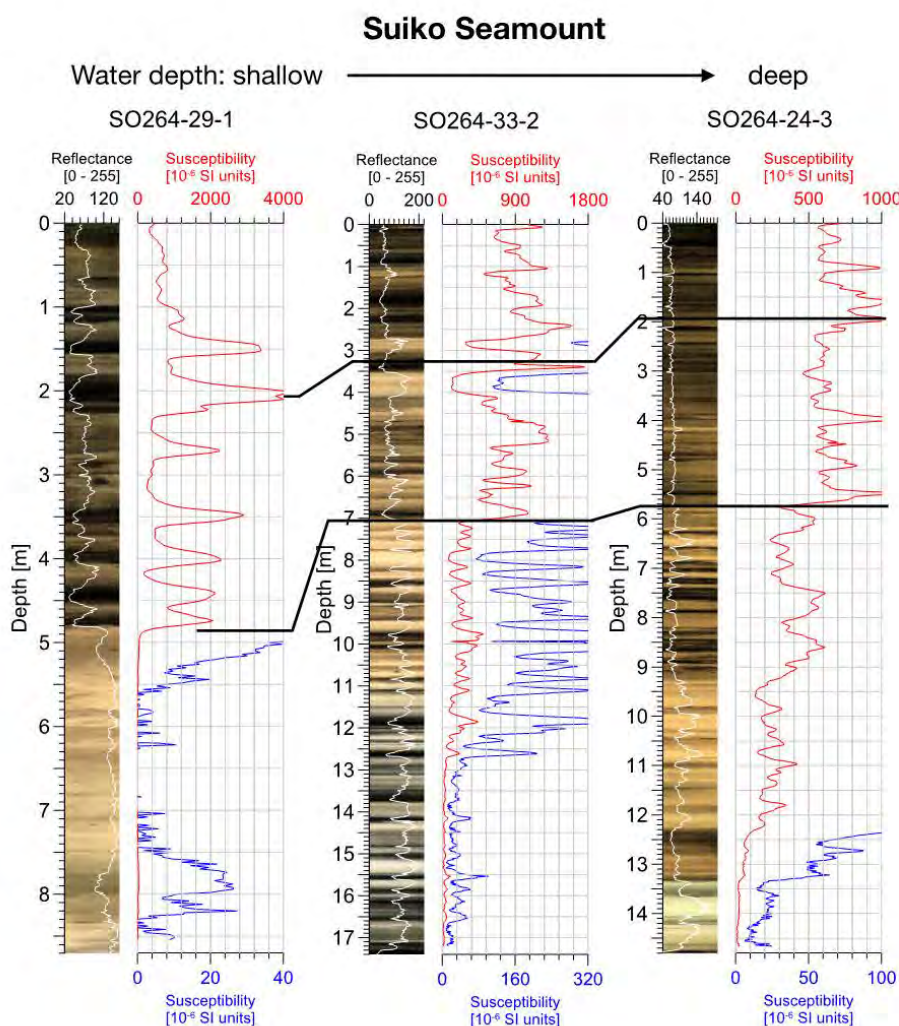


Figure 5.6-22. Preliminary core correlation of selected cores from Suiko Seamount based on magnetic susceptibility datasets. Most apparent is the change from low (blue) to high (red) magnetic susceptibility values (note different scales), which reflect the transition from the 'southernmost calcareous ooze facies' to the 'mid-transect siliciclastic-carbonaceous facies'.

Potential core correlation of Suiko Seamount sediments

Using magnetic susceptibility data for three representative sediment cores spanning the shallow, intermediate, and deep water stations, we provide a preliminary correlation of cores recovered at Suiko Seamount (Fig. 5.6-22). A significant peak in magnetic susceptibility in the upper portion of the three cores allows for first reference point, while a sharp transition to very low magnetic susceptibility values is present within the middle to lower sections of all three cores. Finally, the peaks and the previously mentioned transition are evident in cores from other sampled seamounts to the north and south, meaning the Suiko seamount cores from shallow, intermediate, or deep sites can be used to possibly cross-correlate key cores from the entire Emperor Seamount Chain (c.f. Fig. 5.6-21).

5.6.6 Working Area 3: Jimmu to Minnetonka seamounts (45°-48°N 168°-170°E)

(Cyrus Karas, Dirk Nürnberg)

Jimmu and Minnetonka Seamounts are located on the Emperor Seamount Chain between ~46°N and 48°N and ~170°E and 168°E (Fig. 5.6-23). RV SONNE started station work in this area on July 30, 2018 and left this area on August 07, 2018. We took 6 TV-MUCs, 5 MUCs without telemetry, 14 GCs and 2 PCs from a depth range of 1893 m to 3973 m water depth (Fig. 5.6-24, Tables 5.6-6, 5.6-7). Core recoveries of GCs are on average 64% with a maximum recovery of ~12.66 m at Station 56-2 at 3973 m water depth. The recovery of the two PCs are higher than the GCs with a recovery of ~78% at ~2000-3000 m water depth (Table 5.6-7).

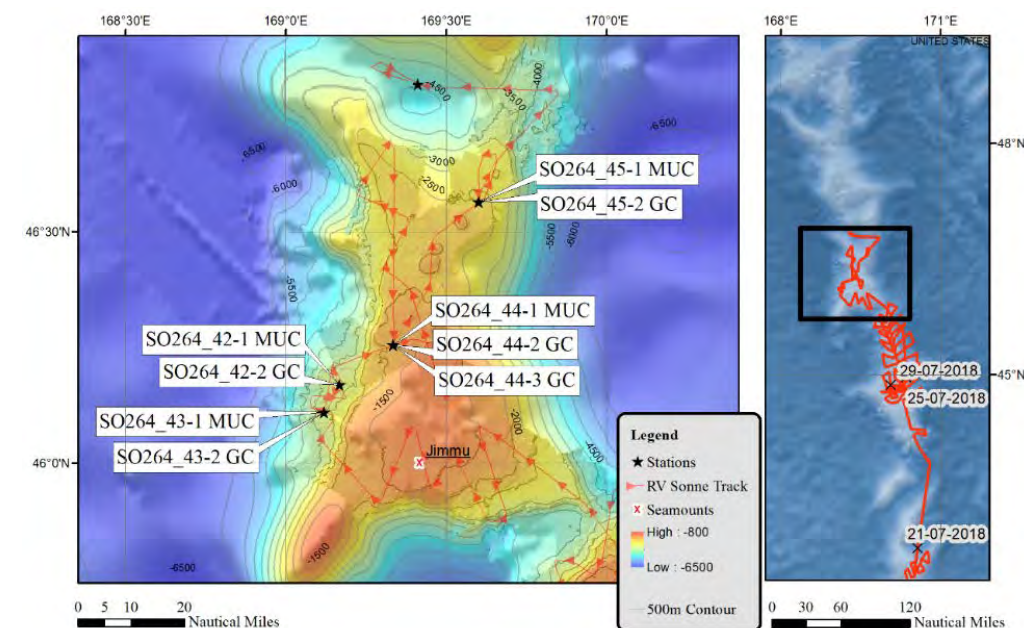


Figure 5.6-23. Bathymetric map showing the geology stations at Jimmu Seamount. Black rectangle in chart to the right indicates the study area on the Emperor Seamount Chain. Red line marks the SO264 cruise track.

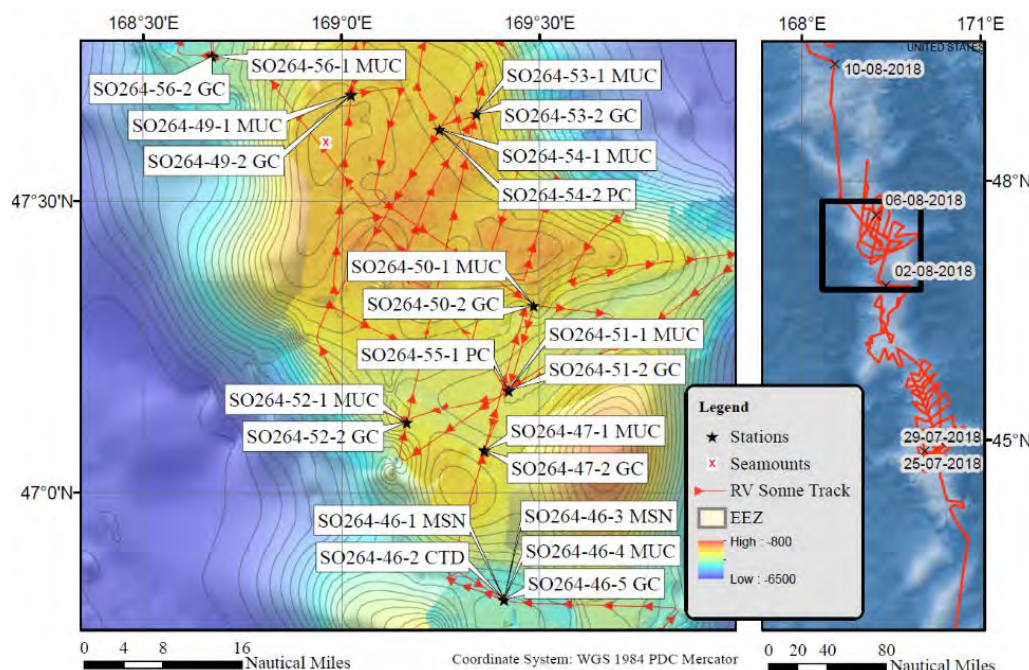


Figure 5.6-24. Bathymetric map showing the geology stations at Minnetonka Seamount. Black rectangle in chart to the right indicates the study area on the Emperor Seamount Chain. Red line marks the SO264 cruise track.

Table 5.6-6. Recovered multicores (MUCs) from Jimmu and Minnetonka seamounts.

Station Nr.	Area/Seamount	Gear	Latitude at depth (deg/min)	Longitude at depth (deg/min)	Water depth (m)	Max Recovery (cm)
SO264-42-1	Jimmu	TV-MUC	46°10,136'N	169°10,067'E	3024	30
SO264-43-1	Jimmu	TV-MUC	46°06,577'N	169°07,190'E	3242	28
SO264-44-1	Jimmu	TV-MUC	46°15,306'N	169°20,064'E	1892	14
SO264-45-1	Jimmu	MUC	46°33,795'N	169°36,072'E	2423	15
SO264-46-4	Minnetonka	MUC	46°48,935'N	169°24,659'E	3992	30
SO264-47-1	Minnetonka	MUC	47°04,386'N	169°21,656'E	2644	30
SO264-48-1	Minnetonka	TV-MUC	47°58,507'N	169°03,865'E	2872	28
SO264-49-1	Minnetonka	TV-MUC	47°40,869'N	169°01,425'E	2433	14
SO264-50-1	Minnetonka	MUC	47°19,301'N	169°29,069'E	2622	30
SO264-51-1	Minnetonka	MUC	47°10,551'N	169°25,283'E	2933	35
SO264-52-1	Minnetonka	MUC	47°07,276'N	169°09,872'E	2754	30
SO264-53-1	Minnetonka	MUC	47°38,930'N	169°20,415'E	2325	28
SO264-54-1	Minnetonka	TV-MUC	47°37,321'N	169°14,898'E	2127	28
SO264-56-1	Minnetonka	MUC	47°44,754'N	168°40,393'E	3946	31

Table 5.6-7. Recovered Gravity Cores (GC) and Piston Cores (PC) from Jimmu and Minnetonka seamounts.

Station Nr.	Area/Seamount	Gear	Latitude at depth (deg/min)	Longitude at depth (deg/min)	Water depth (m)	Recovery (m)	Recovery [%]
SO264-42-2	Jimmu	GC15	46°10,143'N	169°10,069'E	3021	11.55	77
SO264-43-2	Jimmu	GC15	46°06,569'N	169°07,191'E	3239	5.13	34
SO264-44-2	Jimmu	GC 5	46°15,297'N	169°20,066'E	1893	2.31	46
SO264-44-3	Jimmu	GC 10	46°19,304'N	169°20,062'E	1894	9.26	93
SO264-45-2	Jimmu	GC 10	46°33,796'N	169°36,071'E	2425	8.35	84
SO264-46-5	Minnetonka	GC20	46°48,940'N	169°24,653'E	3992	9.00	45
SO264-47-2	Minnetonka	GC10	47°04,392'N	169°21,660'E	2647	6.94	69
SO264-48-2	Minnetonka	GC15	47°58,507'N	169°03,870'E	2872	8.92	59
SO264-49-2	Minnetonka	GC9	47°40,870'N	169°01,420'E	2400	5.90	66
SO264-50-2	Minnetonka	GC15	47°19,295'N	169°29,074'E	2629	3.58	24
SO264-51-2	Minnetonka	GC9	47°10,548'N	169°25,282'E	2933	7.71	86
SO264-52-2	Minnetonka	GC11	47°07,273'N	169°09,874'E	2752	8.00	73
SO264-53-2	Minnetonka	GC11	47°38,931'N	169°20,417'E	2325	8.63	78
SO264-54-2	Minnetonka	PC15	47°37,321'N	169°14,848'E	2139	11.43	76
SO264-55-1	Minnetonka	PC20	47°10,542'N	169°25,292'E	2936	16.11	81
SO264-56-2	Minnetonka	GC20	47°44,754'N	168°40,407'E	3973	12.66	63

PARASOUND studies in Working Area 3

PARASOUND backscatter profiles of the Jimmu and Minnetonka seamounts indicate a much smoother seafloor bathymetry compared to more southern-located seamounts of the Emperor Seamount Chain. On both seamounts vast areas are covered with well-stratified sediments (Fig. 5.6-25). Approaching from the south, the Jimmu Seamount area is characterized by the first appearance of the **'northern siliciclastic-siliceous'** sediment facies at ~46°48'N that is typical for the subarctic North Pacific realm, and gradually replaces the **'mid-transect siliciclastic-carbonaceous facies'**. PARASOUND images for each coring station are given in the Appendix 5.4.

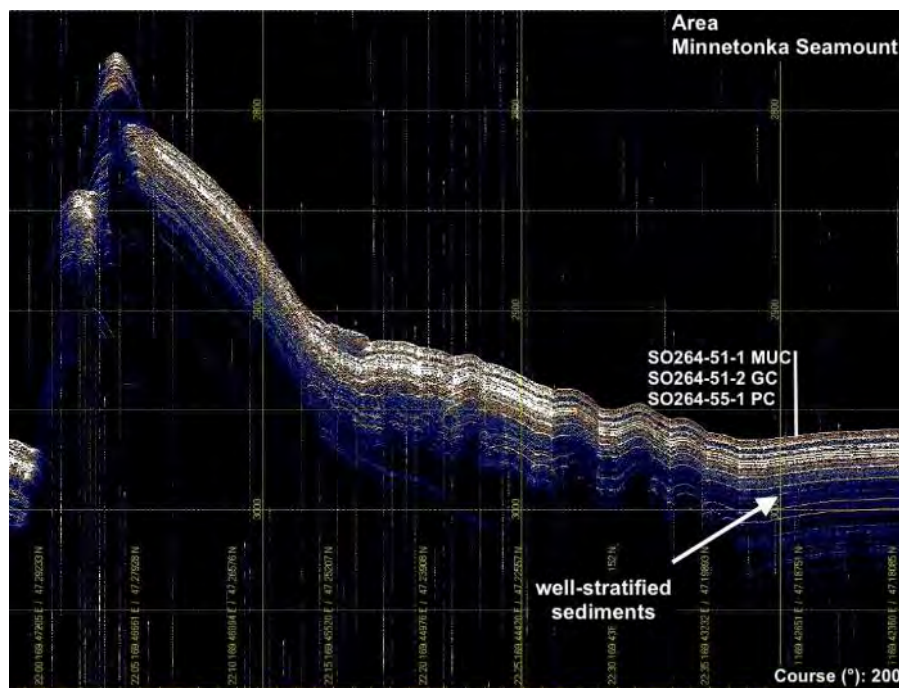


Figure 5.6-25. PARASOUND backscatter profile from Minnetonka Seamount with preliminary sedimentological interpretation (white arrow). Well-stratified, siliciclastic-calcareous and siliceous sediments are typical at Jimmu and Minnetonka seamounts.

Surface sediment lithology

Surface sediments in the Jimmu/Minnetonka area mostly show brownish to grayish foraminiferal sands and/or silty clays. We frequently found volcanic grains in cm-size and partly rounded terrigenous grains, which most likely are related to ice-rafting. Partly, the ice-rafted debris is deposited as IRD layers.

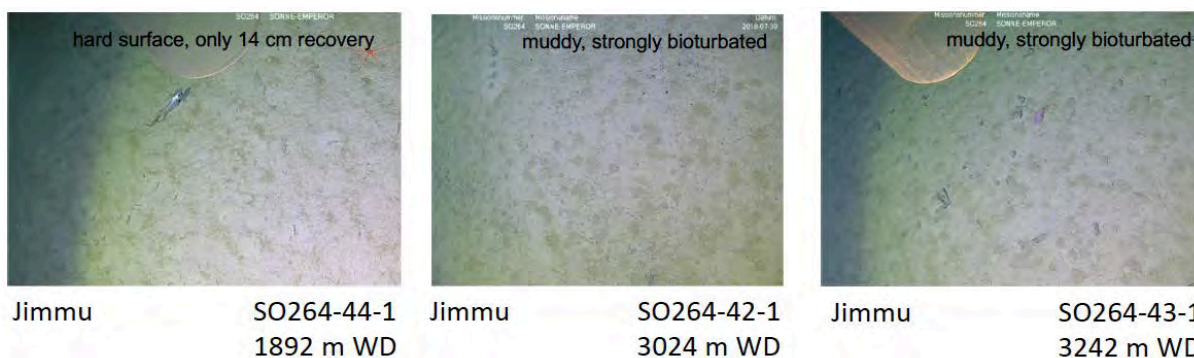


Figure 5.6-26. TV-MUC images of the seafloor at Jimmu Seamount: Station SO264-44-1 at 1892 m water depth, Station SO264-42-1 at 3024 m water depth, and Station SO264-43-1 at 3242 m water depth. While the deep locations are muddy and strongly bioturbated due to intense benthic life, the mid-depth station 44-1 shows a hard, probably ancient seafloor.

Video observations accomplished with the six TV-MUC deployments at Jimmu and Minnetonka seamounts (Figs. 5.6-26 and 5.6-27) indicate that the deeper surface sediments mainly consists of highly bioturbated silty muds. At mid-depths of ~2400 m (e.g. Site SO264-49-1), foraminiferal sands/silts dominate in both the MUC tubes and in the ~6 m long downcore record. The abundant foraminiferal tests in the surface sediments

indicate a relatively good carbonate preservation. Wave ripples observed by TV-MUC at Site SO264-49-1 point to a high-energy environment with relatively strong bottom currents at ~2400 m water depth (Fig. 5.6-27).

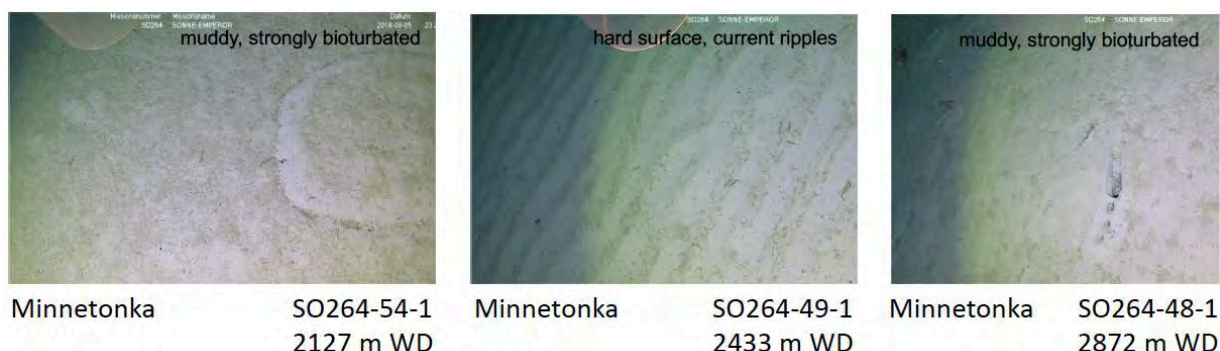


Figure 5.6-27. TV-MUC images of the seafloor at Minnetonka Seamount: Station SO264-54-1 at 2127 m water depth, Station SO264-49-1 at 2433 m water depth, and Station SO264-48-1 at 2872 m water depth. While shallow and deep locations are muddy and strongly bioturbated due to intense benthic life, the mid-depth station 49-1 shows current-induced wave ripples ca. 10 cm apart from each other.

Down-core records from Jimmu Seamount

Gravity (GC) and piston cores (PC) from Jimmu Seamount were recovered from 1893-3239 m water depth (Table 5.6-7). Common to the mid-depth cores between 1893 m and 3021 m water depth (cores SO-264-42-2, 44-3, 45-2) is that they showed the prominent transition between the **southern calcareous ooze facies** (fine, light silty to clayey calcareous coccolithophorides oozes) in the lower parts of the sediment cores on the one hand and the **mid-transect siliciclastic-carbonaceous facies** (foraminiferal coarser sand/silt) in the upper meters of the cores on the other hand (Fig. 5.6-28). Notably, the core depths at which the prominent lithological change takes place is different in the individual cores and varies by a few meters mostly due to different sedimentation rates. In the upper sections of these cores, plenty of volcanic grains in the silt to pebble grain size fraction, distinct volcanic ash layers, and some coarse (sand-sized) terrigenous IRD layers are present. The prominent lithological change is not seen in core SO264-43-2 from 3239 m water depth, as the core was too short. Nonetheless, it can be correlated to core SO264-46-5 (3992 m water depth) to the north of Jimmu Seamount (Fig. 5.6-29). The prominent lithological change is exemplified in core SO264-42-2 (Fig. 5.6-29) from 3021 m water depth. The transition is at ~4.6 m core depth, and is accompanied by a change from whitish towards dark colors and a marked increase in magnetic susceptibility values from <100 to ~2000-4000 Si-units. Paleoceanographically, this lithological change most likely indicates both an increase of terrigenous input (at higher magnetic susceptibility values) and the decrease of low/non magnetic calcareous (coccolithophoride) oozes, mainly due to a rapid and enduring climatic change from warmer and/or higher productive conditions with high coccolith and/or diatom production towards cooler conditions with more terrigenous (dust, ice-rafting) input at a diminished primary (calcite) productivity.

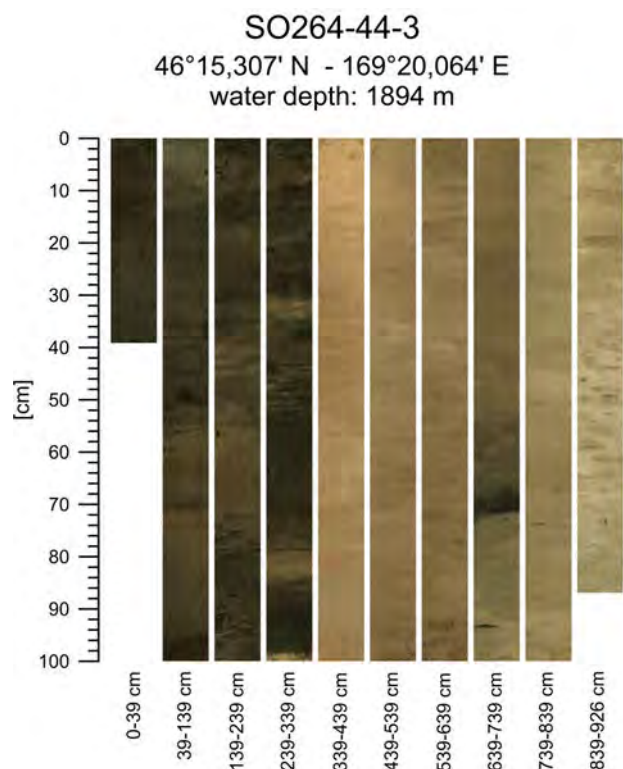


Figure 5.6-28. Core SO264-44-3 exemplarily shows the prominent transition between the southern calcareous ooze facies (fine, light silty to clayey calcareous coccolithophorides oozes) in the lower part and the mid-transect siliciclastic-carbonaceous facies (foraminiferal coarser sand/silt) in the upper meters of the cores.

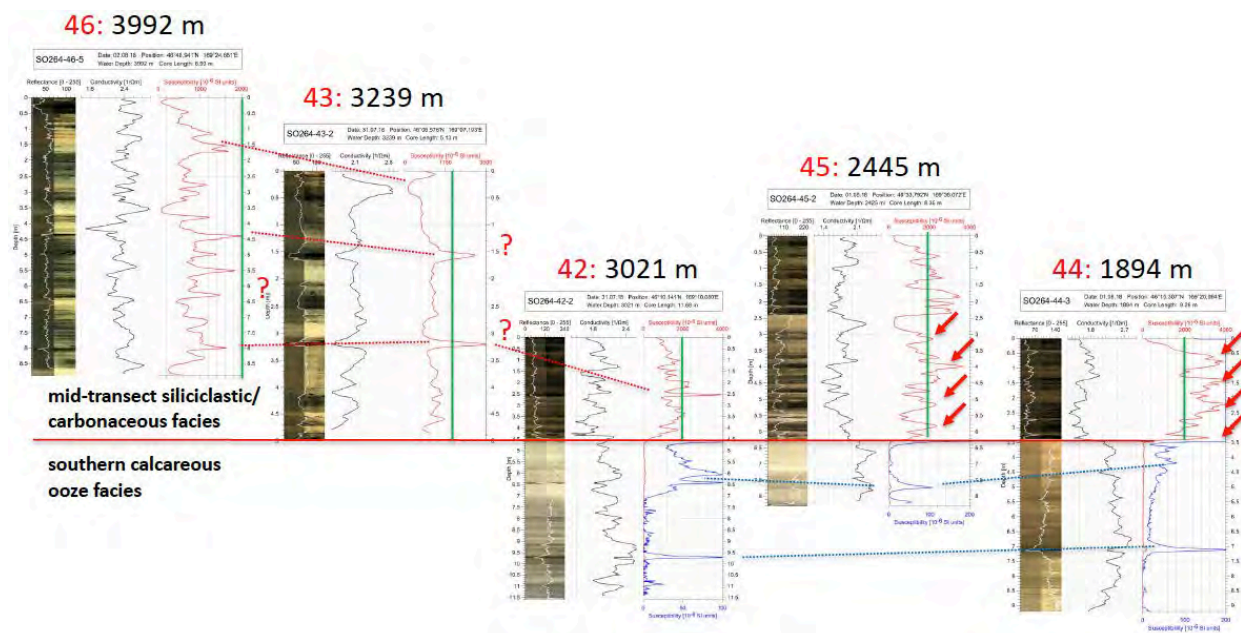


Figure 5.6-29. Tentative core correlation across Jimmu Seamount. Core images, color reflectance (white), conductivity (black), and magnetic susceptibility records (red and blue on different scales) of gravity cores SO264-42-2, -43-2, -44-3, 45-2 (from Jimmu Seamount) and -46-5 (from north of Jimmu Seamount). Red horizontal line marks prominent lithological change between 'southern calcareous ooze facies' in the lower parts of the sediment cores and the 'mid-transect siliciclastic-carbonaceous facies' above. Preliminary core correlations are indicated by dotted lines and red arrows.

Down-core records from Minnetonka Seamount

The sedimentary deposits at Minnetonka Seamount are extraordinarily interesting insofar as different facies types meet in dependence of oceanographic and climatic frontiers, and as a result of the changing depth of the carbonate compensation depth (CCD).

Mid-water depth cores – SO264-47-2, 48-2, 49-2, 50-2, 52-2, 53-2, 54-2: The seven gravity (GC) and piston cores (PC) from mid-water depths from Minnetonka Seamount cover a water depth range of 2139 to 2872 m. Four of them – SO264-48-2, 52-2, 53-2, and 54-2 - exhibit the prominent lithological transition described above from the 'southern calcareous ooze facies' (fine, light silty to clayey calcareous coccolithophorides oozes) in the lower parts of the sediment cores to the 'mid-transect siliciclastic-carbonaceous facies' (foraminiferal coarser sand/silt). The transition is best reflected in the rapid change in magnetic susceptibility and color reflectance values. Above the transition zone, the sedimentary deposits resemble those from Jimmu Seamount further south, and can be easily correlated to those by using the magnetic susceptibility records (Fig. 5.6-30).

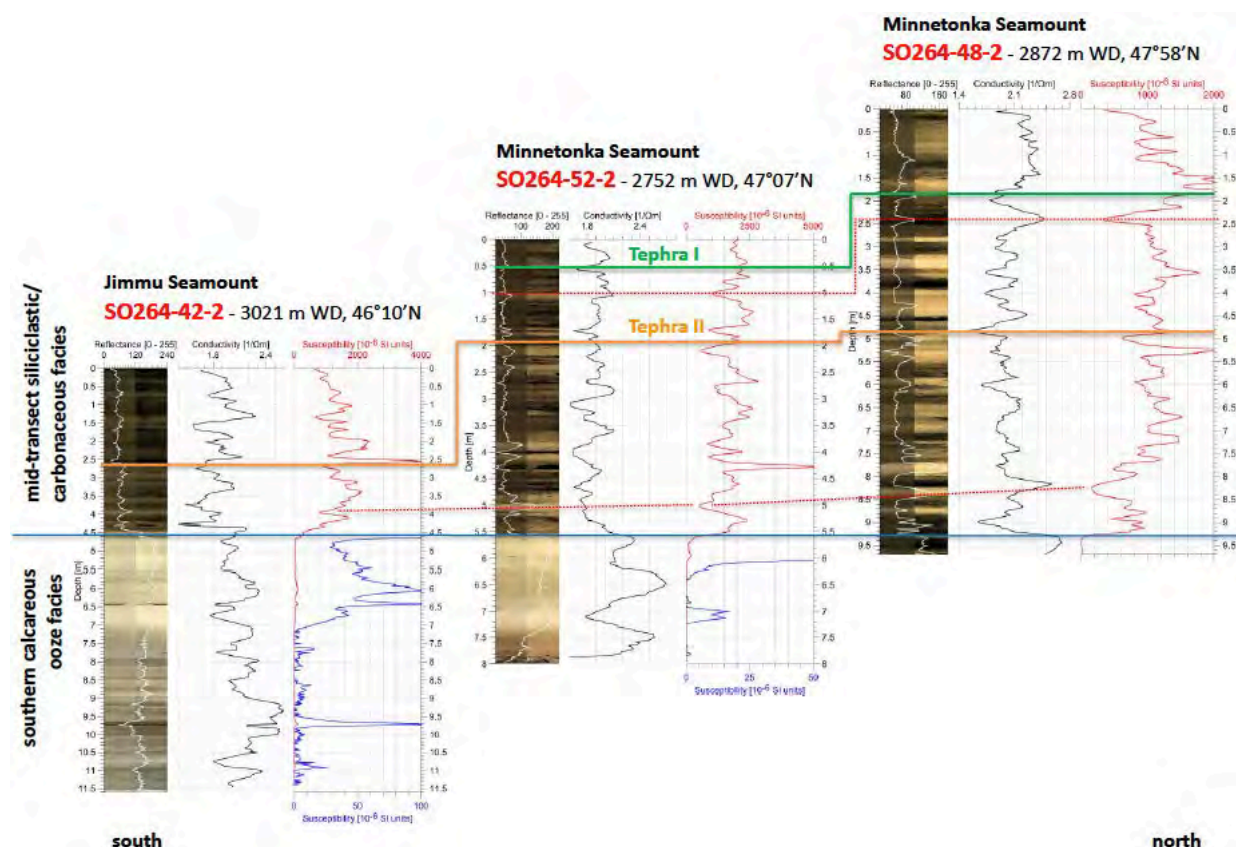


Figure 5.6-30. Tentative south-north-oriented core correlation from Jimmu Seamount (SO264-42-2) to Minnetonka Seamount (SO264-52-2 and -48-2) taking into account the color reflectance (white), conductivity (black), and magnetic susceptibility records (blue/red). Bold blue line indicates the prominent lithological transition between the 'southern calcareous ooze facies' in the lower core sections and the 'mid-transect siliciclastic-carbonaceous facies' on top. Dotted red tielines mark further core correlations. Prominent tephra layers 1 (green) and 2 (orange) are additionally used for core correlation (c.f. Chapter 5.7).

The correlation is convincingly supported by tephrastatigraphic results described in Chapter 5.7. Cores SO264-47-2, 49-2 and 50-2 with core recoveries of maximum ~7 m were most likely too short to reach the lithological transition zone, but exclusively show the ‘mid-transect siliciclastic-carbonaceous facies’ with its typical pattern in high and variable magnetic susceptibilities values. Sediments are abundant in foraminifers.

Deep-water depth cores – SO264-51-2, 55-1, 56-2: Three gravity (GC) and piston cores (PC) from deep-water depths from Minnetonka Seamount cover a water depth range of 2936 to 3946 m. Although these cores exhibit recoveries between 7.7 m and 16.1 m and hence, are markedly longer than the mid-water depth cores, they are lacking the typical older ‘southern calcareous ooze facies’ with the prominent whitish coccolith oozes. Instead, the sediment is largely consisting of grey silty clay or clayey silt, with common foraminifera. Important to note is, however, that for the first time along the Emperor Seamount Chain transect, typical diatomaceous oozes intercalate the dominant siliciclastic sediment type (Fig. 5.6-31). These greenish, foraminifer-bearing diatomaceous oozes, which have already been described by our group further to the north in the Bering and Okhotsk seas at the beginning of late Pleistocene interglacial time periods (e.g., Nürnberg & Tiedemann, 2004; Riethdorf et al., 2013a,b), gradually replace the white and pure calcareous oozes. Notably, coccolith and diatom oozes show both very low magnetic susceptibility values, impeding the differentiation of sediment types from magnetic susceptibility records alone and hence, making core correlation approaches difficult.

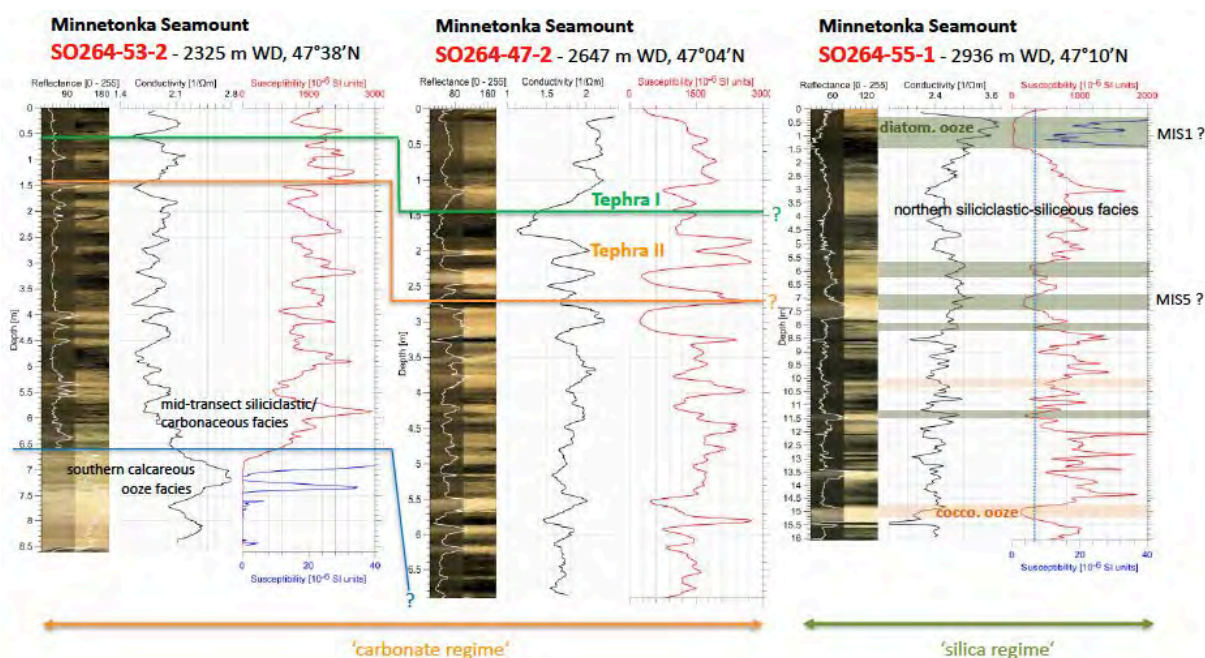


Figure 5.6-31. Comparison of Minnetonka Seamount sediment records within a narrow range of only half a degree latitude (47°04'N-47°38'N). The deepest core SO264-55-1 from below 2900 m water depth is characterized by prominent diatom oozes similar to those observed in the Bering and Okhotsk seas of Late Pleistocene age. Cores from above 2900 m water depth (SO264-53-2 and 47-2) do not show diatom oozes, but are characterized by carbonate-rich sediments. Tephra layers support the tentative core correlation between the latter cores. Green = Tephra I, orange = Tephra II, blue horizontal line marks the lithological transition between the ‘southern calcareous ooze facies’ in the lower core sections and the ‘mid-transect siliciclastic-carbonaceous facies’ on top. Greenish shading = diatom oozes, orange shading = coccolith oozes.

Although both sediment types point to high marine productivity, the change from a more calcareous (coccolithophoride-dominated) deep environment to a biogenic opal/siliciclastic environment implies significantly different environmental conditions. Nutrient availability and consumption is most crucial, as coccolithophorides prefer oligotrophic conditions, while rapid and intense diatom growth is commonly related to high-nutrient environments. In the study area, nutrient availability might have changed along with changes in the climatic and oceanographic frontal system from temperate to subpolar regimes. Lateral migrations of the Subarctic Front were most likely responsible in this respect.

The depositional environment at Minnetonka Seamount, however, is additionally affected by changes in the oceanic carbonate system. Within the very narrow $\sim 1^\circ$ -latitude by 1° -longitude area of Minnetonka Seamount ($47^\circ 04' - 47^\circ 58' \text{N}$ and $168^\circ 40' - 169^\circ 30' \text{E}$), diatom layers are only present in the deep-water locations >2900 m water depth, while the mid-depth cores <2900 m include coccolith oozes which can be traced further southward (Fig. 5.6-13). Further north, coccolith oozes gradually vanish, even at shallower water depths. This water depth and latitude-dependent change to an environment characterized by biogenic opal and siliciclastic-dominated sedimentation is due to a change in the calcite preservation state of the ocean. Apparently, Minnetonka Seamount is directly at the location where the calcite saturation depth changes from deep to shallow (c.f. Chapter 5.3). The Minnetonka cores, thus, will be ideal to reconstruct past changes in the North Pacific carbonate system.

5.6.7 Working Area 4: Tenji to South of Detroit seamounts (48°-50°N 167°30'E-169°30'E)

(Thomas Ronge, Dirk Nürnberg)

The Tenji working area comprises three seamounts. The southernmost but most prominent is Tenji Seamount (Fig. 5.6-32), while the other two seamounts further to the north are clearly smaller and officially remain unnamed. In the following, we refer to them as 'North of Tenji' and 'South of Detroit'.

Nine multicorers (MUC), one TV-MUC (Table 5.6-8), eight piston cores (PC) and three gravity cores (GC) (Table 5.6.9) were deployed along a transect between ~48°50' N and ~50°15' N, in water depths between ~2300 and 5300 m. Station work took place between August 7th and August 13th, 2018. The recovery rates for the piston and gravity corers were on average 77%, but overall ranged between 67% and 91% (Table 5.6-9).

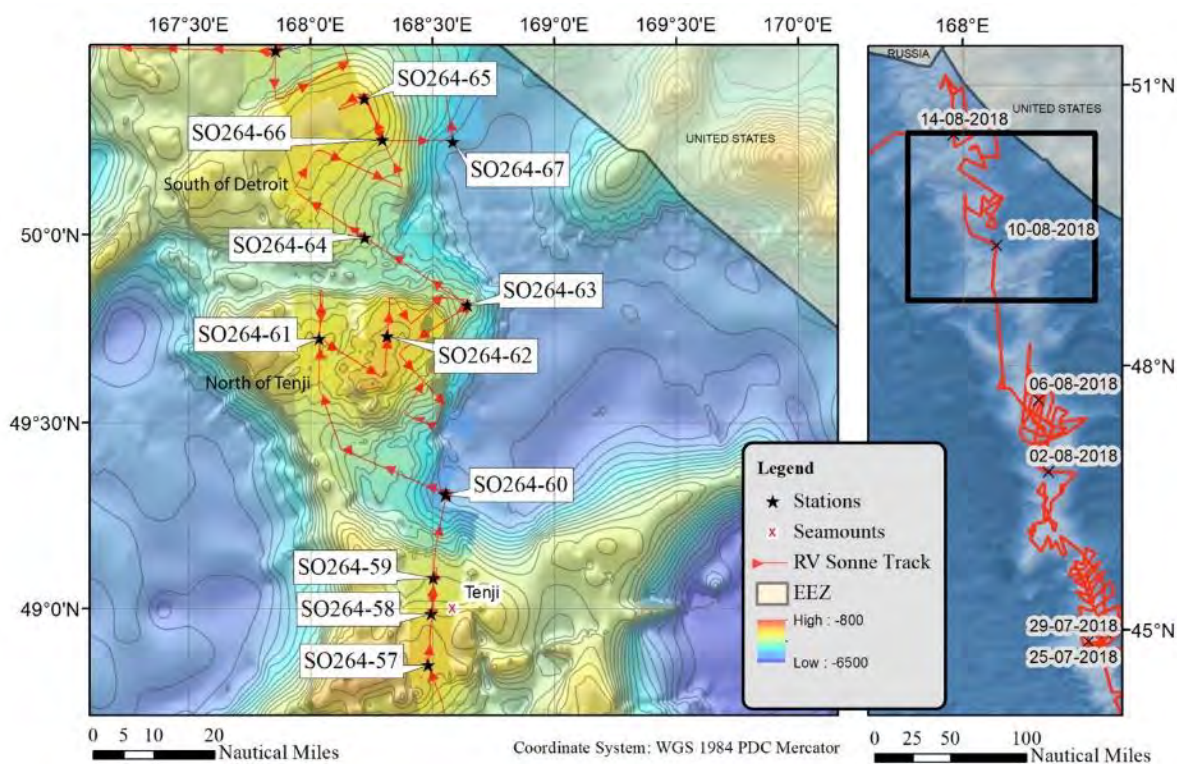


Figure 5.6-32. Bathymetric chart showing the geology stations in the Tenji working area, including the minor seamounts 'North of Tenji' and 'South of Detroit'. Black rectangle in chart to the right indicates the study area on the Emperor Seamount Chain. Red line marks the SO264 cruise track.

Table 5.6-8. List of MUC and TV-MUC deployments in the Tenji, North of Tenji and South of Detroit working areas. SO264-58-1 did not release due to mechanical problems.

Station Nr.	Area/Seamount	Gear	Latitude at depth (deg/min)	Longitude at depth (deg/min)	Water depth (m)	Max Recovery (cm)
SO264-57-1	Tenji	MUC	48°50,814'N	168°29,006'E	2355	28
SO264-58-1	Tenji	MUC	48°59,181'N	168°29,776'E	2588	0
SO264-59-1	Tenji	MUC	49°04,961'N	168°30,319'E	2916	11
SO264-60-14	Tenji	MUC	48°18,442'N	168°33,434'E	5270	35
SO264-61-1	north of Tenji	MUC	49°43,401'N	168°02,272'E	2590	26
SO264-62-1	north of Tenji	MUC	49°43,810'N	168°18,921'E	2378	30
SO264-63-1	Tenji	TV-MUC	49°48,761'N	168°38,731'E	3772	31
SO264-64-2	south of Detroit	MUC	49°59,490'N	168°13,465'E	3492	32
SO264-65-1	south of Detroit	MUC	50°21,535'N	168°13,340'E	2496	30
SO264-66-1	south of Detroit	MUC	50°15,065'N	168°17,834'E	2747	29

Table 5.6-9. List of sediment cores (PC and GC) retrieved in the Tenji, North of Tenji and South of Detroit working areas.

Station Nr.	Area/Seamount	Gear	Latitude at depth (deg/min)	Longitude at depth (deg/min)	Water depth (m)	Recovery (m)	Recovery [%]
SO264-57-2	Tenji	PC20	48°50,814'N	168°29,003'E	2356	15.40	77
SO264-58-2	Tenji	PC20	48°59,186'N	168°29,779'E	2594	17.00	85
SO264-59-2	Tenji	GC20	49°04,957'N	168°30,314'E	2930	13.36	67
SO264-60-12	Tenji	GC15	49°18,447'N	168°33,427'E	5275	10.57	70
SO264-60-13	Tenji	GC15	49°18,445'N	168°33,437'E	5274	10.25	68
SO264-61-2	north of Tenji	PC20	49°43,401'N	168°02,273'E	2591	15.70	79
SO264-62-2	north of Tenji	PC20	49°43,848'N	168°18,922'E	2373	15.50	78
SO264-63-2	Tenji	PC20	49°48,766'N	168°38,731'E	3779	18.22	91
SO264-64-1	south of Detroit	PC20	49°59,488'N	168°13,466'E	3495	18.55	93
SO264-65-2	south of Detroit	PC20	50°21,531'N	168°13,353'E	2498	13.41	67
SO264-66-2	south of Detroit	PC20	50°15,064'N	168°17,818'E	2751	15.04	75

PARASOUND studies in Working Area 4

This working area encompasses three smaller seamounts (from south to north): the Tenji Seamount, 'North of Tenji' Seamount and 'South of Detroit Seamount'. PARASOUND backscatter profiles indicate that thick (>50m thickness) and well-defined sediment deposits cover most areas (Fig. 5.6-33). Sediment cores retrieved from the seamounts show siliciclastic-siliceous sediments that are common in this part of the working area. PARASOUND images for each coring station are given in the Appendix 5.4.

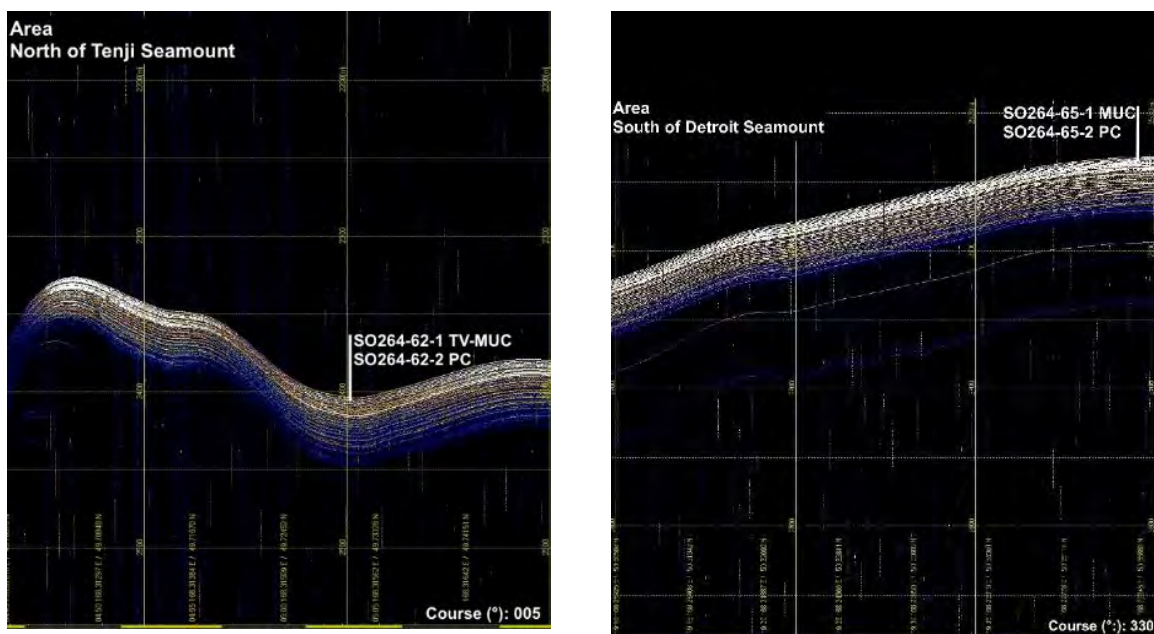


Figure 5.6-33. Selected PARASOUND profiles with coring sites from ‘North of Tenji Seamount’ and ‘South of Detroit Seamount’. Note the thick and layered sediment sequences (>50m thickness), which cover large parts of the seamounts.

Surface sediment lithology

Brown to dark gray terrigenous silty clays constitute the dominant lithology of surface sediments from Tenji, ‘North of Tenji’ and ‘South of Detroit’ seamounts. The TV-MUC seafloor observations at station SO264-62-1 from ~2374 m water depth show an intense bottom life, strongly bioturbating the seafloor sediments (Fig. 5.6-34). The southernmost station SO264-57-1 (2355 m water depth) was the only station, where we still found calcareous foraminifera-bearing silty to sandy oozes. Several cm-sized pebbles, which were interpreted as IRD, were recorded in core SO264-63-1 (3772 m water depth) (Fig. 5.6-35).

Down-core sediment records

Most of the cores from this working area were not opened due to various reasons. Only cores SO264-57-2 and SO264-60-12 were split open (Appendices 5.6-1 and 5.6-2), and show a resembling lithology described below. All unopened cores could be related to these two reference records using the logging data. Lithology was described between the cut 1 m core sections.

The sedimentary regime of the area from the Tenji Seamount to the southern flank of Detroit Seamount (Fig. 5.6-32) is dominated by dark olive-green clays and silty clays that are intercalated with dark greenish to yellowish-brown diatom oozes. The main lithological patterns are best documented in the record of SO265-57-2, which was retrieved from the top of Tenji Seamount from a water depth of 2356 m (Fig. 5.6-32).

Like SO264-57-2, all sediment records from Tenji, ‘North of Tenji’ and ‘South of Detroit’ seamounts lack the prominent shift from the well-defined coccolith oozes (southern calcareous ooze facies) to the more terrigenous, siliciclastic silty clays (mid-transect

siliciclastic-carbonaceous facies), as it was recorded for most cores south of this working area (Fig. 5.6-30).



Figure 3.6-34. Seafloor sediment at Station SO264-62-1 north of Tenji Seamount, view from ~2378 m water depth, a few meters above seafloor. Active benthic life leaving burrows and circular spurs point to the intense bioturbation of sediments. Image taken by TV-MUC.

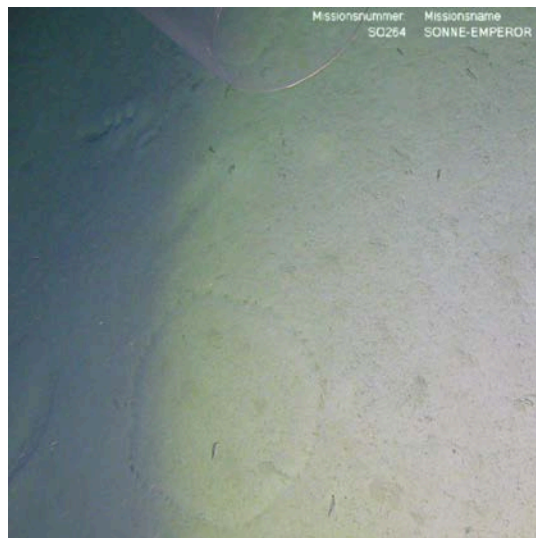


Figure 5.6-35. Seafloor sediment at Station SO264-61-1 north of Tenji Seamount, view from ~2590 m water depth, a few meters above seafloor. Active benthic life leaving burrows and circular spurs point to the intense bioturbation of sediments. Image taken by TV-MUC.

Instead, the sediment cores SO264-57-2 to SO264-66-2 exhibit a very homogenous lithology of dark greenish to dark olive green/gray clays and silty clays, which are repeatedly intercalated with lighter clays and silty clays of the same color (northern siliciclastic-siliceous environment) (Fig. 5.6-36). These terrigenous intervals are characterized by high amounts of siliciclastic material, which is mostly in the silt and clay grain size fraction. The sequences are repeatedly interrupted by prominent dark greenish to yellowish-brown layers of diatom oozes. The contact of biogenic oozes to the terrigenous (silty) clays is predominantly sharp, occasionally gradational, rarely bioturbated. The repeated appearance of these siliceous oozes are most likely associated with maxima in North Pacific biological silica production (Honjo, 1990; Pondaven et al., 2000). According to Riethdorf et al. (2013a,b), these peaks in biogenic productivity might be linked to warm phases of deglacial climate transitions and are associated to increased insolation, the northward propagation of the marginal ice zone, increasing sea-surface temperatures and a prolonged summer season. Notably, the sediment records also showed prominent layers of diagenetically altered greenish compacted clays that do not identify in the magnetic susceptibility.

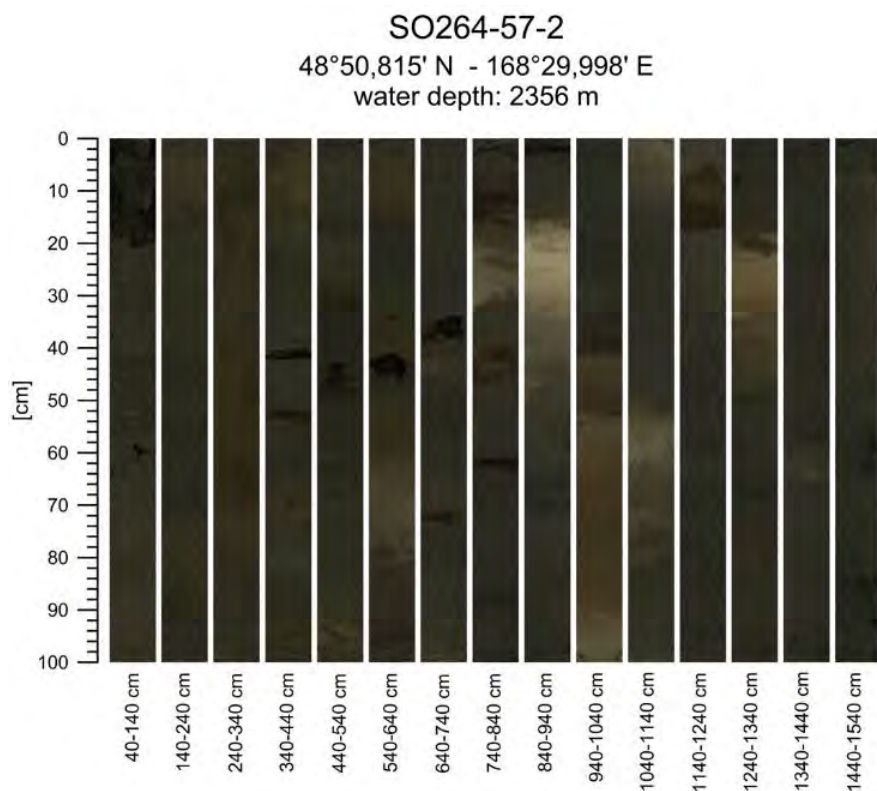


Figure 5.6-36. Core images of piston core SO264-57-2. The succession is dominated by dark olive-green clays and silty clays that are intercalated by dark greenish to yellowish-brown diatom oozes.

It is possible to achieve a very good core-to-core-correlation for most of the cores in Working Area 4, using the shipboard logging data (Fig. 5.6-37). This core correlation across the Tenji working area and the more southerly working areas, indicates higher sedimentation rates at Tenji Seamount and further north towards Detroit Seamount. This might imply that the northern cores cover several glacial-interglacial cycles.

The minor lithological changes between dark olive-green and slightly lighter (silty) clays along with the intercalated diatom oozes might also corroborate the assumption that these sediment cores cover several glacial-interglacial changes of the late Pleistocene. This 'northern siliciclastic-siliceous facies', hence, is presumably younger than the (Pliocene to Pleistocene) sediment facies found in the more southerly records ('southern calcareous ooze facies' and 'mid-transect siliciclastic-carbonaceous facies') (c.f. Fig. 5.6-30).

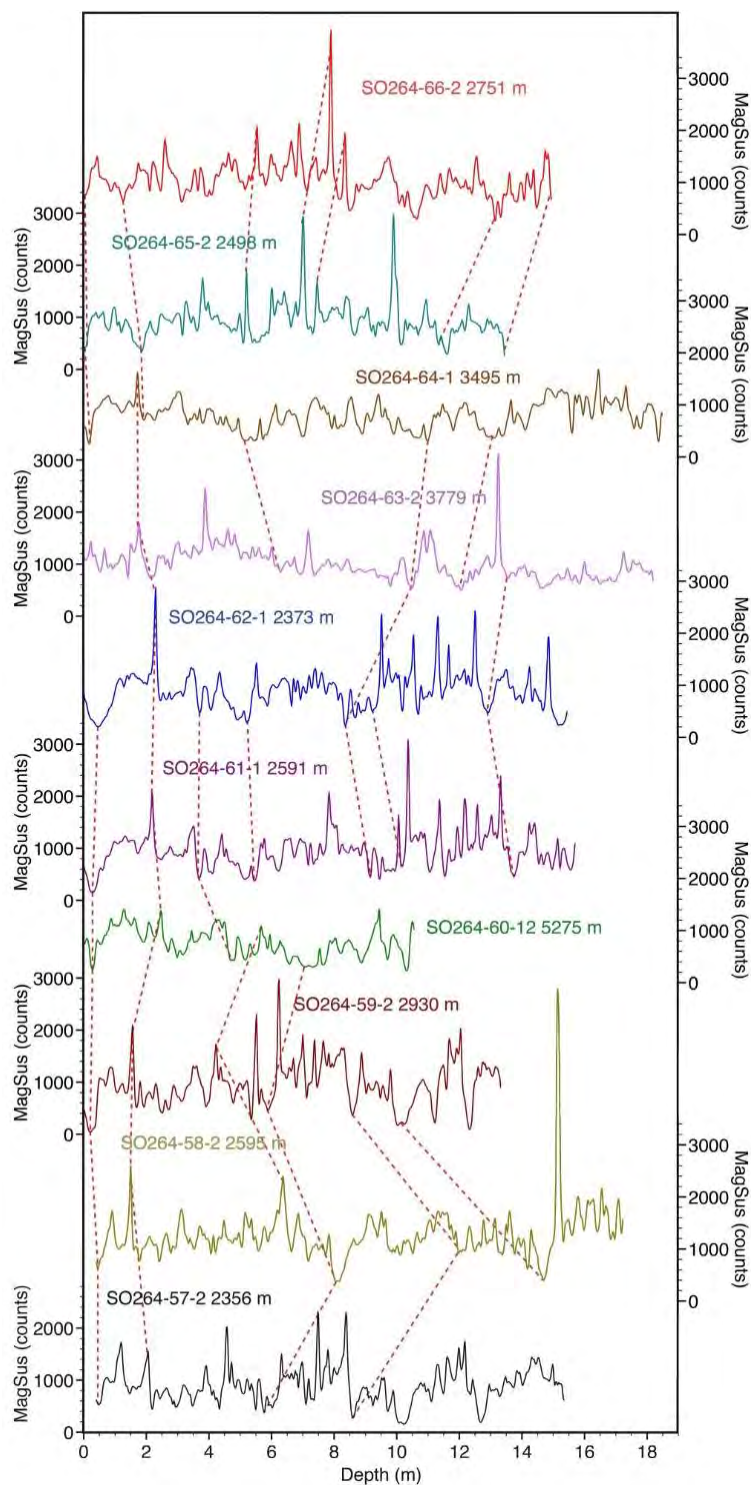


Figure 5.6-37. Magnetic susceptibility records of all sediment cores retrieved on Tenji, 'North of Tenji' and 'South of Detroit' seamounts. The red dashed lines mark preliminary tie-points used to achieve a first core-to-core-correlation.

5.6.8 Working Area 5: Detroit Seamount (50°14'–51°N 166°50'–168°35'E)

(Dirk Nürnberg)

Detroit Seamount is located on the northernmost part of the Emperor Seamount Chain. Our work focussed on the area between ~50°N and 51°N and ~166°30'E and 167°30'E (Fig. 5.6-38). RV SONNE started station work in this area on August 13, 2018 and left this area on August 17, 2018. We took 1 TV-MUC, 5 MUCS without telemetry, 3 GCs, 4 PCs, and 2 BCs from a depth range of 2396 m to 3917 m water depth (Fig. 5.6-38, Tables 5.6-10 and 5.6-11). Core recoveries of PCs were highly variable with maximum ~90% and a maximum core length of ~18.55 m at Station 69-2 from 3473 m water depth. The recovery of the PCs are commonly higher than the GCs, which only showed recoveries of ~50% at ~2400–3000 m water depth. The deployment of two 5.75 m-long BCs at 3200–3900 m water depths (SO264-75-1 and 76-1) was rather successful and provided on average 80% core recovery.

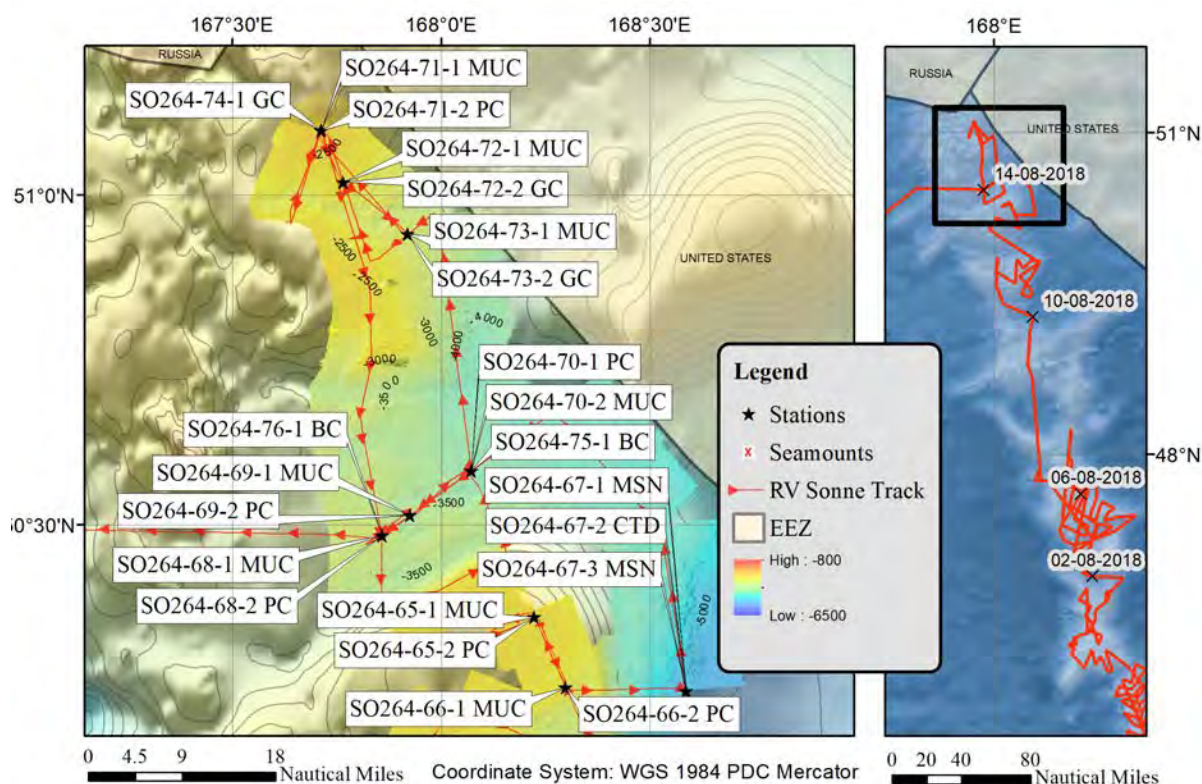


Figure 5.6-38. Bathymetric map showing the geology stations on Detroit Seamount. Black rectangle in chart to the right indicates the study area on the Emperor Seamount Chain. Red line marks the SO264 cruise track.

Table 5.6-10. List of multicorer (MUC and TV-MUC) deployments in the Detroit Seamount working area.

Station Nr.	Area/Seamount	Gear	Latitude at depth (deg/min)	Longitude at depth (deg/min)	Water depth (m)	Max Recovery (cm)
SO264-68-1	Detroit	MUC	50°29,040'N	167°51,501'E	3285	34
SO264-69-1	Detroit	MUC	50°30,869'N	167°55,443'E	3478	33
SO264-70-2	Detroit	MUC	50°34,910'N	168°04,294'E	3916	32
SO264-71-1	Detroit	MUC	51°05,879'N	167°42,751'E	2394	32
SO264-72-1	Detroit	MUC	51°01,206'N	167°45,887'E	2615	33
SO264-73-1	Detroit	TV-MUC	50°56,493'N	167°55,170'E	3039	30

Table 5.6-11. List of box cores, piston cores and gravity cores (BC, PC and GC) retrieved in the Detroit Seamount working area.

Station Nr.	Area/Seamount	Gear	Latitude at depth (deg/min)	Longitude at depth (deg/min)	Water depth (m)	Recovery (m)	Recovery [%]
SO264-68-2	Detroit	PC20	50°29,043'N	167°51,487'E	3284	18.01	90
SO264-69-2	Detroit	PC20	50°30,877'N	167°55,478'E	3473	18.55	93
SO264-70-1	Detroit	PC20	50°34,915'N	168°04,292'E	3917	5.00	25
SO264-71-2	Detroit	PC20	51°05,880'N	167°42,755'E	2397	1.22	6
SO264-72-2	Detroit	GC10	51°01,209'N	167°45,890'E	2626	5.78	58
SO264-73-2	Detroit	GC10	50°56,498'N	167°55,180'E	3047	4.59	46
SO264-74-1	Detroit	GC10	51°05,877'N	167°42,752'E	2396	5.70	57
SO264-75-1	Detroit	BC6	50°34,909'N	168°04,288'E	3919	5.10	85
SO264-76-1	Detroit	BC6	50°29,039'N	167°51,493'E	3297	4.24	71

PARASOUND studies in Working Area 5

The Detroit Seamount is the northernmost seamount area, which was studied during RV SONNE cruise SO264. Detroit Seamount in the pelagic subarctic Pacific is widely covered by thick (> 70m), well-layered and mostly undisturbed sediment sequences, reflecting a high sediment-accumulation regime. The seamount area shows typical sediments of the 'northern siliciclastic-siliceous facies' reflecting the pelagic depositional character in this area (Fig. 5.6-39). PARASOUND images for each coring station are given in the Appendix 5.4.

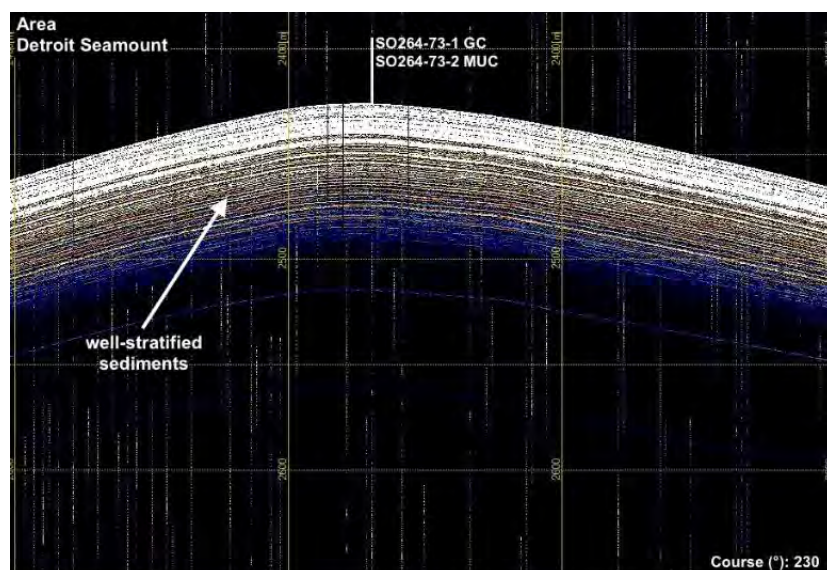


Figure 5.6-39. PARASOUND profile with coring site and preliminary sedimentological interpretation from Detroit Seamount. Note the thick and well-layered, undisturbed, high-accumulation sediment sequences (>70m), which cover large parts of Detroit Seamount.

Surface sediment lithology

Video observations accomplished with the TV-MUC deployments at Detroit Seamount indicate that the seafloor sediments resemble those from Tenji Seamount. Seafloor sediments mainly consists of brown to dark gray terrigenous silty clays. Rich benthic life causes the intense bioturbation of sediments (Fig. 5.6-40). Centimeter-sized pebbles, which were interpreted as IRD, are abundant. Calcareous foraminifera-bearing silty to sandy oozes, which were still present further to the south (Tenji Seamount), are no longer present.

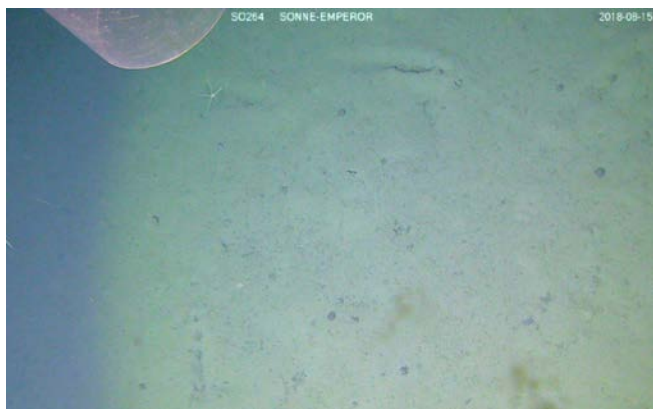


Figure 5.6-40. Seafloor sediment at Station SO264-73-1 at Detroit Seamount, view from ~3039 m water depth, a few meters above seafloor. Active benthic life leaving burrows and circular spurs point to the intense bioturbation of sediments. Ophiroids are present. Black cm-sized pebbles are common. Image taken by TV-MUC.

Downcore sediment records

Due to various reasons, only a few sediment cores from Detroit Seamount were opened. Most of them, however, were logged (GEOTEK core logger) and scanned (Minolta sediment reflectivity). Only two BCs allowed to describe the downcore lithology at Detroit Seamount. We accomplished two depth transects: The first transect at ~50°30'N consists of cores from 3284-3297 m (68-2PC; 76-1BC) to 3473 m (69-2) to 3917-3919 m (70-1PC; 75-1 BC). The second transect is further to the north at ~51°N, consisting of cores from 2396-2397 m (74-1GC; 71-2PC) to 2626 m (72-2GC) to 3047 m (73-2GC) water depth. With these core transects we hence cover a depth range of ~1500 m at relatively close spacing in between core locations (c.f. Appendices 5.6-1 and 5.6-2).

The sediment records from **Detroit Seamount** reveal monotonous diatom-bearing to diatomaceous, mainly siliciclastic silty clay sequences, which are commonly bioturbated (Fig. 5.6-41). The near-surface diatomaceous, light brownish sediment is observed only in the trigger cores und MUCs. With increasing core depth, greenish horizons of diagenetically altered sediment (clay) occur increasingly. The siliciclastic sequence is repeatedly interrupted by diatomaceous oozes, pointing to rapidly enhanced marine productivity most likely in line with climatic improvements. These diatom oozes, which are typical for the 'northern siliciclastic-siliceous facies' are clearly reflected in higher color b^* -values and low magnetic susceptibility values. Ice-rafted detritus is rare although present in most of the sediment profiles pointing to the presence of (seasonal) sea ice and/or icebergs in the Detroit Seamount area. Peaks in biogenic silica production similarly observed in the Bering and Okhotsk seas (Riethdorf et al., 2013a,b; Nürnberg and Tiedemann, 2004) were related to deglacial times of increased insolation, the northward propagation of the marginal ice zone, increasing sea-surface temperatures and a prolonged summer season.

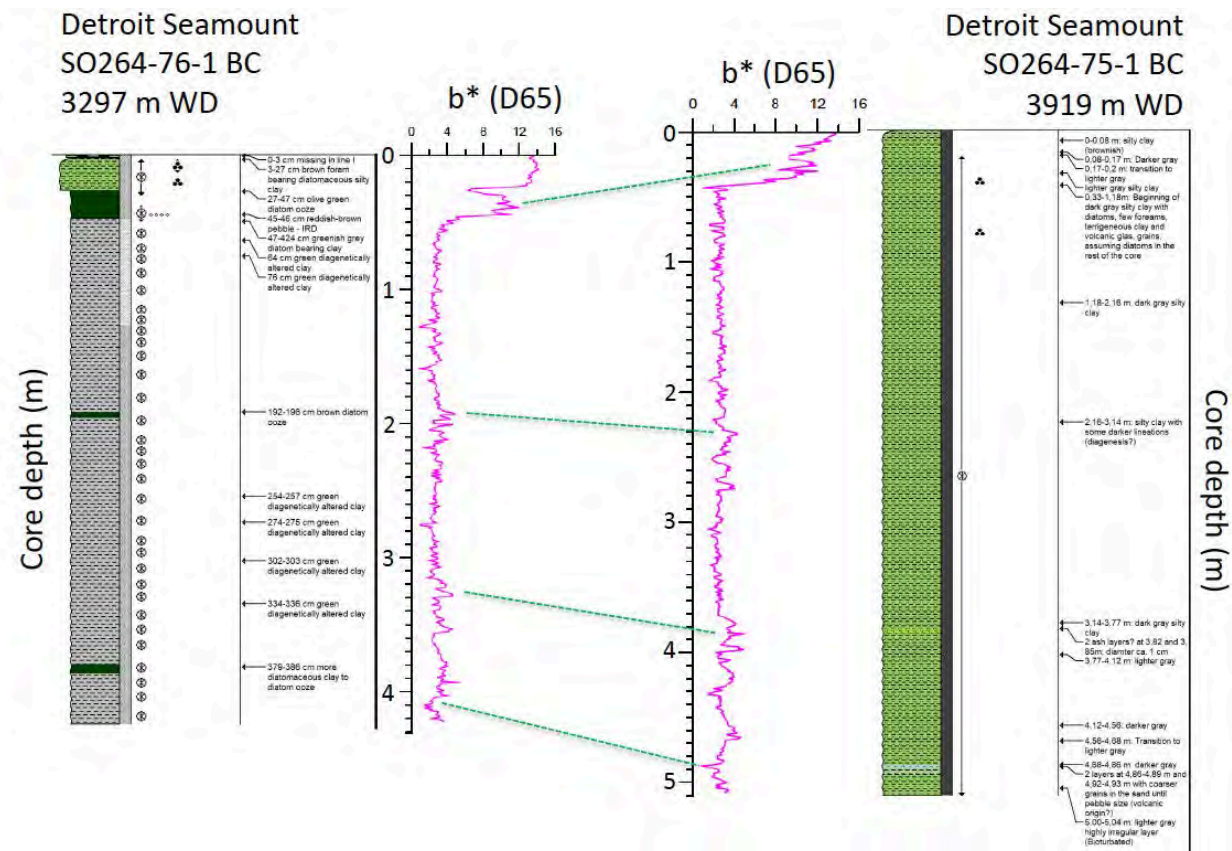


Figure 5.6-41. Tentative correlation (green dotted lines) of BC-cores from Detroit Seamount using Minolta color (b^*) records. Left: Core SO264-76-1 from 3297 m water depth. Right: Core SO264-75-1 from 3919 m water depth. Lithology log, sediment description, and b^* -records are shown.

The magnetic susceptibility records allow to correlate the sediment cores across wide distances. Fig. 5.6-42 shows the tentative correlation of cores from Minnetonka Seamount, the volcanoes from south of Detroit Seamount, and from Detroit Seamount. The correlation of cores, which is a fundamental step to establish core stratigraphies, further proves that the cores are of high quality, without major disturbances. The numerous tephra layers, which are present in these cores, further help to establish detailed core correlations (c.f. Chapter 5.7).

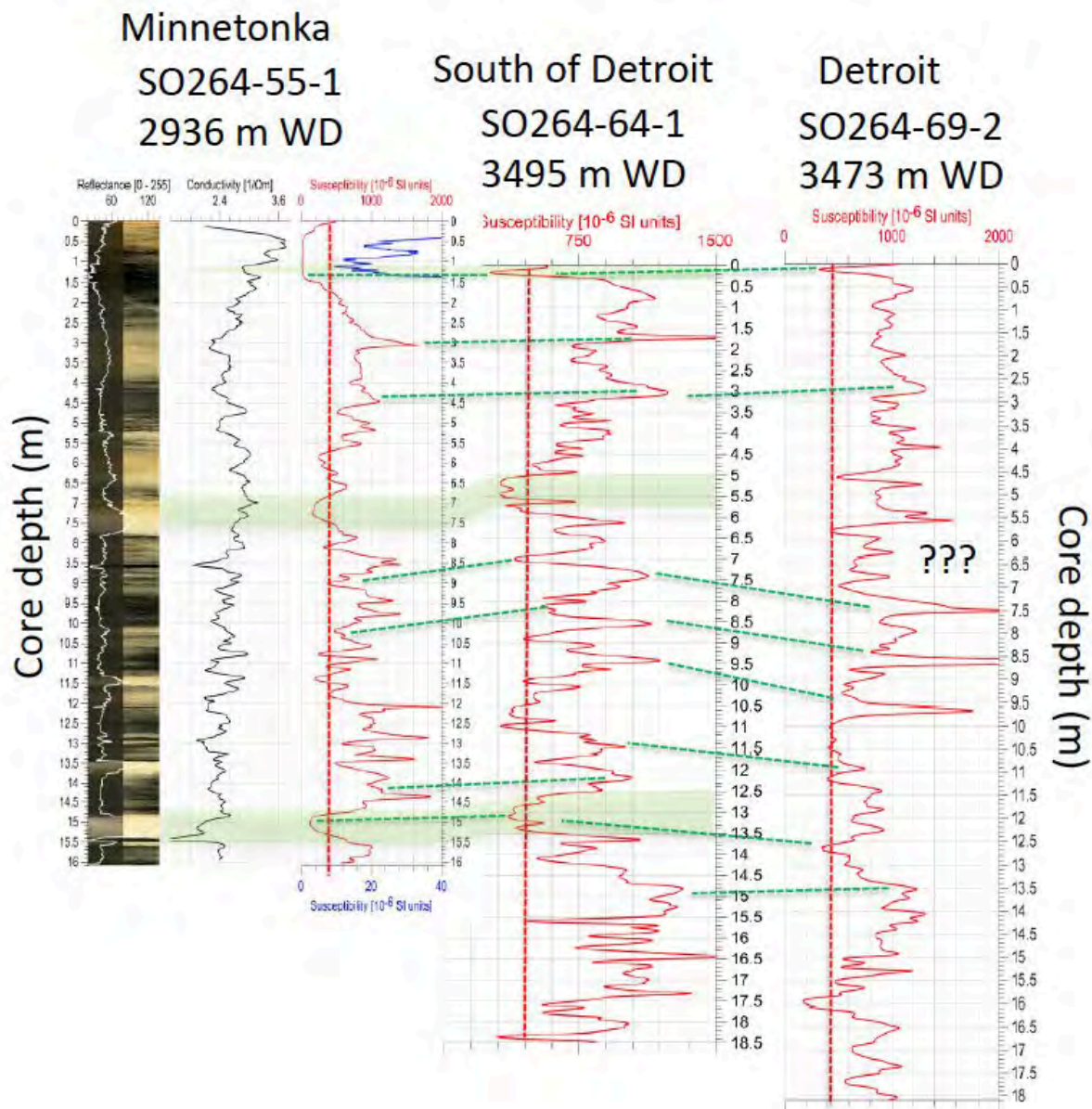


Figure 5.6-42. Tentative core correlation (green dotted lines and green shading) along the Emperor Seamount Chain from $\sim 47^{\circ}\text{N}$ (core SO264-55-1) to $50^{\circ}30'\text{N}$ (SO264-69-2) using magnetic susceptibility records.

5.7 Tephra layers in sediment cores from the Emperor Seamount Chain

(Natalia Bubenshchikova, Dirk Nürnberg)

The Northwest Pacific deep-sea sediments contain numerous tephra layers, which provide the opportunity to reconstruct explosive volcanism in the Kurile-Kamchatka, the Northeastern Japan and Alaska-Aleutian Arcs areas through time (Rea et al., 1993; Prueher and Rea, 2001; Cao et al., 1995; Ponomareva et al., 2013; 2017; 2018). Detailed data on the geochemical composition and ages of tephra layers in the Pleistocene to Holocene sediments of the Okhotsk and Japan Seas have been recently published by Derkachev et al. (2016) and Sagawa et al. (2018). Overall, however, the tephrostratigraphy of the Northwest Pacific deep-sea sediments, including those of the Emperor Seamount Chain, remains unsufficiently explored although tephra markers bear high potential for supra-regional stratigraphical approaches (Ponomareva et al., 2018).

During cruise SO264, visible (>1cm thick) tephra layers and lenses were detected in 25 sediment cores, which were recovered from the Ojin/Jingo, Niningi/Nintoko, Soga, Suiko, Jimmu, and Minnetonka seamounts of the Emperor Seamount Chain (Fig. 5.7-1). The identification of tephra layers was based on three approaches: visual inspection of the sediment cores (description of sedimentary texture/structures, contacts, bioturbation), the microscopic analyses of selected sediment samples >63 µm (binocular), and the analysis of the core logging data.

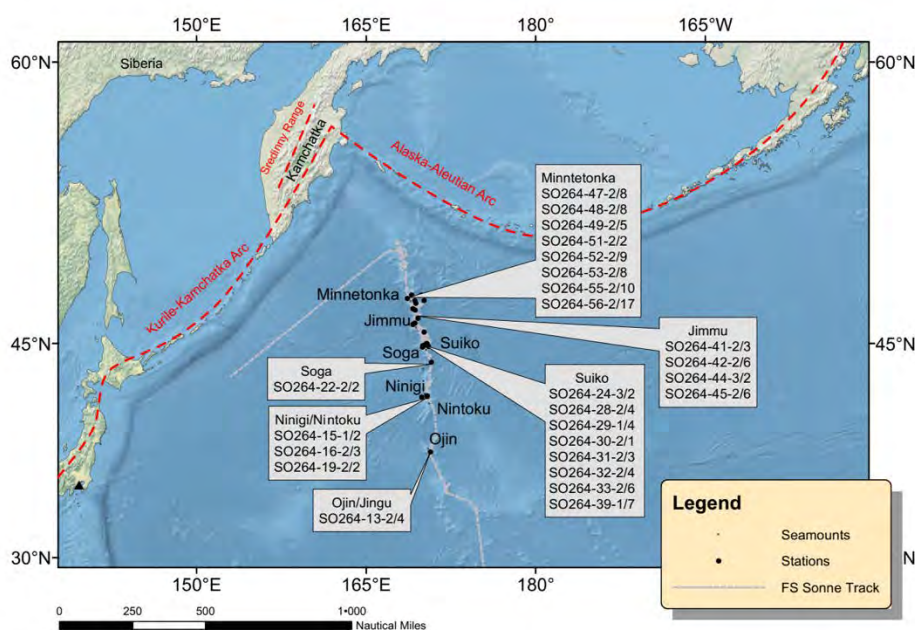


Figure 5.7-1. Bathymetric chart of the North Pacific, showing the locations of the studied SO264 sediment cores, in which tephra layers were preserved. Red dashed line outlines the Kurile-Kamchatka and Alaska-Aleutian volcanic arcs.

Relatively low abundances (from 1 to 4) of tephra layers were found in the southern cores, while a higher number (up to 17) tephra layers was observed in the northern cores, e.g. on Minnetonka Seamount (Fig. 5.7-1, Tables 5.7-1, 5.7-2). The northward increase of tephra layer abundances supports the notion on their probable origin from explosive volcanic eruptions in the Kurile-Kamchatka and Aleutian arcs (Fig. 5.7-1). In total, we have identified 128 visible (>1cm thick) tephra layers and took 262 tephra samples. Tephra layers vary in thickness from 1 to 10 cm (Table 5.7-2) and in color from light to dark gray, beige, and light to dark brown (Figs. 5.7-2, 5.7-3). The tephra layers commonly exhibit sharp to diffuse or strongly tilted basal contacts, and diffuse upper contacts (Figs. 5.7-2, 5.7-3). Some tephra layers are strongly bioturbated.

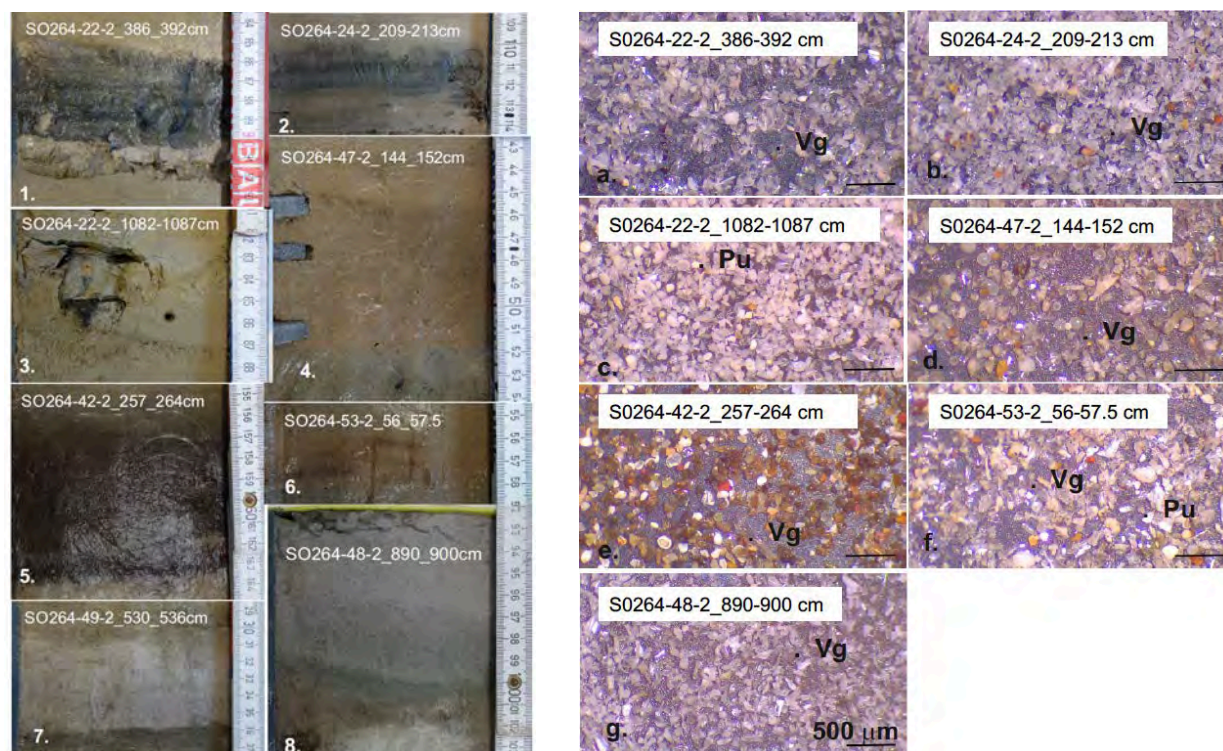


Figure 5.7-2. Photographs of SO264 sediment core sections (left) and binocular images of the grain size fractions >63 μm (right) of visible tephra layers from Soga Seamount (1, 3, a, c), from Suiko Seamount (2, b), from Jimmu Seamount (5, e); and from Minnetonka Seamount (4, 6-8, d, f, g). Note that Tephra V (in Tab. 5.7-1) is supposedly represented in (1), (2), (a) and b; Tephra I (in Tab. 5.7-1) is present in (4), (6), (d) and (f); Tephra III (in Tab. 5.7-1) is present in (7), (8) and (g). Vg – volcanic glasses; Pu – pumices.

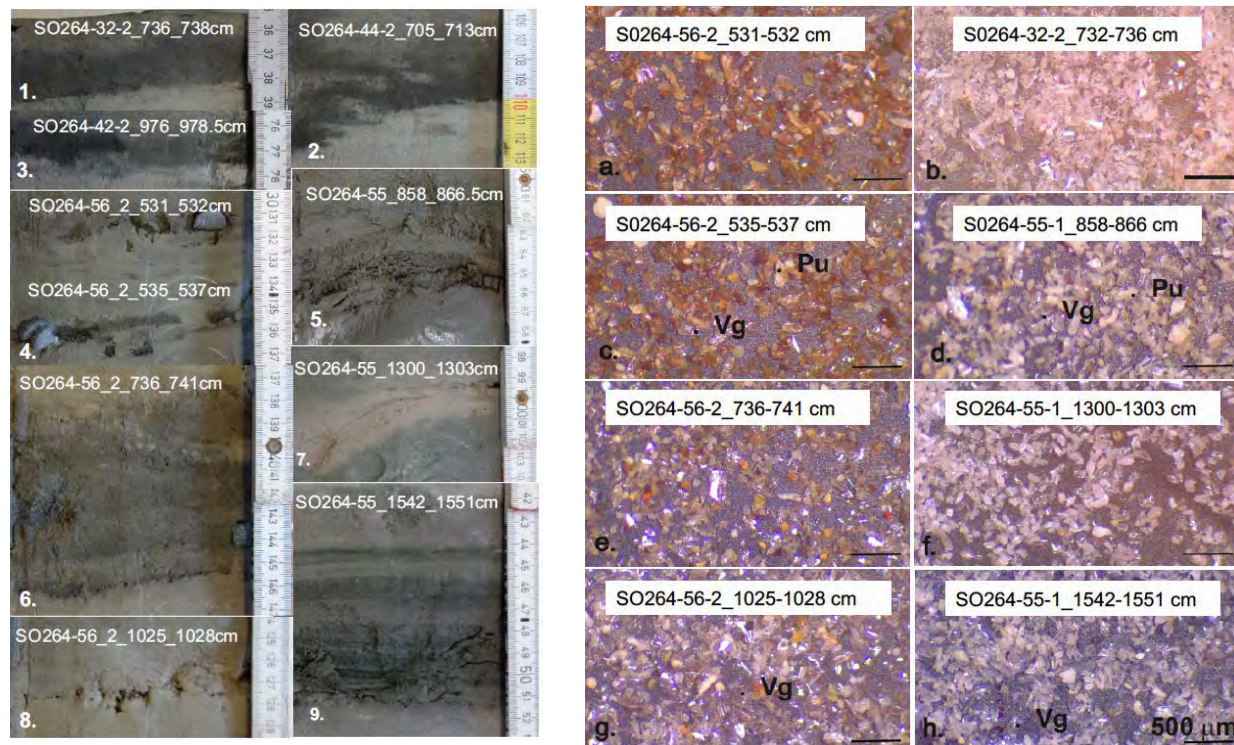


Figure 5.7.3. Photographs of SO264 sediment core sections (left) and binocular images of the sediment grain size fractions >63 μm (right) of visible tephra layers from Suiko Seamount (1, b), from Jimmu Seamount (2, 3), from Minnetonka Seamount (4-9 and c-h). Note, that Tephra IV (in Tab. 5.7-1) is supposedly represented in (1), (2), (3) and (b). Vg – volcanic glasses; Pu – pumices.

Table 5.7-1. Presence of prominent tephra layers in SO264 sediment cores from Soga, Suiko, Jimmu and Minnetonka seamounts, and preliminary core correlation. The different ash layers are color-coded. MS = magnetic susceptibility.

Tephra	Description	Soga	Suiko				Jimmu				Minnetonka						
		SO264-22-2	SO264-24-3	SO264-28-2	SO264-32-2	SO264-31-2	SO264-41-2	SO264-42-2	SO264-44-3	SO264-45-2	SO264-47-2	SO264-48-2	SO264-49-2	SO264-51-2	SO264-52-2	SO264-53-2	SO264-55-1
Tephra I	tephra appears in bright brown color (Plate Xa 4,6,d,f); high red/ blue Ratio, low color b*, reflectance, conductivity and MS									99-103 cm	144-152 cm	180,5-185 cm	56-65,5 cm		56-57,5 cm	55,5-58,5 cm	
Tephra Ia	similar to Tephra I				32-36,5 cm					154-158 cm	246-252 cm		142,5-149,5 cm				
Tephra II	tephra appears in dark brown color (Plate Xa 5,e); high color b* and MS, low reflectance, red/ blue ratio and conductivity			91-93,5 cm	96-99 cm	303,5-306,5 cm	257-264 cm	134-139 cm	229-235 cm	269-273 cm	481,5-488 cm				193-196 cm	142-142,5 cm	
Tephra IIa	similar to Tephra II									324,5-326,5 cm	525-528 cm						
Tephra III	tephra appears in light gray color (Plate Xa 7,8, g); high reflectance, color b* and MS, low red/ blue ratio and conductivity										890-900 cm	530-536 cm				566-571 cm	
Tephra IV	tephra appears in dark gray color (Plate XXa 1-3, b), low reflectance, red/ blue ratio, conductivity and MS, high color b*				736-738 cm		972,5-978 cm	705-713 cm									
Tephra V	tephra appears in dark gray color (Plate Xa 1,2,a,b); low reflectance, red/blue ratio and conductivity, high color b* and MS	386-392 cm	209-213 cm														
Tephra VI	tephra appears in dark gray color (Plate XXa 5,d); low reflectance, color b* and conductivity, high red-blue ratio and MS													554-560,5 cm			858-866,5 cm

The microscopic observation of washed samples taken from the selected tephra layers showed the dominant presence of morphologically different, colorless to light brown volcanic glasses and pumices along with minerals and rock fragments, with very rare diatoms and foraminifers (Figs. 5.7-2, 5.7-3).

Based on the first, still preliminary inspection of tephra layers, we identified a variety of clearly distinguishable tephra layers I to VI (Table 5.7-1). These volcanic ash layers I to VI are defined by their different signatures in the core logging data, including color reflectance, the red/blue ratio, the color b* values, conductivity and magnetic susceptibility (Table 5.7-1). Thereby, Tephra I and Ia as well as Tephra II and IIa appear visually identical and probably originate from the same source volcanoes.

The tephra layers I, Ia, II, IIa, III and IV can be traced among selected sediment cores from the Suiko, Jimmu and Minnetonka seamounts (Fig. 5.7-1). This tephrastratigraphical approach (Fig. 5.7-4) is still preliminary and needs further support from the geochemical analysis of the volcanic glass shards. Subsequent to the cruise, the detected tephra layers will be studied for major and trace element compositions of volcanic glasses with Laser Ablation - Inductively Coupled Plasma - Mass-Spectrometry (LA-ICP-MS) analysis at GEOMAR. The resulting data will be compared with the available North Pacific database to further define source volcanoes and ages of eruptions.

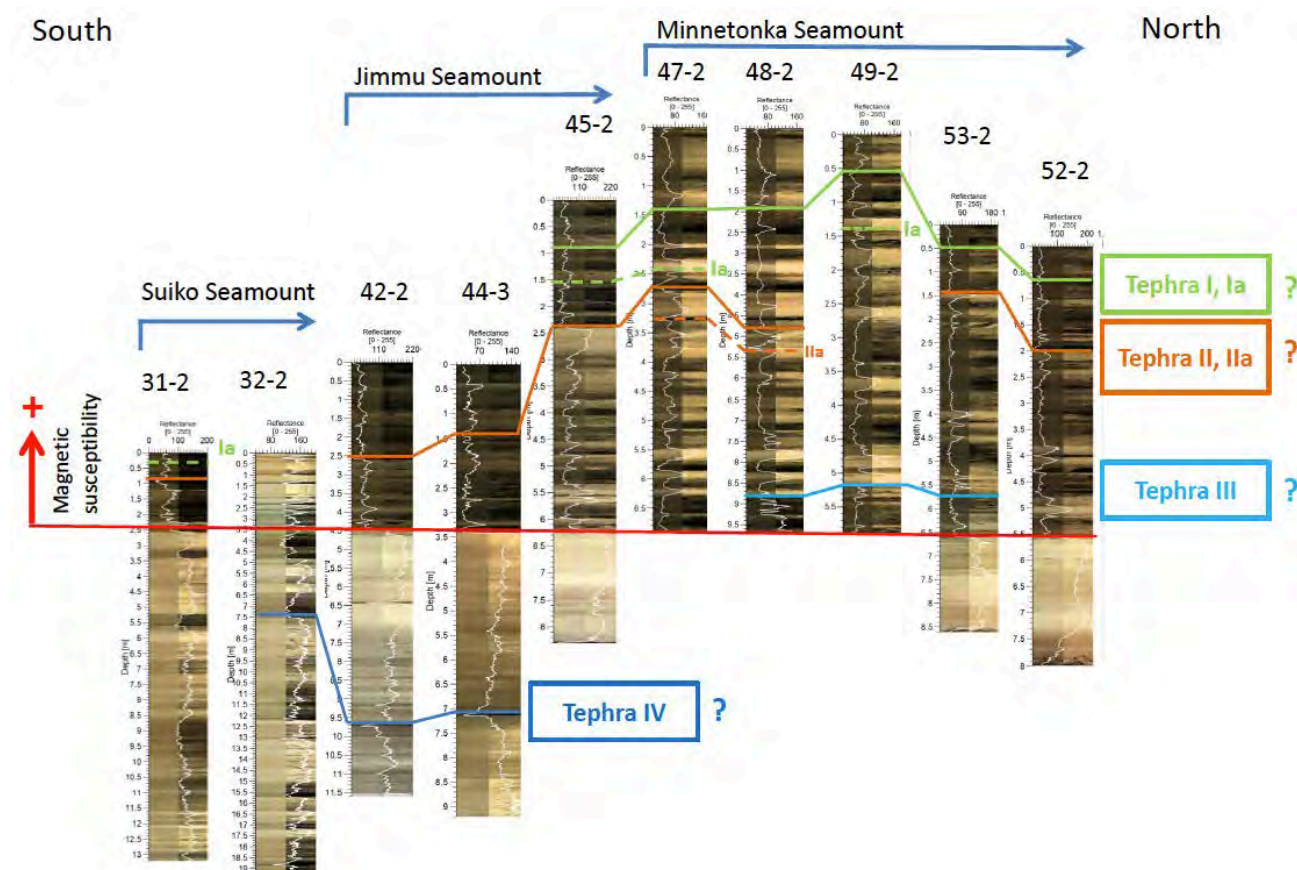


Figure 5.7-4. Preliminary correlation of selected SO264 sediment cores retrieved from Suiko (south), Jimmu and Minnetonka (north) seamounts using the prominent tephra layers I, Ia, II, IIa, III and IV (specified in Table 5.7.1) as time markers. Cores are arranged according to the core depths where the magnetic susceptibility records start to increase.

Table 5.7-2. Volcanic ash (tephra) layers detected in the SO264 sediment cores.

No.	Core No.	Area, Seamount	Tephra Code, No.	Interval, depth in core (cm)	Thickness (cm)	Description
1	SO264-13-2	Ojin/ Jingu	1	514-516	2	Tephra appears in brown color, uneven lower contact
			2	540-548	8	Tephra appears in brown color, uneven lower contact
			3	554-558,5	4.5	Tephra appears in brown color, uneven lower contact
			4	581-586	5	Tephra appears in dark brown color, sharp contact
2	SO264-15-1	Ninigi	1	264-268	4	Tephra lense vertical appears in dark grey greenish color, bioturbated
			2	1327,5-1334,5	7	Tephra appears in dark grey color, tilted lower contact
3	SO264-16-2	Ninigi	1	336-337,5	1.5	Tephra appears in light to dark grey color, uneven lower contact
			2	1007,5-1009,5	2	Tephra appears in light to dark grey color, uneven lower, bioturbated
			3	1420-1426,5	6.5	Tephra appears in dark grey color, tilted lower contact
4	SO264-19-2	Nintoku	1	1220-1224,5	4.5	Tephra appears in brown color, sharp lower contact
			2	1279-1283	4	Tephra appears in dark grey greenish color, sharp lower contact
5	SO264-22-2	Soga	1	386-392	6	Tephra appears in 1 cm thick white layer, 4 cm thick dark grey layer, and 1 cm thick white layer, sharp contact, very dense
			2	1082-1087	5	Tephra appear in pale color, tilted lower contact, very dense
6	SO264-24-3	Suiko	1	209-213	4	Tephra appears in 1 cm thick white layer, 2 cm thick dark grey layer, and 1 cm thick white layer, lower contact uneven, dense
			2	545-550	5	Tephra appears in dark grey layer, bioturbated
7	SO264-28-2	Suiko	1	83-87	4	Tephra appears in dark grey color, sharp lower contact
			2	91-93,5	2.5	Tephra appears in dark brown color, bioturbated
			3	118-126	8	Tephra appears in dark grey color, uneven lower contact
			4	347-350	3	Tephra appears in beige to light brown color, sharp lower contact
8	SO264-29-1	Suiko	1	101-107	6	Tephra appears in dark grey layer, sharp lower contact
			2	146-156	10	Tephra appears in dark grey color, uneven lower contact
			3	295,5-298	2.5	Tephra appears in dark brown color, bioturbated
			4	370-374	4	Tephra appears in beige to light brown color, lower contact tilted

Table 5.7-2. cont. Volcanic ash (tephra) layers detected in the SO264 sediment cores.

9	SO264-30-2	Suiko	1	51-57	6	Tephra appears in dark grey layer, tilted lower contact
10	SO264-31-2	Suiko	1	32-36,5	4.5	Tephra appears in brown layer, bioturbated
			2	63-71	8	Tephra appears in dark grey layer, uneven lower contact
			3	96-99	3	Tephra appears in dark brown color, lower and upper contacts tilted
11	SO264-32-2	Suiko	1	68-69	1	Tephra appears in light grey color, sharp lower and upper contacts
			2	736-738	2	Tephra appears in dark grey color, tilted lower contact dense
			3	1300-1301,5	1.5	Tephra appears in grey color, lower contact sharp and tilted
			4	1875-1877	2	Tephra appears in grey color, bioturbated
12	SO264-33-2	Suiko	1	259,5-261	1.5	Tephra appears in light brown color, sharp lower contacts
			2	297-298	2	Tephra appears in light to dark brown color, bioturbated
			3	338-342	4	Tephra appears in dark brown layer, bioturbated
			4	468,5-470	1.5	Tephra appears in dark brown layer, bioturbated
			5	556,5-558	1.5	Tephra appears in white to brown color, bioturbated
			6	1199-1202	3	Tephra appears in white to grey to greenish color, bioturbated
13	SO264-39-1	Suiko	1	11-15	4	Tephra appears in brownish layer, lower contact tilted
			2	93-95	2	Tephra appears in light brown color, tilted upper and lower contacts
			3	114-118	4	Tephra appears in grey color, bioturbated
			4	153-155	1	Tephra appears in brownish color, bioturbated
			5	155-162	1	Tephra appears in dark grey color, bioturbated
			6	344,5-351	6.5	Tephra appears in white to brown color banding, upper and lower contacts tilted
			7	363-365	3	Tephra layer, appear in white to brown color, sharp contacts
14	SO264-41-2	Jimmu	1	303,5-306,5	3	Tephra appears in brown color, even lower contact, bioturbated
			2	494-501	6	Tephra appears as 2 cm light brown and 4 cm thick brownish layer, sharp lower contact
			3	654-665	11	Tephra appears as 2 cm thick grey and 4 cm thick brownish layer, sharp lower contact
15	SO264-42-2	Jimmu	1	170-175	5	Tephra appears in light brown to dark brown colors, lower contact uneven
			2	208-211	3	Tephra, appears in dark brown color, bioturbated
			3	257-264	7	Tephra layer, appears in bright dark brown color, sharp contacts
			4	309-313,5	4.5	Tephra appears in light to dark brownish color, bioturbated
			5	642,5-649	6.5	Tephra appears as 2 cm thick brownish and 4,5 cm thick beige layers, lower contact sharp, upper contact bioturbated
			6	972,5-978	5.5	Tephra, appears in dark grey color, lower and upper contacts uneven, bioturbated
16	SO264-44-3	Jimmu	1	134-139	5	Tephra appears in dark brown color, bioturbated
			2	705-713	8	Tephra appears in dark grey color, tilted lower contact, dense
			3	99-103	4	Tephra appears in bright brown/ orange color, slightly tilted lower contact, upper bioturbated
17	SO264-45-2	Jimmu	2	154-158	4	Tephra appears in light brownish color, uneven contacts
			3	167-170	3	Tephra appears in dark brown color, bioturbated
			4	209-211	2	Lense of beige tephra
			5	229-235	6	Tephra layer, appears in dark brown color, tilted contacts
			6	472,5-477	4.5	Tephra appears in dark brown dense layer sharp contacts
			7	575-584,5	9.5	Tephra appears in brownish color, coarse, banding, sharp lower contact
18	SO264-47-2	Minnetonka	1	144-152	8	Tephra appears in bright brown/ orange color, tilted lower contact
			2	246-252	6	Tephra appears in bright brown/ orange color, tilted lower contact
			3	269-273	4	Tephra appears in dark brown color, bioturbated
			4	324,5-326,5	2	Tephra appears in dark brown color, bioturbated
			5	401-403	2	Tephra appears in brown reddish color, coarse, tilted contacts
			6	477-481	4	Tephra appears in dark grey color color, tilted contacts
			7	575-584,5	9.5	Tephra appears in brownish color, coarse, banding, sharp lower contact
			8	674-677	3	Tephra appears in dark brown color, bioturbated
19	SO264-48-2	Minnetonka	1	161-162,5	1.5	Tephra appears in white-grey color, tilted lower contact
			2	180,5-185	4.5	Tephra appears in bright brown color, bioturbated, tilted lower contact
			3	481,5-488	6.5	Tephra appears in brown color, even lower contact
			4	525-528	3	Tephra appears in dark brown color, sharp contact
			5	532,5-534,5	2	Tephra appears in dark brown color, coarse, sharp lower contact
			6	890-900	10	Tephra appears in white-grey color, dense, sharp lower contact
			7	901-904	3	Tephra appears in dark brown color, bioturbated
			8	904-911	7	Tephra appears in dark brown color, vertical lense
20	SO264-49-2	Minnetonka	1	56-65,5	9.5	Tephra appears in bright brown/ orange color, even lower contact
			2	93-100	7	Tephra appears in brown color
			3	142,5-149,5	7	Tephra appears in light brown to bright brown to grey, color bending, sharp contact
			4	478-481	3	Tephra appears in dark brown color, tilted contacts, bioturbated
			5	530-536	10	Tephra appears in white grey color, dense, sharp lower contact
21	SO264-51-2	Minnetonka	1	244-247,5	3.5	Tephra appears in light grey to dark grey color, banding, coarse, sharp lower contact
			2	554-560,5	5.5	Tephra appears in dark grey color, dense, sharp contact
22	SO264-52-2	Minnetonka	1	56-57,5	1.5	Tephra appears in bright brown/ orange color, even lower contact
			2	116,5-118,5	2	Tephra appears in dark brown color, bioturbated
			3	147-149	2	Tephra appears in light brown color, bioturbated
			4	155-160	5	Tephra appears in light grey color, tilted upper and lower contacts

Table 5.7-2. cont. Volcanic ash (tephra) layers detected in the SO264 sediment cores.

			5	170-174	4	Tephra appears in light brown color, tilted upper and lower contacts
			6	193-196	3	Tephra appears in dark brown color, bright, lower contact sharp, upper contact bioturbated
			7	266,5-270,5	4	Tephra appears in dark grey color, tilted lower contact, coarse
			8	398-403	5	Tephra appears in brown color, dense, sharp lower contact
			9	468-470	2	Tephra appears in dark brown color, bioturbated
23	SO264-53-2	Minnetonka	1	55,5-58,5	3	Tephra appears in bright brown/ orange color, even lower contact
			2	142-145,5	3.5	Tephra appears in dark brown color, tilted lower contact
			3	155-157	2	Tephra appears in beige color, sharp lower contact
			4	379-381,5	2.5	Tephra appears in brown reddish color, coarse, bioturbated
			5	391-393	2	Tephra appears in peach color, bioturbated
			6	413-416	3	Tephra appears in dark grey color, coarse, even lower contact
			7	566-571	5	Tephra appears in white grey to beige color, tilted lower contact, bioturbated
			8	606-608	2	Tephra appears in brown color, bioturbated
24	SO264-55-1	Minnetonka	1	858-866,5	8.5	Tephra appears in dark grey color, dense, tilted lower contact
			2	950-952	2	Tephra appears in dark grey color, bioturbated
			3	1046-1052	6	Tephra appears in light grey color, tilted lower contact
			4	1193,5-1195	1.5	Tephra appear in grey color, sharp lower contact
			5	1212-1215,5	3.5	Tephra appears in dark brown color, bioturbated
			6	1224-1227,5	3.5	Tephra appears in pale color, coarse, tilted lower contact
			7	1263,5-1265	1.5	Tephra appears in pale color, even lower contact
			8	1298,5-1303,5	5	Tephra appears in pale color, strongly tilted lower contact
			9	1345-1349	4	Tephra appears in dark brown color, bioturbated lower contact
			10	1541,5-1551,5	10	Tephra appears in light to dark grey greenish color, banding, dense, sharp lower contact
25	SO264-56-2	Minnetonka	1	88-91	3	Tephra appears in dark brown color, bioturbated
			2	334-337,5	3.5	Tephra layer appear in dark brown color, bioturbated
			3	372-379	5	Tephra appears in dark brown color, dense, sharp lower contact
			4	417-421	4	Tephra appears in light beige color, sharp lower contact
			5	531-532	1	Tephra appears in dark grey color, coarse, tilted lower contact, bioturbated
			6	535,5-537	1.5	Tephra appears in dark grey color, coarse, tilted lower contact, bioturbated
			7	622-623,5	1.5	Tephra appears in dark brown color, lower contact uneven, bioturbated
			8	657-659,5	2.5	Tephra layers in brown color, lower contact uneven
			9	728-730	2	Tephra appears in dark brown color, bioturbated
			10	737,5-746	8.5	Tephra appears in dark brown color, sharp lower contact
			11	791-795,5	4.5	Tephra appears in pale color, coarse, dense, sharp lower contact
			12	876-878	2	Tephra appears in dark grey color, bioturbated
			13	984,5-986	1.5	Tephra appears in pale color, bioturbated
			14	1025-1028	3	Tephra appears in pale color, dense, uneven lower contact
			15	1036-1039	3	Tephra appears in dark brown color, bioturbated
			16	1043-1045	2	Tephra appears in pale color, coarse, bioturbated
			17	1160,5-1161,5	1	Tephra appears in grey greenish color, tilted lower contact

5.8 Sediment / pore-water geochemistry and microbiology

(Annika Schnakenberg, Jessica Volz)

5.8.1 Objectives

The reduction of ferric iron phases and manganese oxides in marine sediments represents an important metabolic process in marine sediments and releases adsorbed trace metals and nutrients into the pore water of the surrounding sediments. Based on paleomagnetic and geochemical methods, Korff et al. (2016) have identified magnetite-depleted zones in carbonate-free sediments of the northwest Pacific (38°N 164°E) that correspond to glacial periods. The authors suggest that oxygen-depleted bottom water changed the redox conditions in the sediment and therefore trapped organic matter, which caused the dissolution of magnetite by the dissimilatory Fe(III) reduction during glacial periods (Froelich et al., 1979; Berner, 1981). The main objective of the Geochemistry Group during RV SONNE cruise SO264 was to acquire high-resolution pore-water profiles and retrieve sediment samples to investigate the impact of lithology, mode of sedimentation and accumulation rate on the composition and activity of the sub-seafloor biosphere and biogeochemical processes. The main specific goals were 1) to investigate iron- and manganese-reducing processes in the suboxic zone (absence of oxygen and sulphide) of the sediment by the application of inorganic techniques as well as a molecular biological approach, 2) to determine the spatial variability of iron- and manganese reducing processes along the Emperor Seamount Chain from 34°N to 51°N throughout the surface water productivity gradient and 3) to study the iron- and manganese-reducing processes in different water masses from lower intermediate water depth (3000-4000 m) to the deep sea (>5000 m). Furthermore, biologically driven active manganese oxide reduction in the sediment ought to be investigated by incubation studies.

5.8.2 Shipboard methods

Immediately after core recovery, the multi-corer (MUC) sediment cores for geochemical and microbiological studies were transferred into the cold room at a temperature of ~4°C. One MUC core was used for the retrieval of the supernatant bottom water as well as sediment and pore-water sampling. In order to allow for high resolution sampling of the MUC without mixing of the pore water of different depths, all MUC cores were sliced, ~50 mL of fresh sediment were transferred into Falcon tubes and the pore water was extracted by means of rhizons with an average pore size of 0.1 µm (Seeberg-Elverfeldt et al., 2005). If necessary, the headspaces were flushed with Argon gas in order to avoid oxidation. A parallel MUC core was separately used for the later performance of microbiological community analyses. The sampling interval for both MUC cores was every second centimeter in the first 10 cm of the core and every 5 cm below.

The piston cores (PC) and gravity cores (GC) were cut into 1 m segments on deck. After the PC or GC were cut open, the working half was immediately transferred into the cold room at a temperature of ~4°C for the extraction of the pore water by means of rhizons and sediment sampling. After the box cores (BC) were subsampled in the hangar, sub-core Unit I was directly transferred into the cold room at a temperature of ~4°C. The temperature of the sediment in the sub-cores was determined once they have been transferred into the cold room, which did not exceed 9°C. In order to avoid any contamination, the sediment surface in the sub-cores was scraped off with a sterile ceramic knife. Pore-water and sediment sampling for the PC, GC and BC were performed at intervals of 20 cm. In order to avoid any dilution or oxidation during the pore-water sampling of MUC, PC, GC and BC by rhizons, the first mL of the freshly extracted pore water was discarded.

About 10 cc of sediment from MUC, PC, GC and BC were collected for nucleic acid extraction under sterile conditions for subsequent community analyses with Next

Generation Sequencing (NGS) at the same intervals as the samples for pore water and sediment geochemistry. Another 10 cc sediment samples were taken for total acid digestions as well as the extraction of different iron and manganese solid-phase species. All sediment samples were stored under anoxic conditions at -20°C.

Shipboard analyses include the determination of the dissolved iron, dissolved manganese and alkalinity. Pore-water samples were stored for the later determination of the dissolved inorganic carbon (DIC), sulfate, chloride, nitrate, nitrite, ammonium, silica and phosphate concentration as well as the concentration of cations. Sediment samples were stored for the later determination of the bulk element composition, iron speciation as well as trace metal contents.

Dissolved iron (Fe^{2+}) was detected photometrically (DR Lange HACH 2800 photometer) at a wavelength of 565 nm. 1 mL of the extracted pore water was added to 50 μL Ferrospectral solution to complex dissolved Fe for colorimetric measurement. In the case of high concentrations of Fe^{2+} ($>1 \text{ mg L}^{-1}$) the samples were fixed in ascorbic acid and subsequently diluted with oxygen-free artificial seawater.

Dissolved manganese (Mn^{2+}) was measured in a photometric assay based on the complexation of the ions by formaldoxime, which subsequently changes its colour from colourless to pink and can be quantified at a wavelength of 450 nm. 1 ml of sample or diluted (with Milli Q water) sample were placed onto 50 μL of formaldoxime reagent (1 g formaldoxime and 0.5 mL 37% (w/v) formaldehyde in 25 mL Milli Q water) and 90 μL 30% ammonia. The solution was then mixed thoroughly and let to react at room temperature for 2 min. Subsequently, 50 μL 0.1 M EDTA (pH 8) and 100 μL hydroxylamine hydrochloride were added and mixed thoroughly followed by a 10-min centrifugation step at 14000 rpm at room temperature to allow for precipitation of oxidized iron in the pore water. Then, the extinction of the samples was measured with a DR Lange HACH 2800 photometer at a wavelength of 450 nm. The standard was prepared with 179.9 mg/L MnCl_2 and 5 mL concentrated sulfuric acid in H_2O bidest resulting in a final concentration of 50 mg/L Mn^{2+} .

Alkalinity was determined on a 1 mL aliquot of sample by titration with 10 mM HCl. The pH measurements were performed using a Mettler Toledo micro-electrode. The samples were titrated with a digital burette to a pH of approximately 3.8 and both titration volume and final pH were recorded. The alkalinity was calculated using a modified equation from Grasshoff et al. (1999).

Dissolved inorganic carbon (DIC) samples of about 2 mL were transferred into an amber vial filled with 10 μL of HgCl_2 sealed with a PTFE septum-bearing lid and stored at 4°C. Untreated pore-water samples for sulfate (SO_4^{2-}) and chloride (Cl^-) were collected for shore-based analyses and stored at 4°C.

Pore-water cations (Al, Ba, Ca, Mg, Mn, Fe, Si, P, and S) will be analyzed in our home-laboratory at the AWI with Inductively Coupled Plasma Optical Emission Spectrometry (ICP-OES). Sub-samples of ~1 mL of pore water were acidified with 25 μL double sub-boiling distilled hydrochloric acid (HCl) and stored at 4°C.

Bulk sediment composition and iron species samples were collected from MUC, PC and GC cores for shore-based analysis. Samples were collected with cut-off 10 mL syringes or 50 mL centrifuge tubes, respectively and stored frozen at -20°C.

Samples for nucleic acid extraction were collected at 4°C with sterile syringes and transferred into sterile 10 mL cryostable Falcon tubes at -20°C immediately after recovery in order to preserve the in situ microbial community distribution.

For Microbiology specific sampling sediment from 300-325 cm core depth of core GC SO264-60-13 was mixed thoroughly, stored away in an anoxic 2.6-liter sterile glass jars under N_2/CO_2 (80:20, 99.999% purity, Linde, Germany) headspace at 4°C and transported back to Bremen for laboratory based incubation experiments. The remains of

the core were cut in 1 m sections and kept at 4 °C as whole round cores for microbiology purposes. The pore water was then extracted by inserting rhizon samplers in drilled holes in the whole round cores at ca. 50 cm resolution. 2 ml were taken for iron and manganese analysis on board. Rhizon sampling holes were closed with thick rubber tape.

Table 5.8-1 Incubation set-up for sulfur-dependent manganese oxide reduction.

Incubation nr.			
	NaN ₃ (20 mM)	MnO ₂ (30 mM)	S ₈ (30 mM)
1			
2	+	+	+
3		+	
4			+
5		+	+

In order to test for biologically mediated manganese reduction, a slurry incubation setup was performed by mixing 10 ml of sediment with artificial seawater (ASW) in a ratio of 1:4, sealing the mixture in a 60 ml serum bottle with a butyl rubber stopper and subsequently exchanging the headspace to N₂/CO₂ (80:20). The whole set-up was designed to investigate sulphur-dependent manganese oxide reduction resulting in five incubation condition each performed in triplicates (Table 5.8-1). The slurries were incubated at 10°C over the course of five days.

Table 5.8-2 Sites investigated geochemically during cruise SO264 showing parameters analyzed on board and aliquots of samples stored and conserved. If not indicated otherwise, sediment sampling includes sampling for (1) bulk sediment composition and iron species and (2) nucleic acid extraction.

Station	Device	Rhizon sampling	Fe ²⁺	Mn ²⁺	Alkalinity	OES	nutrients	DIC	sediment sampling
SO264-09-1	TV-MUC	X	X	X	X	X			X
SO264-09-2	PC	X	X	X	X	X			X
SO264-16-1	TV-MUC	X	X	X	X	X	X	X	X
SO264-16-2	PC	X	X	X	X	X	X	X	X
SO264-19-1	MUC	X	X	X	X	X	X	X	X
SO264-19-2	GC	X	X	X	X	X	X	X	X
SO264-22-2	GC	X	X	X		X	X		only microbio
SO264-46-4	MUC	X	X		X	X	X		X
SO264-46-5	GC	X	X	X	X	X	X		X
SO264-56-1	MUC	X	X		X	X	X		X
SO264-56-2	GC	X	X	X	X	X	X		X
SO264-60-12	GC	X	X	X	X	X	X		X
SO264-60-13	GC	X	X	X	X	X	X		Whole rounds for microbio
SO264-60-14	MUC	X	X		X	X	X		X
SO264-75-1	BC	X	X	X	X	X	X		X
SO264-76-1	BC	X	X	X	X	X	X		X

Subsamples of 2 mL of the slurry incubation were taken each day, then centrifuged at 12000 rpm for 20 min at room temperature. The supernatant was partly used to immediately measure the dissolved manganese concentration with the photometric approach described above. 500 µl of supernatant were stored in 4.5 ml 0.16 M nitric acid for onshore ICP-OES analysis and further 200 µl of supernatant were mixed with 200 µl of zinc acetate solution (5%, w/v) for onshore ion chromatography analysis. The remaining sediment pellet was stored at -80 °C and will be used for nucleic acid extraction and subsequent next generation sequencing (NGS) onshore.

5.8.3 Shipboard results

Pore-water geochemistry

The susceptibility data collected on board indicate that the availability of magnetite varies significantly at the different study sites of the cruise (Appendix 5.5). This is a result of different lithologies with generally higher carbonate contents above the carbonate compensation depth (CCD) of ~4200 m water depth and the dominance of siliciclastic-carbonaceous sediments south of 48°N. Towards the north, the sediments are dominated by siliciclastic-siliceous sediments with generally higher magnetic susceptibility values (Appendix 5.5).

Sediment core SO264-16-2 PC was taken at intermediate water depth of 3572 m southeast of Ninigi Seamount. As the site is located in a trough enclosed by 3 seamounts, it may act as a depositional trap. Pore-water Fe^{2+} and Mn^{2+} correlate well with the susceptibility data with concentrations of up to 15 μM and 28 μM , respectively (Fig. 5.8-1). Both metals are mainly released at 3-4 m sediment depth, however, due to the close correlation with the magnetic susceptibility the dissimilatory iron and manganese oxide reduction may be dominant throughout the sediment core.

Sediment core SO264-19-2 GC was retrieved southwest of Ninigi Seamount (and northwest of Nintoku Seamount) at a water depth of 5311 m. Except for several high magnetic susceptibility peaks in the upper 4 m of sediment, overall magnetic susceptibility levels are similar to core SO264-16-2 PC (Fig. 5.8-2). Small amounts of pore-water Fe^{2+} (<4 μM) were detected in the lowermost part of the core, where magnetic susceptibility levels are very low while significant pore-water Mn^{2+} concentrations of up to 90 μM were detected throughout the upper 10 m of sediment. As the release of Fe^{2+} coincides with a color change in the sediment from brown above the zone of Fe^{2+} release to green below, we suggest that the release of Fe^{2+} may be associated with the reduction of ferric iron in smectite clays after pore-water nitrate has been consumed (Lyle, 1983).

Sediment core SO264-46-5 GC was taken at intermediate water depth of 3992 m north of Jimmu Seamount and south of Minnetonka Seamount. Similar to site SO264-16-2 PC, site SO264-46-5 GC is located in a trough and may therefore receive high amounts of sediments. However, in contrast to core SO264-16-2 PC, susceptibility levels are up to four times higher in core SO264-46-5 GC (Fig. 5.8-3). Furthermore, pore-water Fe^{2+} concentrations in core SO264-46-5 GC indicate that up to 20 μM Fe^{2+} is released in several layers throughout the sediment core, which are at 50 cm, 2.3 m, 5 m and below 7 m depth.

Sediment core SO264-60-12 GC was retrieved northeast of Tenji Seamount at a water depth of 5275 m. In comparison with the other investigated sites, core SO264-60-12 GC shows much higher alkalinity levels, which indicates that carbonate may be absent in this core. The parallel sediment core SO264-60-13 GC has been taken for microbiological studies. In order to correlate both GC cores, SO264-60-13 GC has been sampled by means of rhizons and pore-water Fe^{2+} and Mn^{2+} have been analyzed. As the pore-water Fe^{2+} profiles from both GC cores are in good agreement, the cores can be well correlated (Fig. 5.8-4). Compared to all investigated sites, both cores (SO264-60-12 GC, SO264-60-13 GC) show the highest pore-water Fe^{2+} and Mn^{2+} concentrations of up to 30 μM and 180 μM , respectively. The susceptibility levels in core SO264-60-12 GC are almost as high as in core SO264-46-5 GC. Pore-water Fe^{2+} is mainly released at 2.5 m depth, while pore-water Mn^{2+} shows high fluctuations throughout the sediment core. The pore-water Fe^{2+} and Mn^{2+} concentrations will be verified later in the home lab using ICP-OES.

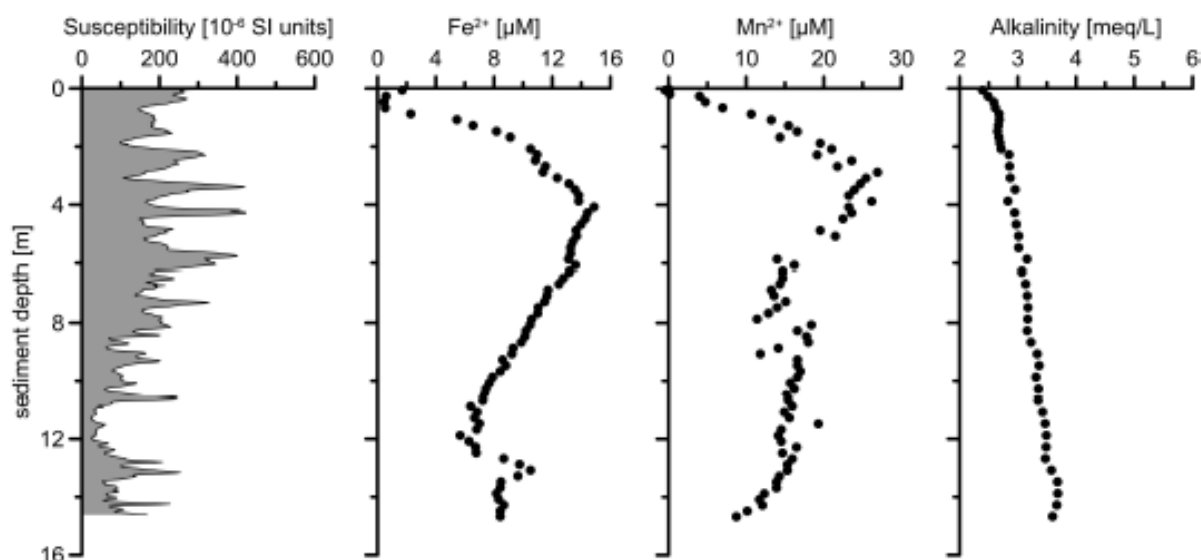


Figure 5.8-1. Preliminary pore-water results for sediment core SO264-16-2 PC taken in the working area 'east of Ninigi Seamount' (41°34,913'N 170°25,787'E) at 3572 m water depth. Magnetic susceptibility data (for more information see Chapter 5.6) indicate the availability of magnetite.

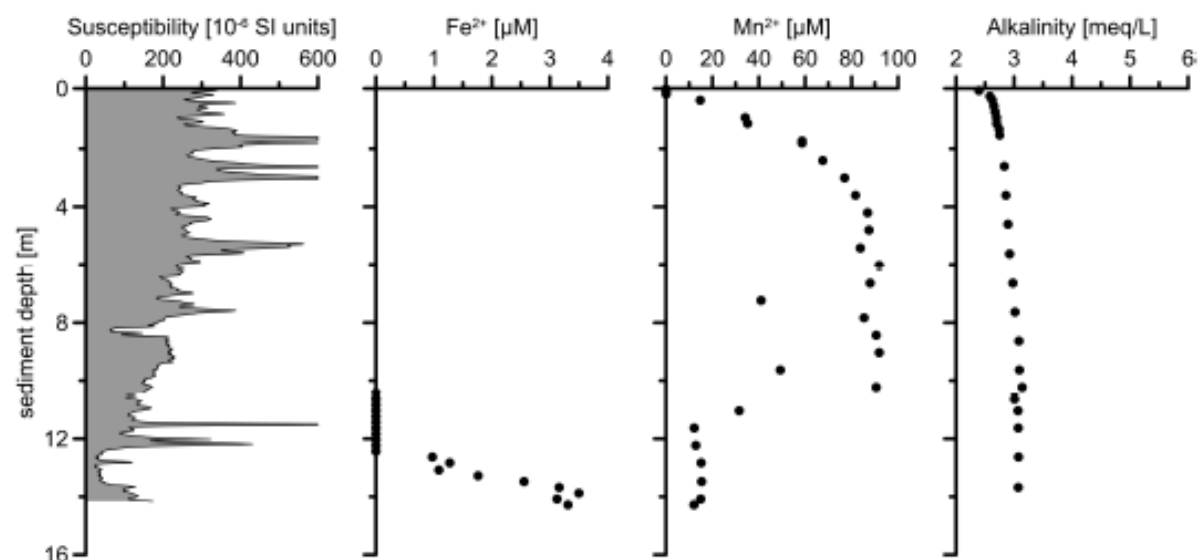


Figure 5.8-2. Preliminary pore-water results for sediment core SO264-19-2 GC taken in the working area 'west of Nintoku Seamount' (41°32,783'N 169°55,733'E) at 5311 m water depth. Magnetic susceptibility data (for more information see Chapter 5.6) exhibit the depth distribution/preservation availability of magnetite. Magnetic susceptibility peaks exceeding 600 10^{-6} SI units in the upper 4 m of sediment were excluded from the graph.

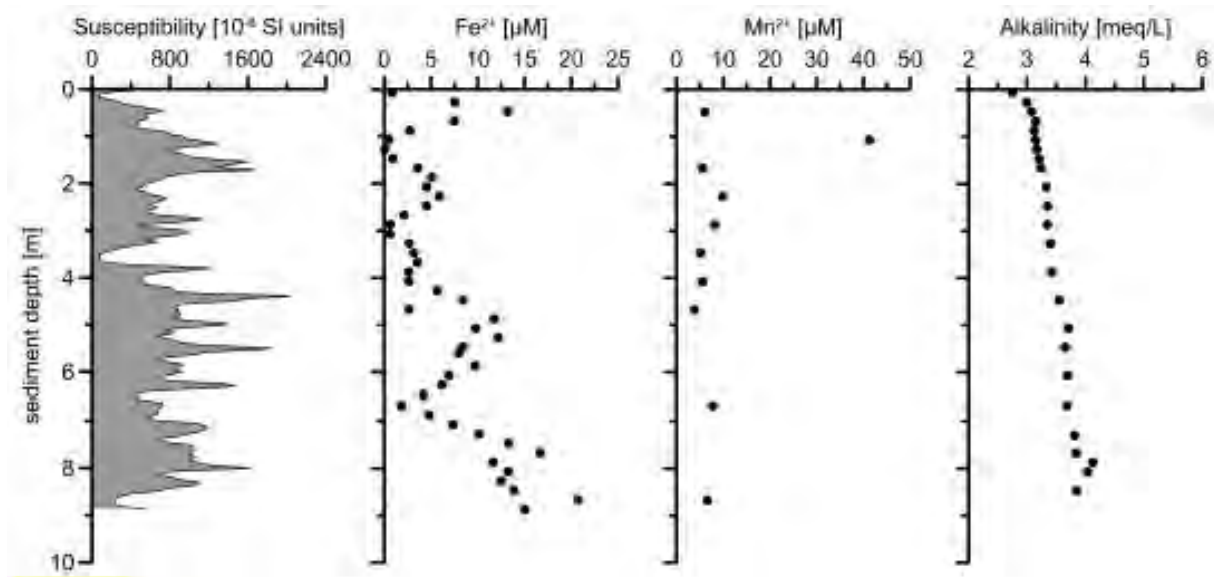


Figure 5.8-3. Preliminary pore-water results for sediment core SO264-46-5 GC taken in the working area 'Minnetonka Seamount' (46°48,940'N 169°24,653'E) at 3992 m water depth. Magnetic susceptibility data (for more information see Chapter 5.6) indicate the availability/preservation of magnetite.

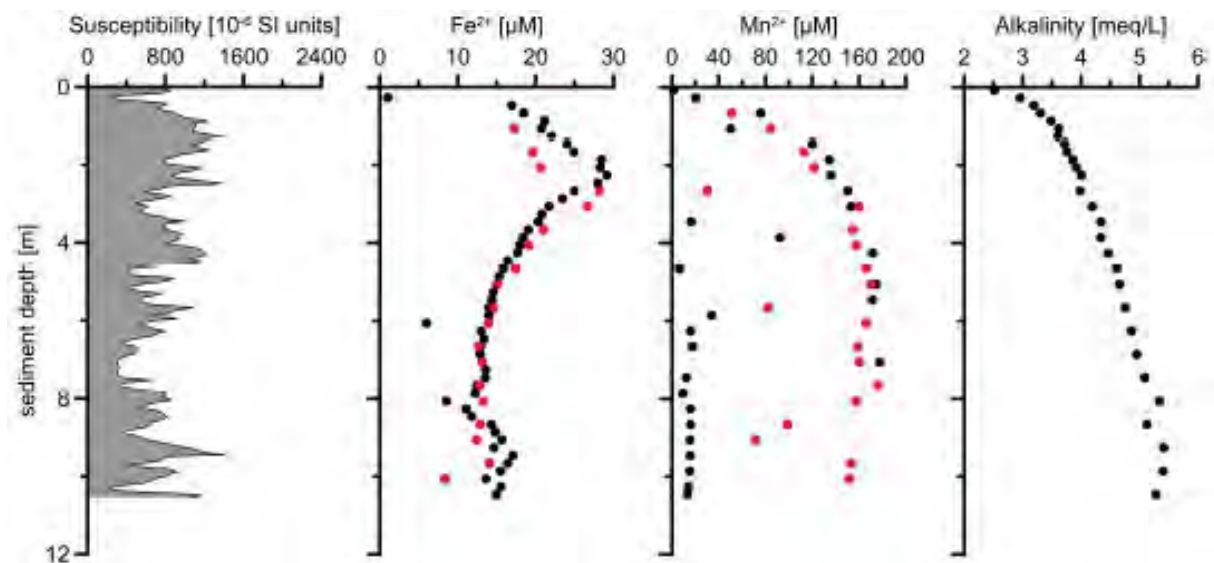


Figure 5.8-4. Preliminary pore-water results for sediment core SO264-60-12 GC (black dots) and SO264-60-13 GC (red dots) taken in the working area 'Tenji Seamount' (49°18,447'N 168°33,427'E) at 5275 m water depth. Magnetic susceptibility data (for more information see Chapter 5.6) indicate the availability/preservation of magnetite.

Manganese reduction incubation experiment

Marine sediments harbor various microorganisms with highly diverse metabolisms. In the surface sediment, where oxygen still penetrates, aerobic respiration occurs. Once oxygen is depleted, alternative substances such as nitrate, manganese oxides, iron oxides, sulfate and methane serve as electron acceptors in microbial respiration in the order free energy released per reaction (Froelich et al., 1979). Manganese oxides in marine sediments serve as potent electron acceptors for microbial respiration and are involved in versatile metabolisms such as organic matter degradation and reduced sulfur compound oxidation (Burdige, 1993; Aller & Rude, 1988). The respiration of metal oxides

in general results in metal dissolution and therefore geochemically detectable dissolved metal ion concentrations in the pore water. Pore water analysis of all GC, PC and BC (Table 5.8-2) sampled during this cruise revealed elevated dissolved Mn concentrations. Subsequently, GC SO264-60-13 was sampled specifically for microbiological study purposes. Sediment from 300–325 cm core depth was used to perform a slurry incubation experiment in which the sediment was mixed with ASW in a 1:4 ratio in order to be incubated in serum bottles under an anoxic atmosphere (N_2/CO_2 , 80:20) at 10°C over five days. The incubations were amended with MnO_2 , S_8 and NaN_3 according to Table 5.8-2. NaN_3 acts as a biohazard and was added to one condition to check for potential chemical MnO_2 reduction. Octahedral sulfur (S_8) on the other hand can potentially serve as an electron donor for Mn-reducers resulting in an increase of the sulfate concentration in the supernatant.

Subsamples of the incubation were retrieved every day and centrifuged at 12000 rpm and room temperature for 20 min. The dissolved Mn concentration was immediately measured photometrically with the Formaldoxime method (Fig. 5.8-5). Moreover, the remaining supernatant was preserved for onshore ICP-OES and ion chromatography analysis. ICP-OES will provide the concentrations of dissolved total sulfur whereas ion chromatography allows the monitoring of the sulfate concentration in the supernatant. The sediment pellet was stored away at -80 °C for subsequent nucleic acid extraction and Illumina HiSeq next generation sequencing onshore in order to monitor the microbial community composition in the incubations and thus detect the active Mn-reducers.

The monitoring of the dissolved Mn concentration revealed an increase from 0.2 μM on day 0 to 7 μM on day 5 in both MnO_2 -amended and MnO_2 and S_8 -amended incubations in contrast to the NaN_3 , MnO_2 and S_8 -amended incubation, which did not reveal a significant increase in dissolved Mn concentration leading to the conclusion that Mn reduction in this type of sediment is indeed biologically mediated (Fig. 5.8-5). Since both incubations show similar concentrations of dissolved Mn, it does not appear that S_8 serves as the main electron donor. Alternatively, the sediment itself might harbor organic carbon substrates which are known electron donors for Mn oxide reduction (Lovely, 1991). Although the S_8 -amended incubations showed slightly more prominent mean increase of dissolved Mn of 1 μM on day 0 to 3 μM on day 5 compared to the unamended incubation (1 μM on day 0 to 2.5 μM on day 5), the error bars of both conditions overlap (Fig. 5.8-5), which might be related to the natural Mn oxide deposits within the sediment.

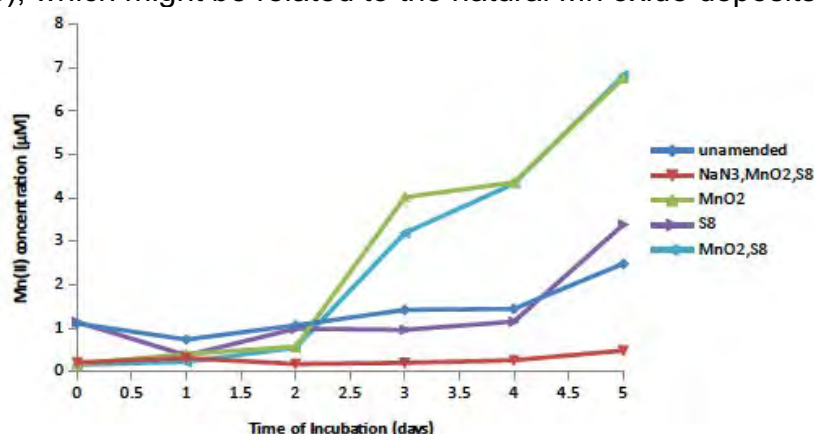


Figure 5.8-5. Monitoring of dissolved Mn concentration in manganese reduction incubation experiment (core SO264-60-13; 300-325 cm core depth).

6. Acknowledgements

RV SONNE cruise SO264 took place in the framework of the BMBF joint project „The Plio/Pleistocene to Holocene development of the pelagic North Pacific from surface to depth – assessing its role for the global carbon budget and Earth’s climate” (BMBF Project No. 03G0264A). The principal investigators Dirk Nürnberg (GEOMAR) and Ralf Tiedemann (AWI) acknowledge generous funding from the “Bundesministerium für Bildung und Forschung”. Additional financial support for the accomplishment of the cruise came from their home institutions, which is greatly appreciated. The chief scientist of cruise SO264, Dirk Nürnberg, thanks the master and crew of RV SONNE and all cruise participants for all their efforts during the expedition. The Projektträger Jülich, represented by Dr. Doreen Rößler, and the Leitstelle Hamburg, represented by Mr. Nils Jakobi, are thanked for kind support.

Danksagung

Die FS SONNE Ausfahrt SO264 fand im Rahmen des BMBF-Verbundprojekts „Die Plio/Pleistozäne bis Holozäne Entwicklung des pelagischen Nordpazifiks von der Oberfläche bis zum Meeresboden – Abschätzung seiner Rolle für die globale Kohlenstoffbilanz und das Erdklima“ (BMBF-Projekt-Nr. 03G0264A) statt. Die Antragsteller und Projektleiter Dirk Nürnberg (GEOMAR) und Ralf Tiedemann (AWI) danken für die großzügige Förderung durch das Bundesministerium für Bildung und Forschung (BMBF). Zusätzliche finanzielle Unterstützung für die Durchführung der SO264-Reise kam von ihren Heimatinstitutionen GEOMAR und AWI, was sehr geschätzt wird. Der Fahrtleiter der Reise SO264, Dirk Nürnberg, dankt dem Kapitän und der Crew von FS SONNE sowie allen Fahrtteilnehmern/innen für ihren Einsatz während der Expedition. Dem Projektträger Jülich, vertreten durch Frau Dr. Doreen Rößler, und der Leitstelle Hamburg, vertreten durch Herrn Nils Jakobi, werden für die freundliche Unterstützung gedankt.

7. References

- Aller, R.C., Rude, P.D. (1988) Complete oxidation of solid phase sulfides by manganese and bacteria in anoxic marine sediments. *Geochimica et Cosmochimica Acta*, 52, 751-765.
- Bednarsek, N., Mozina, J., Vogt, M., O'Brien, C., Tarling, G.A. (2012) The global distribution of pteropods and their contribution to carbonate and carbon biomass in the modern ocean. *Earth Syst. Sci. Data*, 4, 167–186, doi:10.5194/essd-4-167-2012.
- Berner, R.A., Honjo, S. (1981) Pelagic sedimentation of aragonite: its geochemical significance. *Science*, 211, 940–942.
- Berner, R.A. (1981) A new geochemical classification of sedimentary environments. *Journal of Sedimentary Petrology*, 51, 359-365.
- Burdige, D. J. (1993) The biogeochemistry of manganese and iron reduction in marine sediments. *Earth Science Reviews*, 35, 249-284.
- Cao, L.-Q., Arculus, R.J., McKelvey, B.C. (1995) Geochemistry and petrology of volcanic ashes recovered from Sites 881 through 884: a temporal record of Kamchatka and Kurile volcanism. In Rea, D.K., Basov, I.A., Scholl, D.W., and Allan, J.F. (Eds.), *Proc. ODP, Sci. Results*, 145: College Station, TX (Ocean Drilling Program), 345–381. doi:10.2973/odp.proc.sr.145.126.
- Charney, J.G., Flierl, G.R. (1981) Oceanic analogues of atmospheric motions. In *Evolution of Physical Oceanography*, edited by B. A. Warren and C. Wunsch, pp. 504-548, MIT Press, Cambridge, Mass.
- Derkachev, A.N., Nikolaeva, N.A., Gorbarenko, S.A., Portnyagin, M.V., Ponomareva, V.V., Nürnberg, D., et al. (2016) Tephra layers of in the Quaternary deposits of the Sea of Okhotsk: Distribution, composition, age and volcanic sources. *Quaternary International*, 425, 248-272.
- Froelich, P.N., Klinkhammer, G.P., Bender, M.L., Luedke, L.A., Heath, G.R., Cullen, C., Dauphin, P., Hammond, D., Hartmann, B., Maynard, V. (1979) Early oxidation of organic matter in pelagic sediments of the Eastern Equatorial Pacific, suboxic diagenesis. *Geochimica et Cosmochimica Acta*, 43, 1075-1090.
- Garcia, H.E., Locarnini, R.A., Boyer, T.P., Antonov, J.I., Zweng, M.M., Baranova, O.K., Johnson, D.R. (2010) *World Ocean Atlas 2009, Volume 4: Nutrients (phosphate, nitrate, silicate)*. S. Levitus, Ed. NOAA Atlas NESDIS 71, U.S. Government Printing Office, Washington, D.C., 398 pp.
- GEBCO (2008) General Bathymetric Chart of the Oceans (GEBCO) Hom. <http://www.bodc.ac.uk/data/online/delivery/gebco/>.
- Gebhardt H., Sarnthein M., Grootes P.M., Kiefer Th., Kuehn H., Schmieder F., Röhl, U. (2008) Paleonutrient and productivity records from the subarctic North Pacific for Pleistocene glacial terminations I to V. *Paleoceanography*, 23, PA4212. doi:10.1029/2007PA001513.
- Grasshoff, K., Kremling, K., Ehrhardt, M. (eds) (1999) *Methods of seawater analysis*, 3rd edition. Wiley-VCH, Weinheim, New York.
- Honjo, S. (1990) Particle fluxes and modern sedimentation in the polar oceans. In: *Polar Oceanography, Part B. Chemistry, Biology, and Geology*, edited by: Smith, W. D., Academic Press, New York, 687–739.
- Hu, D., Cai, W., Ganachaud, A., Kessler, W., Sprintall, J. (2015) Introduction to special section on Western Pacific Ocean Circulation and Climate. *Journal of Geophysical Research* Vol. 10 Issue 5, 3175-3176.
- Hunt, B.P.V., Pakhomov, E.A., Hosie, G.W., Siegel, V., Ward, P., Bernard, K. (2008) Pteropods in Southern Ocean ecosystems. *Progress in Oceanography*, 78, 193–221. doi:10.1016/j.pocean.2008.06.001.
- Jaccard S.L., Galbraith E.D. (2013) Direct ventilation of the North Pacific did not reach the deep ocean during the last deglaciation. *Geophysical Research Letters*, 40, 199–203.
- Jentzen, A., Schönfeld, J., Schiebel, R. (2018) Assessment of the effect of increasing temperature on the ecology and assemblage structure of modern planktic foraminifers in the Caribbean and surrounding seas. *Journal of Foraminiferal Research*, 48, 251–272. doi:10.2113/gsjfr.48.3.251.
- Kanaya, T., Koizumi, I. (1966) Interpretation of diatom Thanatocoenoses from the north Pacific applied to a study of Core V20-130 (Studies of a deep-sea Core V20-130. Part IV). *Science Reports of the Tohoku University, Second Series (Geology)*, 37(2), 89-130.
- Kawai, H. (1972) Hydrography of the Kuroshio Extension. In *Kuroshio*, edited by H. Stommel and K. Yoshida, pp. 235-352, University of Washington Press, Seattle, Wash..
- Keigwin L.D. (1998) Glacial-age hydrography of the far Northwest Pacific Ocean. *Paleoceanography*, 13: 323-339.
- Korff, L., von Dobeneck, T., Frederichs, T., Kasten, S., Kuhn, G., Gersonde, R., Diekmann, B. (2016) Cycling magnetite dissolution in Pleistocene sediments of the abyssal northwest Pacific Ocean: Evidence for glacial oxygen depletion and carbon trapping. *Paleoceanography*, 31, 600-624. doi:10.1002/2015PA002882.
- Lovley, D. (1991) Dissimilatory Fe(III) and Mn(IV) Reduction. *Microbiology Reviews*, 55, 259-287.

- Lyle, M. (1983) The brown-green color transition in marine sediments: A marker of the Fe(III)-Fe(II) redox boundary. *Limnology and Oceanography*, 28, 1026-1033.
- Mazzullo, J., Meyer, J.A., Kidd, R. (1998) New Sediment Classification Scheme. ODP Shipboard Scientist's Handbook, pp.125-130.
- Nürnberg D., Tiedemann R. (2004) Environmental change in the Sea of Okhotsk over the past 1.1 million years. *Paleoceanography* 19. doi:10.1029/2004PA001023.
- Pierrot, D., Lewis, E., Wallace, D. (2006) MS Excel program developed for CO₂ system calculations, ORNL/CDIAC-105. Carbon Dioxide Information Analysis Center, Oak Ridge National Laboratory, US Department of Energy, Oak Ridge, Tennessee.
- Pondaven, P., Ragueneau, O., Tréguer, P., Hauvespre, A., Dezileau, L., Reyss, J.L. (2000) Resolving the 'opal paradox' in the Southern Ocean. *Nature*, 405, 168–172.
- Ponomareva, V., Portnyagin, M., Derkachev, A., Pendea, I.F., Bourgeois, J., Reimer, P.J., et al. (2013) Early Holocene M~6 explosive eruption from Plosky volcanic massif (Kamchatka) and its tephra as a link between terrestrial and marine paleoenvironmental records. *International Journal of Earth Sciences* 102(6), 1673-1699. doi: 10.1007/s00531-013-0898-0.
- Ponomareva, V., Portnyagin, M., Pendea, F., Zelenin, E., Bourgeois, J., Pinegina, T., et al. (2017) A full Holocene tephrochronology for the Kamchatsky Peninsula region: applications from Kamchatka to North America. *Quaternary Science Reviews*, 168, 101-122. doi: 10.1016/j.quascirev.2017.04.031.
- Ponomareva, V., Portnyagin, M., Derkachev, A., Bazanova, L.I., Bubenshchikova, N.V., Zelenin, E.A., Rogozin, A.N., Plechova, A.A., Gorbarenko S.A. (2018) A ~6 Ma long record of major explosive eruptions from the Kurile-Kamchatka arc inferred from a tephra sequence at the Detroit Seamount, NW Pacific, JKSP-2018.
- Prueher, L.M., Rea, D.K. (2001) Tephrochronology of the Kamchatka–Kurile and Aleutian arcs: evidence for volcanic episodicity. *Journal of Volcanology and Geothermal Research*, 106(1-2), 67-84.
- Rea, D.K., Basov, L.A., Janecek, T.R., Palmer-Julson, A., et al. (1993) Proceedings of the Ocean Drilling Program, Initial Reports, Vol. 145.
- Riethdorf, J.-R., Nürnberg, D., Max, L., Tiedemann, R., Gorbarenko, S.A., Malakhov, M.I. (2013a) Millennial-scale variability of marine productivity and terrigenous matter supply in the western Bering Sea over the past 180 kyr. *Climate of the Past Discussions*, 8, 6135-6198. doi:10.5194/cpd-8-6135-2012.
- Riethdorf, J.R., Max, L., Nürnberg, D., Lembke-Jene, L., Tiedemann, R. (2013b) Deglacial development of (sub) sea surface temperature and salinity in the subarctic northwest Pacific: Implications for upper-ocean stratification. *Paleoceanography*, 28 (1), 91-104. doi:10.1002/palo.20014.
- Roden, G.I. (1977) Oceanic subarctic fronts of the central Pacific: Structure and atmospheric forcing. *Journal of Physical Oceanography*, 7, 761-778.
- Sagawa, T., Nagahashi, Y., Satoguchi, Y., Holbourn, A., Itaki, T., Gallagher, S. J., Saavedra-Pellitero, M., Ikehara, K., Irinod, T., Tada, R. (2018) Integrated tephrostratigraphy and stable isotope stratigraphy in the Japan Sea and East China Sea using IODP Sites U1426, U1427, and U1429, Expedition 346 Asian Monsoon. *Progress in Earth and Planetary Science* 5, 18. DOI 10.1186/s40645-018-0168-7.
- Schiebel, R., Hemleben, C. (2017) *Planktic Foraminifers in the Modern Ocean*. Springer-Verlag, Berlin Heidelberg.
- Schlitzer R. (2010) Ocean Data View. <http://odv.awi.de>.
- Schlitzer R. (2014). Ocean Data View. <http://odv.awi.de>.
- Seeberg-Elverfeldt, J., Schlüter, M., Feseker, T., and Kölling, M. (2005) Rhizon sampling of porewaters near the sediment-water interface of aquatic systems. *Limnology and Oceanography: Methods* 3, 361-371.
- Sverdrup, H., Johnson, M.W., Fleming, R.H. (1942) *The Oceans: Their Physics, Chemistry, and General Biology*. 1087 pp., Prentice-Hall, Englewood Cliffs, N.J..
- Talley, L.D. (1993) Distribution and formation of North Pacific Intermediate Water. *Journal of Physical Oceanography*, 23, 517-537.
- Uda, M. (1963) Oceanography of the Subarctic Pacific Ocean. *Journal of Fisheries Research Board Canada*, 119-179.



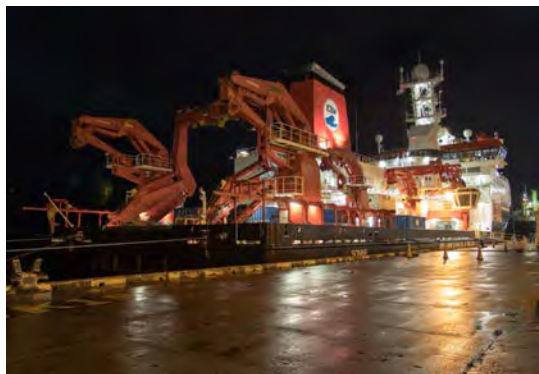
SO264 SONNE-EMPEROR

Weekly Report No. 1
(June 29 – July 1, 2018)

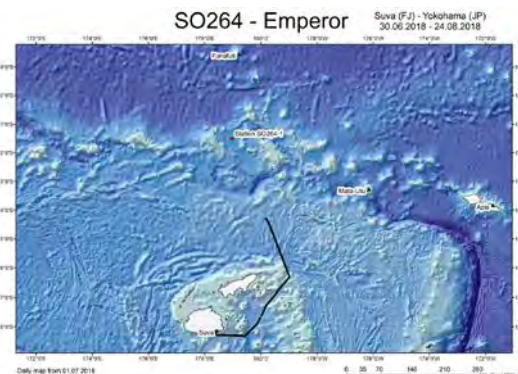
The expedition SO264 with RV SONNE into the North Pacific is the central activity of the BMBF joint project SONNE-EMPEROR of GEOMAR (Kiel) and AWI (Bremerhaven). The subject of this project is the Plio/Pleistocene to Holocene development of the pelagic North Pacific from the surface to depth and its role for the global carbon budget and the Earth's climate.

The starting point of the SO264 was the port city of Suva on the southeastern coast of Fiji's largest island, Viti Levu. On June 29, 2018 at 8:00 a.m., the 38 participants from 11 nations were brought to RV SONNE by the ship's agent. The eight containers sent in advance were already uploaded. The day in port served to prepare the ship for the 54-day lasting journey, including fueling and provisioning. All work was completed in time, so RV SONNE released the lines on June 30, 2018 at 9:30 a.m., accompanied by fresh winds of ~8 Bft, and started its more than 3000 nautical miles long way to the working area of the Emperor Seamount Chain. This very long, approximately 12 days lasting transit became necessary to transfer the ship from the tropical region to the subsequent study areas in the North Pacific.

Although our project-related marine-geological studies will focus on areas north of 30°N, we will use this gigantic transect covering tropical to subarctic climate zones as a unique opportunity to accomplish "en passant" water sampling for nutrient and isotope measurements. For microplankton and organic matter sampling, we will further deploy plankton nets and carry out water filtration studies. Tomorrow, on Monday, July 2, 2018, we will begin the first station work at 6:00 in the morning.



RV SONNE in the port of Suva



Bathymetry around Fiji with SO264 cruise track

With water temperatures of 28°C and air temperatures of only 26°C, we currently set up the laboratories and discuss future sampling protocols. All participants are well, enjoy the extremely pleasant atmosphere aboard RV SONNE, and send best wishes to all relatives at home.

For all cruise participants
Dirk Nürnberg



SO264 SONNE-EMPEROR

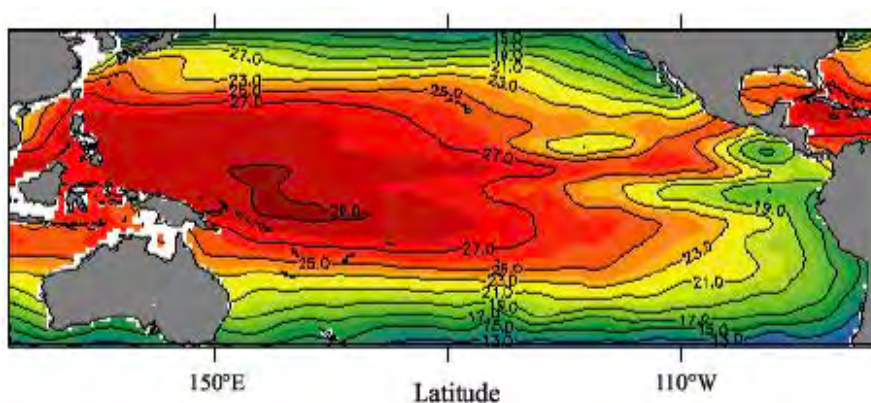
Weekly Report No. 2

(2.7.-8.7.2018)

FS SONNE has begun its ~3000 nautical miles journey to the remote study area of the Emperor Seamount Chain in the North Pacific. The storm from southeasterly directions, already announced the day before, blew us towards the first planned water station at ~11°S and ~179°E. This area belongs to the territory of Tuvalu, for which a research permission has been requested and granted previously. Upon arrival on the morning of July 2, 2018 at 6:00 am, we unfortunately had to cancel station work. A huge wave and winds up to 9 Bft. prevented the safe deployment of the CTD, the multi-net would have been torn by the gusty wind. In order to keep our schedule, we continued to sail to the 2nd planned station. In the afternoon, wind and waves became less, and long-missed faces emerged again from the chambers. Seasickness is unfortunately an everlasting annoying companion.

Since departure, group sessions are held regularly every two days for mutual information and coordination. In addition, the smaller group of team leaders meets daily to discuss the upcoming work. In the morning of July 3, 2018 at 5:00 am we reached the next "water station" at ~7°S and 179°50'E, which became a nice success. The calm weather allowed further unpacking of the containers and setting up of the laboratories.

It remains amazing how RV SONNE manages very long distances at moderate speeds, which are more like those of a cyclist. We are currently in the area of the so-called West Pacific Warmpool, a vast ocean region characterized by extremely high water temperatures of up to 29.5°C (with air temperatures commonly 1-2°C cooler!). This oceanic heat capacity is an important driver for the global climate and controls the heat transfer to high latitudes to a decisive extent. Already during middle Miocene times, i.e. ~7 million years ago, the Pacific proto-warmpool formed due to plate tectonic reorganizations in the Indonesian seaway. With significantly improving weather conditions during the following days, all cruise participants started to realize the gigantic proportions of this oceanic heat storage.



The West Pacific Warmpool with seasurface temperatures >27°C

A highlight of this week was the crossing of the equator at an exact latitude of 0° and longitude of 180°. We suspect that only few people have ever reached this unique position. The awarding of a "Crossing the Line" certificate signed by the god of the sea, Neptun, and the receipt of a bottle of schnapps filled with equatorial water rounded off a happy get-together celebrated by the crew and scientists on the work deck.



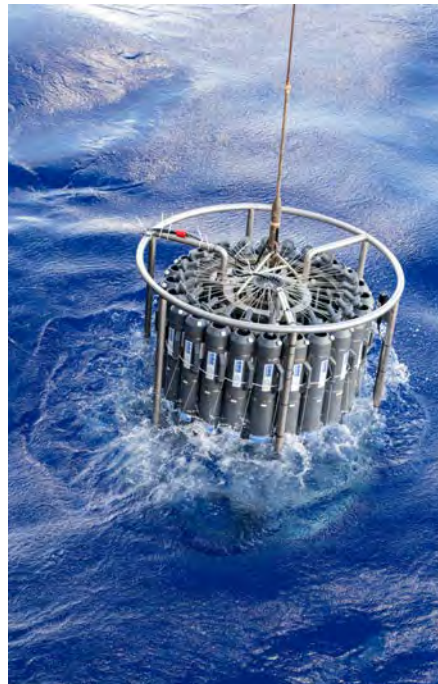
SO264 SONNE-EMPEROR

Weekly Report No. 2
(2.7.-8.7.2018)

During the following days at sea, another 4 water stations between 2°N and 10°N were carried out, thereby crossing the complex area of the equatorial current system. Two westward wind-driven equatorial currents are separated by the eastward north-equatorial countercurrent. Routinely starting with a multinet down to 100 m, insights into the near-surface distribution of planktonic assemblages became possible. Water mass properties such as temperature, salinity, fluorescence, and oxygen content were measured with the subsequent CTD/water rosette equipment, and water samples were collected from depths of up to 5300 m. Subsequent water analyses will focus on stable oxygen and carbon isotopes, silicon and neodymium isotopes, radiocarbon, trace elements, carbonate chemistry, and biomarkers. A multi-net to depths of 600 m terminating the station work documents the deeper vertical distribution of the plankton. The net catches clearly indicate that the plankton communities, especially those of the foraminifera, are influenced by the oceanographically predefined nutrient conditions. The suspended organic material filtered off by continuous pumping "on transit" also points to distinct lateral gradients. All of this work within the water column is necessary to calibrate the proxy parameters used in paleoceanography.



RV SONNE at 8-9 Bft in the tropical W Pacific



Deployment of CTD/water rosette-unit

After crossing the equatorial zone, we slowly but steadily reach the area of the subtropical gyre that circulates in a clockwise direction. The deep blue water reveals that it is a nutrient-poor, oligotrophic ocean area. Accordingly, we will significantly increase the distances between the water stations in the following days, also to be able to meet our strict schedule.

According to the current planning we will arrive next Friday in our study area of the Emperor Seamounts and will start the geology program. The geological devices have now been set up, and the corresponding laboratories are prepared. The sampling of the deep-sea sediments will be done using traditional devices such as TV-Multicorer, large box corer,



SO264 SONNE-EMPEROR

Weekly Report No. 2
(2.7.-8.7.2018)

gravity, piston, and Kasten corers. The international team of technicians, hydrographers, geophysicists, sedimentologists, biologists and tephrastatigraphers, micropalaeontologists, paleoceanographers, and geochemists will guarantee the recovery and processing of these important climate archives.

We learned during the past week that the tropical Pacific can be quite rough, stormy and rainy. Apart from the heat, the weather could be easily compared to the northern German november weather. Even the dreamy South Seas islands hid behind the horizon. A floating plastic canister at 10°03.4'N and 178°26.9'E, ~400 nautical miles away from human settlements closest to us, reminded us that not everything that is found in the ocean belongs there. The spirit on board RV SONNE still remains very good, and we look forward to the coming weeks. All participants are well and send warm greetings from 14° N 178° E to those who stayed at home.

On behalf of all cruise participants

Dirk Nürnberg



SO264 SONNE-EMPEROR

Weekly Report No. 3

(July 9.-15., 2018)

In the course of the past week, FS SONNE has made huge strides in crossing the subtropical vortex of the North Pacific and reaching the actual SO264 study area in time. On Monday, Wednesday and Friday we completed our "Trans-Pacific water sampling program", which already had begun at 7 °S, at 18 °N, 27 °N and 33 °N. The last station was also the beginning of the marine geological work in the area east of the Kimmei volcano in the southernmost area of the north-south oriented Emperor seamount chain.

The sampling of the water column is a small, although exciting program. After crossing the equatorial currents, plankton assemblages have increasingly changed to species communities that can tolerate nutrient-poor conditions. Upon reaching the northern margin of the subtropical gyre, we see a further adaptation of the species to new environmental conditions.



Deployment of the geological core device from FS SONNE

This subtle vortex-like circulation pattern, turning in a clockwise direction and occupying almost the entire North Pacific, became subject of wide discussions: Due to its high amount of floating garbage, it is referred to as the "Great Pacific Garbage Patch". Unfortunately, we also realized that the subtropical gyre is indeed characterized by high proportions of floating trash, and in this respect is different from ocean regions to the south and north. Although being thousands of miles away from human settlements, we observed floating garbage that came along every few minutes on our route between 10 °N and 30 °N, be it plastic bags, light bulbs, fishing net balls, styrofoam, or plastic pieces.

At ~32 °N we leave the influence of the subtopic gyre and slowly enter the realm of the Kuroshio Current, one of the largest current system in the world with a transport volume of ~45 million cubic meters of water per second. The Kuroshio transports tropical heat northward, converges with the southward flowing Oyashio Current off Japan and is deflected



SO264 SONNE-EMPEROR

Weekly Report No. 3

(July 9.-15., 2018)

eastwards into the North Pacific. There, it acts as an oceanographic and climatic barrier - further north, the air and water temperatures will drop significantly.

The focus of our paleoceanographic studies is sampling of sediments on top of submarine volcanoes of the Emperor Seamount Chain, the youngest of which is Hawaii. These volcanoes rise several 1000 m above the deep sea plain, which is at 5-6 km water depth. Interesting for paleoceanographers is that the preservation of tiny calcitic microfossils in these relatively shallow water depths is very good compared to the corrosive regions of the deep North Pacific. The isotope-geochemical signature stored in these calcitic shells provides important insights on how the ocean circulation has changed in the past.

In the first three days of the geological program, various sediment cores from different water depths and areas have already been obtained and processed. Samples from these cores have been collected and archived for a wide variety of analytical approaches. The time-consuming measurements, however, will be made in the home laboratories after the samples have been shipped back home by container from Yokohama (Japan).



Deck work onboard RV SONNE during SO264

Surprisingly, on the summit of the volcano Koko in ~1000 m water depth our coring device got stuck in a sediment deposit, which due to its composition does not belong to a deep sea environment. Visual inspection identified it as a shallow-marine lagoonal deposit enriched with biogenic debris. The initially enigmatic geological finding of such a lagoonal sediment at such great depths was quickly explained. The reef atoll, which formed ~50 million years ago around a volcano towering above sea level, sank to great depth on an aging and cooling lithospheric plate after volcanism declined. It remains questionable in this respect whether these sunken lagoon sediments have never been covered by other deposits since then, or whether erosive ocean currents have incessantly prevented any sedimentation since millions of years until today.

According to our preliminary station planning, we will hit the next volcanic cone, Ojin Seamount, already tomorrow. In good spirits and best support by the SONNE crew, we send cordial greetings from the 36 °N 171 °E to those left at home.

On behalf of the cruise participants
Dirk Nürnberg



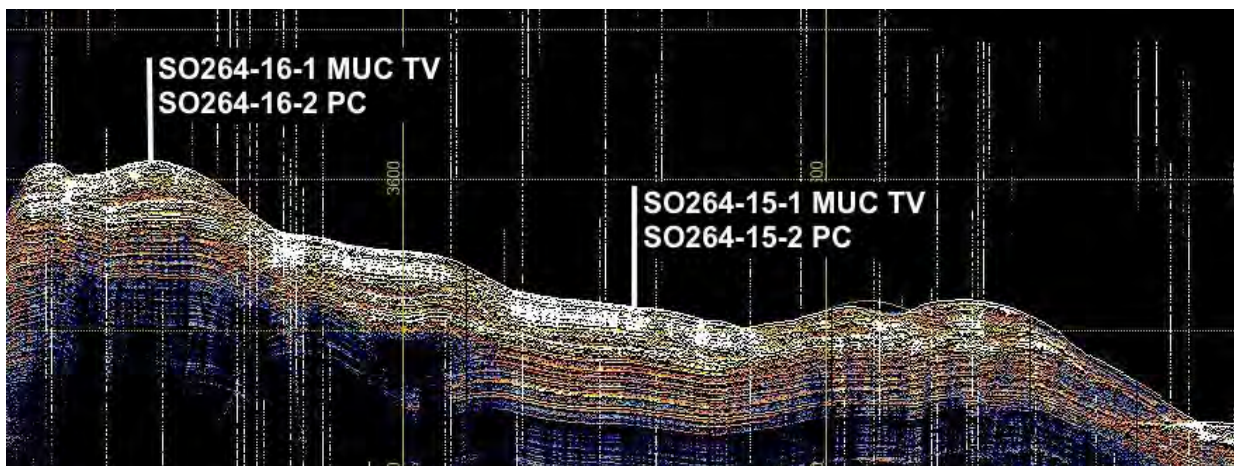
SO264 SONNE-EMPEROR

Weekly Report No. 4
(15.7.-22.7.2018)

Over the past week RV SONNE has left the influence of the Kuroshio Current system and has come into the influence of the counterclockwise rotating Subarctic Gyre. Together with the Subtropical Gyre they represent the two largest vortex systems at mid latitudes of the North Pacific. Both gyres, which are separated by the Kuroshio Current at $\sim 37^\circ\text{N}$ are circulation patterns driven by trade winds and the west wind drift. When entering the sub-polar climate zone, the water and air temperatures decreased significantly and made cruise participants used to more tropical conditions increasingly feel chilly. Today, on Sunday, 22.7.2018, the air temperatures are at only 13°C and the water temperatures are at 11°C . Shorts and T-shirts were meanwhile replaced by long pants and sweaters. Since two days, the North Pacific became foggy and hazy all day, in rather weak winds.

Last week was marked by an intense geology program, several Emperor Seamount Chain volcanoes were mapped and sampled between 37°N and 44°N . These volcanoes are youngest in the south with ages of ~ 55 million years and age towards ~ 65 million years at 44°N . With increasing age, they sink below sea level and are increasingly covered by sediments.

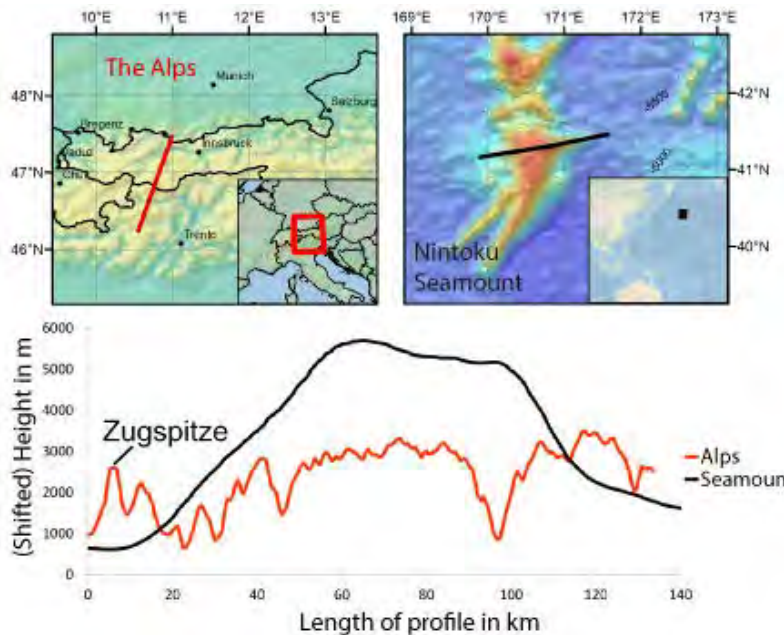
These oceanic deposits have been the focus of this journey: Comparable to the leaves of a book, these individual sediment layers store information about the past evolution of the ocean currents and the associated climate. They can be read out and interpreted by applying most sophisticated measuring techniques and following various scientific approaches. The primary intention of our research field is to understand the natural variability of the ocean-climate system in the context of future climate change.



The mapping of the marine deposits is carried out with the ATLAS PARASOUND sediment echosounder. Here shown, as an example, the seabed region in ~ 3200 m water depth east of the Nintoku volcanic area.

Before sampling the marine sediments, the seabed is mapped with echosounding systems which, on one hand, can display the seafloor three-dimensionally and, on the other hand, penetrate the upper 10s to 100s meters of the sedimentary deposits. These high-tech tools give us the opportunity to select good sampling locations. They also allow us to improve and

to correct existing bathymetric records. Hours and days are spent for intensive and systematic mapping. Using a cruising speed of 6 kn, 60 nautical miles or nearly 120 kilometers can be recorded in 10 hours – which is a time-consuming approach in view of the huge dimensions of the submarine mountains.



The comparative presentation of height profiles across the Nintoku Seamount and the Alps illustrates the gigantic dimensions of the submarine volcanic structures of the Emperor Seamount Chain. The Nintoku volcano overtops the Alps by more than 2000 meters in altitude.

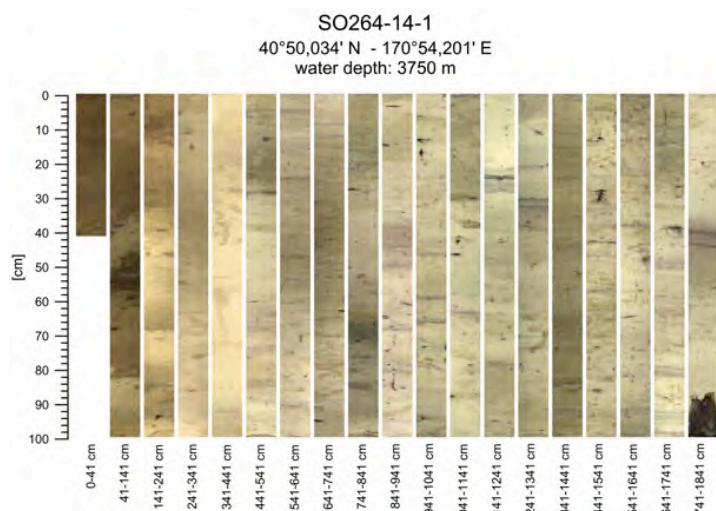
As expected, the search for good sediment deposits turns out to be quite difficult. Our ambition is to recover sediments rich in biogenic calcite that is preserved only rarely in the relatively flat regions of the North Pacific: that's why we focus our work on the "volcanic peaks". During the last few days we worked on the flattest regions of the Ojin, Nintoku, Yomei and Suiko volcanic regions, but also sampled the volcanic flanks down to water depths of ~5700 m.

For the recovery of sediment cores, we use wire-guided, up to 20 m long gravity pipes, which are lowered and retrieved via the ship's lowering gear. Meanwhile, we have gained a large number of high-quality, carbonate-rich sediment cores from various water depths, from which we will produce paleoceanographic and paleoclimatic data series. We must realize, however, that the summit regions often consist of bare basalt rocks, since sediments down to depths of ~1800 m are eroded or transported away by strong bottom currents. The search for sediment pockets is tedious, but not impossible.



SO264 SONNE-EMPEROR

Weekly Report No. 4
(15.7.-22.7.2018)

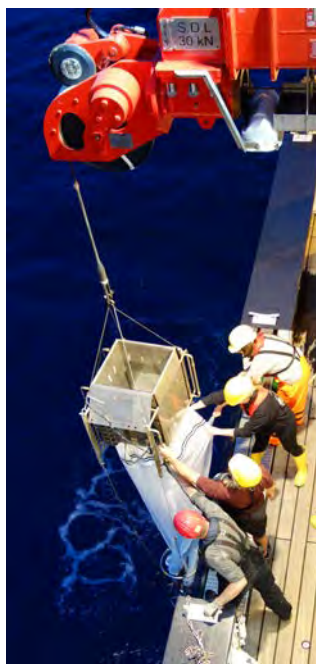


Bright carbonate-rich sediments can be found in large water depths of up to 4200 m. They contain abundant planktonic and benthic unicellular microfossils (foraminifera) - the most important (isotopic) geochemical signal carrier in paleoceanography. Cooler climatic periods are clearly recognizable by darker colors. Also typical are basaltic pebbles and sand layers, which suggest intensive downhill transport. Prominent volcanic ash layers can contribute important information to the age of the deposits.

Our intensive sampling program of the water column will continue at Suiko Seamount, which will serve to calibrate and further underpin the proxy parameters used in paleoceanography. The oceanic mixed layer is commonly sampled by multineets in order to describe calcitic and siliceous plankton communities.



Multinet in continuous use in order to study plankton communities.



The scientific work is in full swing and the various disciplines work hand in hand to quickly process the numerous sediment cores. Even if the busy days become sometimes long, the preparation and analysis of the samples is fun for all of us. Tomorrow, we will "climb" the next summit, in the best mood and greatly supported by the RV SONNE crew. All send cordial greetings from 44 °N 170 °E to those who stayed at home.

On behalf of all cruise participants

Dirk Nürnberg



SO264 SONNE-EMPRESS

Weekly Report Nr. 5
(July 23-29, 2018)

Empress Suiko was the first empress and thirty-third monarch of Japan, followed by seven other empresses in Japanese history. She came to power at the age of 39 in 593 AD until she died at the age of 74. The huge volcano, which we intensively mapped and geologically sampled in the course of this week, is named after her: Suiko Seamount. The Suiko volcano belongs to the Emperor Seamount Chain in the North Pacific, became already inactive about 60 million years ago and sank below sea level. Fossil shallow-water corals of the same age were found on the summit and witness the turbulent history of this volcano.

Previously we had sampled several, mostly younger, volcanoes during the last weeks: Kinmei, Soga, and Yomei, named after family members of the Empress. Suiko was the third daughter of Emperor Kinmei and his wife Soga, and she was the younger sister of Emperor Yomei. Yomei was only in power for two years before he died due to illness. A long and traditional history in Japan, long before the Vikings had their high time in Northern Europe.

The Suiko volcano is located at about 45° north and 170° east and is within the area of the Subarctic Front, which is defined as the 4°C isotherm in 100 m water depth and the approximate boundary between the wind-driven subtropical and subarctic vortex systems. The volcano is interesting in the sense that we continue to hope to be able to recover good sediments on the summit areas located in relatively shallow water. In fact, we are not the first to do geological studies here. The drill ship "Glomar Challenger" already carried out a drilling campaign here in the late seventies with the intention to study the volcanic development of the Emperor seamount chain. In 2001, the French research vessel "Marion Dufresne" retrieved a first paleoceanographically interesting sediment core of ~44 m core length, which had not been worked on until now.



Empress Suiko (554–628 years AD), third and youngest daughter of Emperor Kinmei and his wife Soga (en.wikipedia.org)



Modern drone technology makes it possible: photographed from 500 m height FS SONNE draws its tracks in the vastness of the North Pacific.



SO264 SONNE-EMPRESS

Weekly Report Nr. 5
(July 23-29, 2018)

So far we carried out ten busy stations on Suiko exclusively for sediment sampling. With core recoveries of 80% on average, we brought ~120 m of sediment core to the working deck. These sediment cores were obtained from water depths of 1800 m to 3200 m. A quite successful action, after conditions were significantly worse on the previous volcanoes with their flat and barren summit areas. Although core locations from water depths of ~1800 m are rather too deep to reach into the modern North Pacific Intermediate Water, they should still be ideal for reconstructing the glacial conditions, when North Pacific Intermediate Water was clearly deeper then. The North Pacific Intermediate Water contributes to the ventilation of the deeper Pacific.



The so-called "bananas", gravity cores which bent or partly broke when hitting the seabed, are rare so far, but then make the deck crew very busy. Fortunately, these "bananas" still contain short high-quality sediment sequences.

The sediment cores, some of which are more than 19 m long, are being extensively analyzed on board before they are sent home packed in reefer containers. After sawing the sediment core into pieces of 1 meter, the exact labeling and the division of the sediment cores into work and archive halves continues. Then, the core segments are first logged by various methods, that is: every centimeter geophysical parameters of the sediment are measured, which help determine the characteristics of the sediments, correlate sediment cores from different areas, and get initial ideas on the age of the sediments. Subsequently, the core segments are photographed and described by experienced geologists. Working and measuring in a large number of on-board laboratories requires many hours and above all, a well-coordinated team working hand in hand. This also presupposes that route planning and station planning is carried out in a forward-looking manner in order to be able to use ship, crew and the scientific group effectively.

Our first assessment of the logging data is promising. The different sediment sequences, which contain biogenic calcite down to large water depths, can be correlated very well within the study area. Distinct volcanic ash layers provide additional information for cross-regional correlation and approaches to age dating.



SO264 SONNE-EMPRESS

Weekly Report Nr. 5
(July 23-29, 2018)

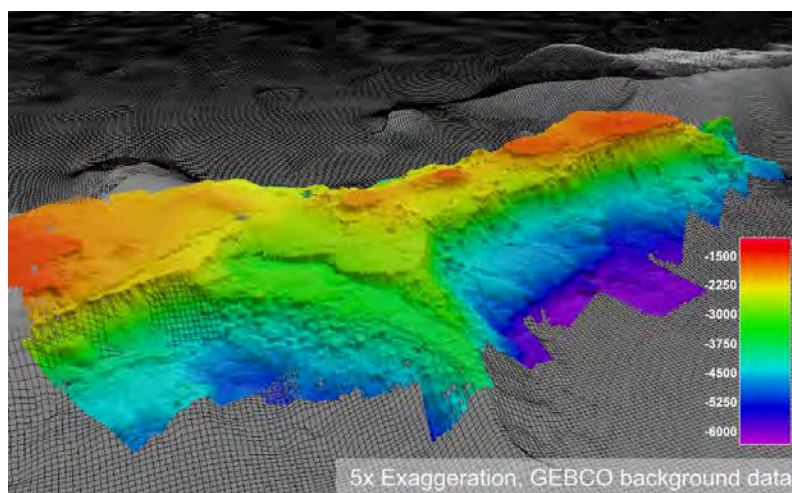


High activity in the geology laboratory. Geologists and biologists work hand in hand on the night station and share the laboratory space.

Apart from sediment coring, a major focus of our work during the last week was bathymetric mapping and profiling with the sediment echosounder. We have significantly expanded this work at Suiko to optimize the difficult search for suitable coring stations. Our work on the previously sampled volcanoes had shown that a systematic recording of the very complex bathymetric conditions and the documentation of existing sediment packages makes the selection of potential core locations much more successful.

On Saturday we had a little celebration: Half of the SO264 expedition is already over and experience shows that the second half will just go by quickly. Nonetheless, there is still much to be done. The next volcano is calling: Jimmu. According to legend, Jimmu is the first emperor of Japan, with a regency from 660 to 585 BC. He should have turned 126 years old. Well, legends! With the best mood and support from the SONNE crew we send warm greetings from 45 ° N 170 ° E to those who stayed at home. On behalf of all cruise participants

Dirk Nürnberg



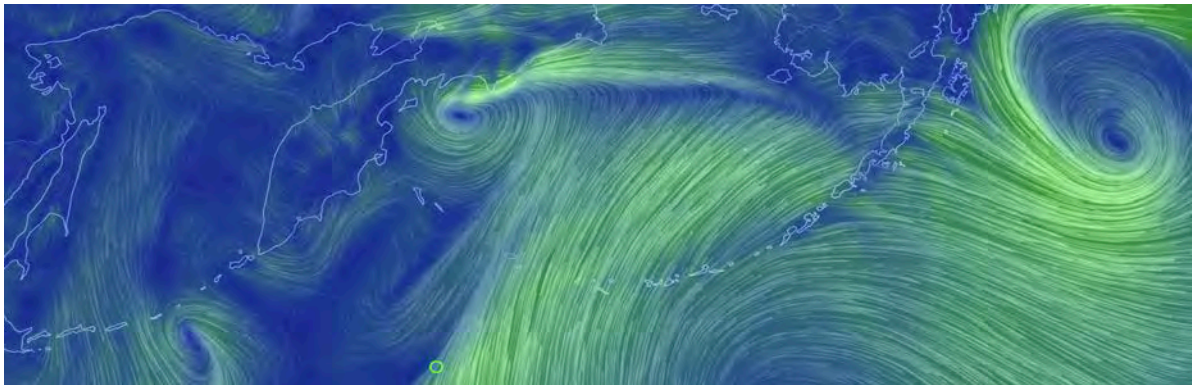
Three-dimensional presentation of the Suiko volcano based on bathymetric datasets created during SO264.



SO264 SONNE-EMPEROR

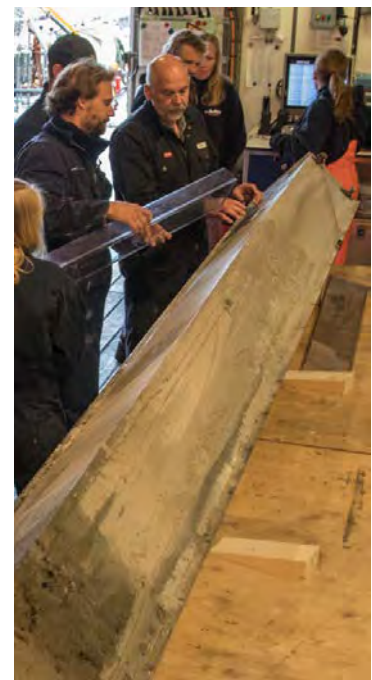
Weekly Report No. 6
(July 30 – August 5, 2018)

During the first days of last week, the Jimmu volcano became focus of our work. Jimmu, named after the first emperor of Japan, is located at about 46°N, comparable to the latitude of Milan (Italy). Here, however, it is quite cool, with air temperatures around 12°C and water temperatures around 10°C. Since many days we work in a dense fog soup, which is even not blown away by strong winds. We have not seen the sun for days.



Presentation of near-surface winds in the North Pacific region on Saturday, August 4, 2018 (www.earth.nullschool.net). The position of FS SONNE is marked as a green circle.

Our coring equipment for sediment sampling was used in water depths of approx. 1800 m to approx. 3200 m. Our intention was again to sample areas of the volcano that are as shallow as possible in order to reach the upper ocean levels and later to reconstruct them. In the shallow areas, the sediment deposits found are clearly thinner, so that we only used relatively short corers. However, due to the lower sedimentation rates, the short cores include more "time" and allow a deeper look into the geological past than the longer sediment cores from the deeper regions. Unfortunately, the conditions are not always optimal, so that one or the other bent or broken "banana" comes on deck and our contingent of steel tubes shrinks significantly. Nevertheless, the core recovery is more than 80% and shows interesting facies changes from biogenic oozes to terrigenous deposits, intercalated by prominent volcanic ash layers, which allow us to correlate cores over large areas.



Processing of sediment cores

The long row of volcanoes in the Emperor Seamount Chain ultimately reflects the movement of oceanic crustal plates above a stationary magma source from the Earth's mantle, called "hot spot" volcanism. This hot spot breaks through the moving lithospheric plate like a cutting torch. The most obvious geological evidence is that the volcanoes are getting older and deeper from south to north. With increasing distance from the magma source volcanoes lose



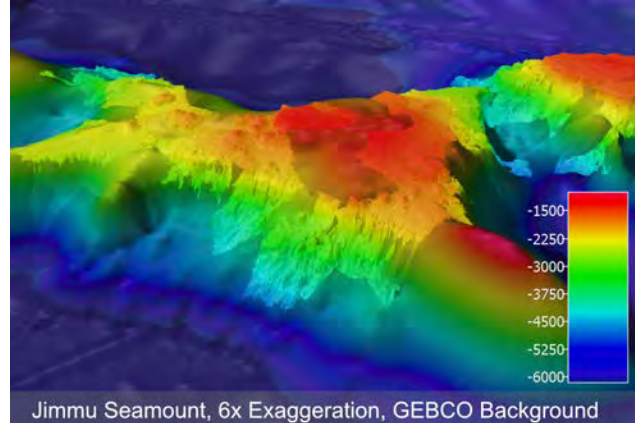
SO264 SONNE-EMPEROR

Weekly Report No. 6
(July 30 – August 5, 2018)

contact with their magma source, become inactive, and subside together with the cooling ocean crust. The volcanic peaks usually appear as flattened and sometimes very extensive plateaus. These are formed when the volcanic cones, which previously lay above sea level, sink to sea level and are leveled by the eroding effect of water. The US geologist Harry H. Hess (1906-1969) described these relationships for the first time in 1945, thus underpinning the theory of plate tectonics. Hess called the flattened submarine volcanic cone 'Guyot'. Not according to the Swiss geographer Arnold H. Guyot (1807-1884), but in reference to the flat-roofed biology and geology building of Princeton University (USA), which in turn was named after Princeton professor Arnold H. Guyot.



*Harry Hammond Hess
(1906-1969), co-
founder of the plate
tectonic theory*



The Jimmu Guyot as part of the Emperor Seamount Chain is located at approx. as 46°N and 169°E. The Guyot with the leveled summit area rises from approx. 5200 m water depth up to approx. 1200 m to the sea surface.



The Guyot Hall of Princeton University (USA)

Our work progress was slowed down last Thursday night. Beginning in the late evening, wind and wave increased markedly, making the deployment of our equipment increasingly difficult. Over night, a violent southwest storm developed with up to 22 m/s wind speed (9 Beaufort) and wave heights up to 6 m. On Friday to Saturday morning, station work had to be cancelled accordingly, and we used the time to map the next volcano. 'Minnetonka' is his name. This name comes from the Indian Dakota Sioux 'mni tanka' and means 'big water'. With continued good mood and great support from the RV SONNE crew, we send the very best regards from 47°N 169°E to those who stayed at home.

On behalf of all SO264 cruise participants

Dirk Nürnberg



SO264 SONNE-EMPEROR

Weekly Report No. 7

(6.8.-12.8.2018)

The seventh week of our little trip is over. It started with the celebration of a round birthday of a crew member, the week ended today with another birthday. You could almost think we are celebrating too much! But: A long journey with the inevitable narrowness and all kind of constrictions needs these small, lovingly celebrated sociable breaks. They motivate for the remaining, almost too short time on board.

At the beginning of the week, the very successful work on the Minnetonka volcano was completed. Ten core stations in water depths of 2100 to 4000 m and sometimes difficult terrain resulted in a core recovery of almost 110 m. The varied sediment sequences are for the first time characterized by increased occurrences of diatomaceous oozes. These are deposits mostly composed of siliceous microplankton (diatoms) that differ significantly from the carbonate-rich sediments to the south. These diatomaceous oozes are typical of the northernmost North Pacific that some of us are very familiar with from previous expeditions to the Bering Sea adjacent to the north, or to the Okhotsk Sea. They will quickly allow us to get an idea about the age of the sediments.



Research Vessel SONNE during SO264.



Crane dancing: The retrieval of bent core equipment on deck requires tact.



The lowering frame used to deploy sediment corers on RV SONNE.

On Wednesday, we jumped over to the next volcano further to the north, Tenji Guyot or Tenji Seamount. Tenji surprises with thick undisturbed sediment sequences even on the shallow plateau areas. With only a few deployments from water depths of 2300 to 5200 m, core recovery increased rapidly to a total of 80 m. These fantastic conditions are very different from what we got to know further south and will probably accompany us up to Detroit Seamount in the northernmost working area. The large core recoveries here in the north of the Emperor Seamount Chain make the geologist's heart beat faster. But it becomes clear that we are reaching our limits with our laboratory and equipment consumables. Much is getting tight and we start to improvise. Just because we continue to bring all variants of



SO264 SONNE-EMPEROR

Weekly Report No. 7

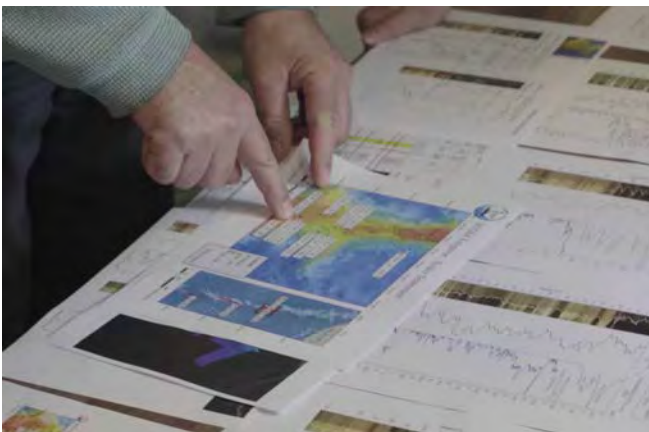
(6.8.-12.8.2018)

"bananas" back on deck. Today, on Sunday, we switched to a core device with a smaller core diameter, for which sufficient packaging material is available and which leaves us a lot of room for station work in the remaining week.



The bow area of RV SONNE with the big spotlights.

Despite the already existing large workload, the cruise report is being tackled. There are more and more discussion groups that transform the results collected so far into diagrams and texts. A tedious, but extremely interesting job. As an "old stager", it is good to see how the "youngsters" get involved, work above average, grow into one team, do not pay attention to overtime, while only earning little money. Is this the way research works?



Long discussions to get clarity.



Working on the sediment core halves.

On Thursday and Friday, plankton productivity in the near-surface ocean for the first time has become so high that biologists started to conduct a variety of plankton captures down to water depths of 800 meters over a time period of 24 hours to get a detailed picture of plankton diversity, activity and their temporal variability. The collected algae samples will probably be the first to arrive in Germany. As soon as we arrive in Yokohama, the sensitive frozen sample material is flown to Germany in a special container. Only 1.5 milligrams per sample are needed for the analysis. Although this is only 1/20 of the weight of a stamp, it took over 24 hours to collect that amount together.

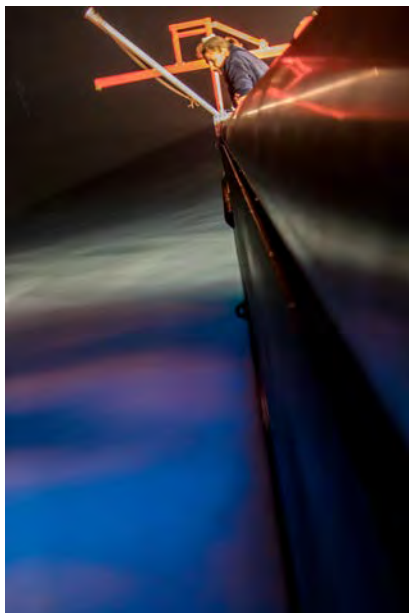
The weather stays well-intentioned meanwhile. Little wind, little wave! The danger of typhoons approaching has faded away. After weeks of dense, cold fog this weekend was sunny and warm again. And oh, almost forgot: Tenji Seamount is named after the 38th Emperor of Japan, who reigned from 661 to 672 AD.



SO264 SONNE-EMPEROR

Weekly Report No. 7

(6.8.-12.8.2018)



Night mist, Night-shift

Tenji, son of Yomei (eponym of an volcano in the south, which we already worked on) distinguished himself - apart from his 14 children - by the fact that he implemented various political reforms that centralized and strengthened Japan. Geologically interesting is that in the 7th year of his reign "flammable water", most likely petroleum, became known and for the first time points to oil deposits in Japan.

In good spirits, the successful continuation of the SO264 cruise in view and backed up by the constant and energetic support of the SONNE crew, we send the very best greetings from 50°N 168°E to those who stayed at home. On behalf of all cruise participants.

天智天皇

(Tenji)

Dirk Nürnberg



SO264 SONNE-EMPEROR

Weekly Report No. 8
(August 13-19, 2018)

The eighth week of the SO264 cruise is over. It started with station work on a small volcanic area south of Detroit Seamount at about 50°N. Three geostations were routinely carried out with the piston corer and the multicorer. The sediment deposits allowed a core recovery of approx. 47 m from 2500-3500 m water depth. We could not have done better! The core logging data suggest that diatomaceous sediment types prevail, which can easily be correlated with each other, but can also be bound to our sedimentary records located further south. In terms of time we cover the last glacial / interglacial cycles. Unfortunately, we were unable to open and visually describe the newly recovered sediment cores. In fact, this very long expedition has brought us an unpredictably large core recovery, so we nearly ran out of packaging material. We decided to just log the cores and postpone the opening of these last cores to the time at home. At the end of the geo-related work, another multi-net/CTD/water program was started east of our study area at 5000 m water depth.



Rolling home.

Most of the past week was spent on Detroit Seamount, at about 50-51°N and 167-168°E. We have reached the US and Russian territorial waters, except for a few miles, to complete our successful coring program. Detroit Seamount, comparable in area to Hawaii, is already a very well studied region with many existing sediment cores and excellent publications. Our US colleague Lloyd Keigwin from the Woods Hole Oceanographic Institution did a great job here in the late 1990s and gave new ideas to the community. We have revisited a few of his important core locations to extract fresh sediment material for new analytical approaches. By email, we were in contact with him and received quite a few good tips.



*Lloyd Keigwin,
paleoceanographer,
Woods Hole Oceanographic
Institution*



SO264 SONNE-EMPEROR

Weekly Report No. 8
(August 13-19, 2018)

A total of ten coring stations were completed in three days in water depths of 2400-3900 m. Unfortunately, we were followed by bad luck at the end of our journey. After two operations with strongly bent piston corers (called "bananas"), this device was no longer usable. We accordingly changed to our gravity and box corers, which unfortunately no longer provided the long core recovery we were used to. But the short and big box corers brought unexpected amounts of sediment and the hangar-laboratory looked pretty "muddy" afterwards. The logging data promise very high-quality sediment records, on which many scientist generations can work. Finally, one last plankton/water station was accomplished west of Detroit Seamount.

In the night from Thursday to Friday, at 02:00 in the morning, we stopped station works, the expedition program ended and the transit towards Yokohama started. Approximately 1500 nautical miles are still ahead of us to the port of disembarkment. Hopefully no typhoons will hinder our backtrip. I think we can say that we have used the ship efficiently, thanks to the fantastic crew, but also thanks to the many technicians, scientists and students, who worked tirelessly and brought the hard and ever-lasting work to an end.



Waves ahead.

Along a north-south-oriented transect along approximately 179°E we finally completed an extensive water sampling program across the North Pacific from 7°N to 50°N as well as a closely-spaced sediment sampling program along the Emperor Seamount Chain from 33°N to 51°N. At 77 stations, we ran 183 devices.



Banana.

Even in the 8th week, the weather remained benign with relatively little wave and moderate winds. It is noteworthy that the northernmost of our volcanoes was not named after a Japanese ruler, but - as unromantic - after the US warship "USS Detroit", which was destroyed in Pearl Harbor last World War. Still with the best mood, the energetic support from the SONNE crew, and especially with the prospect of a fresh beer in Japan, we send the very best greetings from now already 41°N 150°E to those who stayed at home. On behalf of all cruise participants

Dirk Nürnberg

Appendix 4 SO264 station list

Station No.	Gear No.	Station label	Area	Gear	Date (dd.mm.yy) Start	Start UTC	At seafloor/ at depth UTC	End UTC	Duration of station (hrs:min)	Latitude start (deg/min)	Longitude start (deg/min)	Water depth EM122 (m)	Latitude at depth (deg/min)	Longitude at depth (deg/min)	Water depth EM122 (m)	Latitude end (deg/min)	Longitude end (deg/min)	Water depth EM122 (m)	Rope length (m)	Rope tension (kN)	Core recovery (m)
SO264-1	-1	SO264-1-1	Tuvalu	MSN	02.07.18	18:23	18:26			07°00,465'S	179°49,294'W								100		
SO264-1	-2	SO264-1-2	Tuvalu	CTD	02.07.18	19:21				07°00,463'S	179°49,291'W	5338			5338			5338	3000		
SO264-1	-3	SO264-1-3	Tuvalu	MSN	02.07.18	22:00	22:17			07°00,464'S	179°49,289'W								500		
SO264-2	-1	SO264-2-1	Howland & Baker	MSN	04.07.18	20:08	20:11	20:25	0:17	01°46,992'N	179°36,701'E	5612.6	01°46,991'N	179°36,700'E	5622	01°46,998'N	179°36,700'E	5613	100		
SO264-2	-2	SO264-2-2	Howland & Baker	CTD	04.07.18	20:42	21:12	22:03	1:21	01°46,990'N	179°36,697'E	5612	01°46,990'N	179°36,695'E	5612	01°47,002'N	179°36,691'E	5612	1200		
SO264-2	-3	SO264-2-3	Howland & Baker	MSN	04.07.18	22:14	22:33	23:05	0:51	01°47,003'N	179°36,693'E	5620	01°46,990'N	179°36,697'E	5613	01°46,958'N	179°36,739'E	5625	600		
SO264-3	-1	SO264-3-1	Kiribati	MSN	05.07.18	13:03	13:08	13:22	0:19	04°30,572'N	179°08,052'E	5685	04°30,574'N	179°05,050'E	5683	04°30,576'N	179°08,056'E	5684	100		
SO264-3	-2	SO264-3-2	Kiribati	CTD	05.07.18	13:38	14:11	15:05	1:27	04°30,572'N	179°08,052'E	5683	04°30,566'N	179°08,030'E	5683	04°30,566'N	179°08,022'E	5683	1200		
SO264-3	-3	SO264-3-3	Kiribati	MSN	05.07.18	15:14	15:39	16:14	1:00	04°30,563'N	179°08,022'E	5684	04°30,565'N	179°08,026'E	5683	04°30,566'N	179°08,025'E	5682	600		
SO264-4	-1	SO264-4-1	Harrie Island	MSN	06.07.18	06:12	6:15	6:30	0:18	07°19,738'N	178°44,624'E	5429	07°19,740'N	178°44,623'E	5425	07°19,740'N	178°44,621'E	5427	100		
SO264-4	-2	SO264-4-2	Harrie Island	CTD	06.07.18	06:44	8:54	10:37	3:53	07°19,742'N	178°44,617'E	5436	07°19,742'N	178°44,619'E	5436	07°19,746'N	178°44,624'E	5436	5300		
SO264-5	-1	SO264-5-1	Marshall Islands	MSN	07.07.18	00:05	0:11	0:26	0:21	09°59,425'N	178°27,619'E	5738	09°59,420'N	178°27,618'E	5740	09°59,413'N	178°27,621'E	5740	100		
SO264-5	-2	SO264-5-2	Marshall Islands	CTD	07.07.18	00:40	1:13	2:02	1:22	09°59,420'N	178°27,619'E	5738	09°59,422'N	178°27,618'E	5738	09°59,420'N	178°27,618'E	5738	1200		
SO264-5	-3	SO264-5-3	Marshall Islands	MSN	07.07.18	02:15	2:41	3:15	1:00	09°59,419'N	178°27,618'E	5739	09°59,420'N	178°27,618'E	5737	09°59,420'N	178°27,618'E	5739.5	600		
SO264-6	-1	SO264-6-1	Wake Island	MSN	08.07.18	21:23	21:27	21:39	0:16	18°33,602'N	176°55,197'E	3613	18°33,599'N	176°55,200'E	3590	18°33,597'N	176°55,199'E	3587	100		
SO264-6	-2	SO264-6-2	Wake Island	CTD	08.07.18	21:55	23:20	0:37	2:42	18°33,600'N	176°55,202'E	3578	18°33,608'N	176°55,199'E	3578	18°33,596'N	176°55,203'E	3578	3500		
SO264-6	-3	SO264-6-3	Wake Island	MSN	09.07.18	00:47	1:18	1:51	1:04	18°33,597'N	176°55,200'E	3588	18°33,604'N	176°55,207'E	3575.3	18°33,601'N	176°55,200'E	3606.7	700		
SO264-7	-1	SO264-7-1	International	MSN	11.07.18	03:00	3:05	3:19	0:19	27°46,950'N	175°36,525'E	5511	27°46,953'N	175°36,530'E	5532	27°46,952'N	175°36,538'E	5512	100		
SO264-7	-2	SO264-7-2	International	CTD	11.07.18	03:34	4:12	5:08	1:34	27°46,953'N	175°36,531'E	5512	27°46,956'N	175°36,537'E	5512	27°46,953'N	175°36,541'E	5512	1500		
SO264-7	-3	SO264-7-3	International	MSN	11.07.18	05:19	5:41	6:16	0:57	27°46,952'N	175°36,544'E	5512	27°46,957'N	175°36,542'E	5513	27°46,946'N	175°36,542'E	5513	700		
SO264-8	-1	SO264-8-1	E' of Kimmei Seamount	TV-MUC	12.07.18	18:42	19:41	20:35	1:53	33°39,600'N	174°45,063'E	2682	33°39,615'N	174°45,044'E	2682	33°39,614'N	174°45,047'E	2682	2687	29	
SO264-8	-2	SO264-8-2	E' of Kimmei Seamount	GC10	12.07.18	21:28	22:15	23:32	2:04	33°39,614'N	174°45,041'E	2682	33°39,616'N	174°45,044'E	2682	33°39,662'N	174°45,041'E	2682	2712	71	9.72
SO264-8	-3	SO264-8-3	E' of Kimmei Seamount	MSN	12./13.07.18	23:59	0:05	0:18	0:19	33°39,269'N	174°46,160'E	2715	33°39,271'N	174°46,167'E	2716	33°39,271'N	174°46,166'E	2715	100		
SO264-8	-4	SO264-8-4	E' of Kimmei Seamount	CTD	13.07.18	00:40	1:49	2:51	2:11	33°39,272'N	174°46,150'E	2716	33°39,267'N	174°46,164'E	2716	33°39,266'N	174°46,164'E	2716	2682		
SO264-8	-5	SO264-8-5	E' of Kimmei Seamount	MSN	13.07.18	03:01	3:33	4:13	1:12	33°39,270'N	174°46,168'E	2716	33°39,263'N	174°46,165'E	2720	33°39,263'N	174°46,159'E	2715	800		
SO264-9	-1	SO264-9-1	Koko Seamount	TV-MUC	13.07.18	18:39	19:58	21:11	2:32	34°46,964'N	172°20,993'E	3866	34°46,982'N	172°20,986'E	3866	34°46,982'N	172°20,978'E	3866	3871	40	
SO264-9	-2	SO264-9-2	Koko Seamount	PC20	13.07.18	21:48	23:24	0:57	3:09	34°46,977'N	172°20,983'E	3865	34°46,977'N	172°20,987'E	3865	34°46,980'N	172°20,981'E	3865	3859.7	83	15.7
SO264-10	-1	SO264-10-1	Koko Seamount	TV-MUC	14.07.18	05:58	6:27	6:59	1:01	34°55,535'N	172°08,797'E	1599	34°55,551'N	172°08,745'E	1599	34°55,550'N	172°08,754'E	1599	1581	29	
SO264-10	-2	SO264-10-2	Koko Seamount	GC10	14.07.18	07:18	7:45	8:19	1:01	34°55,554'N	172°08,748'E	1573	34°55,752'N	172°08,752'E	1573	34°55,581'N	172°08,749'E	1573	1577	39	0
SO264-11	-1	SO264-11-1	Koko Seamount	MSN	14.07.18	16:29	16:32	16:49	0:20	35°31,574'N	172°23,336'E	4112	35°31,573'N	172°23,333'E	4089	35°31,570'N	172°23,327'E	4096	100		
SO264-11	-2	SO264-11-2	Koko Seamount	CTD	14.07.18	17:08	18:50	20:32	3:24	35°31,571'N	172°23,328'E	4001	35°31,441'N	172°23,220'E	4001	35°31,442'N	172°23,216'E	4001	3976		
SO264-11	-3	SO264-11-3	Koko Seamount	MSN	14.07.18	20:40	21:07	21:46	1:06	35°31,439'N	172°23,216'E	3992	35°31,444'N	172°23,220'E	3997	35°31,440'N	172°23,214'E	3984.6	800		
SO264-12	-1	SO264-12-1	Koko Seamount	TV-MUC	15.07.18	00:46	1:24	1:44	0:58	35°07,278'N	172°02,174'E	1078.9	35°07,251'N	172°02,184'E	1078.9	35°07,254'N	172°02,183'E	1078.9	1091	14.6	
SO264-12	-2	SO264-12-2	Koko Seamount	GC5	15.07.18	02:10	2:31	2:49	0:39	35°07,247'N	172°02,188'E	1077.4	35°07,250'N	172°02,191'E	1077.4	35°07,254'N	172°02,140'E	1077.4	1082	16.6	0
SO264-13	-1	SO264-13-1	Ojin & Jingu Seamount	TV-MUC	16.07.18	00:55	2:17	3:25	2:30	37°47,865'N	170°43,238'E	3933	37°47,860'N	170°43,221'E	3933	37°47,860'N	170°43,224'E	3933	3945	49	
SO264-13	-2	SO264-13-2	Ojin & Jingu Seamount	PC20	16.07.18	04:09	5:32	6:41	2:32	37°47,865'N	170°43,227'E	3935	37°47,865'N	170°43,227'E	3935	37°47,862'N	170°43,217'E	3935	3930	87	13.81
SO264-13	-3	SO264-13-3	Ojin & Jingu Seamount	MSN	16.07.18	07:58	8:03	8:15	0:17	37°47,283'N	170°44,240'E	4026	37°47,283'N	170°44,249'E	4022	37°47,278'N	170°44,250'E	4020	100	1.1	
SO264-13	-4	SO264-13-4	Ojin & Jingu Seamount	CTD	16.07.18	08:30	10:12	11:50	3:20	37°47,275'N	170°44,241'E	4021	37°47,276'N	170°44,251'E	4021	37°47,283'N	170°44,250'E	4021	3999		
SO264-13	-5	SO264-13-5	Ojin & Jingu Seamount	MSN	16.07.18	11:58	12:24	13:04	1:06	37°47,284'N	170°44,250'E	4029	37°47,278'N	170°44,249'E	4016	37°47,276'N	170°44,240'E	4019	700	1.2	
SO264-14	-1	SO264-14-1	Nintoku Seamount	GC20	17.07.18	07:39	8:39	9:47	2:08	40°50,041'N	170°54,191'E	3750	40°50,034'N	170°54,201'E	3750	40°50,033'N	170°54,196'E	3750	3766	94	18.41
SO264-14	-2	SO264-14-2	Nintoku Seamount	MUC	17.07.18	09:51	10:58	13:45	3:54	40°50,041'N	170°54,192'E	3739	40°50,038'N	170°54,189'E	3739	40°50,033'N	170°54,193'E	3739	3765	43	
SO264-15	-1	SO264-15-1	E' of Ninigi Seamount	TV-MUC	17.07.18	18:50	20:03	21:13	2:23	41°36,911'N	170°25,341'E	3668	41°36,914'N	170°25,343'E	3668	41°36,920'N	170°25,344'E	3668	3686	47	
SO264-15	-2	SO264-15-2	E' of Ninigi Seamount	GC20	18.07.18	04:44	5:41	6:49	2:05	41°36,937'N	170°25,359'E	3662	41°36,917'N	170°25,340'E	3662	41°36,912'N	170°25,345'E	3662	3706	82	14.48
SO264-16	-1	SO264-16-1	E' of Ninigi Seamount	TV-MUC	17./18.07.18	21:45	23:00	0:11	2:26	41°34,904'N	170°25,776'E	3570	41°34,910'N	170°25,781'E	3570	41°34,913'N	170°25,781'E	3570	3588	46	
SO264-16	-2	SO264-16-2	E' of Ninigi Seamount	PC20	18.07.18	00:50	1:58	3:45	2:55	41°34,913'N	170°25,787'E	3572	41°34,914'N	170°25,783'E	3572	41°34,914'N	170°25,783'E	3572	3568	77	14.8
SO264-17	-1	SO264-17-1	Godeigo Seamount	TV-MUC	18.07.18	17:58	18:39	19:43	1:45	41°49,766'N	170°29,149'E	2072	41°49,691'N	170°29,236'E	2072	41°49,688'N	170°29,137'E	2072	./.	./.	
SO264-18	-1	SO264-18-1	Nintoku Seamount	TV-MUC	18.07.18	22:39	23:17	23:57	1:18	41°20,040'N	170°22,444'E	1313	41°20,037'N	170°22,438'E	1313	41°20,041'N	170°22,436'E	1313	1321	38.5	
SO264-18	-2	SO264-18-2	Nintoku Seamount	GC5	19.07.18	00:00	0:30	0:56	0:56	41°20,043'N	170°22,443'E	1313	41°20,042'N	170°22,441'E	1313	41°20,041'N	170°22,446'E	1313	1320	21	0
SO264-19	-1	SO264-19-1	W' of Nintoku Seamount	MUC	19.07.18	05:37	7:09	8:52	3:15	41°32,766'N	169°55,724'E	5304	41°32,784'N	169°55,732'E	5304	41°32,784'N	169°55,728'E	5304	5337	59	
SO264-19	-2	SO264-19-2	W' of Nintoku Seamount	GC20	19.07.18	08:55	10:14	11:43	2:48	41°32,783'N	169°55,733'E	5311	41°32,784'N	169°55,7							

SO264-23	-2	SO264-23-2	Suiko Seamount	PC20	22.07.18	04:28	6:01	7:22	2:54	44°48,835'N	170°36,781'E	4245	44°48,832'N	170°36,784'E	4245	44°48,831'N	170°36,781'E	4245	4240	83	16.29
SO264-24	-1	SO264-24-1	Suiko Seamount	MSN	22.07.18	08:59	9:03	9:16	0:17	44°48,051'N	170°35,837'E	4303	44°48,051'N	170°35,841'E	4299	44°48,059'N	170°35,860'E	4298	100		
SO264-24	-2	SO264-24-2	Suiko Seamount	CTD	22.07.18	09:30	11:18	12:52	3:22	44°48,067'N	170°35,864'E	4304	44°48,063'N	170°35,867'E	4304	44°48,065'N	170°35,868'E	4304	4265		
SO264-24	-3	SO264-24-3	Suiko Seamount	GC20	22.07.18	12:59	14:15	15:27	2:28	44°48,066'N	170°35,862'E	4295	44°48,061'N	170°35,877'E	4295	44°48,065'N	170°35,864'E	4295	4345	97	14.8
SO264-24	-4	SO264-24-4	Suiko Seamount	MSN	22.07.18	16:02	16:32	17:09	1:07	44°47,134'N	170°35,442'E	4410	44°47,129'N	170°35,453'E	4411	44°47,129'N	170°35,454'E	4411	750	3.2	
SO264-24	-5	SO264-24-5	Suiko Seamount	MSN	22.07.18	17:45	18:09	19:05	1:20	44°47,127'N	170°35,448'E	4410	44°47,129'N	170°35,449'E	4409	44°47,130'N	170°35,450'E	4411	750	1	
SO264-25	-1	SO264-25-1	Suiko Seamount	TV-MUC	23.07.18	00:08	0:56	1:50	1:42	44°46,353'N	170°07,960'E	1819	44°46,339'N	170°07,987'E	1819	44°46,341'N	170°07,979'E	1819	1804	32.5	
SO264-25	-2	SO264-25-2	Suiko Seamount	PC20	23.07.18	02:03	2:52	3:43	1:40	44°46,341'N	170°07,987'E	1788	44°46,345'N	170°07,978'E	1788	44°46,344'N	170°07,981'E	1788	1780	65	
SO264-26	-1	SO264-26-1	Suiko Seamount	MUC	23.07.18	04:14	4:46	5:20	1:06	44°46,424'N	170°10,287'E	1772	44°46,405'N	170°10,318'E	1772	44°46,413'N	170°10,325'E	1772	1786	33	
SO264-26	-2	SO264-26-2	Suiko Seamount	GC20	23.07.18	05:29	6:00	6:31	1:02	44°46,412'N	170°10,327'E	1771	44°46,412'N	170°10,325'E	1771	44°46,407'N	170°10,320'E	1771	1791	74	16.43
SO264-27 (=25)	-1	SO264-27-1	Suiko Seamount	GC20	23.07.18	07:19	7:50	8:22	1:03	44°46,333'N	170°07,986'E	1788	44°46,338'N	170°07,984'E	1788	44°46,336'N	170°07,973'E	1788	1808	43	0
SO264-28	-1	SO264-28-1	Suiko Seamount	MUC	23.07.18	19:30	20:16	20:56	1:26	44°51,547'N	170°03,912'E	1935	44°51,551'N	170°03,989'E	1935	44°51,547'N	170°03,997'E	1935	1940	38	
SO264-28	-2	SO264-28-2	Suiko Seamount	GC10	23.07.18	20:57	21:31	22:09	1:12	44°51,547'N	170°03,997'E	1935	44°51,546'N	170°03,983'E	1935	44°51,542'N	170°03,984'E	1935	1957	67	7.635
SO264-29	-1	SO264-29-1	Suiko Seamount	GC10	24.07.18	23:05	23:41	0:16	1:11	44°52,027'N	170°03,837'E	1966	44°52,020'N	170°03,835'E	1966	44°52,020'N	170°03,831'E	1966	1994	61	8.7
SO264-29	-2	SO264-29-2	Suiko Seamount	MUC	24.07.18	00:19	1:01	1:39	1:20	44°52,030'N	170°03,830'E	1965	44°52,026'N	170°03,842'E	1965	44°52,022'N	170°03,836'E	1965	1985	38	
SO264-30	-1	SO264-30-1	Suiko Seamount	MUC	24.07.18	02:30	3:08	3:45	1:15	44°46,466'N	170°01,090'E	1857	44°46,466'N	170°01,090'E	1857	44°46,468'N	170°01,090'E	1857	1876	37	
SO264-30	-2	SO264-30-2	Suiko Seamount	GC20	24.07.18	04:03	4:22	4:58	0:55	44°46,467'N	170°01,088'E	1857	44°46,465'N	170°01,094'E	1857	44°46,468'N	170°01,086'E	1857	1874	67	19.23
SO264-31	-1	SO264-31-1	Suiko Seamount	GC20	24.07.18	05:49	6:23	6:58	1:09	44°51,161'N	170°07,699'E	1942	44°51,161'N	170°07,650'E	1942	44°51,151'N	170°07,648'E	1942	1966	61	13.21
SO264-31	-2	SO264-31-2	Suiko Seamount	MUC	24.07.18	07:12	7:48	8:28	1:16	44°51,154'N	170°07,648'E	1941	44°51,159'N	170°07,659'E	1941	44°51,158'N	170°07,659'E	1941	1958	37	
SO264-32	-1	SO264-32-1	Suiko Seamount	MUC	24.07.18	19:06	20:05	21:04	1:58	44°59,774'N	170°24,318'E	3203	44°59,773'N	170°24,285'E	3203	44°59,775'N	170°24,288'E	3203	3231	41	
SO264-32	-2	SO264-32-2	Suiko Seamount	GC20	24.07.18	21:12	22:00	22:52	1:40	44°59,777'N	170°24,285'E	3200	44°59,781'N	170°24,280'E	3200	44°59,781'N	170°24,280'E	3200	3237	86	19.32
SO264-33	-1	SO264-33-1	Suiko Seamount	MUC	24./25.07.18	23:34	0:32	1:30	1:56	44°58,289'N	170°21,032'E	3141	44°58,290'N	170°21,027'E	3141	44°58,286'N	170°21,021'E	3141	3170	36	
SO264-33	-2	SO264-33-2	Suiko Seamount	GC20	25.07.18	01:35	2:30	3:24	1:49	44°58,286'N	170°21,019'E	3141	44°58,290'N	170°21,024'E	3141	44°58,291'N	170°21,018'E	3141	3139	78	17.38
SO264-34	-1	SO264-34-1	Suiko Seamount	MUC	25.07.18	05:09	5:56	6:46	1:37	45°01,852'N	170°13,553'E	2622	45°01,850'N	170°13,549'E	2622	45°01,849'N	170°13,552'E	2622	2648	45	
SO264-34	-2	SO264-34-2	Suiko Seamount	GC10	25.07.18	06:52	7:35	8:19	1:27	45°01,851'N	170°13,548'E	2622	45°01,852'N	170°13,553'E	2622	45°01,853'N	170°13,553'E	2622	2647	51	1.95
SO264-35	-1	SO264-35-1	Suiko Seamount	MSN	25.07.18	18:44	18:50	18:59	0:15	44°46,372'N	170°10,365'E	1769	44°46,372'N	170°10,365'E	1769	44°46,407'N	170°10,327'E	1770	100	1.1	
SO264-35	-2	SO264-35-2	Suiko Seamount	CTD	25./26.07.18	19:16	20:03	4:06	8:50	44°46,142'N	170°10,295'E	1730	44°46,142'N	170°10,290'E	1730	44°46,147'N	170°10,300'E	1730	1730		
SO264-36	-1	SO264-36-1	Suiko Seamount	BC6	28.07.18	21:30	22:00	22:45	1:15	44°46,409'N	170°10,319'E	1771	44°46,409'N	170°10,319'E	1771	44°46,405'N	170°10,319'E	1771	1794	93	4.9
SO264-37	-1	SO264-37-1	Suiko Seamount	BC6	28./29.07.18	23:51	0:30	1:30	1:39	44°52,027'N	170°03,836'E	1966	44°52,027'N	170°03,838'E	1966	44°52,026'N	170°03,834'E	1966	1983	47	
SO264-38 (=36)	-1	SO264-38-1	Suiko Seamount	GKG	29.07.18	02:50	3:22	4:04	1:14	44°46,430'N	170°10,349'E	1771	44°46,414'N	170°10,317'E	1771	44°46,413'N	170°10,323'E	1771	1790	39	
SO264-39	-1	SO264-39-1	Suiko Seamount	BC6	29.07.18	05:28	6:26	7:29	2:01	44°58,283'N	170°21,053'E	3143	44°58,296'N	170°21,025'E	3143	44°58,286'N	170°21,022'E	3143	3176	85	5.17
SO264-39	-2	SO264-39-2	Suiko Seamount	GKG	29.07.18	07:52	8:49	9:49	1:57	44°58,288'N	170°21,023'E	3141	44°58,294'N	170°21,028'E	3141	44°58,290'N	170°21,027'E	3141	3166	37	
SO264-39	-3	SO264-39-3	Suiko Seamount	GKG	29.07.18	09:59	10:55	11:56	1:57	44°58,286'N	170°21,022'E	3142	44°58,295'N	170°21,025'E	3142	44°58,290'N	170°21,021'E	3142	3173	59	
SO264-40	-1	SO264-40-1	Suiko Seamount	MSN	29.07.18	15:22	15:28	15:43	0:21	45°34,024'N	170°18,018'E	5401	45°34,007'N	170°18,008'E	5401	45°33,997'N	170°18,010'E	5406	100	1.1	
SO264-40	-2	SO264-40-2	Suiko Seamount	CTD	29.07.18	15:57	18:13	20:01	4:04	45°34,003'N	170°18,005'E	5401	45°34,002'N	170°18,003'E	5401	45°33,995'N	170°18,004'E	5401	5367	27.7	
SO264-40	-3	SO264-40-3	Suiko Seamount	MSN	29.07.18	20:07	20:33	21:11	1:04	45°33,993'N	170°18,007'E	5401	45°34,004'N	170°18,003'E	5409.3	45°34,003'N	170°18,000'E	5401	700	3.3	
SO264-41	-1	SO264-41-1	Suiko Seamount	MUC	29/30.07.18	22:33	23:43	0:51	2:18	45°41,968'N	170°09,314'E	3641	45°41,947'N	170°09,306'E	3641	45°41,947'N	170°09,305'E	3641	3672	43	
SO264-41	-2	SO264-41-2	Suiko Seamount	GC20	30.07.18	00:52	2:04	3:08	2:16	45°41,947'N	170°09,305'E	3645	45°41,942'N	170°09,300'E	3645	45°41,942'N	170°09,296'E	3645	3678	84	9.47
SO264-42	-1	SO264-42-1	Jimmu Seamount	TV-MUC	30.07.18	21:31	22:33	23:34	2:03	46°10,139'N	169°10,072'E	3024	46°10,136'N	169°10,067'E	3024	46°10,139'N	169°10,067'E	3024	3036	33.7	
SO264-42	-2	SO264-42-2	Jimmu Seamount	GC15	30./31.07.18	23:44	0:37	1:28	1:44	46°10,143'N	169°10,069'E	3021	46°10,140'N	169°10,067'E	3021	46°10,140'N	169°10,067'E	3021	3058	72	11.55
SO264-43	-1	SO264-43-1	Jimmu Seamount	TV-MUC	31.07.18	02:16	3:23	4:28	2:12	46°06,564'N	169°07,184'E	3242	46°06,577'N	169°07,190'E	3242	46°06,577'N	169°07,187'E	3242	3299	36.1	
SO264-43	-2	SO264-43-2	Jimmu Seamount	GC15	31.07.18	04:42	5:36	6:33	1:51	46°06,569'N	169°07,191'E	3239	46°06,576'N	169°07,193'E	3239	46°06,574'N	169°07,186'E	3239	3271	76	5.13
SO264-44	-1	SO264-44-1	Jimmu Seamount	TV-MUC	31.07.18	21:12	21:58	22:39	1:27	46°15,301'N	169°20,063'E	1892	46°15,306'N	169°20,064'E	1892	46°15,299'N	169°20,056'E	1892	1904	23.1	
SO264-44	-2	SO264-44-2	Jimmu Seamount	GC 5	31.07./01.08.18	22:50	23:51	0:02	1:12	46°15,297'N	169°20,066'E	1893	46°15,298'N	169°20,062'E	1893	46°15,305'N	169°20,061'E	1893	1917	32	2.31
SO264-44	-3	SO264-44-3	Jimmu Seamount	GC 10	01.08.18	00:07	0:38	1:27	1:20	46°19,304'N	169°20,062'E	1894	46°15,307'N	169°20,064'E	1894	46°15,305'N	169°20,059'E	1894	1913	60	9.26
SO264-45	-1	SO264-45-1	Minnetonka Seamount	MUC	01.08.18	07:18	8:03	8:49	1:31	46°33,744'N	169°36,710'E	2423	46°33,745'N	169°36,072'E	2423	46°33,802'N	169°36,069'E	2423	2446	42	
SO264-45	-2	SO264-45-2	Minnetonka Seamount	GC 10	01.08.18	08:58	9:33	10:13	1:15	46°33,796'N	169°36,071'E	2425	46°33,792'N	169°36,072'E	2425	46°33,800'N	169°36,069'E	2425	2449	60	8.35
SO264-46	-1	SO264-46-1	Minnetonka Seamount	MSN	01.08.18	18:29	18:33	18:46	0:17	46°48,924'N	169°24,709'E	3992	46°48,922'N	169°24,707'E	4000	46°48,918'N	169°24,707'E	3993	100	1.1	
SO264-46	-2	SO264-46-2	Minnetonka Seamount	CTD	01.08.18	19:02	20:42	22:18	3:16	46°48,942'N	169°24,653'E	3992	46°48,942'N	169°24,660'E	3992	46°48,937'N	169°24,668'E	3992	3960	21.5	
SO264-46	-3	SO264-46-3	Minnetonka Seamount																		

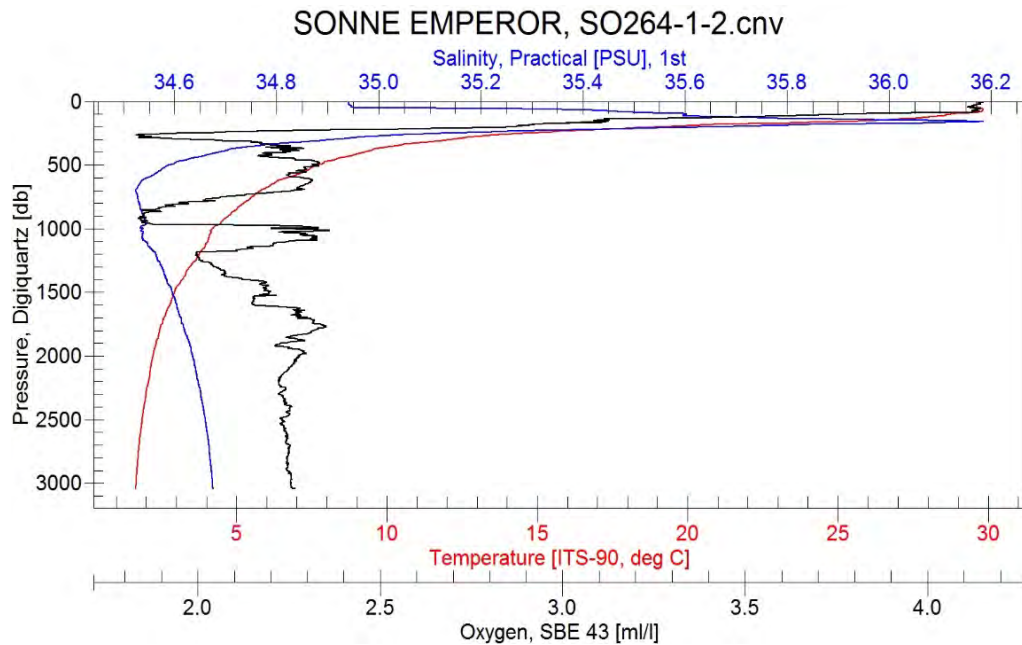
SO264-52	-2	SO264-52-2	Minnetonka Seamount	GC11	05.08.18	05:38	6:23	7:11	1:33	47°07,273'N	169°09,874'E	2752	47°07,271'N	169°09,869'E	2752	47°07,270'N	169°09,873'E	2752	2790	65	8
SO264-53	-1	SO264-53-1	Minnetonka Seamount	MUC	05.08.18	18:36	19:20	20:04	1:28	47°38,940'N	169°20,429'E	2325	47°38,930'N	169°29,415'E	2325	47°38,929'N	169°20,418'E	2325	2347	32	
SO264-53	-2	SO264-53-2	Minnetonka Seamount	GC11	05.08.18	20:10	20:49	21:50	1:40	47°38,931'N	169°20,417'E	2325	47°38,934'N	169°20,417'E	2325	47°38,933'N	169°20,425'E	2325	2360	63	8.63
SO264-54	-1	SO264-54-1	Minnetonka Seamount	TV-MUC	05./06.08.18	22:37	23:25	0:08	1:31	47°37,321'N	169°14,898'E	2127	47°37,319'N	169°14,853'E	2127	47°37,321'N	169°14,848'E	2127	2145	30	
SO264-54	-2	SO264-54-2	Minnetonka Seamount	PC15	06.08.18	00:12	1:22	2:16	2:04	47°37,321'N	169°14,848'E	2139	47°37,318'N	169°14,852'E	2139	47°37,324'N	169°14,847'E	2139	2129	62	11.43
SO264-55 (=51)	-1	SO264-55-1	Minnetonka Seamount	PC20	06./07.08.18	22:07	23:15	0:23	2:16	47°10,542'N	169°25,292'E	2936	47°10,553'N	169°25,291'E	2936	47°10,548'N	169°25,284'E	2936	2925	94	16.11
SO264-56	-1	SO264-56-1	Minnetonka Seamount	MUC	07.08.18	07:54	9:06	10:19	2:25	47°44,766'N	168°40,383'E	3946	47°44,754'N	168°40,397'E	3946	47°44,759'N	168°40,409'E	3946	3978	47	
SO264-56	-2	SO264-56-2	Minnetonka Seamount	GC20	07.08.18	10:24	11:26	12:31	2:07	47°44,754'N	168°40,407'E	3973	47°44,752'N	168°40,398'E	3973	47°44,758'N	168°40,404'E	3973	3989	92	12.66
SO264-57	-1	SO264-57-1	Tenji Seamount	MUC	07.08.18	20:01	20:45	21:30	1:29	48°50,730'N	168°28,972'E	2355	48°50,814'N	168°29,006'E	2355	48°50,814'N	168°29,001'E	2355	2377	33	
SO264-57	-2	SO264-57-2	Tenji Seamount	PC20	07.08.18	21:32	22:38	23:30	1:58	48°50,814'N	168°29,003'E	2356	48°50,815'N	168°29,998'E	2356	48°50,817'N	168°29,006'E	2356	2347	76	15.4
SO264-58	-1	SO264-58-1	Tenji Seamount	MUC	08.08.18	03:14	4:03	5:00	1:46	48°59,166'N	168°29,719'E	2588	48°59,181'N	168°29,776'E	2588	48°59,184'N	168°29,780'E	2588	2609	33	
SO264-58	-2	SO264-58-2	Tenji Seamount	PC20	08.08.18	05:15	6:20	7:15	2:00	48°59,186'N	168°29,779'E	2594	48°59,189'N	168°29,773'E	2594	48°59,185'N	168°29,780'E	2594	2578	67	17
SO264-59	-1	SO264-59-1	Tenji Seamount	MUC	08.08.18	10:02	10:59	11:55	1:53	49°04,963'N	168°30,304'E	2916	49°04,961'N	168°30,319'E	2916	49°04,957'N	168°30,316'E	2916	2938	35	
SO264-59	-2	SO264-59-2	Tenji Seamount	GC20	08.08.18	11:58	12:45	13:35	1:37	49°04,957'N	168°30,314'E	2930	49°04,960'N	168°30,299'E	2930	49°04,958'N	168°30,316'E	2930	2943	84	13.36
SO264-60	-1	SO264-60-1	Tenji Seamount	MSN	08.08.18	16:05	16:35	17:12	1:07	49°18,438'N	168°33,411'E	5269.9	49°18,436'N	168°33,423'E	5270	49°18,443'N	168°33,416'E	5285	700	3.1	
SO264-60	-2	SO264-60-2	Tenji Seamount	CTD	08.08.18	17:30	19:31	21:33	4:03	49°18,442'N	168°33,426'E	5270	49°18,448'N	168°33,431'E	5270	49°18,452'N	168°33,426'E	5270	5240	28.6	
SO264-60	-3	SO264-60-3	Tenji Seamount	MSN	08.08.18	21:45	22:08	22:45	1:00	49°18,449'N	168°33,422'E	5273.6	49°18,446'N	168°33,440'E	5270.1	49°18,450'N	168°33,428'E	5269.3	700	3.1	
SO264-60	-4	SO264-60-4	Tenji Seamount	MSN	08./09.08.18	23:09	23:23	1:48	2:39	49°18,451'N	168°33,429'E	5278.6	49°18,441'N	168°33,435'E	5277	49°18,444'N	168°33,415'E	5276	700	3.1	
SO264-60	-5	SO264-60-5	Tenji Seamount	MSN	09.08.18	02:09	2:34	5:27	3:18	49°18,447'N	168°33,427'E	5266	49°18,446'N	168°33,430'E	5273	49°18,447'N	168°33,424'E	5269	700	3.1	
SO264-60	-6	SO264-60-6	Tenji Seamount	MSN	09.08.18	05:58	6:24	9:07	3:09	49°18,444'N	168°33,416'E	5273.6	49°18,450'N	168°33,427'E	5274.9	49°18,448'N	168°33,420'E	5280.1	700	3.1	
SO264-60	-7	SO264-60-7	Tenji Seamount	MSN	09.08.18	09:31	9:56	12:44	3:13	49°18,444'N	168°33,434'E	5275.3	49°18,445'N	168°33,428'E	5269	49°18,445'N	168°33,431'E	5270.5	700	1.2	
SO264-60	-8	SO264-60-8	Tenji Seamount	MSN	09.08.18	13:01	13:30	16:29	3:28	49°18,443'N	168°33,435'E	5275	49°18,447'N	168°33,418'E	5272	49°18,448'N	168°33,431'E	5269	700	1.3	
SO264-60	-9	SO264-60-9	Tenji Seamount	MSN	09.08.18	16:45	17:11	20:01	3:16	49°18,448'N	168°33,471'E	5268	49°18,450'N	168°33,434'E	5266	49°18,449'N	168°33,422'E	5261	700	2.1	
SO264-60	-10	SO264-60-10	Tenji Seamount	MSN	09.08.18	20:20	20:47	23:32	3:12	49°18,449'N	168°33,425'E	5268.7	49°18,441'N	168°33,434'E	5264.9	49°18,441'N	168°33,436'E	5261.3	700	1.1	
SO264-60	-11	SO264-60-11	Tenji Seamount	MSN	09./10.08.2018	23:51	0:18	3:05	3:14	49°18,444'N	168°33,431'E	5277.3	49°18,445'N	168°33,433'E	5263.4	49°18,448'N	168°33,425'E	5281.4	700	1.1	
SO264-60	-12	SO264-60-12	Tenji Seamount	GC15	10.08.18	03:25	4:47	6:40	3:15	49°18,447'N	168°33,427'E	5275	49°18,444'N	168°33,426'E	5275	49°18,446'N	168°33,422'E	5275	5313	102	10.57
SO264-60	-13	SO264-60-13	Tenji Seamount	GC15	10.08.18	06:56	8:18	9:45	2:49	49°18,445'N	168°33,437'E	5274	49°18,448'N	168°33,430'E	5274	49°18,448'N	168°33,423'E	5274	5316	95	10.25
SO264-60	-14	SO264-60-14	Tenji Seamount	MUC	10.08.18	09:52	11:25	13:00	3:08	49°18,450'N	168°33,422'E	5270	49°18,442'N	168°33,434'E	5270	49°18,450'N	168°33,419'E	5270	5308	60	
SO264-61	-1	SO264-61-1	N' of Tenji Seamount	MUC	10.08.18	22:01	23:04	23:54	1:53	49°43,399'N	168°02,282'E	2590	49°43,401'N	168°02,272'E	2590	49°43,401'N	168°02,273'E	2590	2604	40.2	
SO264-61	-2	SO264-61-2	N' of Tenji Seamount	PC20	10./11.08.18	23:39	1:11	2:13	2:26	49°43,401'N	168°02,273'E	2591	49°43,399'N	168°02,272'E	2591	49°43,400'N	168°02,273'E	2591	2582	85	15.7
SO264-62	-1	SO264-62-1	N' of Tenji Seamount	TV-MUC	11.08.18	05:35	6:22	7:08	1:33	49°43,810'N	168°18,878'E	2378	49°43,847'N	168°18,921'E	2378	49°43,845'N	168°18,927'E	2378	2384	32.5	
SO264-62	-2	SO264-62-2	N' of Tenji Seamount	PC20	11.08.18	07:22	8:22	9:11	1:49	49°43,848'N	168°18,922'E	2373	49°43,840'N	168°18,918'E	2373	49°43,841'N	168°18,920'E	2373	2363	76	15.5
SO264-63	-1	SO264-63-1	Tenji Seamount	MUC	11.08.18	21:30	22:39	23:50	2:20	49°48,762'N	168°38,731'E	3772	49°48,761'N	168°38,731'E	3772	49°48,767'N	168°38,732'E	3772	3802	46	
SO264-63	-2	SO264-63-2	Tenji Seamount	PC20	11./12.08.18	23:51	1:25	2:48	3:57	49°48,766'N	168°38,731'E	3779	49°48,760'N	168°38,731'E	3779	49°48,762'N	168°38,720'E	3779	3774	66	18.22
SO264-64	-1	SO264-64-1	S' of Detroit Seamount	PC20	12.08.18	06:14	7:22	8:29	2:15	49°59,488'N	168°13,466'E	3495	49°59,494'N	168°13,468'E	3495	49°59,495'N	168°13,467'E	3495	3486	63	18.55
SO264-64	-2	SO264-64-2	S' of Detroit Seamount	MUC	12.08.18	08:43	9:47	10:55	2:12	49°59,487'N	168°13,467'E	3492	49°59,490'N	168°13,465'E	3492	49°59,492'N	168°13,472'E	3492	3513	43	
SO264-65	-1	SO264-65-1	S' of Detroit Seamount	MUC	12.08.18	21:10	22:02	22:50	1:40	50°21,501'N	168°13,328'E	2496	50°21,503'N	168°13,340'E	2496	50°21,530'N	168°13,355'E	2496	2522	34	
SO264-65	-2	SO264-65-2	S' of Detroit Seamount	PC20	12./13.08.13	22:53	23:56	0:53	2:00	50°21,531'N	168°13,353'E	2498	50°21,537'N	168°13,356'E	2498	50°21,534'N	168°13,344'E	2498	2492	56	13.41
SO265-66	-1	SO264-66-1	S' of Detroit Seamount	MUC	13.08.18	01:50	2:42	3:35	1:45	50°15,068'N	168°17,812'E	2747	50°15,065'N	168°17,834'E	2747	50°15,064'N	168°17,818'E	2747	2747	38	
SO265-66	-2	SO264-66-2	S' of Detroit Seamount	PC20	13.08.18	03:33	4:41	5:33	2:00	50°15,064'N	168°17,818'E	2751	50°15,067'N	168°17,821'E	2751	50°15,065'N	168°17,827'E	2751	2742	69	15.04
SO264-67	-1	SO264-67-1	Detroit Seamount	MSN	13.08.18	07:50	7:54	8:06	0:16	50°14,677'N	168°35,180'E	5034	50°14,680'N	168°35,175'E	5031	50°14,696'N	168°35,161'E	5031	100	0.9	
SO264-67	-2	SO264-67-2	Detroit Seamount	CTD	13.08.18	08:18	10:22	12:02	3:44	50°14,698'N	168°35,153'E	5034	50°14,701'N	168°35,172'E	5034	50°14,703'N	168°35,154'E	5034	4993	27.5	
SO264-67	-3	SO264-67-3	Detroit Seamount	MSN	13.08.18	12:05	12:26	12:59	0:54	50°14,702'N	168°35,160'E	5029	50°14,702'N	168°35,163'E	5033.4	50°14,701'N	168°35,161'E	5032	5030.3	2.7	
SO264-68	-1	SO264-68-1	Detroit Seamount	MUC	13.08.18	19:17	20:18	21:22	2:05	50°29,039'N	167°51,577'E	3285	50°29,040'N	167°51,501'E	3285	50°29,040'N	167°51,494'E	3285	3306	40	
SO264-68	-2	SO264-68-2	Detroit Seamount	PC20	13.08.18	21:22	22:42	23:58	2:36	50°29,040'N	167°51,494'E	3284	50°29,043'N	167°51,487'E	3284	50°29,033'N	167°51,496'E	3284	3275	71	18.01
SO264-69	-1	SO264-69-1	Detroit Seamount	MUC	14.08.18	00:38	1:40	2:44	2:06	50°30,874'N	167°55,488'E	3478	50°30,869'N	167°55,493'E	3478	50°30,881'N	167°55,487'E	3478	3508	42	
SO264-69	-2	SO264-69-2	Detroit Seamount	PC20	14.08.18	02:45	4:05	5:09	2:24	50°30,881'N	167°55,487'E	3473	50°30,877'N	167°55,478'E	3473	50°30,880'N	167°55,491'E	3473	3478	69	18.55
SO264-70	-1	SO264-70-1	Detroit Seamount	PC20	14.08.18	06:18	7:34	8:50	2:32	50°34,909'N	168°04,275'E	3917	50°34,915'N	168°04,292'E	3917	50°34,911'N	168°04,282'E	3917	3928	55	5
SO264-70	-2	SO264-70-2	Detroit Seamount	MUC	14.08.18	09:35	10:43	11:56	2:21	50°34,915'N	168°04,301'E	3916	50°34,910'N	168°04,294'E	3916	50°34,910'N	168°04,283'E	3916			

Appendix 5.2.1. Bottle summary and station plots.**A.5.2.1-1 SONNE EMPEROR SO264-1-2 CTD**

Latitude = 07° 00.46 S UTC (Time) = Jul 02 2018 19:18

Longitude = 179° 49.29 W Water depth 5338 m.

Bottle	Depth (m)	Pressure (dB)	Salinity (PSU)	Temp. (°C)	Oxygen (ml/l)	Density (Kg/m ³)	Fluo
1	3001.432	3040.021	34.675	1.652	2.257	27.754	0.015
2	3000.439	3039.008	34.675	1.653	2.256	27.754	0.011
3	3001.720	3040.314	34.675	1.652	2.258	27.754	0.016
4	2001.824	2022.774	34.636	2.209	2.278	27.674	0.010
5	2001.645	2022.592	34.636	2.210	2.277	27.674	0.027
6	2003.213	2024.184	34.636	2.210	2.276	27.674	0.014
7	1503.028	1516.950	34.594	2.933	2.201	27.577	0.013
8	1502.692	1516.610	34.594	2.934	2.205	27.577	0.020
9	1504.157	1518.094	34.594	2.933	2.196	27.577	0.014
10	1002.031	1010.096	34.535	4.199	2.237	27.404	0.000
11	1002.644	1010.716	34.536	4.199	2.226	27.404	0.007
12	1002.777	1010.850	34.536	4.200	2.220	27.404	0.001
13	501.222	504.645	34.573	7.470	2.305	27.023	-0.027
14	501.555	504.981	34.574	7.471	2.306	27.023	-0.024
15	501.219	504.642	34.573	7.471	2.303	27.023	-0.025
16	301.703	303.617	34.910	12.221	1.975	26.485	-0.066
17	301.567	303.480	34.909	12.216	1.956	26.485	-0.069
18	302.758	304.679	34.910	12.207	1.972	26.487	-0.067
19	126.303	127.050	35.839	27.179	3.160	23.302	0.489
20	127.616	128.371	35.838	27.183	3.134	23.300	0.454
21	127.056	127.808	35.831	27.217	3.154	23.284	0.491
22	27.679	27.836	34.943	29.620	4.134	21.815	-0.082
23	27.378	27.534	34.943	29.620	4.151	21.815	-0.080
24	27.805	27.963	34.943	29.621	4.136	21.815	-0.084



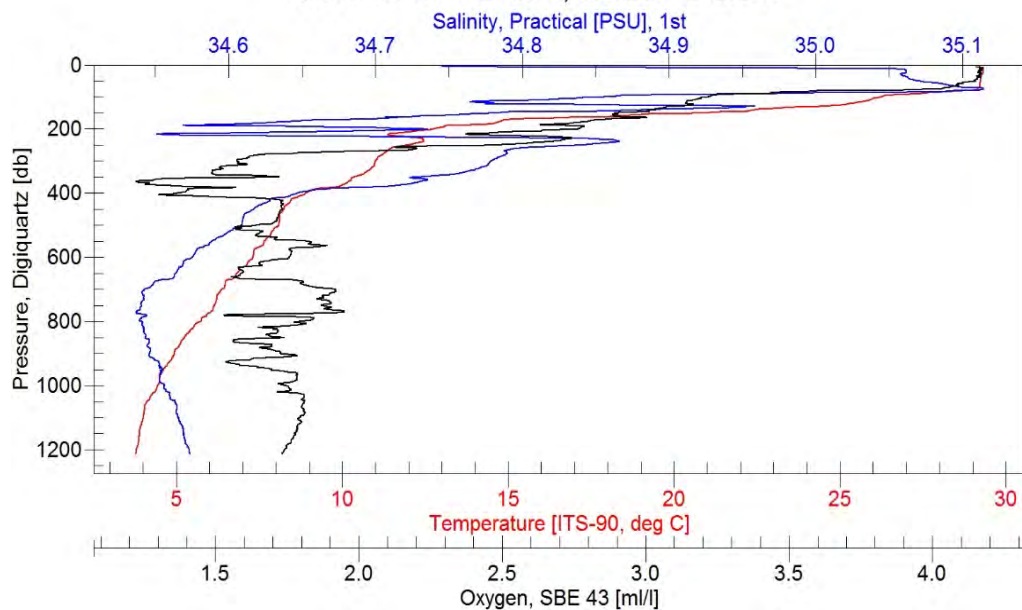
A.5.2.1-2 SONNE EMPEROR SO264-2-2 CTD

Latitude = 01° 46.99 N UTC (Time) = Jul 04 2018 20:40

Longitude = 179° 36.70 W Water depth 5612 m.

Bottle	Depth (m)	Pressure (dB)	Salinity (PSU)	Temp. (°C)	Oxygen (ml/l)	Density (Kg/m³)	Fluo
1	1202.412	1212.586	34.574	3.779	1.730	27.479	0.010
2	1003.486	1011.492	34.556	4.367	1.728	27.403	0.007
3	802.303	808.312	34.539	5.466	1.680	27.263	0.000
4	702.777	707.870	34.537	6.260	1.893	27.162	0.006
5	602.721	606.942	34.566	7.188	1.720	27.059	0.007
6	502.536	505.933	34.603	8.030	1.646	26.965	-0.005
7	402.063	404.681	34.641	8.943	1.391	26.853	-0.021
8	376.693	379.123	34.710	10.002	1.282	26.733	-0.038
9	351.835	354.083	34.727	10.388	1.616	26.679	-0.055
10	301.337	303.225	34.775	11.010	1.563	26.605	-0.035
11	251.229	252.773	34.840	12.084	2.541	26.455	-0.067
12	202.114	203.332	34.713	12.617	2.716	26.252	-0.069
13	180.998	182.079	34.605	14.490	2.724	25.783	-0.090
14	160.366	161.316	34.707	18.018	2.881	25.050	-0.090
15	140.229	141.053	34.873	22.641	3.019	23.948	-0.013
16	120.360	121.061	34.745	25.427	3.121	23.026	0.171
17	100.262	100.841	34.865	26.337	3.219	22.833	0.288
18	82.895	83.370	35.028	28.002	3.537	22.421	0.421
19	62.807	63.164	35.091	29.223	4.081	22.063	0.387
20	43.093	43.336	35.066	29.253	4.171	22.033	0.340
21	23.067	23.196	35.062	29.308	4.171	22.009	0.254
22	13.122	13.195	34.942	29.244	4.174	21.940	0.176
23	13.139	13.212	34.880	29.196	4.175	21.910	0.143
24	13.194	13.267	34.885	29.200	4.179	21.912	0.140

SONNE EMPEROR, SO264-2-2.cnv

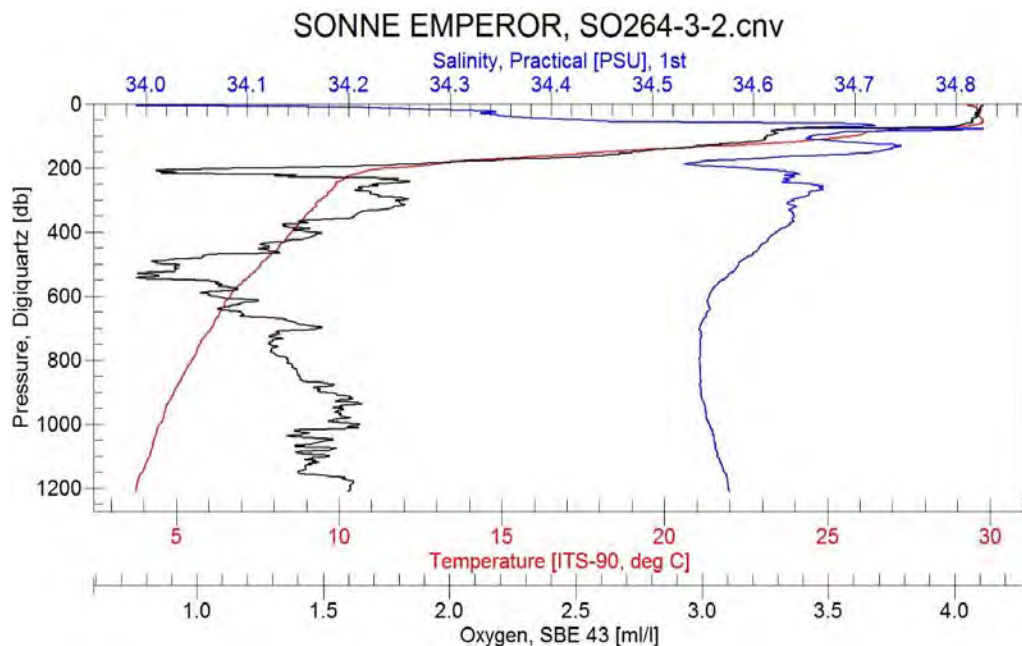


A.5.2.1-3 SONNE EMPEROR SO264-3-2 CTD

Latitude = 04° 30.57 N UTC (Time) = Jul 05 2018 13:38

Longitude = 179° 08.05 E Water depth 5683 m.

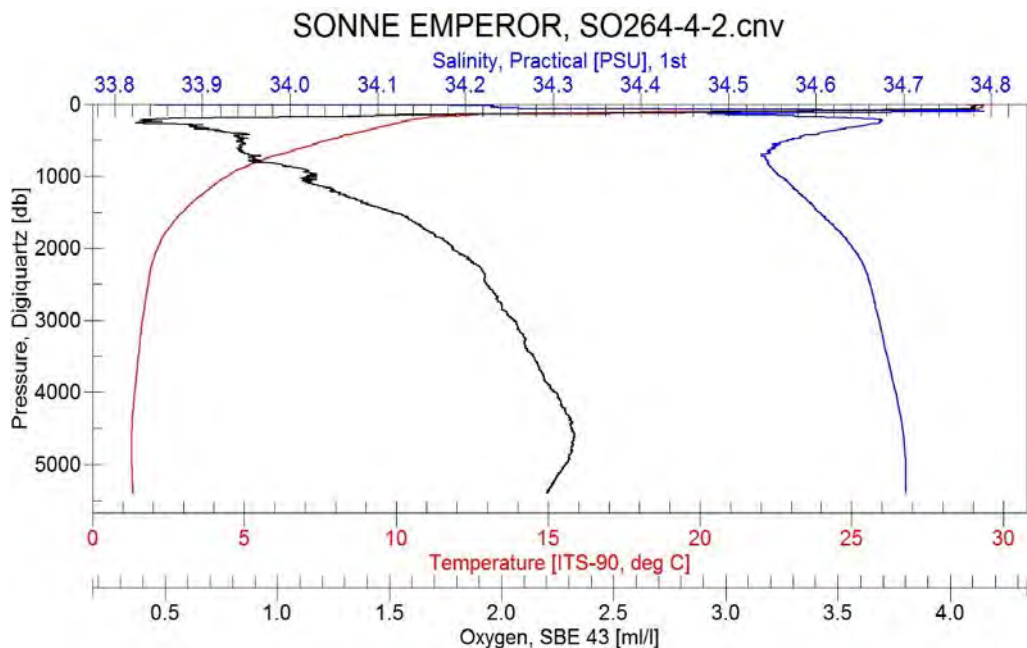
Bottle	Depth (m)	Pressure (dB)	Salinity (PSU)	Temp. (°C)	Oxygen (ml/l)	Density (Kg/m³)	Fluo
1	1200.394	1210.578	34.576	3.758	1.601	27.483	-0.001
2	1001.697	1009.712	34.556	4.446	1.610	27.394	-0.001
3	801.486	807.509	34.544	5.442	1.360	27.270	0.008
4	702.154	707.261	34.545	6.020	1.334	27.199	0.011
5	601.640	605.869	34.552	6.608	1.121	27.127	-0.004
6	502.316	505.725	34.580	7.551	0.917	27.017	-0.005
7	402.095	404.725	34.616	8.501	1.479	26.902	-0.023
8	377.219	379.663	34.628	8.680	1.348	26.884	-0.024
9	352.290	354.551	34.633	8.942	1.552	26.846	-0.031
10	302.026	303.927	34.631	9.320	1.797	26.783	-0.045
11	252.550	254.109	34.655	9.886	1.699	26.707	-0.055
12	202.165	203.388	34.626	10.682	0.909	26.546	-0.091
13	182.642	183.738	34.539	12.544	1.709	26.131	-0.082
14	162.197	163.163	34.605	15.525	2.400	25.557	0.025
15	142.508	143.350	34.703	18.811	2.773	24.848	0.072
16	122.295	123.012	34.697	22.347	3.073	23.897	0.154
17	102.066	102.659	34.655	25.926	3.246	22.803	0.391
18	81.993	82.465	34.603	28.089	3.791	22.073	0.514
19	62.555	62.912	34.559	29.743	4.071	21.489	0.075
20	42.162	42.401	34.354	29.699	4.081	21.348	-0.042
21	22.087	22.211	34.289	29.658	4.102	21.311	-0.089
22	12.312	12.381	34.209	29.557	4.105	21.284	-0.101
23	12.810	12.882	34.213	29.562	4.119	21.286	-0.113
24	12.919	12.991	34.212	29.562	4.107	21.285	-0.115



A.5.2.1-4 SONNE EMPEROR SO264-4-2 CTD

Latitude = 07° 19.74 N UTC (Time) = Jul 06 2018 06:44
 Longitude = 178° 44.61 E Water depth 5436 m.

Bottle	Depth (m)	Pressure (dB)	Salinity (PSU)	Temp. (°C)	Oxygen (ml/l)	Density (Kg/m³)	Fluo
1	5299.909	5396.738	34.703	1.334	2.199	27.816	0.019
2	5301.614	5398.495	34.703	1.334	2.196	27.816	0.014
3	5300.404	5397.249	34.703	1.334	2.205	27.816	0.013
4	4506.532	4580.523	34.700	1.289	2.329	27.810	0.017
5	4507.289	4581.301	34.700	1.289	2.324	27.810	0.015
6	4506.244	4580.227	34.700	1.289	2.327	27.810	0.016
7	3505.744	3555.040	34.683	1.492	2.158	27.775	0.021
8	3505.994	3555.295	34.682	1.492	2.155	27.775	0.022
9	3505.365	3554.652	34.683	1.492	2.160	27.775	0.019
10	2504.613	2533.863	34.662	1.825	1.942	27.728	0.037
11	2504.999	2534.256	34.662	1.825	1.944	27.728	0.023
12	2503.832	2533.068	34.662	1.825	1.943	27.728	0.020
13	1502.804	1516.735	34.605	2.874	1.559	27.591	0.034
14	1504.378	1518.329	34.605	2.875	1.557	27.591	0.039
15	1502.463	1516.389	34.605	2.877	1.556	27.590	0.035
16	1003.240	1011.325	34.558	4.375	1.180	27.404	0.036
17	1002.685	1010.765	34.558	4.376	1.183	27.403	0.032
18	1002.688	1010.768	34.558	4.377	1.184	27.403	0.041
19	503.138	506.580	34.564	7.825	0.842	26.965	0.004
20	502.169	505.603	34.566	7.790	0.841	26.971	0.004
21	502.743	506.182	34.565	7.800	0.842	26.970	0.013
22	102.621	103.223	34.714	19.531	2.888	24.671	0.353
23	102.733	103.336	34.717	19.444	2.903	24.696	0.347
24	102.587	103.189	34.709	19.604	2.911	24.648	0.349

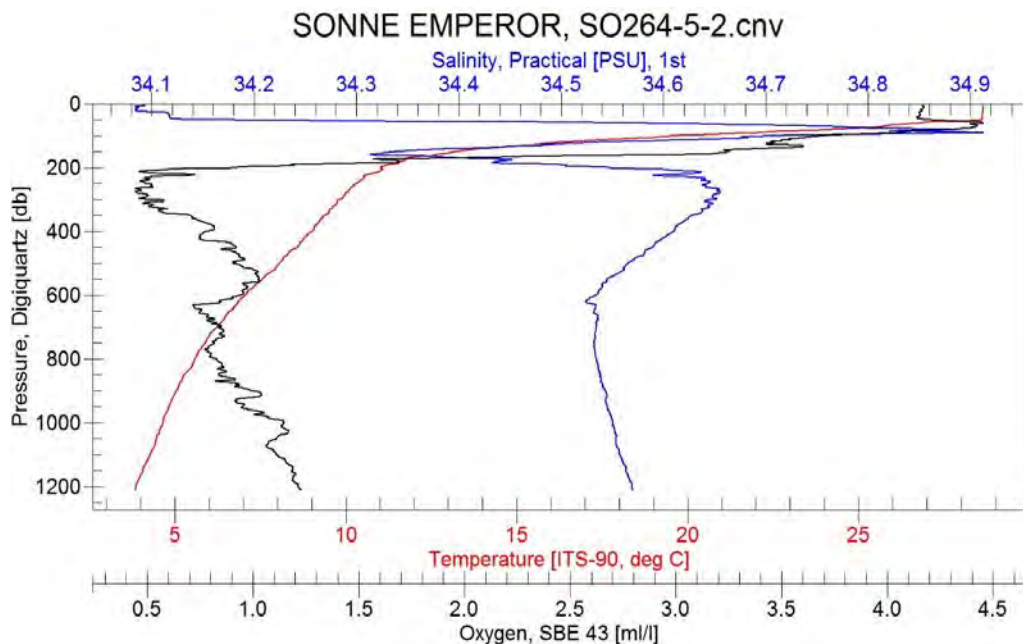


A.5.2.1-5 SONNE EMPEROR SO264-5-2 CTD

Latitude = 09° 59.42 N UTC (Time) = Jul 07 2018 00:40

Longitude = 178° 27.62 E Water depth 5738 m.

Bottle	Depth (m)	Pressure (dB)	Salinity (PSU)	Temp. (°C)	Oxygen (ml/l)	Density (Kg/m³)	Fluo
1	1200.394	1210.731	34.569	3.839	1.223	27.469	0.008
2	1004.491	1012.663	34.551	4.564	1.155	27.377	0.026
3	803.773	809.920	34.534	5.519	0.857	27.252	0.006
4	703.426	708.634	34.530	6.012	0.832	27.188	0.011
5	603.383	607.703	34.522	6.864	0.832	27.068	-0.004
6	502.916	506.393	34.557	7.908	0.993	26.947	0.003
7	403.221	405.911	34.600	8.858	0.750	26.834	-0.066
8	379.322	381.831	34.609	9.079	0.797	26.806	-0.074
9	354.511	356.833	34.620	9.324	0.712	26.775	-0.090
10	303.943	305.897	34.638	9.746	0.535	26.718	-0.061
11	254.269	255.873	34.639	10.293	0.470	26.625	-0.184
12	204.135	205.398	34.586	11.035	0.627	26.452	-0.258
13	184.251	185.382	34.442	11.705	1.525	26.216	-0.241
14	163.948	164.945	34.324	12.527	2.793	25.967	-0.143
15	144.011	144.880	34.395	14.139	3.483	25.695	-0.017
16	131.186	131.973	34.470	15.535	3.382	25.450	0.120
17	103.487	104.101	34.664	19.165	3.599	24.727	0.521
18	84.468	84.966	34.800	22.698	4.115	23.874	0.156
19	64.329	64.705	34.793	25.320	4.391	23.092	-0.022
20	43.713	43.966	34.248	28.267	4.236	21.745	-0.133
21	23.424	23.558	34.125	28.632	4.141	21.531	-0.313
22	14.503	14.586	34.109	28.655	4.161	21.511	-0.330
23	13.553	13.631	34.110	28.650	4.153	21.513	-0.321
24	14.438	14.520	34.109	28.655	4.156	21.511	-0.336



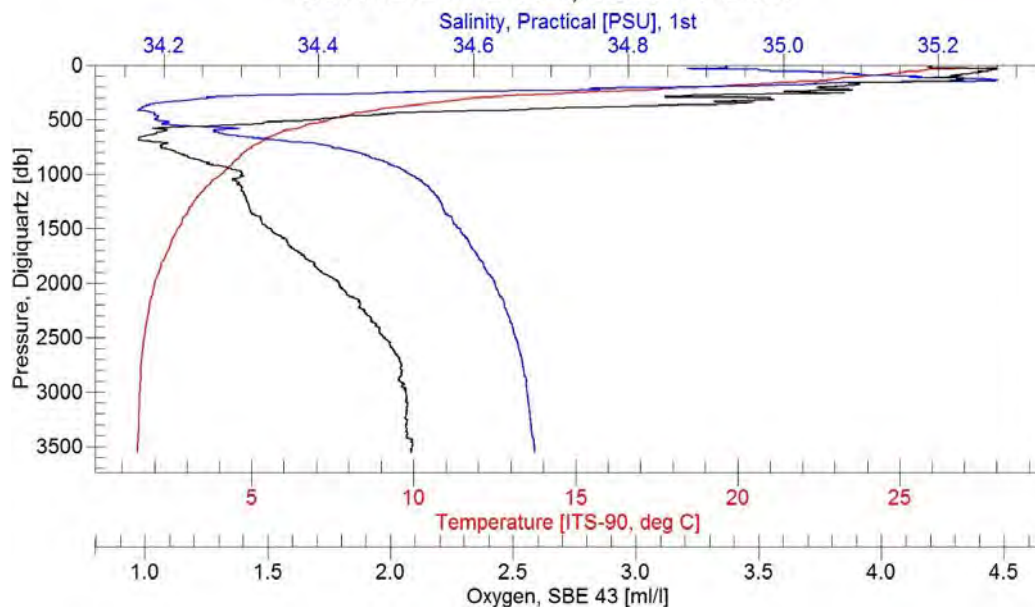
A.5.2.1-6 SONNE EMPEROR SO264-6-2 CTD

Latitude = 18° 33.60 N UTC (Time) = Jul 08 2018 21:55

Longitude = 176° 55.20 E Water depth 3578 m.

Bottle	Depth (m)	Pressure (dB)	Salinity (PSU)	Temp. (°C)	Oxygen (ml/l)	Density (Kg/m³)	Fluo
1	3503.238	3554.086	34.679	1.484	2.087	27.773	0.018
2	3502.983	3553.825	34.679	1.484	2.083	27.773	0.014
3	3502.626	3553.460	34.679	1.484	2.083	27.773	0.018
4	3006.543	3046.633	34.670	1.545	2.062	27.758	0.014
5	3005.475	3045.543	34.670	1.546	2.073	27.758	0.022
6	3005.980	3046.059	34.670	1.546	2.071	27.758	0.018
7	2005.413	2027.347	34.628	1.991	1.810	27.685	0.028
8	2004.858	2026.783	34.628	1.992	1.810	27.685	0.027
9	2005.605	2027.542	34.628	1.992	1.811	27.685	0.011
10	1002.814	1011.350	34.522	3.948	1.408	27.419	0.016
11	1004.556	1013.111	34.523	3.946	1.407	27.420	0.016
12	1004.452	1013.006	34.522	3.947	1.408	27.420	0.024
13	703.861	709.340	34.376	5.269	1.076	27.156	0.009
14	703.558	709.034	34.375	5.278	1.074	27.154	0.013
15	703.835	709.313	34.375	5.277	1.072	27.154	0.012
16	354.141	356.596	34.181	10.376	3.349	26.255	-0.065
17	353.978	356.431	34.182	10.421	3.339	26.248	-0.063
18	353.272	355.719	34.183	10.472	3.346	26.240	-0.074
19	123.776	124.564	35.230	23.185	4.315	24.062	0.442
20	123.882	124.670	35.233	23.180	4.300	24.066	0.466
21	124.732	125.526	35.248	23.158	4.315	24.083	0.398
22	53.829	54.162	34.980	25.605	4.443	23.144	-0.194
23	54.593	54.932	34.981	25.600	4.457	23.147	-0.228
24	54.021	54.356	34.980	25.602	4.451	23.145	-0.212

SONNE EMPEROR, SO264-6-2.cnv

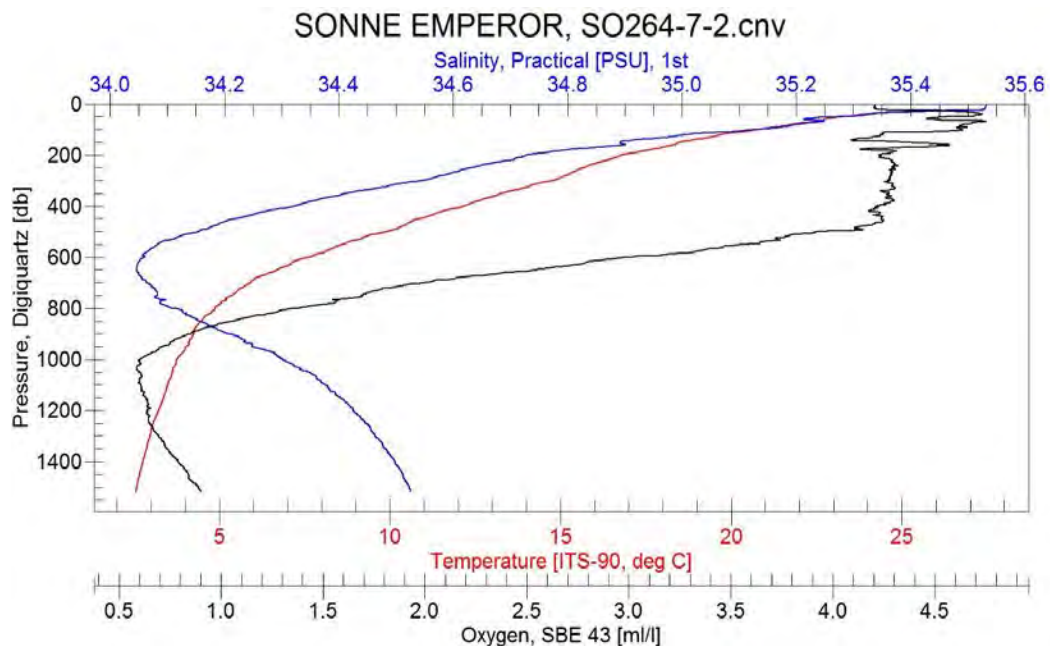


A.5.2.1-7 SONNE EMPEROR SO264-7-2 CTD

Latitude = 27° 46.95 N UTC (Time) = Jul 11 2018 03:34

Longitude = 175° 36.53 E Water depth 5512 m.

Bottle	Depth (m)	Pressure (dB)	Salinity (PSU)	Temp. (°C)	Oxygen (ml/l)	Density (Kg/m³)	Fluo
1	1501.351	1516.878	34.526	2.567	0.900	27.554	0.027
2	1000.536	1009.667	34.310	3.731	0.595	27.272	0.029
3	801.050	807.971	34.123	4.817	1.265	27.008	0.025
4	701.616	707.508	34.060	5.908	1.979	26.829	0.005
5	600.953	605.852	34.055	7.666	2.984	26.589	0.003
6	501.281	505.245	34.150	9.936	3.926	26.309	-0.005
7	401.132	404.206	34.324	12.274	4.243	26.022	-0.019
8	376.351	379.211	34.360	12.733	4.276	25.960	-0.022
9	352.083	354.738	34.402	13.209	4.271	25.898	-0.023
10	301.924	304.164	34.522	14.561	4.236	25.708	-0.042
11	251.363	253.196	34.610	15.488	4.299	25.572	-0.061
12	201.401	202.845	34.718	16.727	4.240	25.370	-0.019
13	182.351	183.650	34.778	17.424	4.316	25.250	0.022
14	161.787	162.931	34.867	18.080	4.532	25.158	0.032
15	141.537	142.531	34.889	18.521	4.293	25.064	0.153
16	121.926	122.777	34.979	19.464	4.214	24.891	0.406
17	102.414	103.124	35.093	20.447	4.627	24.719	0.361
18	81.830	82.393	35.189	21.733	4.662	24.441	0.066
19	60.792	61.207	35.223	22.745	4.478	24.179	0.033
20	41.916	42.200	35.308	23.875	4.674	23.915	-0.001
21	22.075	22.224	35.528	27.444	4.212	22.975	-0.050
22	11.825	11.904	35.533	27.464	4.212	22.971	-0.058
23	12.058	12.139	35.533	27.465	4.217	22.971	-0.056
24	12.083	12.164	35.533	27.465	4.214	22.971	-0.058

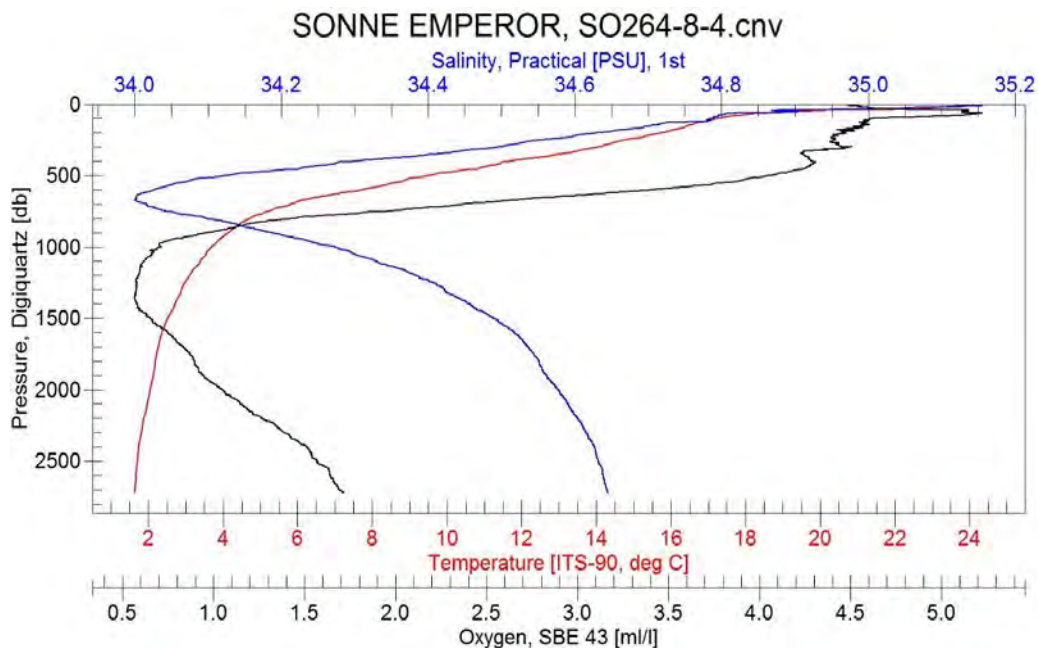


A.5.2.1-8 SONNE EMPEROR SO264-8-2 CTD

Latitude = 33° 39.27 N UTC (Time) = Jul 13 2018 00:40

Longitude = 174° 46.15 E Water depth 2716 m.

Bottle	Depth (m)	Pressure (dB)	Salinity (PSU)	Temp. (°C)	Oxygen (ml/l)	Density (Kg/m³)	Fluo
1	2686.659	2723.410	34.645	1.636	1.712	27.729	-0.003
2	2687.056	2723.815	34.645	1.636	1.714	27.729	0.001
3	2686.600	2723.350	34.645	1.636	1.711	27.729	-0.005
4	2004.549	2028.684	34.580	2.034	1.077	27.643	0.033
5	2004.129	2028.257	34.580	2.034	1.079	27.643	0.041
6	2004.482	2028.615	34.580	2.035	1.078	27.643	0.036
7	1503.579	1519.860	34.490	2.511	0.665	27.530	0.025
8	1504.293	1520.585	34.491	2.510	0.667	27.531	0.038
9	1502.907	1519.179	34.490	2.510	0.668	27.530	0.027
10	1003.978	1013.631	34.272	3.678	0.691	27.247	0.025
11	1002.772	1012.410	34.272	3.679	0.692	27.246	0.038
12	1003.293	1012.938	34.272	3.679	0.693	27.246	0.033
13	672.856	678.781	33.997	5.993	2.541	26.769	0.004
14	672.803	678.728	33.998	5.995	2.540	26.769	-0.005
15	672.692	678.616	33.997	5.997	2.547	26.768	0.004
16	352.826	355.657	34.386	12.815	4.242	25.964	-0.043
17	352.512	355.339	34.386	12.816	4.249	25.963	-0.041
18	352.803	355.633	34.386	12.813	4.249	25.964	-0.039
19	93.402	94.092	34.780	17.408	4.834	25.252	1.184
20	93.125	93.813	34.779	17.410	4.838	25.251	1.123
21	93.279	93.968	34.781	17.403	4.842	25.253	1.156
22	53.412	53.801	34.821	18.892	5.220	24.914	0.022
23	53.021	53.408	34.823	18.929	5.219	24.906	0.030
24	53.190	53.578	34.819	18.890	5.232	24.913	0.018



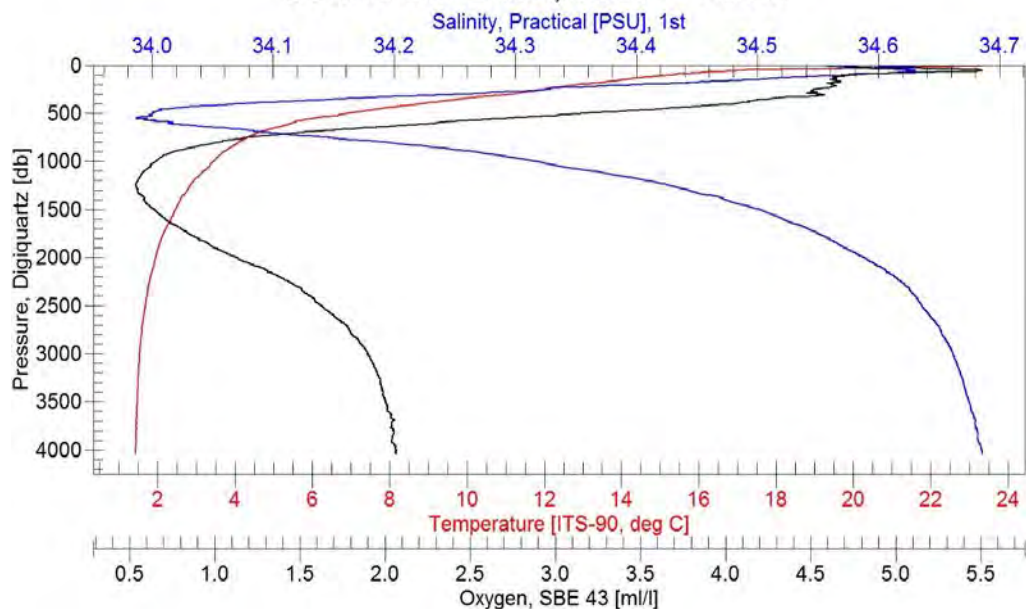
A.5.2.1-9 SONNE EMPEROR SO264-11-2 CTD

Latitude = 35° 31.57 N UTC (Time) = Jul 14 2018 17:08

Longitude = 172° 23.32 E Water depth 4001 m.

Bottle	Depth (m)	Pressure (dB)	Salinity (PSU)	Temp. (°C)	Oxygen (ml/l)	Density (Kg/m³)	Fluo
1	3975.832	4043.069	34.686	1.433	2.059	27.785	-0.011
2	3506.509	3561.909	34.675	1.474	2.004	27.771	0.021
3	3255.952	3305.453	34.670	1.496	1.971	27.763	0.025
4	3005.328	3049.223	34.662	1.532	1.910	27.753	0.017
5	2754.929	2793.517	34.652	1.585	1.819	27.739	0.021
6	2505.080	2538.669	34.640	1.650	1.698	27.723	0.013
7	2256.048	2284.948	34.623	1.757	1.501	27.700	0.015
8	2004.267	2028.726	34.597	1.908	1.237	27.666	0.024
9	1755.836	1776.209	34.560	2.078	0.938	27.623	0.034
10	1504.301	1520.839	34.513	2.383	0.701	27.559	0.019
11	1253.971	1266.995	34.443	2.761	0.562	27.469	0.032
12	1003.696	1013.509	34.325	3.377	0.638	27.318	0.043
13	703.184	709.543	34.092	4.600	1.477	27.006	0.026
14	603.452	608.762	34.025	5.333	2.135	26.870	0.002
15	503.123	507.426	33.995	6.646	2.987	26.681	-0.004
16	403.240	406.590	34.043	8.425	3.871	26.465	-0.057
17	303.652	306.101	34.194	10.492	4.555	26.244	-0.049
18	253.648	255.662	34.281	11.496	4.513	26.131	-0.039
19	203.533	205.125	34.396	12.870	4.604	25.957	-0.036
20	123.141	124.079	34.514	14.476	4.703	25.715	0.120
21	93.253	93.956	34.575	15.473	4.917	25.543	0.820
22	53.305	53.703	34.608	16.783	5.453	25.267	0.912
23	23.862	24.038	34.576	20.974	4.811	24.180	-0.153
24	13.424	13.523	34.604	21.847	4.748	23.960	-0.175

SONNE EMPEROR, SO264-11-2.cnv

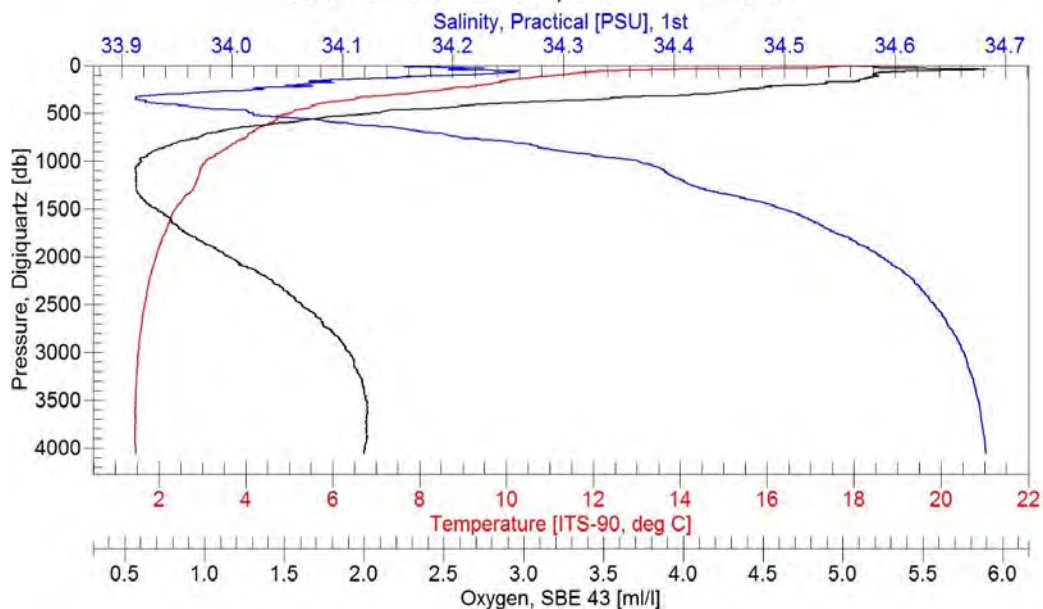


A.5.2.1-10 SONNE EMPEROR SO264-13-4 CTD

Latitude = 37° 47.27 N UTC (Time) = Jul 16 2018 08:30
 Longitude = 170° 44.24 E Water depth 4021 m.

Bottle	Depth (m)	Pressure (dB)	Salinity (PSU)	Temp. (°C)	Oxygen (ml/l)	Density (Kg/m³)	Fluo
1	3999.024	4067.693	34.682	1.468	1.995	27.780	-0.013
2	3505.613	3561.710	34.677	1.461	2.030	27.773	0.024
3	3005.154	3049.659	34.664	1.518	1.932	27.755	0.018
4	2754.791	2793.939	34.651	1.594	1.788	27.737	0.019
5	2504.424	2538.510	34.636	1.676	1.621	27.718	0.016
6	2254.505	2283.835	34.617	1.779	1.438	27.694	0.019
7	2003.138	2027.984	34.586	1.949	1.155	27.655	0.021
8	1754.202	1774.906	34.548	2.131	0.923	27.609	0.030
9	1503.824	1520.660	34.497	2.385	0.720	27.546	0.029
10	1253.374	1266.644	34.421	2.807	0.587	27.448	0.021
11	1002.687	1012.691	34.370	3.068	0.607	27.382	0.029
12	902.955	911.744	34.293	3.492	0.701	27.281	0.011
13	702.778	709.275	34.193	4.055	0.992	27.144	0.029
14	602.820	608.245	34.101	4.563	1.462	27.016	0.006
15	402.644	406.071	33.920	6.175	3.117	26.682	-0.055
16	302.721	305.223	33.960	7.897	4.206	26.476	-0.074
17	252.787	254.845	34.021	8.816	4.489	26.385	-0.047
18	202.837	204.463	34.057	9.444	4.750	26.312	-0.032
19	152.812	154.018	34.105	10.208	5.107	26.221	-0.028
20	102.838	103.637	34.181	11.089	5.193	26.124	0.160
21	73.092	73.655	34.239	11.875	5.253	26.023	1.079
22	52.730	53.133	34.216	12.573	5.690	25.872	1.952
23	27.867	28.079	34.215	16.939	5.262	24.927	0.527
24	12.881	12.978	34.201	17.284	5.190	24.834	0.273

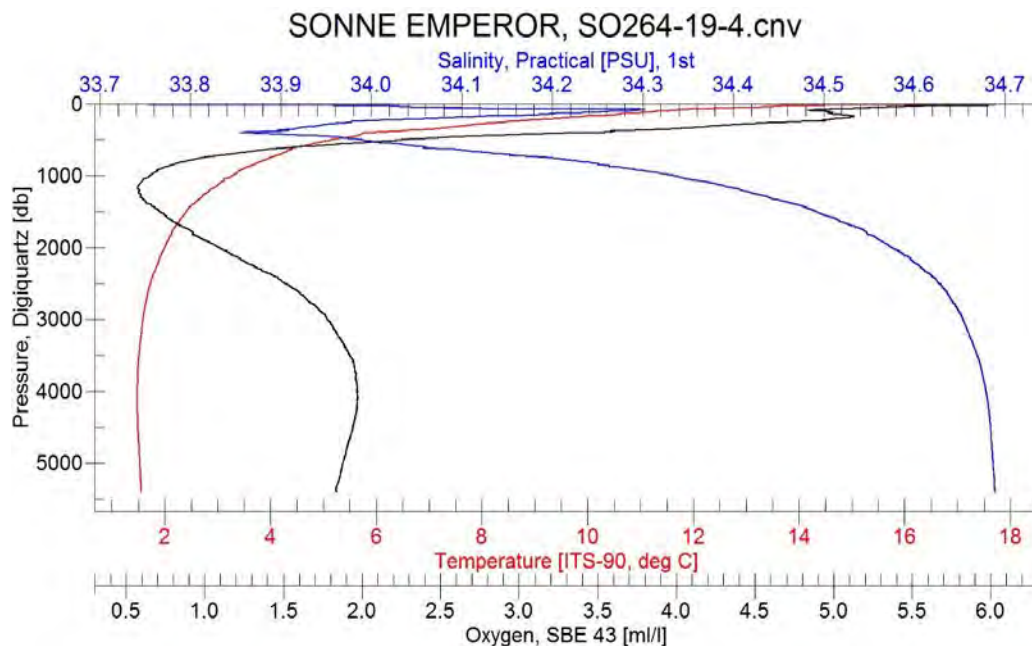
SONNE EMPEROR, SO264-13-4.cnv



A.5.2.1-11 SONNE EMPEROR SO264-19-4 CTD

Latitude = 41° 31.76 N UTC (Time) = Jul 19 2018 13:32
 Longitude = 169° 55.70 E Water depth 5308 m.

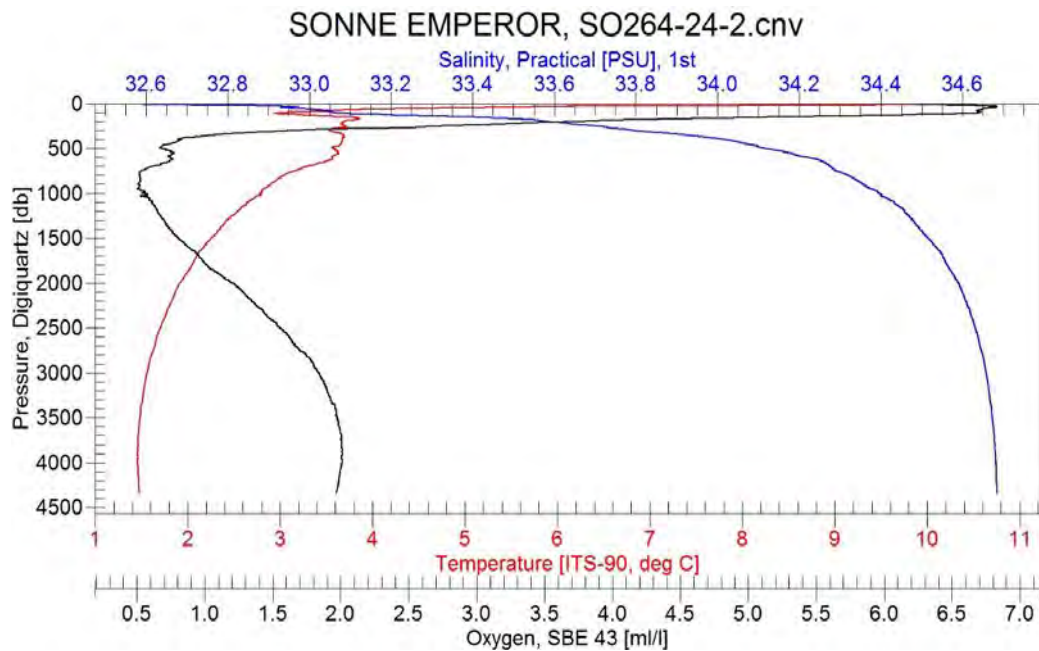
Bottle	Depth (m)	Pressure (dB)	Salinity (PSU)	Temp. (°C)	Oxygen (ml/l)	Density (Kg/m³)	Fluo
1	5284.971	5393.531	34.689	1.559	1.836	27.791	-0.008
2	5009.374	5109.045	34.688	1.537	1.871	27.789	0.015
3	4509.538	4593.974	34.685	1.499	1.931	27.785	0.020
4	4009.064	4079.396	34.681	1.479	1.976	27.779	0.012
5	3508.426	3565.809	34.672	1.501	1.943	27.766	0.022
6	3007.533	3053.133	34.656	1.575	1.809	27.745	0.027
7	2507.918	2542.939	34.630	1.717	1.539	27.710	0.031
8	2007.314	2032.925	34.576	1.993	1.119	27.643	0.037
9	1756.815	1778.165	34.545	2.146	0.924	27.605	0.033
10	1506.623	1524.019	34.494	2.390	0.738	27.543	0.048
11	1255.772	1269.506	34.426	2.747	0.603	27.457	0.023
12	1006.230	1016.623	34.337	3.247	0.645	27.340	0.042
13	905.730	914.863	34.295	3.440	0.705	27.287	0.035
14	705.250	712.016	34.183	4.043	1.018	27.137	0.018
15	605.716	611.380	34.076	4.407	1.426	27.014	0.029
16	406.011	409.609	33.890	5.735	3.069	26.712	-0.005
17	305.017	307.644	33.925	7.425	4.132	26.517	-0.027
18	205.504	207.223	34.083	9.649	5.036	26.299	-0.025
19	156.150	157.438	34.205	10.755	4.928	26.203	-0.027
20	105.579	106.436	34.278	11.599	4.999	26.107	0.056
21	75.062	75.666	34.241	12.104	5.015	25.982	0.159
22	55.487	55.931	33.998	12.369	5.346	25.742	0.718
23	29.544	29.778	33.985	13.438	5.538	25.519	2.209
24	15.534	15.657	33.711	17.294	5.586	24.456	2.302



A.5.2.1-12 SONNE EMPEROR SO264-24-2 CTD

Latitude = 44° 48.06 N UTC (Time) = Jul 22 2018 09:30
 Longitude = 170° 35.86 E Water depth 4304 m.

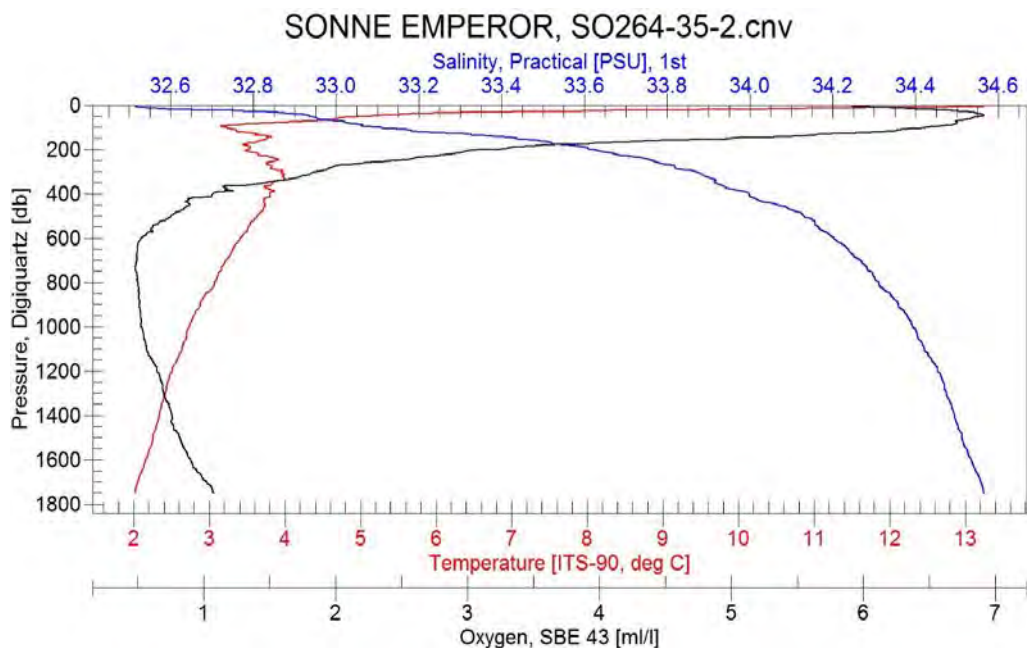
Bottle	Depth (m)	Pressure (dB)	Salinity (PSU)	Temp. (°C)	Oxygen (ml/l)	Density (Kg/m³)	Fluo
1	4265.981	4344.729	34.684	1.479	1.968	27.783	-0.008
2	4266.507	4345.271	34.684	1.479	1.969	27.783	-0.001
3	4265.646	4344.385	34.684	1.479	1.970	27.783	-0.005
4	3005.681	3052.164	34.660	1.555	1.862	27.749	0.023
5	2005.752	2031.950	34.592	1.908	1.234	27.663	0.025
6	2005.677	2031.873	34.592	1.908	1.231	27.663	0.022
7	2005.345	2031.536	34.592	1.907	1.232	27.663	0.028
8	1004.593	1015.272	34.400	2.753	0.546	27.434	0.024
9	1004.102	1014.775	34.399	2.750	0.547	27.434	0.034
10	1005.177	1015.863	34.400	2.755	0.544	27.434	0.023
11	804.181	812.335	34.316	3.050	0.521	27.339	0.030
12	603.731	609.556	34.215	3.565	0.731	27.209	0.019
13	604.615	610.451	34.211	3.574	0.731	27.205	0.008
14	603.908	609.735	34.213	3.573	0.731	27.207	0.006
15	403.861	407.560	33.985	3.679	0.853	27.014	-0.010
16	404.353	408.056	33.985	3.679	0.852	27.014	-0.016
17	403.539	407.235	33.985	3.679	0.853	27.014	-0.018
18	203.938	205.706	33.644	3.677	3.159	26.741	-0.054
19	153.741	155.055	33.460	3.851	4.758	26.577	-0.071
20	104.299	105.177	33.067	3.213	6.596	26.324	-0.092
21	53.766	54.212	32.919	5.377	6.763	25.983	1.591
22	28.821	29.058	32.901	7.703	6.543	25.668	1.686
23	28.795	29.032	32.866	7.683	6.526	25.644	1.725
24	28.757	28.994	32.857	7.971	6.504	25.595	1.694



A.5.2.1-13 SONNE EMPEROR SO264-35-2 CTD

Latitude = 44° 46.14 N UTC (Time) = Jul 25 2018 19:16
 Longitude = 170° 10.29 E Water depth 1763 m.

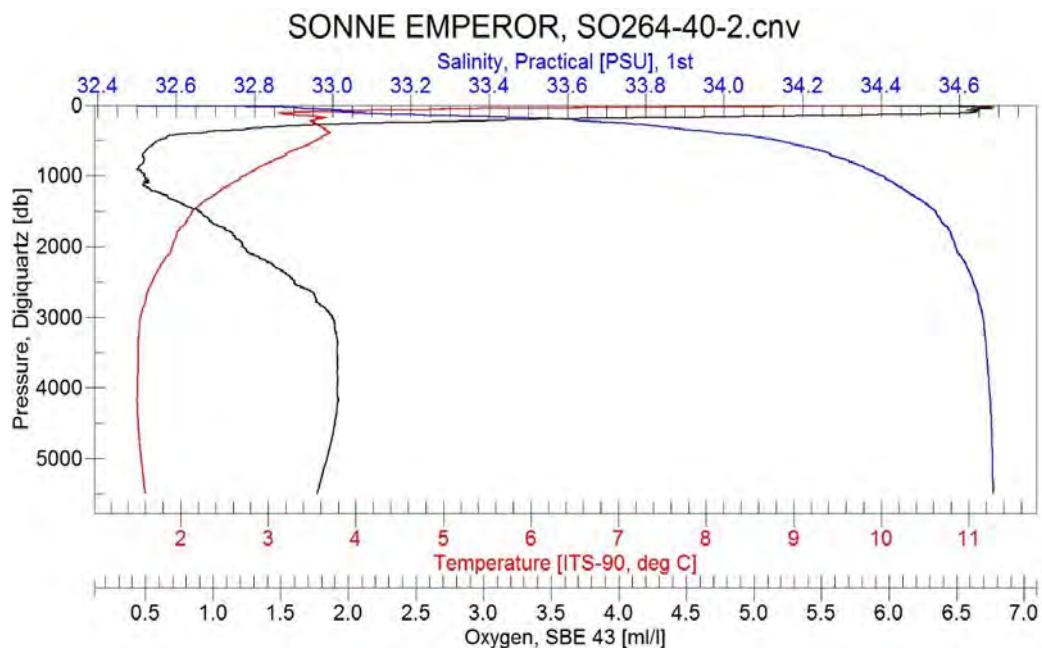
Bottle	Depth (m)	Pressure (dB)	Salinity (PSU)	Temp. (°C)	Oxygen (ml/l)	Density (Kg/m³)	Fluo
1	1730.436	1751.880	34.565	2.021	1.076	27.630	0.023
2	1602.106	1621.461	34.538	2.142	0.917	27.599	0.038
3	1502.461	1520.248	34.514	2.249	0.832	27.571	0.033
4	1402.568	1418.832	34.498	2.317	0.768	27.552	0.034
5	1302.645	1317.434	34.480	2.395	0.715	27.530	0.030
6	1201.831	1215.181	34.462	2.470	0.672	27.509	0.043
7	1102.502	1114.482	34.429	2.610	0.582	27.470	0.034
8	1002.816	1013.468	34.399	2.714	0.534	27.437	0.032
9	902.816	912.186	34.359	2.874	0.510	27.390	0.034
10	800.368	808.474	34.338	2.954	0.502	27.365	0.023
11	697.751	704.642	34.255	3.249	0.473	27.272	0.017
12	599.654	605.433	34.211	3.388	0.513	27.223	0.022
13	498.744	503.427	34.128	3.638	0.718	27.132	0.002
14	398.753	402.399	34.019	3.760	0.924	27.033	-0.018
15	349.352	352.504	33.931	3.851	1.337	26.953	-0.043
16	297.421	300.066	33.871	3.924	1.673	26.898	-0.043
17	247.265	249.434	33.809	3.944	2.098	26.846	-0.058
18	197.923	199.635	33.658	3.609	2.863	26.758	-0.049
19	147.918	149.179	33.466	3.626	4.314	26.604	-0.070
20	98.530	99.358	33.058	3.182	6.307	26.320	-0.114
21	80.221	80.891	33.008	4.070	6.561	26.195	0.543
22	49.691	50.103	32.904	5.593	6.749	25.946	1.418
23	19.923	20.087	32.741	8.230	6.535	25.467	0.626
24	9.994	10.076	32.526	11.278	6.269	24.801	0.314



A.5.2.1-14 SONNE EMPEROR SO264-40-2 CTD

Latitude = 45° 34.00 N UTC (Time) = Jul 29 2018 15:57
 Longitude = 170° 18.00 E Water depth 5401 m.

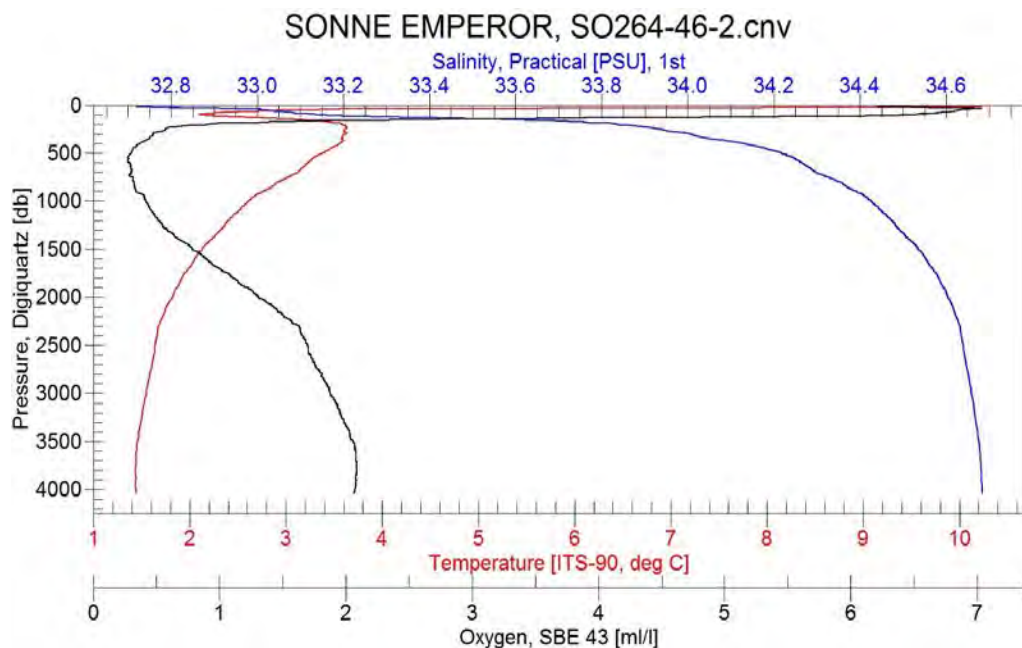
Bottle	Depth (m)	Pressure (dB)	Salinity (PSU)	Temp. (°C)	Oxygen (ml/l)	Density (Kg/m³)	Fluo
1	5375.012	5488.614	34.687	1.597	1.774	27.787	-0.006
2	5374.666	5488.257	34.687	1.597	1.773	27.787	-0.014
3	5375.429	5489.045	34.687	1.597	1.769	27.787	-0.005
4	3506.312	3564.978	34.670	1.519	1.908	27.764	0.023
5	3506.487	3565.158	34.671	1.519	1.911	27.764	0.015
6	3505.981	3564.640	34.670	1.518	1.911	27.764	0.028
7	2005.662	2032.002	34.591	1.907	1.242	27.662	0.030
8	2004.234	2030.549	34.591	1.907	1.238	27.662	0.033
9	2005.062	2031.391	34.591	1.907	1.241	27.662	0.028
10	1004.031	1014.774	34.402	2.721	0.512	27.439	0.041
11	1004.208	1014.954	34.401	2.727	0.517	27.437	0.043
12	1004.381	1015.129	34.400	2.729	0.512	27.436	0.040
13	503.913	508.688	34.132	3.546	0.590	27.144	0.033
14	503.729	508.502	34.132	3.547	0.594	27.144	0.032
15	503.764	508.538	34.132	3.547	0.592	27.144	0.030
16	303.400	306.126	33.832	3.602	1.464	26.899	-0.016
17	304.110	306.842	33.833	3.603	1.465	26.899	-0.015
18	303.303	306.028	33.833	3.602	1.463	26.899	-0.019
19	103.615	104.495	33.074	3.194	6.463	26.331	-0.047
20	103.848	104.730	33.072	3.195	6.457	26.330	-0.035
21	103.550	104.429	33.079	3.210	6.462	26.334	-0.053
22	13.711	13.824	32.525	10.957	6.057	24.857	0.873
23	13.400	13.511	32.525	10.962	6.056	24.856	0.942
24	13.520	13.632	32.525	10.957	6.054	24.857	0.890



A.5.2.1-15 SONNE EMPEROR SO264-46-2 CTD

Latitude = 46° 48.94 N UTC (Time) = Aug 01 2018 19:02
 Longitude = 169° 24.65 E Water depth 3992 m.

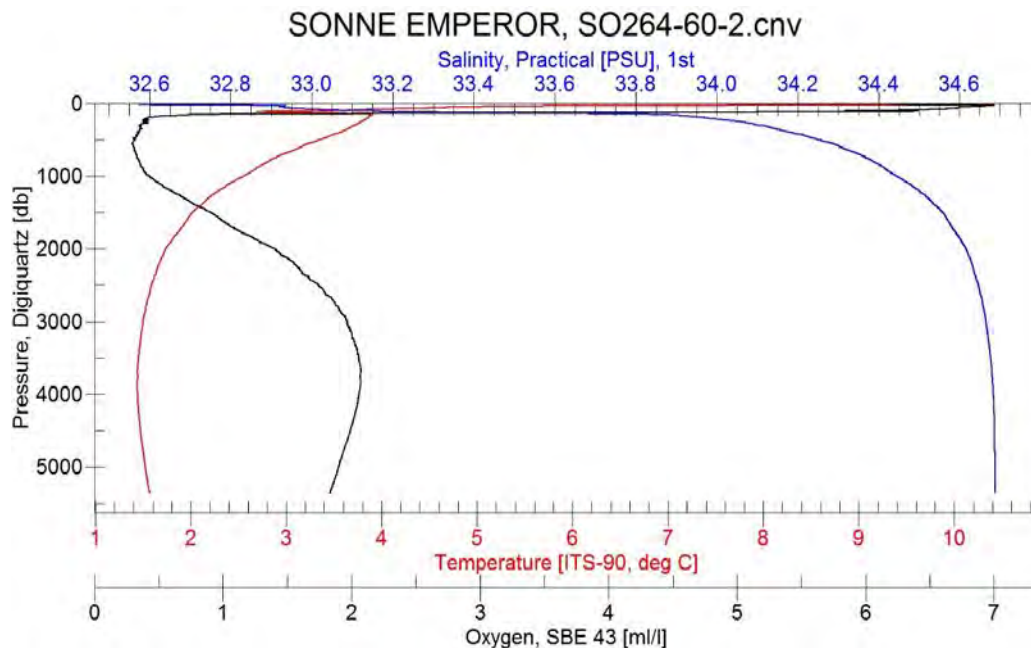
Bottle	Depth (m)	Pressure (dB)	Salinity (PSU)	Temp. (°C)	Oxygen (ml/l)	Density (Kg/m³)	Fluo
1	3967.375	4038.567	34.684	1.446	2.065	27.783	-0.010
2	3507.640	3566.753	34.678	1.448	2.082	27.775	0.027
3	3007.453	3054.548	34.661	1.539	1.907	27.751	0.025
4	2706.256	2746.681	34.649	1.598	1.797	27.736	0.029
5	2506.278	2542.511	34.641	1.639	1.713	27.725	0.027
6	2205.929	2236.224	34.625	1.713	1.550	27.705	0.026
7	2006.164	2032.749	34.608	1.797	1.368	27.684	0.025
8	1705.710	1727.072	34.576	1.944	1.078	27.645	0.021
9	1506.028	1524.160	34.544	2.087	0.862	27.608	0.045
10	1205.180	1218.807	34.483	2.354	0.568	27.535	0.036
11	1004.463	1015.330	34.426	2.608	0.427	27.467	0.045
12	904.384	913.946	34.391	2.758	0.346	27.426	0.045
13	704.302	711.403	34.308	3.080	0.301	27.329	0.021
14	604.478	610.426	34.272	3.198	0.289	27.290	0.034
15	404.517	408.299	34.124	3.565	0.376	27.136	0.007
16	304.353	307.124	34.018	3.612	0.438	27.046	-0.053
17	254.063	256.344	33.937	3.600	0.564	26.982	-0.016
18	204.433	206.244	33.833	3.572	0.891	26.902	0.009
19	154.349	155.697	33.434	2.783	3.915	26.655	-0.021
20	103.433	104.324	33.146	2.133	6.577	26.477	-0.046
21	73.900	74.530	33.073	2.298	6.875	26.405	0.193
22	54.350	54.811	33.003	3.136	6.961	26.279	0.875
23	29.194	29.440	32.767	8.673	6.644	25.421	2.244
24	13.926	14.042	32.718	10.250	6.405	25.129	2.178



A.5.2.1-16 SONNE EMPEROR SO264-60-2 CTD

Latitude = 49° 18.44 N UTC (Time) = Aug 08 2018 17:30
 Longitude = 168° 33.42 E Water depth 5270 m.

Bottle	Depth (m)	Pressure (dB)	Salinity (PSU)	Temp. (°C)	Oxygen (ml/l)	Density (Kg/m³)	Fluo
1	5240.645	5351.624	34.688	1.568	1.833	27.788	-0.008
2	5240.994	5351.985	34.688	1.568	1.833	27.789	0.001
3	3505.259	3565.134	34.678	1.452	2.060	27.774	0.015
4	3506.107	3566.004	34.678	1.452	2.056	27.774	0.031
5	2004.028	2031.040	34.612	1.759	1.367	27.690	0.034
6	2005.142	2032.175	34.612	1.759	1.365	27.690	0.034
7	1003.763	1014.852	34.442	2.560	0.436	27.484	0.049
8	1004.308	1015.405	34.442	2.560	0.434	27.484	0.034
9	703.047	710.297	34.343	2.997	0.319	27.365	0.042
10	702.568	709.812	34.343	2.997	0.320	27.365	0.044
11	502.544	507.479	34.260	3.319	0.290	27.268	0.041
12	503.238	508.180	34.261	3.318	0.288	27.269	0.035
13	303.266	306.096	34.097	3.731	0.312	27.097	0.013
14	303.186	306.014	34.097	3.731	0.312	27.097	0.015
15	203.537	205.386	33.964	3.858	0.376	26.978	0.035
16	202.773	204.615	33.961	3.860	0.366	26.976	0.022
17	122.672	123.763	33.445	3.214	3.851	26.626	0.018
18	123.194	124.289	33.445	3.219	3.866	26.625	0.029
19	52.711	53.171	32.917	4.753	6.625	26.051	0.655
20	53.336	53.801	32.920	4.721	6.638	26.058	0.650
21	27.364	27.601	32.841	7.503	6.820	25.650	2.198
22	28.290	28.535	32.826	7.695	6.740	25.611	2.213
23	12.642	12.751	32.570	10.399	6.198	24.988	1.813
24	13.717	13.835	32.569	10.409	6.186	24.986	1.817

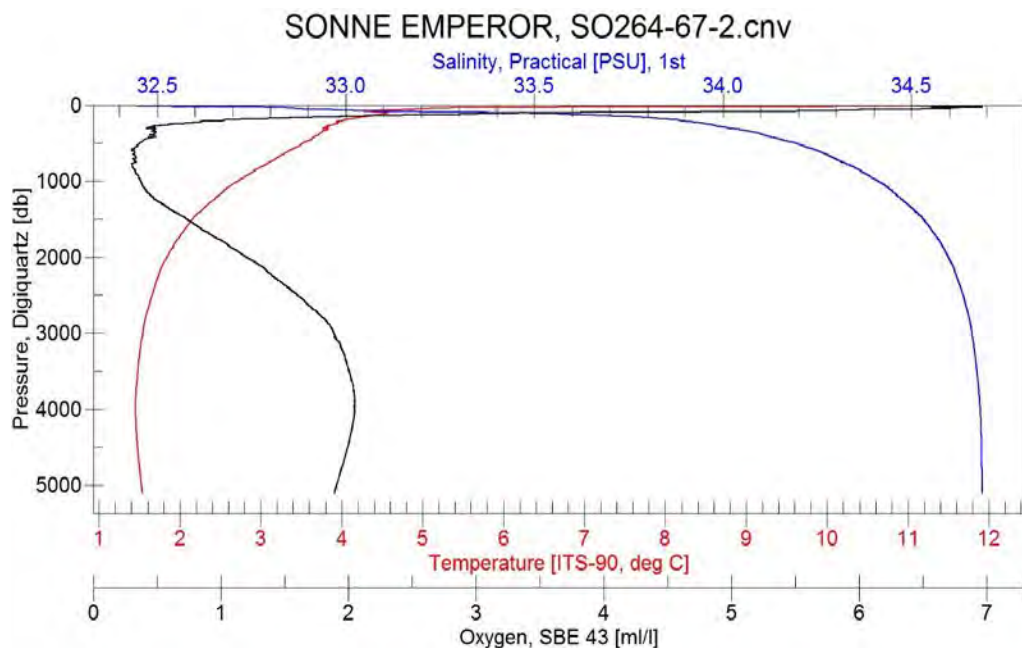


A.5.2.1-17 SONNE EMPEROR SO264-67-2 CTD

Latitude = 50° 14.69 N UTC (Time) = Aug 13 2018 08:18

Longitude = 168° 35.15 E Water depth 5034 m.

Bottle	Depth (m)	Pressure (dB)	Salinity (PSU)	Temp. (°C)	Oxygen (ml/l)	Density (Kg/m³)	Fluo
1	5000.488	5104.010	34.688	1.537	1.890	27.788	-0.003
2	5000.638	5104.165	34.688	1.537	1.887	27.788	0.027
3	5000.992	5104.530	34.688	1.537	1.890	27.788	0.009
4	3506.576	3566.792	34.676	1.471	2.031	27.772	0.021
5	3507.703	3567.948	34.676	1.471	2.030	27.771	0.027
6	3506.067	3566.270	34.676	1.471	2.033	27.771	0.025
7	2006.412	2033.642	34.602	1.818	1.259	27.677	0.035
8	2004.881	2032.084	34.602	1.819	1.261	27.677	0.042
9	2004.952	2032.156	34.602	1.820	1.257	27.677	0.030
10	1004.289	1015.472	34.409	2.720	0.383	27.444	0.045
11	1005.032	1016.226	34.409	2.720	0.384	27.444	0.043
12	1003.826	1015.003	34.409	2.720	0.383	27.444	0.053
13	503.904	508.898	34.192	3.517	0.356	27.195	0.038
14	503.895	508.889	34.192	3.517	0.355	27.195	0.019
15	503.984	508.978	34.192	3.517	0.355	27.195	0.033
16	203.970	205.841	33.888	4.002	0.980	26.903	0.019
17	203.868	205.738	33.887	4.002	0.968	26.902	0.001
18	203.142	205.005	33.887	4.004	0.974	26.902	0.014
19	54.479	54.959	32.887	4.853	6.334	26.017	0.245
20	53.277	53.745	32.881	4.871	6.386	26.011	0.199
21	53.168	53.636	32.876	4.887	6.439	26.004	0.256
22	13.509	13.627	32.433	11.104	6.499	24.759	4.870
23	13.648	13.767	32.431	11.119	6.471	24.755	5.134
24	13.885	14.006	32.431	11.122	6.484	24.755	5.251

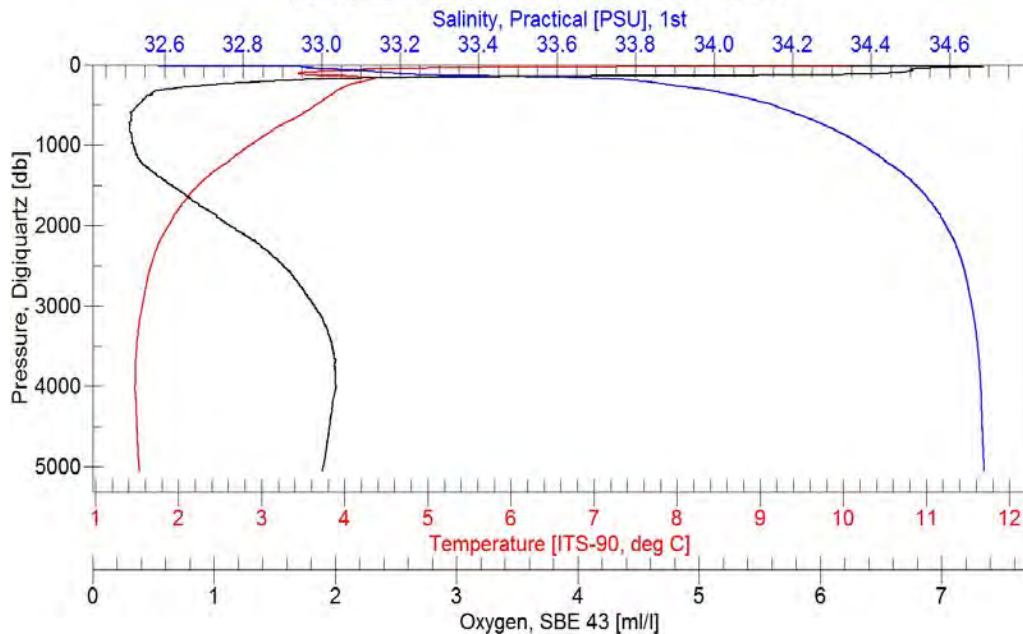


A.5.2.1-18 SONNE EMPEROR SO264-77-2 CTD

Latitude = 50° 29.71 N UTC (Time) = Aug 16 2018 08:23
 Longitude = 166° 52.73 E Water depth 4978 m.

Bottle	Depth (m)	Pressure (dB)	Salinity (PSU)	Temp. (°C)	Oxygen (ml/l)	Density (Kg/m³)	Fluo
1	4951.462	5053.516	34.687	1.531	1.893	27.788	-0.008
2	4506.216	4594.376	34.684	1.505	1.948	27.784	0.025
3	4005.913	4079.548	34.680	1.481	1.999	27.778	0.015
4	3505.517	3565.788	34.673	1.492	1.991	27.768	0.026
5	3005.359	3053.441	34.659	1.556	1.856	27.748	0.021
6	2504.625	2541.686	34.637	1.656	1.615	27.720	0.032
7	2004.016	2031.249	34.593	1.869	1.169	27.666	0.034
8	1503.857	1522.469	34.519	2.213	0.695	27.578	0.041
9	1303.207	1318.699	34.474	2.425	0.506	27.523	0.046
10	1002.751	1013.937	34.387	2.820	0.354	27.418	0.046
11	902.206	912.048	34.349	2.979	0.334	27.373	0.049
12	802.449	811.007	34.305	3.140	0.311	27.322	0.047
13	701.974	709.288	34.261	3.325	0.314	27.269	0.043
14	602.523	608.653	34.214	3.476	0.318	27.217	0.028
15	502.416	507.405	34.153	3.644	0.363	27.151	0.042
16	402.684	406.583	34.073	3.794	0.420	27.073	0.015
17	301.930	304.779	33.966	3.942	0.585	26.971	-0.006
18	252.696	255.050	33.893	4.032	0.864	26.904	-0.034
19	152.636	154.020	33.579	4.256	2.918	26.631	-0.024
20	102.939	103.861	33.160	3.477	6.369	26.374	-0.040
21	53.025	53.493	32.976	4.608	6.683	26.114	0.434
22	32.957	33.246	32.934	5.579	7.118	25.971	3.050
23	13.086	13.200	32.587	11.457	6.219	24.816	1.832
24	-	-	-	-	-	-	-

SONNE EMPEROR, SO264-77-2.cnv



Appendix Table 5.2.2. Instrument configuration and calibration report sheet from SBE 911 onboard RV SONNE during cruise SO264.

PSA file: D:\CTDDData\Config\SeasaveSO264.psa

Date: 06/30/2018

Instrument configuration file: D:\CTDDData\Config\Config-2018-Apr-11.xmlcon

Configuration report for SBE 911plus/917plus CTD

Frequency channels suppressed : 0
Voltage words suppressed : 0
Computer interface : RS-232C
Deck unit : SBE11plus Firmware Version >= 5.0
Scans to average : 1
NMEA position data added : Yes
NMEA depth data added : No
NMEA time added : Yes
NMEA device connected to : PC
Surface PAR voltage added : No
Scan time added : No

1) Frequency 0, Temperature

Serial number : 5708
Calibrated on : 29-Nov-17
G : 4.34672016e-003
H : 6.30541503e-004
I : 1.89017921e-005
J : 1.16692170e-006
F0 : 1000.000
Slope : 1.00000000
Offset : 0.0000

2) Frequency 1, Conductivity

Serial number : 4261
Calibrated on : 14-Dec-17
G : -9.81926846e+000
H : 1.34574018e+000
I : -2.13843774e-003
J : 2.21056804e-004
CTcor : 3.2500e-006
CPcor : -9.57000000e-008
Slope : 1.00000000
Offset : 0.00000

3) Frequency 2, Pressure, Digiquartz with TC

Serial number : 1184
Calibrated on : 12-Dec-17
C1 : -3.923755e+004
C2 : -2.831515e-001
C3 : 1.211200e-002
D1 : 3.402400e-002
D2 : 0.000000e+000
T1 : 3.027916e+001
T2 : -4.427000e-004
T3 : 4.118300e-006

T4 : 2.652680e-009
T5 : 0.000000e+000
Slope : 1.00003279
Offset : -0.70932
AD590M : 1.280690e-002
AD590B : -8.805580e+000

4) Frequency 3, Temperature, 2

Serial number : 5938
Calibrated on : 29-Nov-17
G : 4.31999730e-003
H : 6.27126800e-004
I : 1.91838404e-005
J : 1.34572740e-006
F0 : 1000.000
Slope : 1.00000000
Offset : 0.0000

5) Frequency 4, Conductivity, 2

Serial number : 4262
Calibrated on : 05-Dec-17
G : -9.66469630e+000
H : 1.34554639e+000
I : -1.91814055e-003
J : 2.01820078e-004
CTcor : 3.2500e-006
CPcor : -9.57000000e-008
Slope : 1.00000000
Offset : 0.00000

6) A/D voltage 0, Oxygen, SBE 43

Serial number : 2829
Calibrated on : 09-Dec-17
Equation : Sea-Bird
Soc : 4.91300e-001
Offset : -4.99100e-001
A : -3.81630e-003
B : 1.86100e-004
C : -2.54620e-006
E : 3.60000e-003
Tau20 : 1.41000e+000
D1 : 1.92634e-004
D2 : -4.64803e-002
H1 : -3.30000e-002
H2 : 5.00000e+003
H3 : 1.45000e+003

7) A/D voltage 1, Oxygen, SBE 43, 2

Serial number : 2813
Calibrated on : 29 Dec 2017
Equation : Sea-Bird
Soc : 4.35900e-001
Offset : -4.75900e-001
A : -4.43210e-003
B : 2.07560e-004
C : -3.03460e-006

E : 3.60000e-002
Tau20 : 1.30000e+000
D1 : 1.92634e-004
D2 : -4.64803e-002
H1 : -3.30000e-002
H2 : 5.00000e+003
H3 : 1.45000e+003

8) A/D voltage 2, PAR/Irradiance, Biospherical/Licor

Serial number : 70549
Calibrated on : 27 Nov 2017
M : 1.00000000
B : 0.00000000
Calibration constant : 18975000000.00000000
Multiplier : 1.00000000
Offset : -0.05332251

9) A/D voltage 3, Free**10) A/D voltage 4, Fluorometer, WET Labs ECO-AFL/FL**

Serial number : FLNTURTD 3332
Calibrated on : 6 Feb 2018
Dark output : 0.0710
Scale factor : 6.00000000e+000

11) A/D voltage 5, Turbidity Meter, WET Labs, ECO-NTU

Serial number : FLNTURTD 3332
Calibrated on : 6 Feb 2018
ScaleFactor : 2.000000
Dark output : 0.076000

12) A/D voltage 6, Altimeter

Serial number : 62237
Calibrated on :
Scale factor : 15.000
Offset : 0.000

13) A/D voltage 7, Free

Scan length : 41

Pump Control

This setting is only applicable to a custom build of the SBE 9plus.
Enable pump on / pump off commands: NO

Data Acquisition:

Archive data: YES
Delay archiving: NO
Data archive: D:\CTDDData\SO264\test.hex
Timeout (seconds) at startup: 60
Timeout (seconds) between scans: 10

Instrument port configuration:

Port = COM1
Baud rate = 19200
Parity = N
Data bits = 8

Stop bits = 1

Water Sampler Data:

Water Sampler Type: SBE Carousel
 Number of bottles: 24
 Port: COM4
 Enable remote firing: NO
 Firing sequence: Sequential
 Tone for bottle fire confirmation uses PC sound card.

Header information:

Header Choice = Prompt for Header Information
 prompt 0 = Cruise:
 prompt 1 = Ship:
 prompt 2 = Station:
 prompt 3 = Depth:
 prompt 4 = Operator:

TCP/IP - port numbers:

Data acquisition:
 Data port: 49163
 Status port: 49165
 Command port: 49164
 Remote bottle firing:
 Command port: 49167
 Status port: 49168
 Remote data publishing:
 Converted data port: 49161
 Raw data port: 49160

Miscellaneous data for calculations

Depth, Average Sound Velocity, and TEOS-10
 Latitude when NMEA is not available: 0.000
 Longitude when NMEA is not available: 0.000

Average Sound Velocity
 Minimum pressure [db]: 20.000
 Minimum salinity [psu]: 20.000
 Pressure window size [db]: 20.000
 Time window size [s]: 60.000

Descent and Acceleration
 Window size [s]: 2.000

Plume Anomaly
 Theta-B: 0.000
 Salinity-B 0.000
 Theta-Z / Salinity-Z 0.000
 Reference pressure [db] 0.000

Oxygen
 Window size [s]: 2.000
 Apply hysteresis correction: 1
 Apply Tau correction: 1

Potential Temperature Anomaly
 A0: 0.000
 A1: 0.000
 A1 Multiplier: Salinity

Serial Data Output:

Output data to serial port: NO

Mark Variables:

Variables:

Digits Variable Name [units]

0	Scan Count
4	Depth [salt water, m]
7	Conductivity [S/m]
5	Salinity, Practical [PSU]

Shared File Output:

Output data to shared file: NO

TCP/IP Output:

Raw data:

Output raw data to socket: NO
XML wrapper and settings: NO
Seconds between raw data updates: 0.000

Converted data:

Output converted data to socket: NO
XML format: NO

SBE 11plus Deck Unit Alarms

Enable minimum pressure alarm: NO
Enable maximum pressure alarm: NO
Enable altimeter alarm: NO

SBE 14 Remote Display

Enable SBE 14 Remote Display: NO

PC Alarms

Enable minimum pressure alarm: NO
Enable maximum pressure alarm: NO
Enable altimeter alarm: NO
Enable bottom contact alarm: NO
Alarm uses PC sound card.

Options:

Prompt to save program setup changes: YES
Automatically save program setup changes on exit: NO
Confirm instrument configuration change: YES
Confirm display setup changes: YES
Confirm output file overwrite: YES
Check scan length: NO
Compare serial numbers: NO
Maximized plot may cover Seasave: NO

Appendix Table 5.3.1. Plankton net stations, sampling intervals and sample destinations during RV Sonne cruise SO264.

Destination: A = Shell geochemistry and faunal assemblages: Anna Jentzen/MPIC (Planktic Foraminifers) and Nina Keul/IFG/Univ. Kiel (Pteropods); B = Katja Peijneburg/Naturalis Leiden (Phylogenetic analyses of the Gastropods); C =Andrea Abelmann-Gersonde/AWI (Diatoms, Radiolaria); X = Sample lost							
Station	Date	Time	Longitude	Latitude	Water depth (m)	Sampling depth intervals (m)	Destinat.
SO264-1-1	2.7.2018	18:23	179°49.294' W	07°00.465' S		100–80	A
						80–60	A
						60–40	A
						40–20	A
						20–0	A
SO264-1-3	2.7.2018	22:00	179°49.289' W	07°00.464' S		500–350	A
						350–200	A
						200–140	A
						140–60	A
						60–0	B
SO264-2-1	4.7.2018	20:08	179°36.701' E	01°46.992' N	5612	100–80	A
						80–60	A
						60–40	A
						40–20	A
						20–0	A
SO264-2-3	4.7.2018	22:14	179°36.693' E	01°47.003' N	5620	600–375	X
						375–220	A
						220–160	A
						160–80	A
						80–0	B
SO264-3-1	5.7.2018	13:03	179°08.052' E	04°30.572' N	5685	100–80	A
						80–60	A
						60–40	A
						40–20	A
						20–0	A
SO264-3-3	5.7.2018	15:14	179°08.022' E	04°30.563' N	5684	600–400	A
						400–200	A
						200–160	A
						160–80	A
						80–0	B
SO264-4-1	6.7.2018	06:12	178°44.624' E	07°19.738' N	5429	100–80	A
						80–60	A
						60–40	A
						40–20	A
						20–0	A
SO264-5-1	7.7.2018	00:05	178°27.619' E	09°59.425' N	5738	100–80	A

Appendix 5.3 Water column sampling

SO264 Cruise Report

						80–60	A
						60–40	A
						40–20	A
						20–0	A
SO264-5-3	7.7.2018	02:15	178°27.618' E	09°59.419' N	5739	600-400	A
						400-250	A
						250-160	A
						160-40	A
						40-0	B
SO264-6-1	8.7.2018	21:23	176°55.197' E	18°33.602' N	3613	100–80	A
						80–60	A
						60–40	A
						40–20	A
						20–0	A
SO264-6-3	9.7.2018	00:47	176°55.200' E	18°33.597' N	3588	700-500	A
						500-300	A
						300-160	A
						160-80	A
						80-0	B
SO264-7-1	11.7.2018	03:00	175°36.525' E	27°46.950' N	5511	100–80	A
						80–60	A
						60–40	A
						40–20	A
						20–0	A
SO264-7-3	11.7.2018	05:19	175°36.544' E	27°46.952' N	5512	700-500	A
						500-350	A
						350-160	A
						160-80	A
						80-0	B
SO264-8-3	12.7.2018	23:59	174°46.160' E	33°39.269' N	2715	100–80	A
						80–60	A
						60–40	A
						40–20	A
						20–0	A
SO264-8-5	13.7.2018	03:01	174°46.168' E	33°39.270' N	2716	800-500	A
						500-350	A
						350-160	A
						160-40	A
						40-0	B
SO264-11-1	14.7.2018	16:29	172°23.336' E	35°31.574' N	4112	100–80	A
						80–60	A
						60–40	A
						40–20	A

Appendix 5.3 Water column sampling

SO264 Cruise Report

						20-0	A
SO264-11-3	14.7.2018	20:40	172°23.216' E	35°31.439' N	3992	800-500	A
						500-350	A
						350-160	A
						160-40	A
						40-0	B
SO264-13-3	16.7.2018	07:58	170°44.240' E	37°47.283' N	4026	100-80	A
						80-60	A
						60-40	A
						40-20	A
						20-0	A
SO264-13-5	16.7.2018	11:58	170°44.250' E	37°47.284' N	4029	700-500	A
						500-250	A
						250-100	A
						100-40	A
						40-0	B
SO264-19-3	19.7.2018	12:57	169°55.711' E	41°31.768' N	5308	100-80	A
						80-60	A
						60-40	A
						40-20	A
						20-0	A
SO264-19-5	19.7.2018	17:57	169°55.710' E	41°31.766' N	5304	700-500	A
						500-250	A
						250-150	A
						150-60	A
						60-0	B
SO264-24-1	22.7.2018	08:59	170°35.837' E	44°48.051' N	4303	100-80	A
						80-60	A
						60-40	A
						40-20	A
						20-0	A
SO264-24-4	22.7.2018	16:02	170°35.442' E	44°47.134' N	4410	750-500	A
						500-300	A
						300-150	A
						150-60	A
						60-0	B
SO264-24-5	22.7.2018	17:45	170°35.448' E	44°47.127' N	4410	750-500	B
						500-300	A
						300-150	A
						150-60	A
						60-0	A
SO264-35-1	25.7.2018	18:44	170°10.365' E	44°46.372' N	1769	100-80	A
						80-60	A

Appendix 5.3 Water column sampling

SO264 Cruise Report

						60–40	A
						40–20	A
						20–0	A
SO264-40-1	29.7.2018	15:22	170°18.018' E	45°34.024' N	5401	100–80	A
						80–60	A
						60–40	A
						40–20	A
						20–0	A
SO264-40-3	29.7.2018	20:07	170°18.007' E	45°33.993' N	5401	700-500	A
						500-250	A
						250-100	A
						100-20	B
						20-0	B
SO264-46-1	1.8.2018	18:29	169°24.709' E	46°48.924' N	3992	100–80	A
						80–60	A
						60–40	A
						40–20	A
						20–0	A
SO264-46-3	1.8.2018	22:25	169°24.664' E	46°48.944' N	3991	700-500	A
						500-250	A
						250-160	A
						160-40	A
						40-0	B
SO264-60-3	8.8.2018	21:45	168°33.422' E	49°18.449' N	5273	700-500	C
						500-250	C
						250-160	C
						160-40	C
						40-0	C
SO264-60-4	8.8.2018	23:09	168°33.429' E	49°18.451' N	5278	400-50	C
						700-300	C
						700-300	C
						700-50	C
						50-0	C
SO264-60-5	9.8.2018	02:09	168°33.427' E	49°18.447' N	5266	700-300	C
						700-300	C
						700-300	C
						700-50	C
						50-0	C
SO264-60-6	9.8.2018	05:58	168°33.416' E	49°18.444' N	5273	700-300	C
						700-300	C
						700-300	C
						700-50	C
						50-0	C

Appendix 5.3 Water column sampling

SO264 Cruise Report

SO264-60-7	9.8.2018	09:31	168°33.434' E	49°18.444' N	5275	700-300	C
						700-300	C
						700-300	C
						700-50	C
						50-0	C
SO264-60-8	9.8.2018	13:01	168°33.435' E	49°18.443' N	5275	700-300	C
						700-300	C
						700-300	C
						700-50	C
						50-0	C
SO264-60-9	9.8.2018	16:45	168°33.471' E	49°18.448' N	5268	700-300	C
						700-300	C
						700-300	C
						700-50	C
						50-0	C
SO264-60-10	9.8.2018	20:20	168°33.425' E	49°18.449' N	5269	700-300	C
						700-300	C
						700-300	C
						700-50	C
						50-0	C
SO264-60-11	9.8.2018	23:51	168°33.431' E	49°18.444' N	5277	700-300	C
						700-300	C
						700-300	C
						700-50	C
						50-0	C
SO264-67-1	13.8.2018	07:50	168°35.180' E	50°14.677' N	5034	100-80	A
						80-60	A
						60-40	A
						40-20	A
						20-0	A
SO264-67-3	13.8.2018	12:05	168°35.160' E	50°14.702' N	5029	550-300	A
						300-100	A
						100-35	A
						35-15	B
						15-0	B
SO264-77-1	16.8.2018	07:54	166°52.653' E	50°29.700' N	4977	100-80	A
						80-60	A
						60-40	A
						40-20	A
						20-0	A
SO264-77-3	16.8.2018	12:23	166°52.809' E	50°29.725' N	4976	700-500	A
						500-300	A
						300-160	A

						160-60	A
						60-0	B

Appendix Table 5.3.2. Start and end of plankton filter (PF) samples for foraminiferal and pteropod analyses (sieve mesh size >63 µm) during RV Sonne cruise SO264. * samples for diatom analyses (sieve mesh size >40 µm). ** no end time/seawater volume due to overflow during pumping.

P F #	Start Date (UTC)	Start Time (UTC)	Start Latitude	Start Longitude	End Date (UTC)	End Time (UTC)	End Latitude	End Longitude	Sea- water volu me (m ³)
1	01.07. 2018	15:20	11°58,009' S	179°09,315 ' E	01.07.18	17:28	11°33,432' S	178°58,884' E	0.51
2	02.07. 18	00:10	10°23,441' S	179°12,635 'E	02.07.18	02:47	09°54,050' S	179°19,162'E	1.30
3	02.07. 18	02:57	09°52,137' S	179°19,592 'E	02.07.18	08:04	08°50,607' S	179°36,236' E	2.92
4	02.07. 18	19:42	07°00,460' S	179°49,289 'W	03.07.18	00:38	06°44,176' S	179°48,595' W	2.26
5	03.07. 18	09:40	04°52,755' S	179°43,887 ' W	03.07.18	19:52	02°59,112' S	179°39,09' W	5.10
6	04.07. 18	01:30	01°59,890' S	179°48,864 ' W	04.07.18	03:59	01°30,300' S	179°48,610' W	1.25
7	04.07. 18	04:09	01°28,242' S	179°48,869 ' W	04.07.18	11:57	00°08,981' N	179°58,024' E	3.86
8	04.07. 18	17:55	01°25,285' N	179°41,417 ' E	05.07.18	00:23	01°57,662' N	179°34,821' E	2.82
9 **	05.07. 18	00:36	02°00,234' N	179°34,374 ' E	—	—	—	—	1.28
10	05.07. 18	13:43	04°30,569' N	179°08,027 ' E	05.07.18	16:56	04°36,972' N	179°07,119' E	1.93
11	05.07. 18	17:35	04°45,031' N	179°06,004 ' E	06.07.18	05:52	07°17,883' N	178°44,841' E	2.91
12	06.07. 18	07:15	07°19,742' N	178°44,624 ' E	06.07.18	10:51	07°19,739' N	178°44,651' E	1.50
13	06.07. 18	11:51	07°29,838' N	178°43,544 ' E	06.07.18	19:41	09°08,189' N	178°33,082' E	3.29
14	07.07. 18	04:25	10°10,105' N	178°25,721 'E	08.07.18	00:20	14°16,718' N	177°41,811' E	8.28
15	08.07. 18	00:28	14°18,416' N	177°41,509 ' E	08.07.18	07:51	15°49,728' N	177°25,044' E	3.15
16	08.07. 18	08:02	15°52,013' N	177°24,636 ' E	08.07.18	20:45	18°29,184' N	176°55,997' E	5.57
17	08.07. 18	22:34	18°33,596' N	176°55,204 ' E	09.07.18	02:06	18°33,600' N	176°55,205' E	1.43
18	09.07. 18	05:10	19°07,432' N	176°50,532 ' E	09.07.18	08:48	19°47,642' N	176°44,967' E	1.51
19 **	09.07. 18	22:00	22°10,707' N	176°24,987 ' E	—	—	—	—	—
20	10.07. 18	08:53	23°35,596' N	176°12,967 ' E	10.07.18	10:51	24°37,698' N	176°04,095' E	1.41
21	10.07. 18	21:51	26°47,958' N	175°45,231 ' E	11.07.18	02:34	27°44,059' N	175°36,997' E	1.83
22	11.07. 18	04:01	27°46,950' N	175°36,541 ' E	11.07.18	06:32	27°47,330' N	175°36,592' E	1.18
23	11.07. 18	07:27	27°58,388' N	175°34,935 ' E	11.07.18	12:12	28°57,093' N	175°26,497' E	2.42
24	11.07. 18	12:34	28°57,400' N	175°26,285 ' E	11.07.18	20:50	30°37,817' N	175°11,806' E	3.26
25	11.07. 18	21:44	30°48,702' N	175°10,201 ' E	12.07.18	04:15	32°07,291' N	174°58,548' E	1.06
26	12.07. 18	04:23	32°08,997' N	174°58,289 ' E	12.07.18	10:32	33°21,074' N	174°47,007' E	2.48

27	12.07.18	20:38	33°39.612' N	174°45.045' E	13.07.18	00:37	33°39.267' N	174°46.160' E	1.77
28**	13.07.18	08:02	34°07.851' N	174°11.066' E	13.07.18	17:27	34°36.336' N	172°22.810' E	–
29	14.07.18	03:46	34°53.977' N	172°00.105' E	14.07.18	08:36	34°55.356' N	172°08.790' E	2.12
30	14.07.18	08:49	34°56.487' N	172°07.572' E	14.07.18	16:06	35°30.403' N	172°21.765' E	1.14
31	14.07.18	17:15	35°31.488' N	172°23.263' E	14.07.18	21:59	35°31.421' N	172°23.233' E	2.13
32**	15.07.18	06:31	35°44.994' N	171°46.293' E	–	–	–	–	–
33	16.07.18	03:07	37°47.859' N	170°43.228' E	16.07.18	08:45	37°47.278' N	170°44.243' E	0.76
34	16.07.18	22:30	39°03.599' N	171°12.749' E	17.07.18	02:26	40°00.196' N	171°06.090' E	0.93
35	17.07.18	02:47	40°04.732' N	171°05.555' E	17.07.18	06:33	40°49.210' N	170°58.111'E	0.61
36	18.07.18	09:45	41°49.633' N	170°21.815' E	18.07.18	12:05	41°50.617' N	170°35.841' E	0.37
37	20.07.18	23:24	42°31.749' N	170°32.638' E	21.07.18	01:50	43°01.631' N	170°38.423' E	0.41
38	23.07.18	09:08	44°44.730' N	170°09.450' E	23.07.18	10:49	44°43.464' N	170°03.225' E	0.67
39**	23.07.18	10:44	44°45.345' N	170°01.962' E	–	–	–	–	–
40	24.07.18	09:35	44°52.925' N	170°14.278' E	24.07.18	12:03	45°04.240' N	170°08.462' E	0.42
41**	24.07.18	12:15	45°03.928' N	170°09.159' E	24.07.18	14:07	44°57.471' N	170°22.772' E	–
42	24.07.18	14:32	44°55.999' N	170°25.864' E	24.07.18	17:27	45°07.102' N	170°22.880' E	0.68
43	25.07.18	09:10	45°01.848' N	170°13.552' E	25.07.18	11:03	45°00.652' N	170°33.858' E	0.76
44	26.07.18	07:15	44°55.760' N	170°31.524' E	26.07.18	11:30	45°15.484' N	170°28.166' E	0.77
45	27.07.18	03:57	45°21.108' N	169°59.591' E	27.07.18	08:55	45°32.758' N	170°11.582' E	0.78
46	28.07.18	02:48	45°41.641' N	169°57.748' E	28.07.18	07:55	45°48.703' N	169°59.446' E	0.77
47	30.07.18	03:53	45°45.282' N	170°05.813' E	30.07.18	08:21	46°00.734' N	169°37.764' E	0.52
48	30.07.18	12:29	45°58.143' N	169°28.702' E	30.07.18	15:01	46°00.816' N	169°21.181' E	1.00
49**	30.07.18	15:07	46°00.269' N	169°20.864' E	30.07.18	22:02	46°10.133' N	169°10.073' E	–
50	01.08.18	04:17	46°29.937' N	169°28.887' E	01.08.18	06:42	46°39.379' N	169°36.184' E	0.41
51*	01.08.18	06:45	46°38.815' N	169°36.024' E	01.08.18	08:14	46°33.796' N	169°36.064' E	0.16
52	03.08.18	03:27	47°25.254' N	169°15.848' E	03.08.18	08:32	47°47.155' N	169°14.702' E	0.83
53	04.08.18	05:07	47°58.507' N	169°03.868' E	04.08.18	06:42	47°48.065' N	169°04.175' E	0.51
54	08.08.18	01:01	48°52.794' N	168°29.173' E	08.08.18	03:14	48°59.167' N	168°29.721' E	0.49
55	11.08.18	01:56	49°43.399' N	168°02.275' E	11.08.18	04:33	49°40.885' N	168°18.621' E	0.72
56	11.08.18	04:44	49°41.920' N	168°18.724' E	11.08.18	06:02	49°43.842' N	168°18.912' E	0.30

57	11.08. 18	10:29	49°46.858' N	168°19.214' E	11.08.18	12:04	49°46.097' N	168°25.338' E	0.30
58	16.08. 18	00:28	50°34.357' N	168°03.367' E	16.08.18	01:24	50°29.052' N	167°51.471' E	0.13
59	17.08. 18	01:13	48°48.677' N	163°38.621' E	17.08.18	05:36	48°09.896' N	162°25.866' E	0.97
60	17.08. 18	05:54	48°07.696' N	162°21.778' E	17.08.18	09:04	47°39.660' N	161°29.785' E	0.72
61	17.08. 18	09:27	47°36.215' N	161°23.363' E	17.08.18	11:53	47°14.807' N	160°44.082' E	0.60
62	17.08. 18	12:05	47°13.092' N	160°40.922' E	17.08.18	13:45	46°58.648' N	160°14.559' E	0.29
63	18.08. 18	00:19	45°33.036' N	157°40.602' E	18.08.18	02:38	45°13.474' N	157°05.841' E	0.72
64	18.08. 18	03:06	45°09.464' N	156°58.906' E	18.08.18	07:19	44°38.921' N	156°05.301' E	0.74
65	19.08. 18	00:45	42°29.724' N	152°23.663' E	19.08.18	02:59	42°12.701' N	151°53.232' E	0.41
66	19.08. 18	05:22	41°52.791' N	151°21.722' E	19.08.18	09:20	41°21.718' N	150°30.082' E	1.30
67	19.08. 18	11:40	41°02.801' N	149°58.845' E	19.08.18	13:57	40°44.553' N	149°28.834' E	0.55
68	19.08. 18	23:08	39°47.122' N	147°55.348' E	20.08.18	01:29	39°39.059' N	147°42.297' E	0.46

Appendix Table 5.3.3. Data from the Thermosalinograph during plankton filter (PF) sampling (see Appendix Table 5.2.1).

PF sample #	Temperature (°C)	Salinity (psu)	Chlorophyll (µg/l)
PF4	29.63	34.98	
PF5	29.29	35.16	
PF6	29.04	35.33	0.36
PF7	29.22	35.35	0.79
PF8	29.13	34.92	0.42
PF10	29.43	34.18	0.14
PF11	29.27	34.14	0.10
PF12	28.83	33.91	0.10
PF13	28.76	34.10	0.10
PF14	28.49	34.15	0.09
PF15	28.47	34.20	0.09
PF16	28.14	34.62	0.10
PF17	28.09	35.00	0.09
PF18	28.13	34.92	0.10
PF20	28.03	35.37	0.09
PF21	27.39	31.75	0.07
PF22	27.46		0.05
PF23	27.11		0.05
PF24	26.02		0.07
PF25	25.24		0.07
PF26	24.93		0.07
PF27	24.62	35.23	0.09
PF28	24.25	34.71	0.09
PF29	24.08	34.59	0.09
PF30	23.46	34.46	0.09
PF31	23.26	34.54	0.13
PF33	20.43	34.25	0.33
PF34	21.53	34.37	0.18
PF35	20.43	34.10	0.91
PF36	17.48	33.65	3.12
PF37	17.31	33.77	1.63
PF38	11.25	32.59	1.34
PF40	11.76		
PF41	11.72	32.44	1.26
PF42	11.64	32.27	1.07
PF43	12.27	32.61	1.09
PF44	12.80	32.53	1.35
PF45	12.66	32.66	0.86
PF46	10.83	32.77	0.94
PF47	10.27	32.76	1.02

PF48	10.59	32.46	1.03
PF49	10.52	32.38	0.96
PF50	10.36	32.79	2.23
PF51	10.42	32.78	3.01
PF53	10.07	32.69	1.55
PF54	10.43	32.63	1.58
PF55	10.93	32.42	1.15
PF56	10.85	32.64	0.96
PF57	11.24	32.20	2.11
PF58	11.32	32.59	2.10
PF59	11.70	32.63	1.00
PF60	11.86	32.53	1.28
PF61	12.04	32.46	1.72
PF62	12.18	32.50	1.80
PF63	13.18	32.41	1.00
PF64	13.29	32.26	0.83
PF65	15.90	32.63	0.90
PF66	17.78	33.01	1.79
PF67	20.41	33.78	0.36
PF68	21.11	33.65	0.20

Appendix Table 5.3.4 Water samples taken from CTD rosette.

Sonne cruise SO264 (Fiji - Yokohama)											
SO264 Rosette Sampling Protocol											
Cruise: SO264		Station-Nr: SO264-1-2				Area: Transit water depth (m): 5342.9					
Date: 2018-07-02		Bordtime (UTC): 19:21				Lat.: 07° 0.4675' S Long.: 179° 49.291 'W					
Bottle No.	Rope length (m)	DIC	TA& pH	$\delta 18O$	$\delta 13C$ DIC	14C	TE	Nd	sili- cate	plastic	comments
1	3000	X	X	X	X	X			X		Filter 4 (TE)
2	3000						X	X			
3	3000							X			
4	2000	X	X	X	X	X			X		Filter 4 (TE)
5	2000						X	X			
6	2000							X			
7	1500	X	X	X	X	X			X		Filter 3 (TE)
8	1500						X	X			
9	1500							X			
10	1000	X	X	X	X	X			X		Filter 3 (TE)
11	1000						X	X			
12	1000							X			
13	500	X	X	X	X	X			X		Filter 2 (TE)
14	500						X	X			
15	500							X			
16	300	X	X	X	X	X			X		Filter 2 (TE)
17	300						X	X			
18	300							X			
19	125	X	X	X	X	X			X		Filter 1 (TE)
20	125						X	X			
21	125							X			
22	25	X	X	X	X	X			X		Filter 1 (TE)
23	25						X	X			
24	25							X			

Sonne cruise SO264												
(Fiji - Yokohama)												
SO264 Rosette												
Sampling Protocol												
Cruise: SO264		Station-Nr: SO264-2-2				Area: Transit						
						water depth (m): 5612						
Date: 2018-07-04		Bordtime (UTC): 20:42				Lat.: 01° 46.990' N						
						Long.: 179° 36.697'E						
Bottle No.	Rope length (m)	DIC	TA& pH	$\delta^{18}O$	$\delta^{13}C$ DIC	14C	TE	Nd	sili-cate	plastic	comments	
1	1200	X	X	X	X		X		X	X	TE not taken	
2	1000			X	X				X	X		
3	800	X	X	X	X		X		X	X		
4	700			X	X				X	X		
5	600	X	X	X	X		X		X	X		
6	500	X	X	X	X				X	X		
7	400			X	X				X	X		
8	375			X	X				X	X		
9	350	X	X	X	X		X		X	X		
10	300			X	X				X	X		
11	250	X	X	X	X		X		X	X		
12	200			X	X				X	X		
13	180			X	X				X	X		
14	160	X	X	X	X		X		X	X		
15	140			X	X				X	X		
16	120			X	X				X	X		
17	100	X	X	X	X		X		X	X		
18	80	X	X	X	X		X		X	X		
19	60	X	X	X	X		X		X	X		
20	40	X	X	X	X		X		X	X		
21	20	X	X	X	X		X		X	X		
22	10						X	X				
23	10							X				
24	10	X	X	X	X				X	X		
Sonne cruise SO264 (Fiji - Yokohama)												

SO264 Rosette Sampling Protocol											
Cruise: SO264		Station-Nr: SO264-3-2				Area: Transit water depth (m): 5683					
Date: 2018-07-05		Bordtime (UTC): 13:38				Lat.: 04° 30.572' N Long.: 179° 08.052 'E					
Bottle No.	Rope length (m)	DIC	TA& pH	$\delta 18O$	$\delta 13C$ DIC	14C	TE	Nd	sili- cate	plastic	comments
1	1200	X	X	X	X		X		X	X	
2	1000			X	X				X	X	
3	800	X	X	X	X		X		X	X	
4	700			X	X				X	X	
5	600	X	X	X	X		X		X	X	
6	500	X	X	X	X				X	X	
7	400			X	X				X	X	
8	375			X	X				X	X	
9	350	X	X	X	X		X		X	X	
10	300			X	X				X	X	
11	250	X	X	X	X		X		X	X	
12	200			X	X				X	X	
13	180			X	X				X	X	
14	160	X	X	X	X		X		X	X	
15	140			X	X				X	X	
16	120			X	X				X	X	
17	100	X	X	X	X		X		X	X	
18	80	X	X	X	X		X		X	X	
19	60	X	X	X	X		X		X	X	
20	40	X	X	X	X		X		X	X	
21	20	X	X	X	X		X		X	X	
22	10						X	X			
23	10							X			
24	10	X	X	X	X				X	X	
Sonne cruise SO264 (Fiji - Yokohama)											
SO264 Rosette Sampling											

Protocol											
Cruise: SO264			Station-Nr: SO264-3-2				Area: Transit water depth (m): 5683				
Date: 2018-07-05			Bordtime (UTC): 13:38				Lat.: 04° 30.572' N Long.: 179° 08.052 'E				
Bottle No.	Rope length (m)	DIC	TA& pH	$\delta 18O$	$\delta 13C$ DIC	14C	TE	Nd	sili-cate	Plas-tic	Com-ments
1	1200	X	X	X	X		X		X	X	
2	1000			X	X				X	X	
3	800	X	X	X	X		X		X	X	
4	700			X	X				X	X	
5	600	X	X	X	X		X		X	X	
6	500	X	X	X	X				X	X	
7	400			X	X				X	X	
8	375			X	X				X	X	
9	350	X	X	X	X		X		X	X	
10	300			X	X				X	X	
11	250	X	X	X	X		X		X	X	
12	200			X	X				X	X	
13	180			X	X				X	X	
14	160	X	X	X	X		X		X	X	
15	140			X	X				X	X	
16	120			X	X				X	X	
17	100	X	X	X	X		X		X	X	
18	80	X	X	X	X		X		X	X	
19	60	X	X	X	X		X		X	X	
20	40	X	X	X	X		X		X	X	
21	20	X	X	X	X		X		X	X	
22	10						X	X			
23	10							X			
24	10	X	X	X	X				X	X	

Sonne cruise SO264 (Fiji - Yokohama) SO264 Rosette Sampling Protokoll											
Cruise: SO264		Station-Nr: SO264-4-2			Area: Transit water depth (m): 5436						
Date: 2018-07-06		Bordtime (UTC): 06:44			Lat.: 07° 19.745' N Long.: 178° 44.617 'E						
Bottle No.	Rope length (m)	DIC	TA& pH	$\delta 18O$	$\delta 13C$ DIC	14 C	TE	Nd	sili-cate	plastic	comments
1	5300	X	X	X	X	X			X		
2	5300						X	X			
3	5300							X			
4	4500	X	X	X	X	X			X		not taken from CTD, but taken from cubitainer
5	4500						X	X			
6	4500							X			
7	3500	X	X	X	X	X			X		
8	3500						X	X			
9	3500							X			
10	2500	X	X	X	X	X			X		
11	2500						X	X			
12	2500							X			
13	1500	X	X	X	X	X			X		
14	1500						X	X			
15	1500							X			
16	1000	X	X	X	X	X			X		
17	1000						X	X			
18	1000							X			
19	500	X	X	X	X	X			X		
20	500						X	X			
21	500							X			
22	100					X	X	X			
23	100	X	X	X	X				X		
24	100							X			

Sonne cruise SO264 (Fiji - Yokohama)											
SO264 Rosette Sampling Protocol											
Cruise: SO264			Station-Nr: SO264-5-2			Area: Transit water depth (m): 5738					
Date: 2018-07-07			Bordtime (UTC): 0:40			Lat.: 09° 59.420' N Long.: 178° 27.619 'E					
Bottle No.	Rope length (m)	DIC	TA& pH	$\delta^{18}O$	$\delta^{13}C$ DIC	14 C	TE	Nd	sili-cate	Plas-tic	comments
1	1200	X	X	X	X		X		X	X	
2	1000			X	X				X	X	
3	800	X	X	X	X		X		X	X	
4	700			X	X				X	X	
5	600	X	X	X	X		X		X	X	
6	500	X	X	X	X				X	X	
7	400			X	X				X	X	
8	375			X	X				X	X	
9	350	X	X	X	X		X		X	X	
10	300			X	X				X	X	
11	250	X	X	X	X		X		X	X	
12	200			X	X				X	X	
13	180			X	X				X	X	
14	160	X	X	X	X		X		X	X	
15	140			X	X				X	X	
16	120			X	X				X	X	
17	100	X	X	X	X		X		X	X	
18	80	X	X	X	X		X		X	X	
19	60	X	X	X	X		X		X	X	
20	40	X	X	X	X		X		X	X	
21	20	X	X	X	X		X		X	X	
22	10						X	X			
23	10	X	X	X	X				X		
24	10							X			

Sonne cruise SO264 (Fiji - Yokohama)												
SO264 Rosette Sampling Protocol												
Cruise: SO264		Station-Nr: SO264-6-2				Area: Transit						
						water depth (m): 3578						
Date: 2018-07-08		Bordtime (UTC): 21:55				Lat.: 18° 33.600' N Long.: 176° 55.202 'E						
Bottle No.	Rope length (m)	DIC	TA&pH	$\delta^{18}O$	$\delta^{13}C$ DIC	14C	T E	Nd	sili-cate	Plas-tic	Com-ments	
1	3500	X	X	X	X				X			
2	3500						X	X				
3	3500							X				
4	3000	X	X	X	X				X			
5	3000						X	X				
6	3000							X				
7	2000	X	X	X	X				X			
8	2000						X	X				
9	2000							X				
10	1000	X	X	X	X				X			
11	1000						X	X				
12	1000							X				
13	700	X	X	X	X				X			
14	700						X	X				
15	700							X				
16	350	X	X	X	X				X			
17	350						X	X				
18	350							X				
19	120	X	X	X	X				X			
20	120						X	X				
21	120							X				
22	50						X	X				
23	50	X	X	X	X				X			
24	50							X				

Sonne cruise SO264 (Fiji - Yokohama)											
SO264 Rosette Sampling Protocol											
Cruise: SO264		Station-Nr: SO264-7-2				Area: Transit					
Date: 2018-07-11		Bordtime (UTC): 03:34				water depth (m): 5512					
						Lat.: 27° 46.953' N					
						Long.: 175° 36.531 'E					
Bottle No.	Rope length (m)	DIC	TA& pH	$\delta^{18}O$	$\delta^{13}C$ DIC	14 C	TE	Nd	sili-cate	Plas-tic	Com-ments
1	1500	X	X	X	X		X		X	X	
2	1000			X	X				X	X	
3	800	X	X	X	X		X		X	X	
4	700			X	X				X	X	
5	600	X	X	X	X		X		X	X	
6	500	X	X	X	X				X	X	
7	400			X	X				X	X	
8	375			X	X				X	X	
9	350	X	X	X	X		X		X	X	
10	300			X	X				X	X	
11	250	X	X	X	X		X		X	X	
12	200			X	X				X	X	
13	180			X	X				X	X	
14	160	X	X	X	X		X		X	X	
15	140			X	X				X	X	
16	120			X	X				X	X	
17	100	X	X	X	X		X		X	X	
18	80	X	X	X	X		X		X	X	
19	60	X	X	X	X		X		X	X	
20	40	X	X	X	X		X		X	X	
21	20	X	X	X	X		X		X	X	
22	10						X	X			
23	10	X	X	X	X				X		
24	10							X			

Sonne cruise SO264 (Fiji - Yokohama)											
SO264 Rosette Sampling Protocol											
Cruise: SO264		Station-Nr: SO264-8-4				Area: Transit water depth (m): 2716					
Date: 2018-07-13		Bordtime (UTC): 00:40				Lat.: 33° 39.272' N Long.: 174° 46.150 'E					
Bottle No.	Rope length (m)	DIC	TA& pH	$\delta^{18}O$	$\delta^{13}C$ DIC	14 C	TE	Nd	sili-cate	Plas-tic	Com-ments
1	2687	X	X	X	X				X		
2	2687						X	X			
3	2687							X			
4	2000	X	X	X	X				X		
5	2000						X	X			
6	2000							X			
7	1500	X	X	X	X				X		
8	1500						X	X			
9	1500							X			
10	1000	X	X	X	X				X		
11	1000						X	X			
12	1000							X			
13	670	X	X	X	X				X		
14	670						X	X			
15	670							X			
16	350	X	X	X	X				X		
17	350						X	X			
18	350							X			
19	90	X	X	X	X				X		
20	90						X	X			
21	90							X			
22	50						X	X			
23	50	X	X	X	X				X		
24	50							X			

Sonne cruise SO264 (Fiji - Yokohama) SO264 Rosette Sampling Protocol											
Cruise: SO264		Station-Nr: SO264-11-2				Area: Koko Seamount water depth (m): 4096					
Date: 2018-07-14		Bordtime (UTC): 03:34				Lat.: 35° 31.571' N Long.: 172° 23.328 'E					
Bottle No.	Rope length (m)	DIC	TA& pH	$\delta^{18}O$	$\delta^{13}C$ DIC	14 C	TE	Nd	sili-cate	Plas-tic	comments
1	3976	X	X	X	X		X		X	X	
2	3500	X	X	X	X				X	X	
3	3250			X	X				X	X	
4	3000	X	X	X	X				X	X	
5	2750			X	X				X	X	
6	2500	X	X	X	X				X	X	
7	2250			X	X				X	X	
8	2000	X	X	X	X				X	X	
9	1750			X	X				X	X	
10	1500	X	X	X	X				X	X	
11	1250			X	X				X	X	
12	1000	X	X	X	X				X	X	
13	700	X	X	X	X		X		X	X	
14	600			X	X				X	X	
15	500	X	X	X	X		X		X	X	
16	400			X	X				X	X	
17	300	X	X	X	X		X		X	X	
18	250			X	X				X	X	
19	200	X	X	X	X		X		X	X	
20	120	X	X	X	X		X		X	X	
21	90	X	X	X	X		X		X	X	
22	50	X	X	X	X		X		X	X	
23	20	X	X	X	X		X		X	X	
24	10	X	X	X	X		X		X	X	

SO264 Rosette Sampling Protocol											
Cruise: SO264		Station-Nr: SO264-13-4				Area: Ojin & Jingu Seamount water depth (m): 4021					
Date: 2018-07-16		Bordtime (UTC): 08:30				Lat.: 37° 47.275' N Long.: 170° 44.241 'E					

Bottle No.	Rope length (m)	DIC	TA & pH	$\delta 18O$	$\delta 13C$ DIC	14 C	TE	Nd	sili-cate	Plas-tic	comments
1	3999	X	X	X	X		X		X	X	
2	3500	X	X	X	X				X	X	
3	3000			X	X				X	X	
4	2750			X	X				X	X	
5	2500	X	X	X	X				X	X	
6	2250			X	X				X	X	
7	2000			X	X				X	X	
8	1750			X	X				X	X	
9	1500	X	X	X	X				X	X	
10	1250			X	X				X	X	
11	1000	X	X	X	X				X	X	
12	900			X	X				X	X	
13	700			X	X						
14	600			X	X				X	X	
15	400	X	X	X	X						
16	300			X	X						
17	250			X	X				X	X	
18	200	X	X	X	X		X				
19	150			X	X						
20	100	X	X	X	X		X		X	X	
21	70			X	X						
22	50	X	X	X	X		X		X	X	
23	25			X	X						
24	10	X	X	X	X		X				

Sonne cruise SO264 (Fiji - Yokohama)

SO264 Rosette Sampling Protocol											
Cruise: SO264		Station-Nr: SO264-19-4			Area: west of Nintoku Seamoun water depth (m): 5208						
Date: 2018-07-20		Bordtime (UTC): 13:32			Lat.: 41° 31.769' N Long.: 169° 55.707'E						
Bottle No.	Rope length (m)	DI C	TA&pH	$\delta 18O$	$\delta 13C$ DIC	14 C	TE	Nd	sili-cate	plastic	comment s
1	5284	X	X	X	X	X	X		X	X	
2	5000	X	X	X	X	X			X	X	
3	4500			X	X	X			X	X	
4	4000			X	X	X			X	X	
5	3500	X	X	X	X	X			X	X	
6	3000			X	X	X			X	X	
7	2500			X	X	X			X	X	
8	2000			X	X	X			X	X	
9	1750	X	X	X	X	X			X	X	
10	1500			X	X	X			X	X	
11	1250	X	X	X	X	X			X	X	
12	1000			X	X	X			X	X	
13	900			X	X	X			X	X	
14	700			X	X	X			X	X	
15	600	X	X	X	X	X			X	X	
16	400			X	X	X			X	X	
17	300			X	X	X			X	X	
18	200	X	X	X	X	X	X		X	X	
19	150			X	X	X			X	X	
20	100	X	X	X	X	X	X		X	X	
21	70			X	X	X			X	X	
22	50	X	X	X	X	X	X		X	X	
23	25			X	X	X			X	X	
24	10	X	X	X	X	X	X		X	X	
Sonne cruise SO264 (Fiji - Yokohama)											
SO264 Rosette											

Sampling Protocol											
Cruise: SO264		Station-Nr: SO264-24-2				Area: 5- Suiko Seamount water depth (m): 4294					
Date: 2018-07-22		Bordtime (UTC): 09:30				Lat.: 44° 48.067' N Long.: 170° 35.864' E					
Bottle No.	Rope length (m)	DIC	TA&pH	$\delta 18O$	$\delta 13C$ DIC	14C	T E	Nd	sili-cate	Plas-tic	comments
1	4265	X	X				X	X			
2	4265							X			
3	4265			X	X				X	X	
4	3000	X	X	X	X				X	X	
5	2000	X	X				X	X			
6	2000							X			
7	2000			X	X				X	X	
8	1000	X	X				X	X			
9	1000							X			
10	1000			X	X				X	X	
11	800	X	X	X	X		X		X	X	
12	600	X	X				X	X			
13	600							X			
14	600			X	X				X	X	
15	400	X	X				X	X			
16	400							X			
17	400			X	X				X	X	
18	200	X	X	X	X		X		X	X	
19	150			X	X				X	X	
20	100	X	X	X	X		X		X	X	
21	50	X	X	X	X		X		X	X	
22	25	X	X				X	X			
23	25								X		
24	25			X	X			X		X	

Sonne cruise SO264 (Fiji - Yokohama)											
SO264 Rosette Sampling Protokol											
Cruise: SO264		Station-Nr: SO264-35-2				Area: Suiko water depth (m): 1763					
Date: 2018-07-25		Bordtime (UTC): 19:16				Lat.: 44° 46.142' N Long.: 170° 10.295'E					
Bottle No.	Rope length (m)	DI C	TA& pH	$\delta 18O$	$\delta 13C$ DIC	14 C	T E	Nd	sili-cate	Plastic	Comments
1	1730	X	X	X	X	X	X		X	X	
2	1600			X	X					X	
3	1500			X	X	X			X	X	
4	1400	X	X	X	X					X	
5	1300			X	X	X			X	X	
6	1200			X	X	X			X	X	
7	1100			X	X					X	
8	1000	X	X	X	X	X	X		X	X	
9	900			X	X					X	
10	800			X	X	X			X	X	bottles 10-24
11	700			X	X					X	closed on
12	600	X	X	X	X	X	X		X	X	the way- not
13	500			X	X					X	stopped due
14	400			X	X	X			X	X	to technical
15	350	X	X	X	X		X			X	problems
16	300			X	X					X	
17	250			X	X					X	
18	200	X	X	X	X	X	X		X	X	
19	150			X	X					X	
20	100	X	X	X	X	X	X		X	X	
21	80			X	X					X	
22	50	X	X	X	X		X			X	
23	25			X	X	X			X	X	
24	10	X	X	X	X		X			X	

Sonne cruise SO264 (Fiji - Yokohama)											
SO264 Rosette Sampling Protokol											
Cruise: SO264		Station-Nr: SO264-46-2				Area: Minnetonka water depth (m): 3992					
Date: 2018-08-01		Bordtime (UTC): 21:02				Lat.: 46° 48.942' N Long.: 169° 24.653'E					
Bottle No.	Rope length (m)	DI C	TA& pH	$\delta^{18}O$	$\delta^{13}C$ DIC	14 C	TE	Nd	sili-cate	Plas-tic	comme nts
1	3967	X	X	X	X	X			X	X	
2	3500			X	X				X	X	
3	3000			X	X	X			X	X	
4	2700			X	X				X	X	
5	2500	X	X	X	X	X			X	X	
6	2200			X	X				X	X	
7	2000			X	X	X			X	X	
8	1700			X	X				X	X	
9	1500	X	X	X	X	X			X	X	
10	1200			X	X				X	X	
11	1000	X	X	X	X	X			X	X	
12	900			X	X				X	X	
13	700			X	X	X	X		X	X	
14	600			X	X				X	X	
15	400	X	X	X	X	X	X		X	X	
16	300			X	X				X	X	
17	250			X	X	X			X	X	
18	200	X	X	X	X		X		X	X	
19	150			X	X	X			X	X	
20	100	X	X	X	X		X		X	X	
21	70			X	X	X			X	X	
22	50	X	X	X	X		X		X	X	
23	25			X	X	X			X	X	
24	10	X	X	X	X	X	X		X	X	

Sonne cruise SO264 (Fiji - Yokohama)

SO264 Rosette Sampling Protokol											
Cruise: SO264		Station-Nr: SO264-60-2				Area: Tenji water depth (m): 5270					
Date: 2018-08-08		Bordtime (UTC): 17:30				Lat.: 49° 18.442' N Long.: 168° 33.426'E					
Bottle No.	Rope length (m)	DIC	TA&pH	$\delta^{18}O$	$\delta^{13}C$ DIC	14 C	TE	Nd	sili-cate	Plas-tic	Com-ments
1	B			X					X	X	
2	B	X	X	X	X	X	X		X	X	
3	3500			X					X	X	
4	3500	X	X	X	X	X	X		X	X	
5	2000			X					X	X	
6	2000	X	X	X	X	X	X		X	X	
7	1000			X					X	X	
8	1000	X	X	X	X	X	X		X	X	
9	700			X					X	X	
10	700	X	X	X	X	X	X		X	X	
11	500			X					X	X	
12	500	X	X	X	X	X	X		X	X	
13	300			X					X	X	
14	300	X	X	X	X	X	X		X	X	
15	200			X					X	X	
16	200	X	X	X	X	X	X		X	X	
17	120			X					X	X	
18	120	X	X	X	X	X	X		X	X	
19	50			X					X	X	
20	50	X	X	X	X	X	X		X	X	
21	25			X					X	X	
22	25	X	X	X	X	X	X		X	X	
23	10			X					X	X	
24	10	X	X	X	X	X	X		X	X	

Sonne cruise SO264 (Fiji - Yokohama)

SO264 Rosette Sampling Protocol											
Cruise: SO264		Station-Nr: SO264-67-2				Area: Detroit Seamount water depth (m): 5034					
Date: 2018-08-13		Bordtime (UTC):08:18				Lat.: 50° 14.698' N Long.: 168° 35.153 'E					
Bottle No.	Rope length (m)	DIC	TA& pH	$\delta^{18}O$	$\delta^{13}C$ DIC	14 C	TE	Nd	sili-cate	Plas-tic	Com-ments
1	5000	X	X	X	X	X			X		
2	5000						X	X			
3	5000							X			
4	3500			X	X	X			X		
5	3500	X	X				X	X			
6	3500							X			
7	2000	X	X	X	X	X			X		
8	2000						X	X			
9	2000							X			
10	1000	X	X	X	X	X			X		
11	1000						X	X			
12	1000							X			
13	500	X	X	X	X	X			X		
14	500						X	X			
15	500							X			
16	200	X	X	X	X	X			X		
17	200						X	X			
18	200							X			
19	50	X	X	X	X	X			X		
20	50						X	X			
21	50							X			
22	10						X	X			
23	10	X	X	X	X	X			X		
24	10							X			

Sonne cruise SO264 (Fiji - Yokohama)

SO264 Rosette

Sampling Protocol											
Cruise: SO264		Station-Nr: SO264-77-2				Area: Detroit Seamount water depth (m): 4978m					
Date: 2018-08-16		Bordtime (UTC): 8:23				Lat.: 50° 29.732'N Long.: 166° 52.734' E					
Bottle No.	Rope length (m)	DIC	TA & pH	$\delta^{18}\text{O}$	$\delta^{13}\text{C}$ DIC	^{14}C	TE	Nd	silicate	Plastic	Comments
1	4950	X	X	X	X	X			X	X	
2	4500			X	X				X	X	
3	4000	X	X	X	X	X			X	X	
4	3500			X	X				X	X	
5	3000	X	X	X	X	X			X	X	
6	2500			X	X				X	X	
7	2000	X	X	X	X	X			X	X	
8	1500			X	X				X	X	
9	1300	X	X	X	X				X	X	
10	1000			X	X	X			X	X	
11	900	X	X	X	X				X	X	
12	800			X	X				X	X	
13	700	X	X	X	X	X			X	X	
14	600			X	X				X	X	
15	500	X	X	X	X	X			X	X	
16	400			X	X				X	X	
17	300	X	X	X	X				X	X	
18	250			X	X	X			X	X	
19	150	X	X	X	X				X	X	
20	100			X	X	X	X		X	X	
21	50	X	X	X	X	X	X		X	X	
22	30			X	X				X	X	
23	10	X	X	X	X		X		X	X	
24	CAMPARI										

DIC = dissolved inorganic carbon; TA & pH = total alkalinity, pH; $\delta^{18}\text{O}$ = light stable oxygen isotopes, $\delta^{13}\text{C}$ = light stable carbon isotopes; TE = trace elements / radiocarbon (not at all stations); Nd = Neodymium / Nd-isotopes (not at all stations); silicate = Silicate / Si isotopes; plastic = microplastic.

Appendix Table 5.3.5. Locations, timing, and flow volumes of microplastic samples.

Sample Name	Start Date	Start Time	Lat1 (-S/+N)	Long1 (-W/+E)	End Date	End Time	Lat2 (-S/+N)	Long2 (-W/+E)	Flow Volume (m ³)
SO264-2/MP-Transect1	2018-07-05	2:17:16	2°20,9 86'	179°30, 735'	2018-07-05	6:37:54	3°14,7 33'	179°21, 313'	1.101
SO264-2/MP-Transect2	2018-07-05	7:04:42	3°20,2 77'	179°20, 344'	2018-07-05	13:02:10	4°30,5 68'	179°08, 056'	1.558
SO264-3/MP-Station	2018-07-05	13:16:43	4°30,5 76'	179°08, 050'	2018-07-05	16:18:02	4°30,5 55'	179°08, 024'	1.084
SO264-3/MP-Transect1	2018-07-05	16:54:41	4°30,5 78'	179°07, 051'	2018-07-06	1:47:47	6°27,1 63'	178°51, 899'	2.351
SO264-3/MP-Transect2	2018-07-06	2:04:36	6°30,6 41'	178°51, 415'	2018-07-06	6:15:29	7°19,7 38'	178°44, 623'	1.349
SO264-4/MP-Station	2018-07-06	6:40:37	7°19,7 45'	178°44, 619'	2018-07-06	10:27:54	7°19,7 44'	178°44, 625'	1.332
SO264-4/MP-Transect1	2018-07-06	11:45:22	7°28,6 45'	178°43, 680'	2018-07-06	19:27:54	9°11,5 52'	178°32, 722'	1.945
SO264-5/MP-Station	2018-07-07	0:03:40	9°59,4 20'	178°27, 619'	2018-07-07	3:42:06	10°01, 404'	178°27, 359'	1.406
SO264-5/MP-Transect1	2018-07-07	6:50:19	10°40, 158'	178°20, 405'	2018-07-07	11:48:54	11°41, 810'	178°09, 473'	2.191
SO264-5/MP-Transect2	2018-07-07	13:33:58	12°03, 548'	178°05, 604'	2018-07-07	19:22:00	13°15, 260'	177°52, 820'	2.332
SO264-5/MP-Transect3	2018-07-07	21:07:32	13°36, 804'	177°48, 961'	2018-07-08	2:37:00	14°44, 951'	177°36, 820'	1.913
SO264-5/MP-Transect4	2018-07-08	7:51:05	15°49, 736'	177°25, 043'	2018-07-08	13:02:21	16°54, 053'	177°13, 387'	2.041
SO264-6/MP-Station	2018-07-08	21:40:40	18°33, 596'	176°55, 197'	2018-07-09	1:49:14	18°33, 607'	176°55, 198'	1.877
SO264-6/MP-Transect3	2018-07-09	23:32:33	22°28, 194'	176°22, 523'	2018-07-10	1:32:49	22°51, 346'	176°19, 247'	0.573
SO264-6/MP-Transect4	2018-07-10	21:12:19	23°21, 861'	176°14, 918'	2018-07-10	10:49:26	24°34, 302'	176°04, 103'	1.094
SO264-6/MP-Transect5	2018-07-10	11:02:54	24°39, 983'	176°03, 754'	2018-07-10	12:53:00	25°01, 482'	176°00, 678'	2.216
SO264-6/MP-Transect6	2018-07-10	22:00:13	26°49, 771'	175°44, 965'	2018-07-11	2:46:42	27°46, 349'	175°36, 631'	2.106
SO264-7/MP-Station	2018-07-11	3:06:12	27°46, 953'	175°36, 536'	2018-07-11	6:32:28	27°47, 410'	175°36, 573'	NA
SO264-7/MP-Transect1	2018-07-11	11:40:15	28°47, 776'	175°28, 218'	2018-07-11	17:07:23	29°52, 918'	175°18, 381'	NA
SO264-7/MP-Transect2	2018-07-11	21:54:18	30°50, 706'	175°09, 911'	2018-07-12	4:36:28	32°11, 458'	174°57, 925'	2.718
SO264-7/MP-Transect3	2018-07-12	5:05:16	32°17, 279'	174°57, 055'	2018-07-12	10:10:22	33°19, 232'	174°47, 823'	1.539
SO264-8/MP-Survey	2018-07-12	10:31:50	33°21, 054'	174°47, 046'	2018-07-12	18:03:12	33°35, 689'	174°43, 023'	2.863
SO264-8/MP-Station	2018-07-13	0:14:13	33°39, 273'	174°46, 166'	2018-07-13	5:27:42	33°45, 924'	174°37, 804'	1.736
SO264-9/SPM-Survey	2018-07-13	15:32:17	34°43, 164'	172°34, 754'	2018-07-13	19:03	34°46, 982'	172°34, 754'	1.443
SO264-12/MP-Survey	2018-07-15	19:10:53	37°50, 968'	170°27, 608'	NA	NA	NA	NA	NA
SO264-13/MP-Survey	2018-07-15	21:19:08	38°00, 027'	170°31, 627'	2018-07-16	1:04:37	37°47, 863'	170°43, 220'	1.638
SO264-13/MP-Transect1	2018-07-16	12:47:10	37°47, 275'	170°44, 275'	2018-07-16	16:04:15	38°16, 108'	170°52, 977'	0.726

SO264-13/MP-Transect2	2018-07-17	6:50:45	40°49, 647'	170°56, 039'	2018-07-17	7:28:59	40°50, 580'	170°54, 016'	0.223
SO264-18/MP-Transect1	2018-07-18	21:31:00	41°31, 565'	170°25, 031'	2018-07-18	22:36:17	41°20, 120'	170°22, 408'	0.1
SO264-21/MP-Survey	2018-07-20	11:17:54	42°22, 206'	170°32, 853'	2018-07-20	12:18:29	42°18, 501'	170°32, 853'	0.097
SO264-28/Survey	2018-07-23	9:47:32	44°41, 974'	170°10, 023'	2018-07-23	11:22:32	44°46, 469'	170°01, 196'	0.223
SO264-35/MP-Station	2018-07-26	1:18:20	44°46, 141'	170°10, 291'	2018-07-26	4:05:26	44°46, 146'	170°10, 298'	0.291
SO264-36/MP-Survey	2018-07-27	20:34:54	45°45, 619'	170°11, 702'	2018-07-28	3:23	45°44, 092'	170°00, 904'	0.915
SO264-46/MP-Survey	2018-08-01	11:17:21	46°36, 723'	169°37, 556'	2018-08-01	12:34:52	46°43, 616'	169°45, 457'	0.085
SO264-46/MP-Station	2018-08-01	21:11:00	46°48, 940'	169°24, 661'	2018-08-01	23:24:08	46°48, 939'	169°24, 653'	0.191
SO264-50/MP-Survey	2018-08-03	10:15:29	47°30, 777'	169°08, 813'	2018-08-03	11:30:05	47°26, 563'	169°04, 918'	0.162
SO264-56/MP-Survey	2018-08-07	6:24:03	47°47, 528'	168°36, 398'	2018-08-07	8:07:46	47°44, 754'	168°40, 402'	0.417
SO264-60/MP-Station	2018-08-08	20:41:27	49°18, 449'	168°33, 419'	2018-08-08	22:26:31	49°18, 443'	168°33, 419'	0.171
SO264-67/MP-Station	2018-08-13	7:52:50	50°14, 677'	168°35, 179'	2018-08-13	9:29:33	50°14, 698'	168°35, 167'	0.224
SO264-77/MP-Transect1	2018-08-17	1:03:00	48°50, 063'	163°41, 242'	2018-08-17	3:48:01	48°26, 146'	162°56, 333'	0.212
SO264-77/MP-Transect2	2018-08-17	11:30:43	47°18, 218'	160°50, 332'	2018-08-17	12:32:33	47°09, 139'	160°33, 709'	0.097
SO264-77/MP-Transect3	2018-08-18	2:10:46	45°16, 999'	157°12, 180'	2018-08-18	4:23:09	45°00, 292'	156°42, 750'	0.482
SO264-77/MP-Transect4	2018-08-18	9:43:39	44°21, 405'	155°02, 102'	2018-08-18	12:14:32	44°02, 558'	155°02, 102'	0.257
SO264-77/MP-Transect5	2018-08-19	0:21:00	42°32, 959'	152°29, 121'	2018-08-19	2:39:12	42°14, 793'	151°58, 230'	0.175

Appendix Table 5.3.6. Locations, timing, and flow volumes of biomarker filters collected from the surface ocean along the cruise track of SO264.

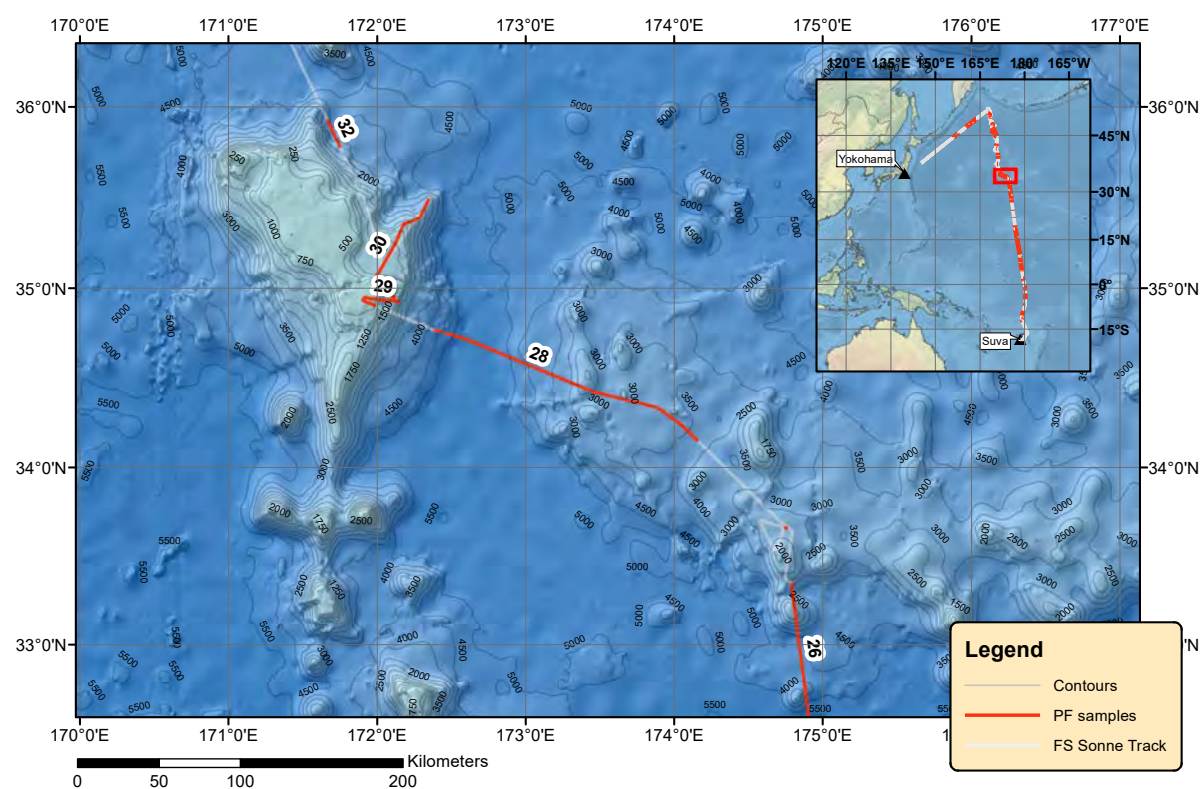
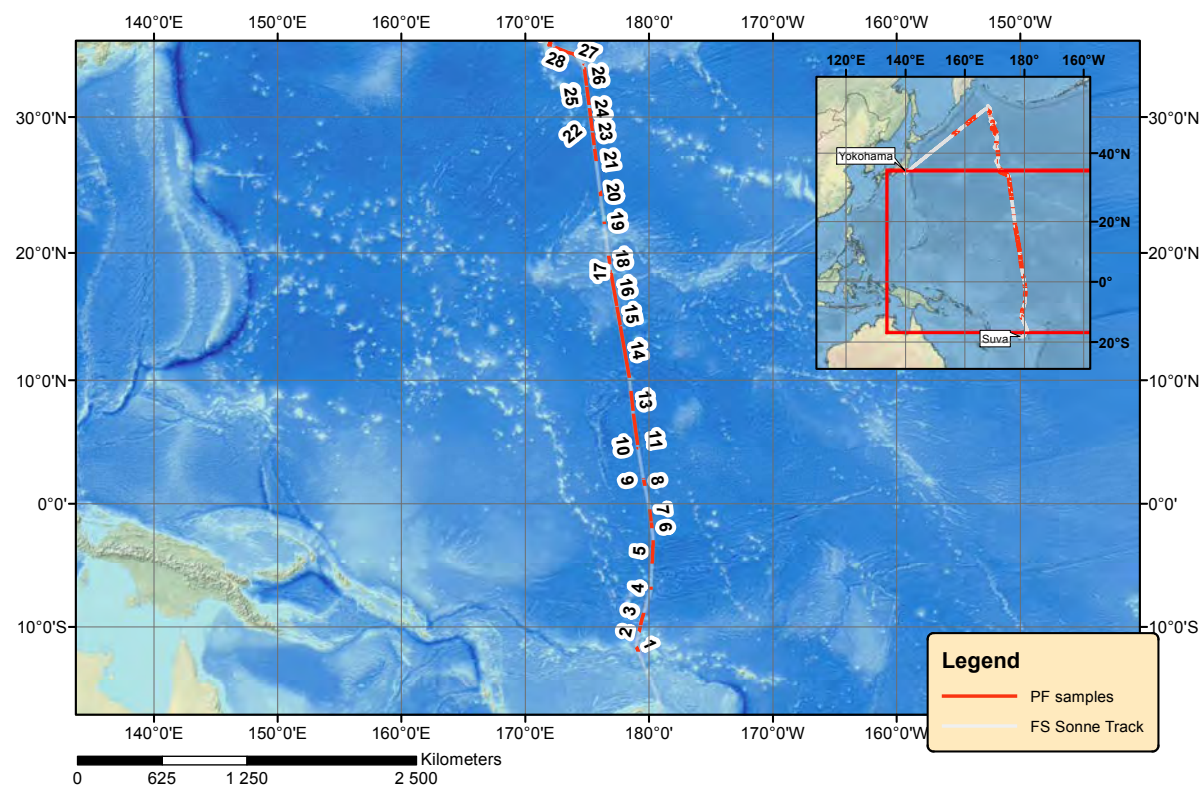
Sampl. #	Start Date	Start Time	Start Lat (-S/+N)	Start Long (-W/+E)	End Date	End Time	End Lat (-S/+N)	End Long (-W/+E)	Flow Vol. (m ³)
1	2018-07-01	15:05:25	-12°00,84'	179°09,30'	2018-07-01	21:00:47	-10°57,692'	179°04,999'	0.249
2	2018-07-01	23:04:53	-10°34,653'	179°10,138'	2018-07-02	3:21:57	-9°47,263'	179°20,692'	0.353
3	2018-07-02	4:24:40	-9°34,820'	179°23,447'	2018-07-02	8:52:52	-8°40,913'	179°39,281'	0.219
4	2018-07-02	8:57:15	-8°40,058'	179°39,550'	2018-07-02	17:06:18	-7°02,958'	179°50,061'	0.585
5	2018-07-02	17:41:19	-7°00,463'	179°49,233'	2018-07-02	21:24:50	-7°00,463'	179°41,291'	0.343
6	2018-07-02	23:51:25	-6°54,907'	179°49,612'	2018-07-03	4:56:06	-5°51,794'	179°46,392'	0.391
7	2018-07-03	5:06:55	-5°49,569'	179°46,286'	2018-07-03	9:43:00	-4°52,131'	179°43,860'	0.47
8	2018-07-03	9:55:03	-4°49,693'	179°43,758'	2018-07-03	13:05:34	-4°12,579'	179°42,191'	0.177
9	2018-07-03	13:12:22	-4°11,406'	179°42,172'	2018-07-03	16:57:43	-3°31,296'	179°40,445'	0.088
10	2018-07-03	17:05:11	-3°29,930'	179°40,391'	2018-07-03	21:06:05	-2°47,651'	179°38,838'	0.289
11	2018-07-03	21:10:53	-2°45,990'	179°39,055'	2018-07-04	1:40:04	-1°58,332'	179°45,074'	1.3
12	2018-07-04	1:42:00	-1°58,332'	179°45,074'	2018-07-04	5:16:15	-1°14,661'	179°50,584'	0.244
13	2018-07-04	5:32:33	-1°11,343'	179°50,997'	2018-07-04	8:36:06	-0°33,337'	179°55,797'	0.202
14	2018-07-04	8:41:41	-0°32,222'	179°55,940'	2018-07-04	14:08:48	0°37,080'	179°51,912'	0.366
15	2018-07-04	14:16:31	0°38,747'	179°51,549'	2018-07-04	18:02:12	1°26,588'	179°41,150'	0.193
16	2018-07-04	20:20:42	01°46,997'	179°36,699'	2018-07-04	23:08:23	1°46,947'	179°36,750'	0.127
17	2018-07-05	2:17:16	2°20,986'	179°30,735'	2018-07-05	6:37:54	3°14,733'	179°21,313'	0.25
18	2018-07-05	7:04:42	3°20,277'	179°20,344'	2018-07-05	13:02:10	4°30,568'	179°08,056'	0.244
19	2018-07-05	13:16:43	4°30,576'	179°08,050'	2018-07-05	16:18:02	4°30,555'	179°08,056'	0.26
20	2018-07-05	16:54:41	4°30,578'	179°07,051'	2018-07-06	1:47:47	6°27,163'	178°51,899'	0.391
21	2018-07-06	6:27:27	7°19,736'	178°44,622'	2018-07-06	10:27:54	7°19,744'	178°44,625'	0.305
22	2018-07-06	11:45:22	7°28,645'	178°43,680'	2018-07-06	19:27:54	9°11,552'	178°32,722'	0.358
23	2018-07-07	0:03:40	9°59,420'	178°27,619'	2018-07-07	6:35:21	10°37,079'	178°20,995'	0.601

24	2018-07-07	6:50:19	10°40,1 58'	178°20,4 05'	2018-07-07	13:28:0 4	12°02,5 98'	178°05,77 5'	0.415
25	2018-07-07	13:33:5 8	12°03,5 48'	178°05,6 04'	2018-07-07	20:49:1 4	13°33,0 32'	177°49,63 3'	0.498
26	2018-07-07	21:07:3 2	13°36,8 04'	177°48,9 61'	2018-07-08	3:46:29	14°59,3 00'	177°34,15 4'	0.447
27	2018-07-08	7:51:05	15°49,7 36'	177°25,0 43'	2018-07-08	15:12:1 9	17°21,3 56'	177°08,40 6'	0.481
28	2018-07-08	21:25:2 6	18°33,6 00'	176°55,2 01'	2018-07-09	1:49:14	18°33,6 07'	176°55,19 8'	0.266
29	2018-07-09	4:36:19	19°00,9 42'	176°51,4 28'	2018-07-09	12:10:2 7	20°23,0 41'	176°40,06 5'	0.434
30	2018-07-09	12:19:3 2	20°24,7 01'	176°39,0 28'	2018-07-09	18:08:3 8	21°27,0 79'	176°31,12 7'	0.237
31	2018-07-09	23:32:3 3	22°28,1 94'	176°22,5 23'	2018-07-10	4:11:06	23°21,6 38'	176°14,95 0'	0.273
32	2018-07-10	21:12:1 9	23°21,8 61'	176°14,9 18'	2018-07-10	10:49:2 6	24°34,3 02'	176°04,10 3'	0.319
33	2018-07-10	11:02:5 4	24°39,9 83'	176°03,7 54'	2018-07-10	16:23:0 2	25°43,5 93'	175°54,59 5'	0.28
34	2018-07-10	22:00:1 3	26°49,7 71'	175°44,9 65'	2018-07-11	2:46:42	27°46,3 49'	175°36,63 1'	0.313
35	2018-07-11	3:06:12	27°46,9 53'	175°36,5 36'	2018-07-11	11:04:2 1	28°40,8 88'	175°28,82 6'	0.457
36	2018-07-11	11:40:1 5	28°47,7 76'	175°28,2 18'	2018-07-11	19:24:2 2	30°20,7 01'	175°14,31 9'	0.392
37	2018-07-11	21:54:1 8	30°50,7 06'	175°09,9 11'	2018-07-12	4:26:28	32°09,4 89'	174°58,21 8'	0.321
38	2018-07-12	5:05:16	32°17,2 79'	174°57,0 55'	2018-07-12	10:10:2 2	33°19,2 32'	174°47,82 3'	0.232
39	2018-07-12	10:31:5 0	33°21,0 54'	174°47,0 46'	2018-07-12	18:03:1 2	33°35,6 89'	174°43,02 3'	0.32
40	2018-07-13	0:14:13	33°39,2 73'	174°46,1 66'	2018-07-13	7:31:08	34°03,3 35'	174°16,58 0'	0.294
41	2018-07-13	15:32:1 7	34°43,1 64'	172°34,7 54'	2018-07-13	19:03	34°46,9 82'	172°34,75 4'	0.214
42	2018-07-15	12:47:0 4	36°57,4 28'	171°04,0 00'	2018-07-15	21:05:0 3	37°59,8 89'	170°31,19 3'	0.346
43	2018-07-16	8:03:13	37°47,2 83'	170°44,2 54'	2018-07-16	12:41:5 2	37°47,2 78'	170°44,24 8'	0.294
44	2018-07-18	10:39:1 2	41°49,7 57'	170°38,9 82'	2018-07-18	13:21:2 1	41°51,7 39'	170°24,43 7'	0.077
45	2018-07-21	3:34:34	43°22,9 53'	170°42,5 68'	2018-07-21	4:49:28	43°38,7 44'	170°45,65 2'	0.056
46	2018-07-22	9:43:18	44°48,0 64'	170°35,8 73'	2018-07-22	12:56	44°48,0 64'	170°35,86 5'	0.075
47	7-29-2018	15:33:4 5	45°33,9 99'	170°18,0 04'	2018-07-29	19:11:2 8	45°33,9 97'	170°18,00 4'	0.081
48	8-1-2018	18:54:2 8	46°48,9 37'	169°24,6 68'	2018-08-01	20:59:2 0	46°48,9 35'	169°24,65 4'	0.058
49	8-7-2018	1:51:24	47°17,2 49'	169°17,6 73'	2018-08-07	3:22:31	47°31,7 80'	169°01,13 3'	0.083
50	8-8-2018	19:05:3 4	49°18,4 45'	168°33,4 28'	2018-08-08	20:37:1 8	49°18,4 45'	168°33,41 3'	0.091
51	8-9-2018	9:58:12	49°18,4 44'	168°33,4 28'	2018-08-09	11:41:4 2	49°18,4 43'	168°33,43 6'	0.089
52	8-10-2018	00:17:0 6	49°18,4 46'	168°33,4 33'	2018-08-10	3:30:56	49°18,4 45'	168°33,42 4'	0.09
53	8-13-2018	9:37:05	50°14,7 01'	168°35,1 66'	2018-08-13	11:11:5 9	50°14,7 00'	168°35,10 5'	0.032
54	8-16-2018	10:32:1 8	50°29,7 35'	166°52,8 04'	2018-08-16	12:54:3 6	50°29,7 26'	166°52,80 7'	0.097
55	8-17-2018	5:21:14	48°12,6 49'	162°30,9 76'	2018-08-17	7:48:28	47°50,8 28'	161°50,43 1'	0.113
56	8-17-2018	12:35:2 7	47°08,6 90'	160°32,1 90'	2018-08-17	14:30:1 9	46°51,9 66'	160°02,38 9'	0.097

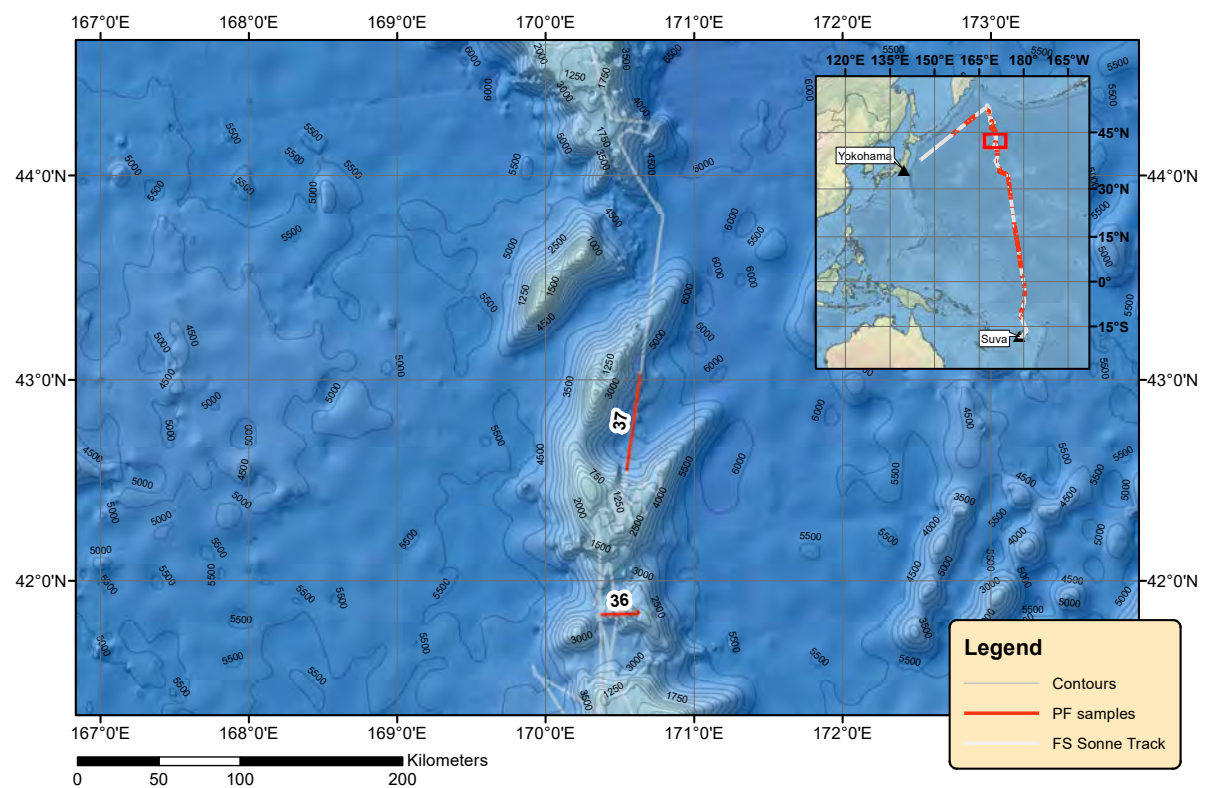
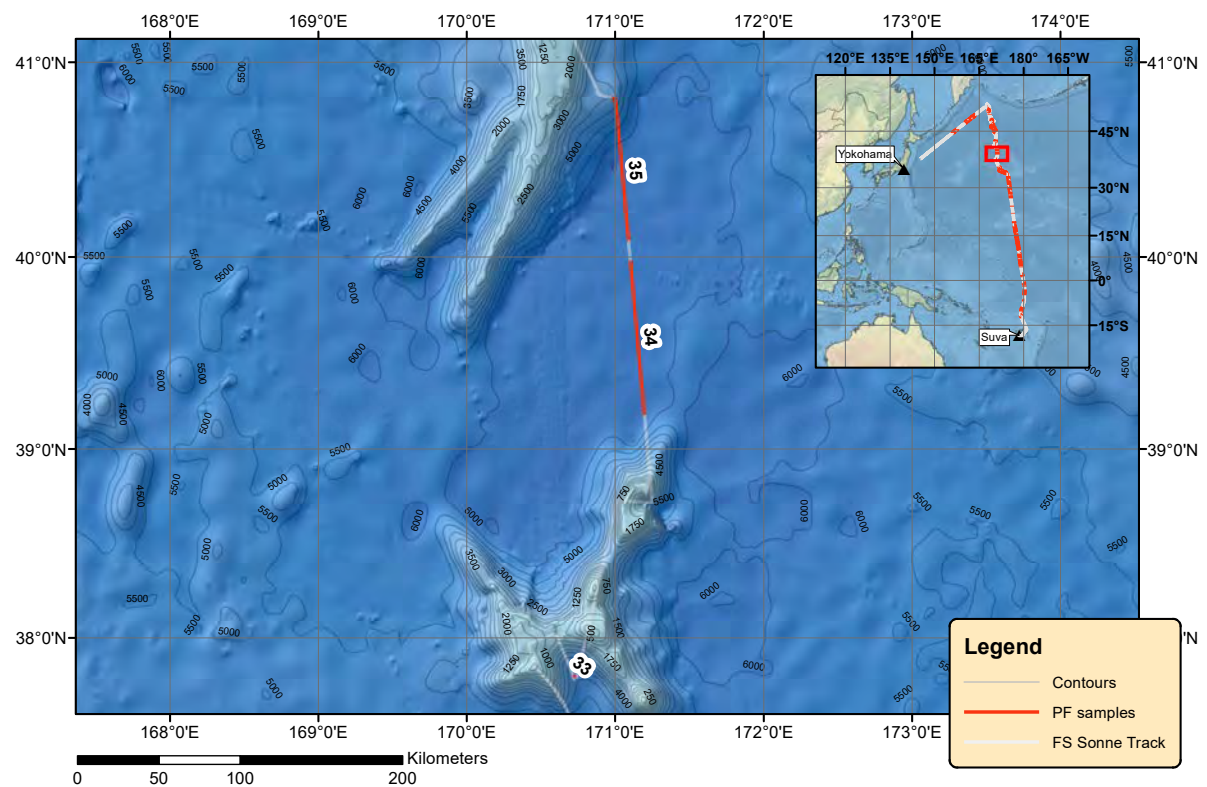
57	8-17-2018	23:27:05	45°40,402'	157°53,675'	2018-08-18	1:55:25	45°19,351'	157°16,350'	0.106
58	8-18-2018	7:16:40	44°39,235'	156°05,847'	2018-08-18	9:30:10	44°23,063'	155°37,668'	0.086
59	8-19-2018	2:53:52	42°13,383'	151°54,415'	2018-08-19	4:39:55	41°58,423'	151°31,119'	0.091
60	8-20-2018	00:23:15	39°42,830'	147°48,419'	2018-08-20	1:51:30	39°37,765'	147°40,253'	0.12

Appendix Table 5.3.7. Locations and timing of surface water collection of samples for DIC, pH, alkalinity, trace elements, $\delta^{18}\text{O}$, and $\delta^{13}\text{C}$ measurements. All samples were collected from the ships seawater intake (membrane pump).

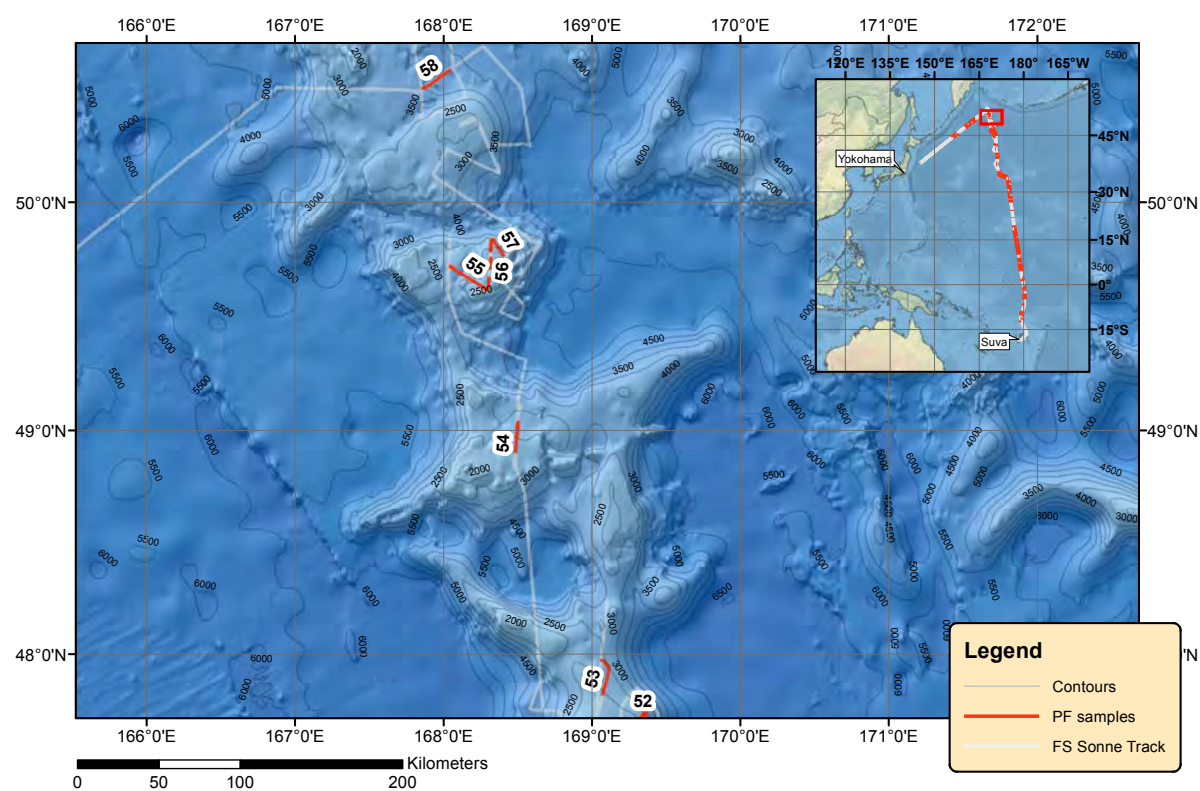
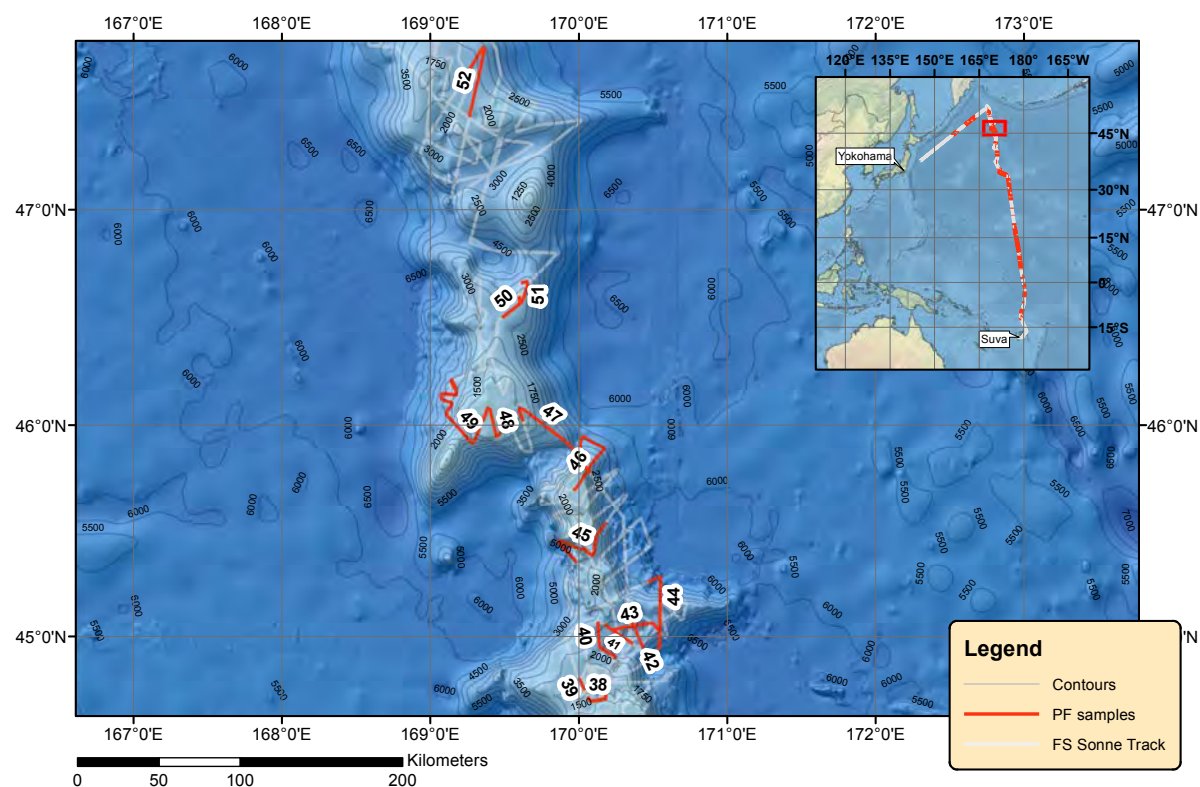
ID	Sample Name	Date	Time	LAT (- °S/+ °N)	LON (- °W/+ °E)
1	SO264/SW	7/2/18	23:34:13	-6°57,790'	-179°49,178'
2	SO264-3/SW	7/5/18	13:04:00	4°30,570'	179°08,054'
3	SO264-4/SW	7/6/18	6:15:29	7°19,738'	178°44,623'
4	SO264-5/SW	7/7/18	0:02:00	9°59,424'	178°27,359'
5	SO264-6/SW	7/8/18	21:15:32	18°33,587'	176°55,110'
6	SO264-7/SW- transect1	7/11/18	11:04:21	28°40,888'	175°28,826'
7	SO264-7/SW- transect2	7/12/18	4:36:00	32°11,458'	174°57,925'
8	SO264-8/SW	7/13/18	0:03:00	33°39,266'	174°46,169'
9	SO264-9/SW- transect1	7/14/18	5:18:05	34°56,195'	172°01,363'
10	SO264-17/SW-survey	7/18/18	10:28:38	41°49,735'	170°27,586'
11	SO264-21/SW- transect1	7/21/18	3:45	NA	NA
12	SO264-40/SW	7/29/2018	20:55	45°33,997'	170°18,005'
13	SO264-77/SW- transect1	8/17/18	3:48:01	48°15,619'	162°36,543'
14	SO264-77/SW- transect2	8/17/18	14:33:00	46°51,564'	160°01,664'
15	SO264-77/SW- transect3	8/18/18	2:10:00	45°16,999'	157°12,180'
16	SO264-77/SW- transect4	8/18/18	9:36:00	44°02,558'	155°02,102'
17	SO264-77/SW- transect5	8/19/2018	2:39:12	42°14,793'	151°58,230'
18	SO264-77/SW- transect6	8/20/18	1:00:00	39°40,709'	147°45,000'



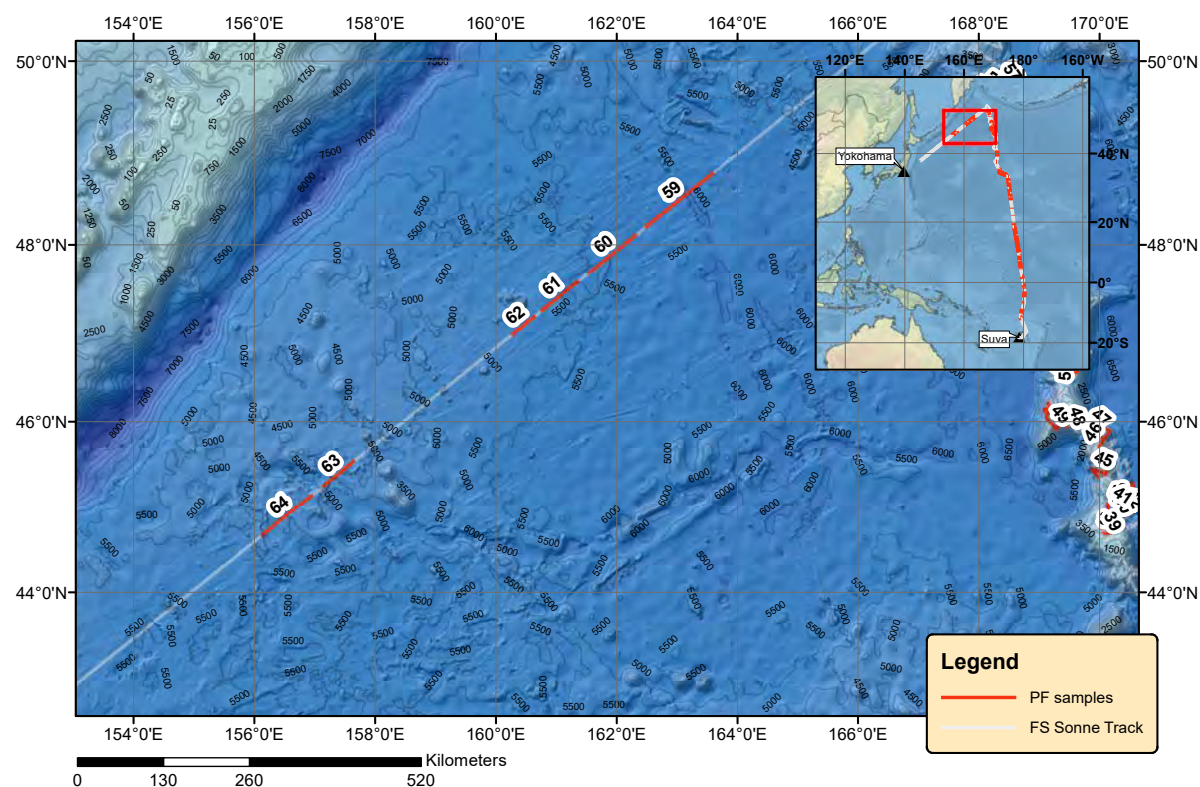
Appendix Figure 5.3.1. PF sample tracks for foraminifers and pteropods analyses (c.f. Appendix Table 5.3.1).



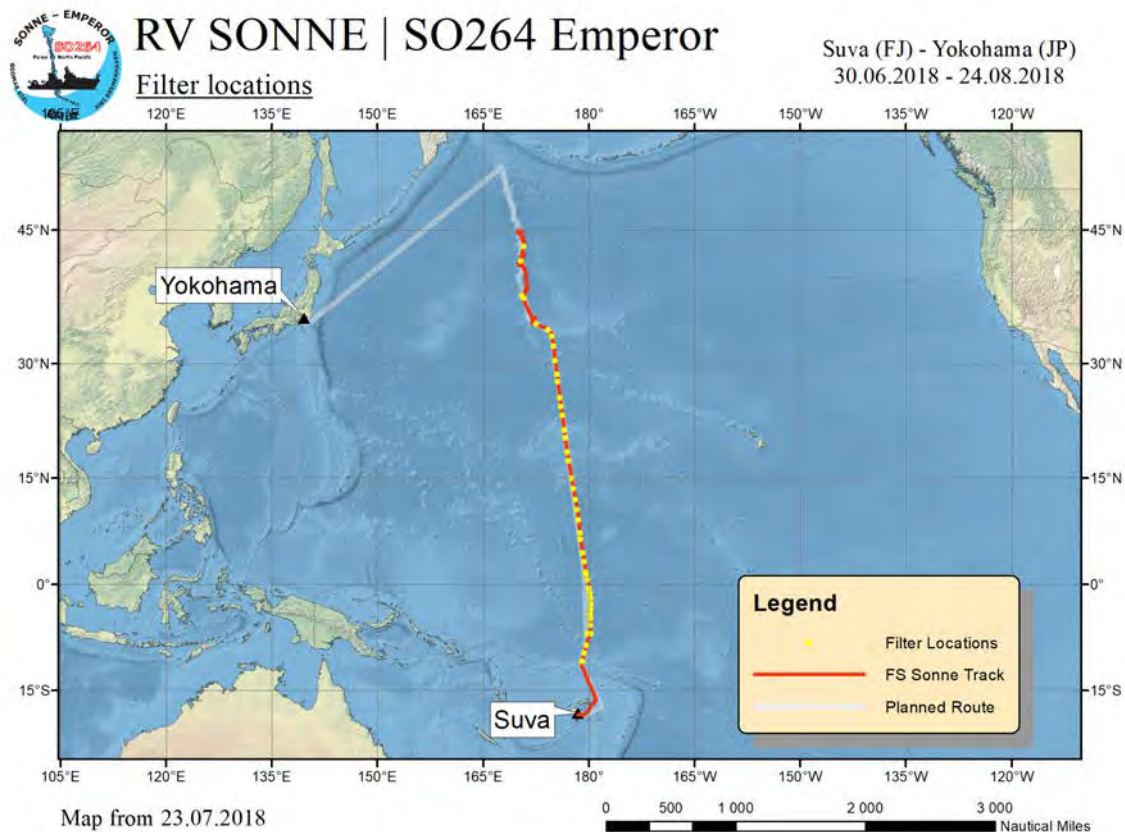
Appendix Figure 5.3.1 continued. PF sample tracks for foraminifers and pteropods analyses (c.f. Appendix Table 5.3.1).



Appendix Figure 5.3.1 continued. PF sample tracks for foraminifers and pteropods analyses (c.f. Appendix Table 5.3.1).



Appendix Figure 5.3.1 continued. PF sample tracks for foraminifers and pteropods analyses (c.f. Appendix Table 5.3.1).



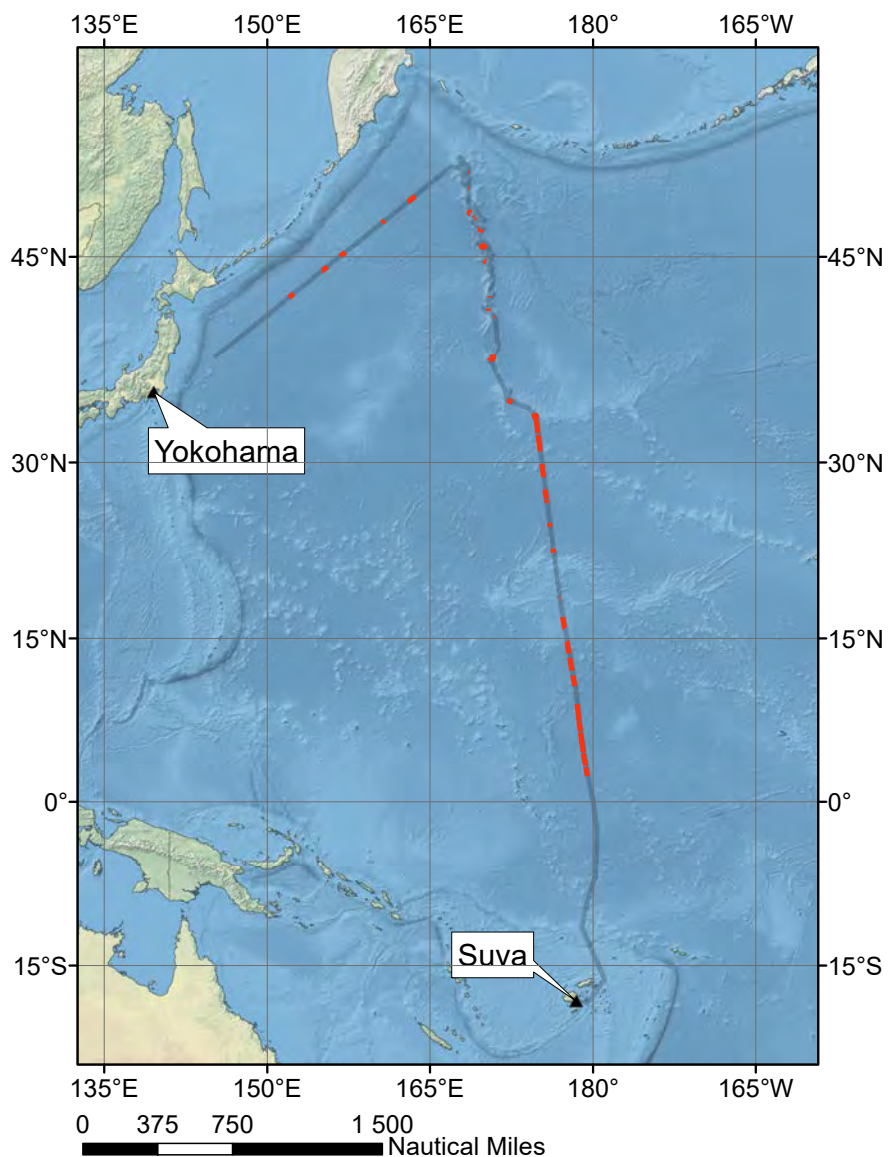
Appendix Figure 5.3.2. Locations of all filter samples collected for suspended particles from the seawater intake (membrane pump) during cruise SO264.



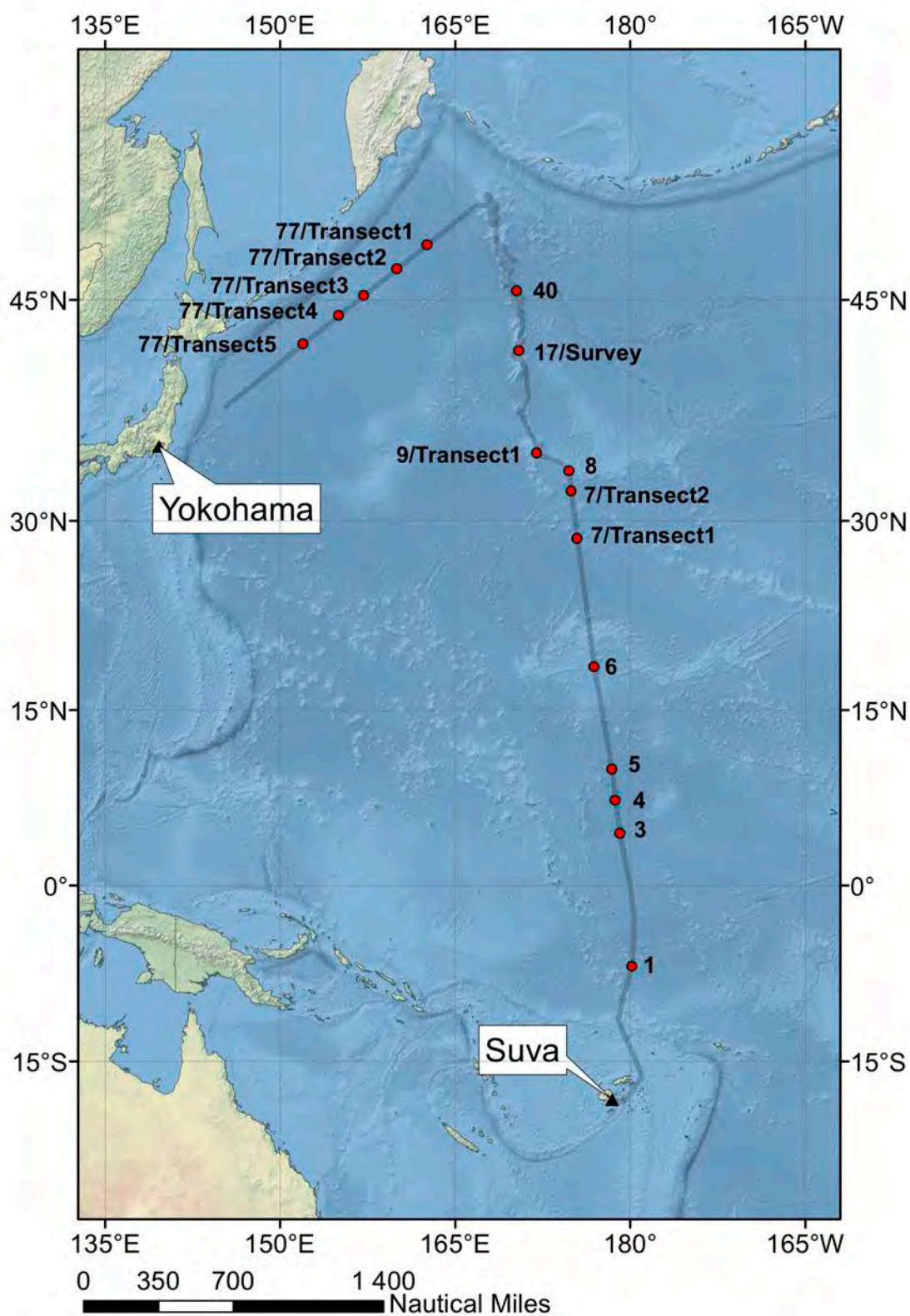
RV SONNE | SO264 Emperor

Micro plastic

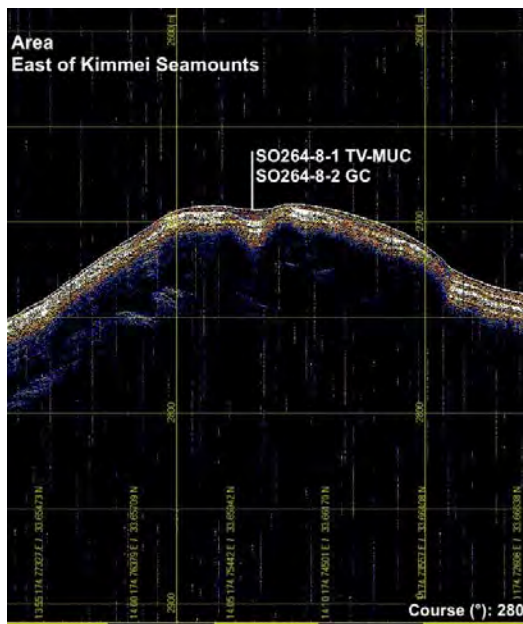
Suva (FJ) - Yokohama (JP)
30.06.2018 - 24.08.2018



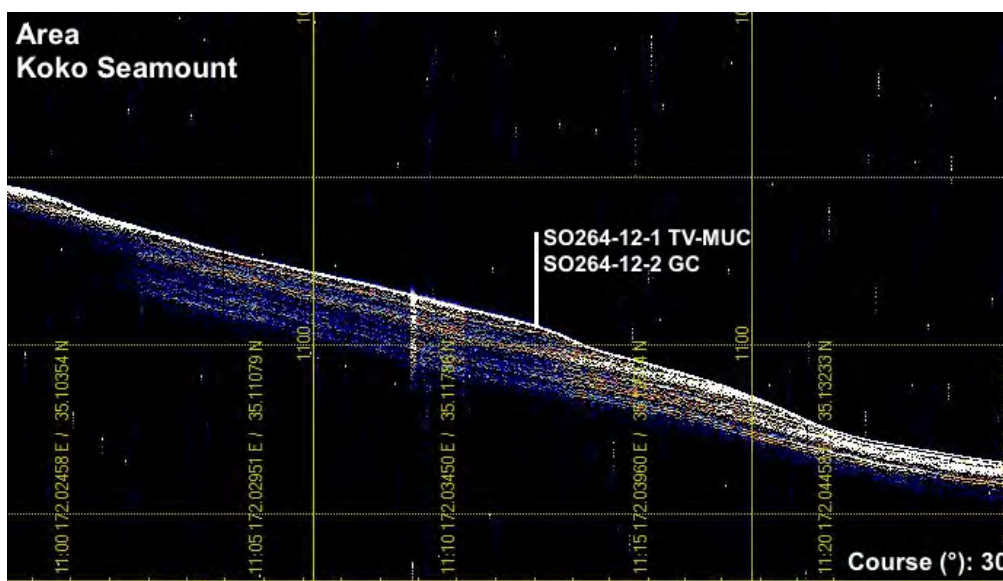
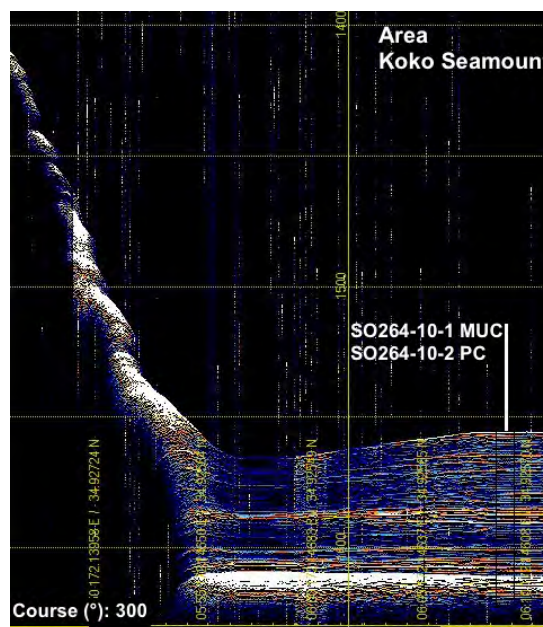
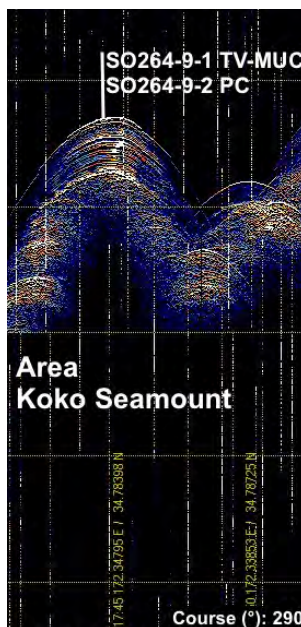
Appendix Figure 5.3.3. Locations of Microplastic samples along SO264 cruise route.

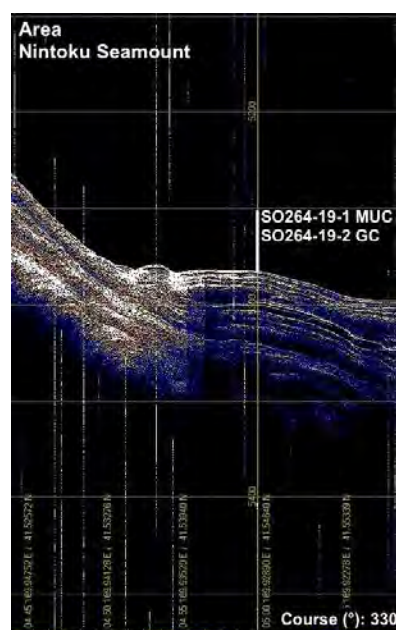
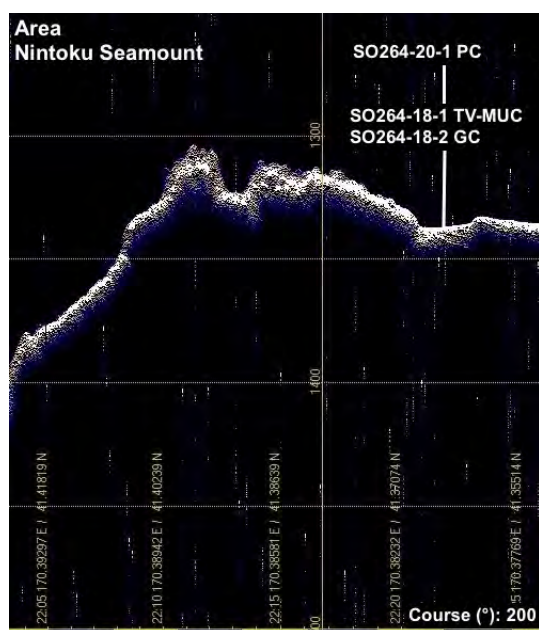
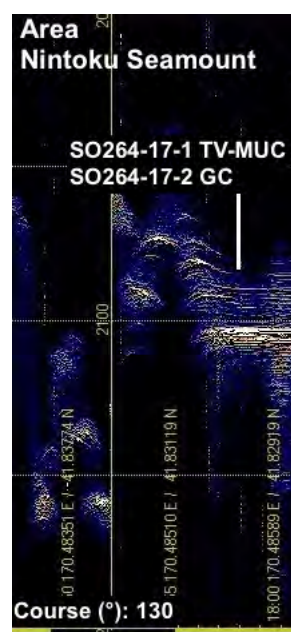
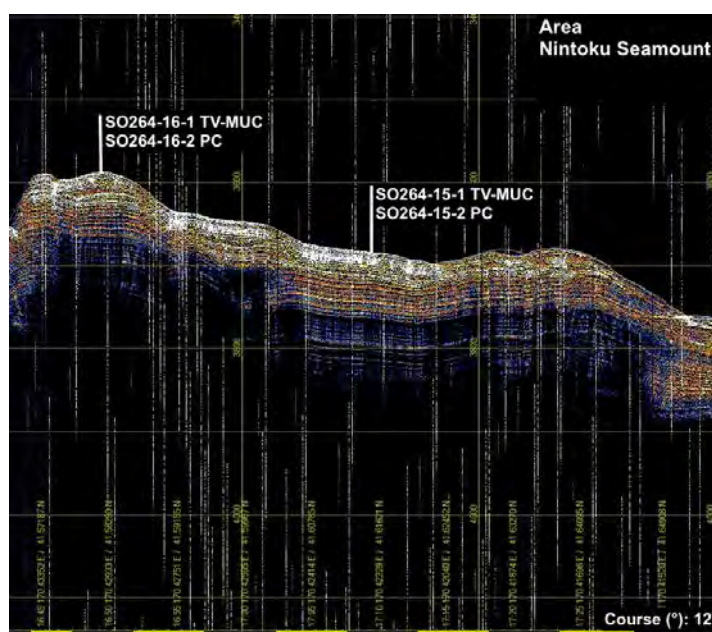
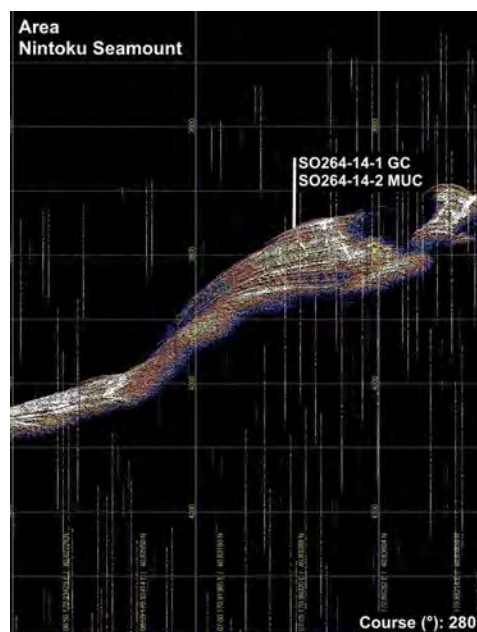
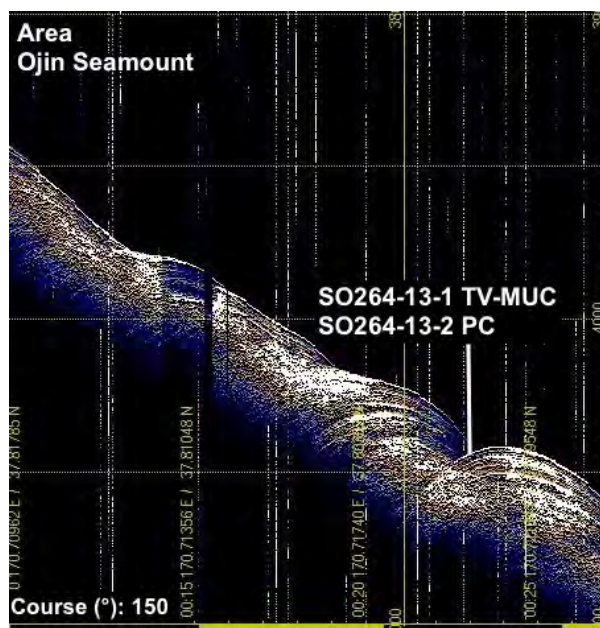


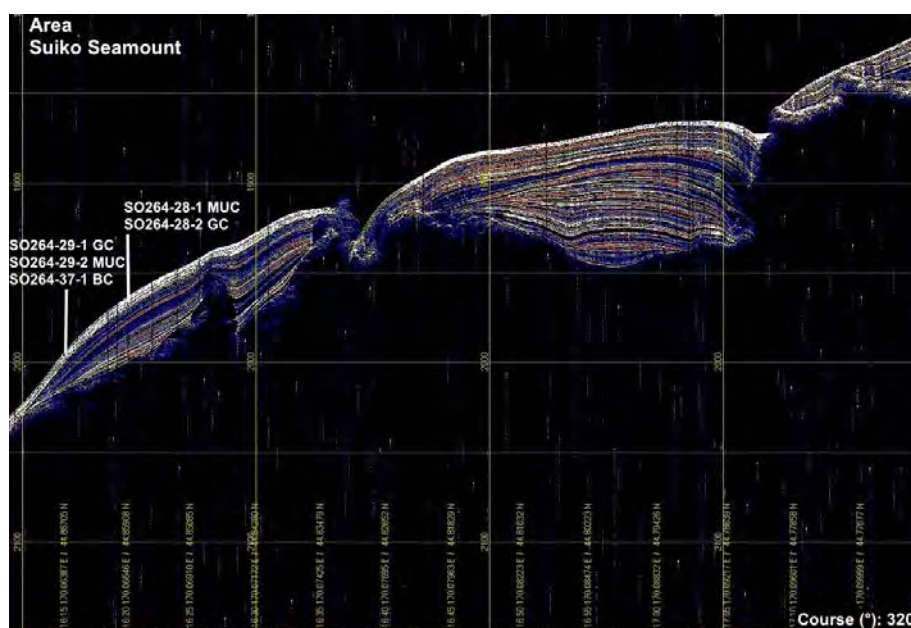
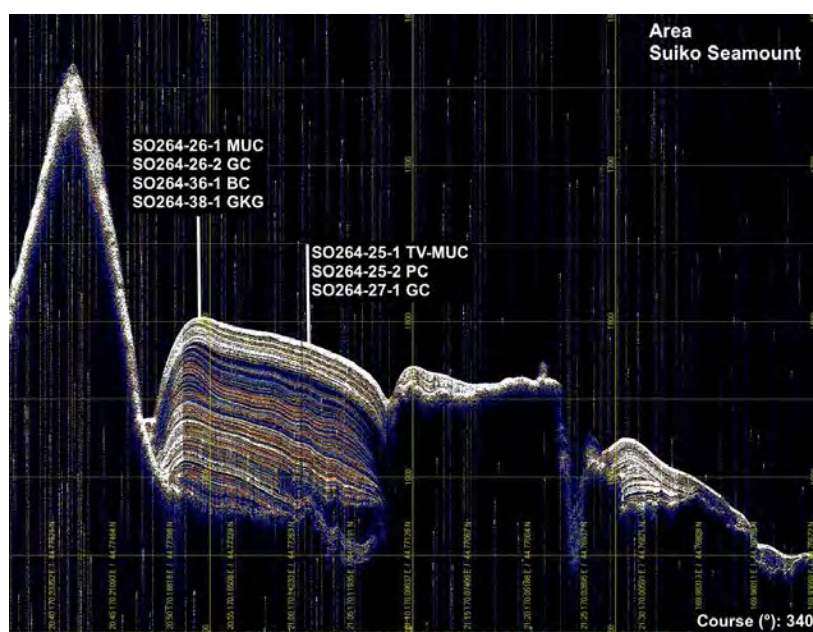
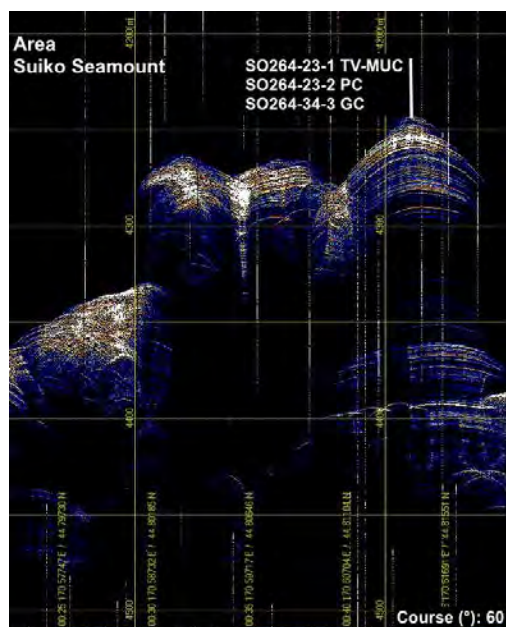
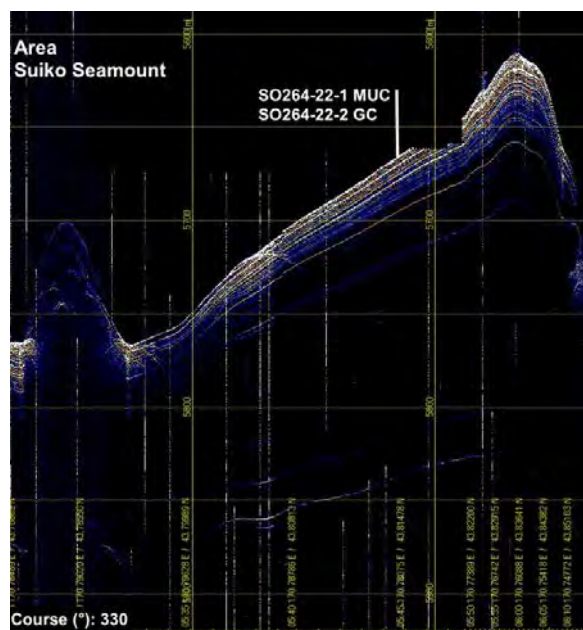
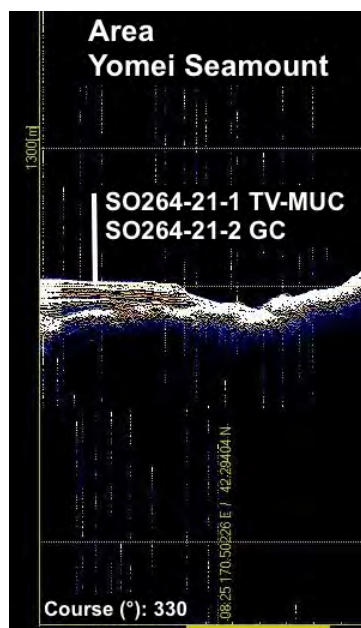
Appendix Figure 5.3.4. Locations of surface water samples for DIC, pH, alkalinity, trace elements, $\delta^{18}\text{O}$, and $\delta^{13}\text{C}$ measurements.

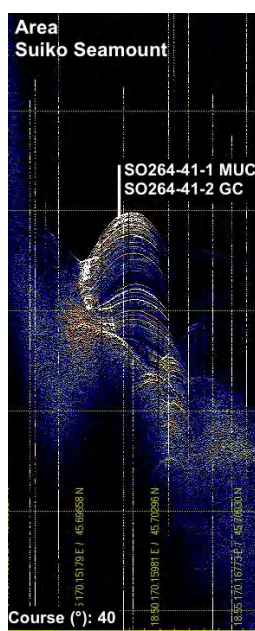
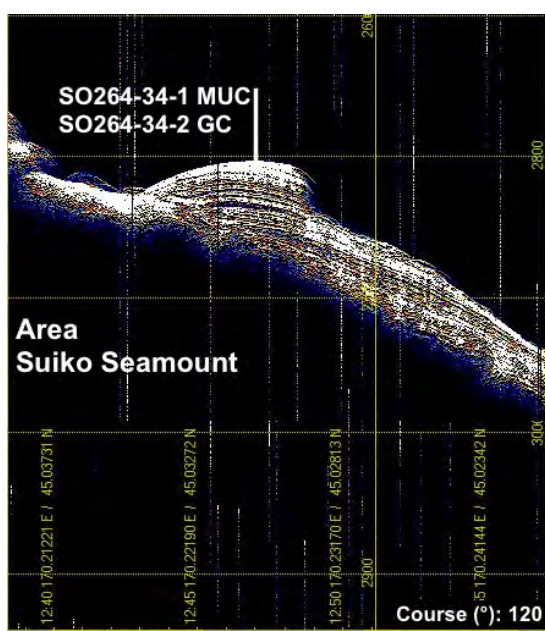
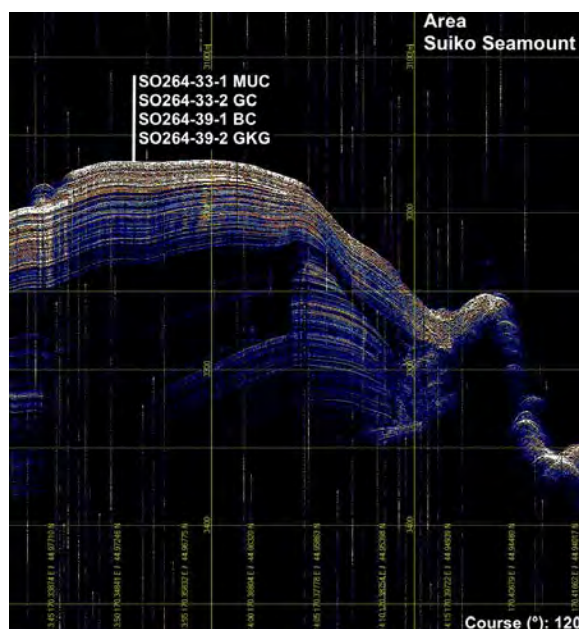
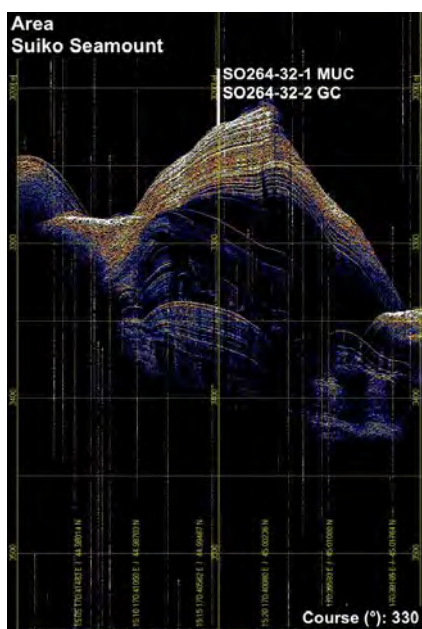
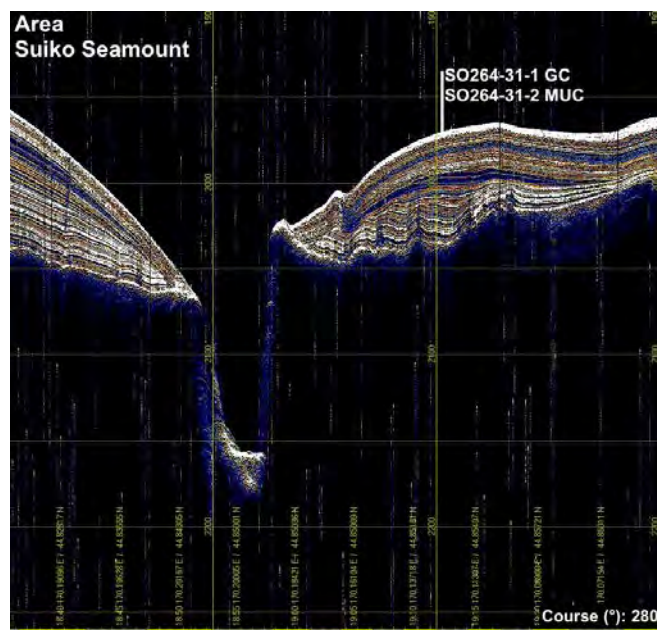
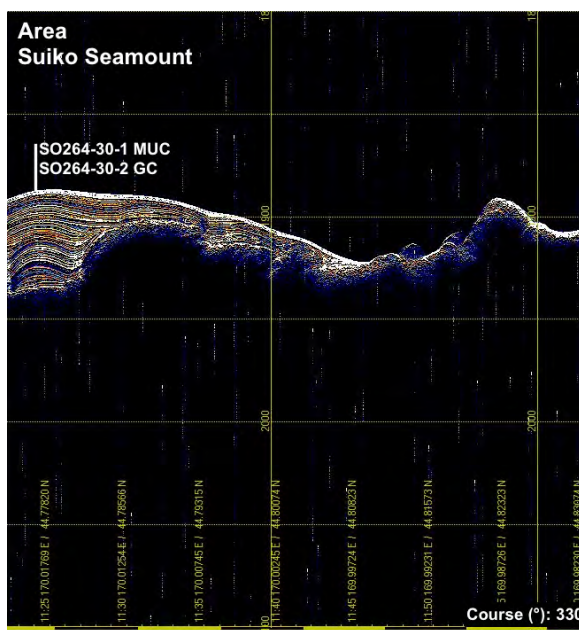


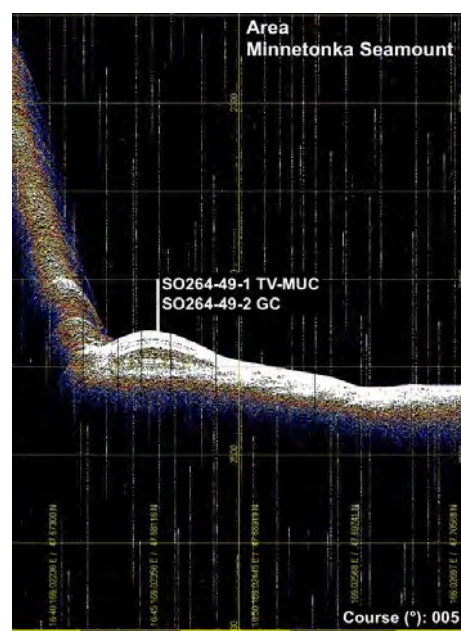
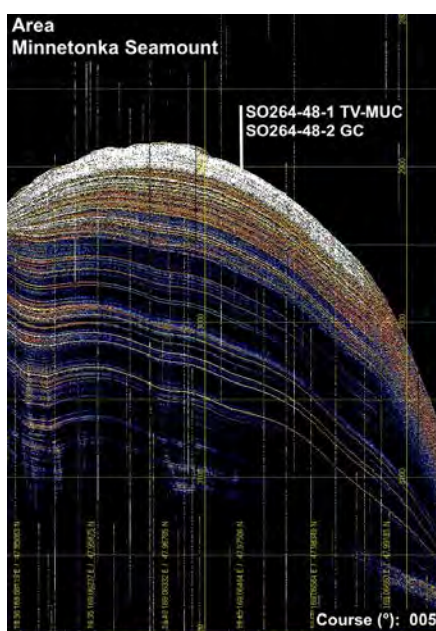
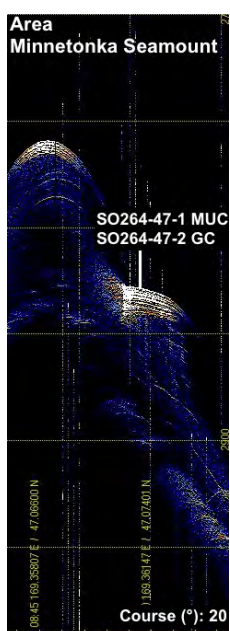
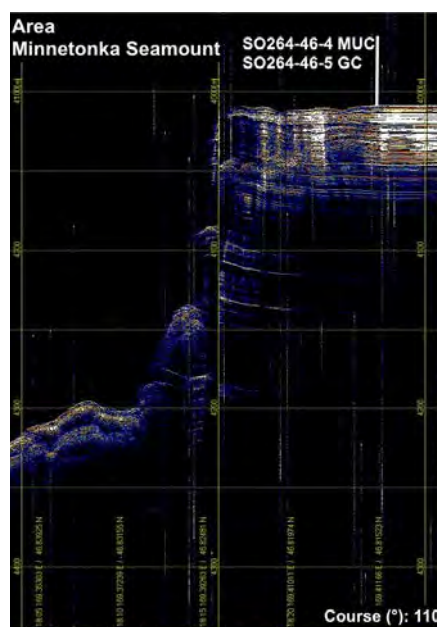
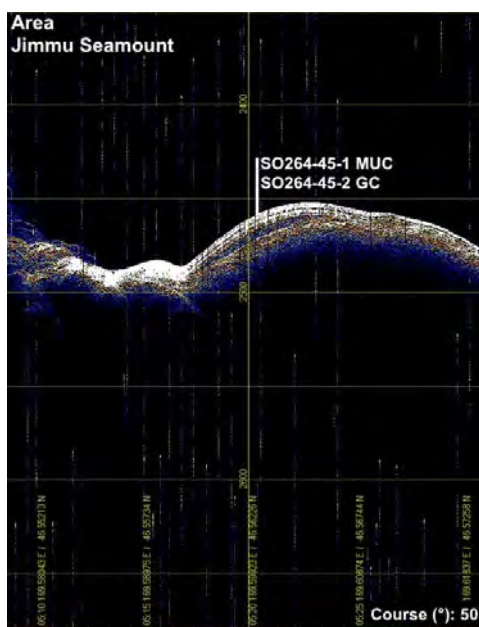
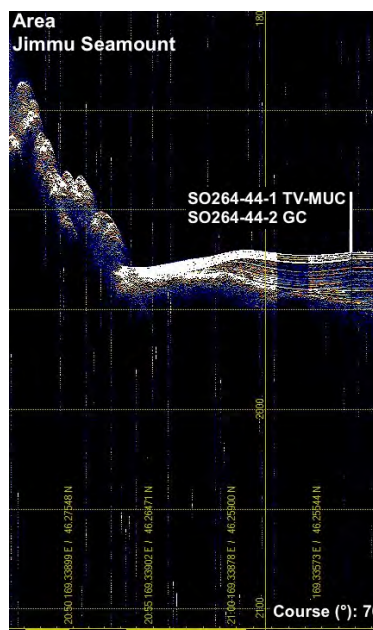
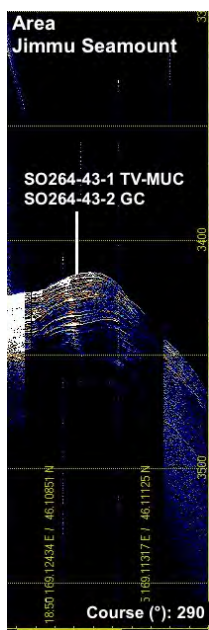
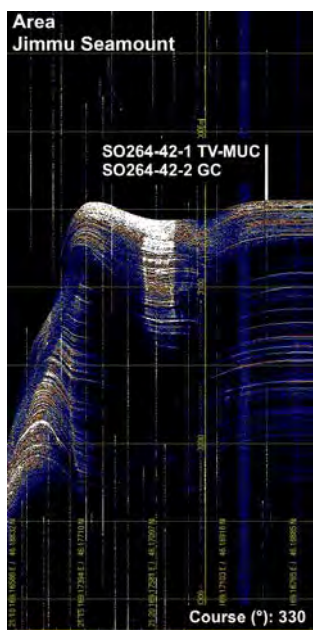
The following images present the PARASOUND profiles across the SO264 coring locations. Area and core numbers are indicated. The orientation of the PARASOUND profile is given at the bottom of each image.

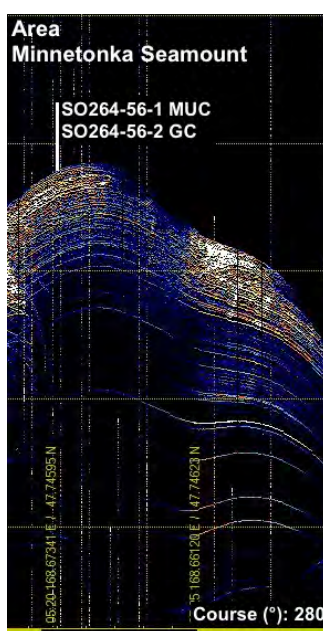
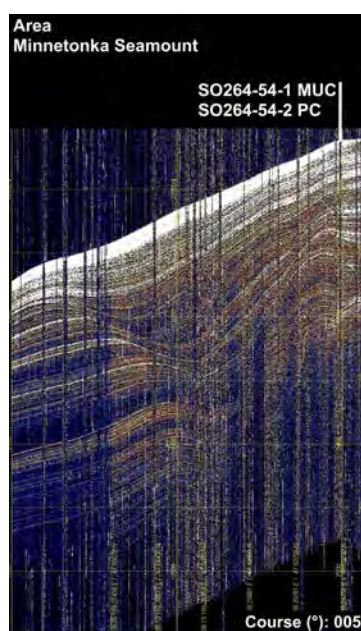
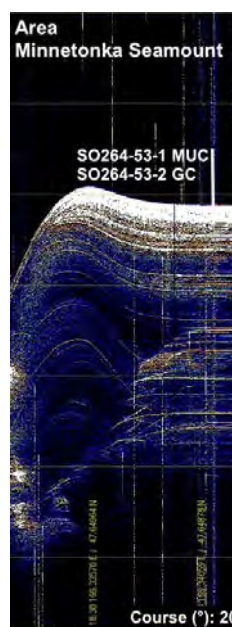
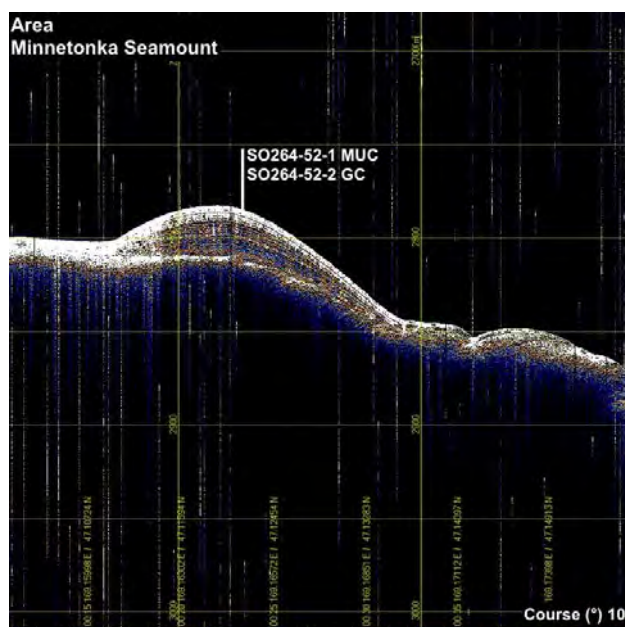
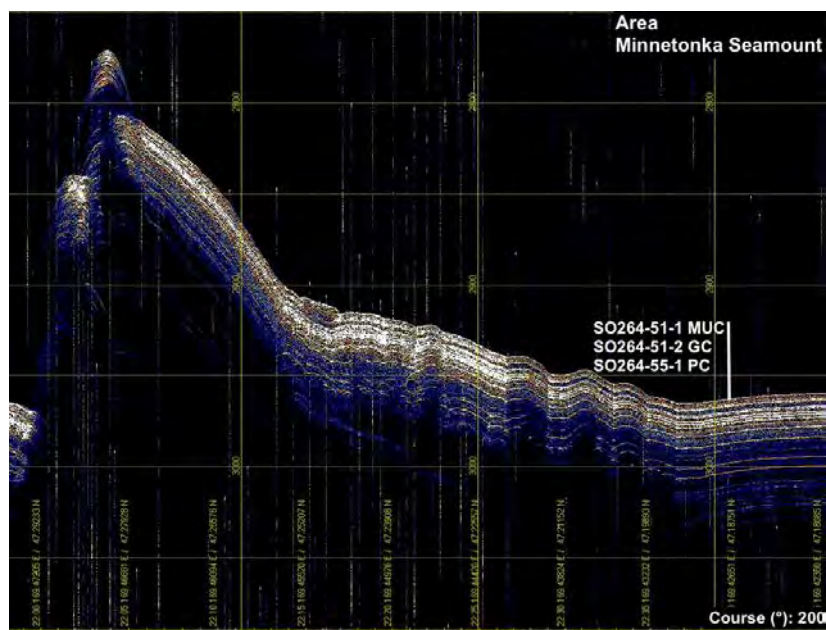
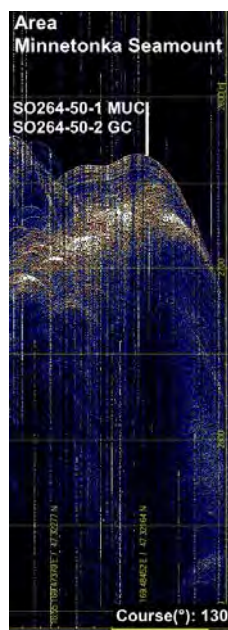


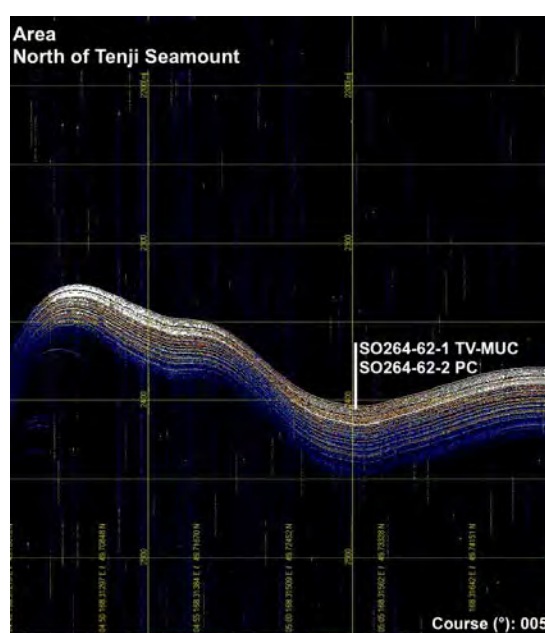
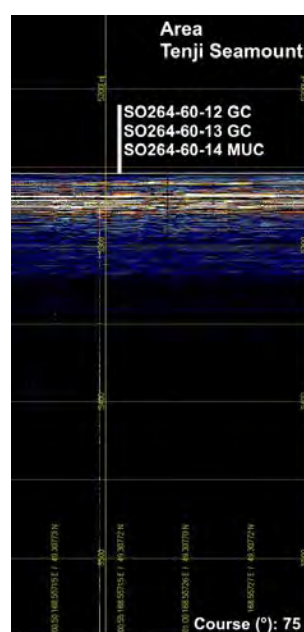
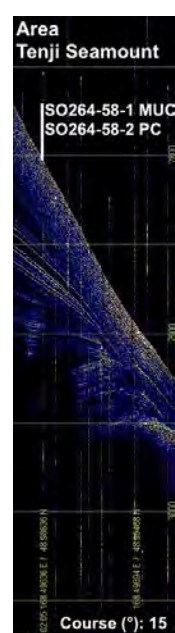


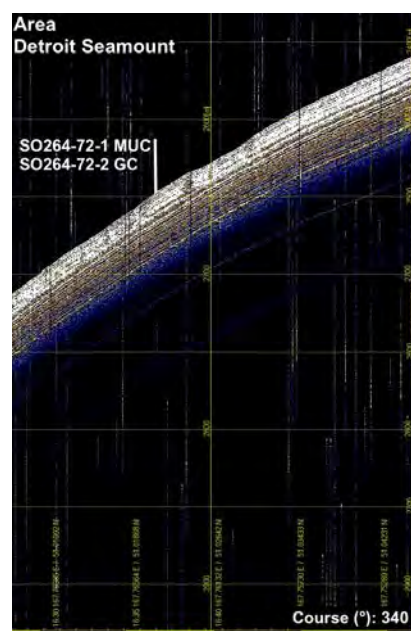
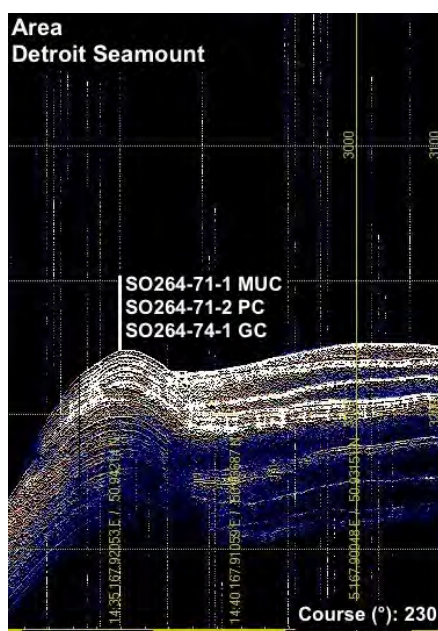
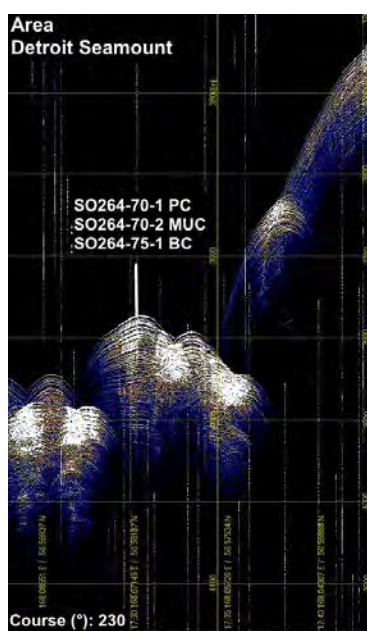
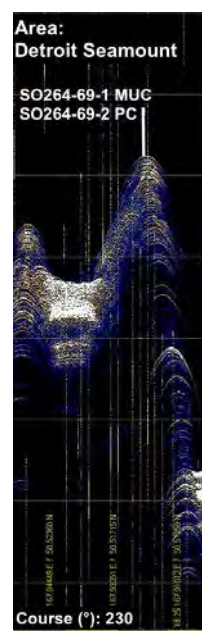
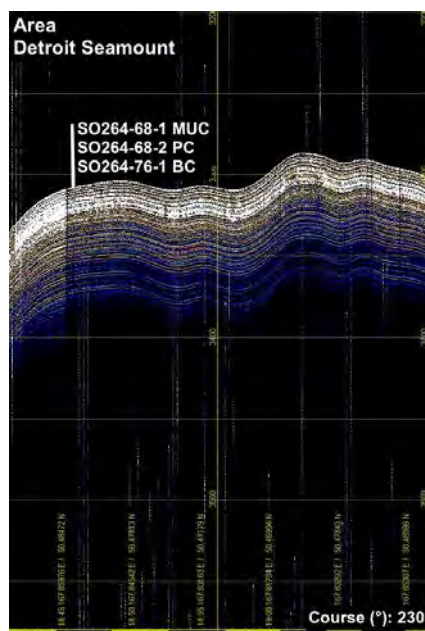
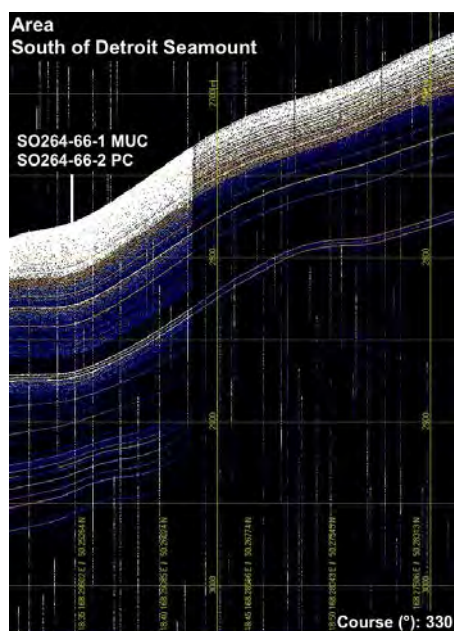
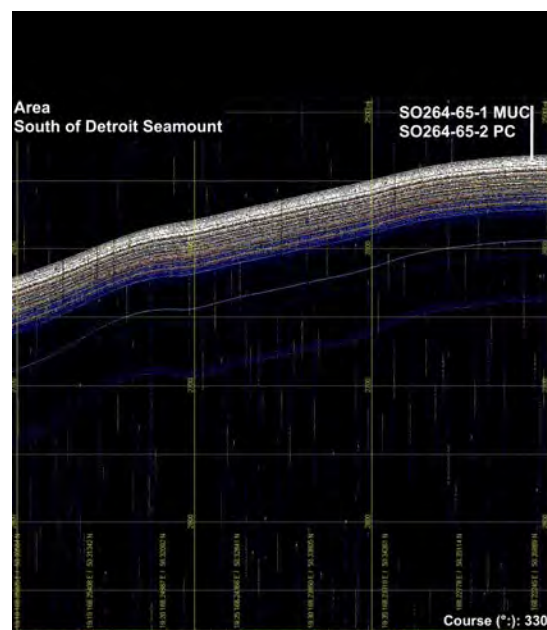
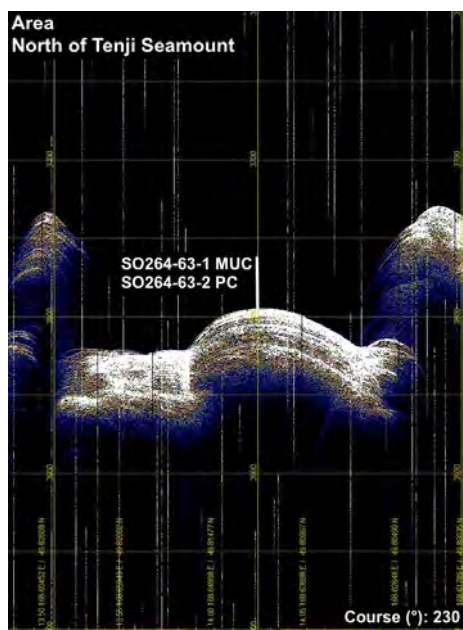


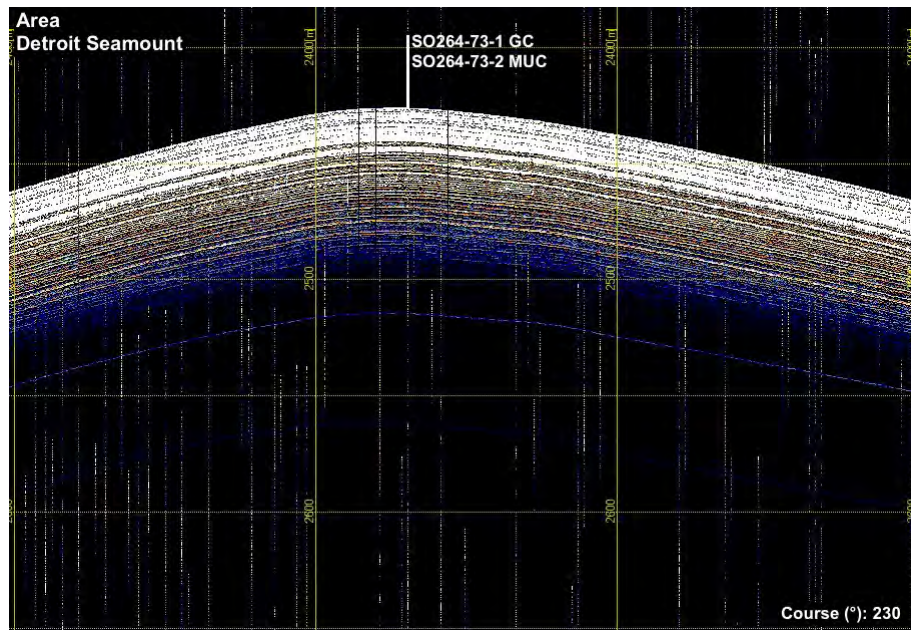


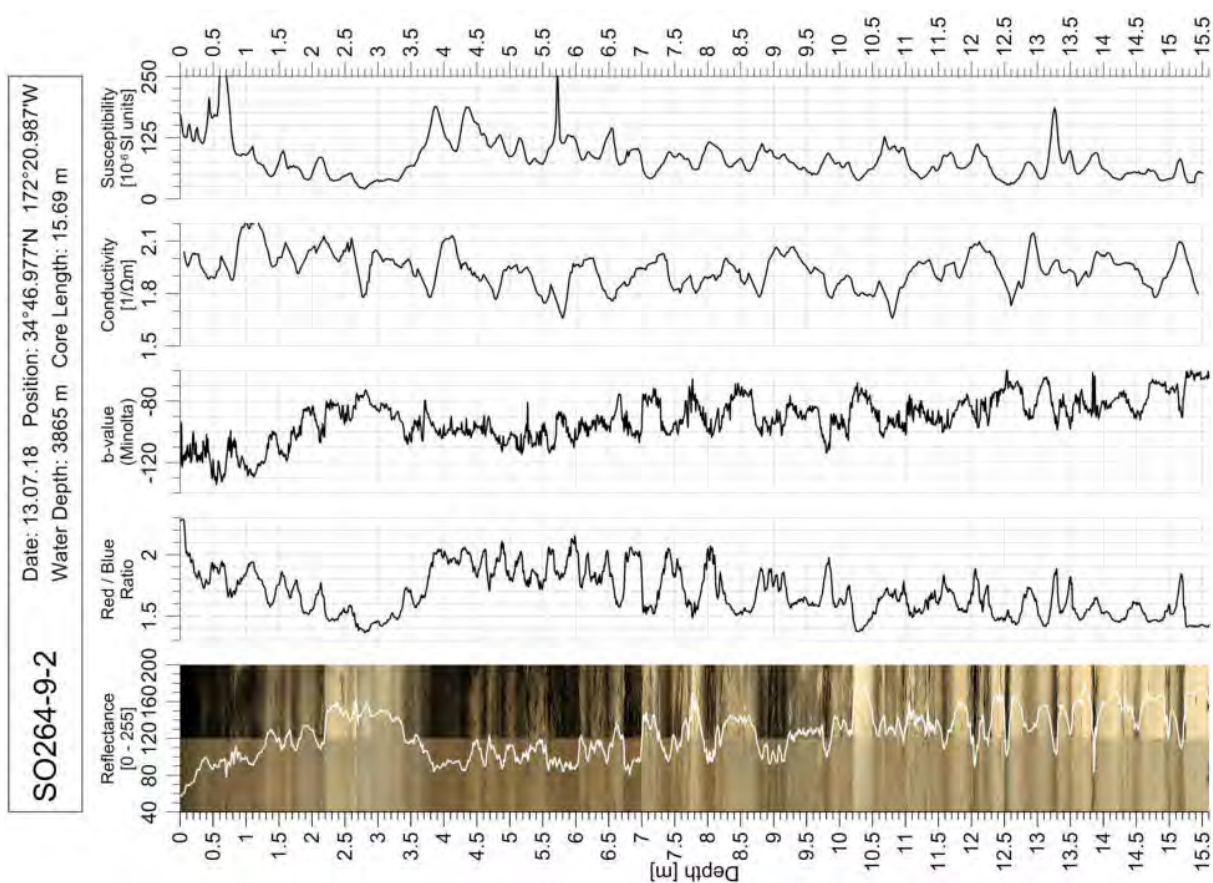
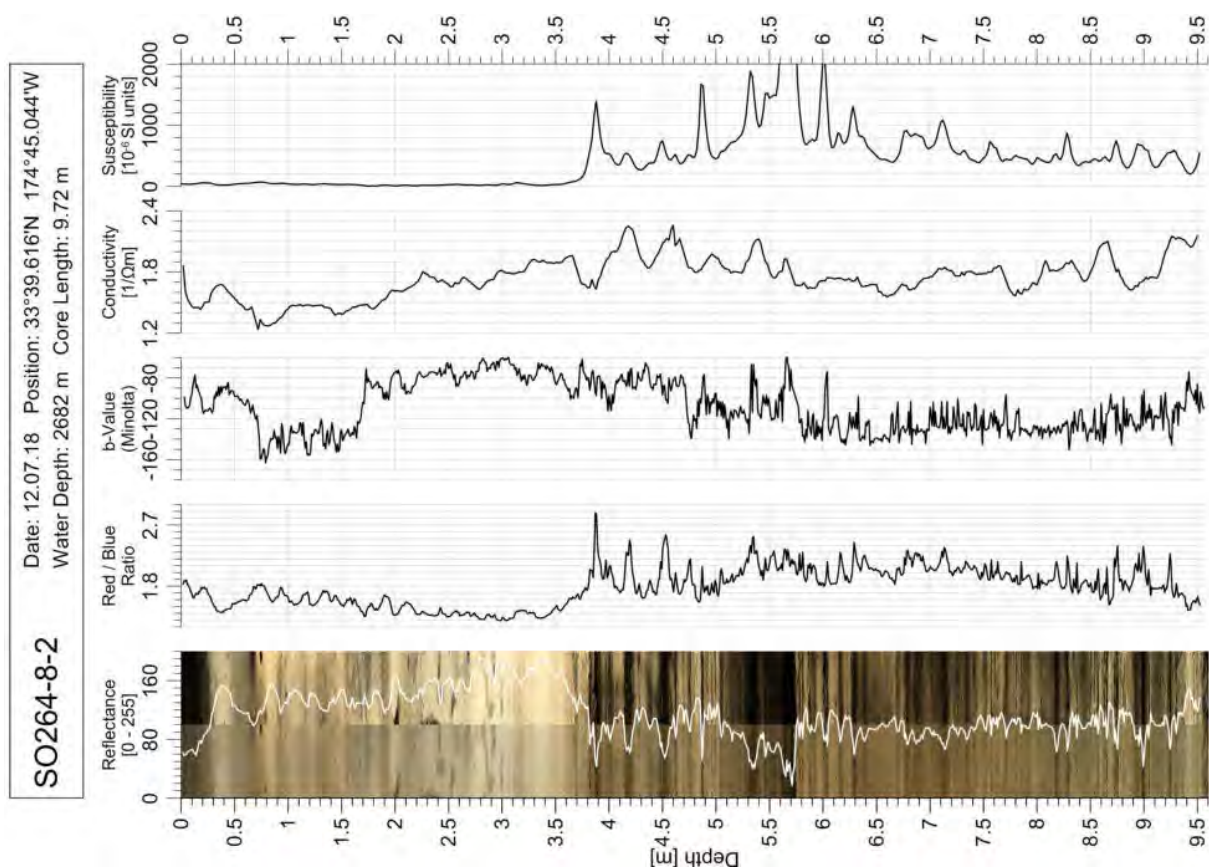






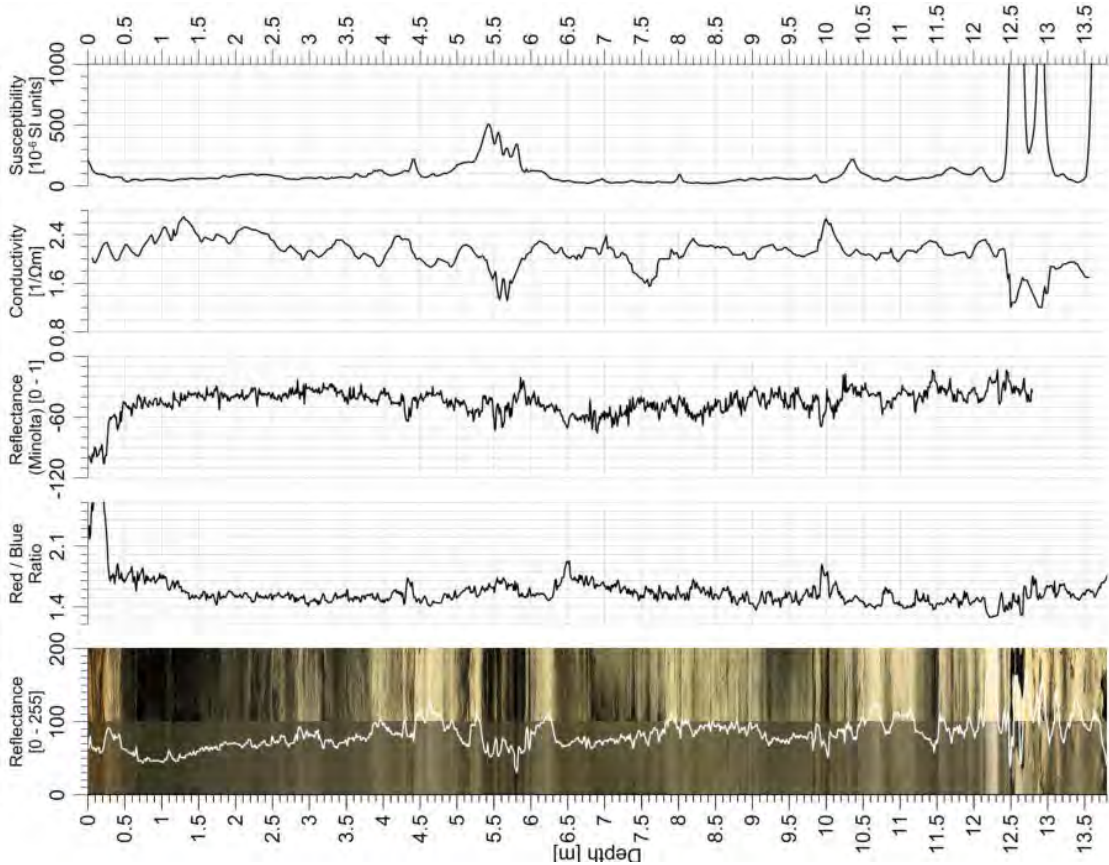






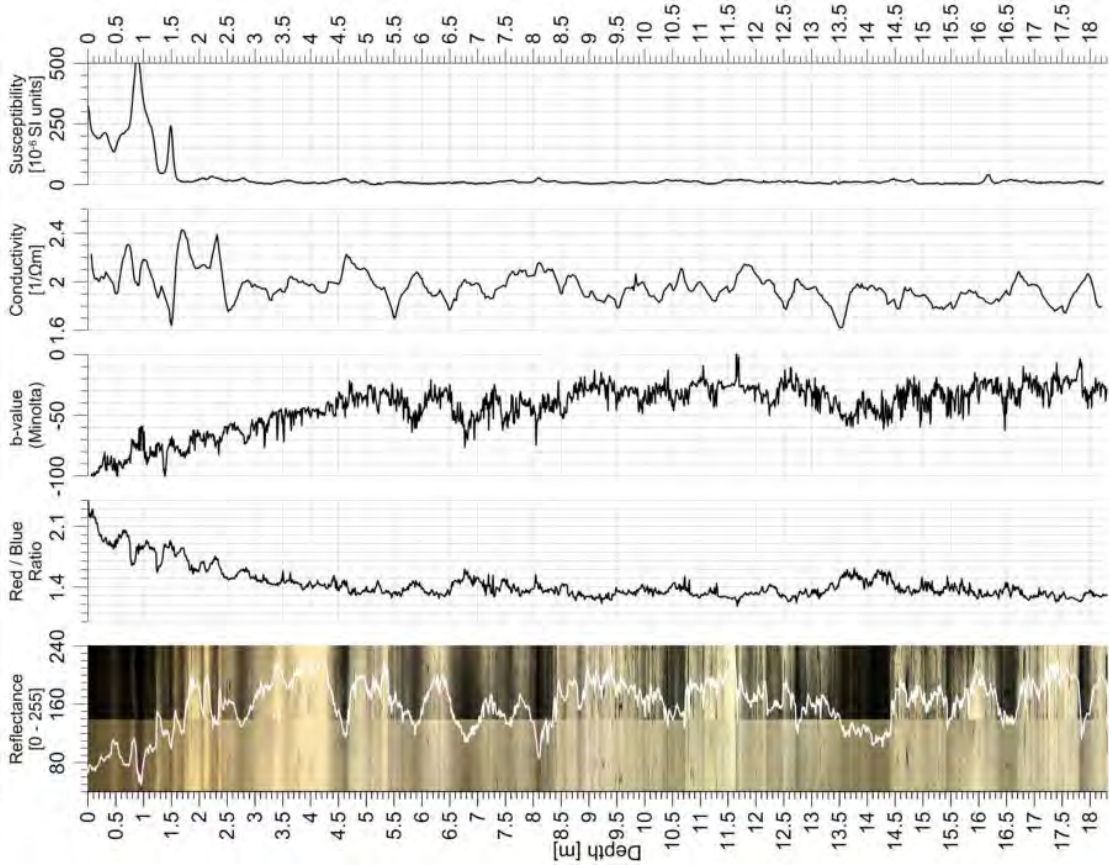
SO264-13-2

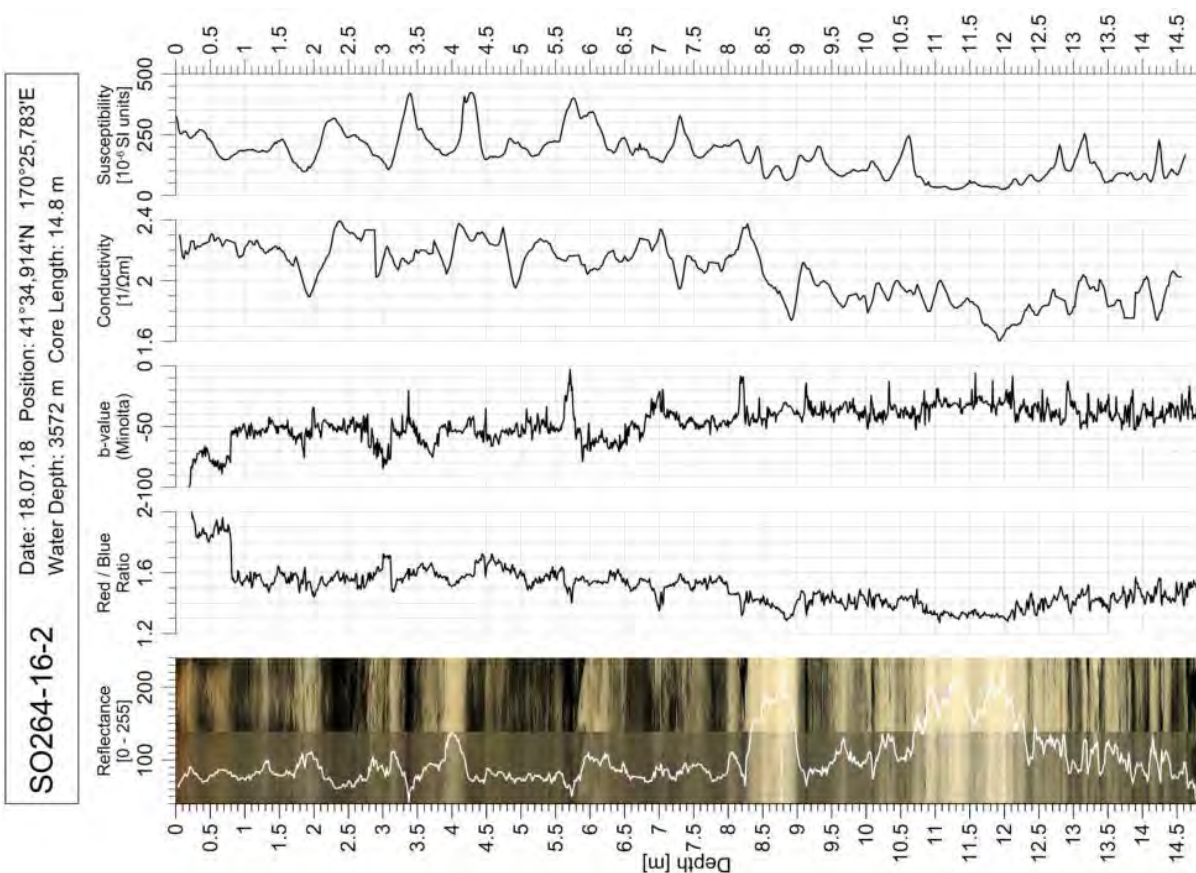
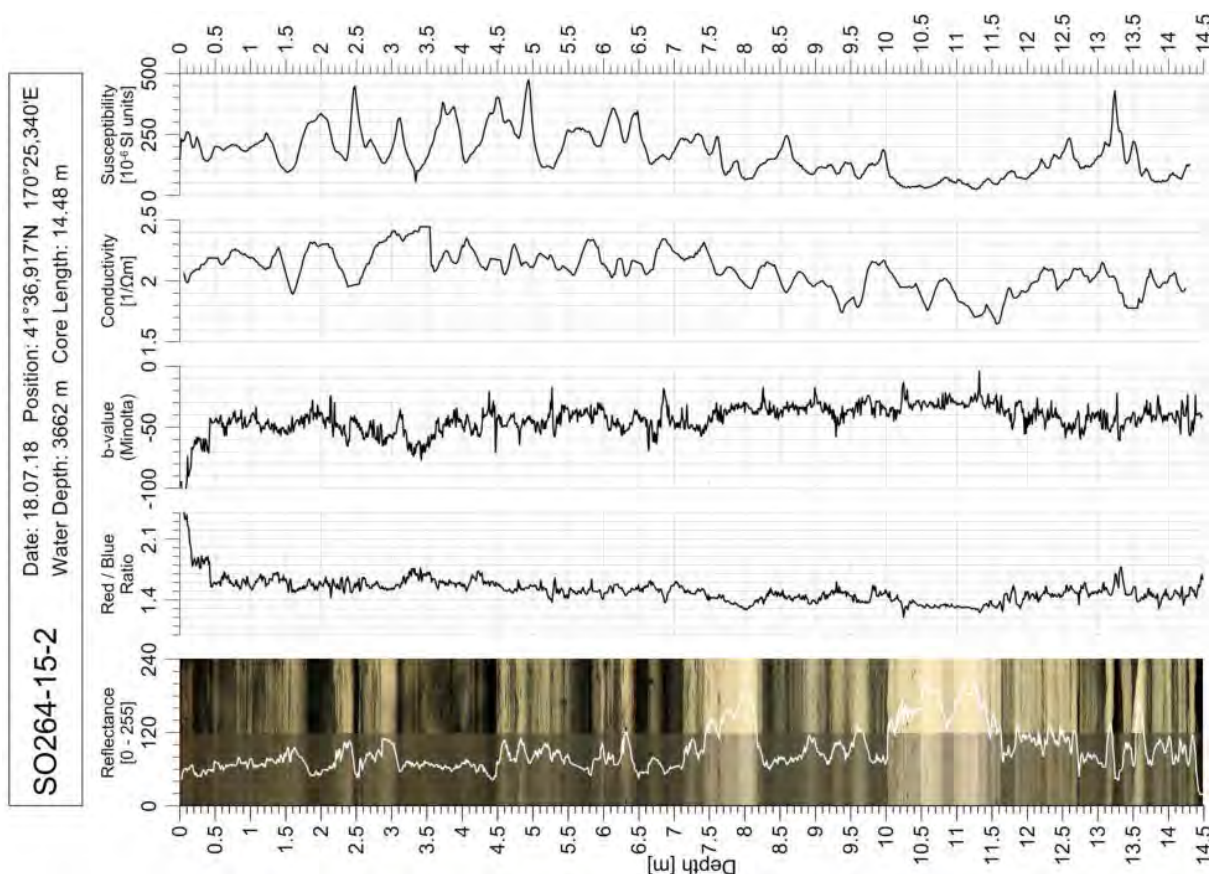
Date: 16.07.18 Position: 37°47.865'N 170°43.327'E
Water Depth: 3935 m Core Length: 13.81 m

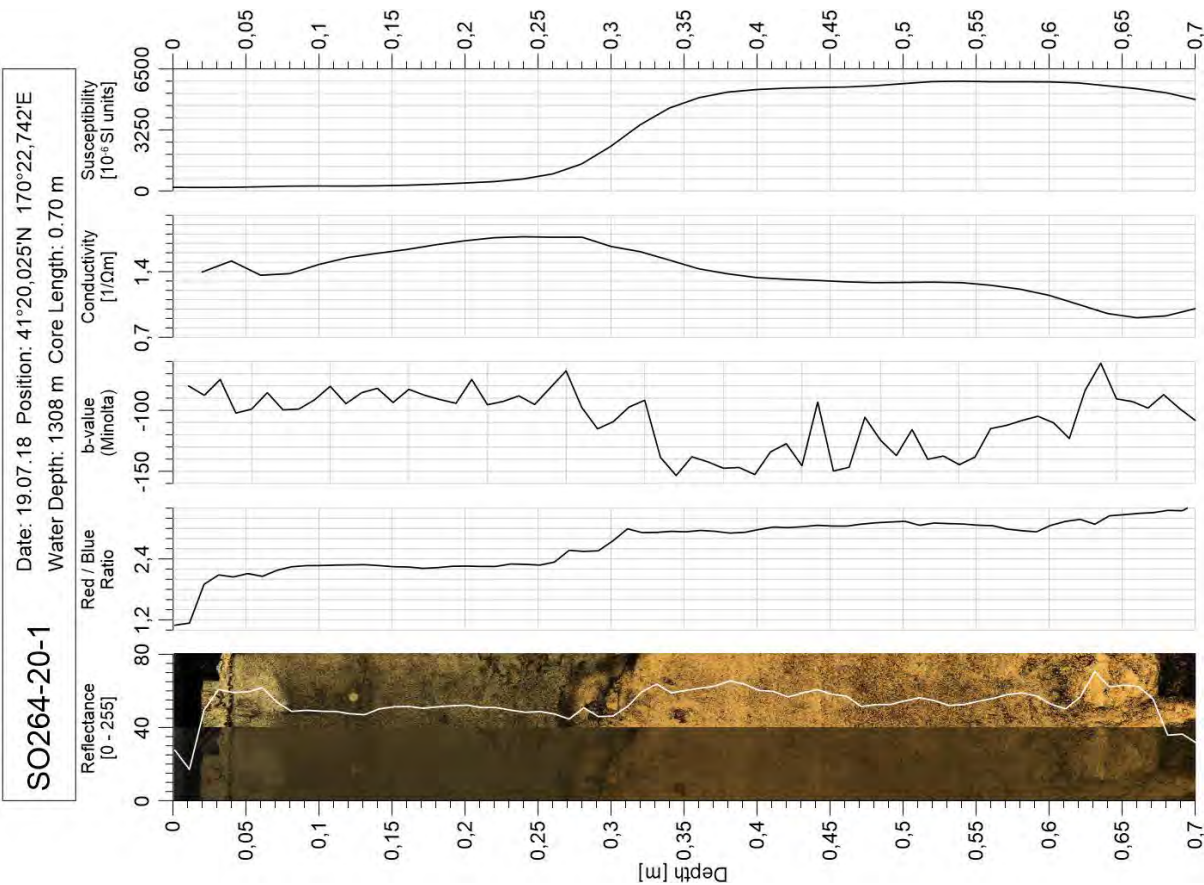
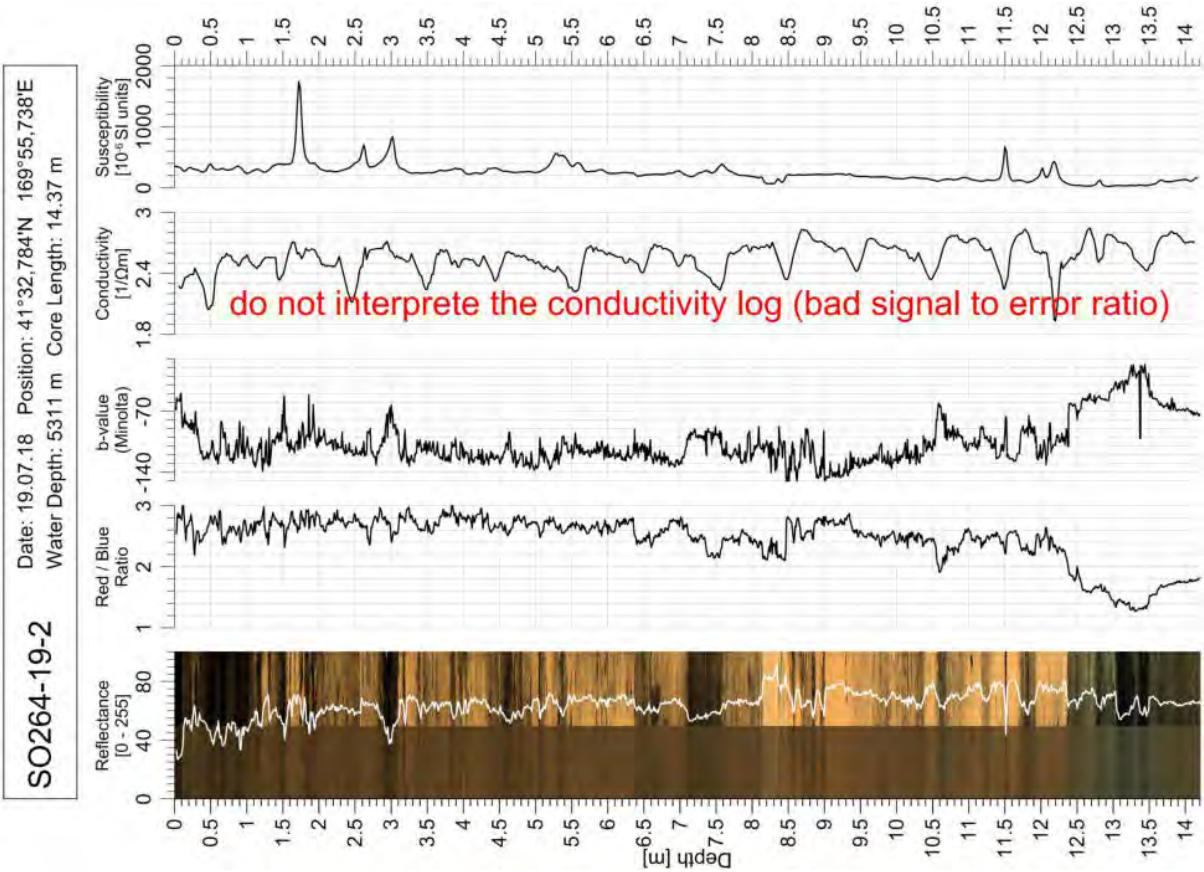


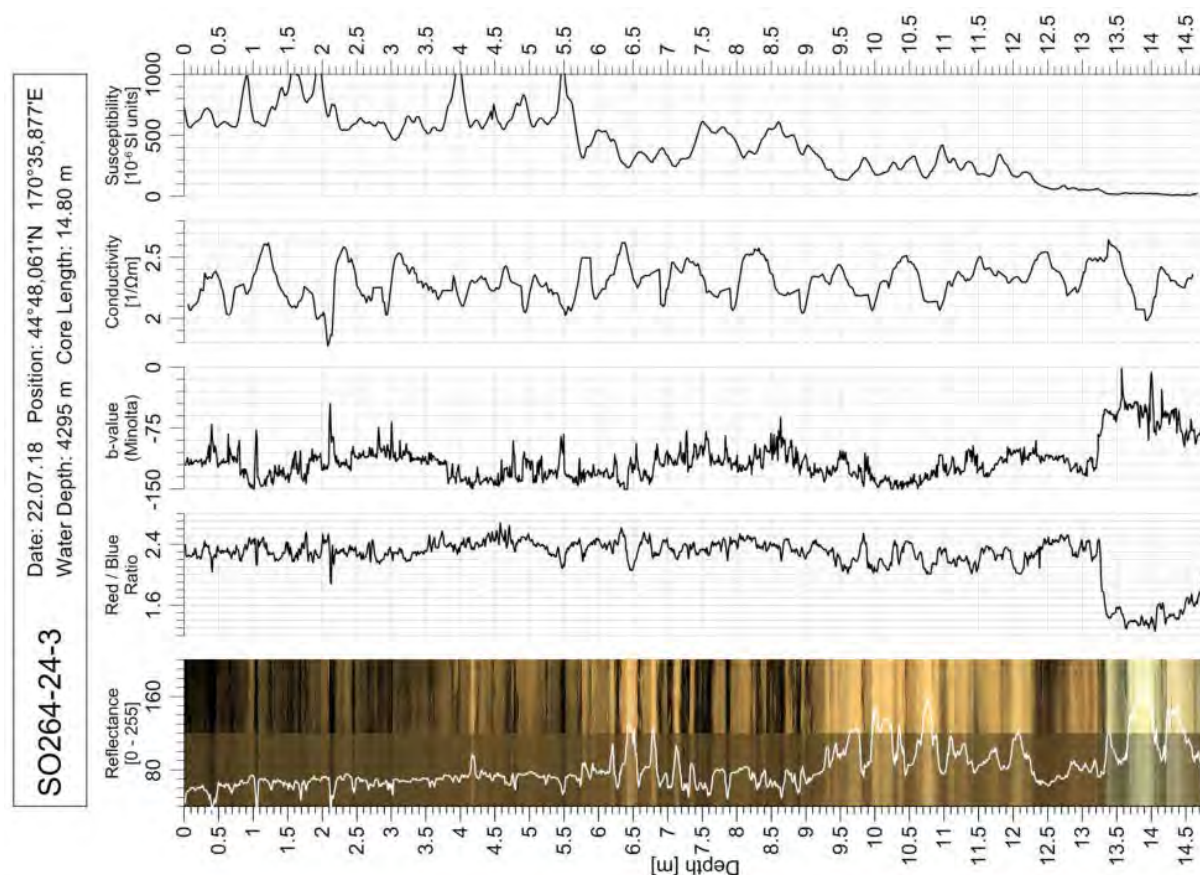
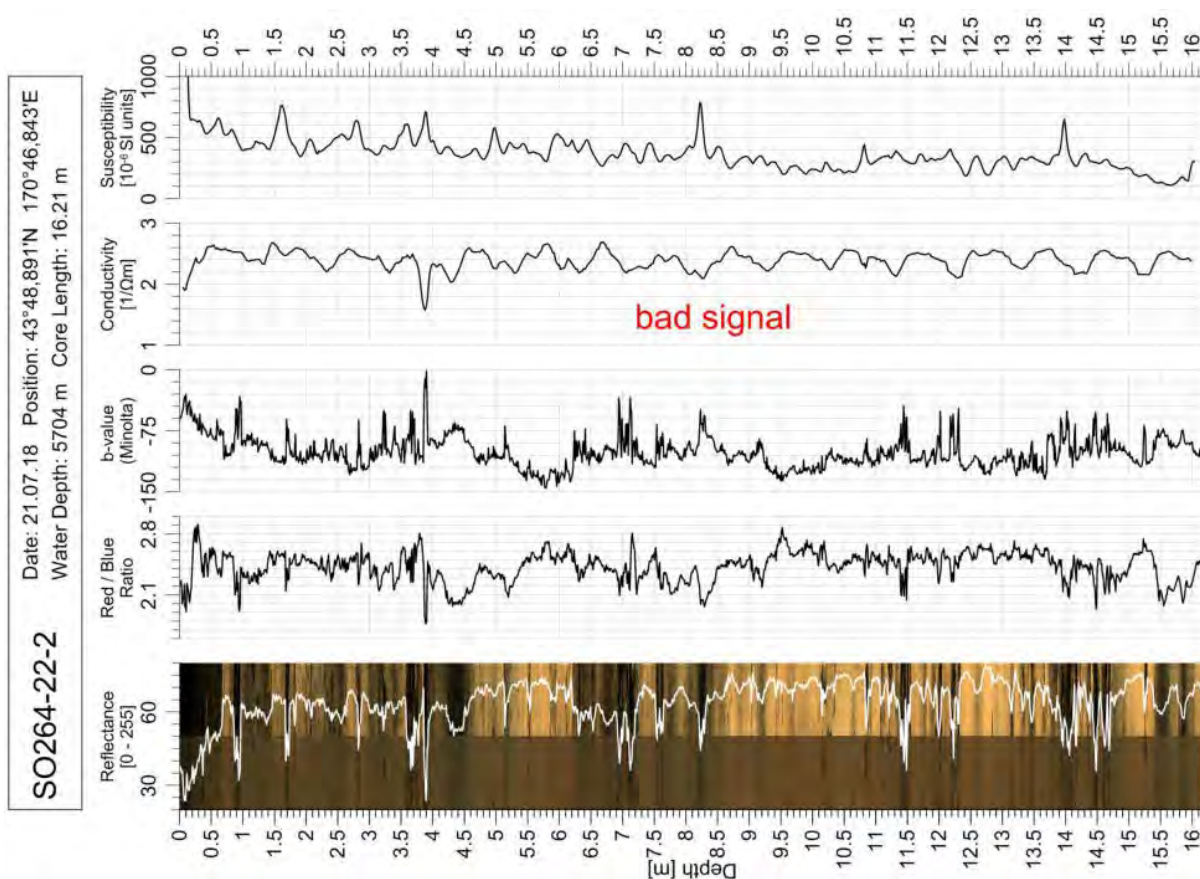
SO264-14-1

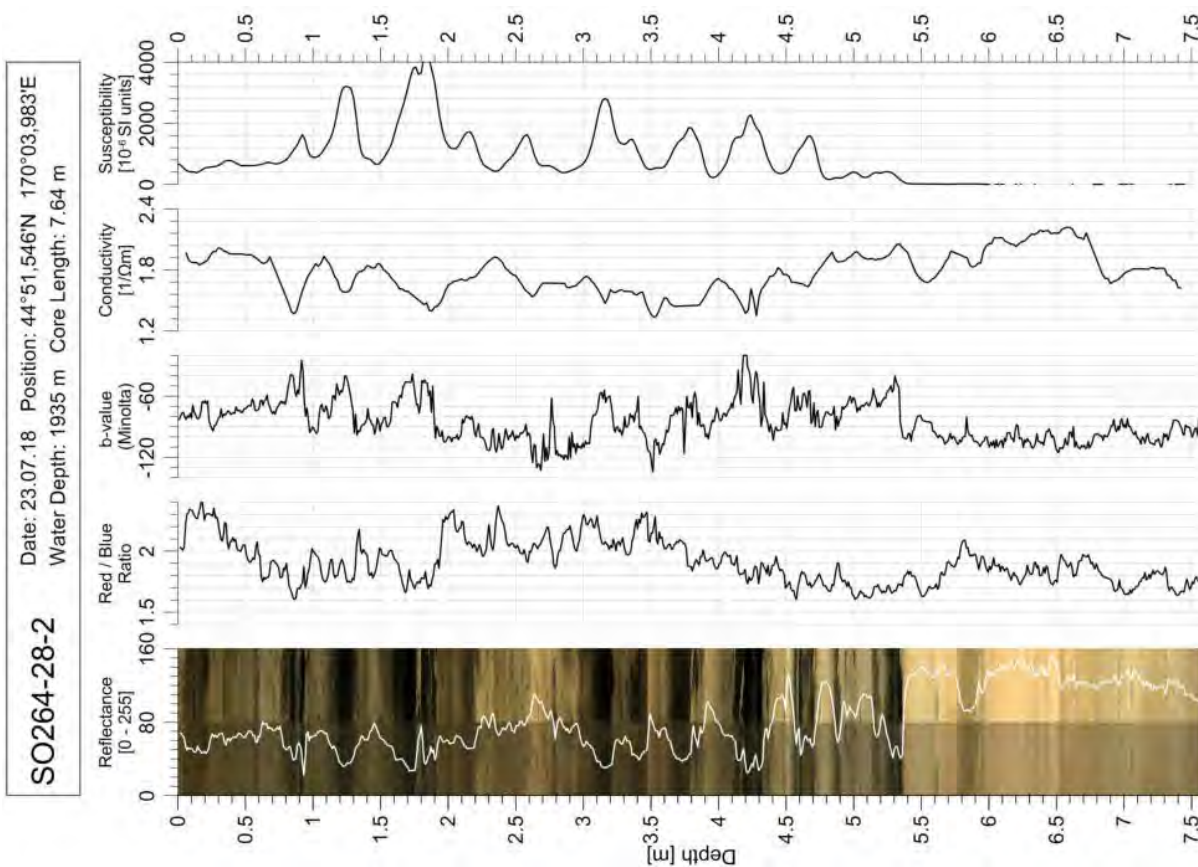
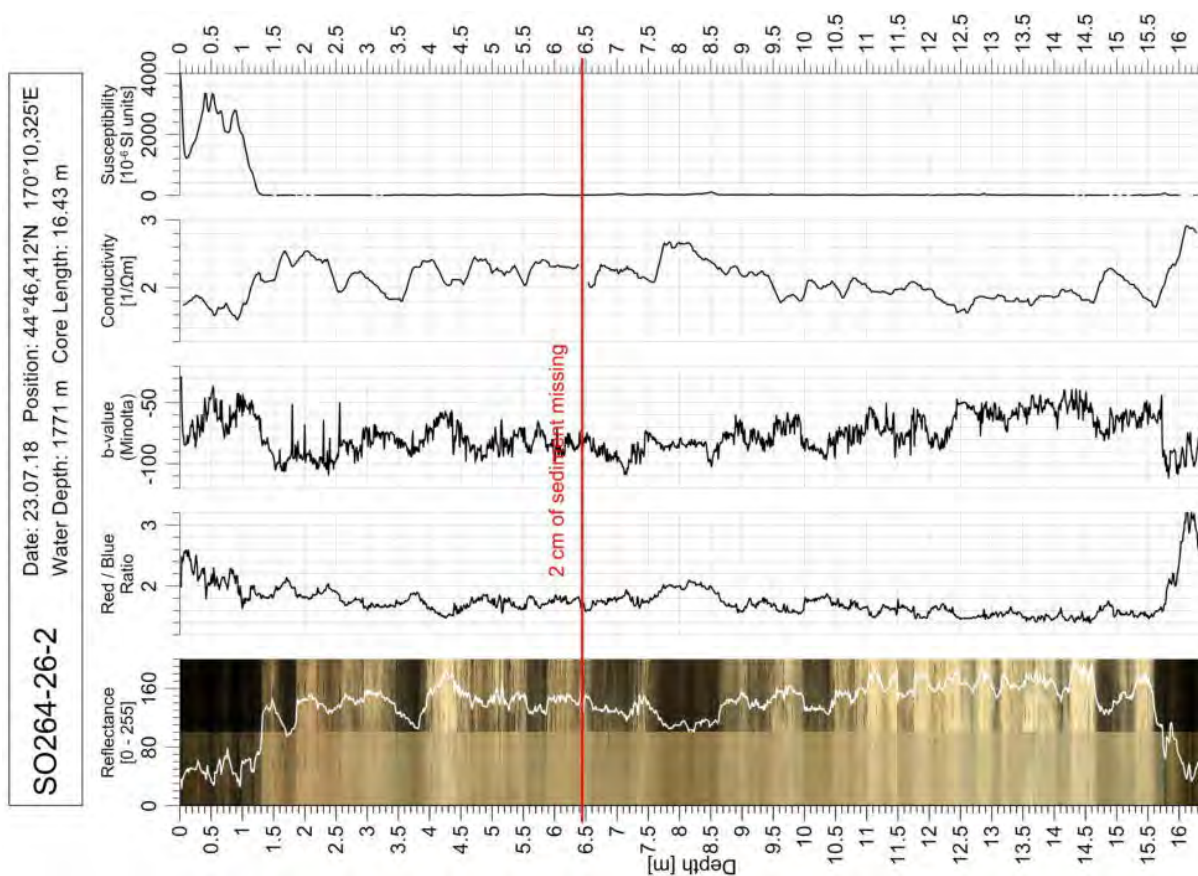
Date: 17.07.18 Position: 40°50.034'N 170°54.201'E
Water Depth: 3750 m Core Length: 18.4 m

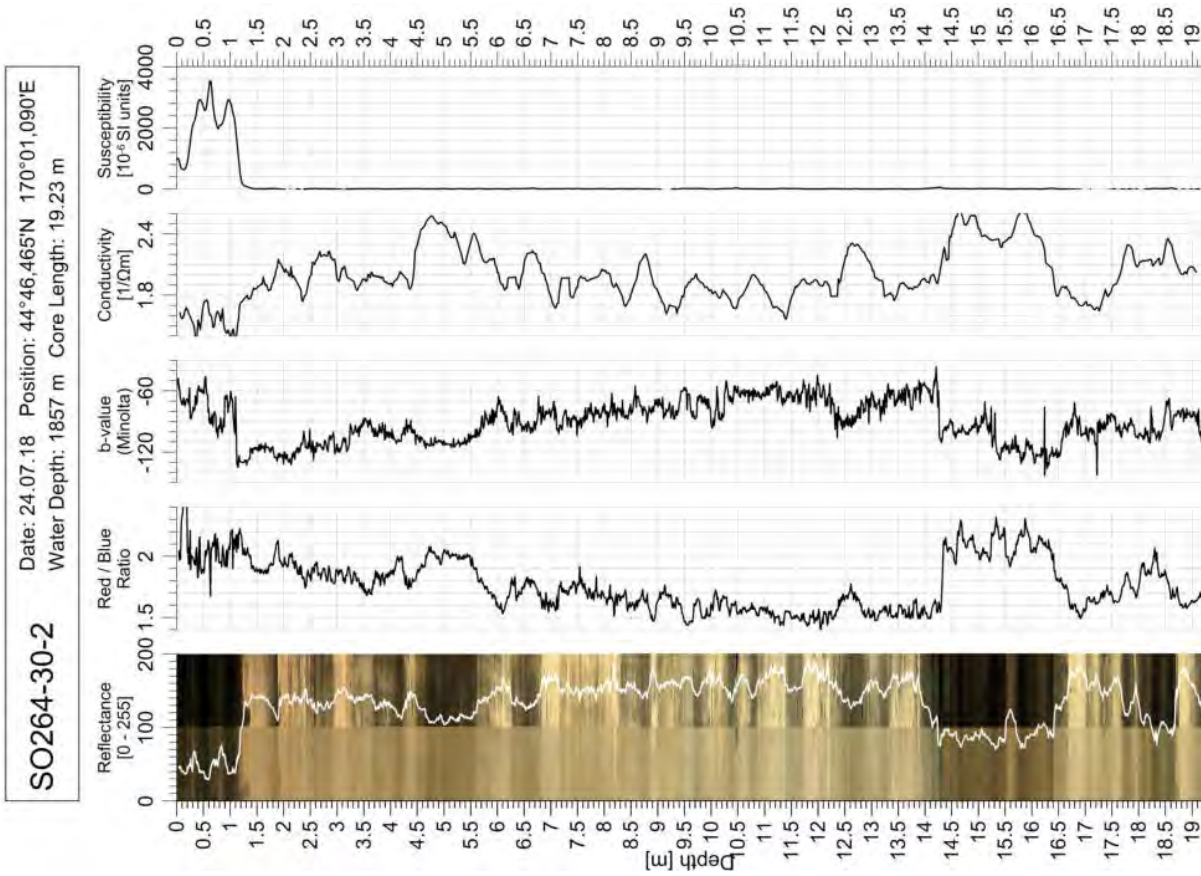
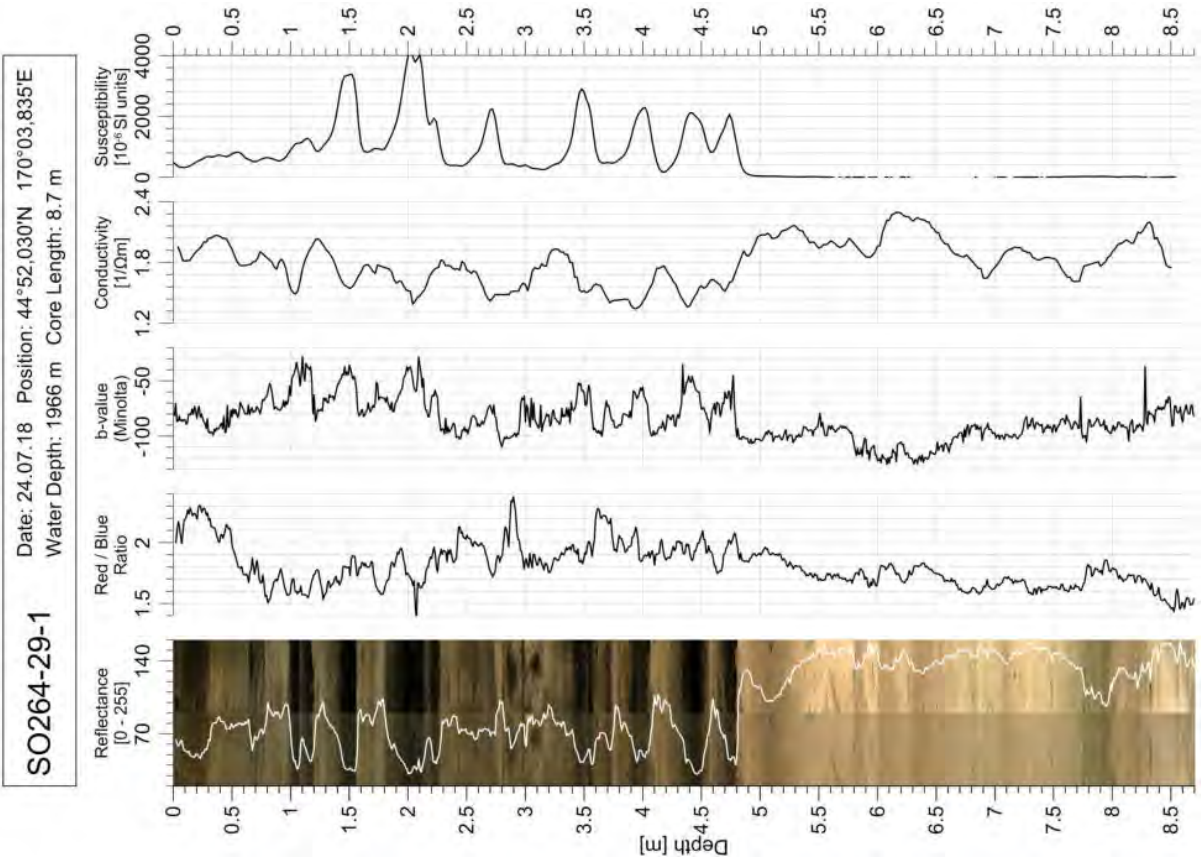


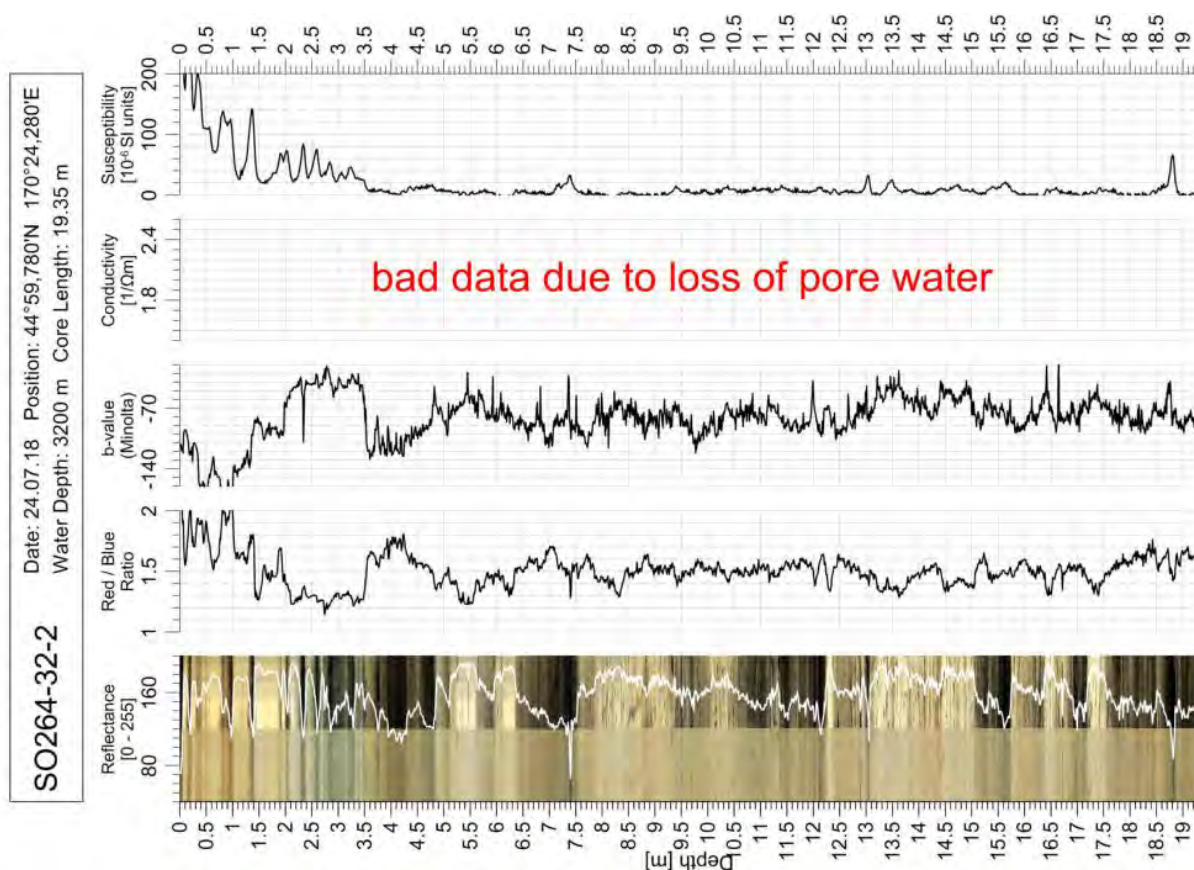
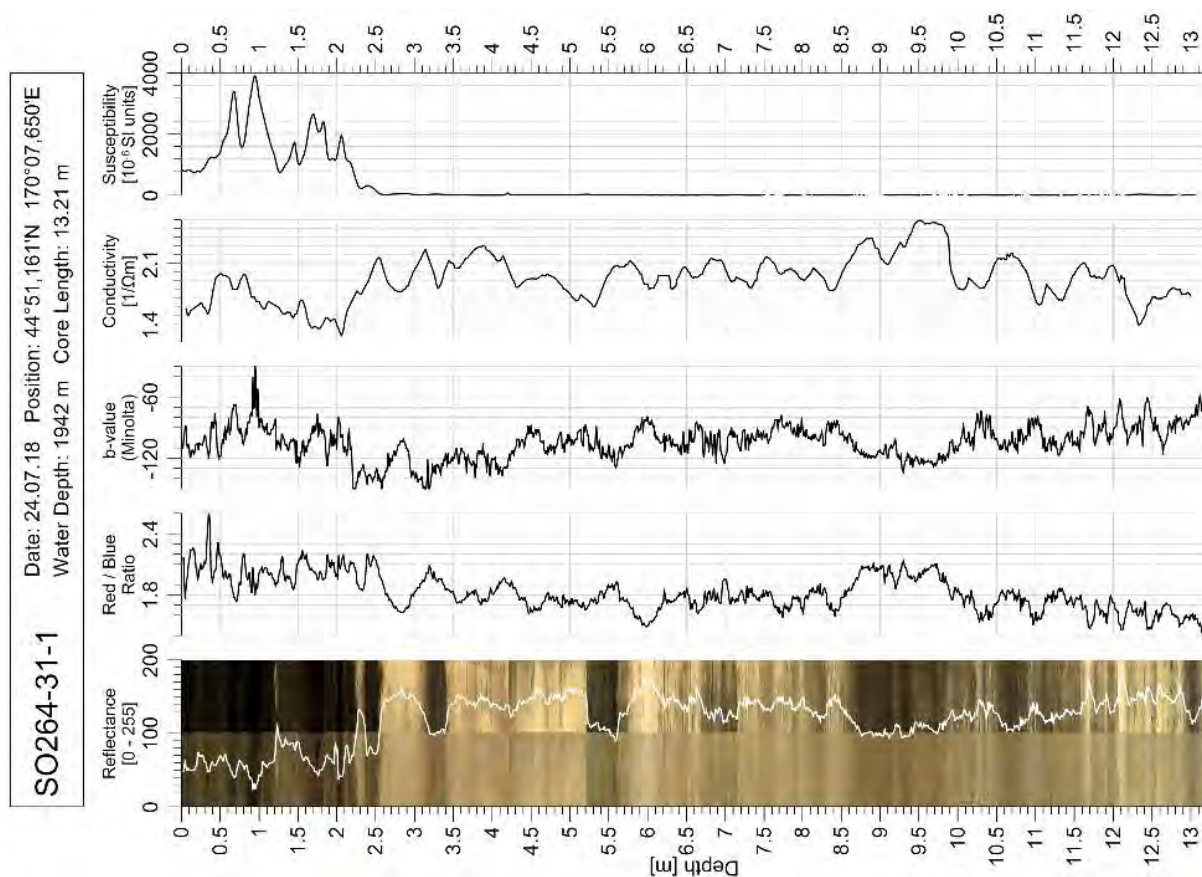


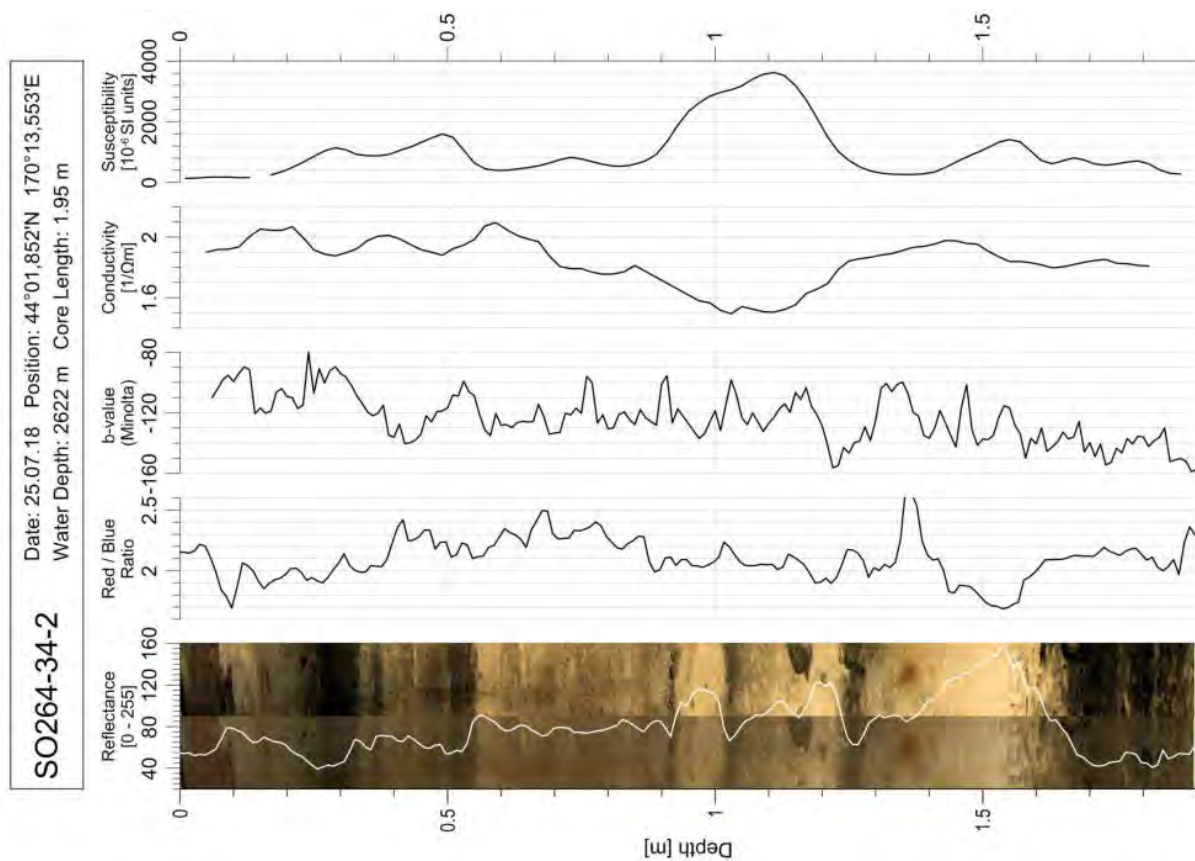
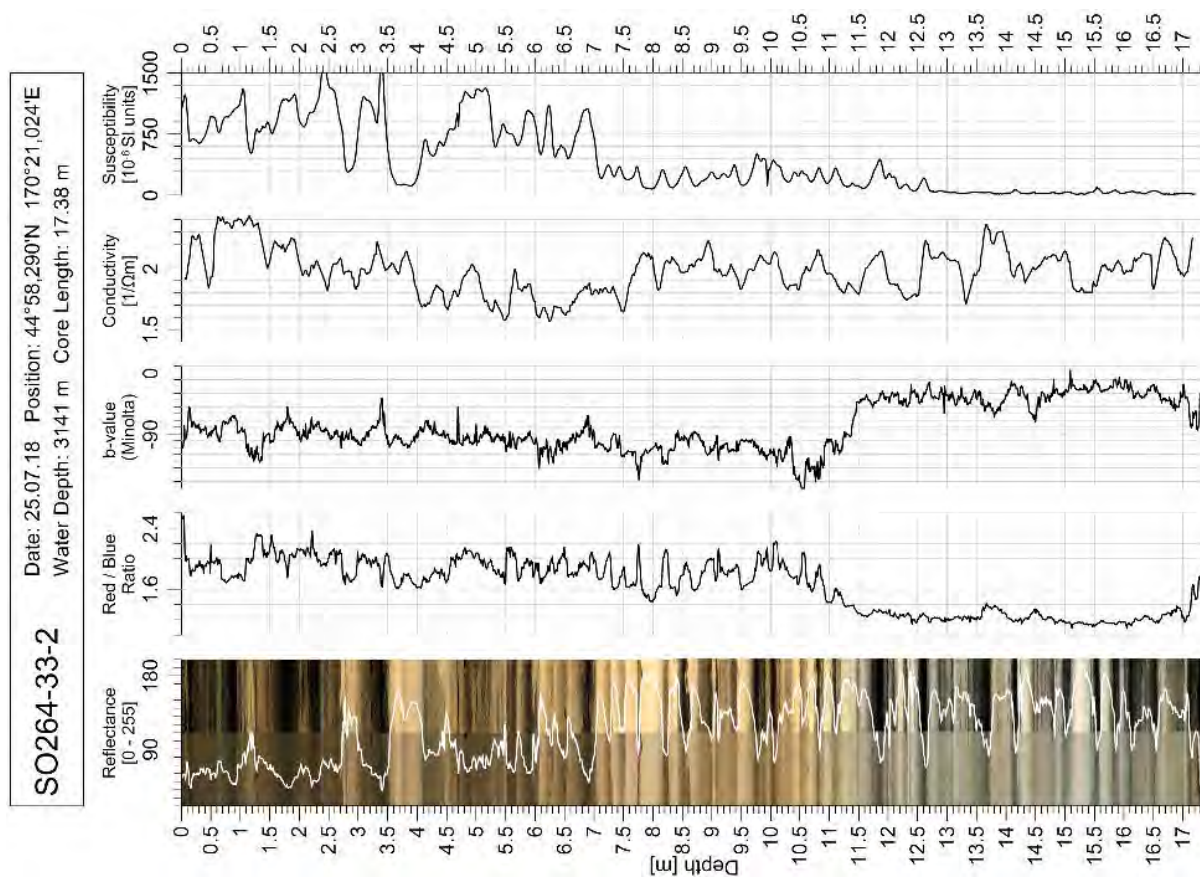


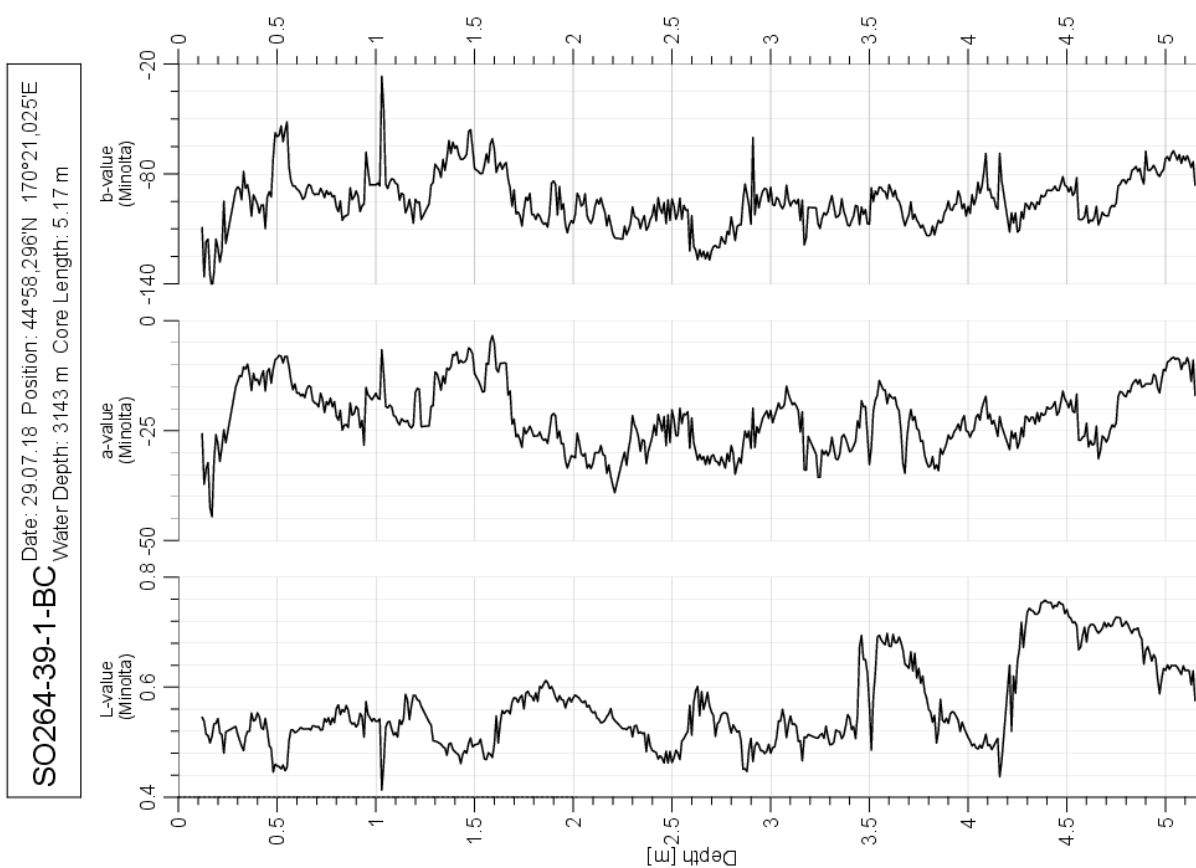
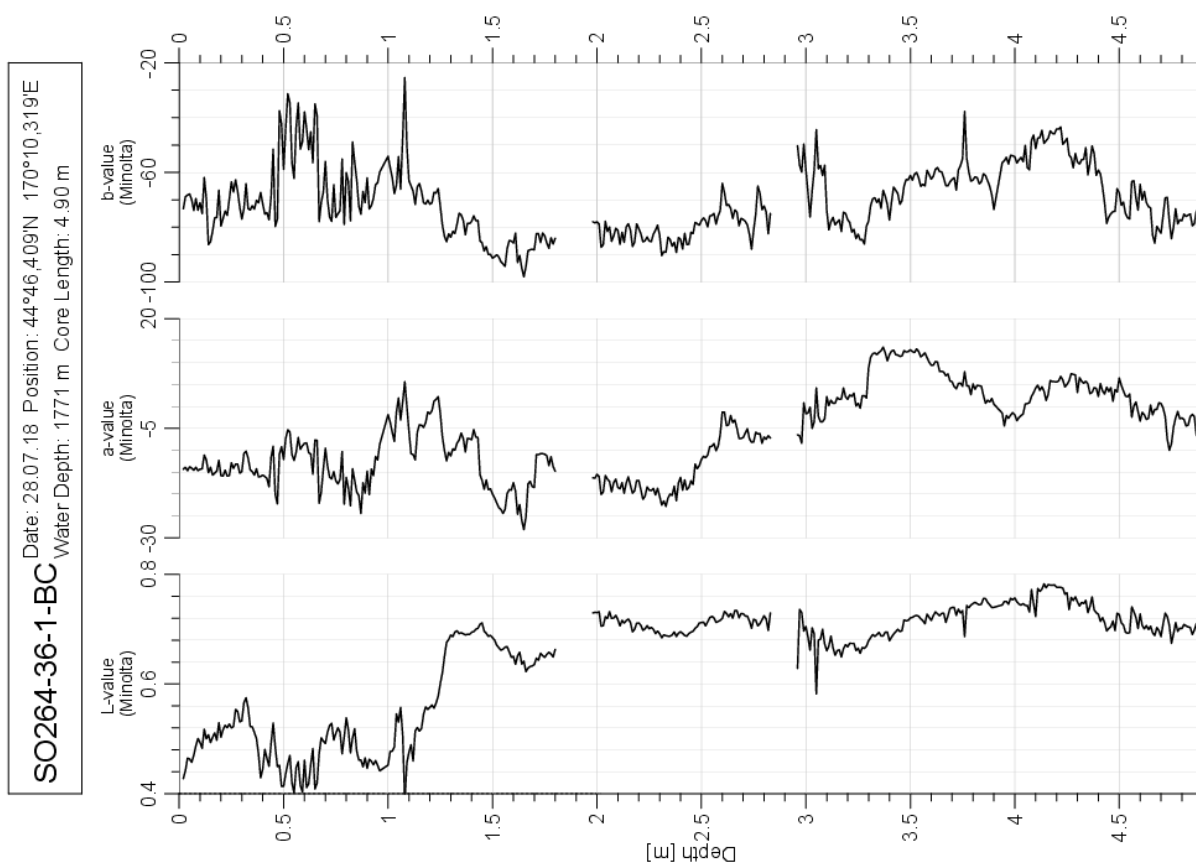


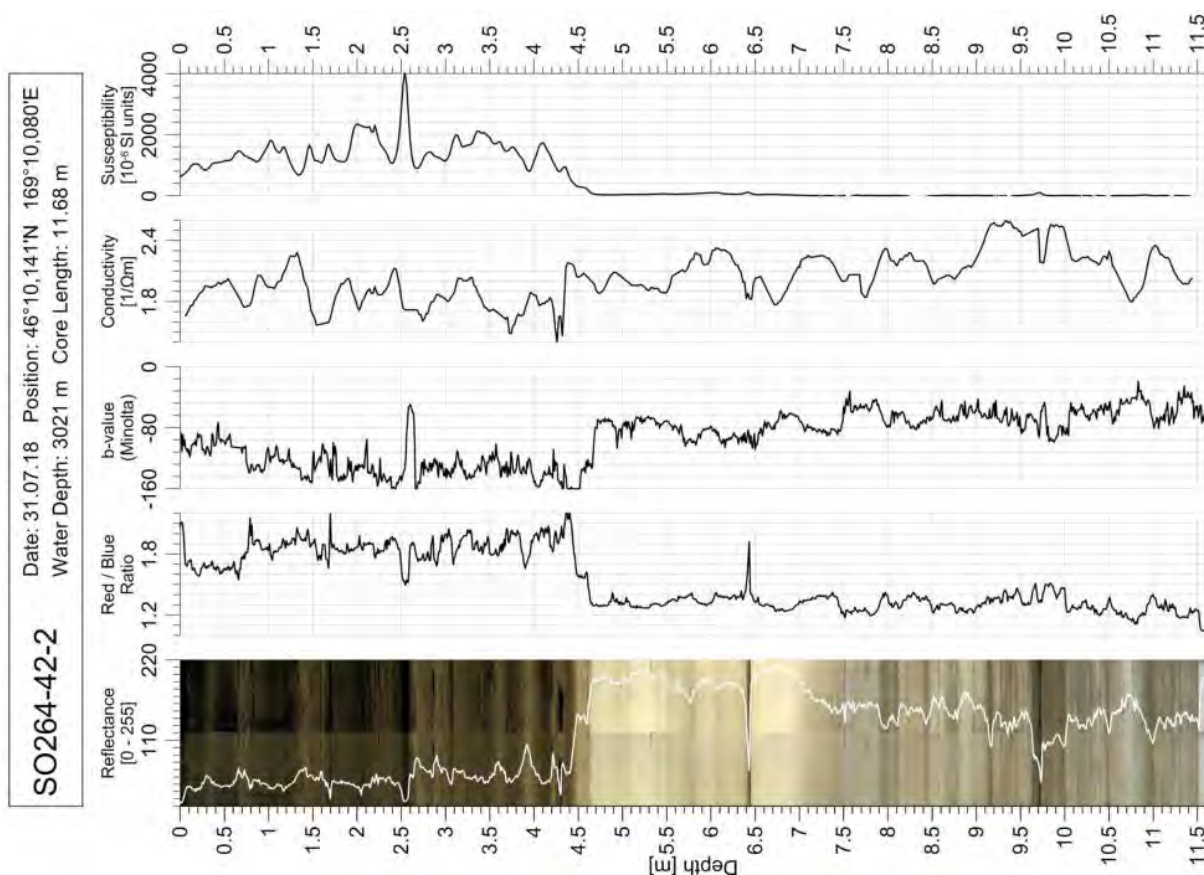
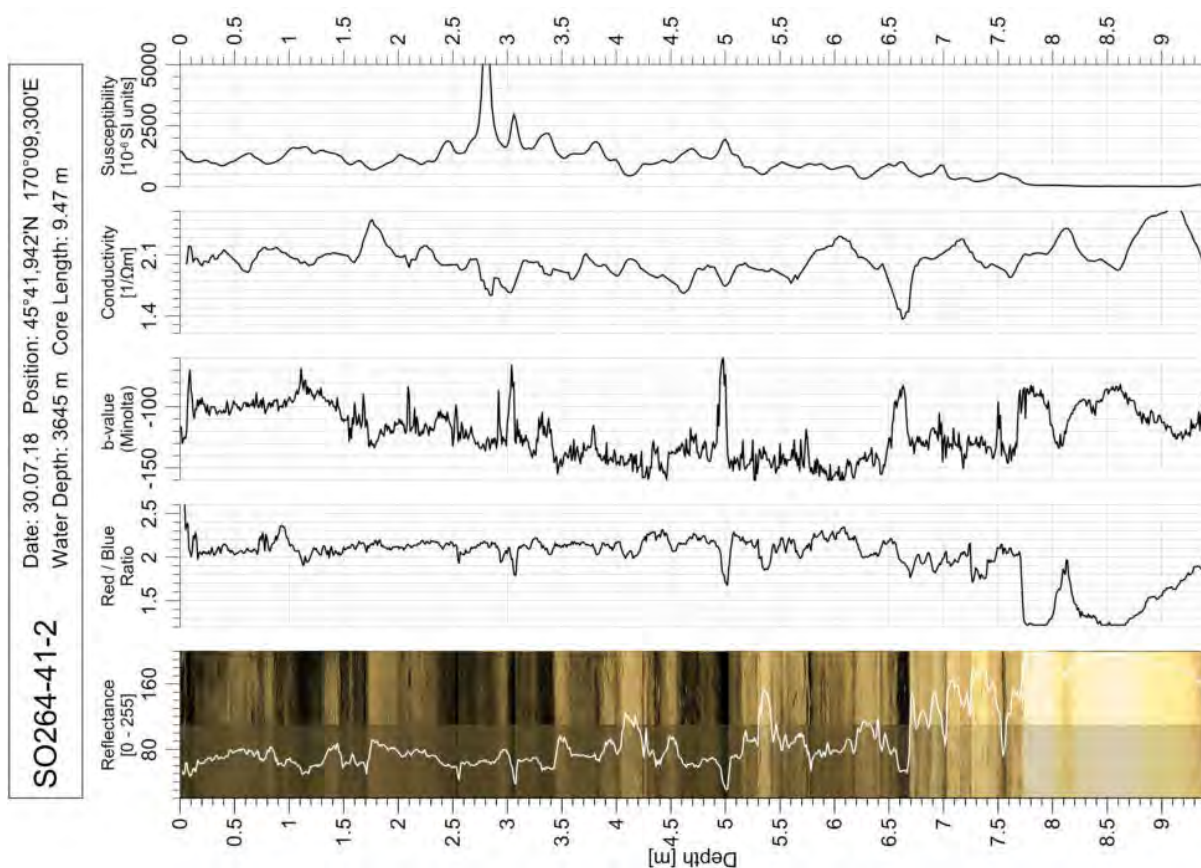


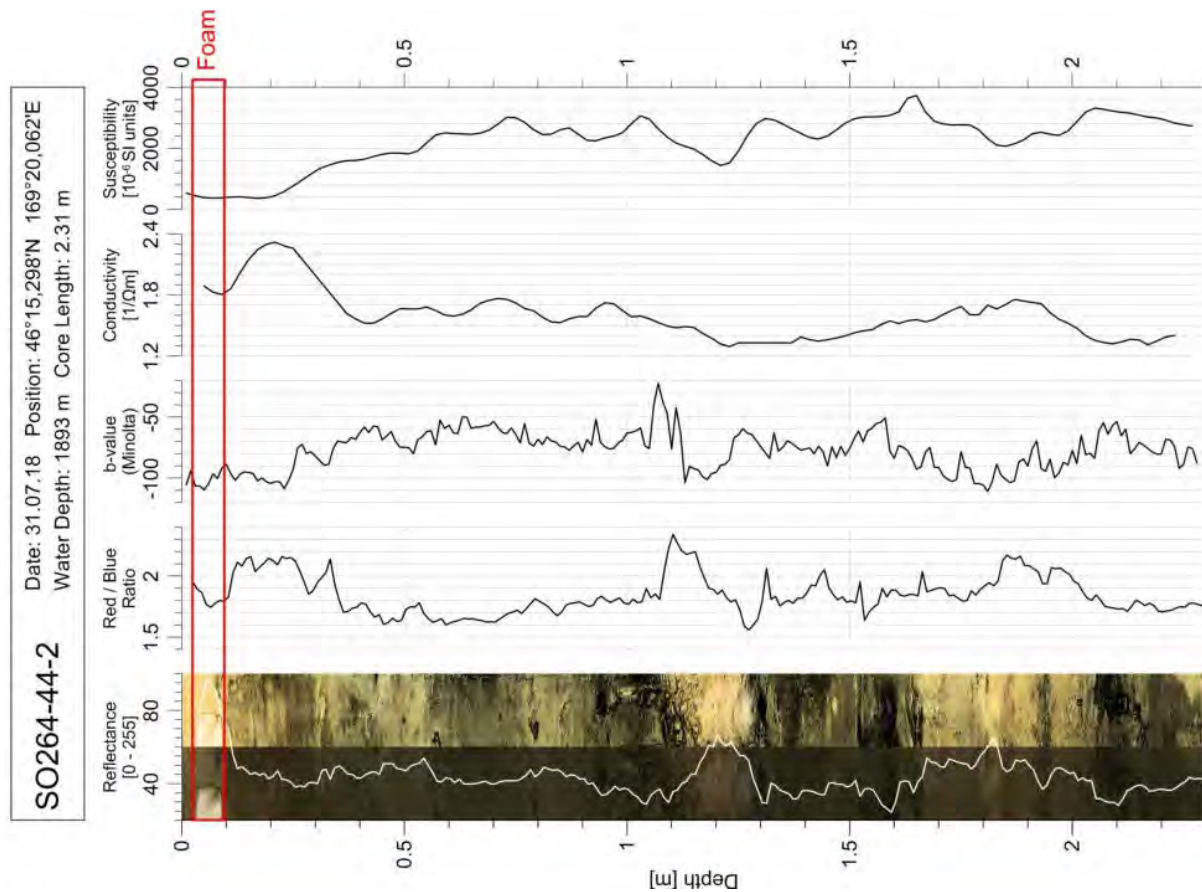
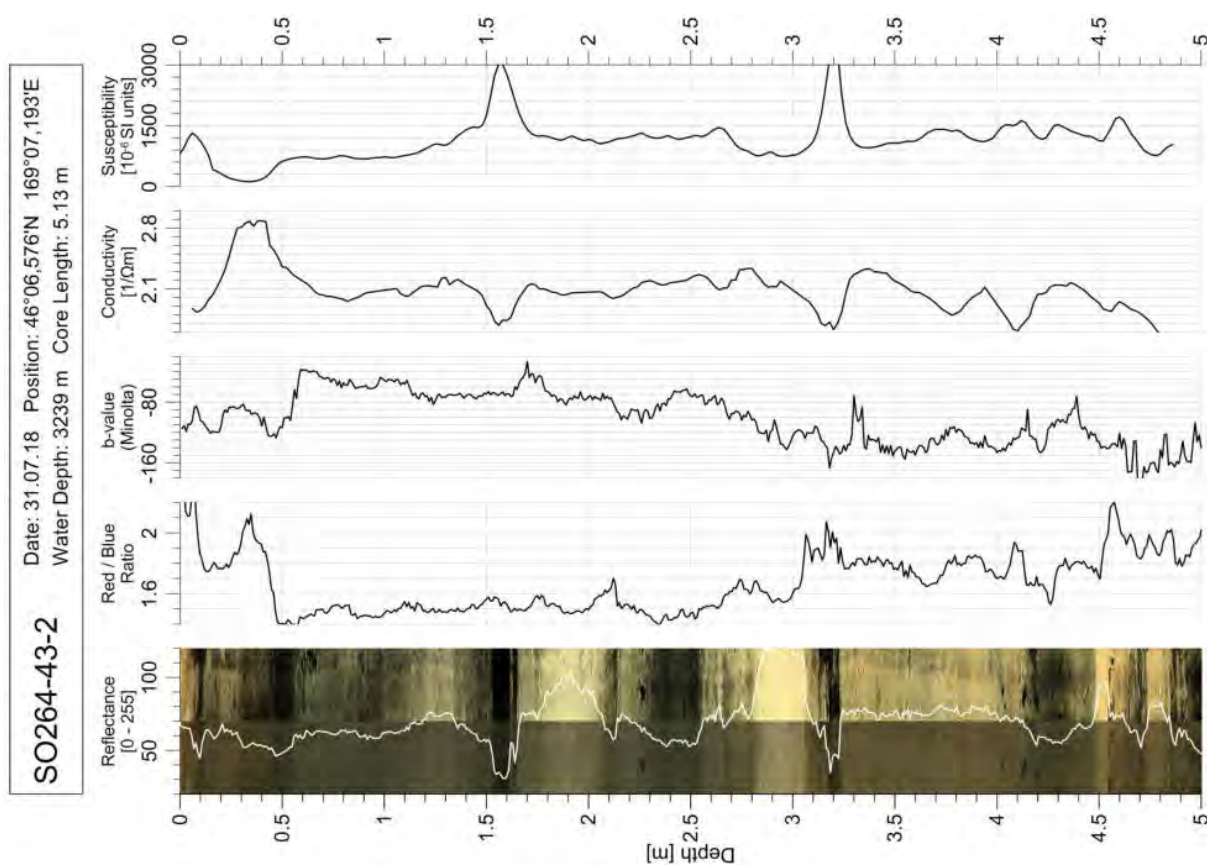


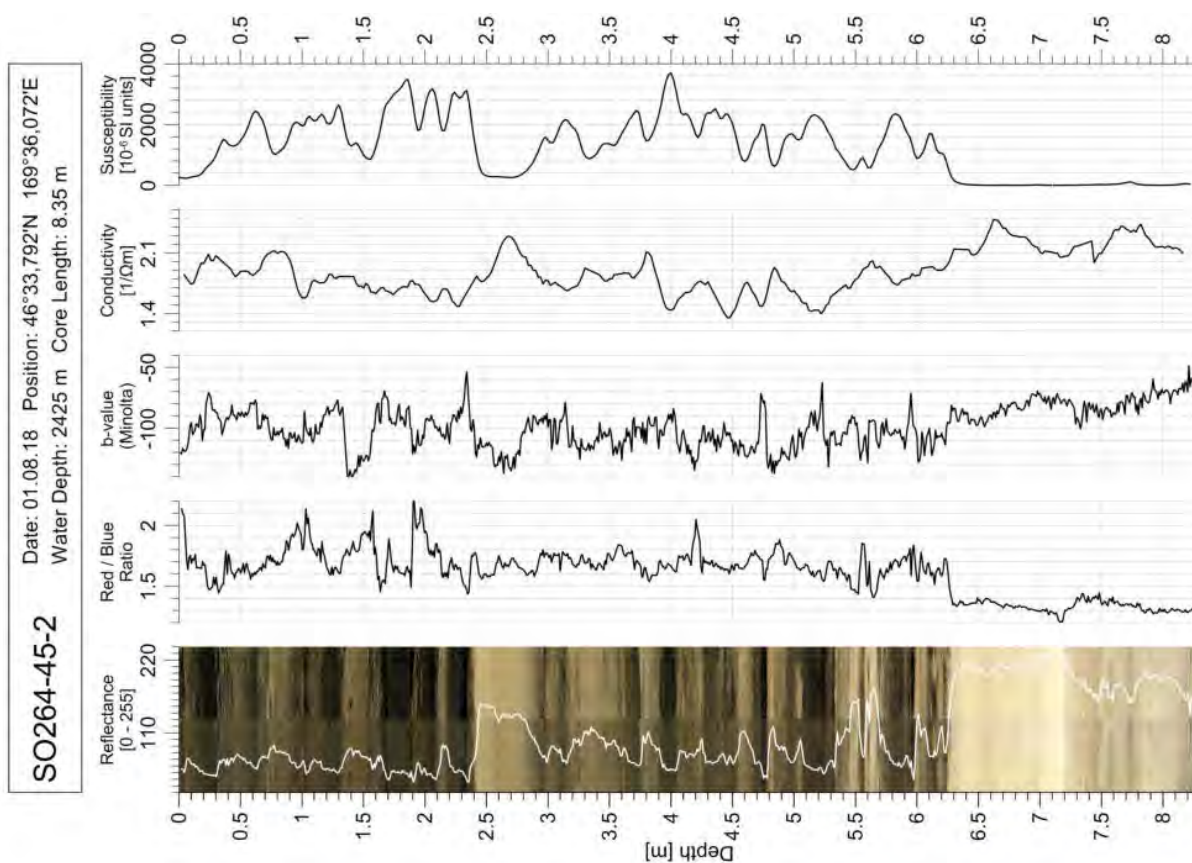
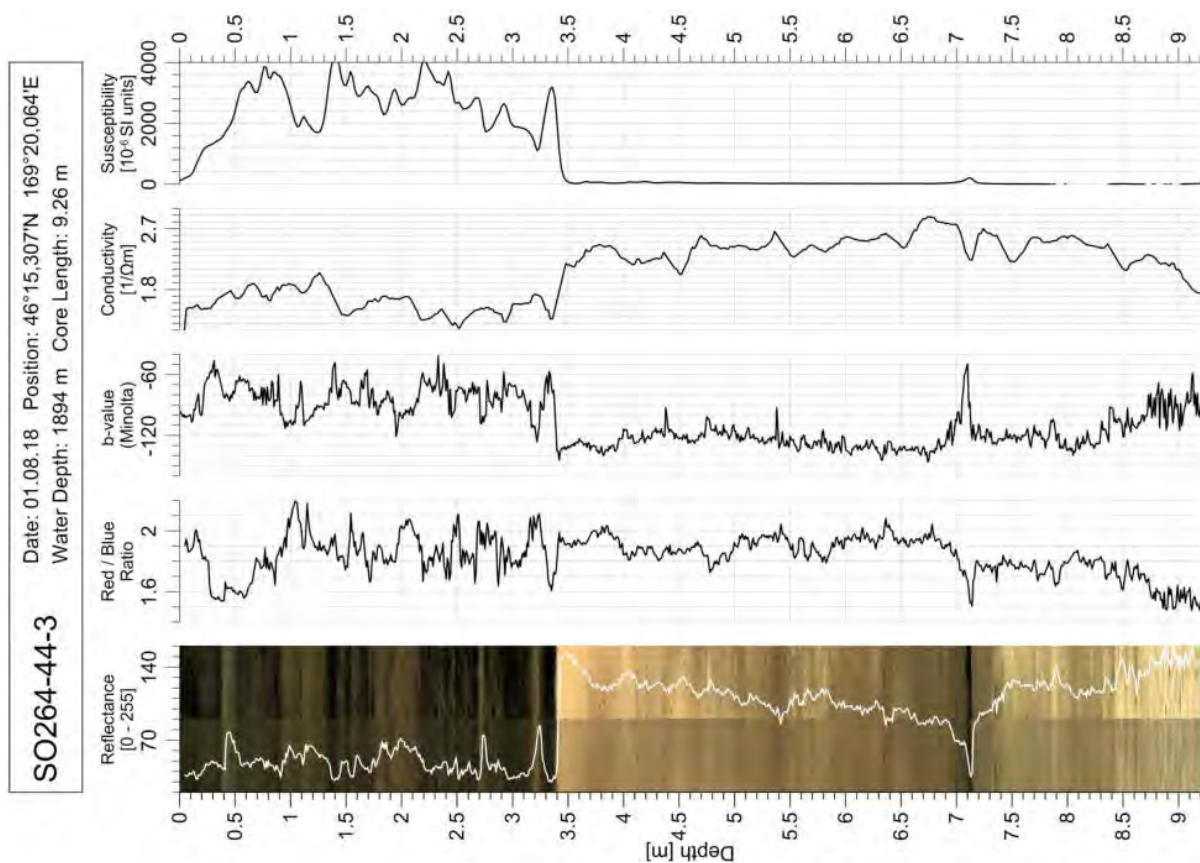


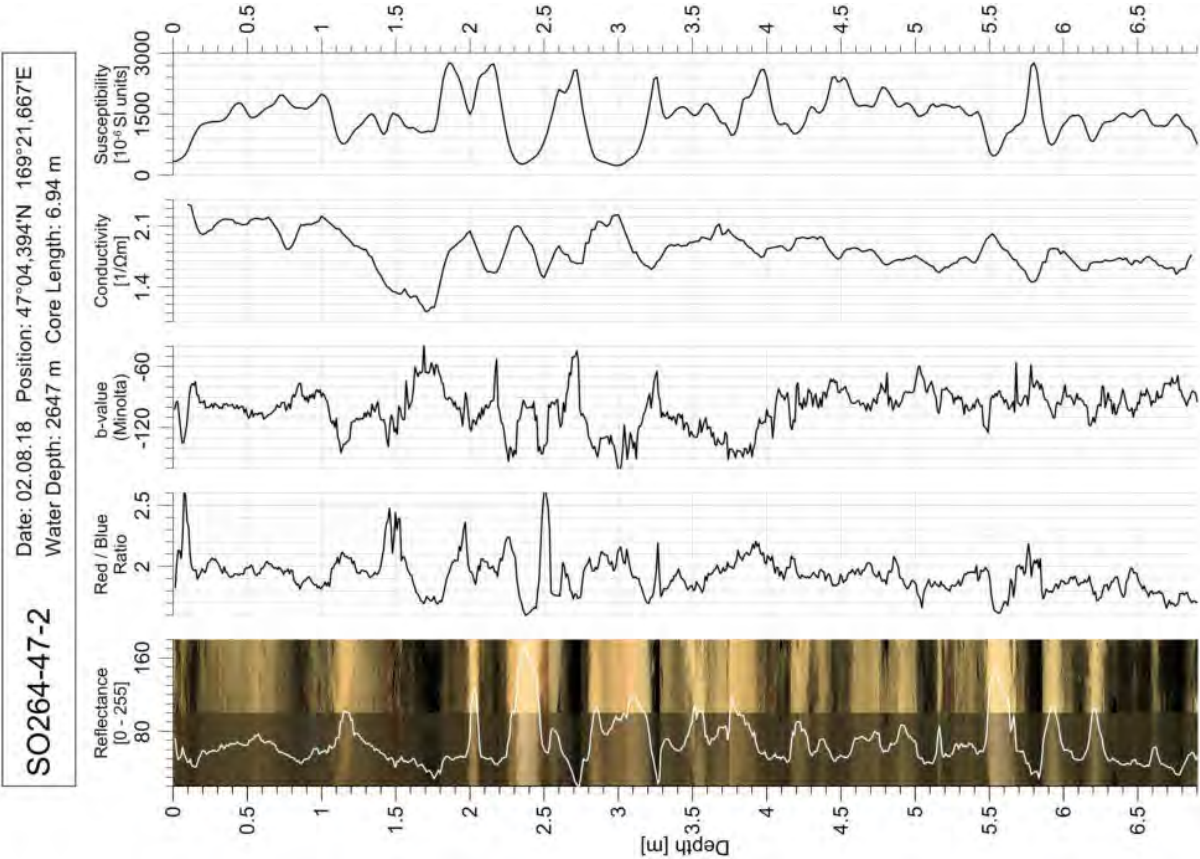
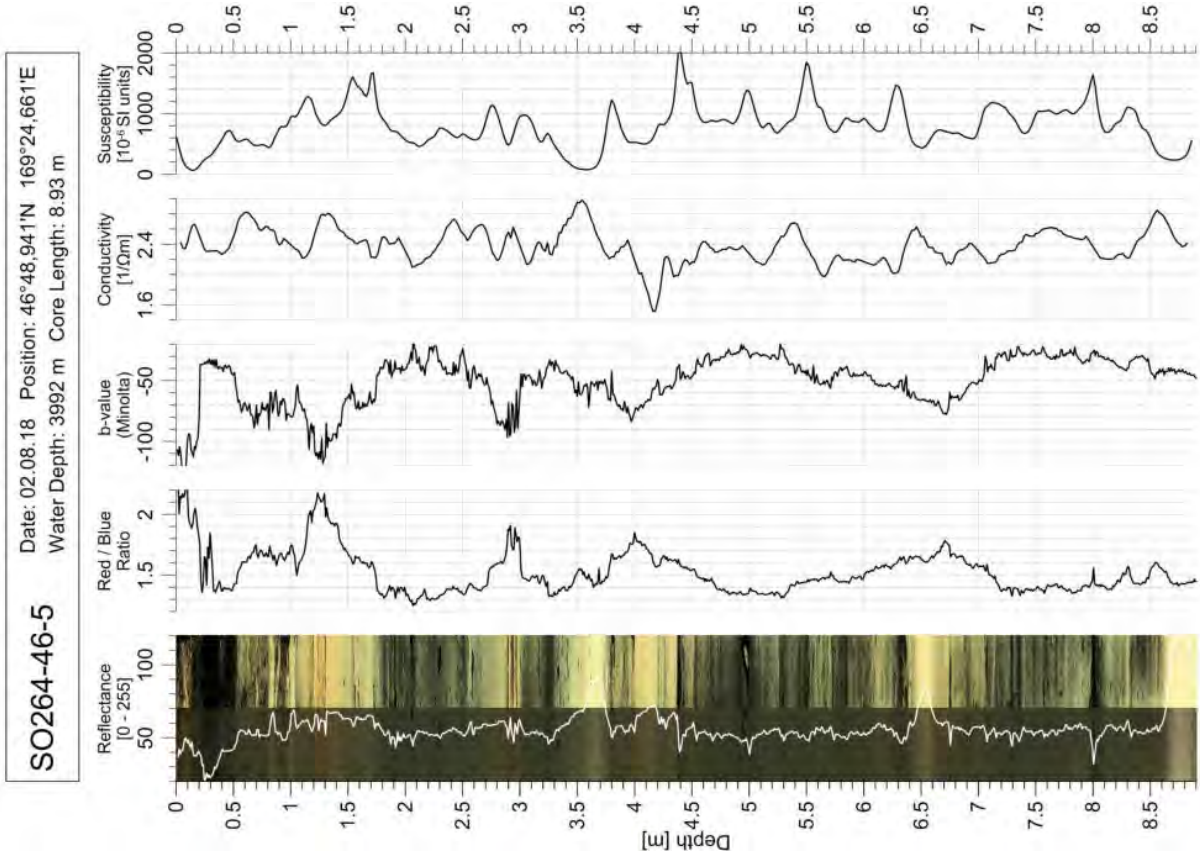


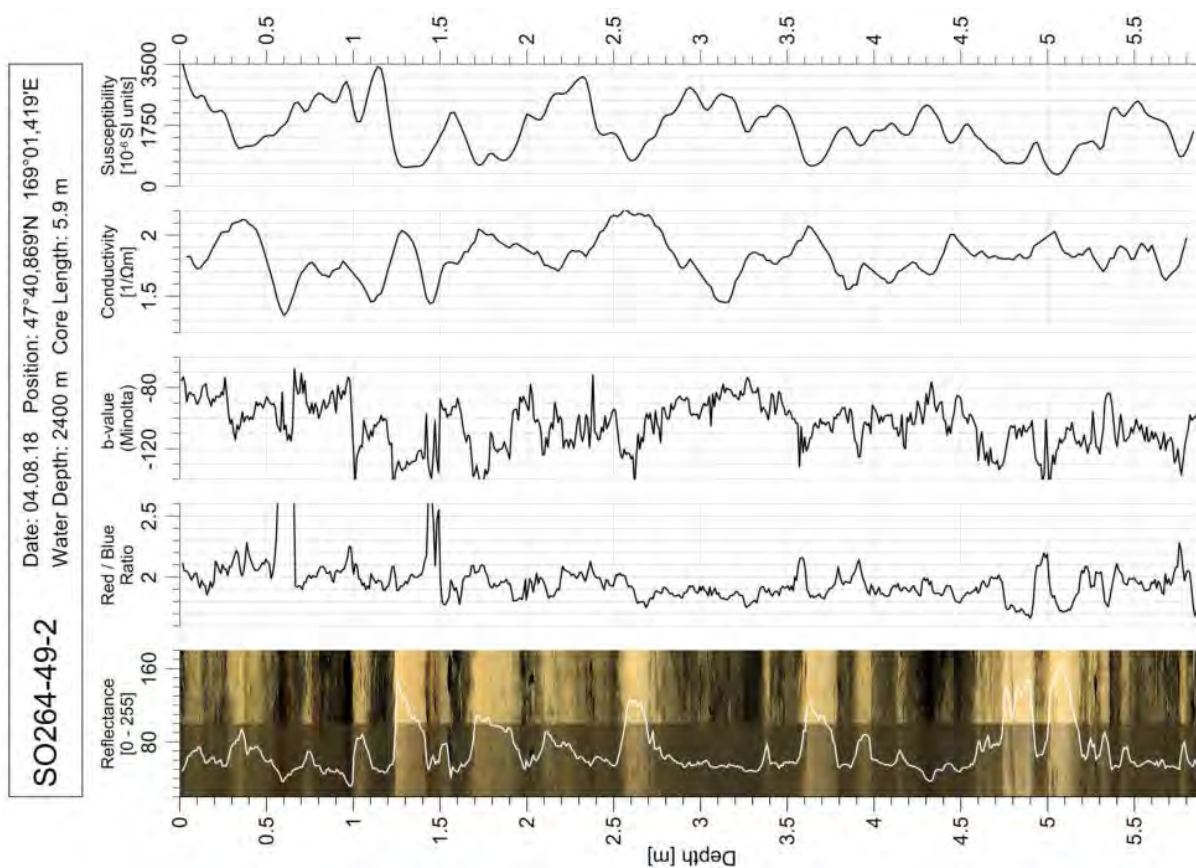
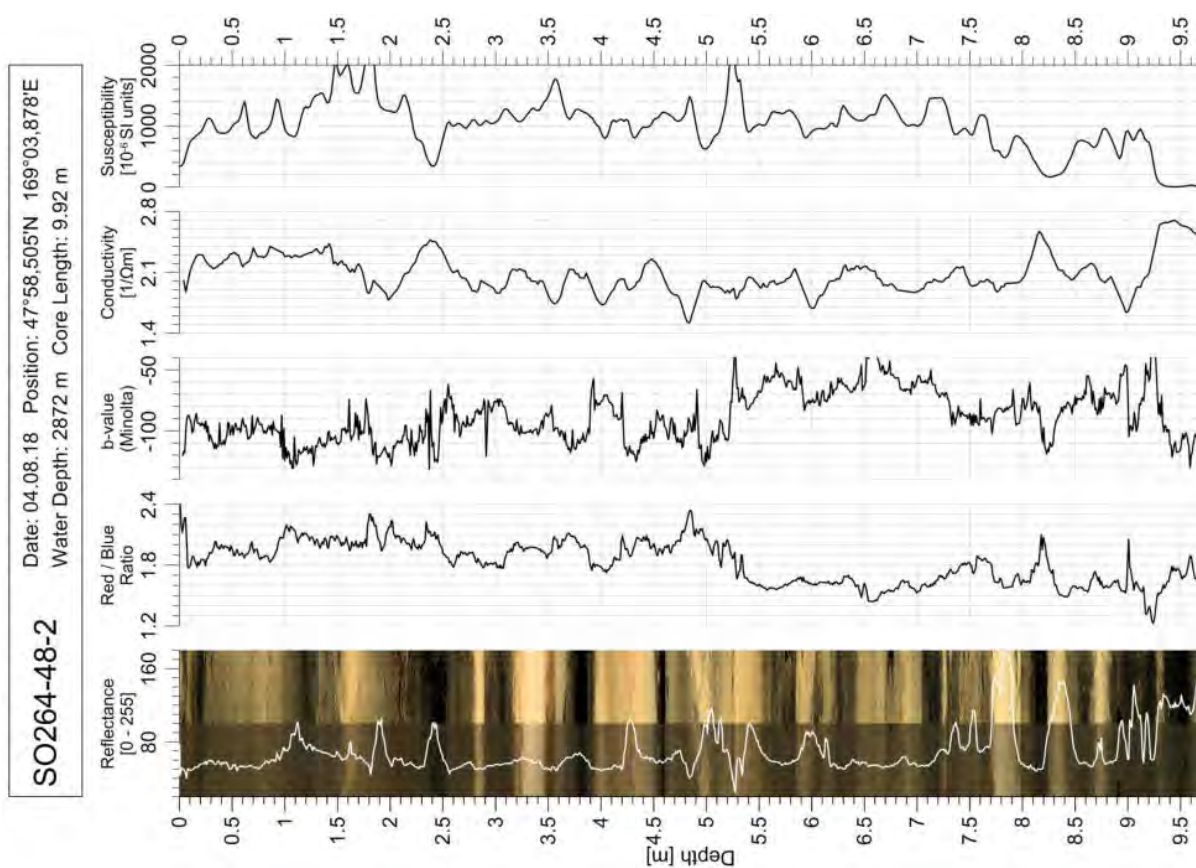


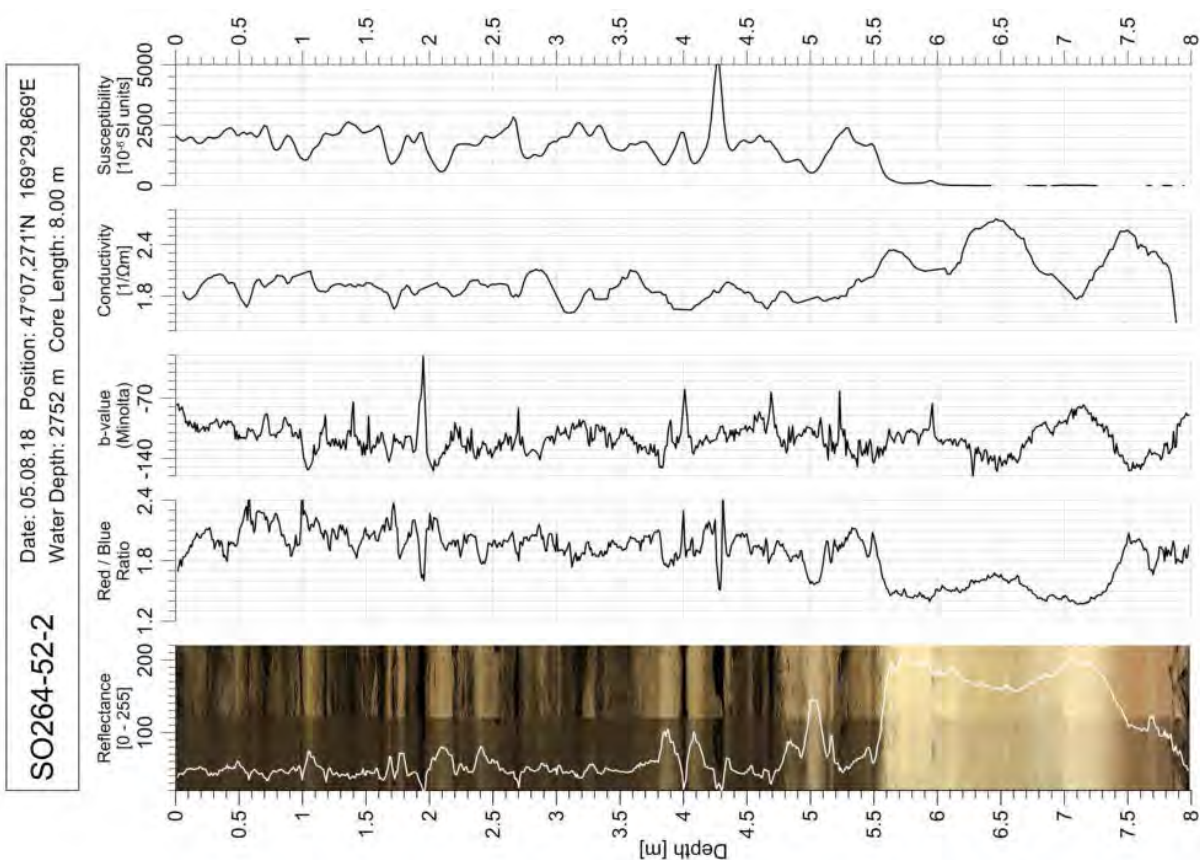
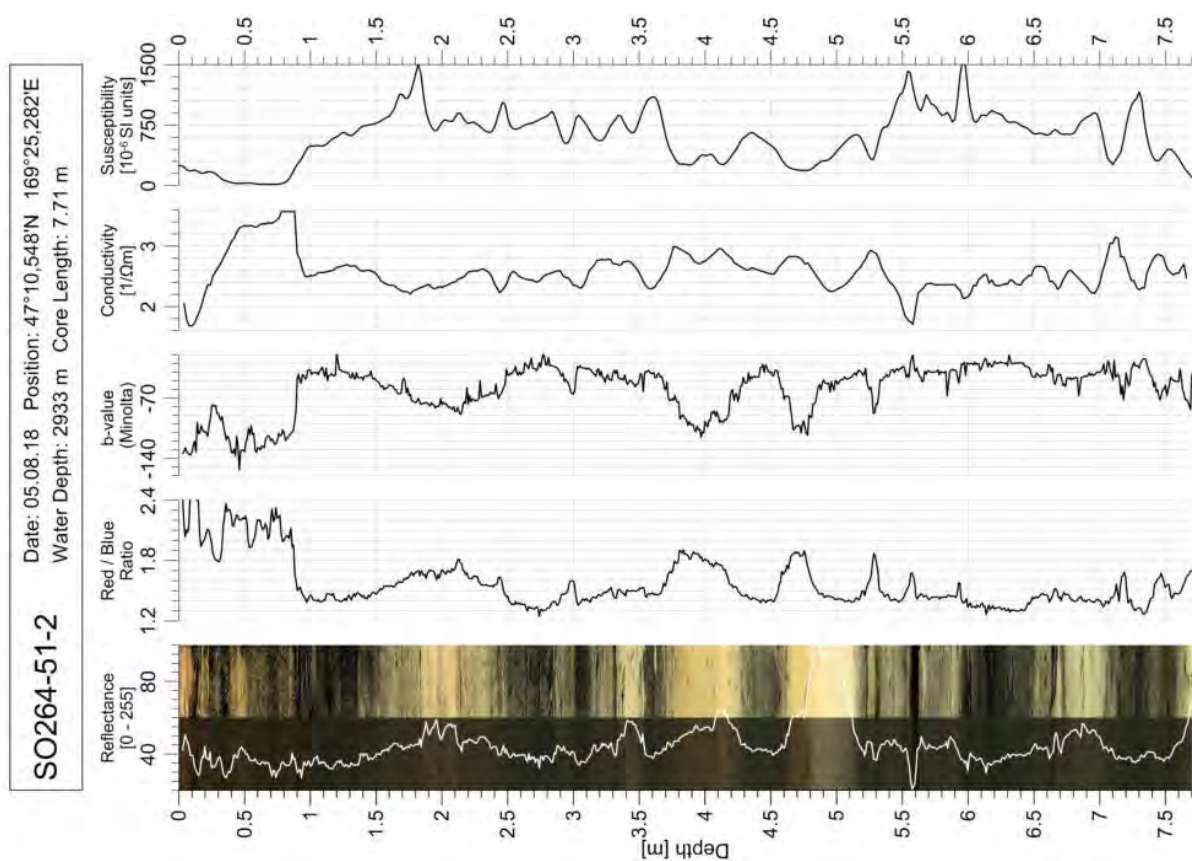


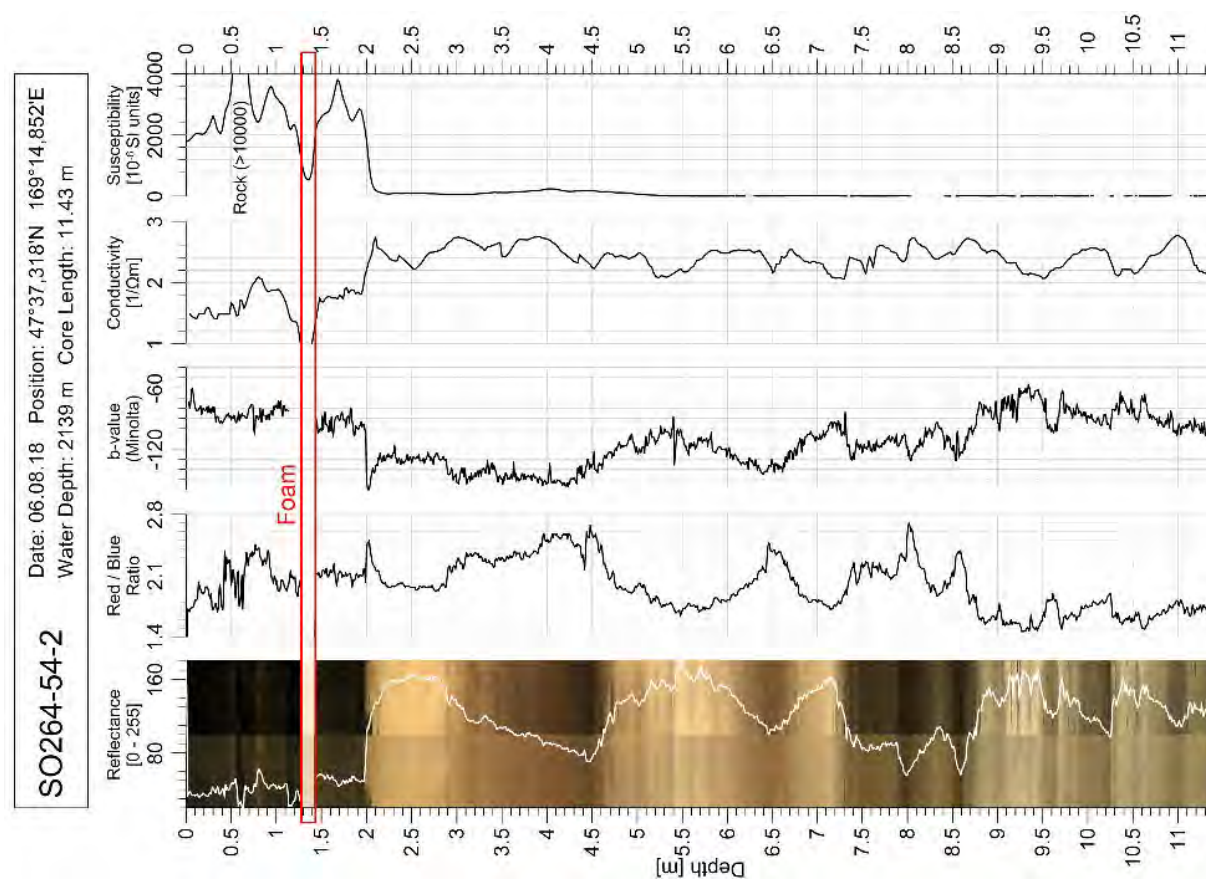
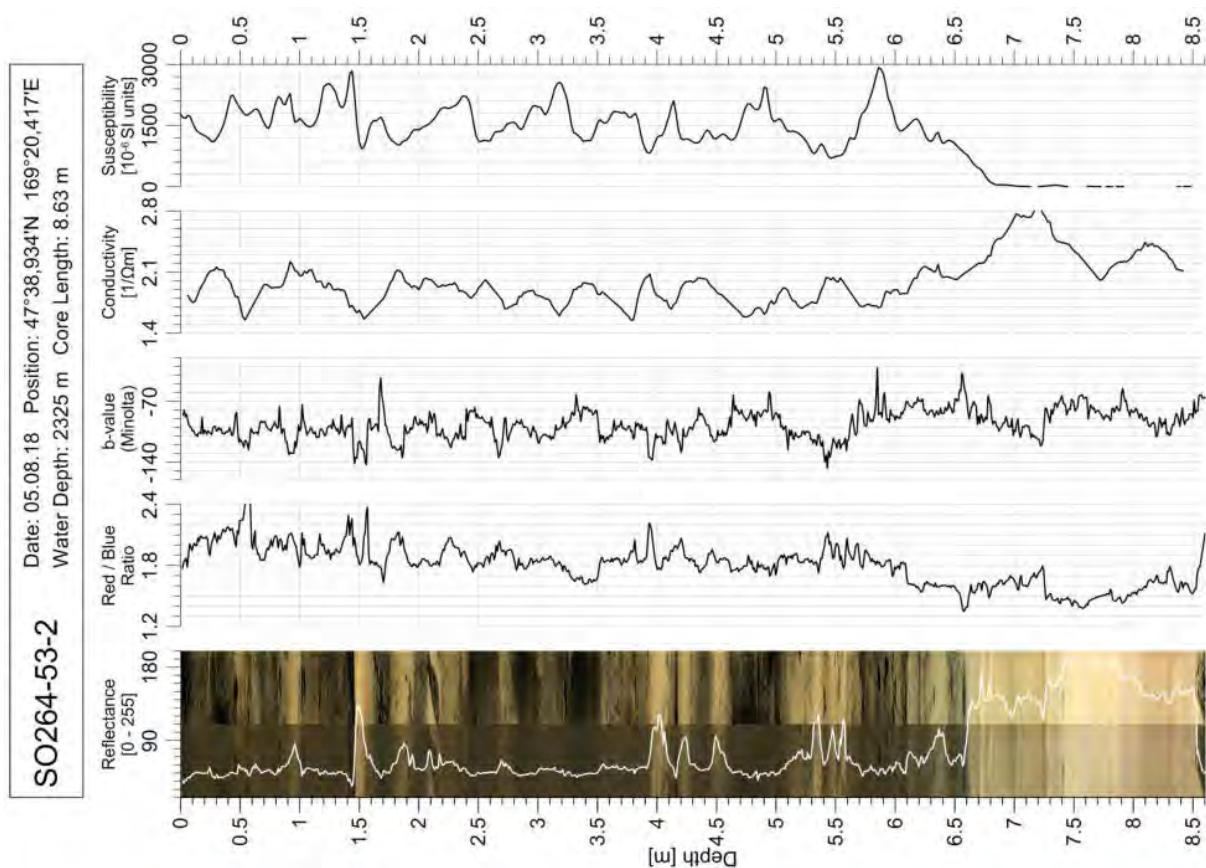


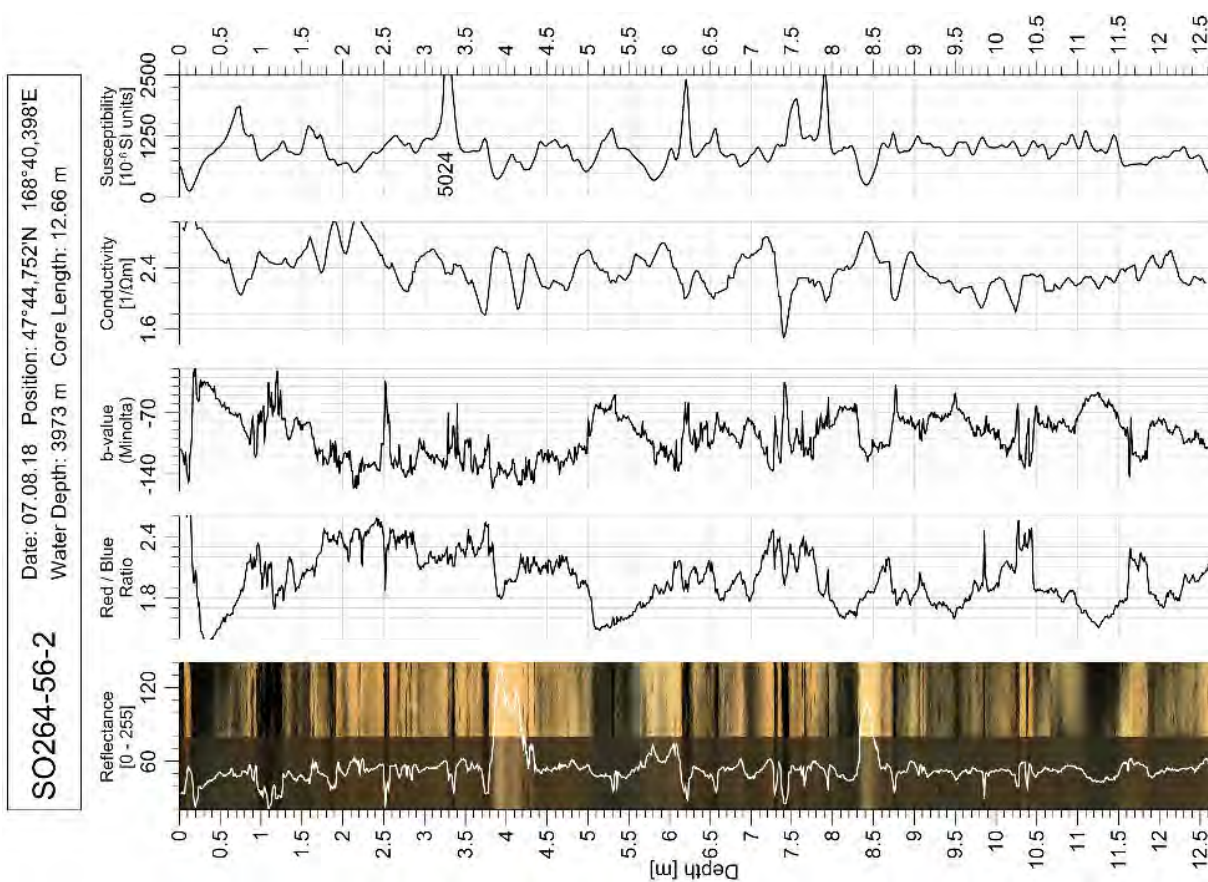
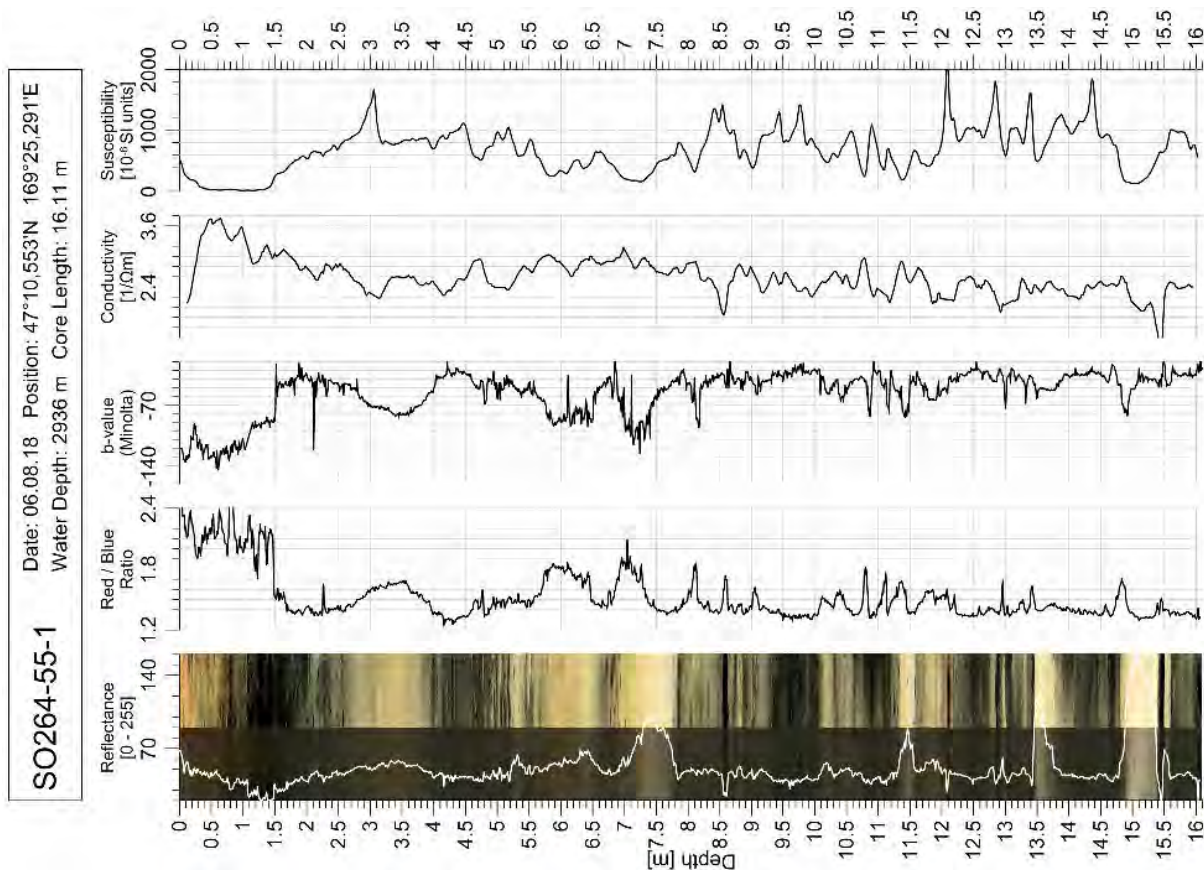


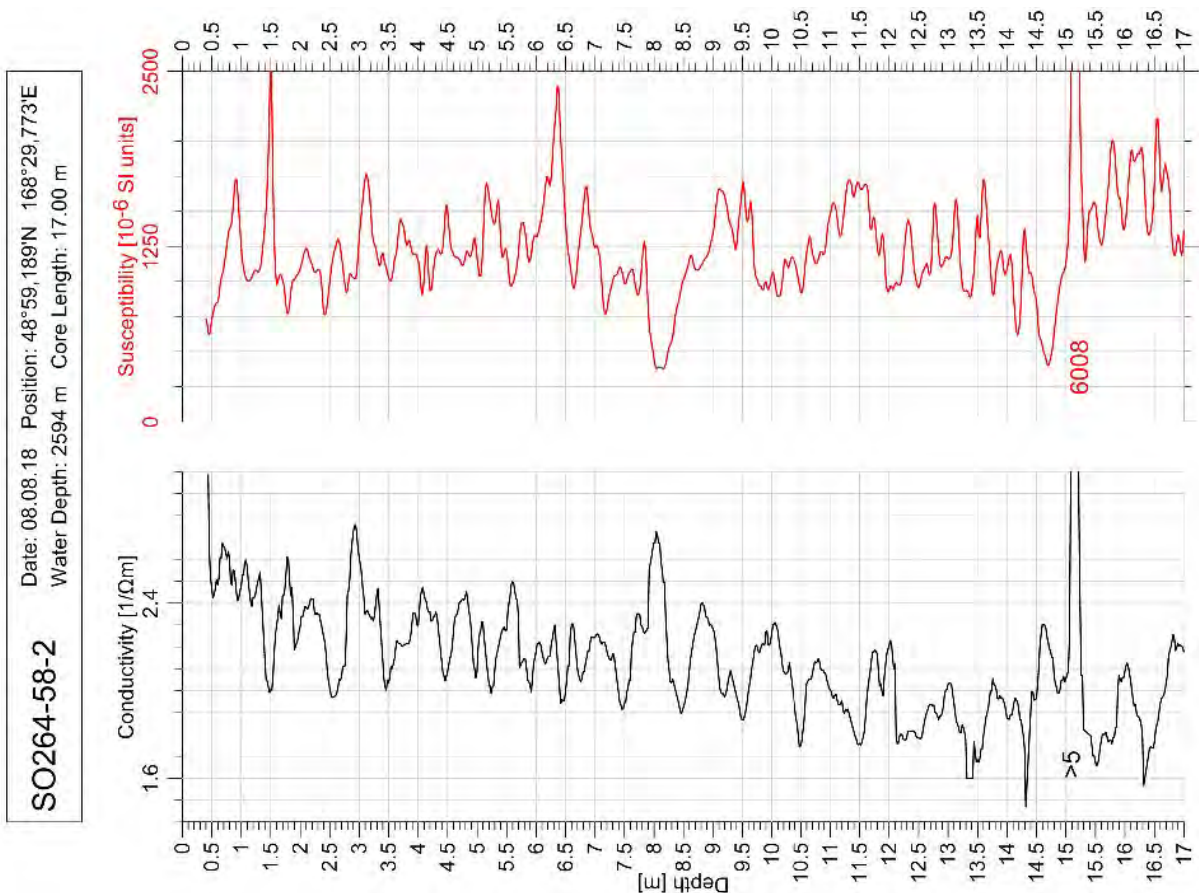
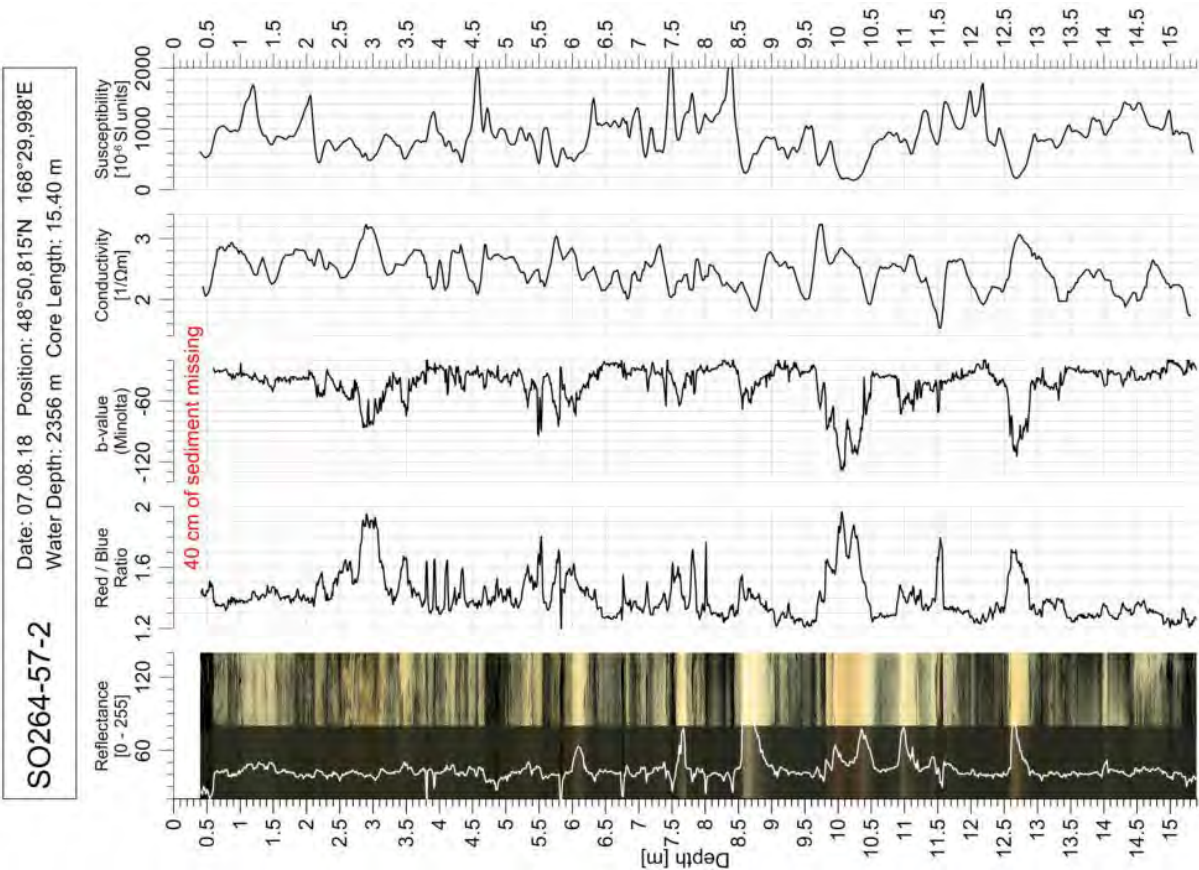




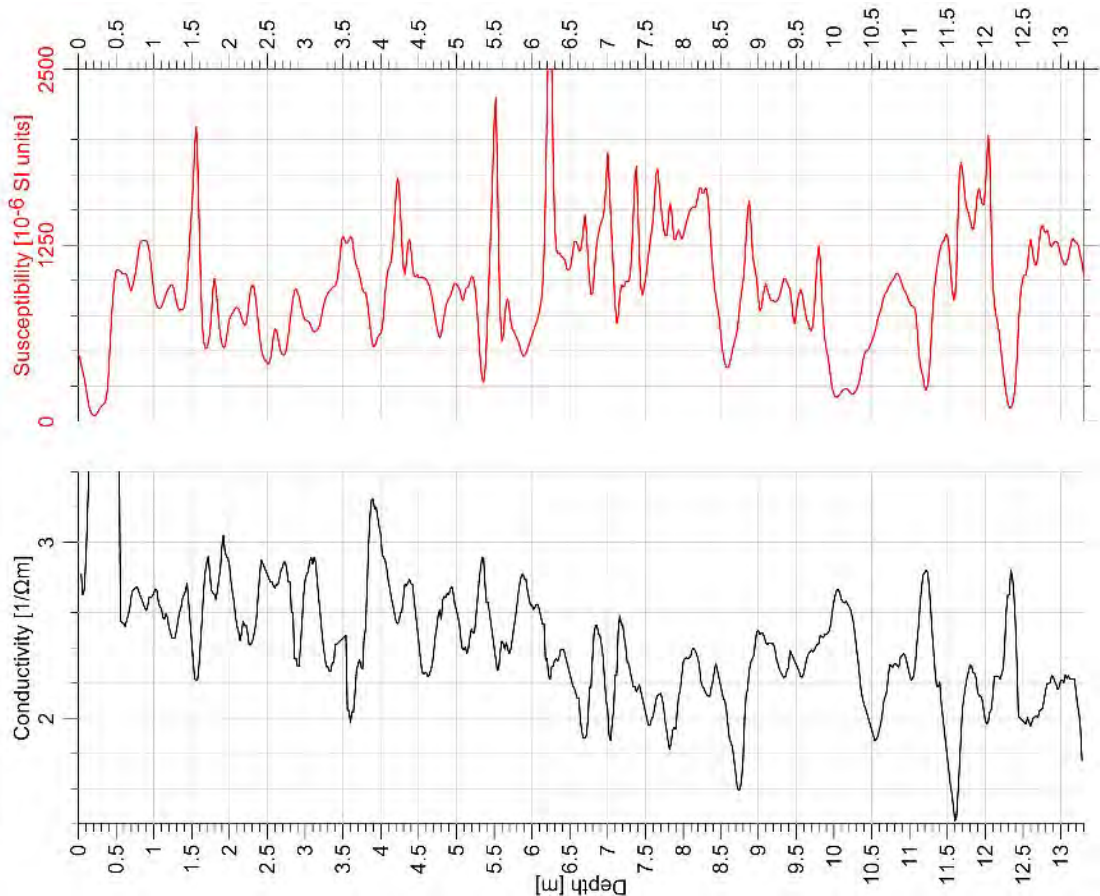




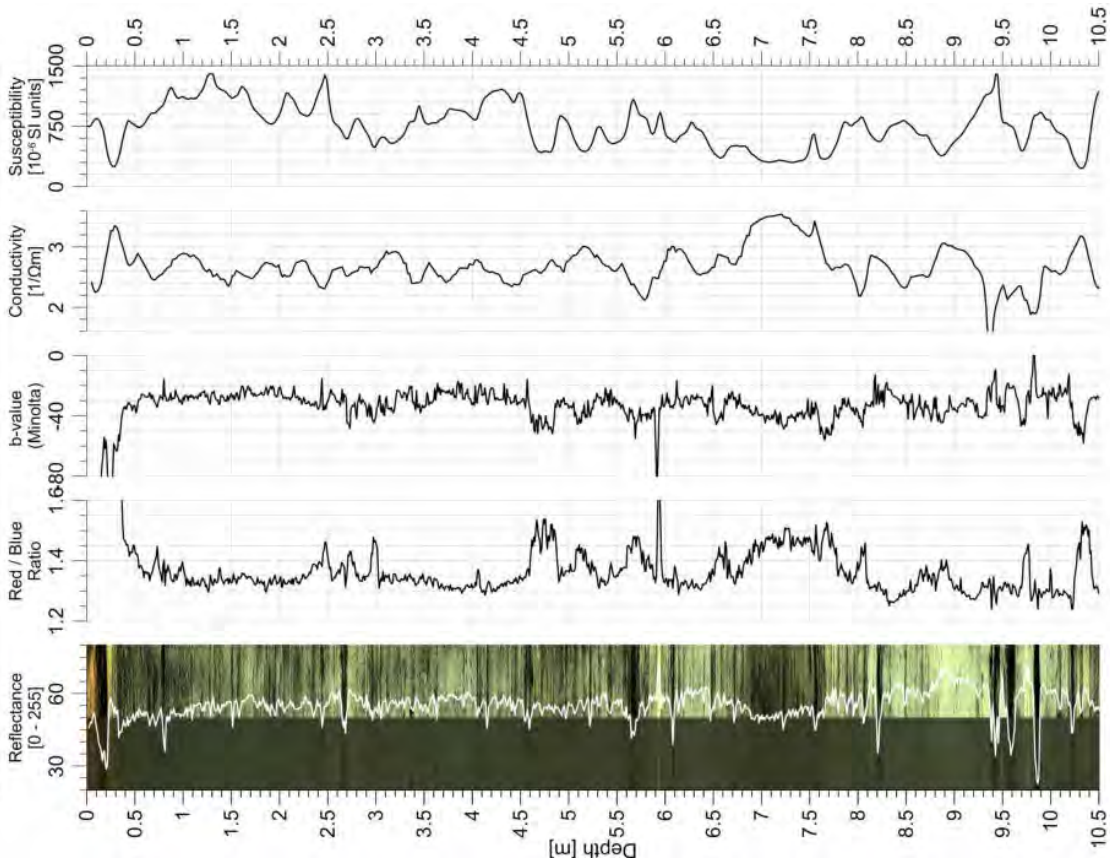


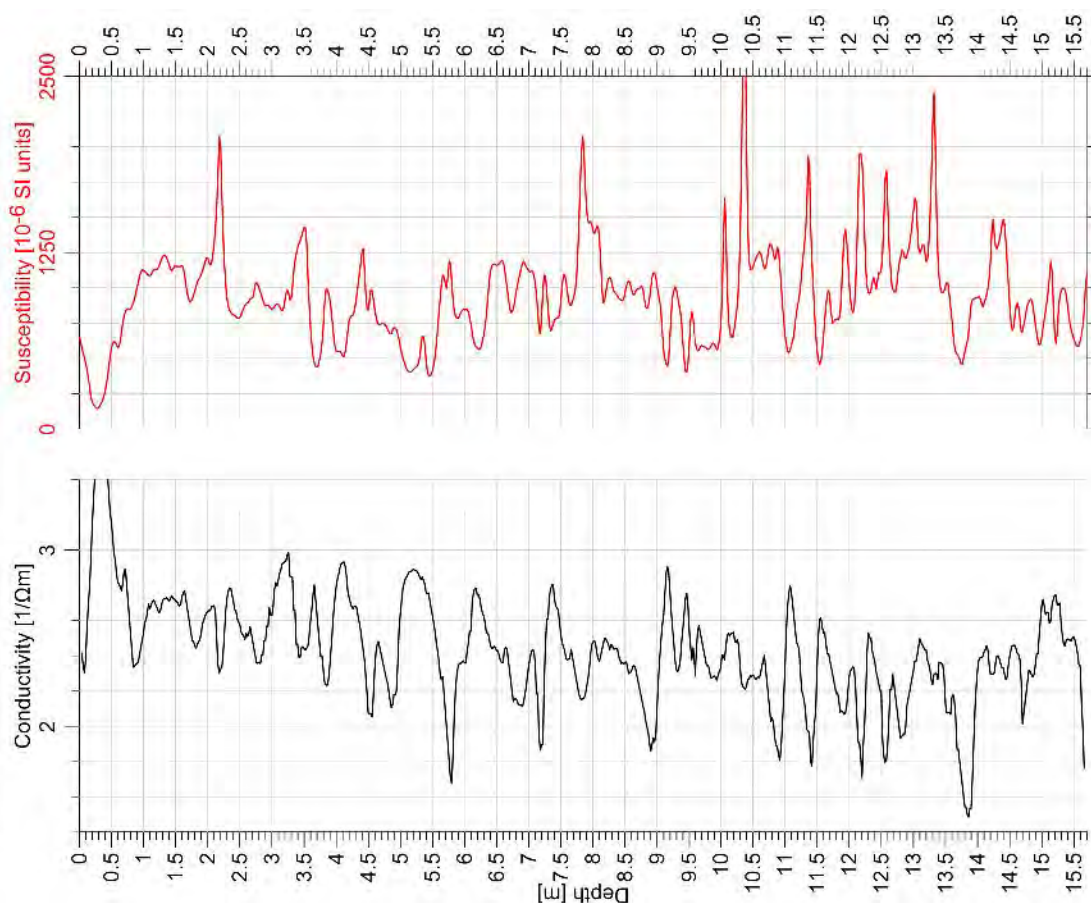
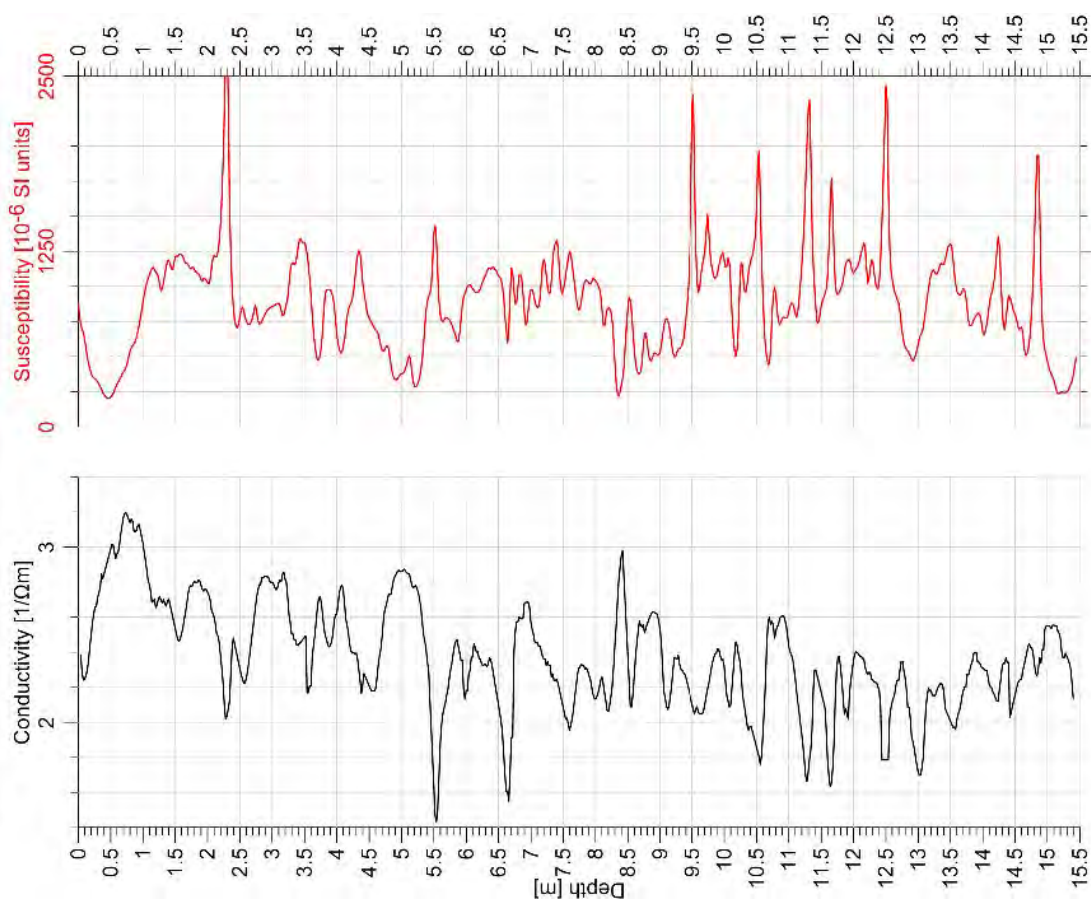


SO264-59-2
Date: 08.08.18 Position: 49°04.96'N 168°30.299'E
Water Depth: 2930 m Core Length: 13.36 m

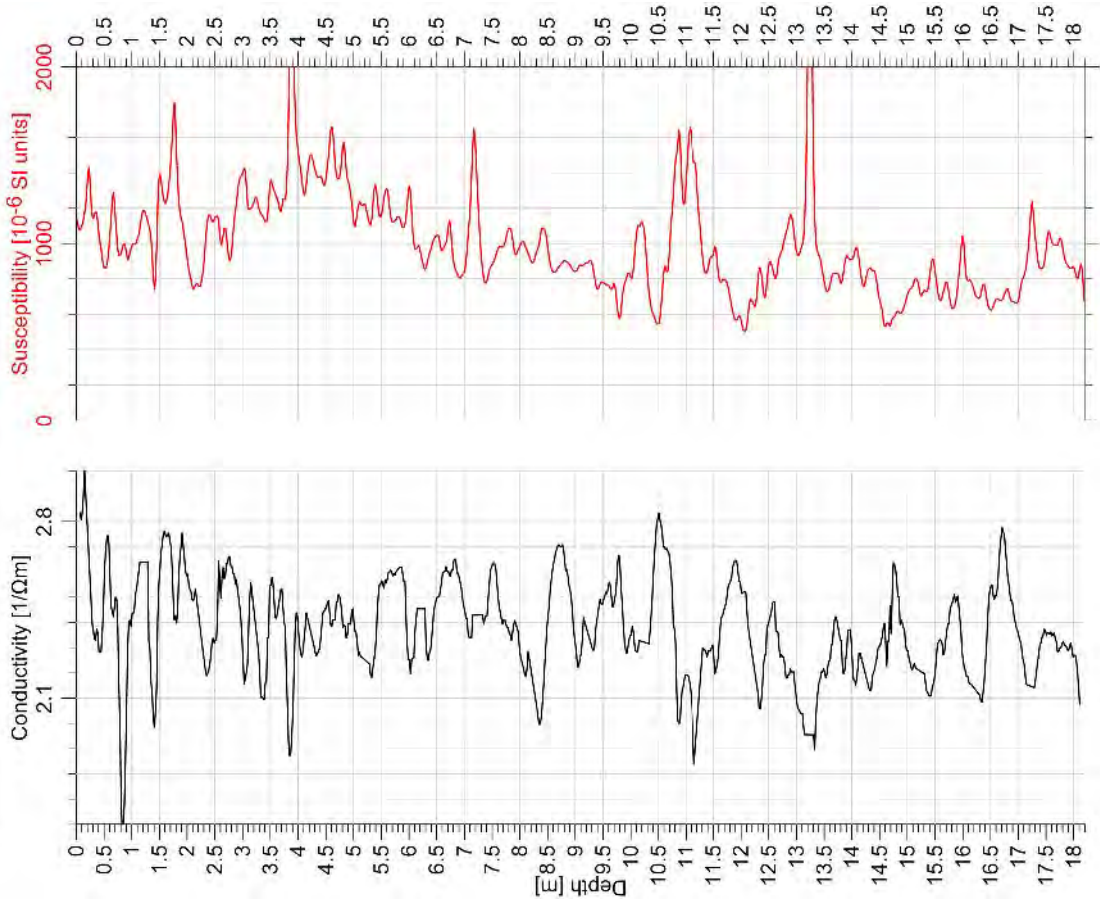


SO264-60-12
Date: 10.08.18 Position: 49°18.444'N 168°33.426'E
Water Depth: 5275 m Core Length: 10.57 m

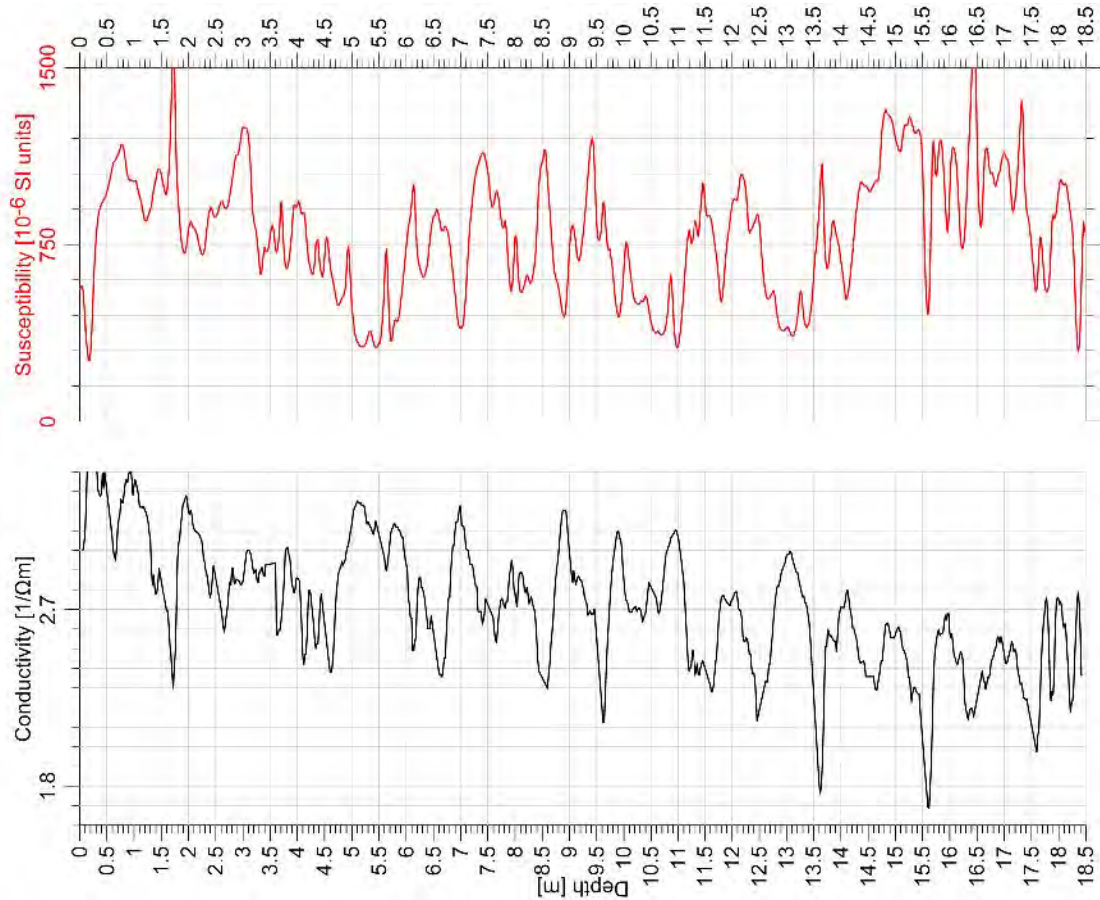


SO264-61-2Date: 11.08.18 Position: 49°43.399'N 168°02.272'E
Water Depth: 2591 m Core Length: 15.70 m**SO264-62-2**Date: 11.08.18 Position: 49°43.840'N 168°18.918'E
Water Depth: 2373 m Core Length: 15.50 m

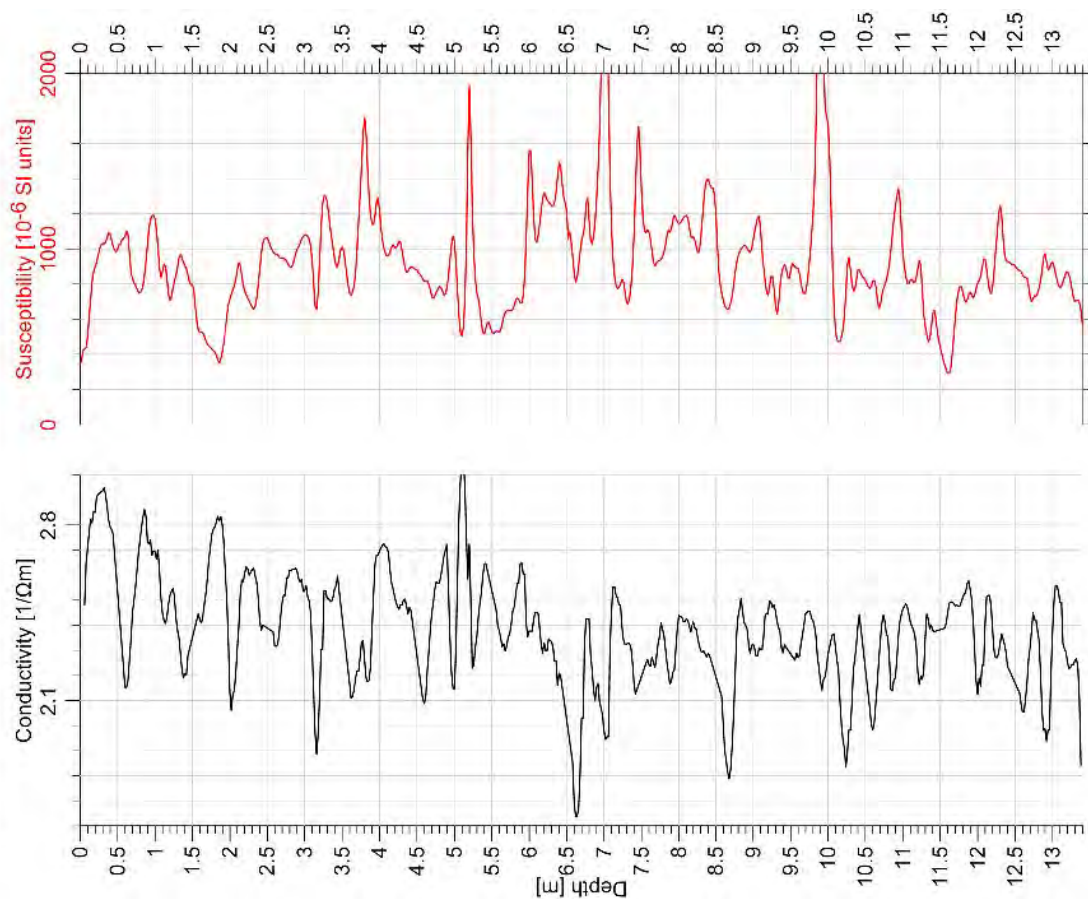
SO264-63-2
Date: 12.08.18 Position: 49°48,760'N 168°38,731'E
Water Depth: 3779 m Core Length: 18.22 m



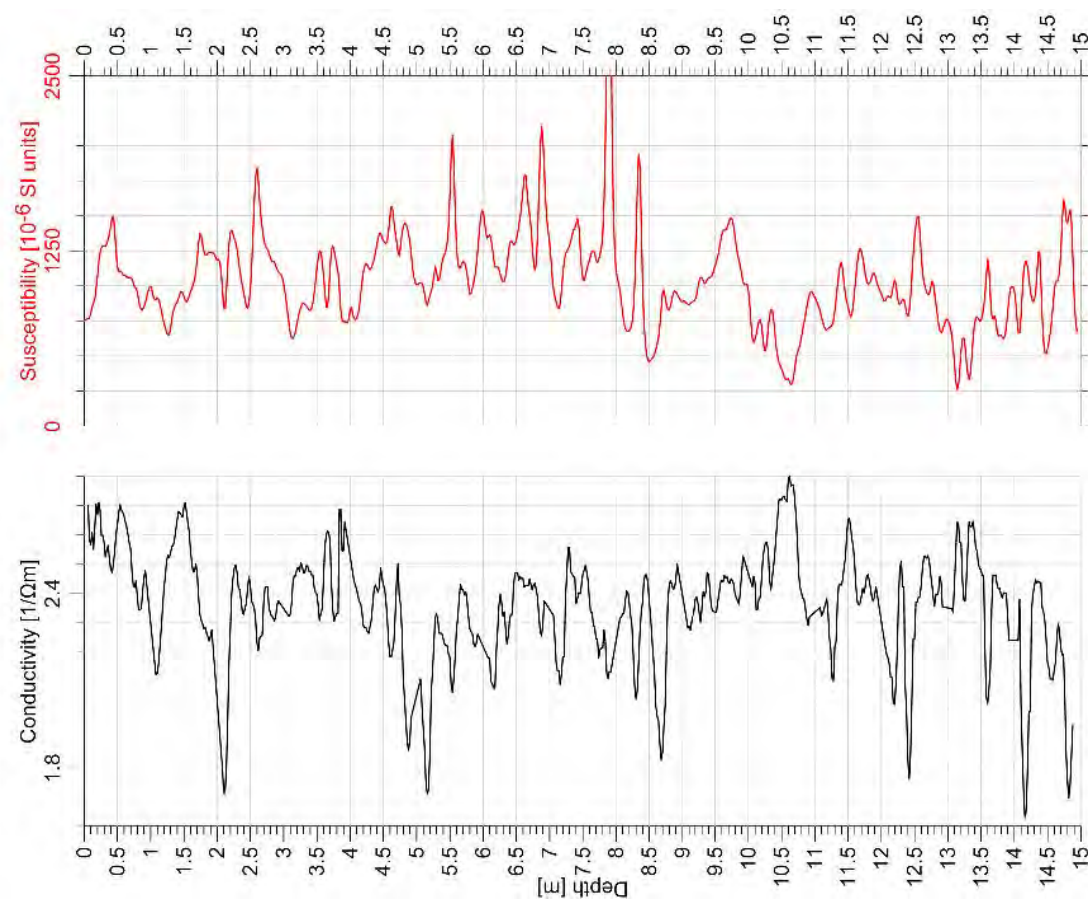
SO264-64-1
Date: 12.08.18 Position: 49°59,494'N 168°13,468'E
Water Depth: 3495 m Core Length: 18.55 m



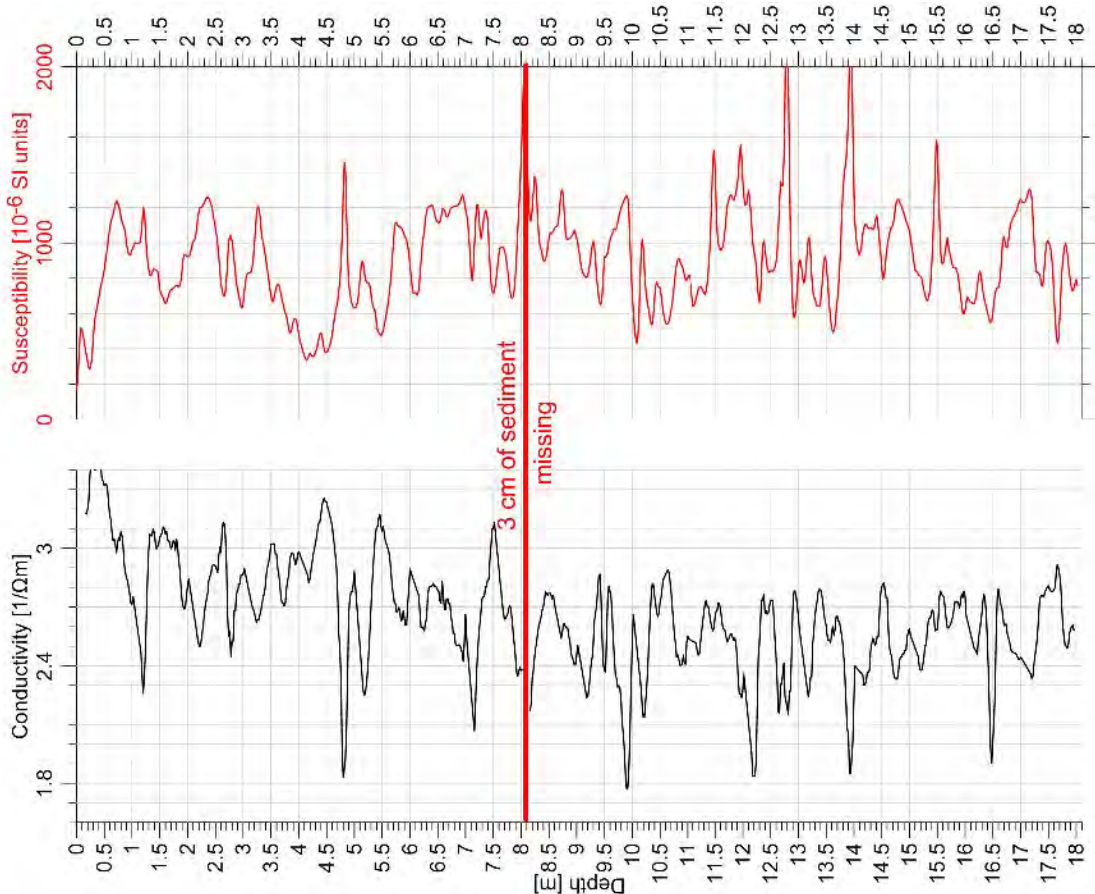
SO264-65-2 Date: 13.08.18 Position: 50°21.537'N 168°13.353'E
Water Depth: 2498 m Core Length: 13.41 m



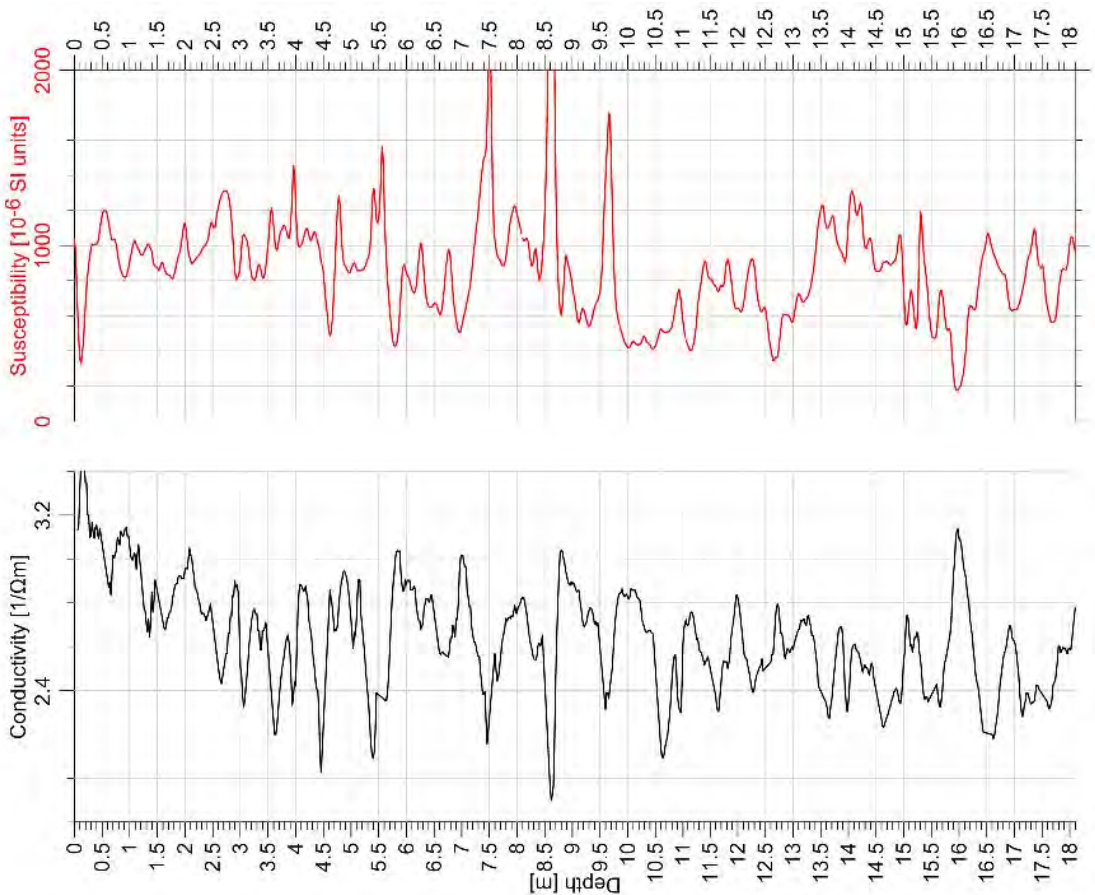
SO264-66-2 Date: 13.08.18 Position: 50°15.067'N 168°17.821'E
Water Depth: 2751 m Core Length: 15.04 m



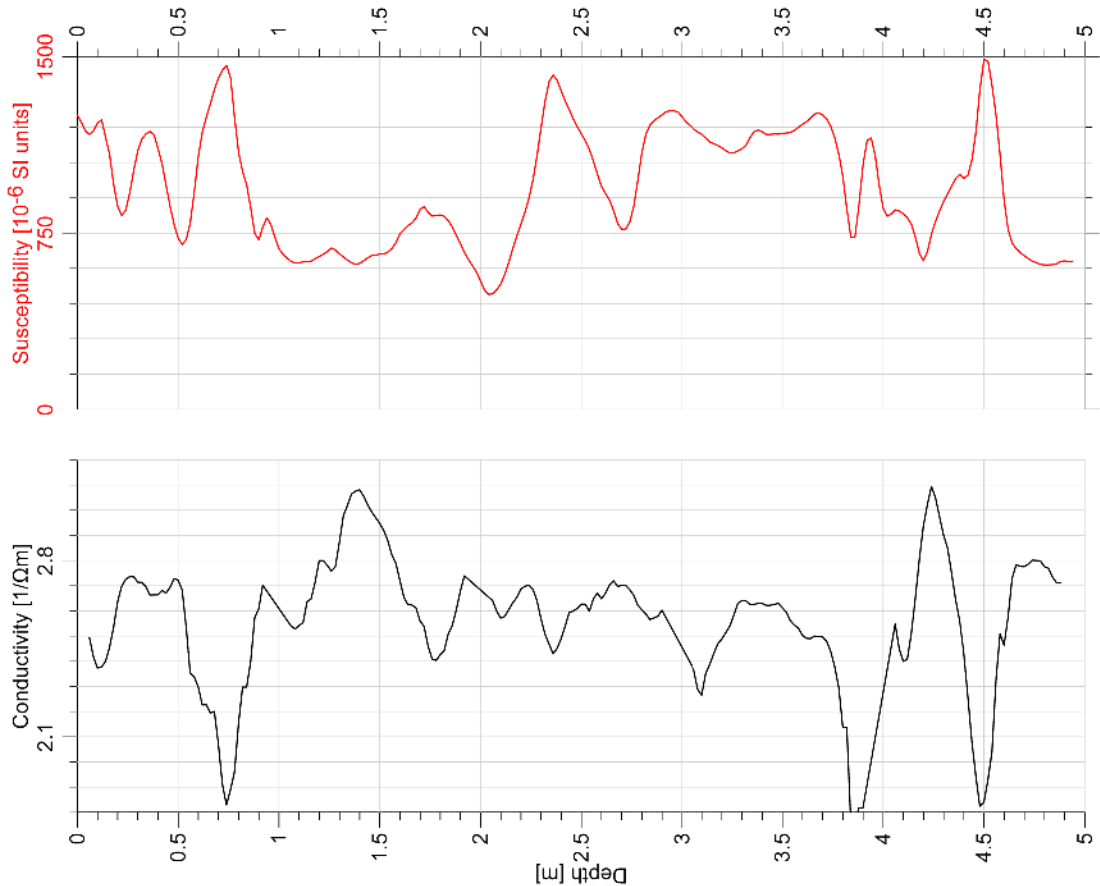
SO264-68-2 Date: 13.08.18 Position: 50°29,043N 167°51,487E
Water Depth: 3284 m Core Length: 18.01 m



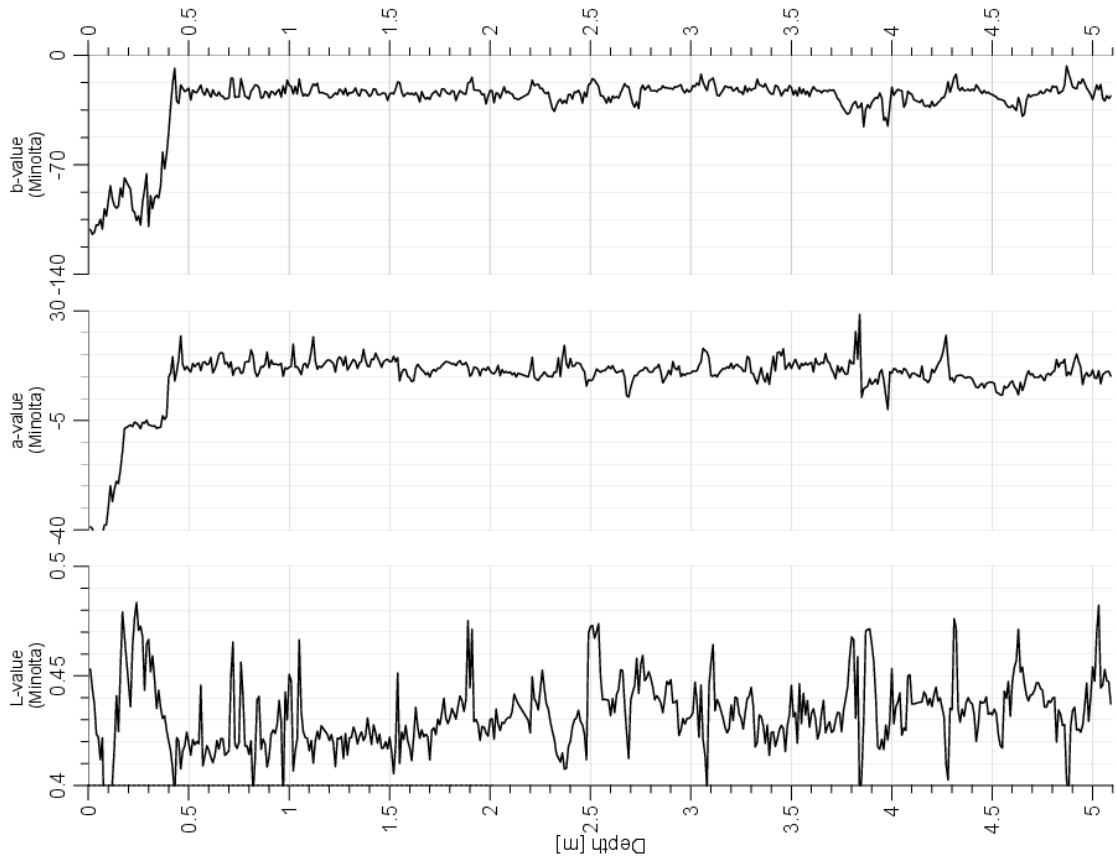
SO264-69-2 Date: 14.08.18 Position: 50°30,877N 167°55,478E
Water Depth: 3473 m Core Length: 18.55 m

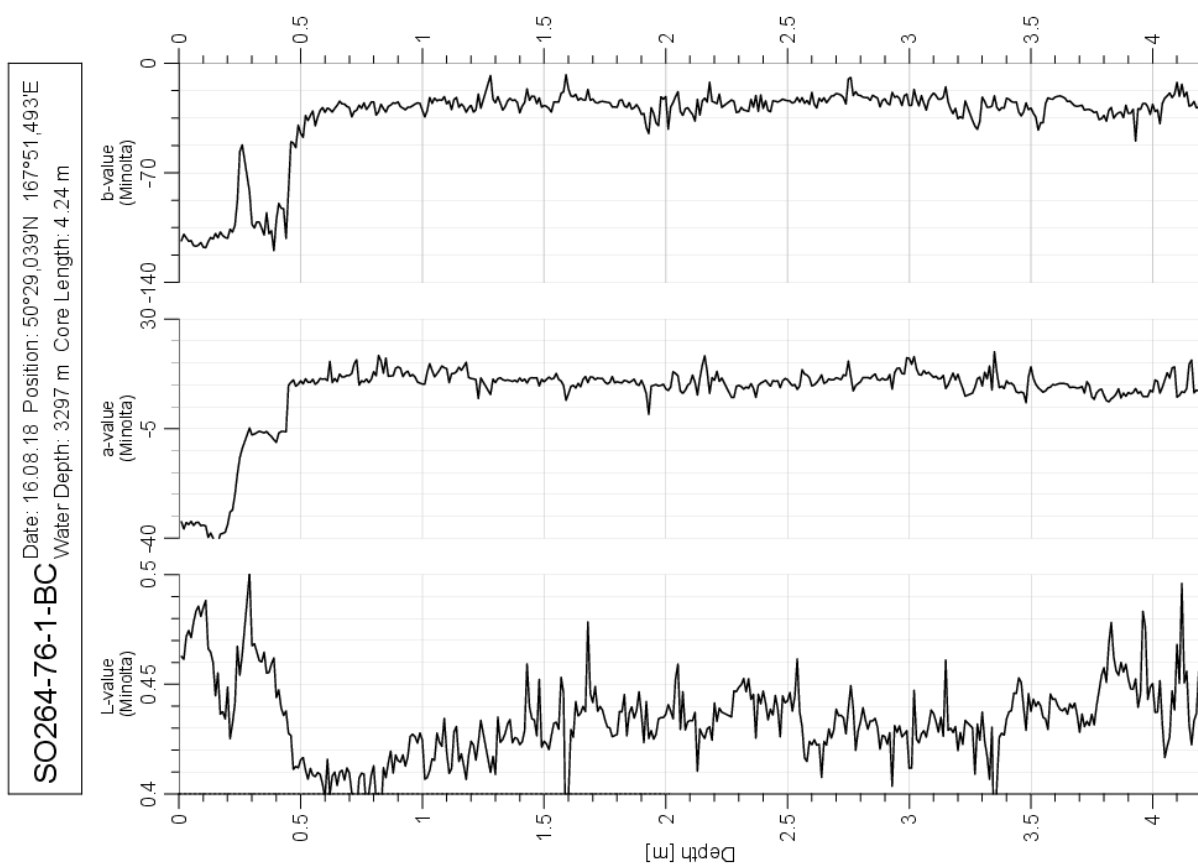


SO264-70-1
Date: 14.08.18 Position: 50°34,915N 168°04,292'E
Water Depth: 3917 m Core Length: 5.00 m







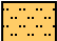

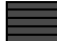
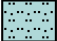










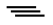
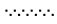
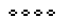






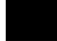






SO264-75-1-BC
Date: 15.08.18 Position: 50°34,909N 168°04,288'E
Water Depth: 3919 m Core Length: 5.10 m





Legend for core description

LITHOLOGY		
 sand	 sandy ooze	 Red clay
 silty sand	 silty ooze	 Diatom Ooze
 silt	 Tephra fine	 Gravel
 sandy silt	 diagenetic layer	 Laminated
 clayey silt	 diagenetic layer (fine)	 Lost Core
 Ooze/Clay	 Turbidite	
 silty clay	 Tephra	
CORE DISTURBANCE		
 - Very Disturbed		
PHYSICAL STRUCTURES		
 - Planar Tabular Bedding		
ACCESSORIES		
 - Sand Lamina	 - Pebbles/Granules	Py - Pyrite
ICHTHOFOSSILS		
 - Zoophycos		
FOSSILS		
 - Corals (solitary)	 - Diatoms	 - Foraminifera (undifferentiated)
BIOTURBATION INDEX		
 Barren	 Moderate	 Complete
 Sparse	 Abundant	
 Low	 Intense	

Appendix 5.6.1 Lithology logs

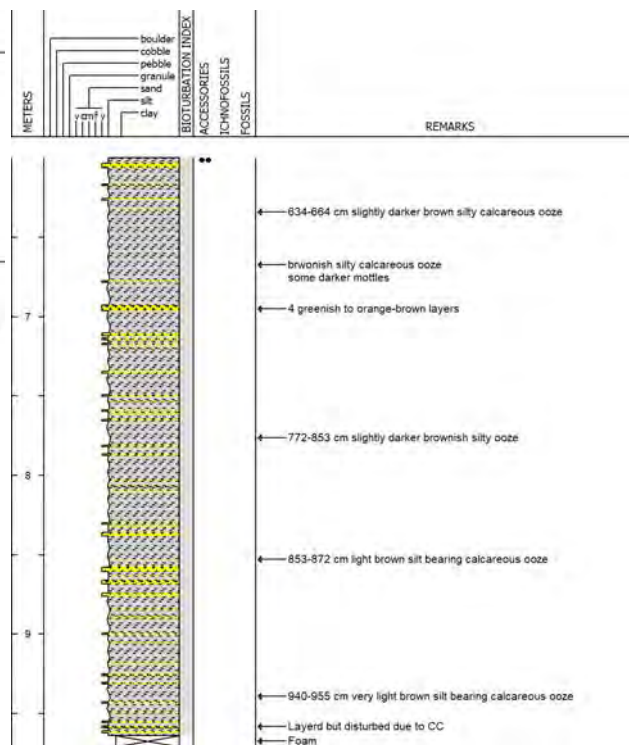
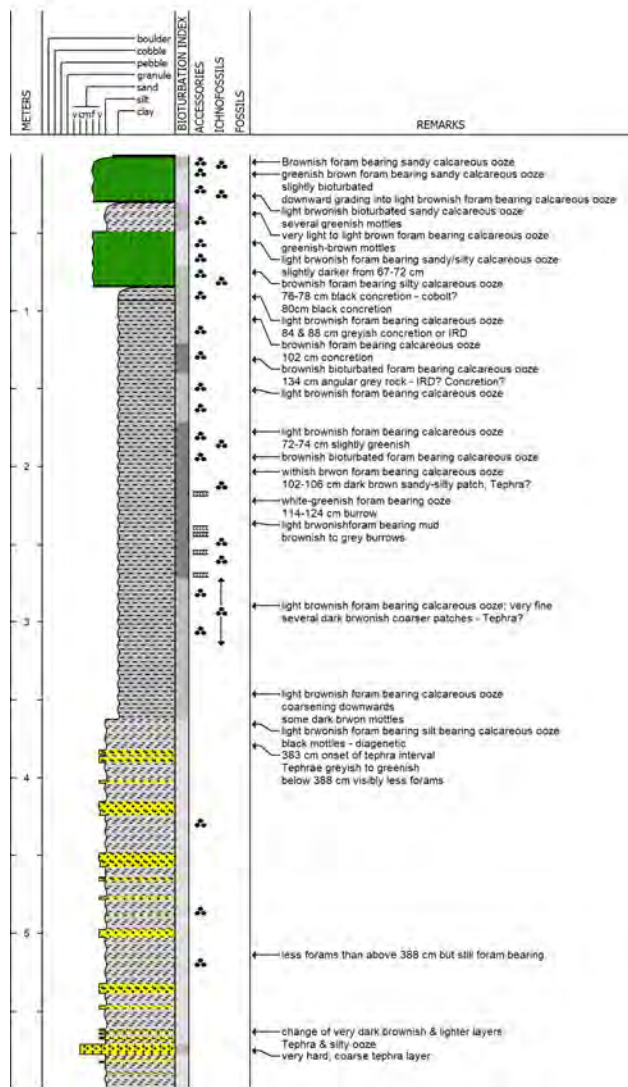
SO264 Cruise Report

SO264-08-2

Date Logged: July 12, 2018

Logged by: T. Ronge

Remarks: 33°39,616'N 174°45,044'E 2682 mbsl



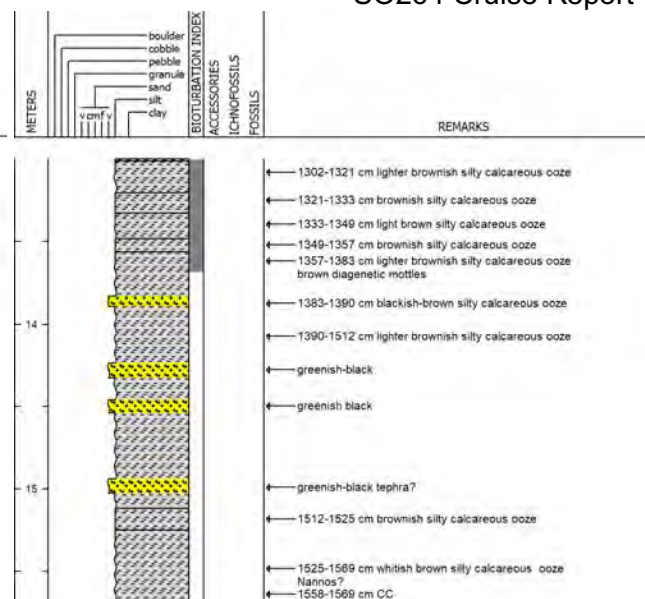
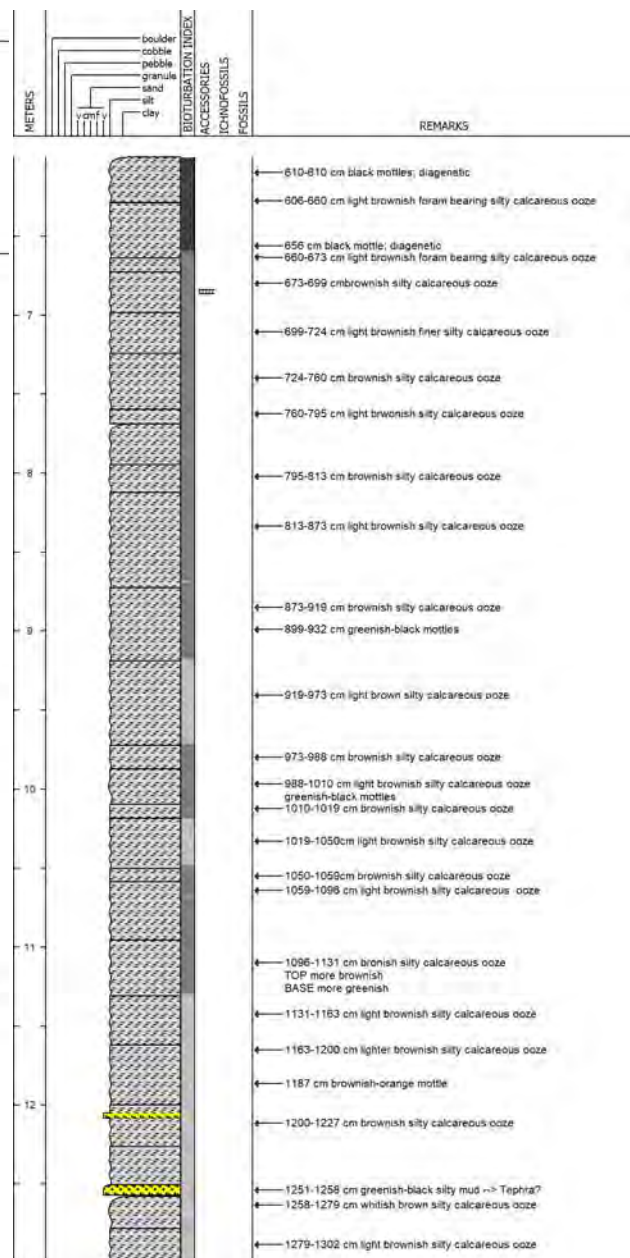
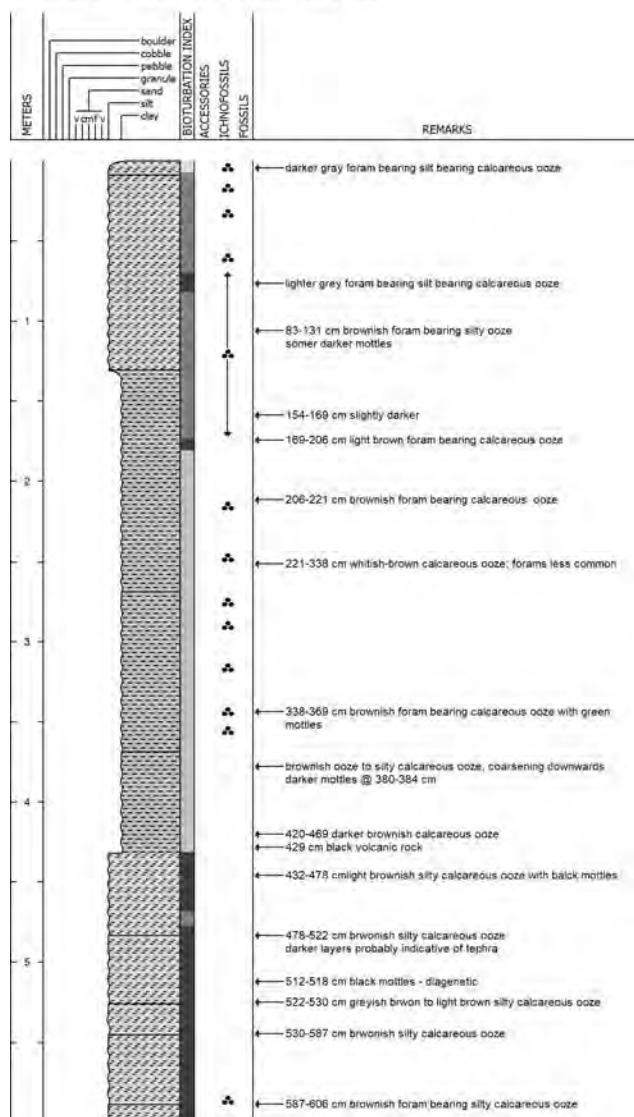
Appendix 5.6.1 Lithology logs

SO264-09-2

Date Logged: July 13, 2018

Logged by: T. Ronge

Remarks: 34°46,977'N 172°20,987'E 3865 mbsl



SO264 Cruise Report

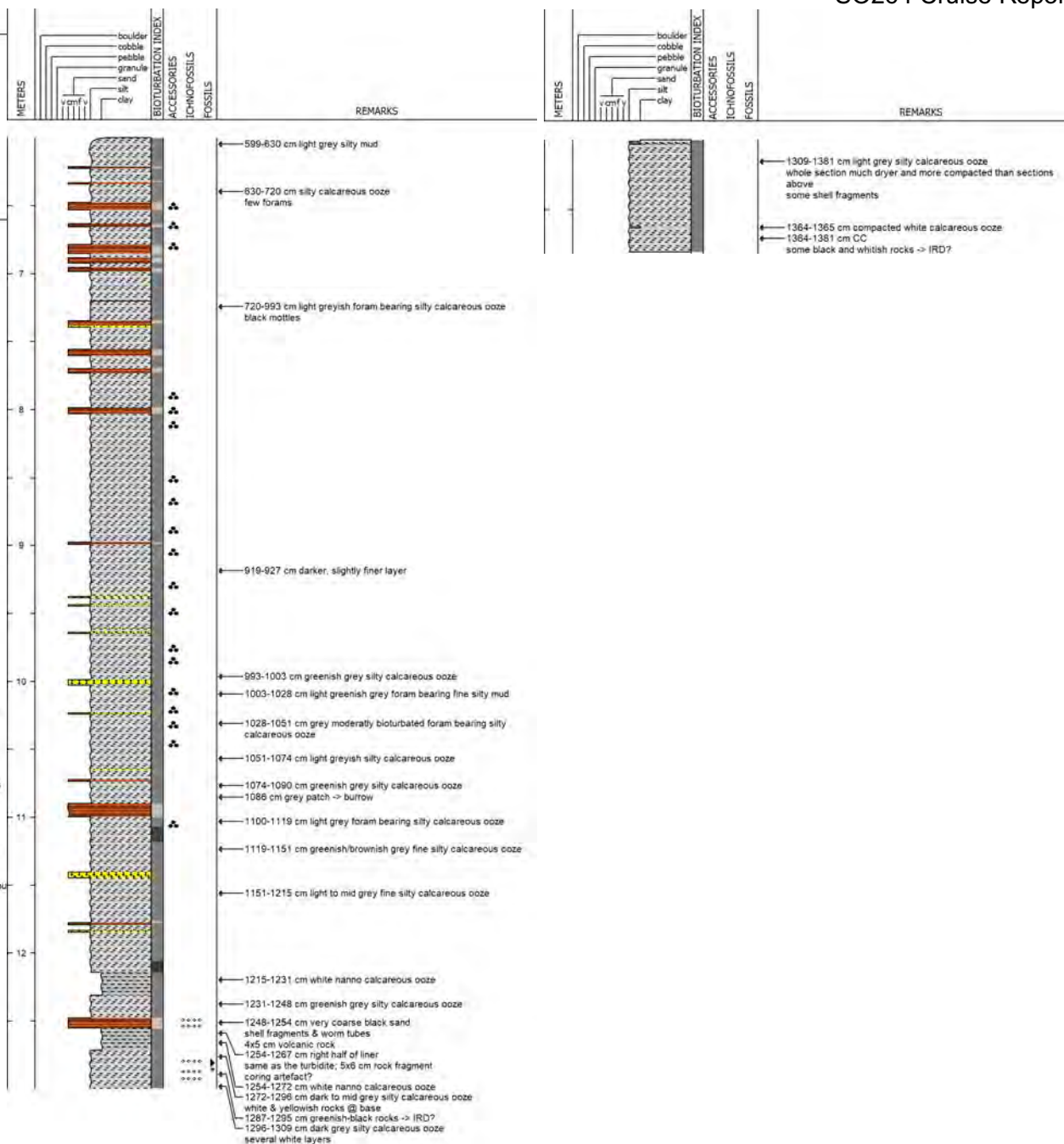
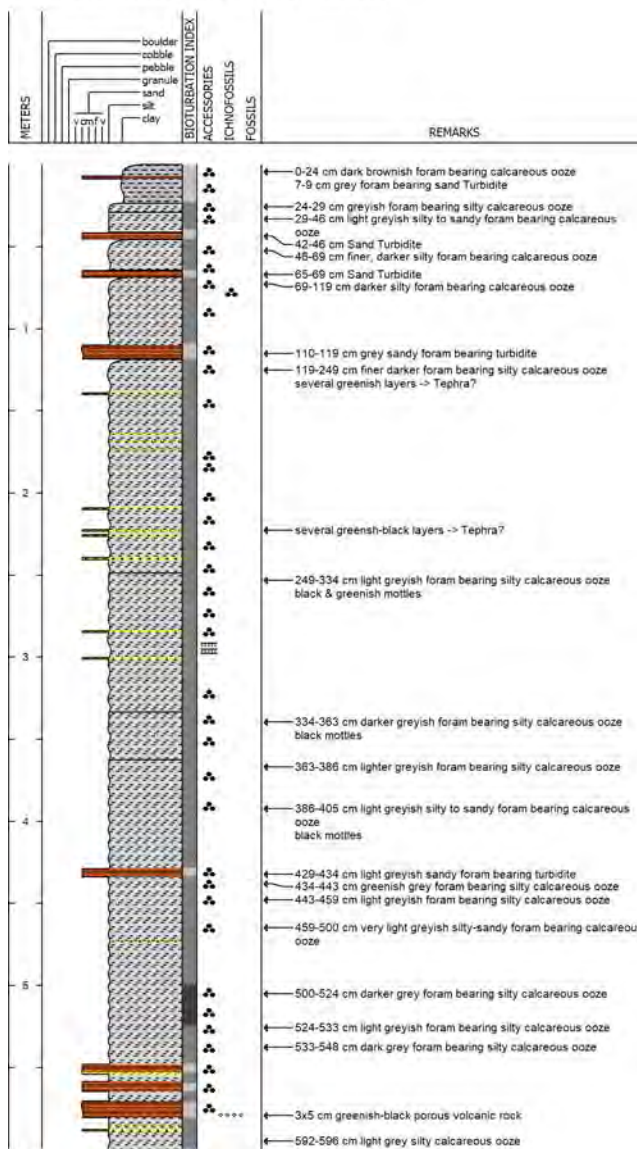
Appendix 5.6.1 Lithology logs

SO264-13-2

Date Logged: July 15, 2018

Logged by: T.Ronge

Remarks: 37°47,865'N 170°43,327'E 3935 mbsl



SO264 Cruise Report

Appendix 5.6.1 Lithology logs

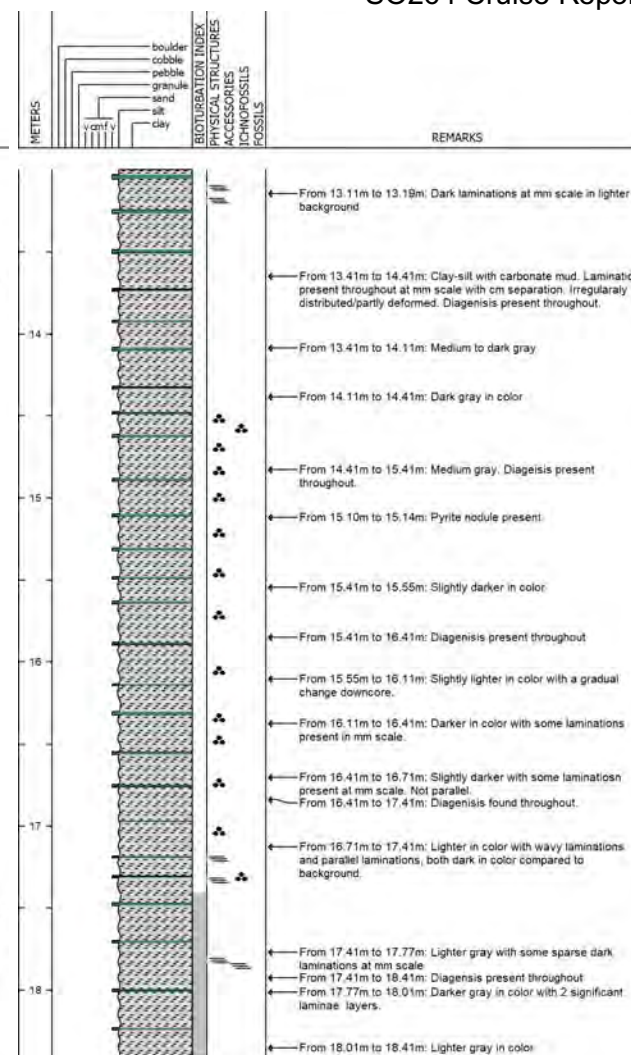
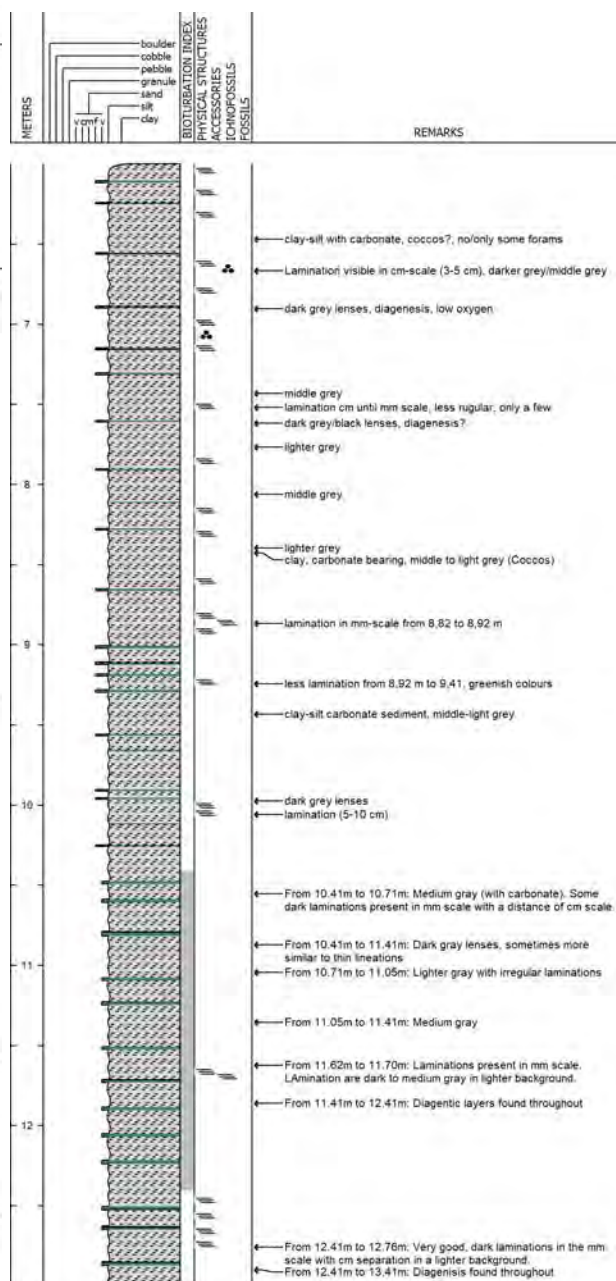
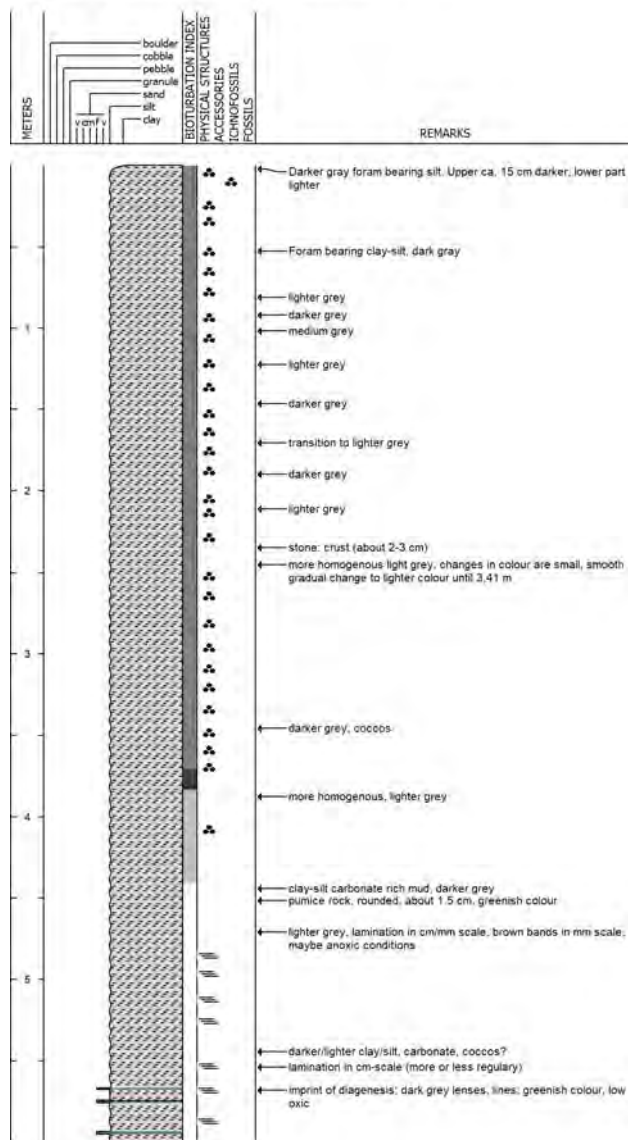
SO264 Cruise Report

SO264-14-1

Date Logged: July 17, 2018

Logged by: C. Karas

Remarks: 40°50,034'N 170°54,201'E 3930 mbsl



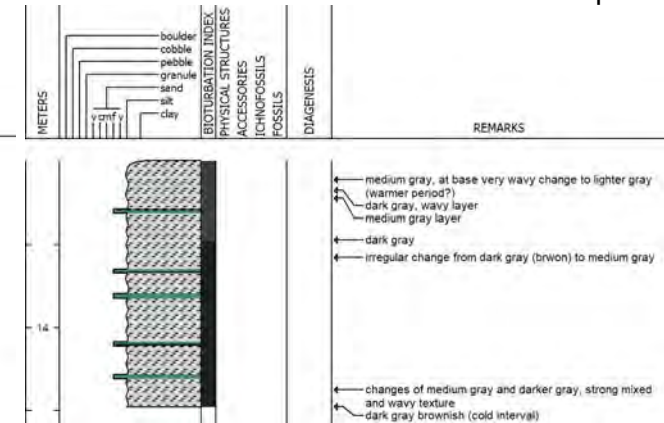
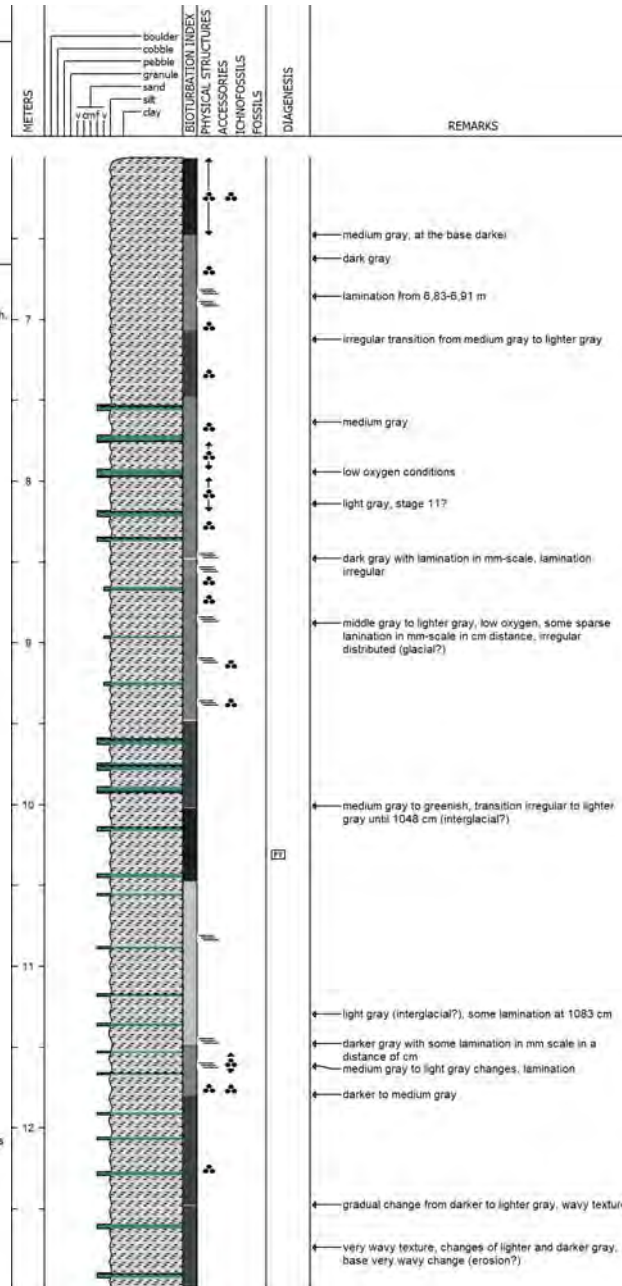
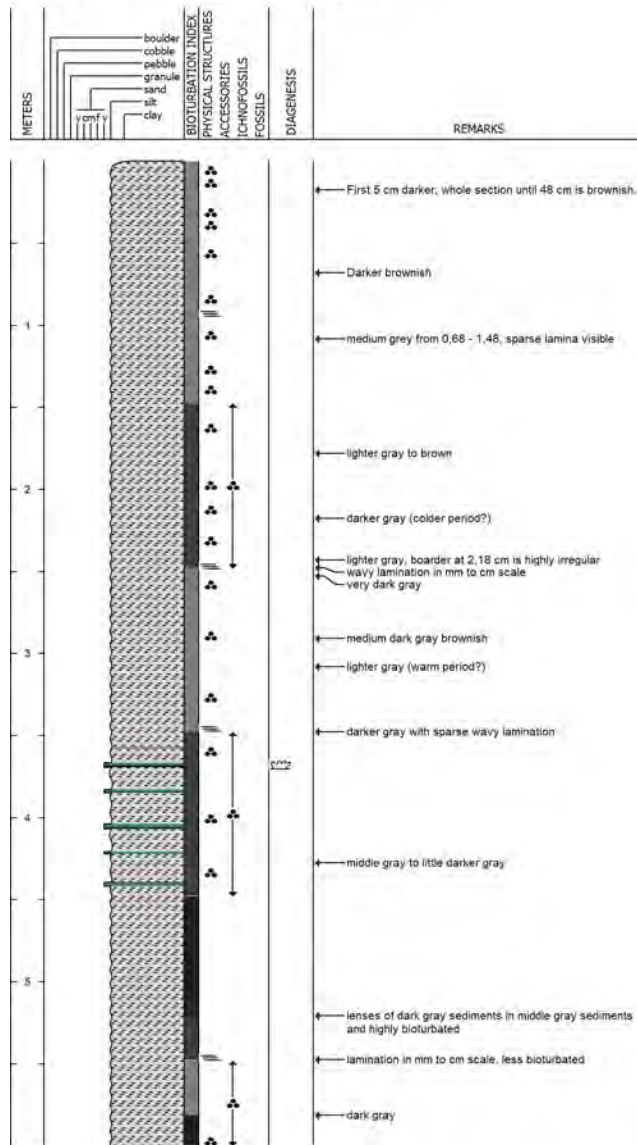
Appendix 5.6.1 Lithology logs

SO264-15-2

Date Logged: July 22, 2018

Logged by: C. Karas

Remarks: 41°36,917'N 170°25,340'E 3662 mbsl



SO264 Cruise Report

Appendix 5.6.1 Lithology logs

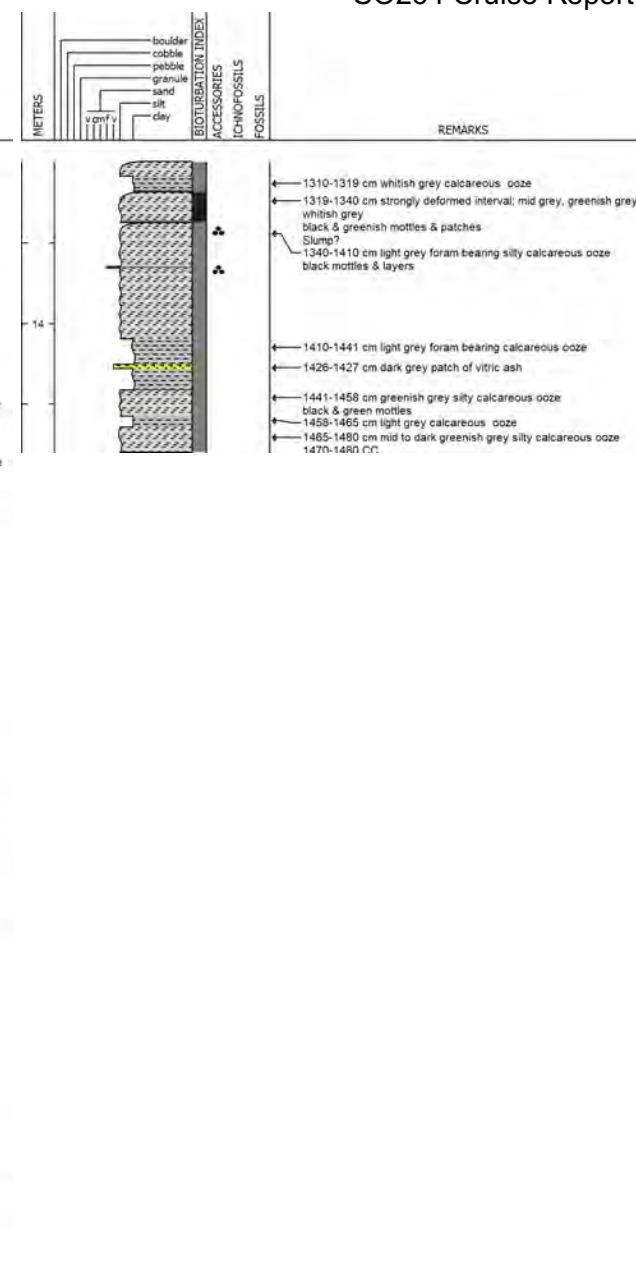
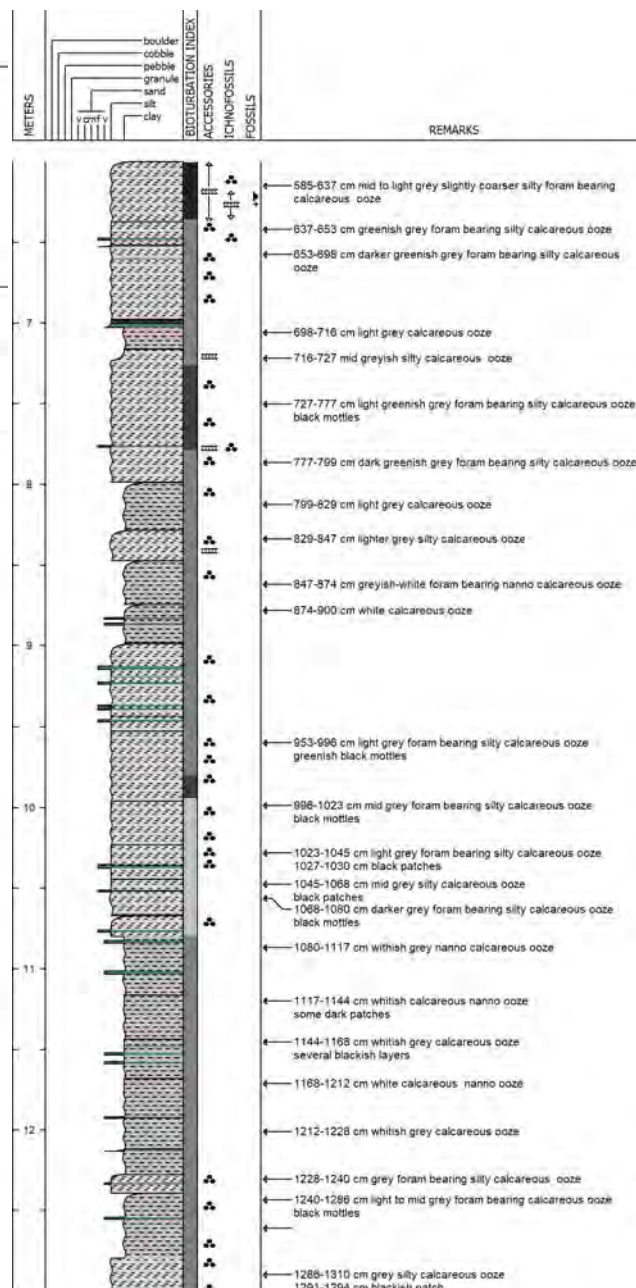
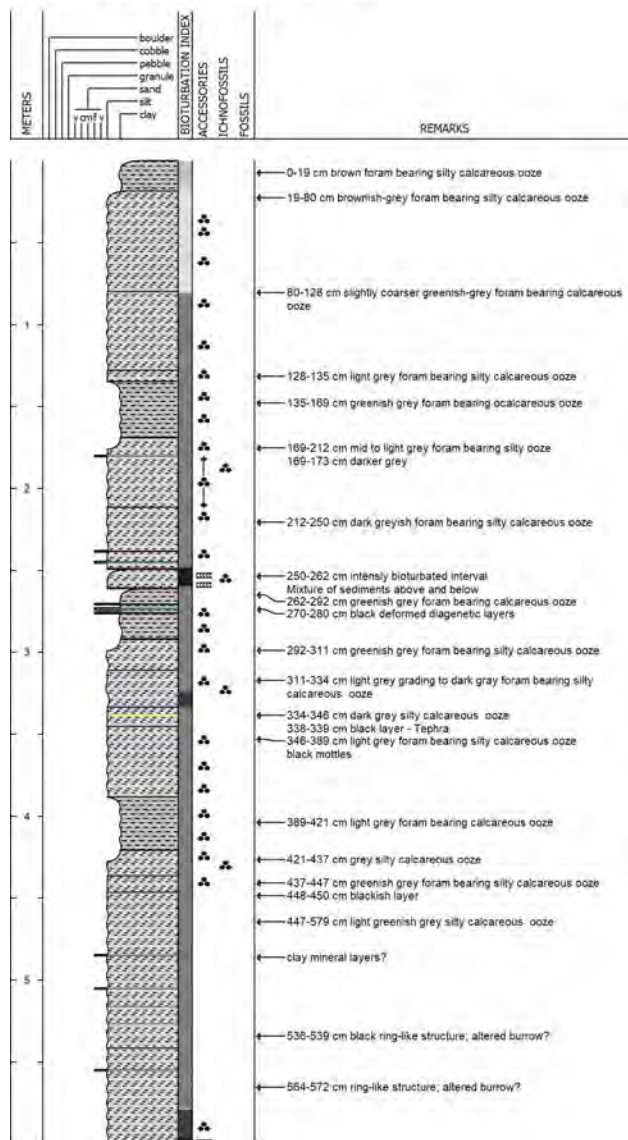
SO264 Cruise Report

SO264-16-2

Date Logged: July 18, 2018

Logged by: T. Ronge

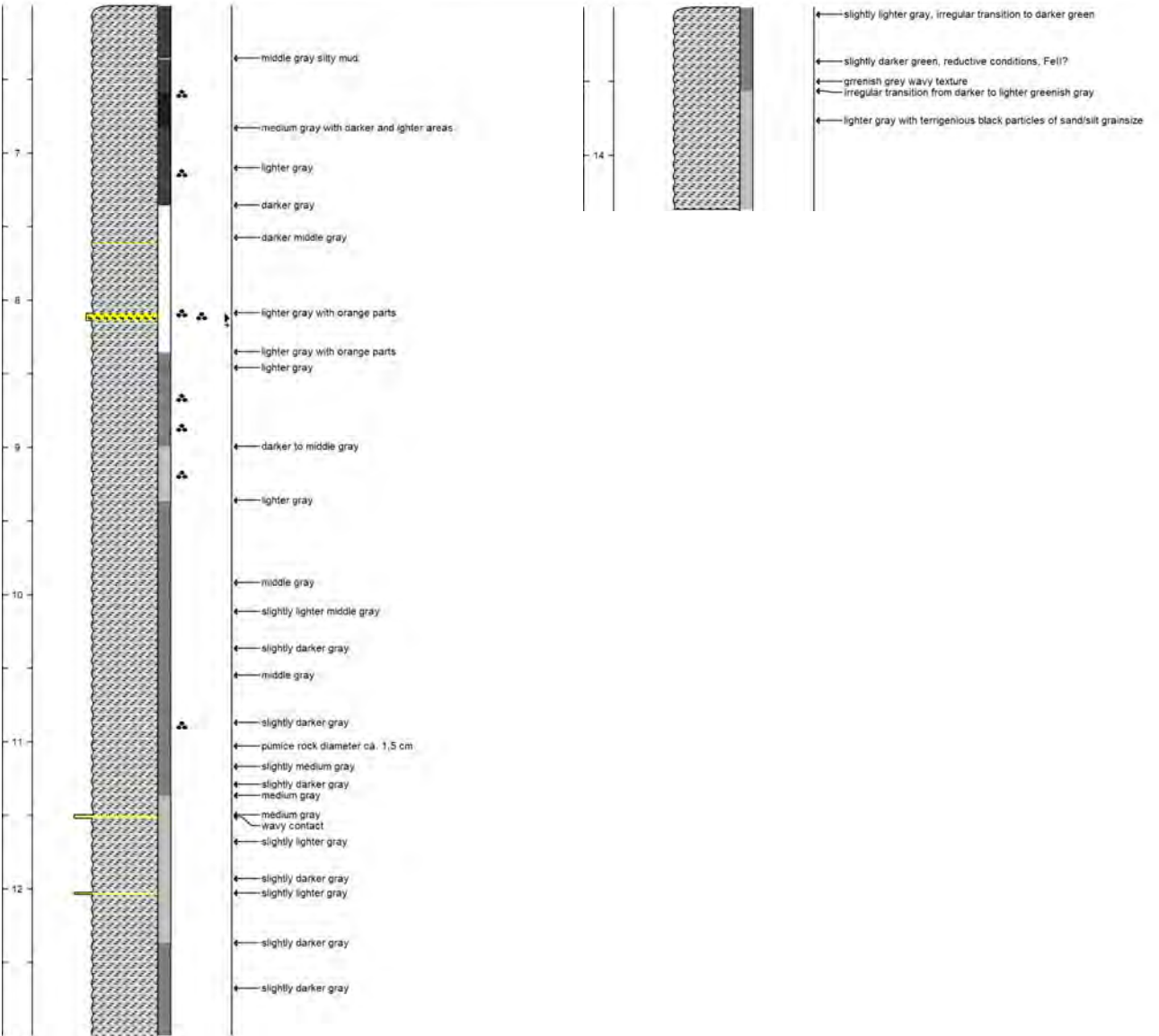
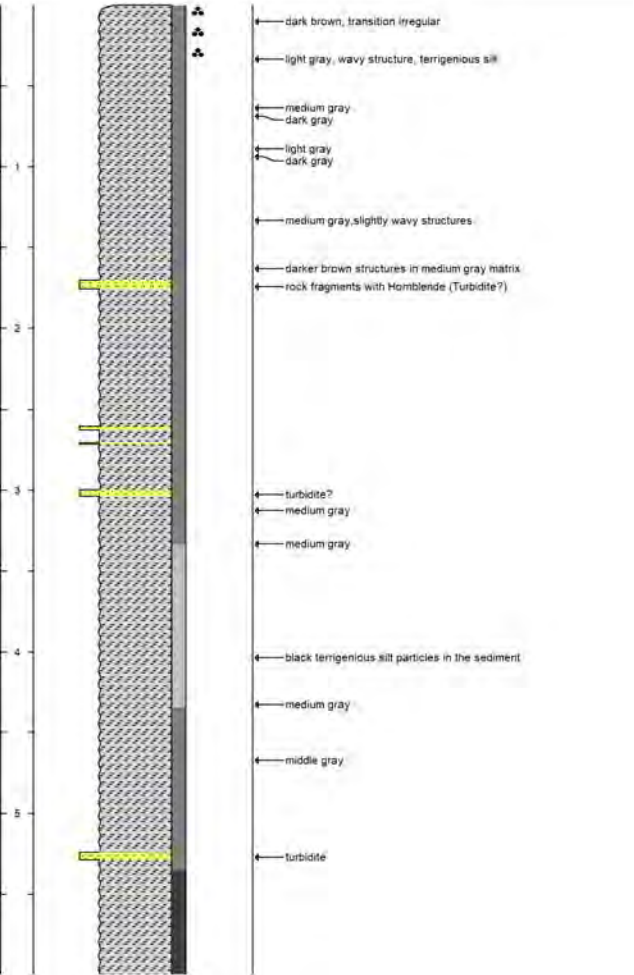
Remarks: 41°34,914'N 170°25,783'E 3572 mbsl



Appendix 5.6.1 Lithology logs

SO264-19-2

Date Logged: July 22, 2018
Logged by: C. Karas
Remarks: 43°48,891'N 170°46,843'E 5704 mbsl



Appendix 5.6.1 Lithology logs

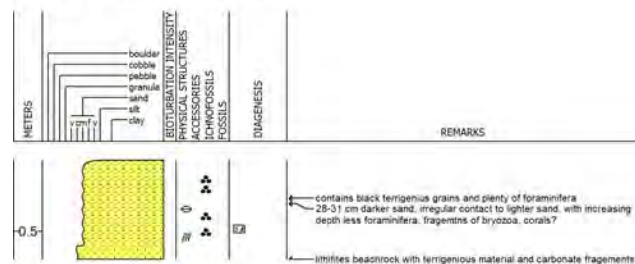
SO264 Cruise Report

SO264-20-1

Date Logged: July 22, 2018

Logged by: C. Karas

Remarks: 41°20,025'N 170°22,742'E 1308 mbsl



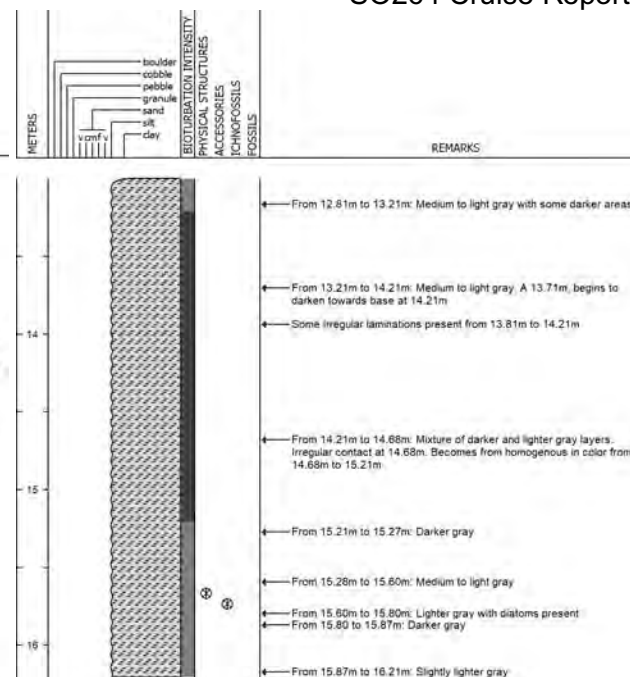
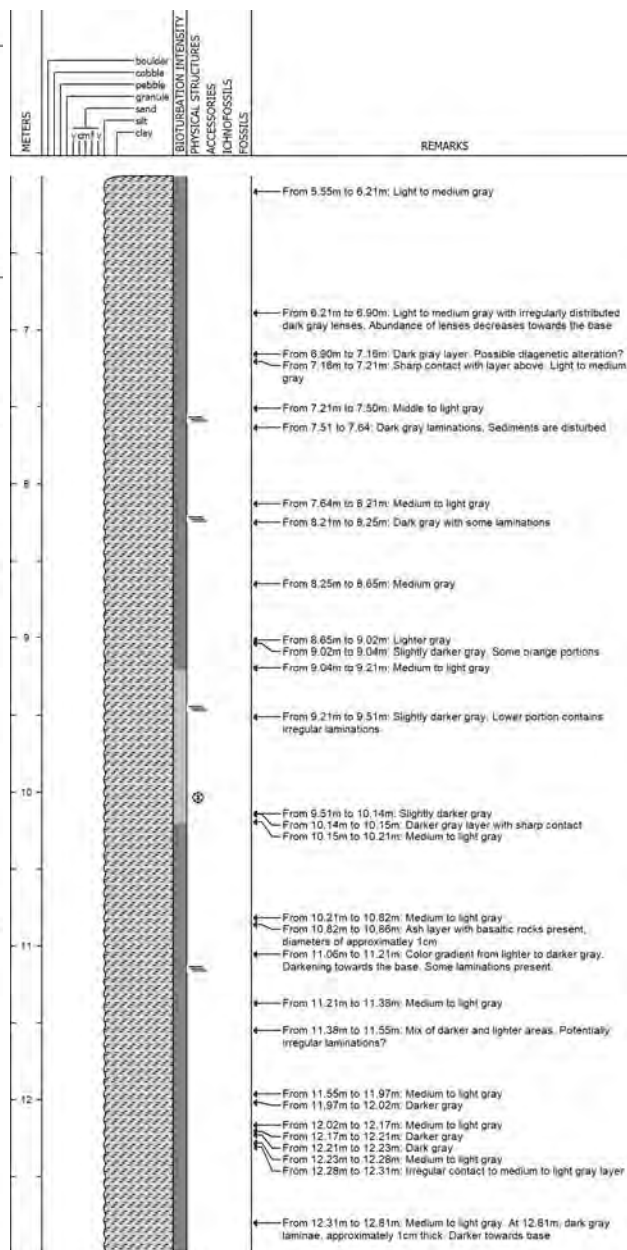
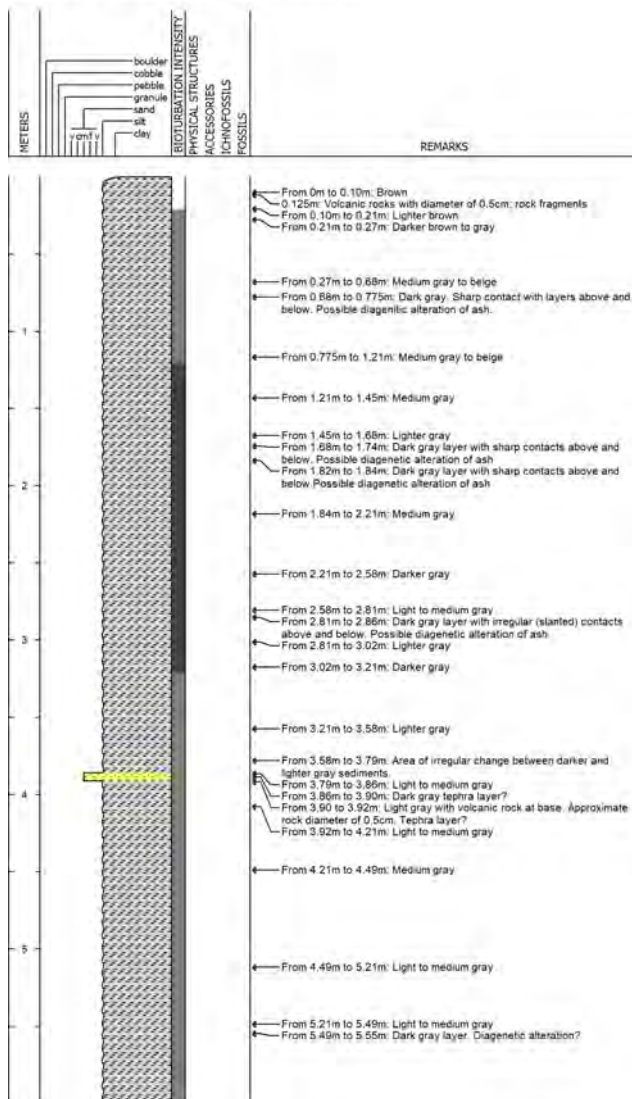
Appendix 5.6.1 Lithology logs

SO264-22-2

Date Logged: July 22, 2018

Logged by: C. Karas

Remarks: 43°48,891'N 170°46,843'E 5704 mbsl



SO264 Cruise Report

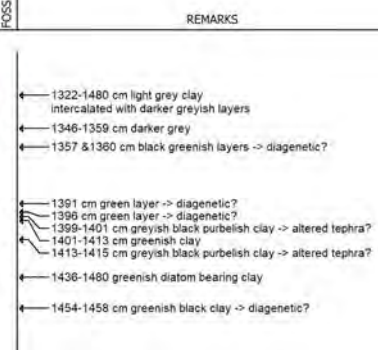
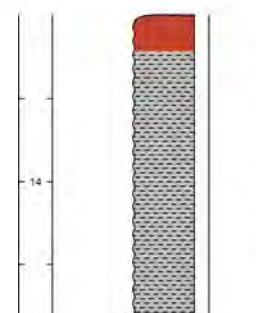
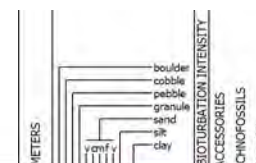
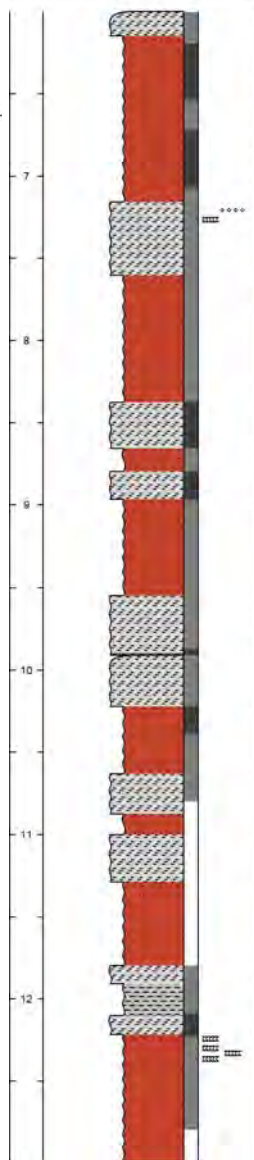
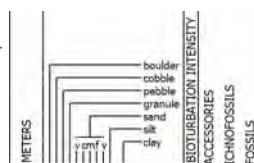
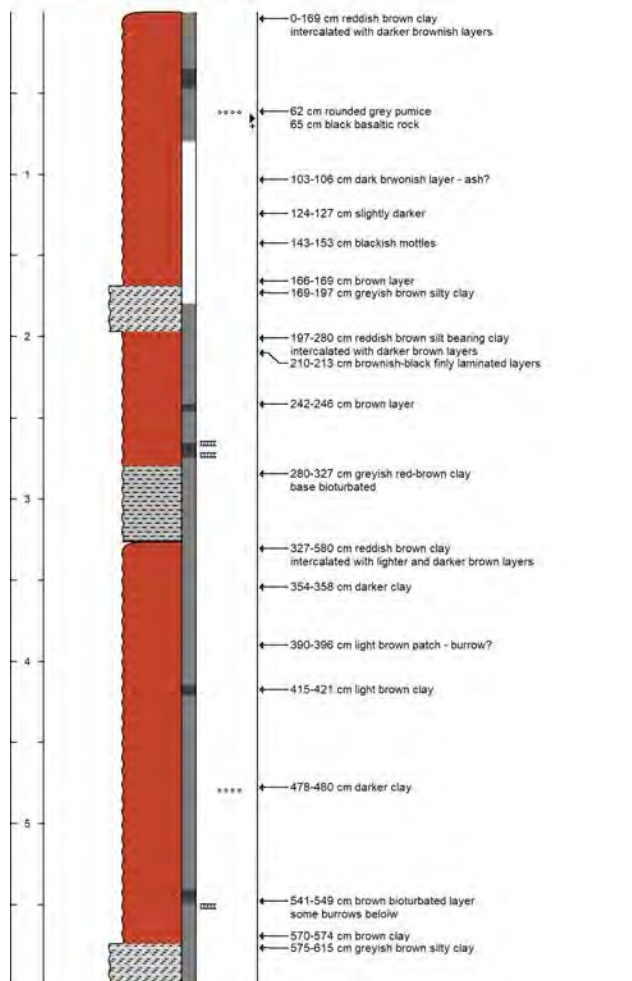
Appendix 5.6.1 Lithology logs

SO264-24-3

Date Logged: July 26, 2018

Logged by: T. Ronge

Remarks: 44°48,061'N 170°35,877'E 4295 mbsl



SO264 Cruise Report

Appendix 5.6.1 Lithology logs

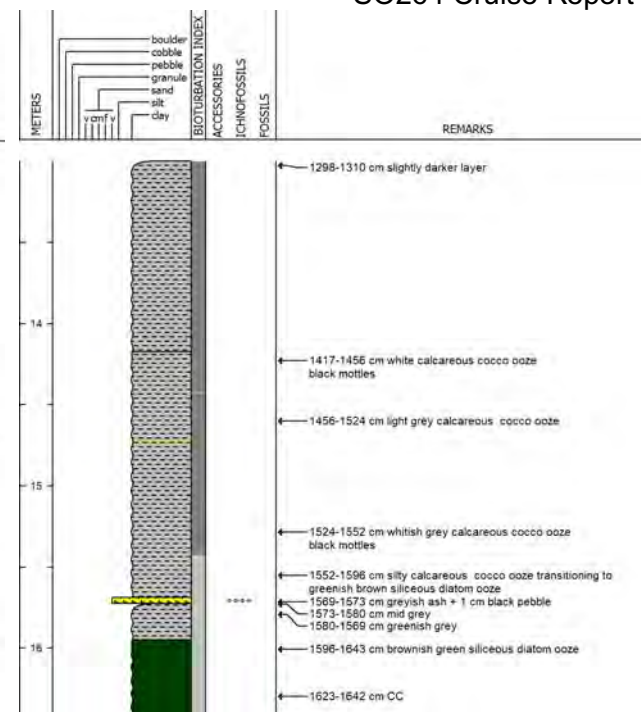
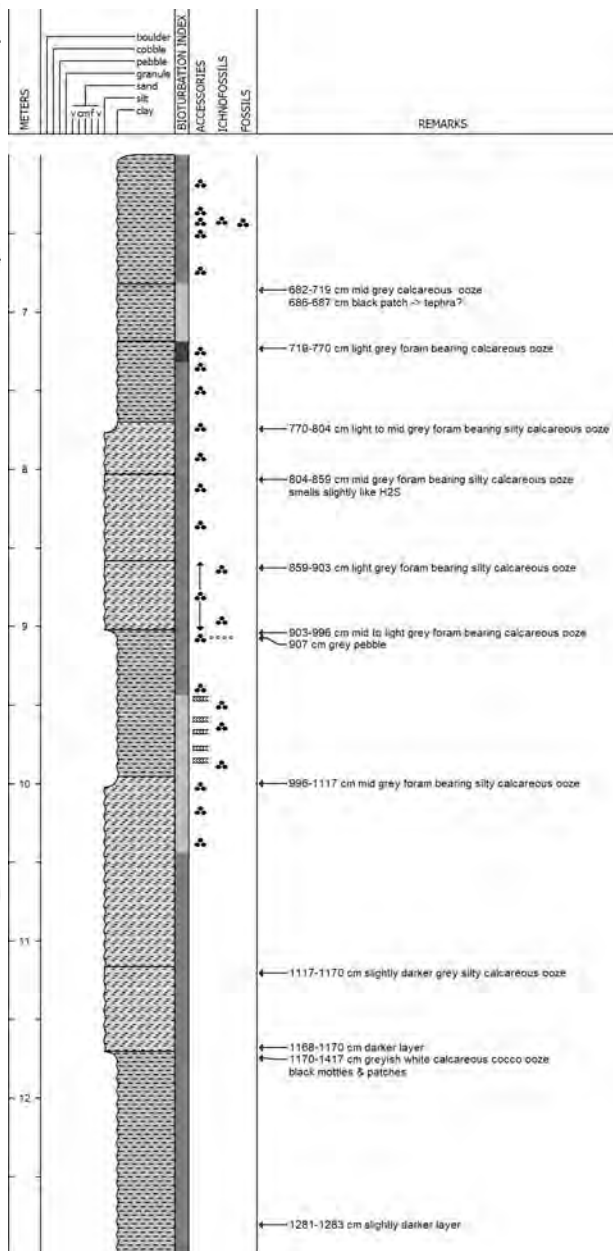
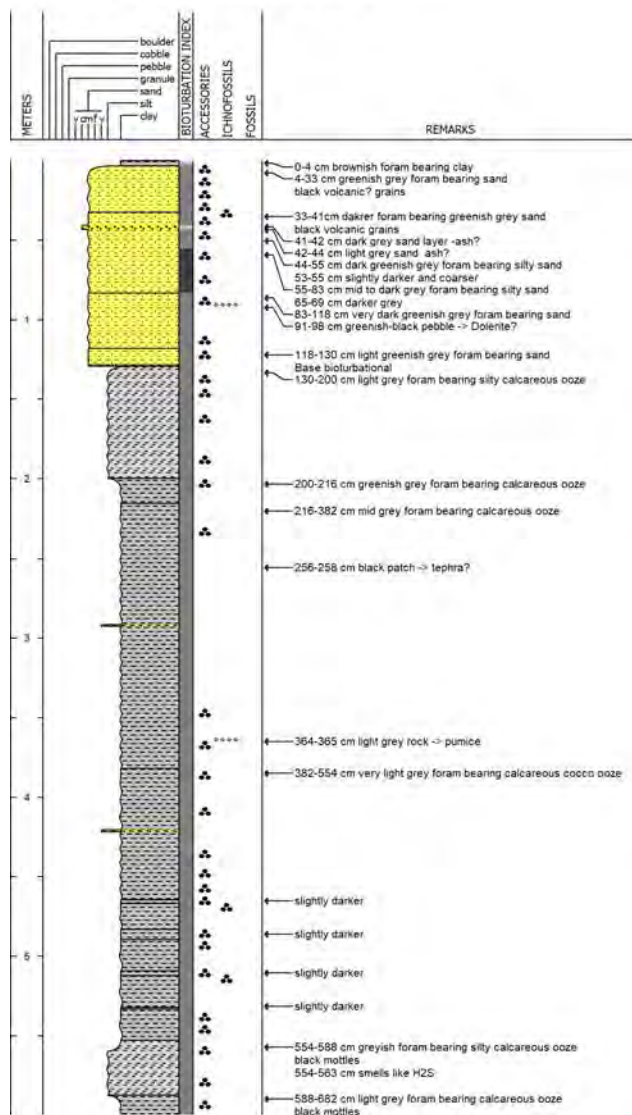
SO264 Cruise Report

SO264-26-2

Date Logged: July 23, 2018

Logged by: T. Ronge

Remarks: 44°46,412'N 170°10,325'E 1771 mbsl



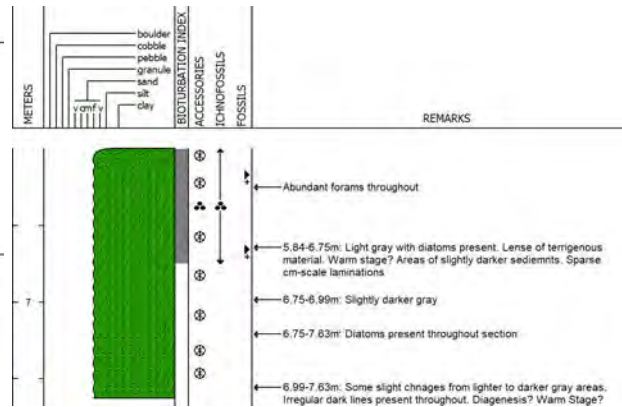
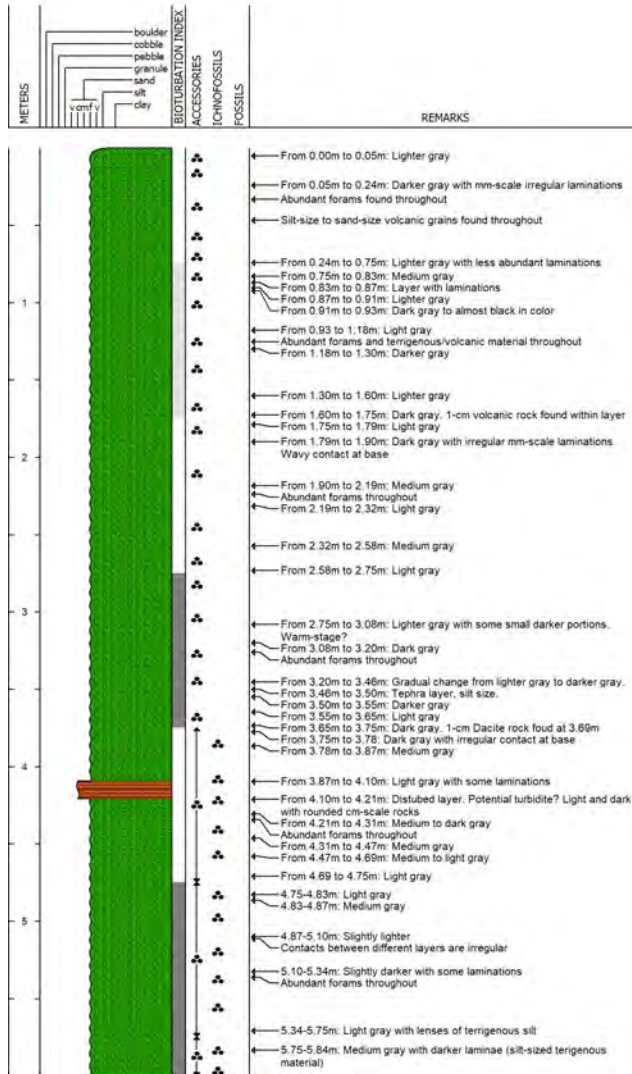
Appendix 5.6.1 Lithology logs

SO264-28-2

Date Logged: July 27, 2018

Logged by: C. Karas

Remarks: 44°51,546'N 170°03,983'E 1935 mbsl



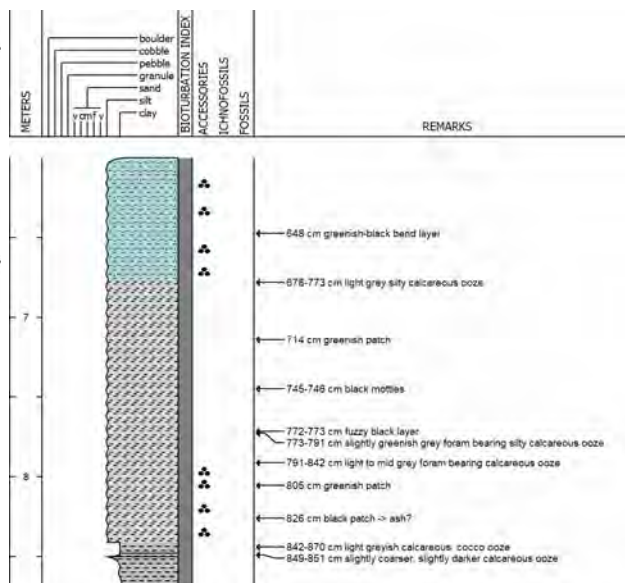
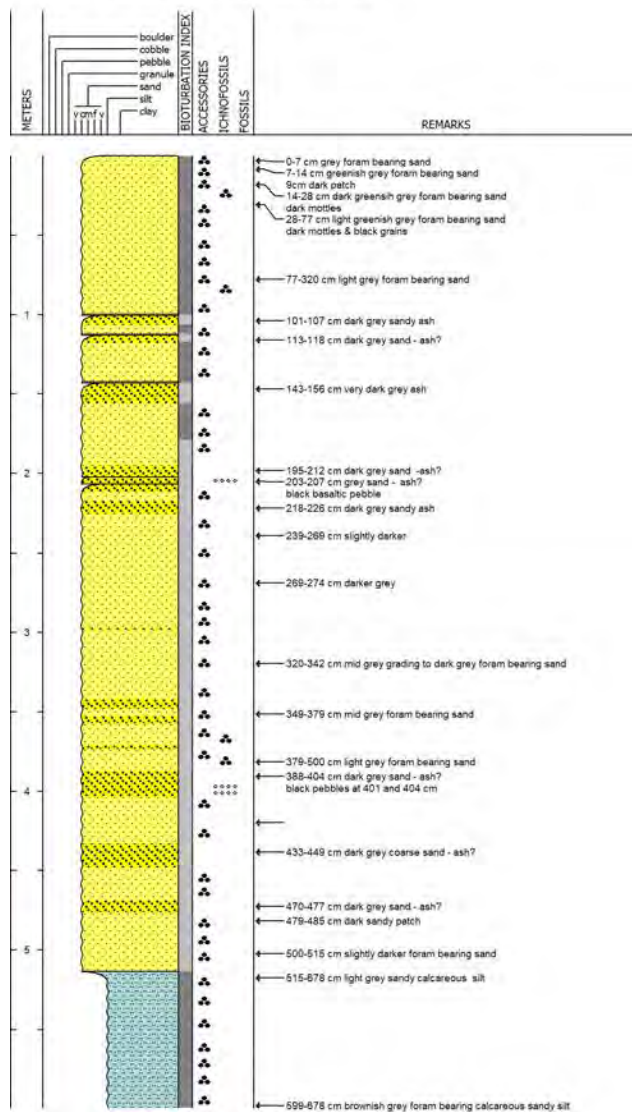
Appendix 5.6.1 Lithology logs

SO264-29-1

Date Logged: July 24, 2018

Logged by: T. Ronge

Remarks: 44°52,030'N 170°03,835'E 1966 mbsl



SO264 Cruise Report

Appendix 5.6.1 Lithology logs

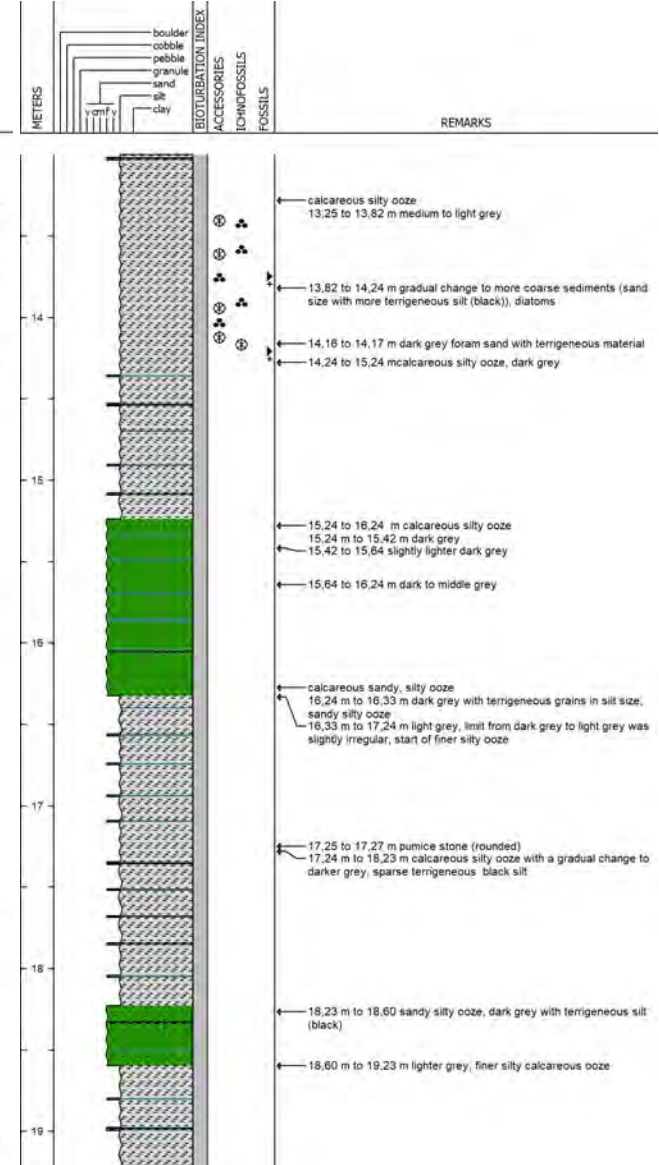
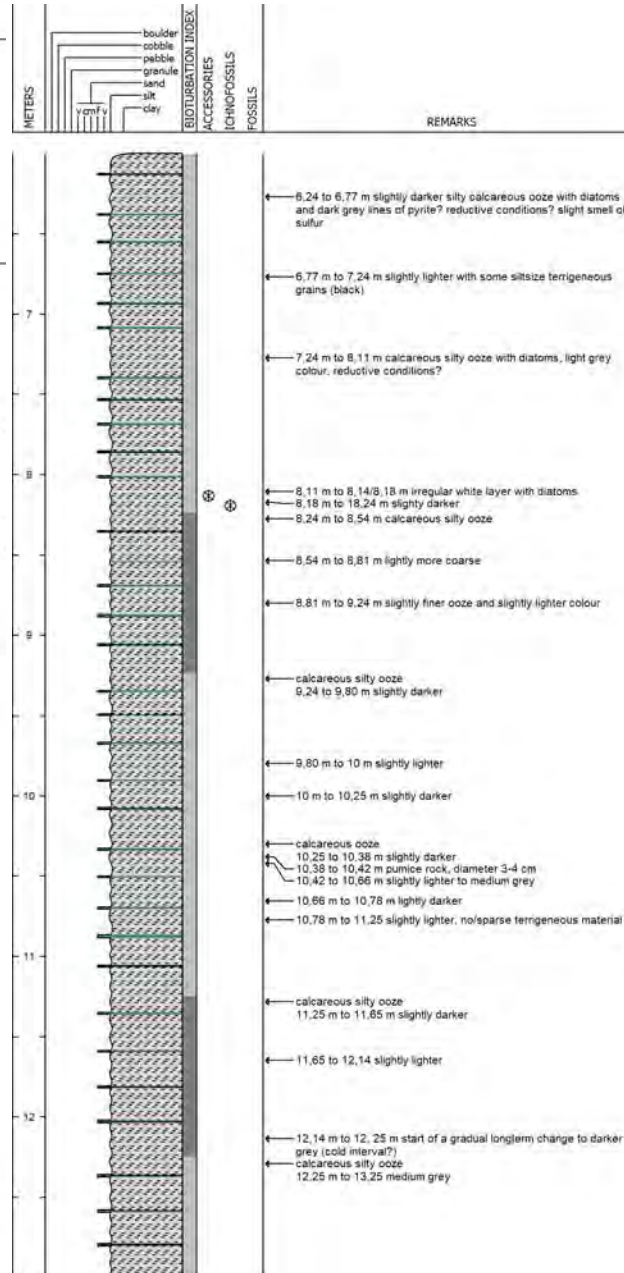
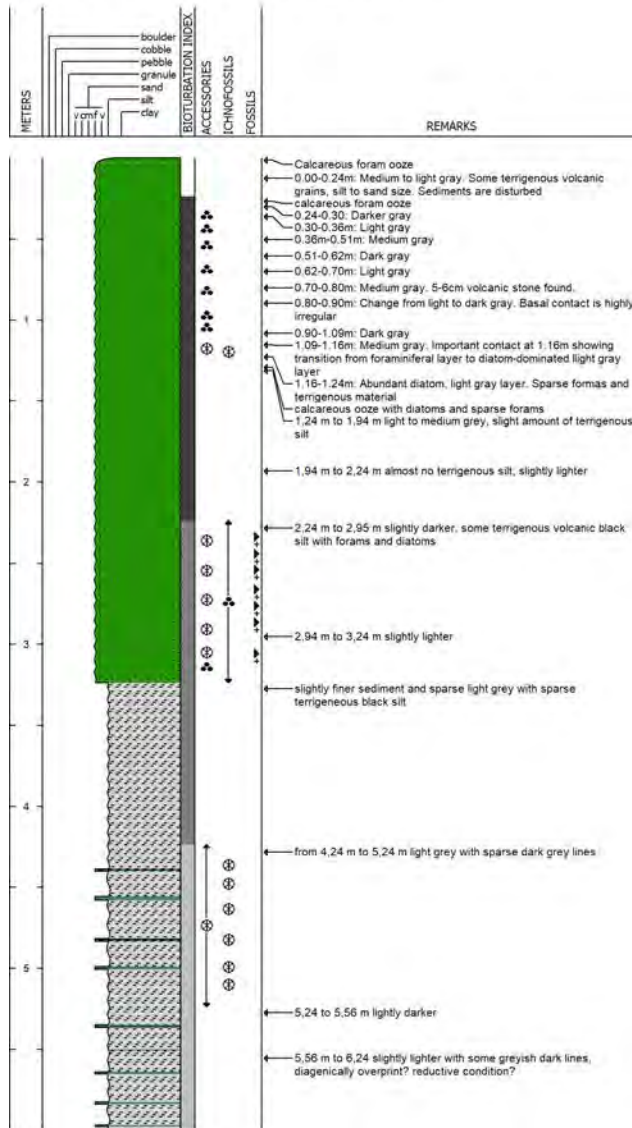
SO264 Cruise Report

SO264-30-2

Date Logged: Juli 28, 2018

Logged by: C. Karas

Remarks: 44°46,465'N 170°01,090'E 1857 mbsl



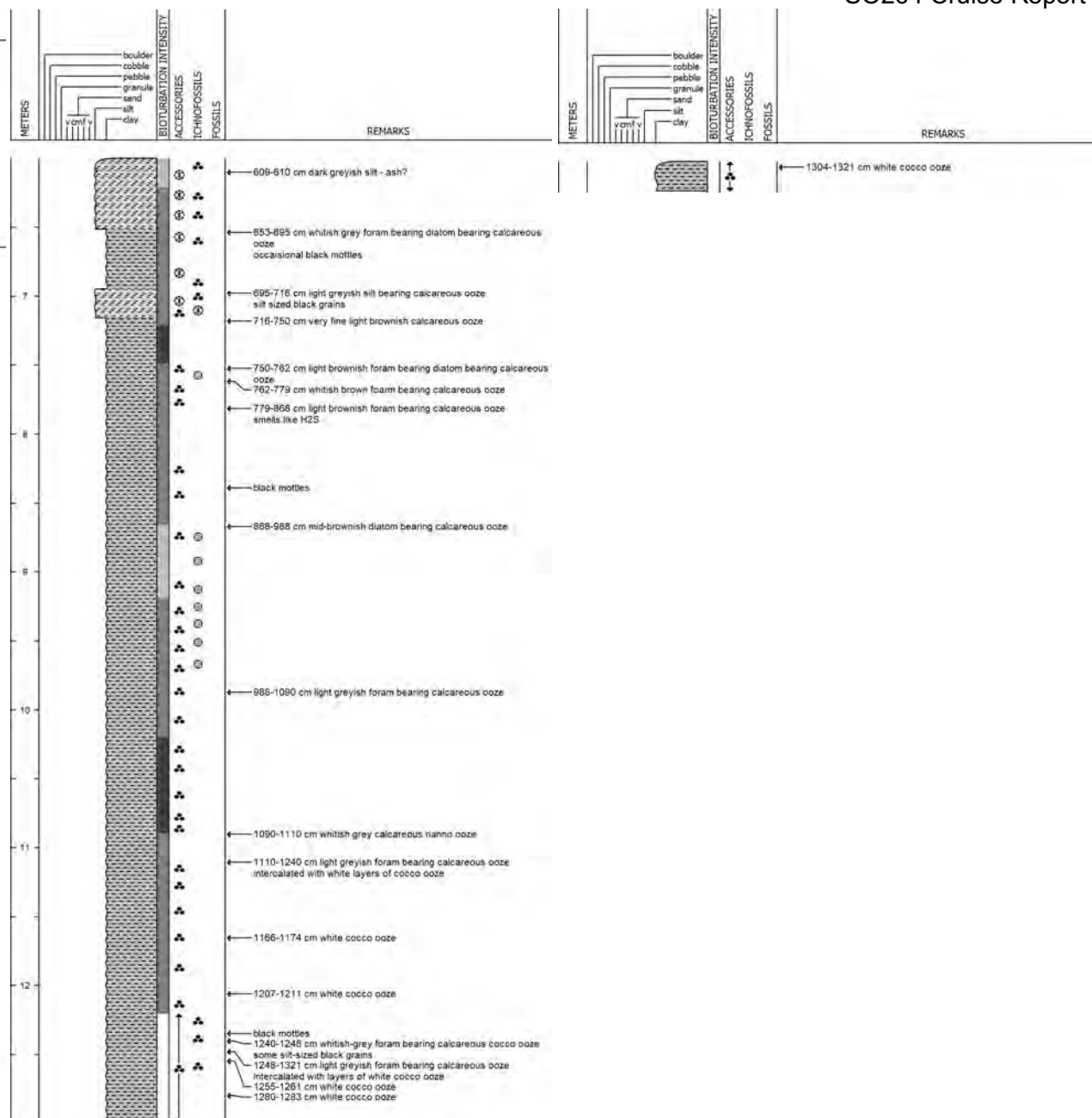
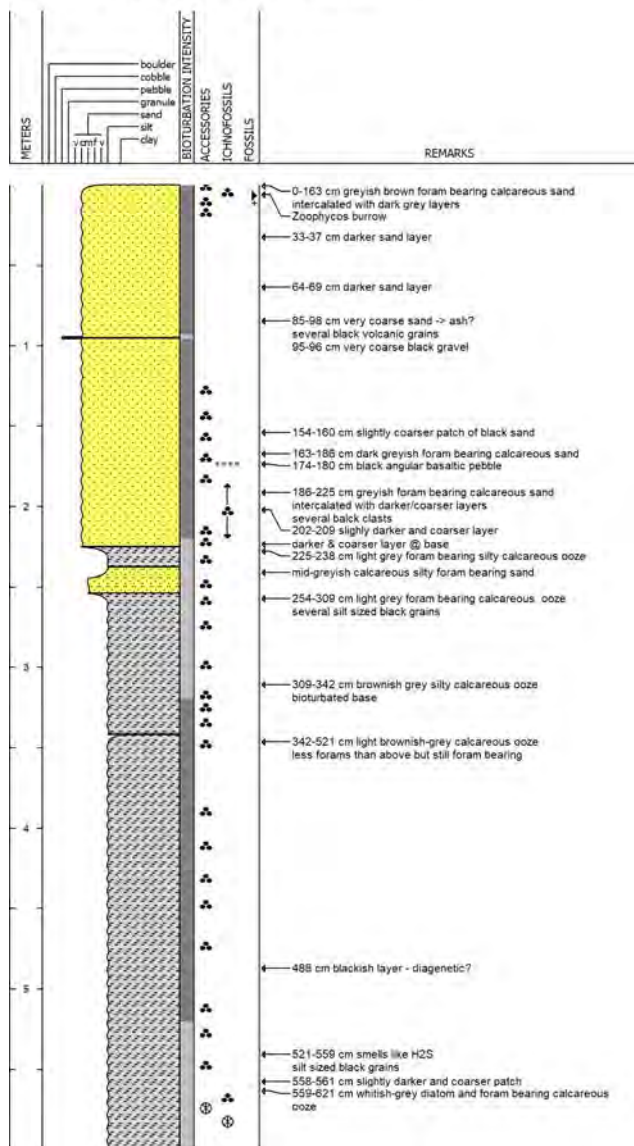
Appendix 5.6.1 Lithology logs

SO264-31-1

Date Logged: July 27, 2018

Logged by: T. Ronge

Remarks: 44°51,161'N 170°07,650'E 1942 mbsl



SO264 Cruise Report

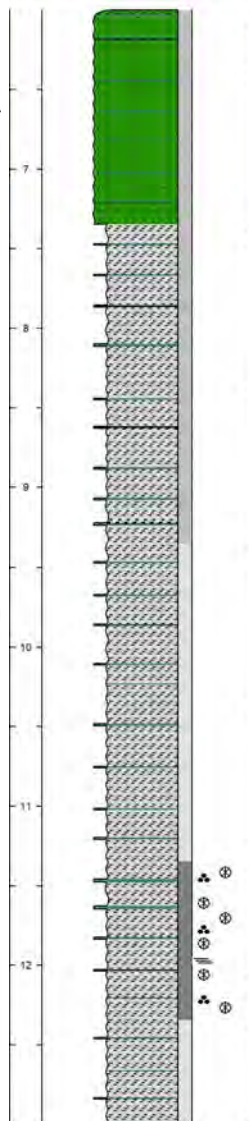
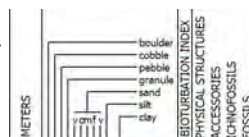
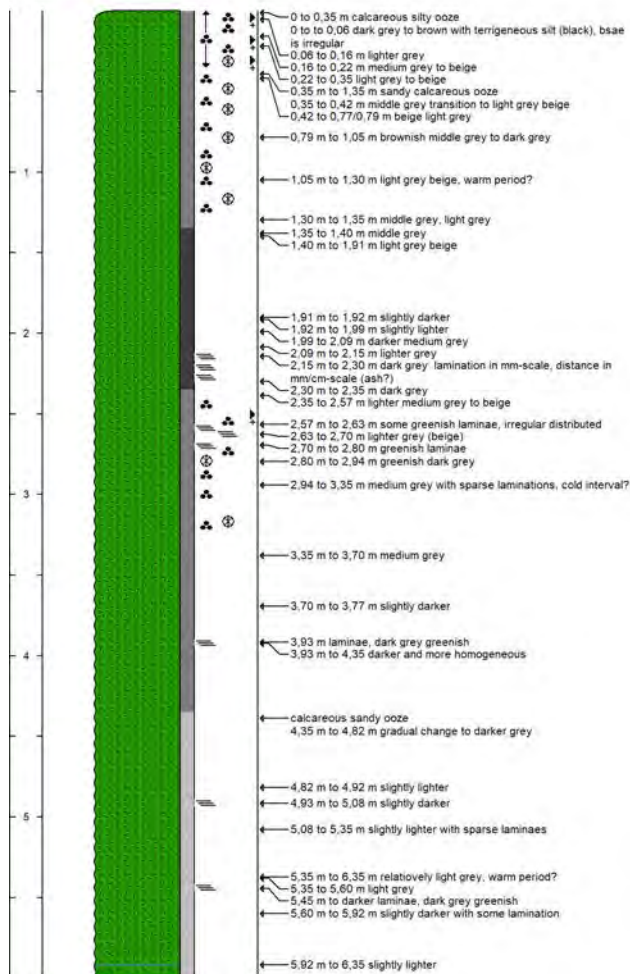
Appendix 5.6.1 Lithology logs

SO264-32-2

Date Logged: July 17, 2018

Logged by: C. Karas

Remarks: 44°59,780'N 170°24,280'E 3200 mbsl



dark grey lines, reductive conditions?

6.35 m to 7.35 m dark grey, cold period?

7.35 m to 7.38 m dark grey

7.38 m to 7.50 m very dark grey, sharp contact

7.50 to 8.35 m middle grey

8.35 m to 9.35 m medium grey with smell of sulfur, reductive conditions?, diagenesis?

9.35 m to 10.35 m medium grey with diagenesis

10.35 m to 11.35 m medium grey

11.35 m to 11.97 m medium grey

11.97 m to 12.00 m laminae, dark grey

12.00 m to 12.08 m lighter

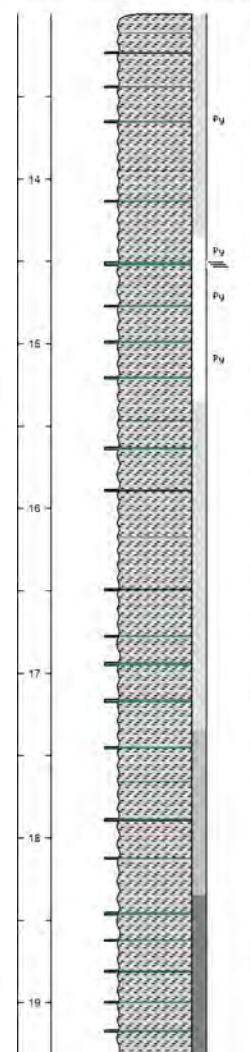
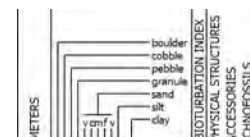
12.08 m to 12.20 m darker, base is bioturbated/disturbed

12.20 m to 12.35 m lighter

12.35 m to 12.97 m medium grey

12.97 m to 13.00 m dark with a slightly wavy base

13.00 m to 13.35 m lighter



13.00 m to 13.35 m lighter

13.35 m to 14.35 calcareous silty ooze, medium grey

14.35 m to 14.97 medium grey

14.97 m to 15.35 m gradual change to slightly darker

15.35 to 15.68 m darker grey

15.68 m to 16.05 m transition to slightly lighter grey

16.05 to 16.35 m slightly darker

16.35 m to 16.70 m medium to slightly darker grey

16.70 to 17.08 slightly darker

17.08 to 17.35 slightly lighter

17.35 m to 17.80 slightly lighter grey

17.80 to 18.35 m slightly darker with some sparse lamination with a thickness of 1 cm in irregular distances of 5-10 cm

18.35 m to 18.70 m medium grey

18.70 to 19.75 dark grey with a highly irregular transition to lighter grey

19.75 to 19.32 m lighter

SO264 Cruise Report

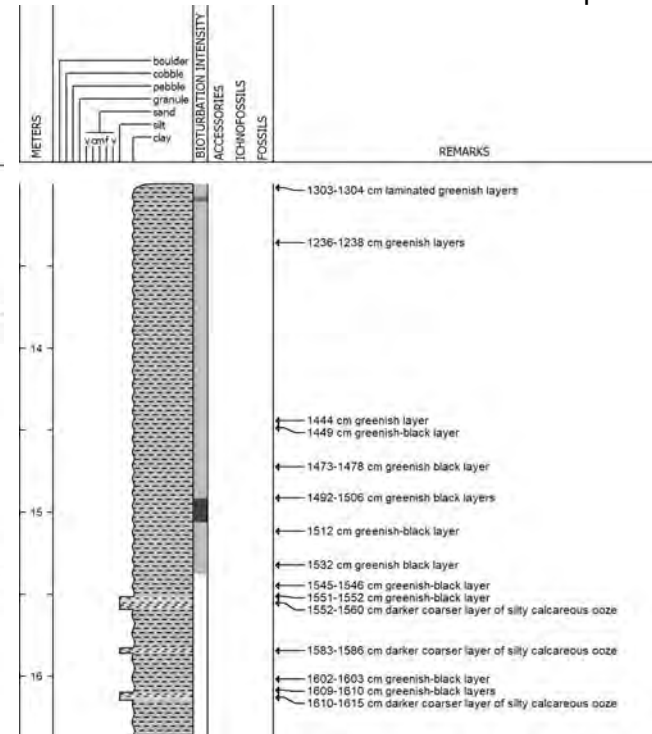
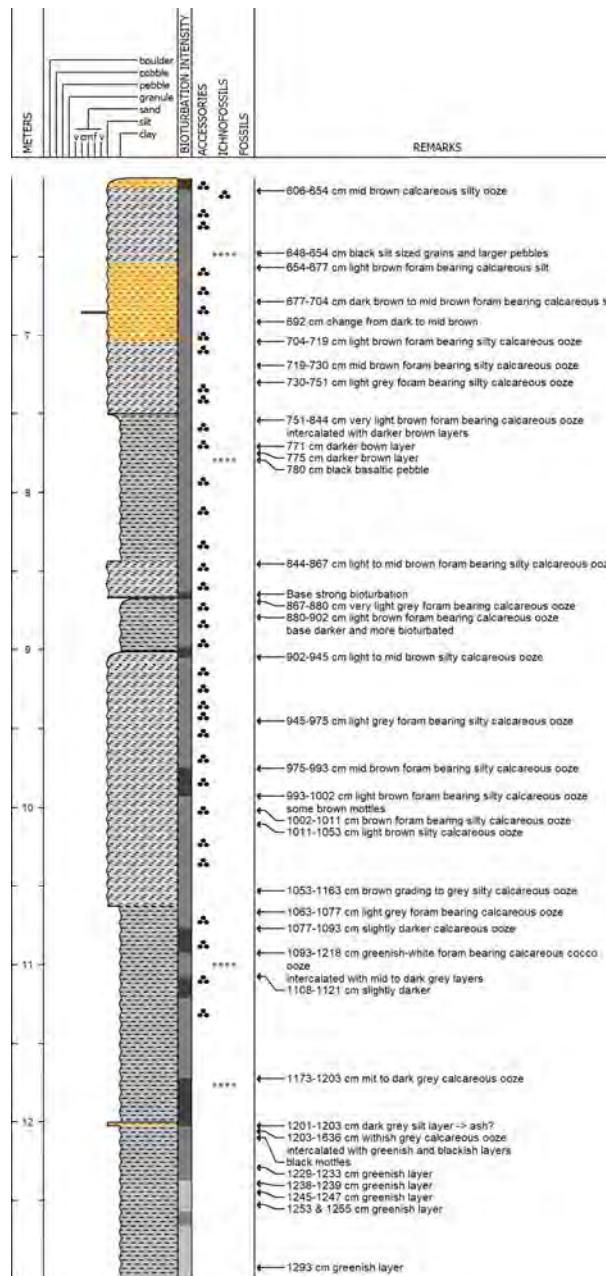
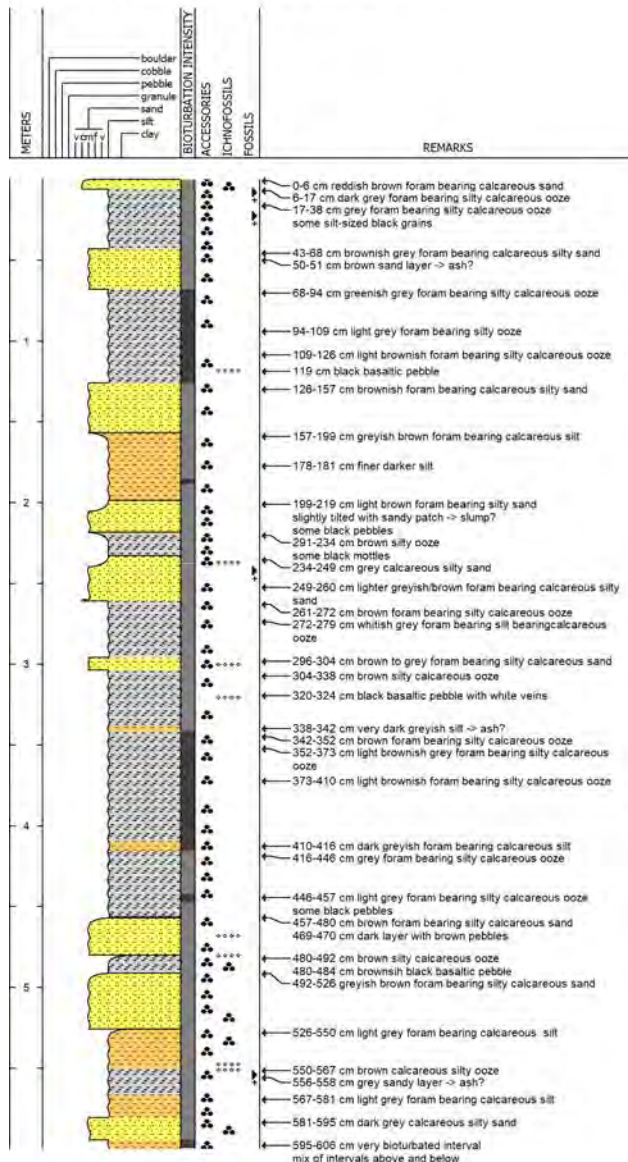
Appendix 5.6.1 Lithology logs

SO264-33-2

Date Logged: July 26, 2018

Logged by: T. Ronge

Remarks: 44°58,290'N 170°21,024'E 3141 mbsl



SO264 Cruise Report

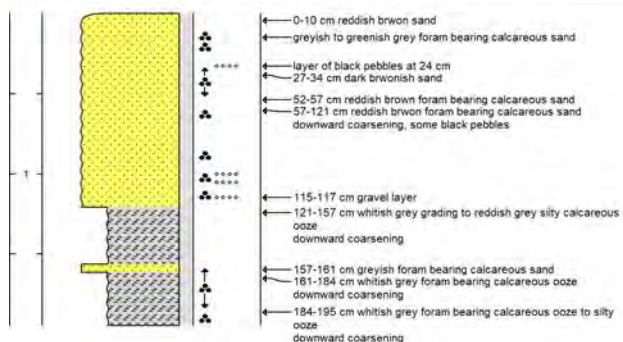
Appendix 5.6.1 Lithology logs

SO264-34-2

Date Logged: July 27, 2018

Logged by: T. Ronge

Remarks: 45°01,852'N 170°13,553'E 2622 mbsl

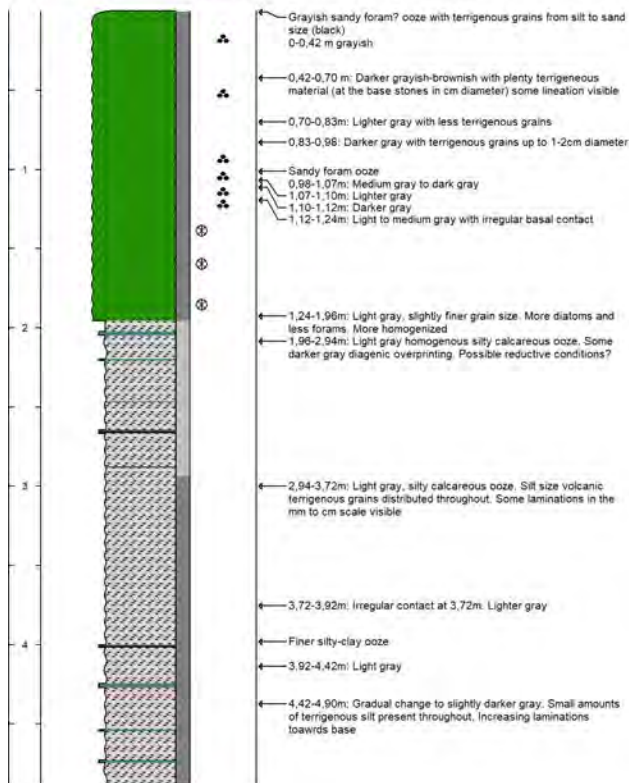


SO264-36-1 (BC)

Date Logged: July 28, 2018

Logged by: C. Karas

Remarks: 44°46,409'N 170°10,319'E 1771 mbsl



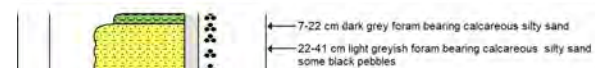
SO264 Cruise Report

SO264-38-1 (=36) GKG

Date Logged: July 30, 2018

Logged by: T. Ronge

Remarks: 44°46,414'N 170°10,317'E 1771 mbsl



Appendix 5.6.1 Lithology logs

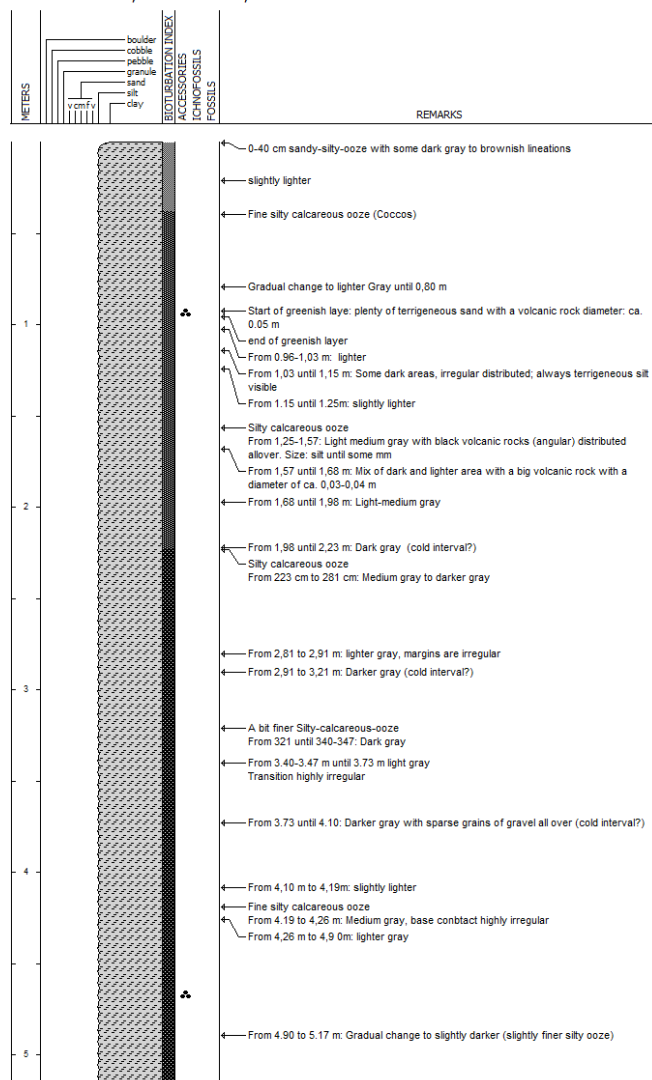
SO264 Cruise Report

SO264-39-1 (BC)

Date Logged: July 28, 2018

Logged by: C. Karas

Remarks: 44° 58, 290 N 170° 21, 025 E

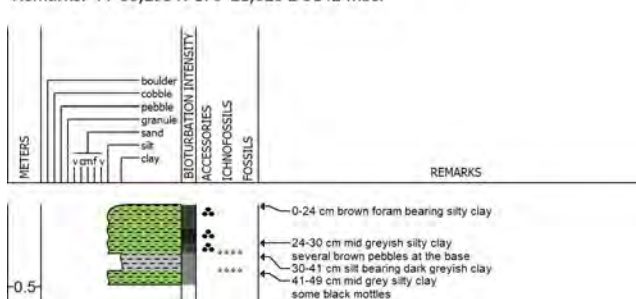


SO264-39-3 GKG

Date Logged: July 30, 2018

Logged by: T. Ronge

Remarks: 44°58,295'N 170°21,025'E 3142 mbsl



Appendix 5.6.1 Lithology logs

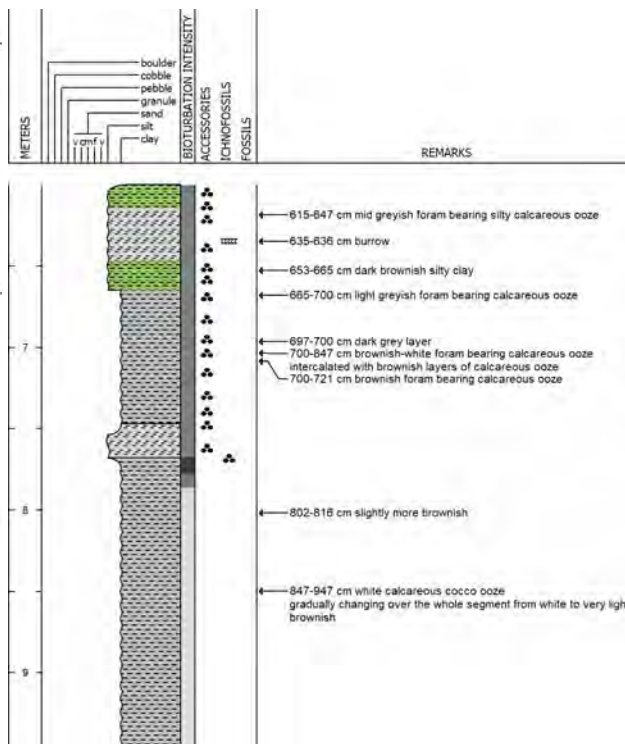
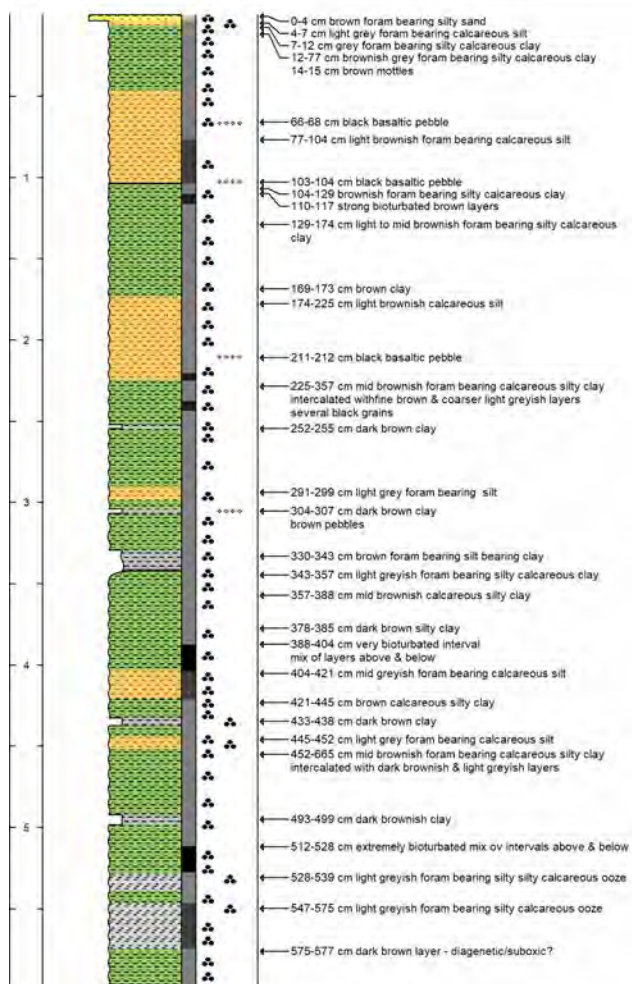
SO264 Cruise Report

SO264-41-2

Date Logged: July 30, 2018

Logged by: T. Ronge

Remarks: 45°41,942'N 170°09,300'E 3645 mbsl



Appendix 5.6.1 Lithology logs

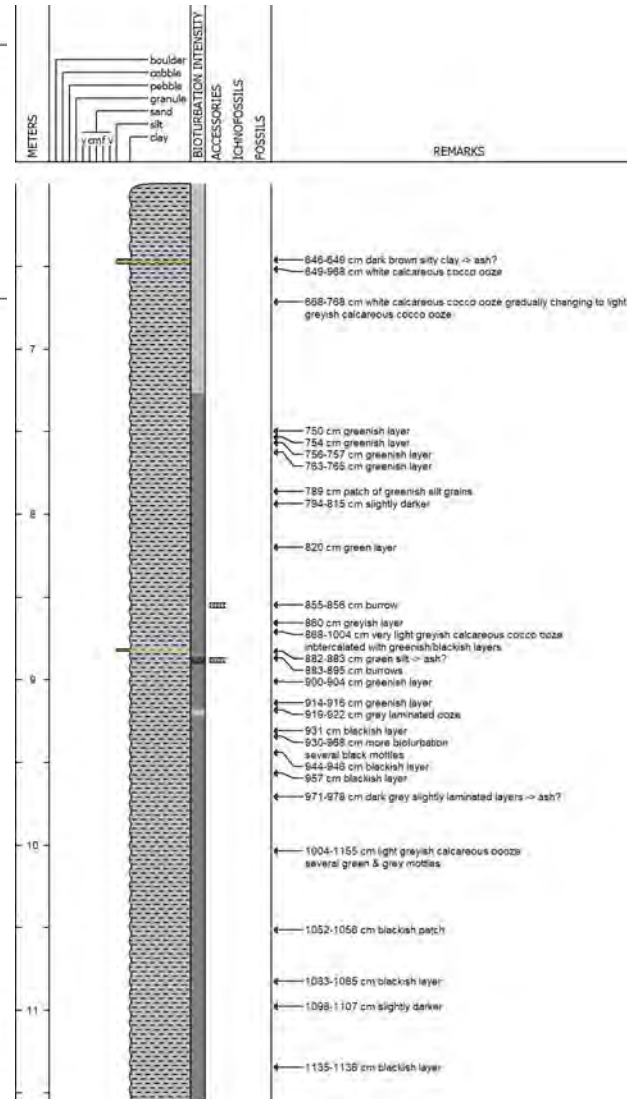
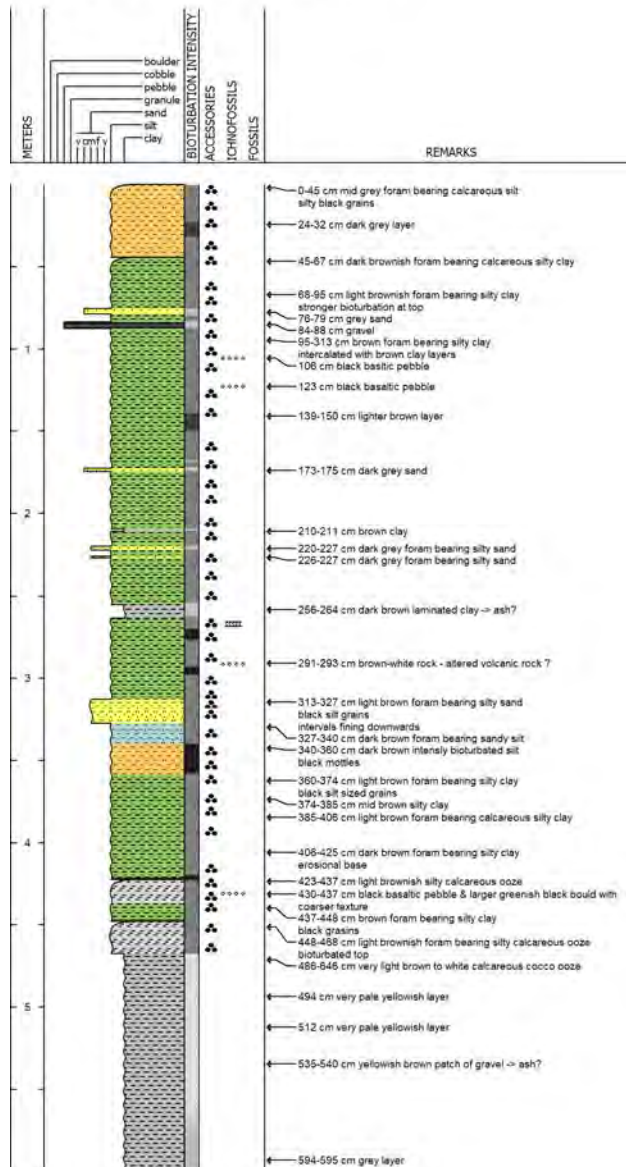
SO264 Cruise Report

SO264-42-2

Date Logged: July 31, 2018

Logged by: T. Ronge

Remarks: 46°06,576'N 169°07,193'E 3239 mbsl



Appendix 5.6.1 Lithology logs

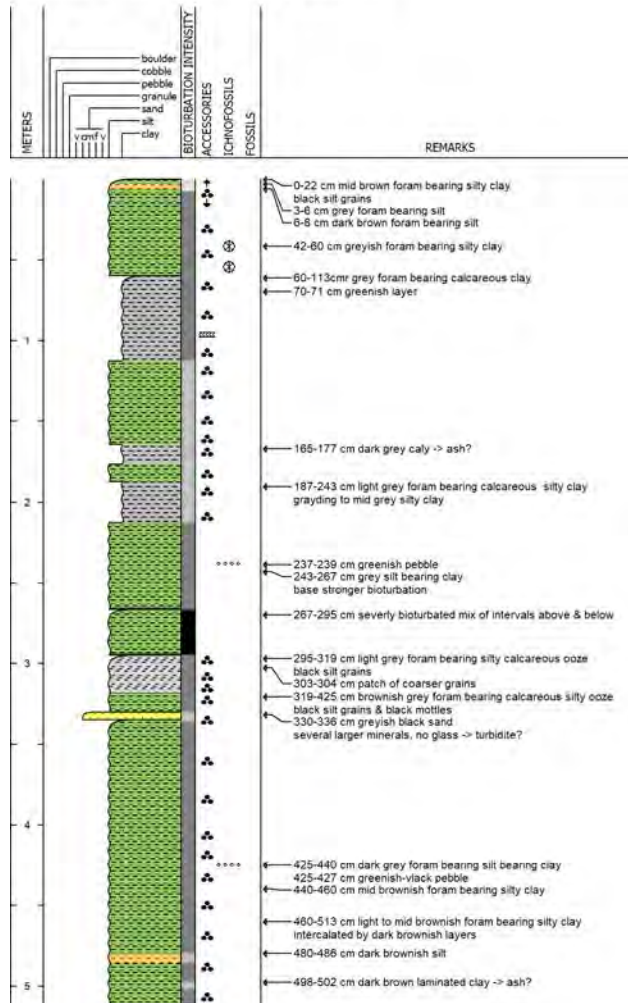
SO264 Cruise Report

SO264-43-2

Date Logged: July 31, 2018

Logged by: T. Ronge

Remarks: 46°06,576'N 169°07,193'E 3239 mbsl



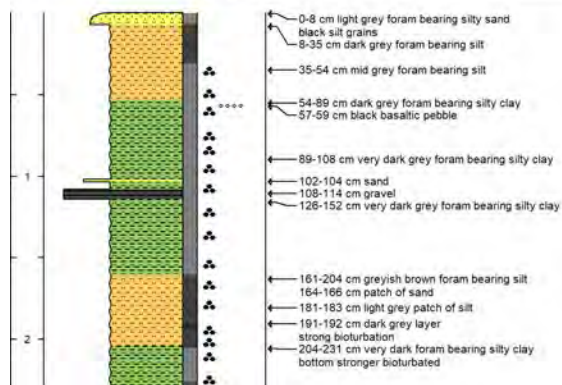
Appendix 5.6.1 Lithology logs

SO264-44-2

Date Logged: Aug 1, 2018

Logged by: T. Ronge

Remarks: 46°15,298'N 169°20,062'E 1893 mbsl

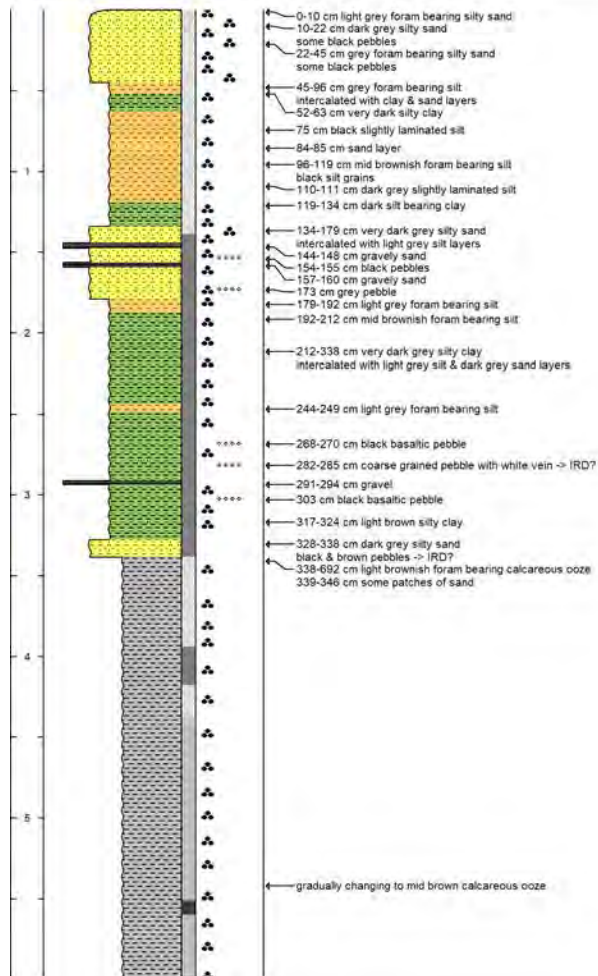


SO264-44-3

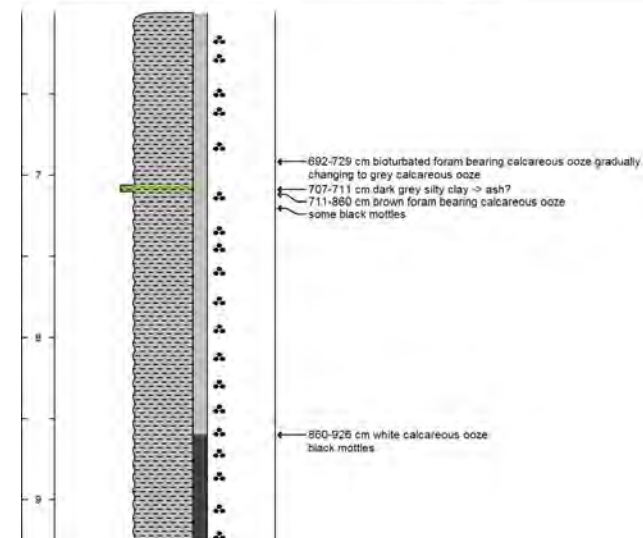
Date Logged: Aug 1, 2018

Logged by: T. Ronge

Remarks: 46°15,307'N 169°20,064'E 1894 mbsl



SO264 Cruise Report



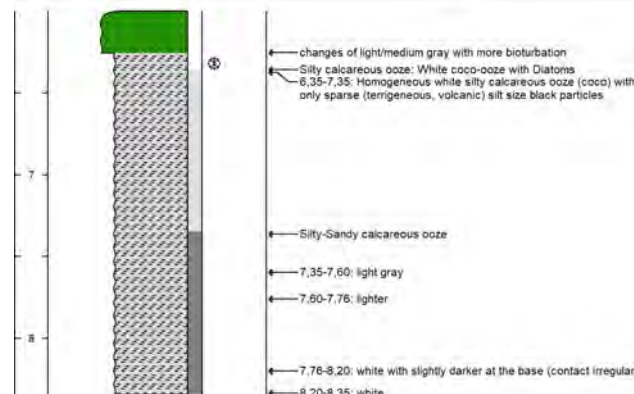
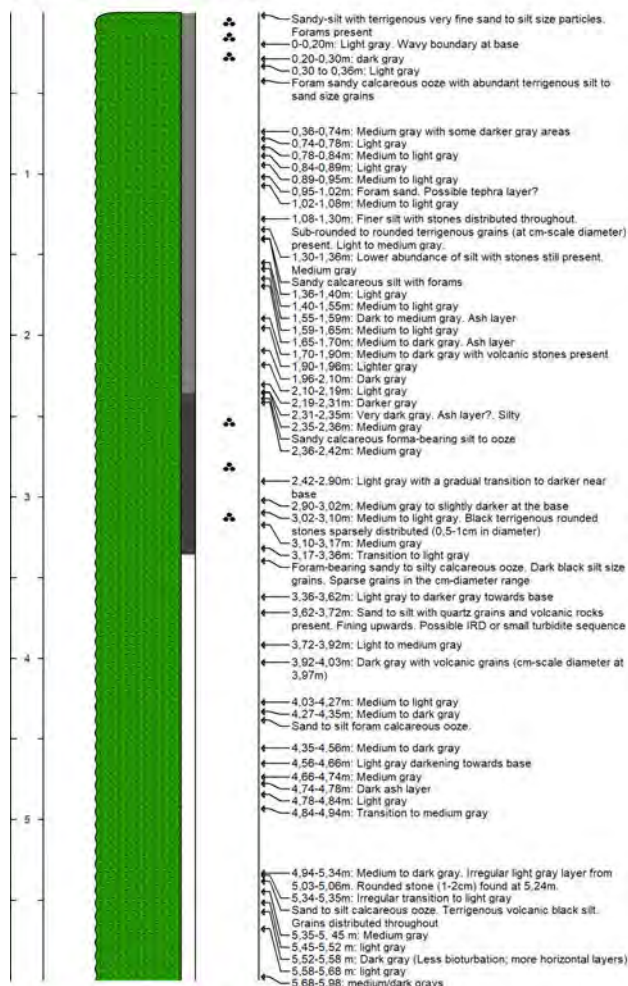
Appendix 5.6.1 Lithology logs

S0264-45-2

Date Logged: Aug 10, 2018

Logged by: C. Karas

Remarks: 46°33,792'N 169°36,072'E 2425 mbsl



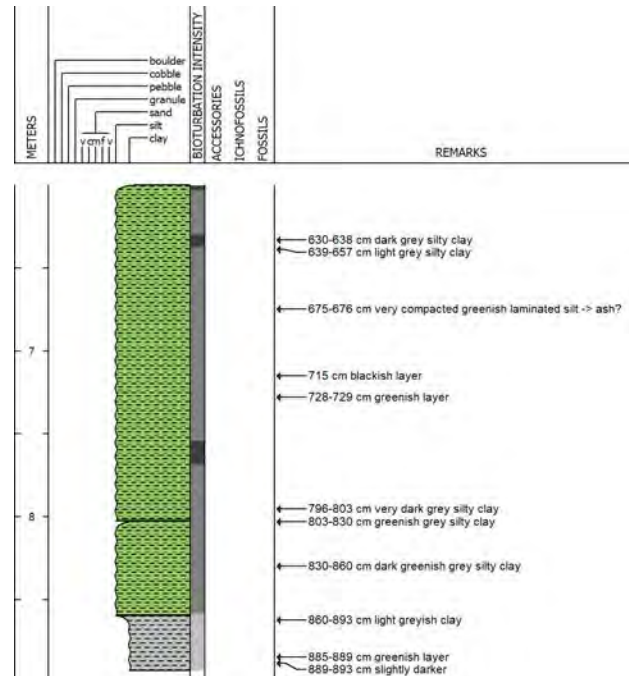
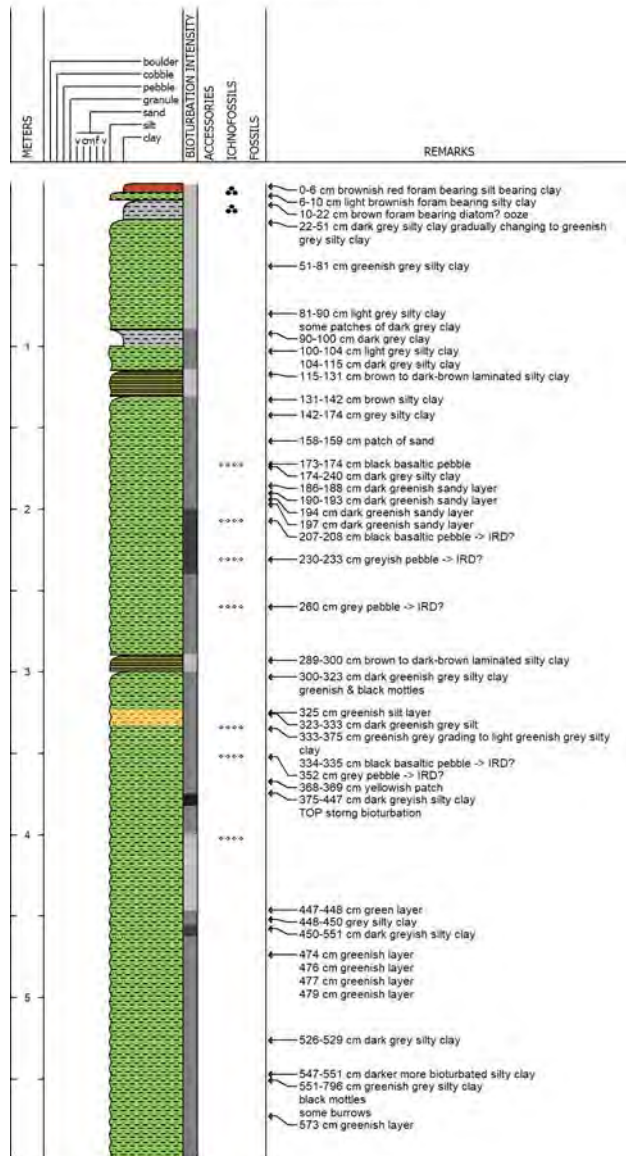
Appendix 5.6.1 Lithology logs

S0264-46-5

Date Logged: Aug 2, 2018

Logged by: T. Ronge

Remarks: 46°48,941'N 169°24,661'E 3992 mbsl



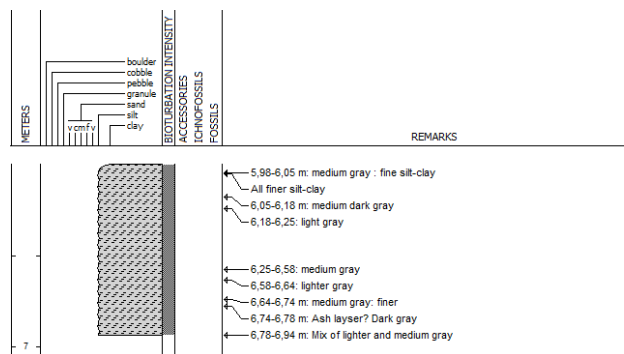
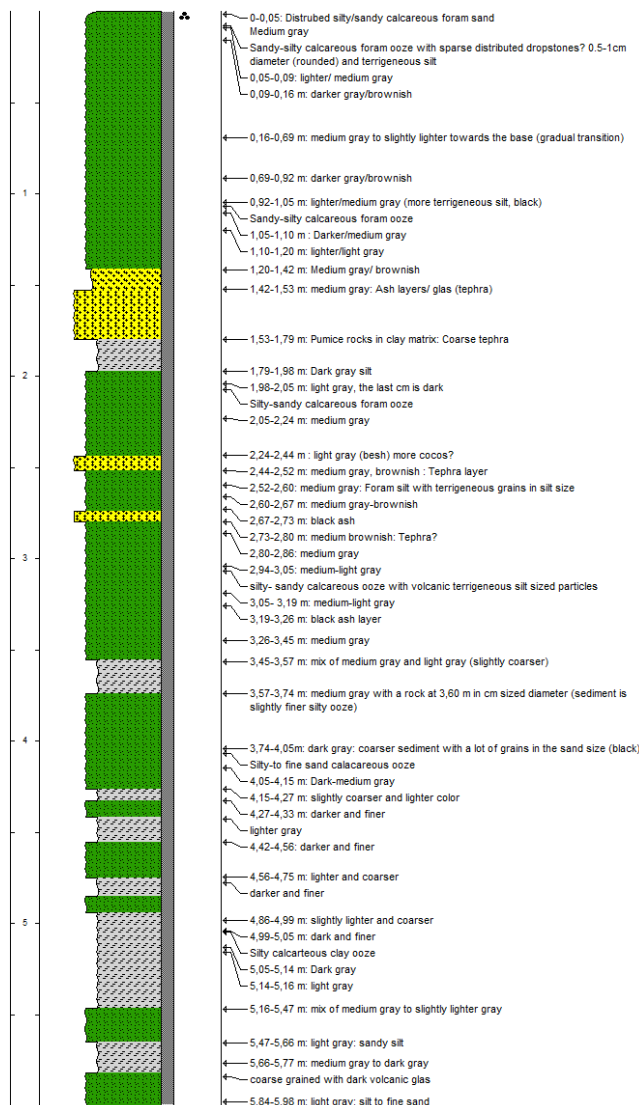
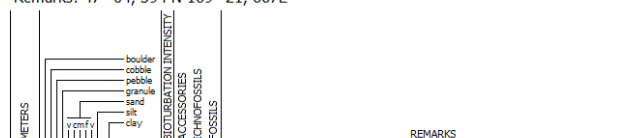
Appendix 5.6.1 Lithology logs

SO264-47-2

Date Logged: July 2018

Logged by: C. Karas

Remarks: 47° 04, 394 N 169° 21, 667E



SO264 Cruise Report

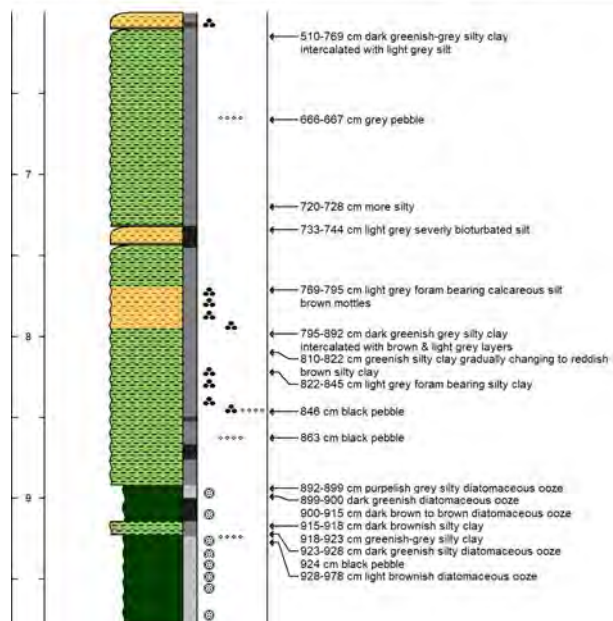
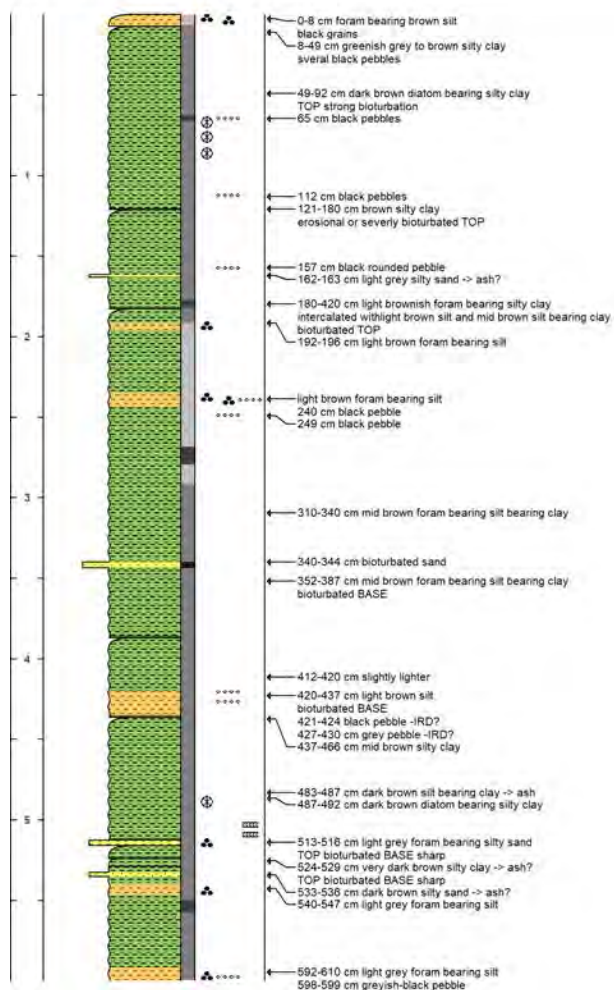
Appendix 5.6.1 Lithology logs

SO264-48-2

Date Logged: Aug 4, 2018

Logged by: T. Ronge

Remarks: 47°58,50'S/N 169°03,87'E 2872 mbsl



SO264 Cruise Report

Appendix 5.6.1 Lithology logs

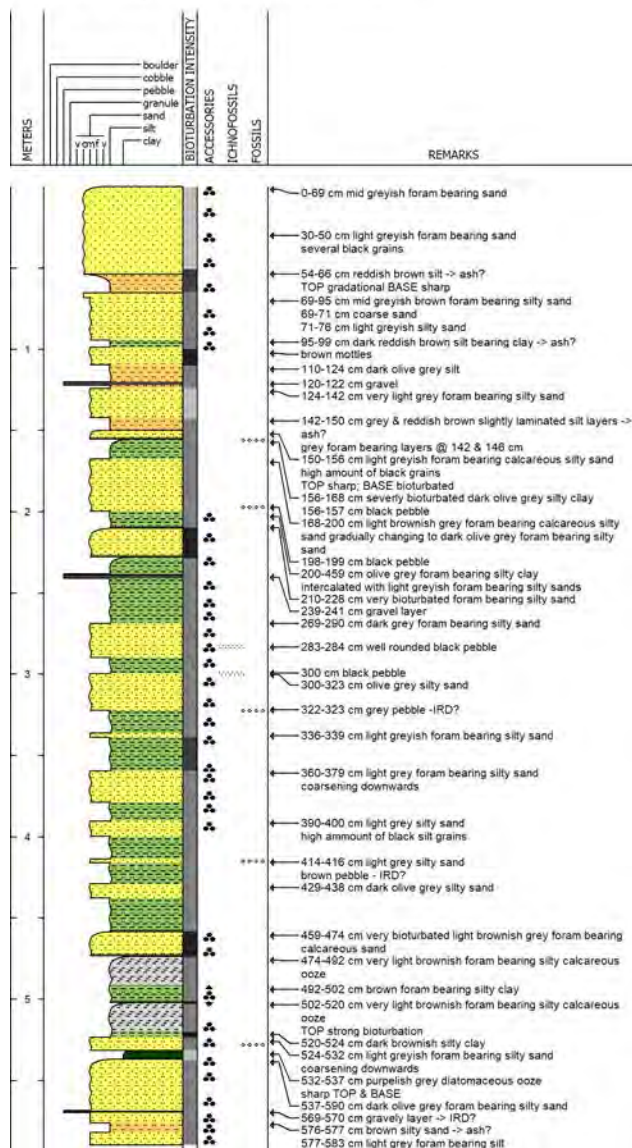
SO264 Cruise Report

SO264-49-2

Date Logged: Aug 4, 2018

Logged by: T. Ronge

Remarks: 47°40,869'N 169°01,419'E 2400 mbsl



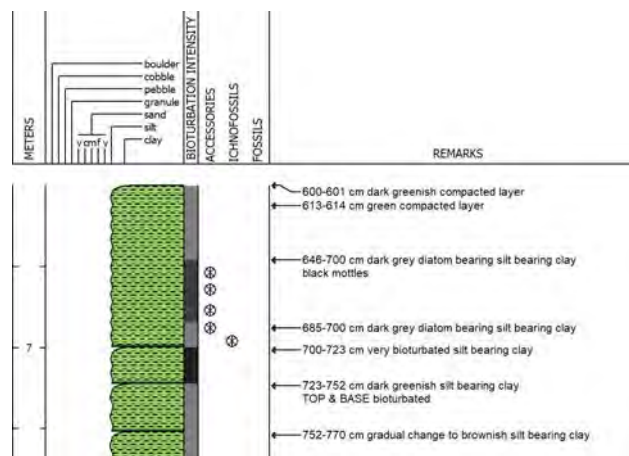
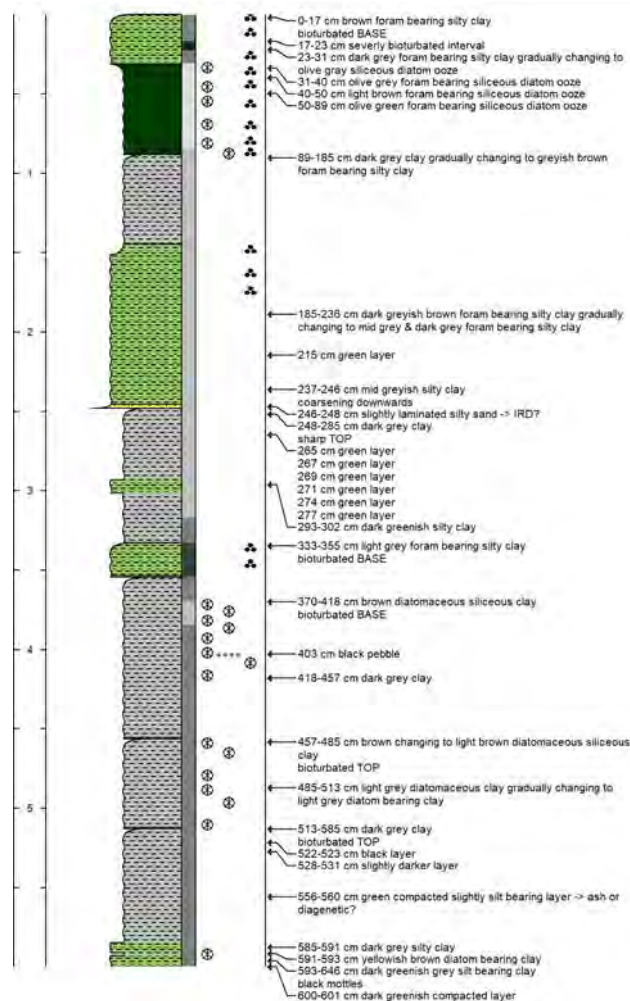
Appendix 5.6.1 Lithology logs

SO264-51-2

Date Logged: Aug 5, 2018

Logged by: T. Ronge

Remarks: 47°10,547'N 169°25,282'E 2933 mbsl



SO264 Cruise Report

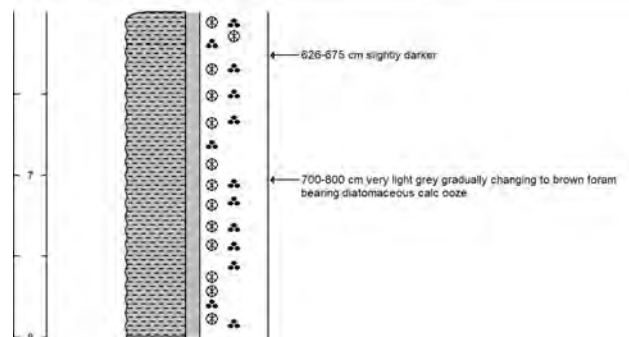
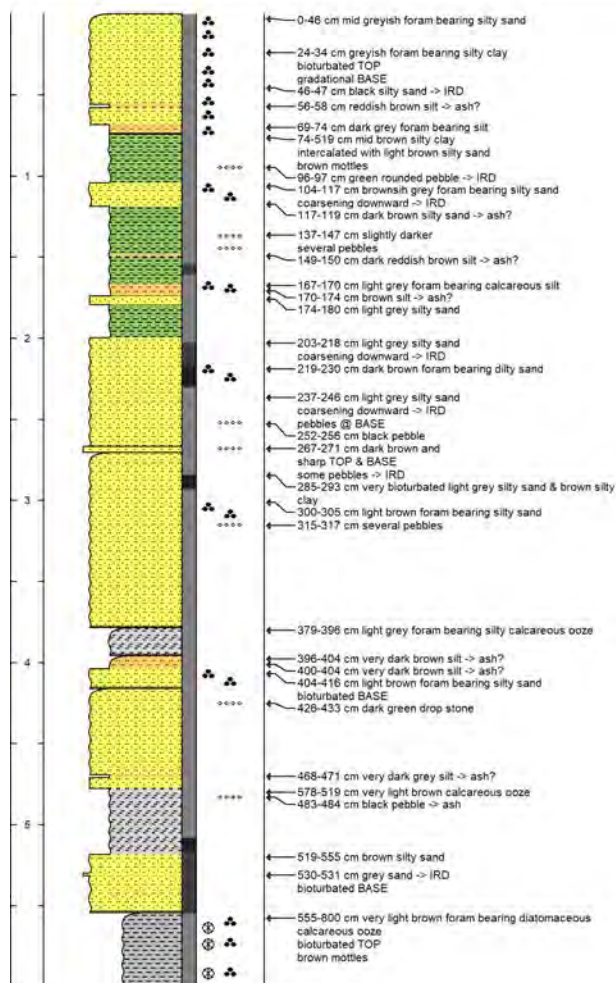
Appendix 5.6.1 Lithology logs

SO264-52-2

Date Logged: Aug 7, 2018

Logged by: T. Ronge

Remarks: 47°07,273'N 169°09,874'E 2752 mbsl



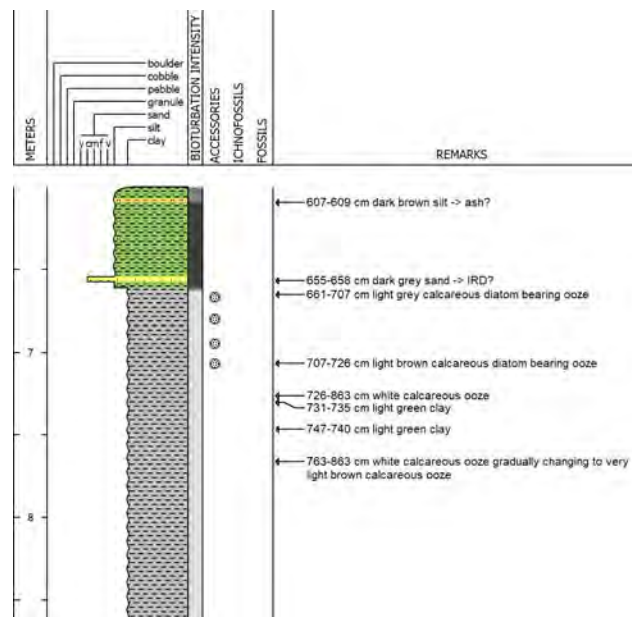
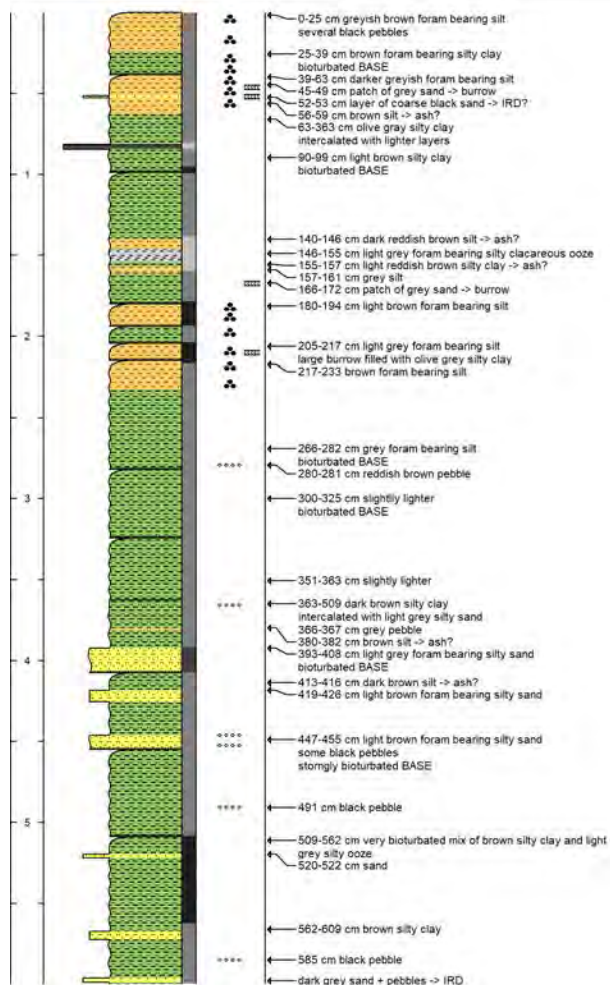
Appendix 5.6.1 Lithology logs

SO264-53-2

Date Logged: Aug 7, 2018

Logged by: T. Ronge

Remarks: 47°38,931'N 169°20,417'E 2325 mbsl



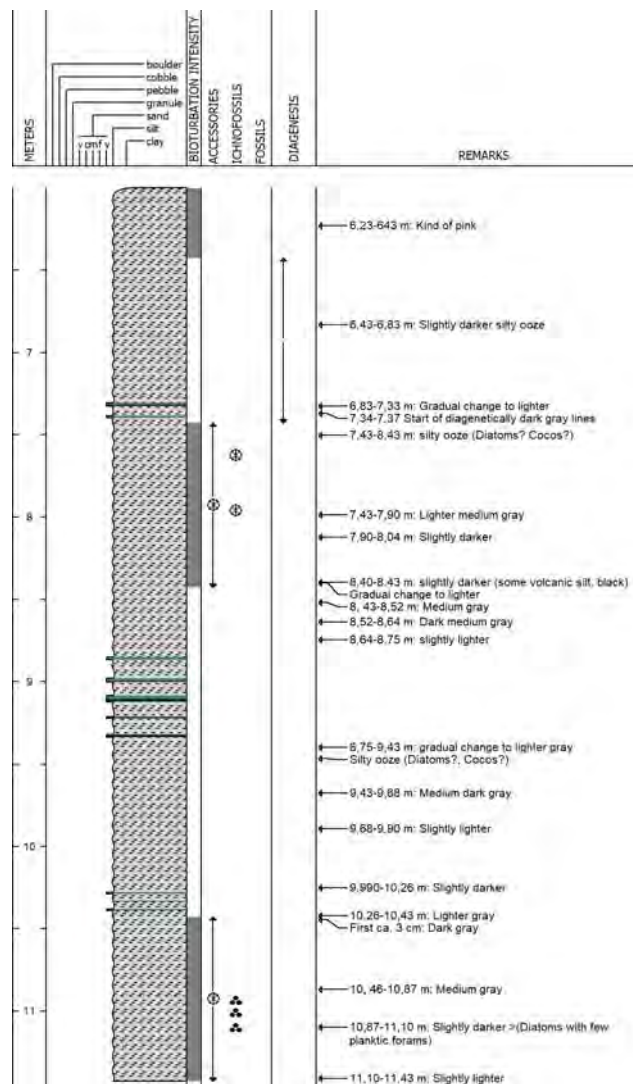
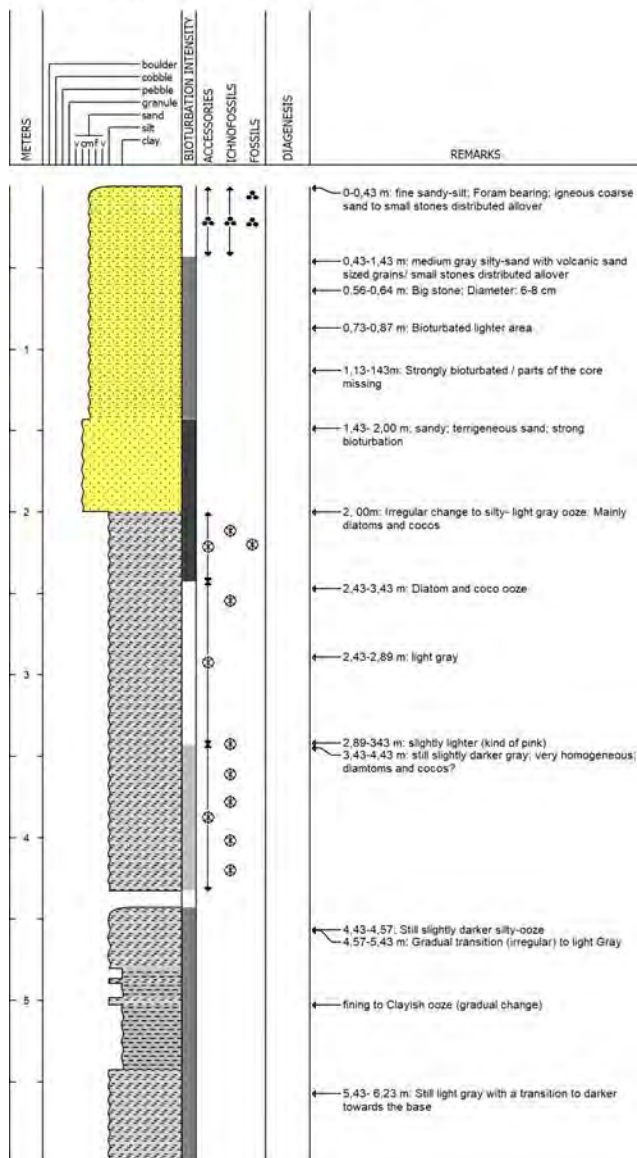
Appendix 5.6.1 Lithology logs

SO264-54-2

Date Logged: Aug 2018

Logged by: C. Karas

Remarks: 47°37,318'N 169°14,852'E 2139 mbsl



SO264 Cruise Report

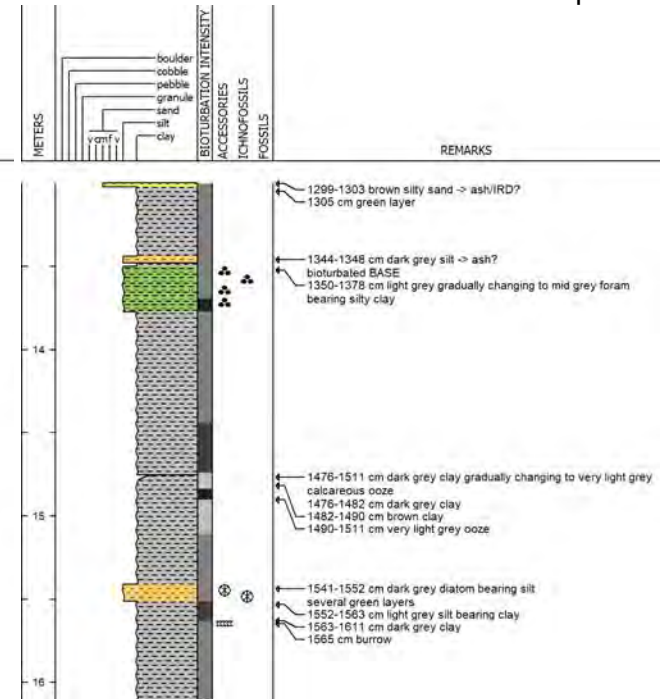
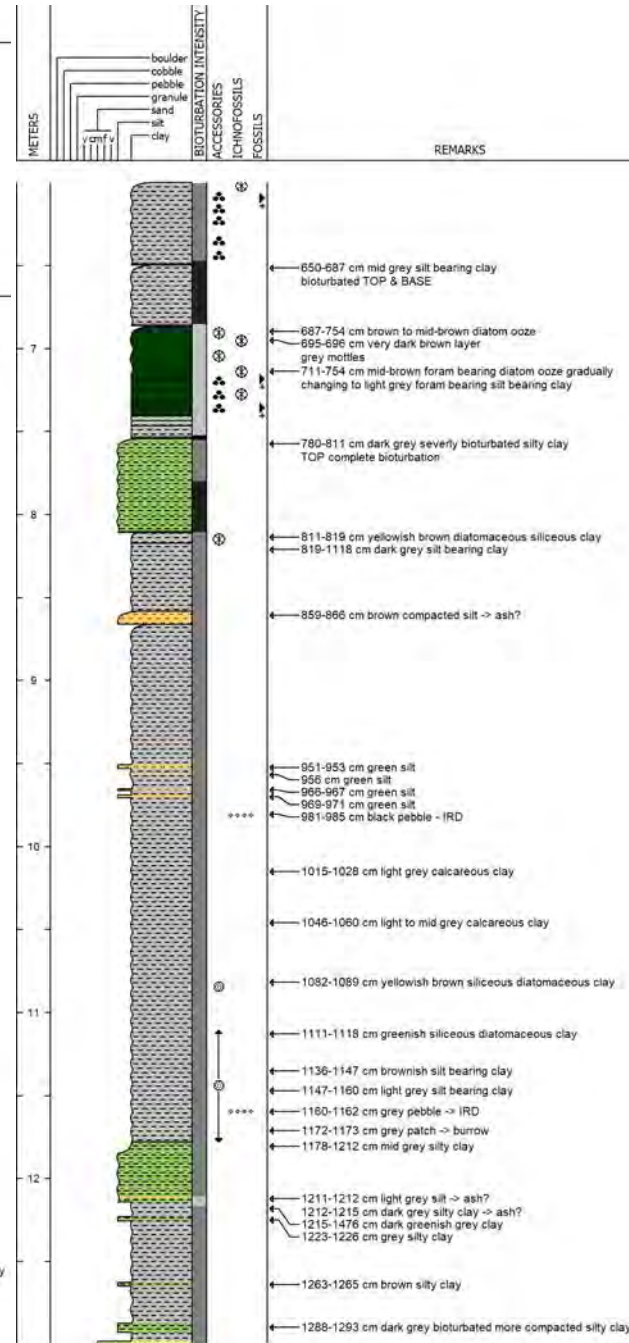
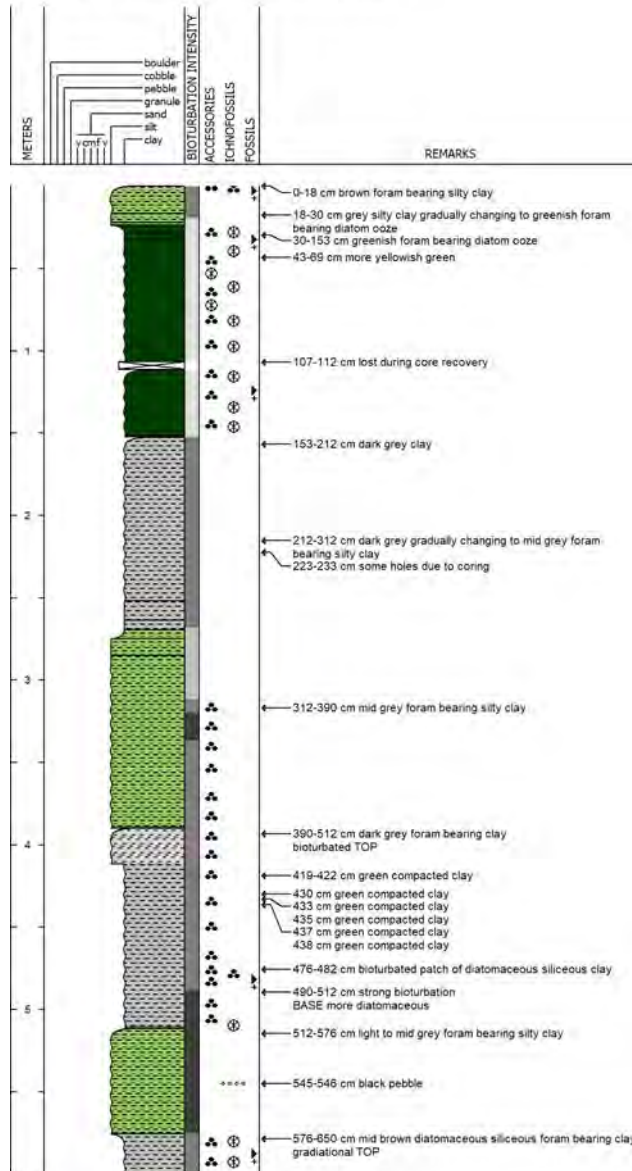
Appendix 5.6.1 Lithology logs

SO264-55-1

Date Logged: Aug 7, 2018

Logged by: T. Ronge

Remarks: 47°10,542'N 169°25,292'E 2936 mbsl



SO264 Cruise Report

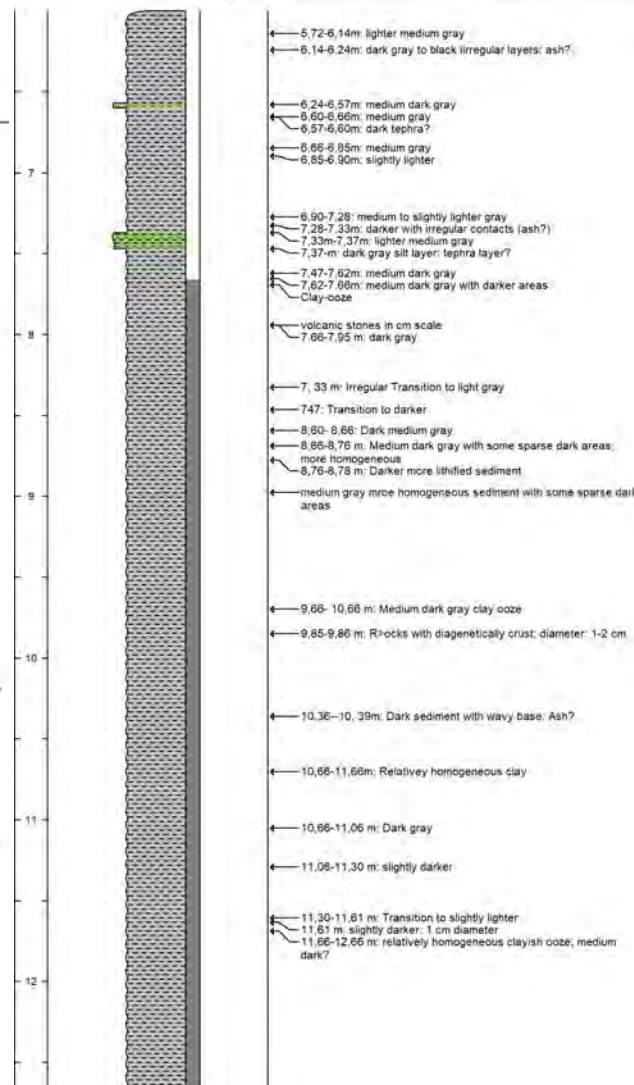
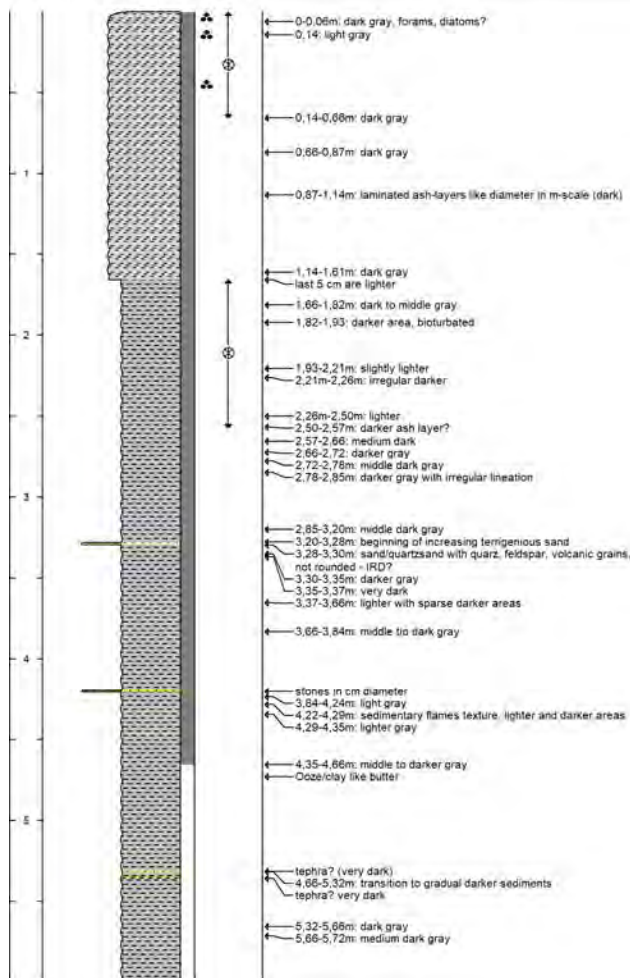
Appendix 5.6.1 Lithology logs

S0264-56-2

Date Logged: Aug 2018

Logged by: C. Karas

Remarks: 47°44,752'N 168°40,398'E 3973 mbsl



SO264 Cruise Report

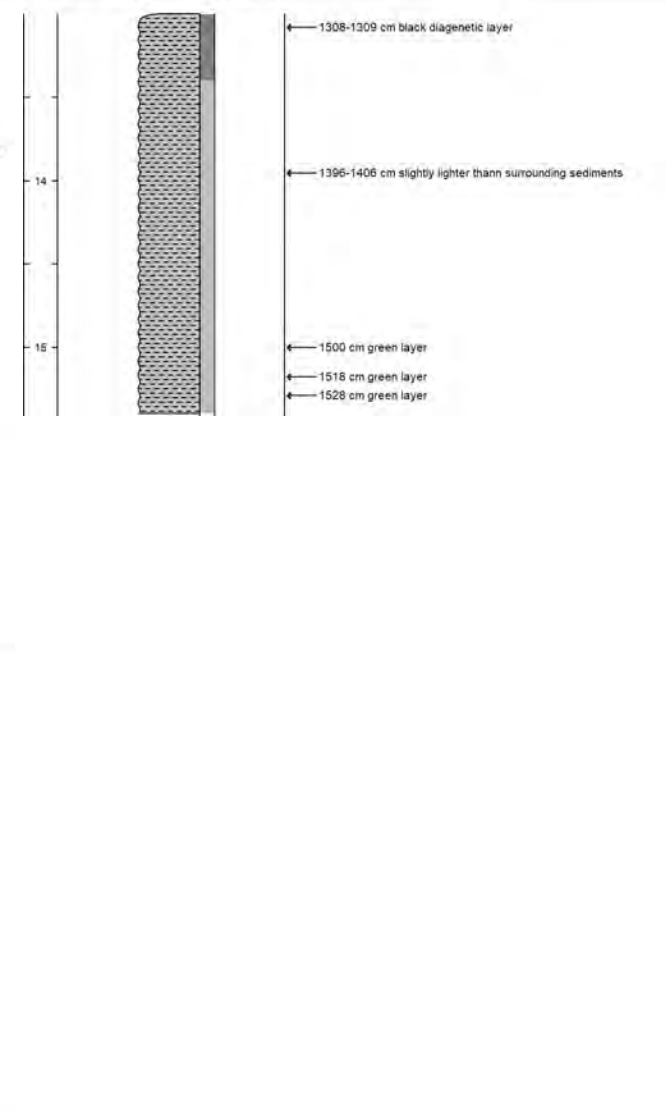
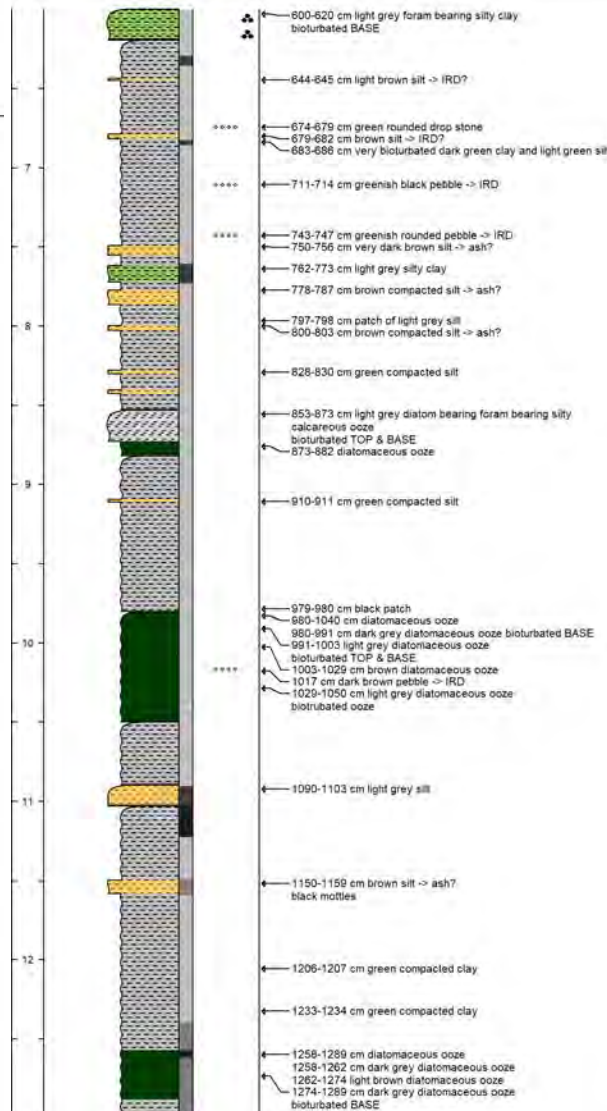
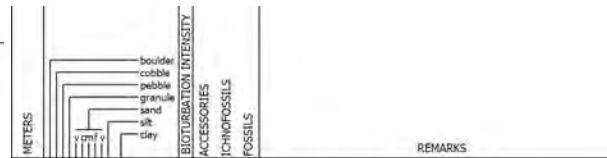
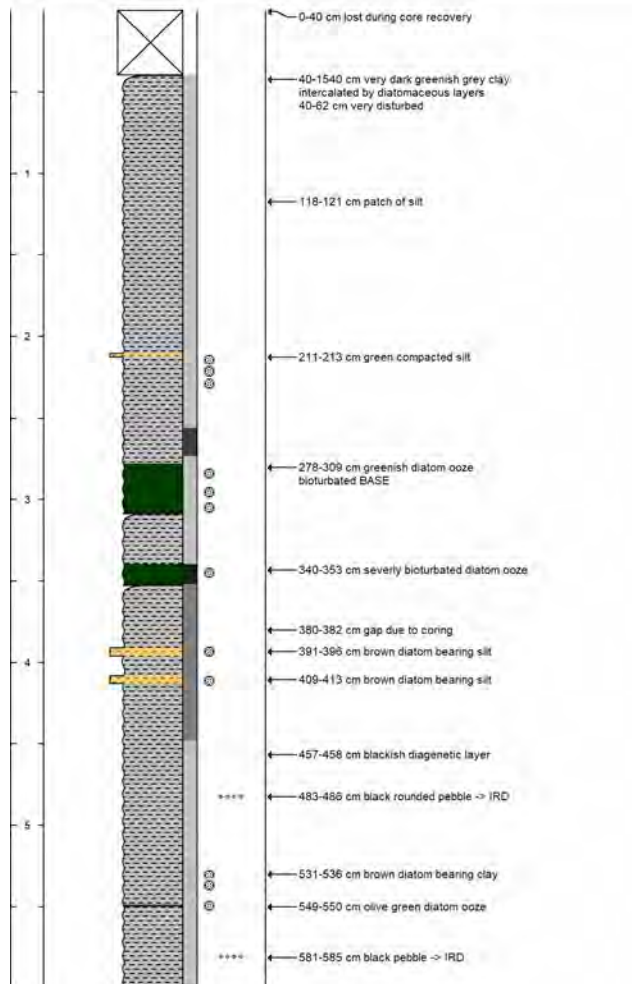
Appendix 5.6.1 Lithology logs

SO264-57-2

Date Logged: Aug 8, 2018

Logged by: T. Ronge

Remarks: 48°50,814'N 168°29,003'E 2356 mbsl



SO264 Cruise Report

Appendix 5.6.1 Lithology logs

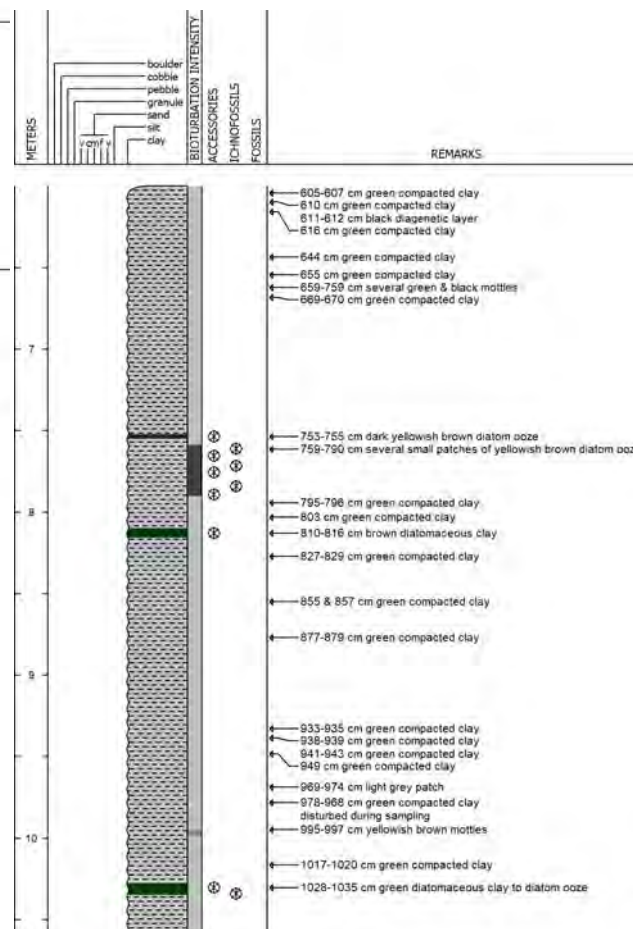
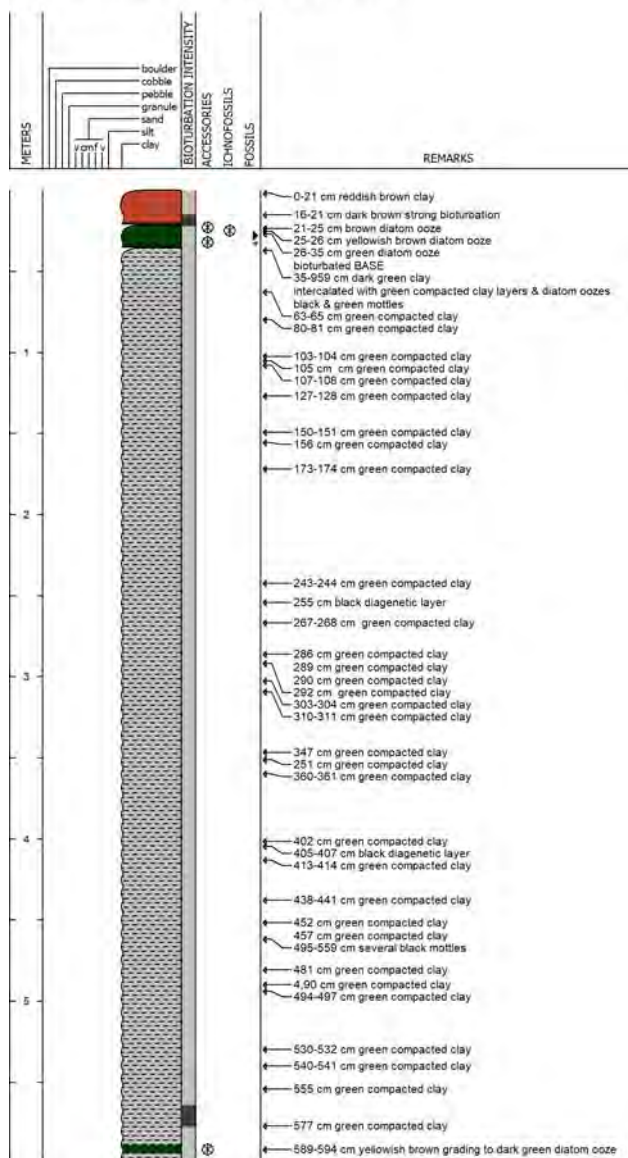
SO264 Cruise Report

SO264-60-12

Date Logged: Aug 10, 2018

Logged by: T. Ronge

Remarks: 49°18,447'N 168°33,427'E 5275 mbsl



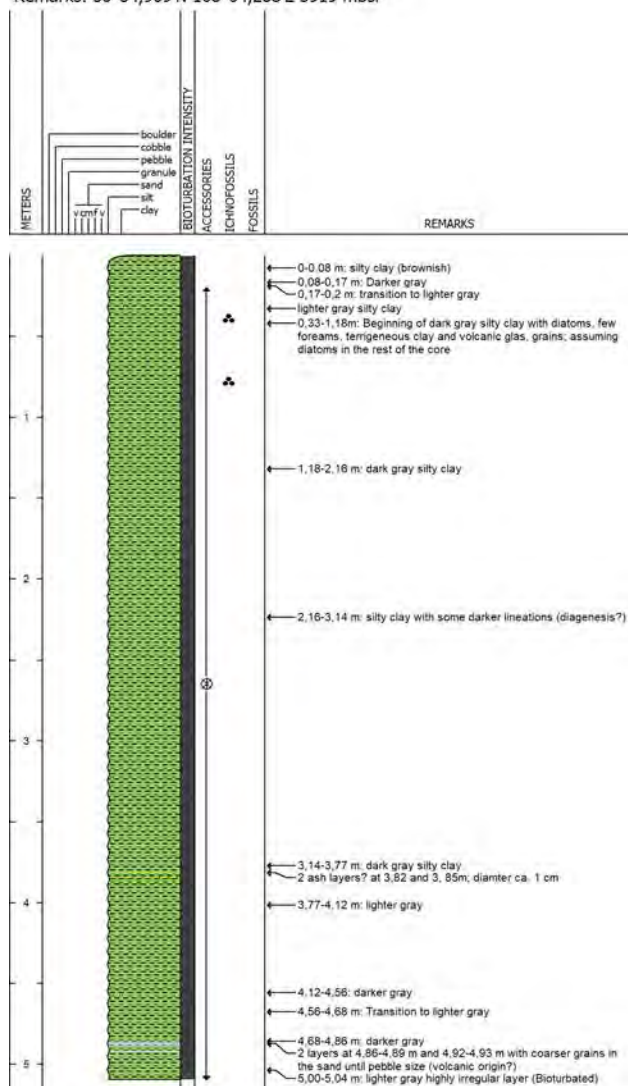
Appendix 5.6.1 Lithology logs

SO264-75-1(BC)

Date Logged: Aug 2018

Logged by: C. Karas

Remarks: 50°34,909'N 168°04,288'E 3919 mbsl

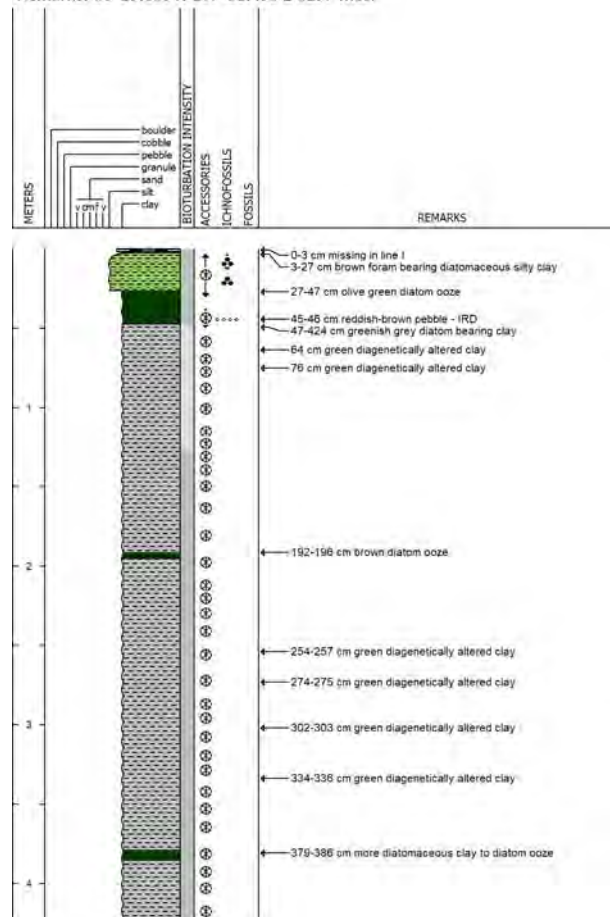


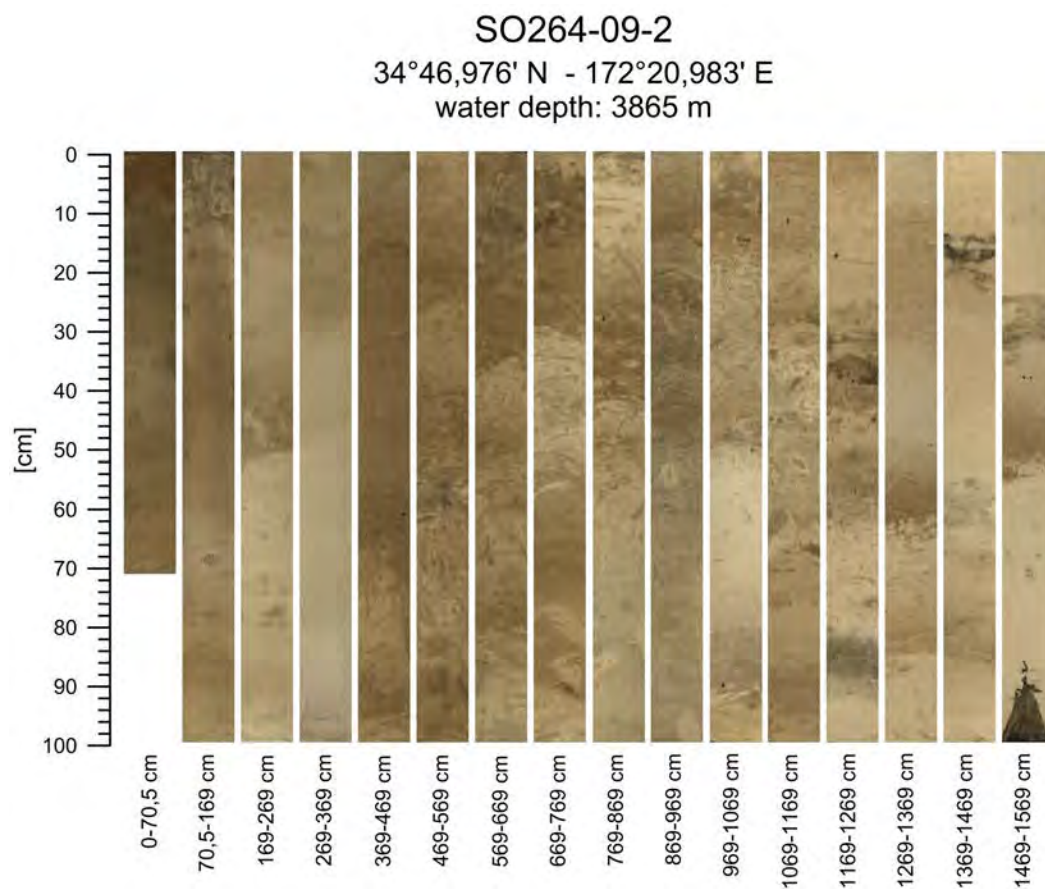
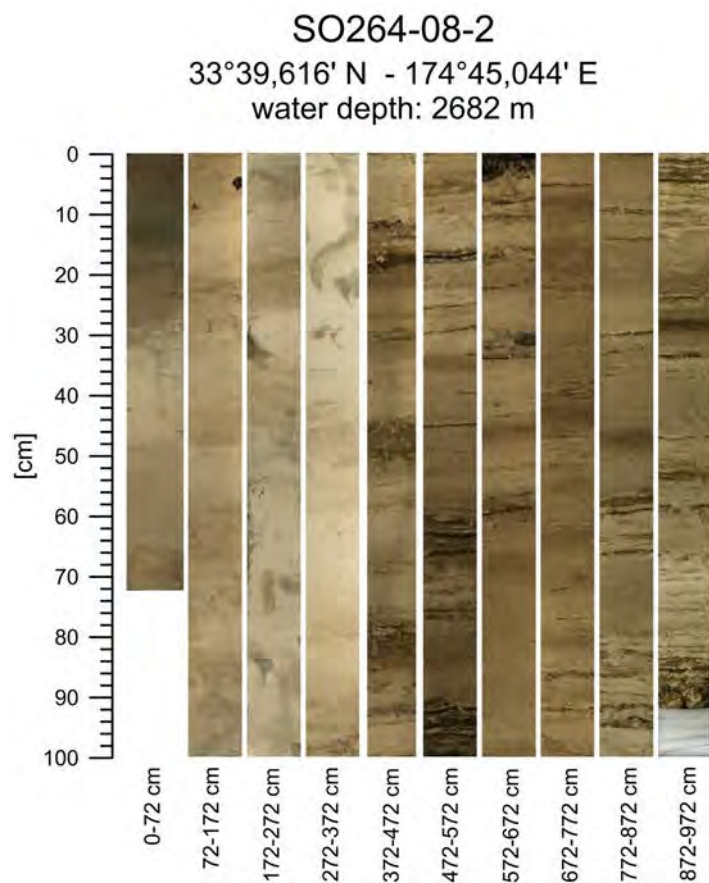
SO264-76-1(BC) Line I

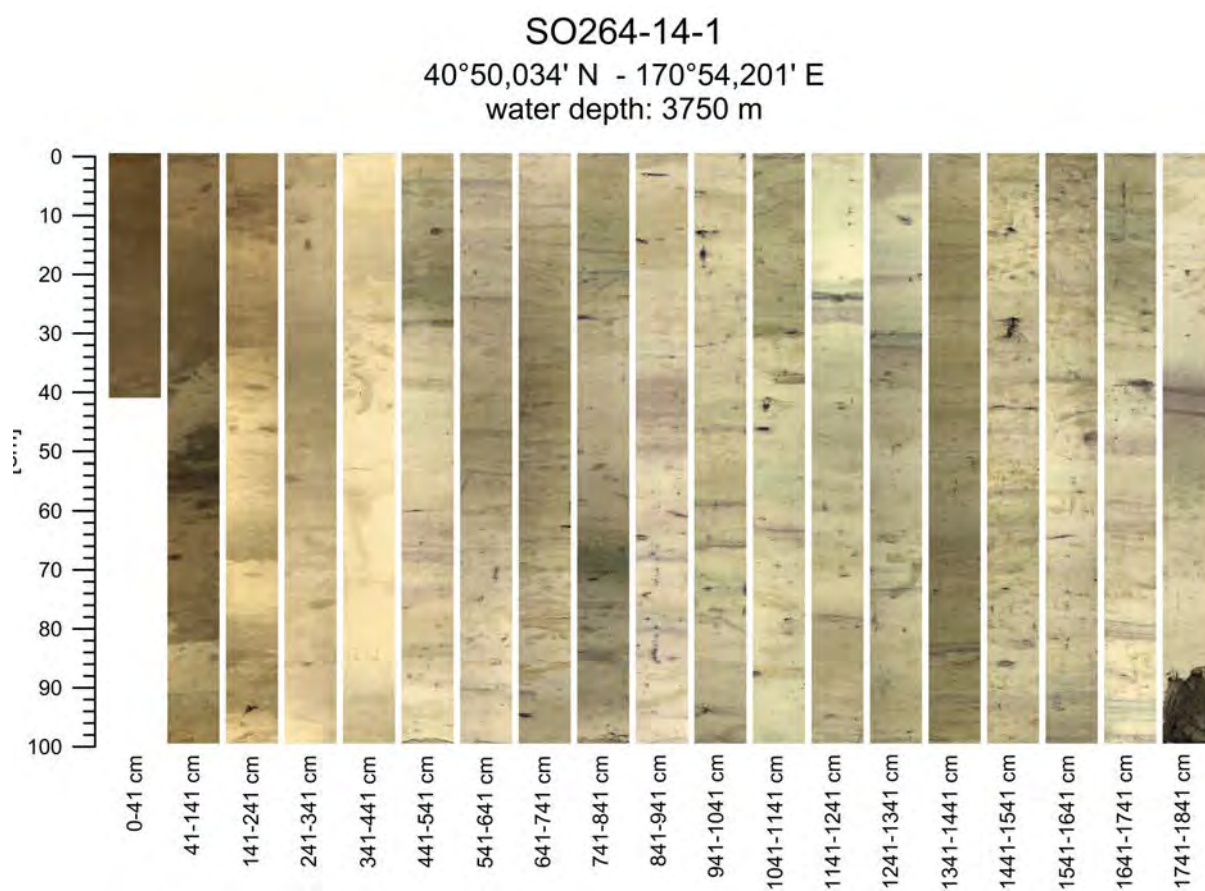
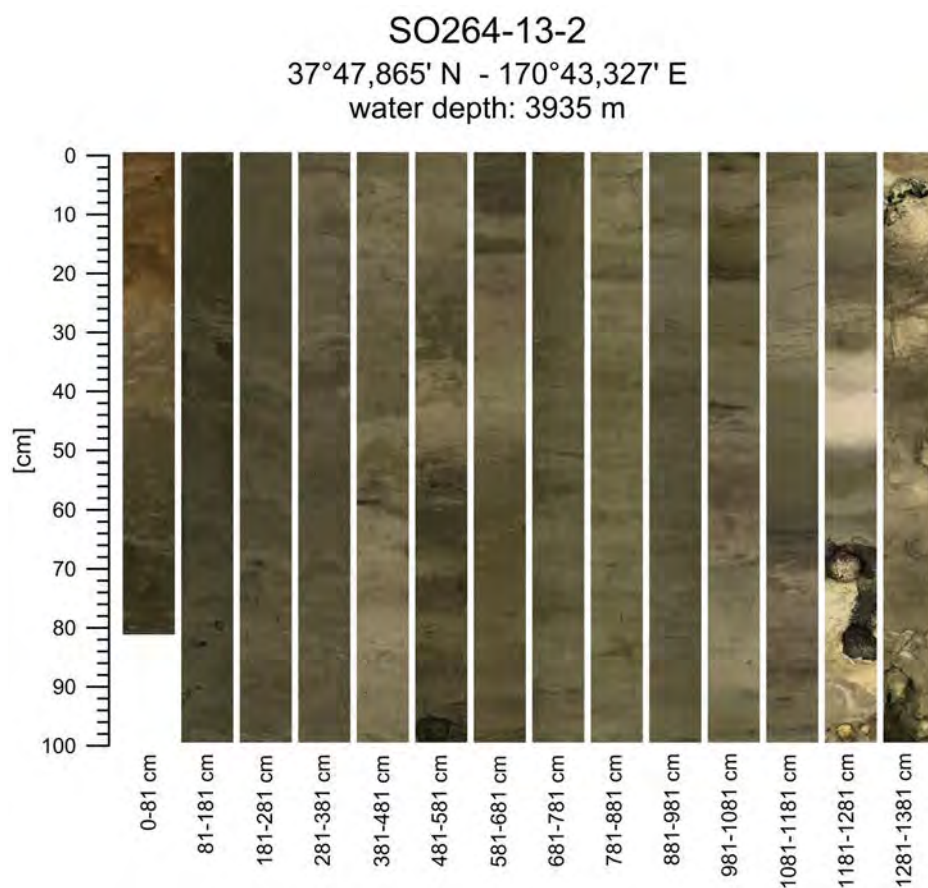
Date Logged: Aug 16, 2018

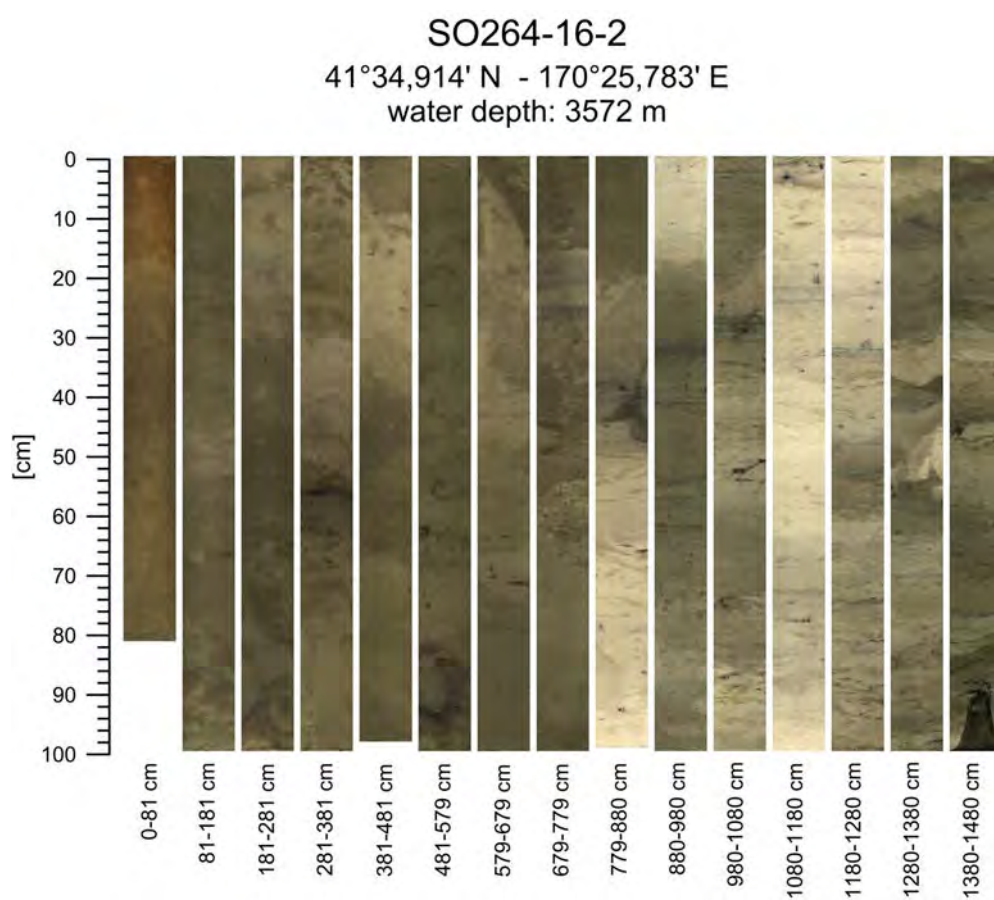
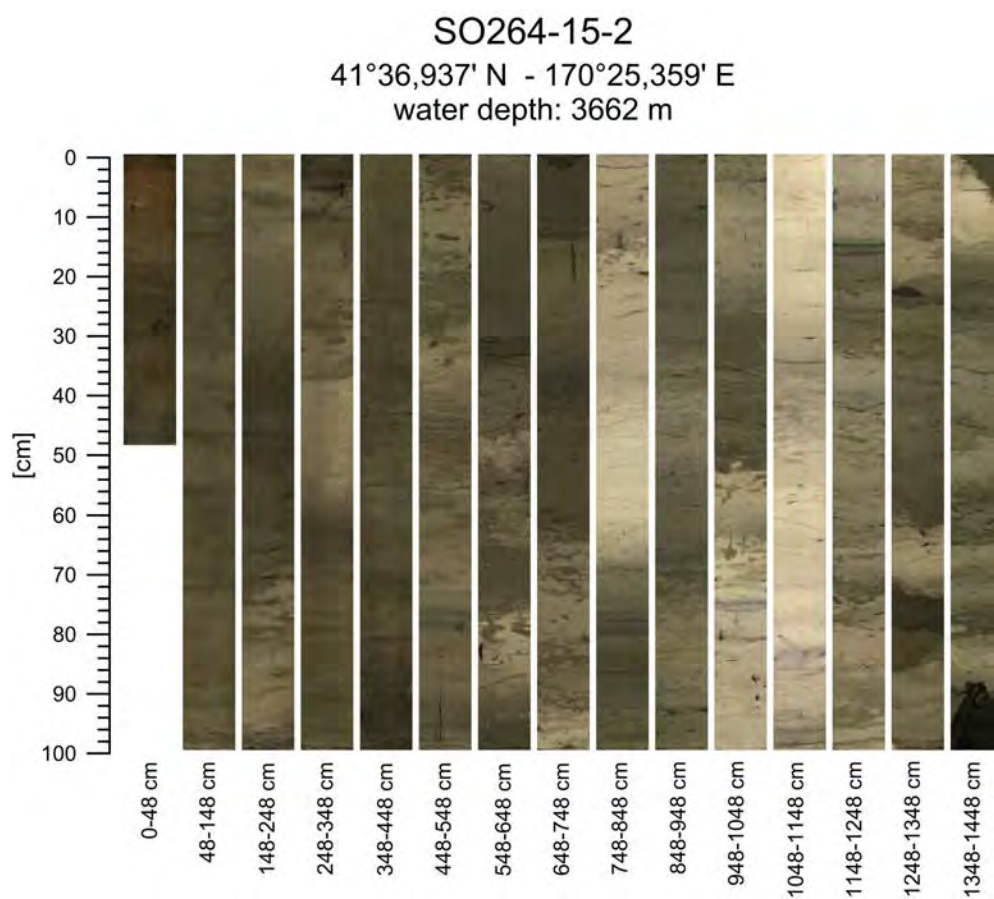
Logged by: T. Ronge

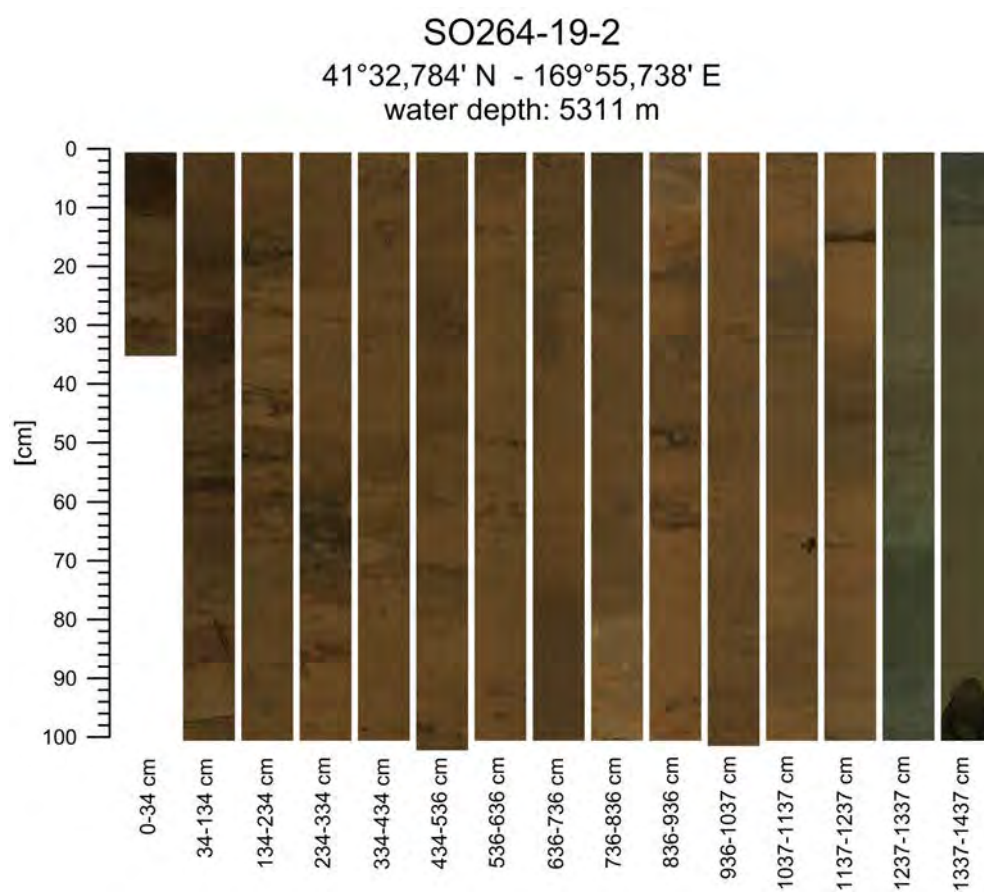
Remarks: 50°29.039'N 167°51.493'E 3297 mbsl



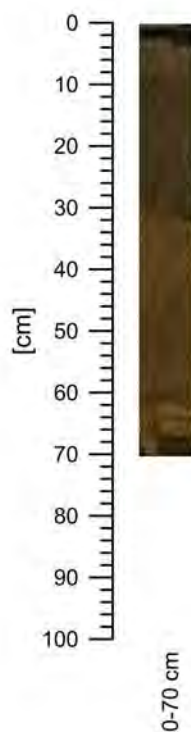


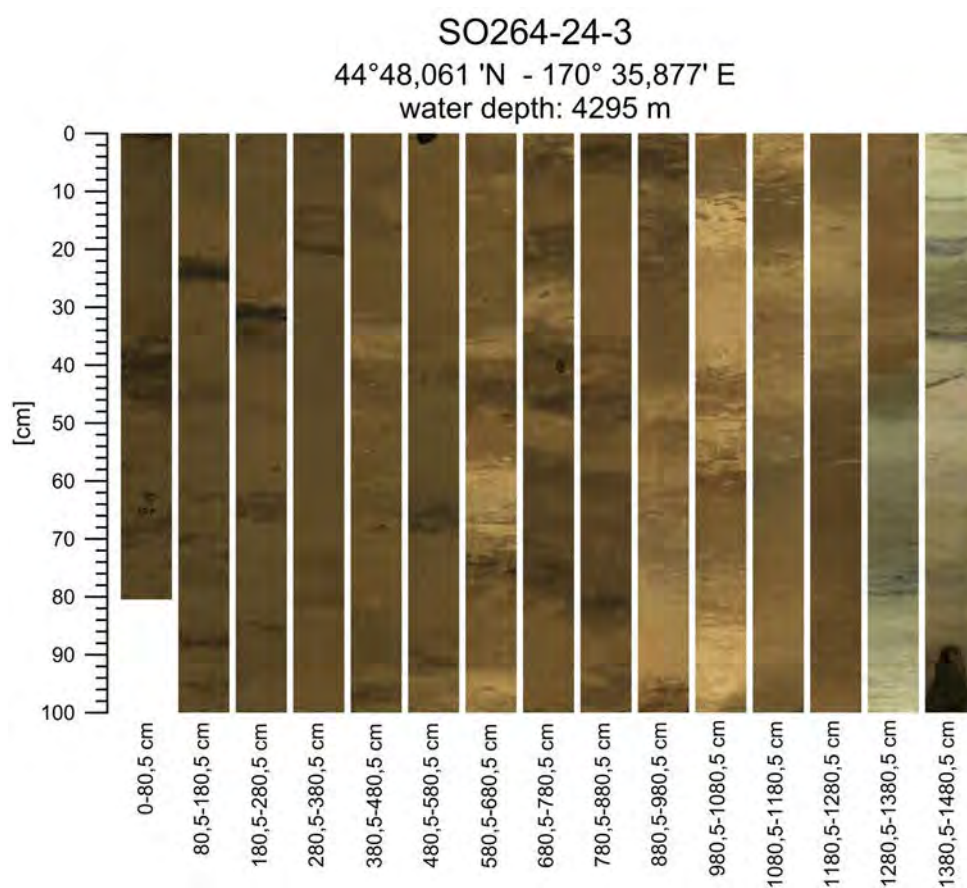
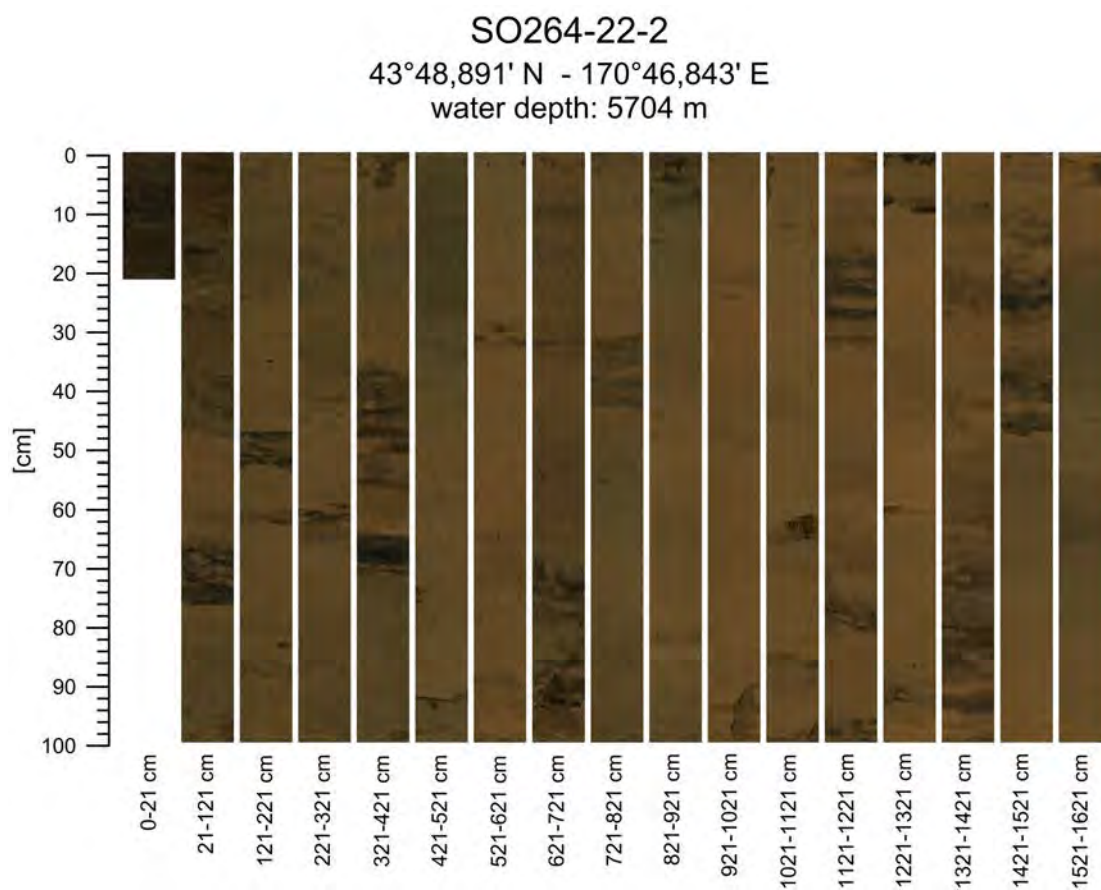


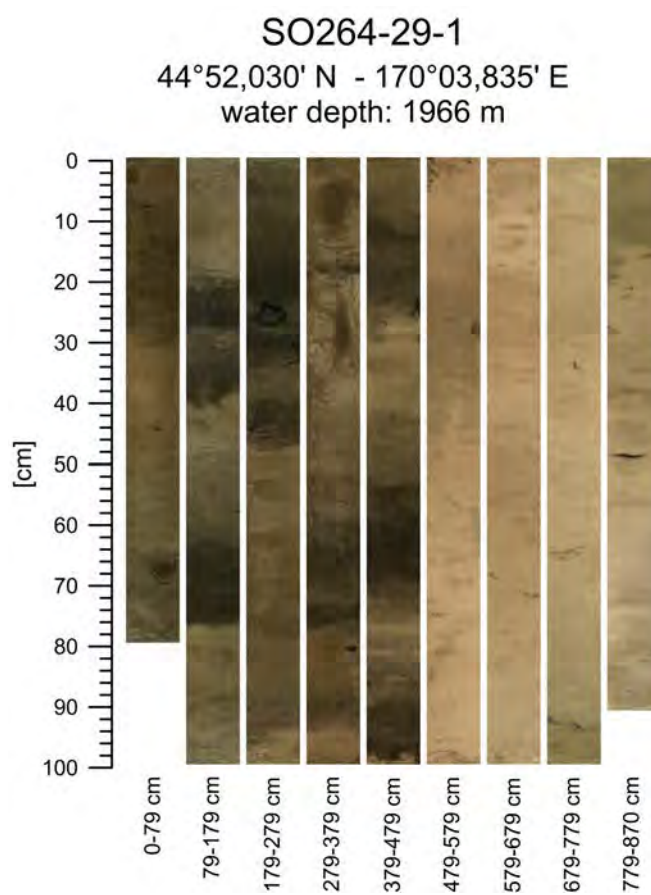
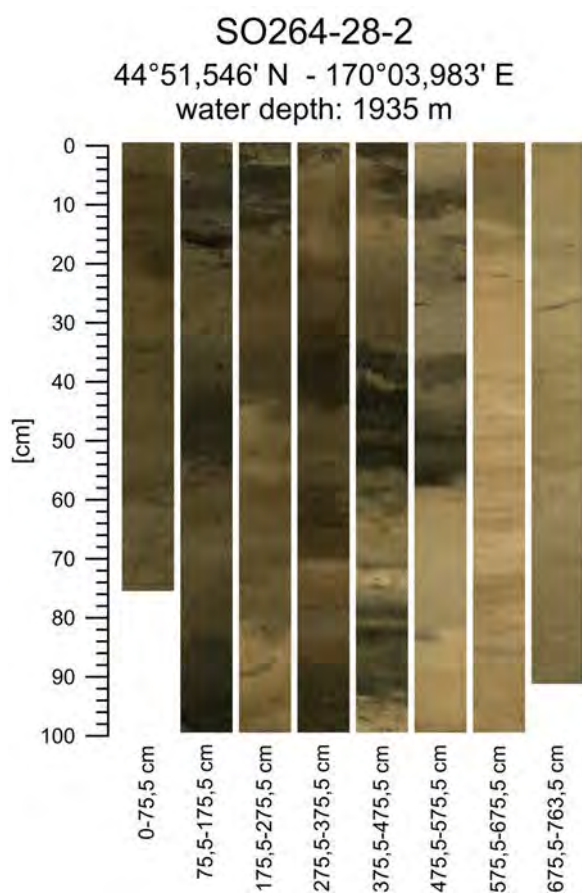
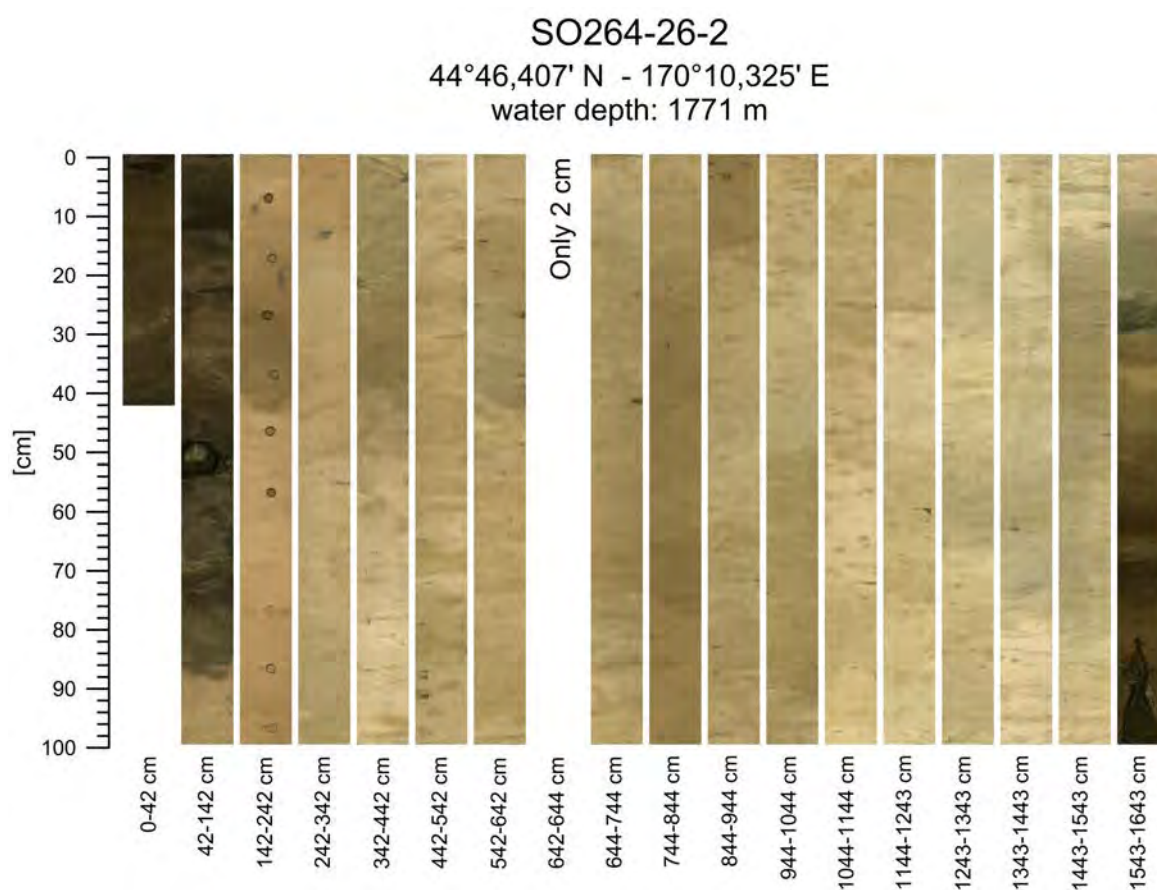


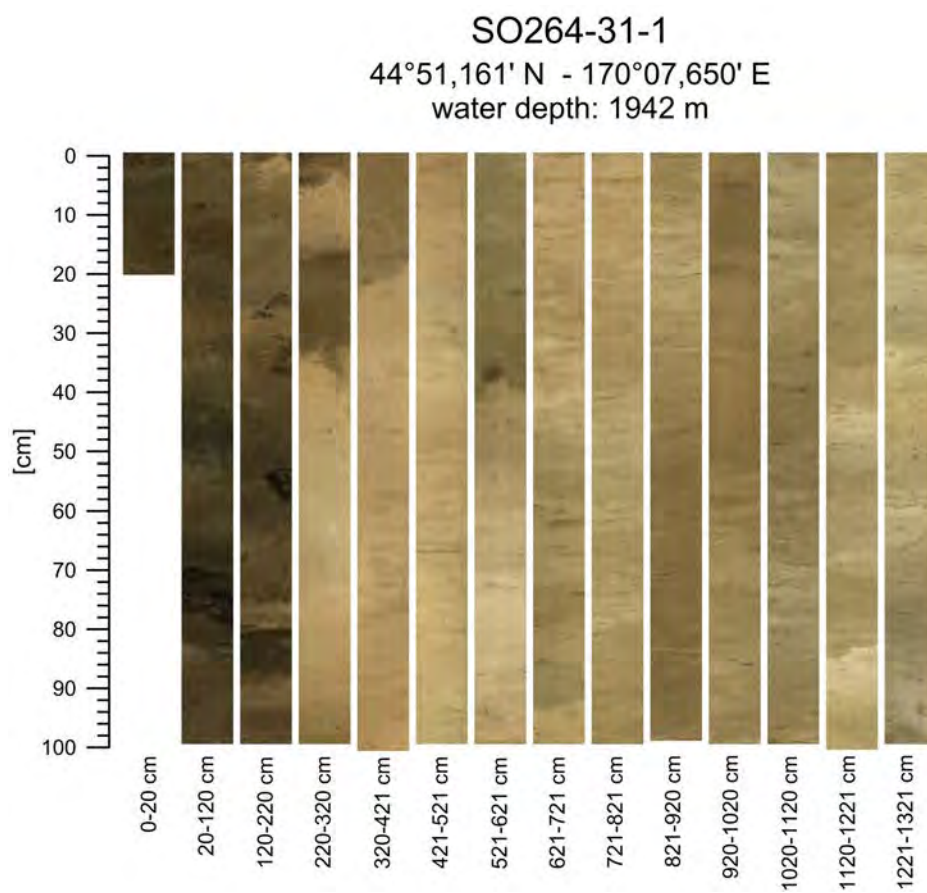
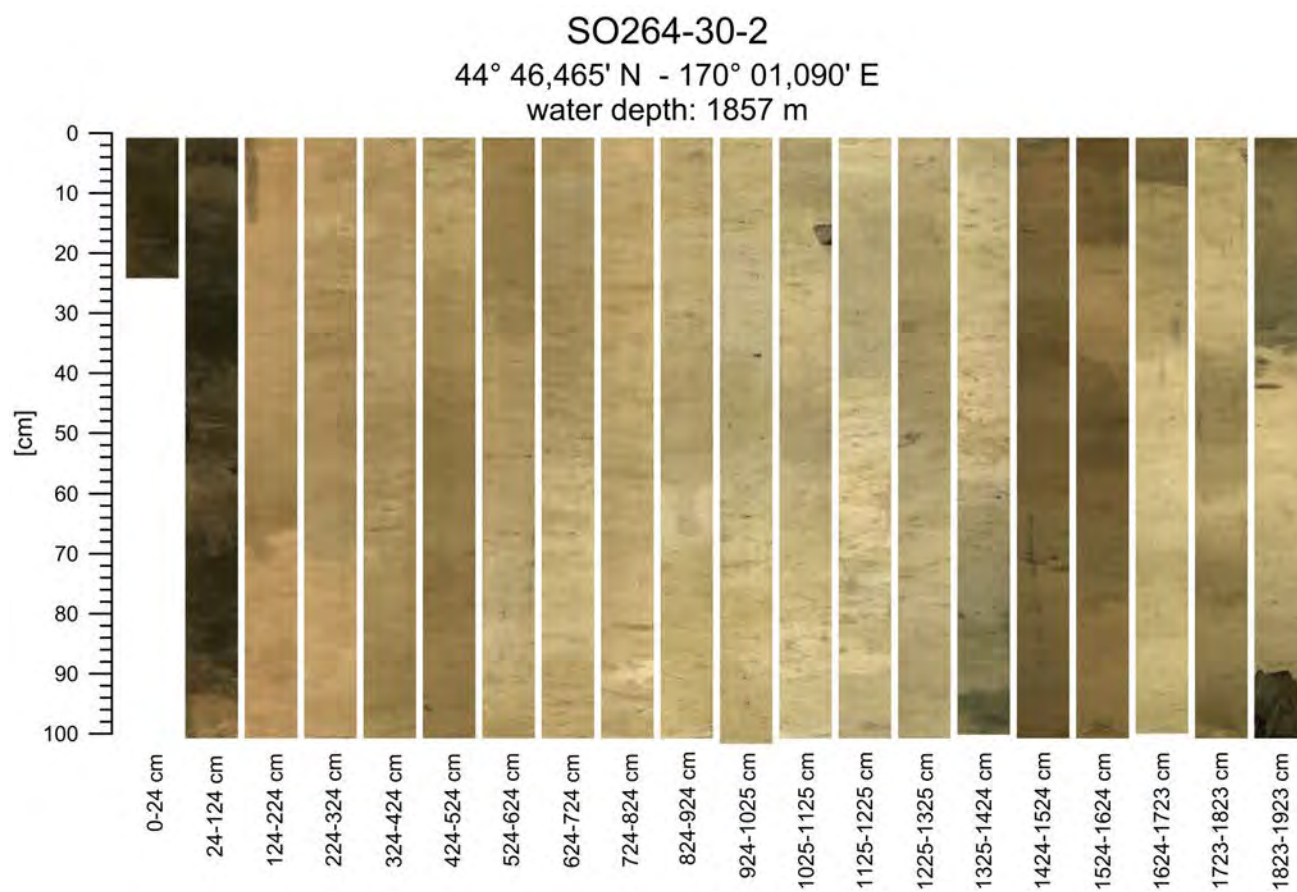


SO264-20-1
41°20,030' N - 170°22,734' E
water depth: 1308 m





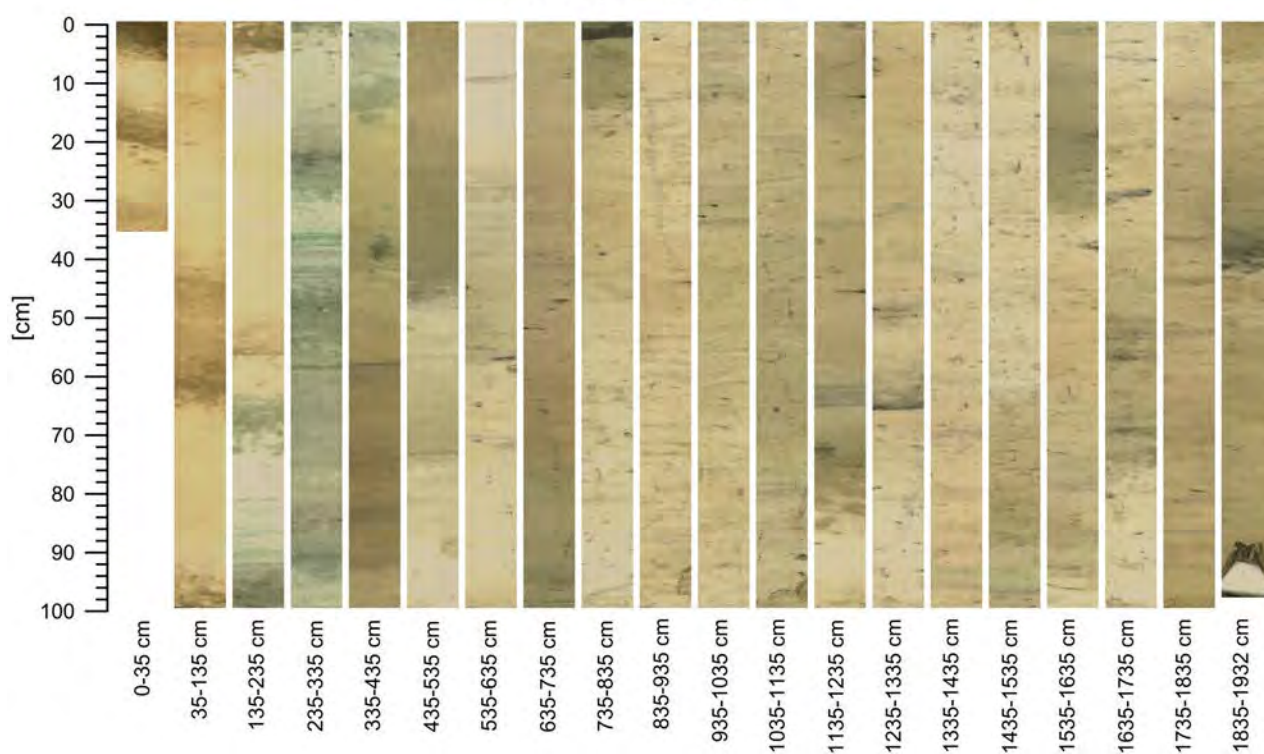




SO264-32-2

44°59,780' N - 170°24,280' E

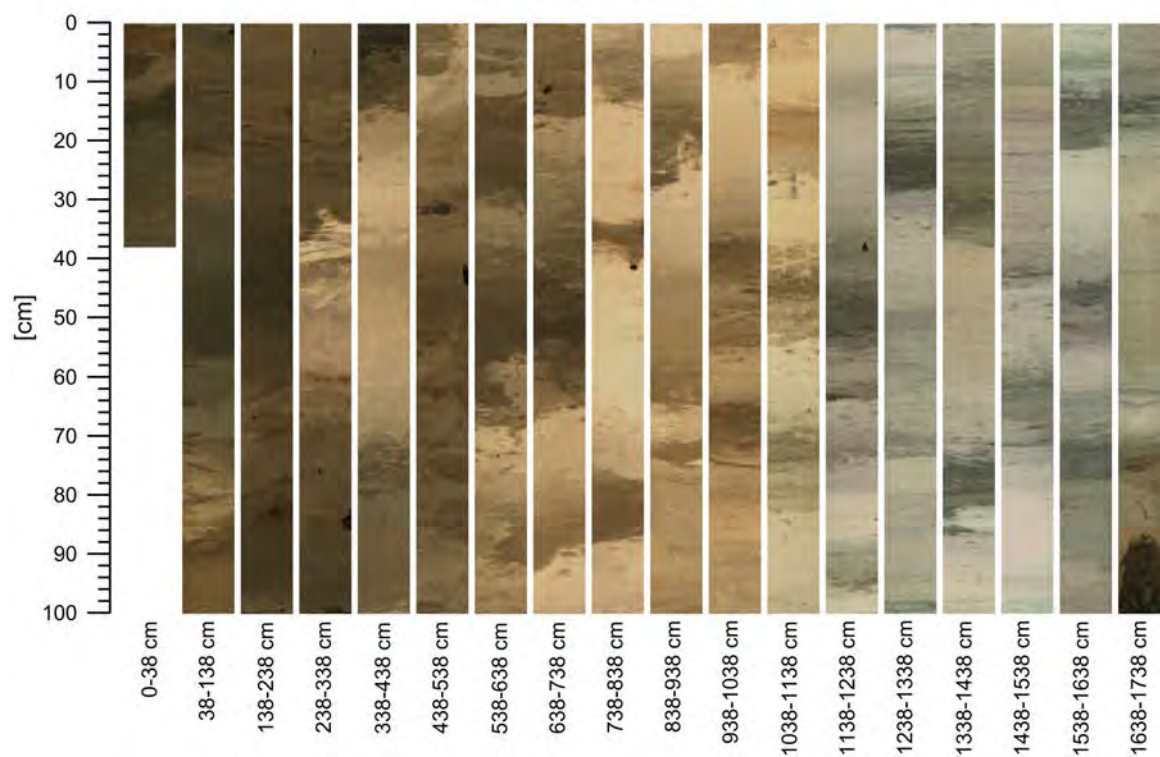
water depth: 3200 m



SO264-33-2

44°58,291' N - 170°21,023' E

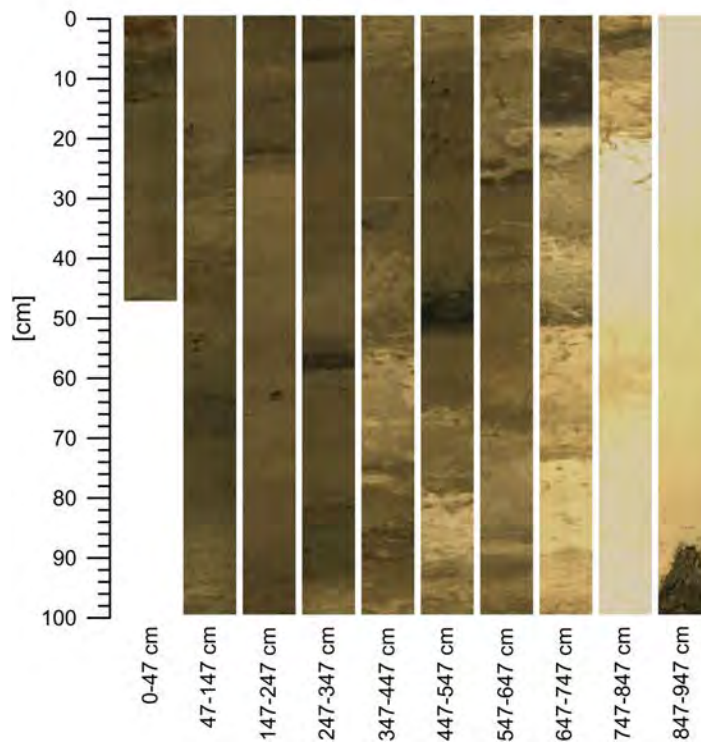
water depth: 3141 m



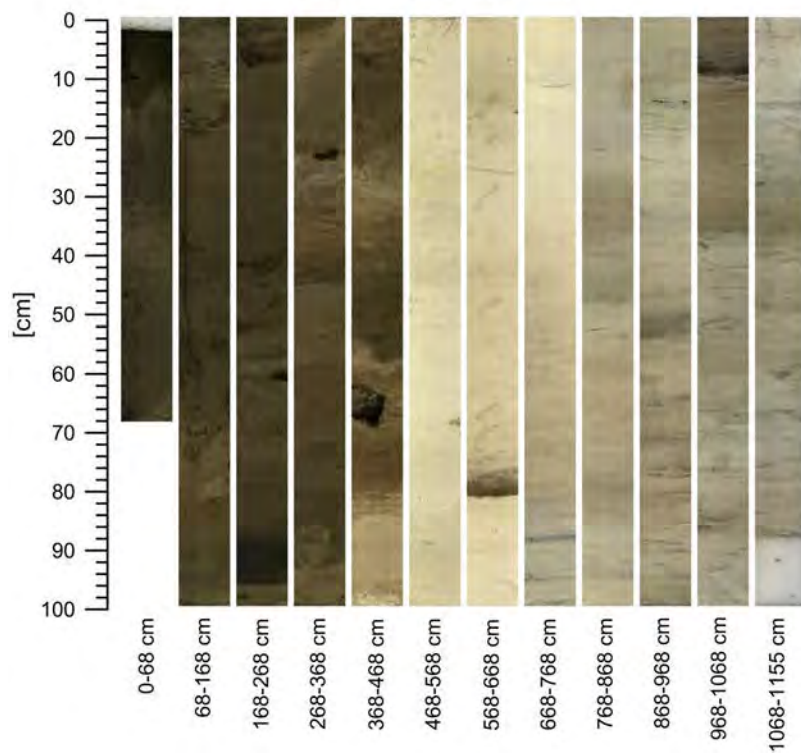
SO264-34-2
45°01,852' N - 170°13,533' E
water depth: 2622 m



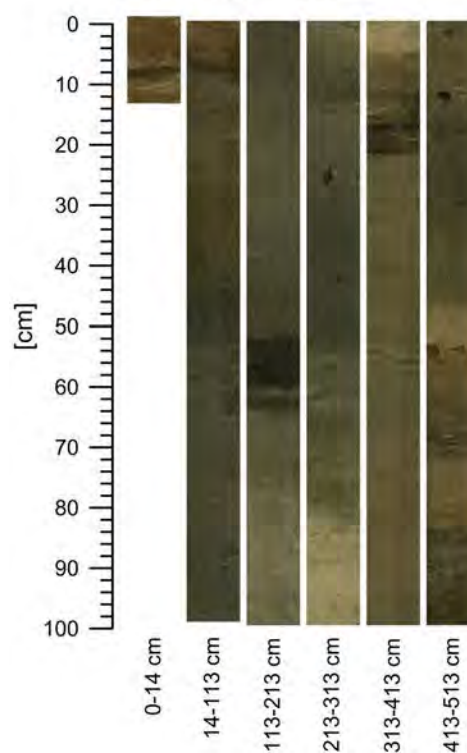
SO264-41-2
45°41,948' N - 170°09,300' E
water depth: 3645 m



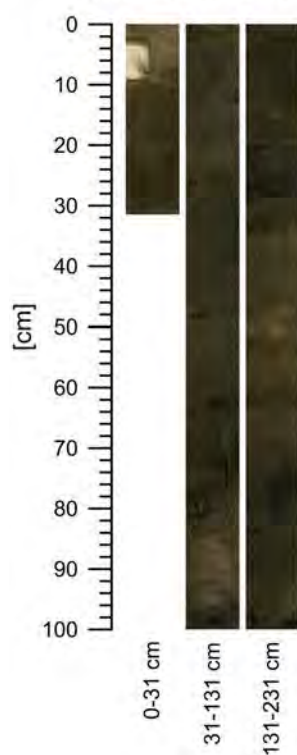
SO264-42-2
46°10,141' N - 169°10,080' E
water depth: 3021 m



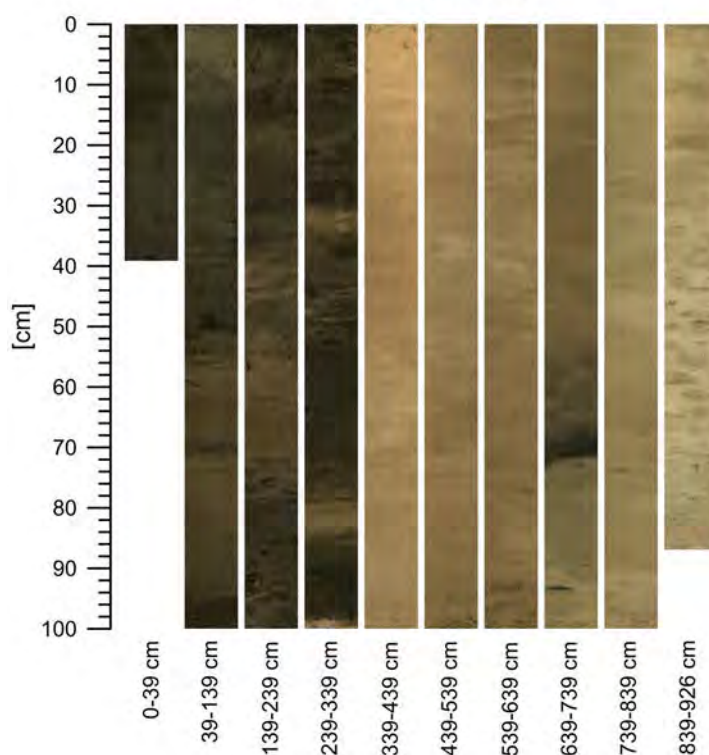
SO264-43-2
46°06,576' N - 169°07,193' E
water depth: 3239 m



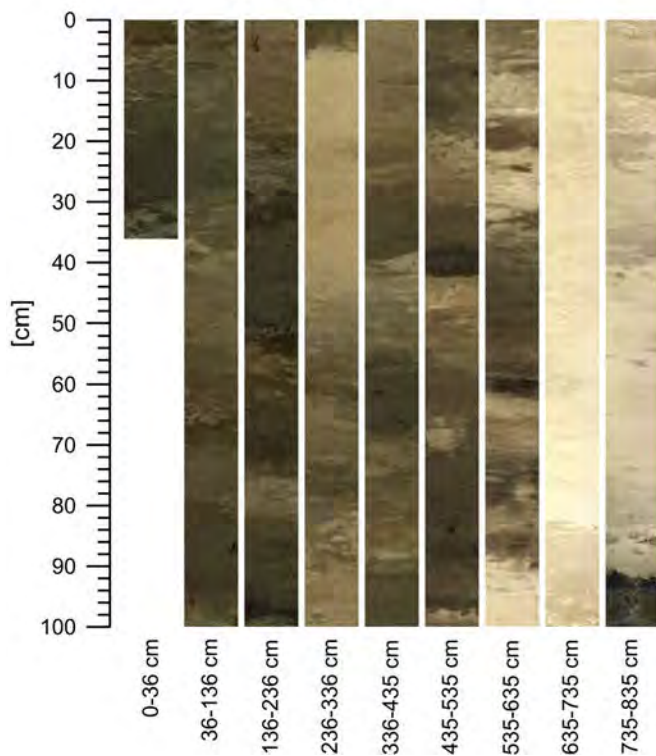
SO264-44-2
46°15,298' N - 169°20,062' E
water depth: 1893 m



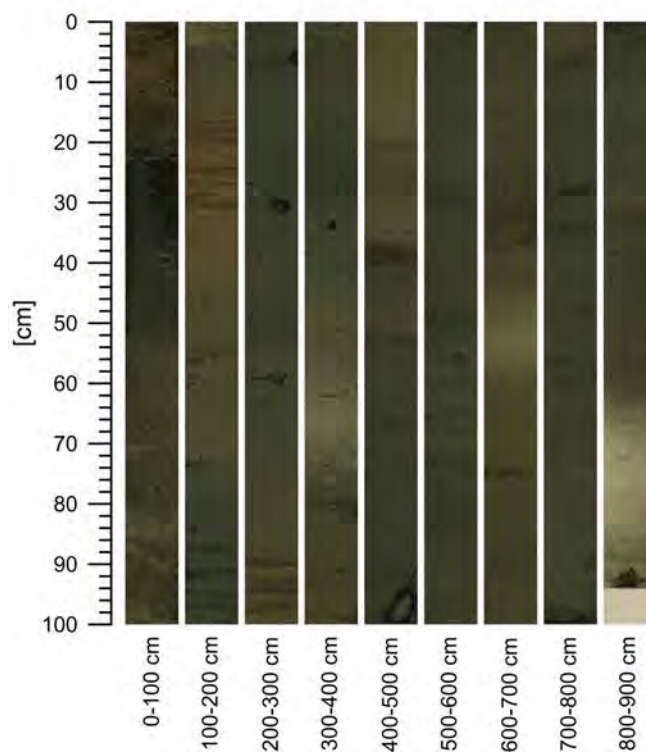
SO264-44-3
46°15,307' N - 169°20,064' E
water depth: 1894 m



SO264-45-2
46°33,792' N - 169°36,072' E
water depth: 2425 m

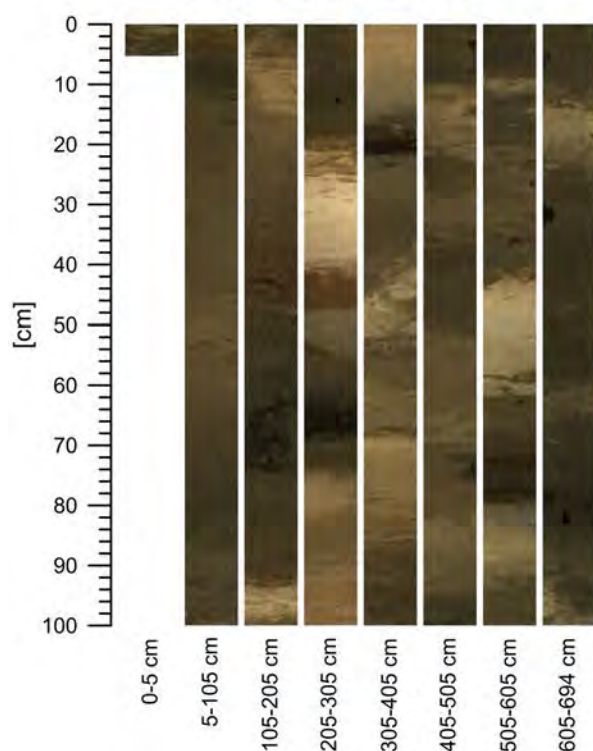


SO264-46-5
46°48,941' N - 169°24,661' E
water depth: 3992 m



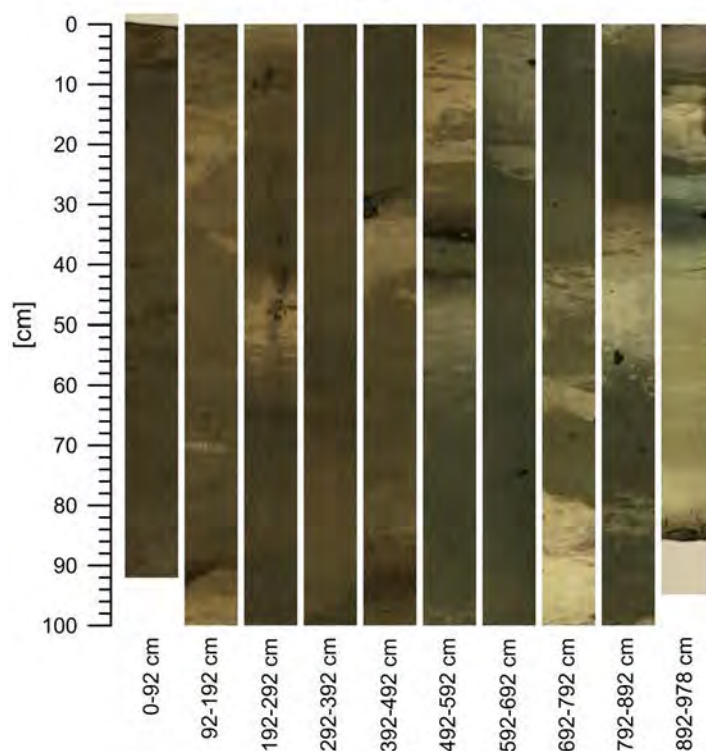
SO264-47-2

47°04,394' N - 169°21,667' E
water depth: 2647 m



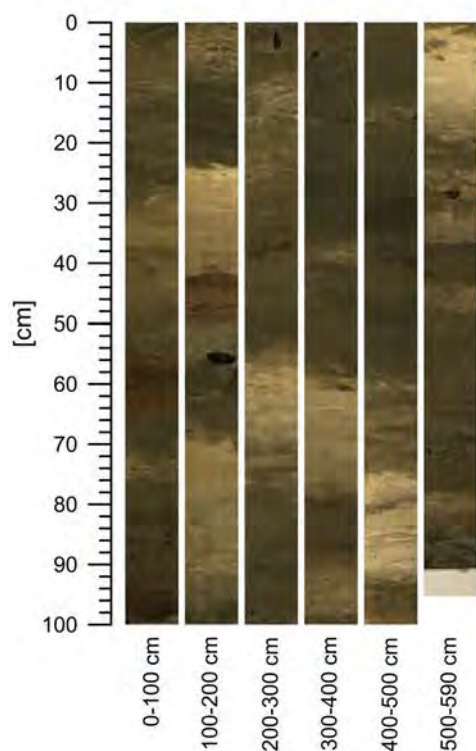
SO264-48-2

47°58,505' N - 169°03,878' E
water depth: 2872 m



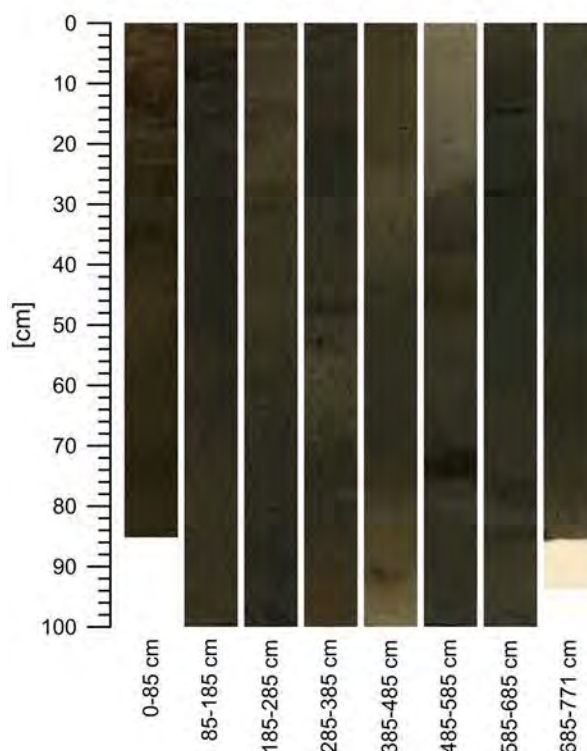
SO264-49-2

47°40,869' N - 169°01,419' E
water depth: 2400 m



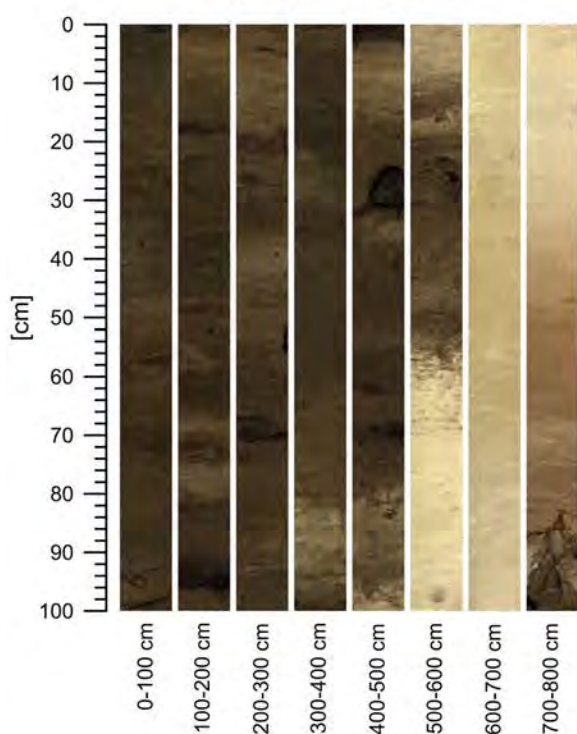
SO264-51-2

47°07,271' N - 169°09,869' E
water depth: 2752 m



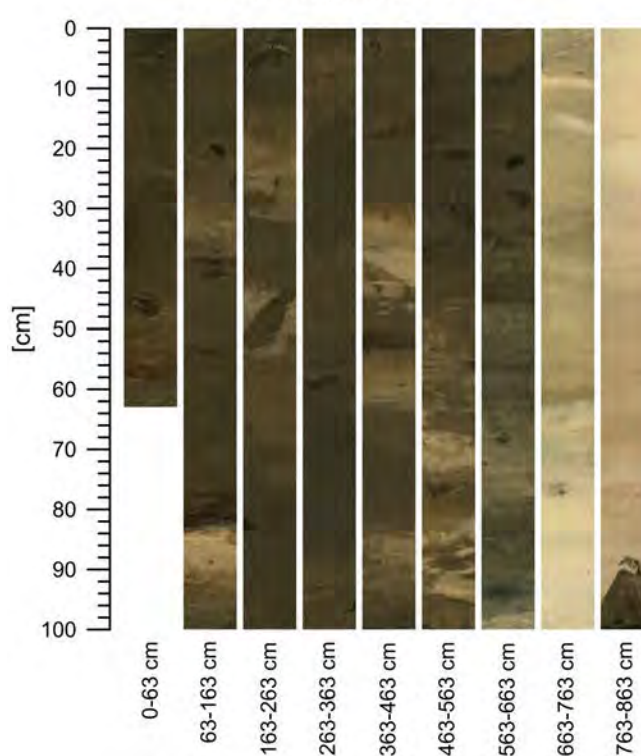
SO264-52-2

47°07,271' N - 169°09,869' E
water depth: 2752 m



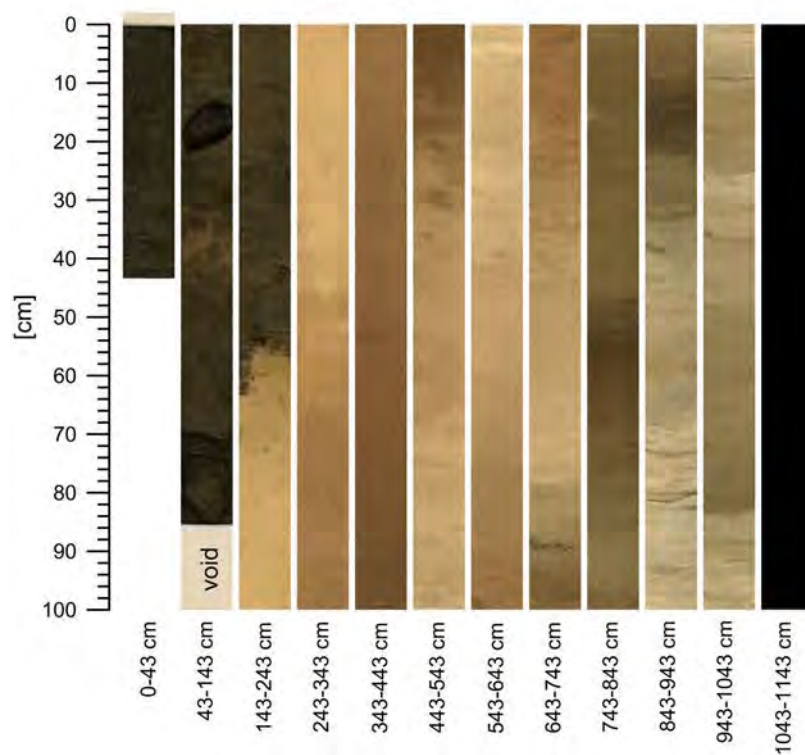
SO264-53-2

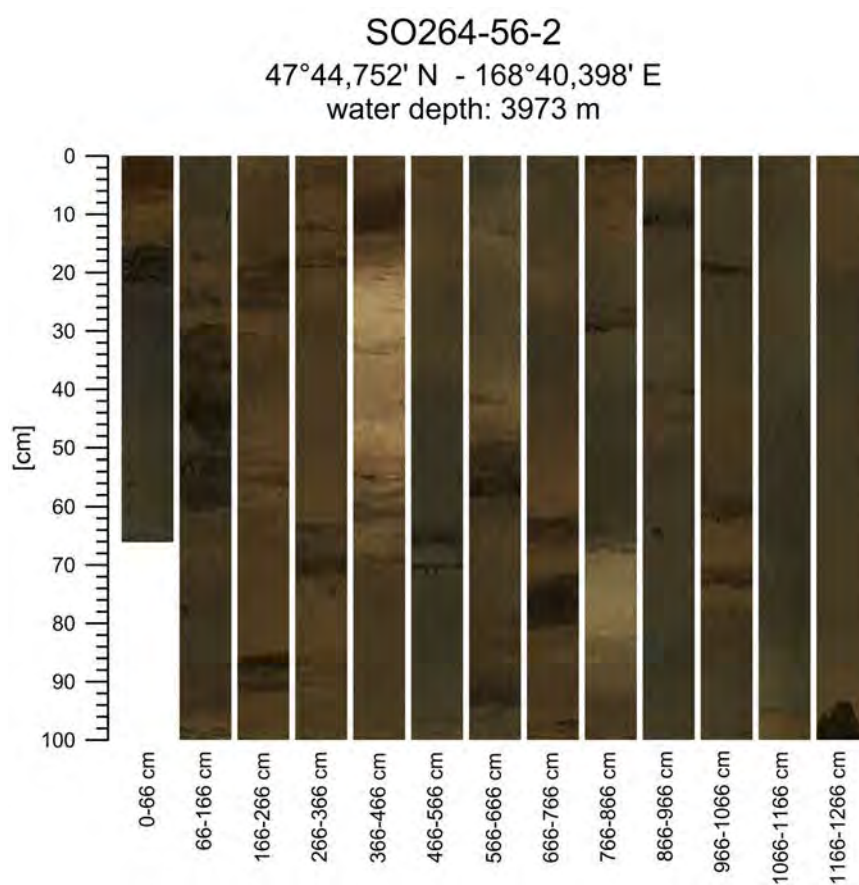
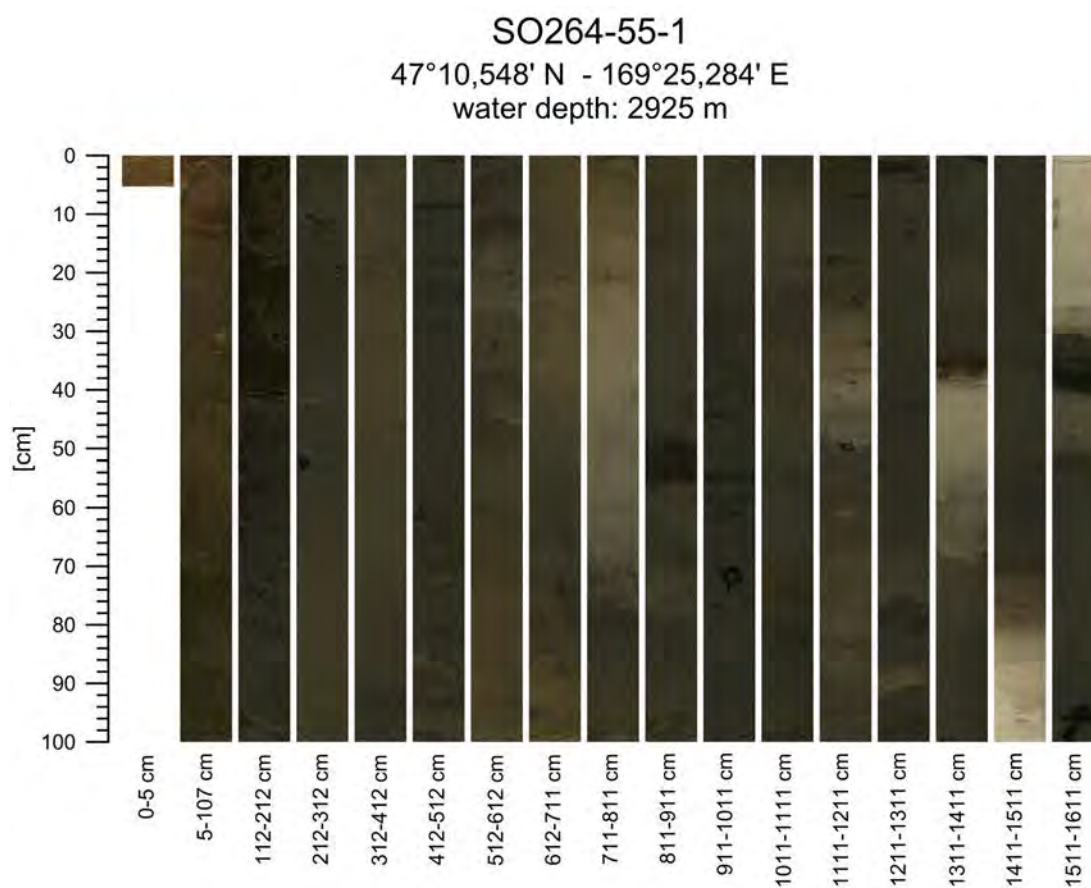
47°38,934' N - 169°20,417' E
water depth: 2325 m

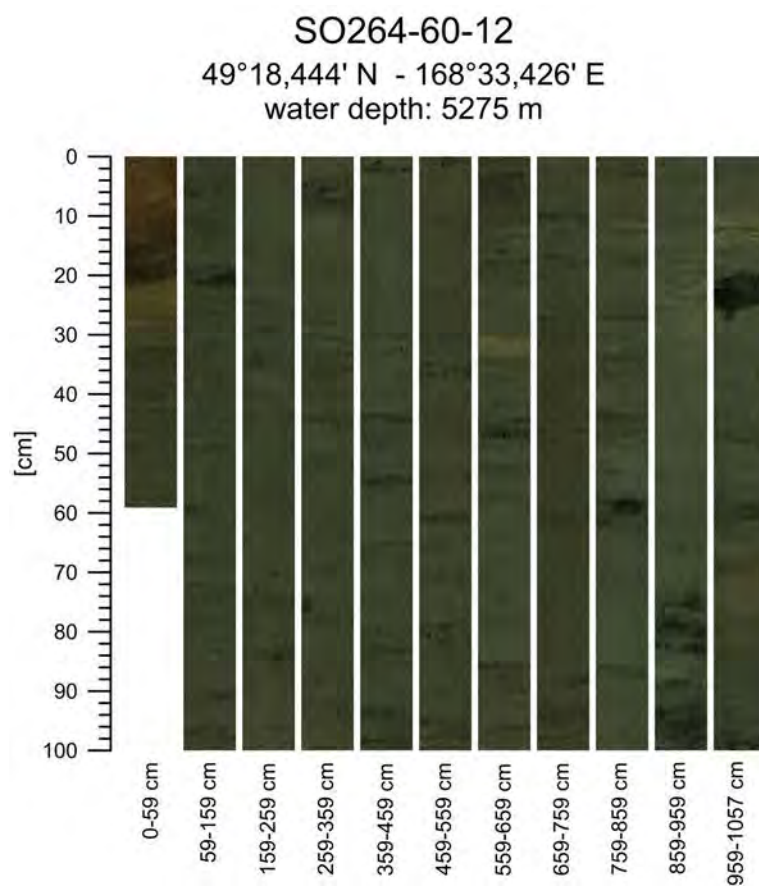
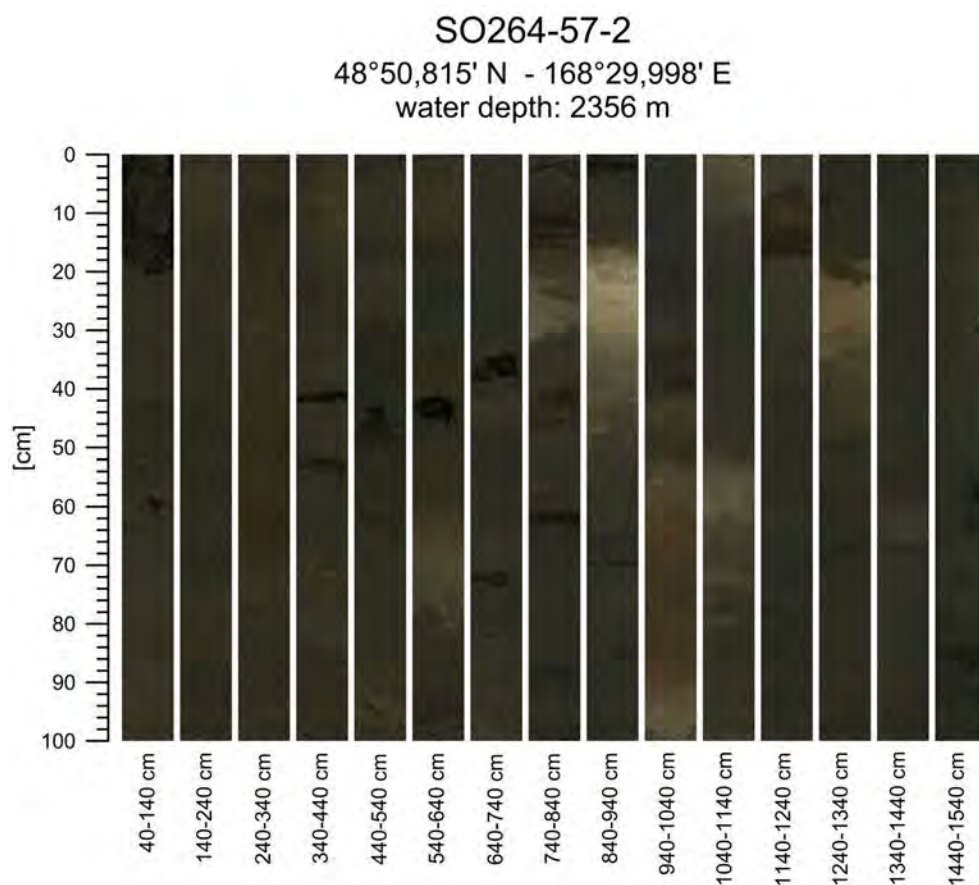


SO264-54-2

47°37,318' N - 169°14,852' E
water depth: 2139 m







GEOMAR Reports

No.	Title
1	FS POSEIDON Fahrtbericht / Cruise Report POS421, 08. – 18.11.2011, Kiel - Las Palmas, Ed.: T.J. Müller, 26 pp, DOI: 10.3289/GEOMAR_REP_NS_1_2012
2	Nitrous Oxide Time Series Measurements off Peru – A Collaboration between SFB 754 and IMARPE –, Annual Report 2011, Eds.: Baustian, T., M. Graco, H.W. Bange, G. Flores, J. Ledesma, M. Sarmiento, V. Leon, C. Robles, O. Moron, 20 pp, DOI: 10.3289/GEOMAR_REP_NS_2_2012
3	FS POSEIDON Fahrtbericht / Cruise Report POS427 – Fluid emissions from mud volcanoes, cold seeps and fluid circulation at the Don-Kuban deep sea fan (Kerch peninsula, Crimea, Black Sea) – 23.02. – 19.03.2012, Burgas, Bulgaria - Heraklion, Greece, Ed.: J. Bialas, 32 pp, DOI: 10.3289/GEOMAR_REP_NS_3_2012
4	RV CELTIC EXPLORER EUROFLEETS Cruise Report, CE12010 – ECO2@NorthSea, 20.07. – 06.08.2012, Bremerhaven – Hamburg, Eds.: P. Linke et al., 65 pp, DOI: 10.3289/GEOMAR_REP_NS_4_2012
5	RV PELAGIA Fahrtbericht / Cruise Report 64PE350/64PE351 – JEDDAH-TRANSECT –, 08.03. – 05.04.2012, Jeddah – Jeddah, 06.04 - 22.04.2012, Jeddah – Duba, Eds.: M. Schmidt, R. Al-Farawati, A. Al-Aidaros, B. Kürten and the shipboard scientific party, 154 pp, DOI: 10.3289/GEOMAR_REP_NS_5_2013
6	RV SONNE Fahrtbericht / Cruise Report SO225 - MANIHIKI II Leg 2 The Manihiki Plateau - Origin, Structure and Effects of Oceanic Plateaus and Pleistocene Dynamic of the West Pacific Warm Water Pool, 19.11.2012 - 06.01.2013 Suva / Fiji – Auckland / New Zealand, Eds.: R. Werner, D. Nürnberg, and F. Hauff and the shipboard scientific party, 176 pp, DOI: 10.3289/GEOMAR_REP_NS_6_2013
7	RV SONNE Fahrtbericht / Cruise Report SO226 – CHRIMP CHatham RIse Methane Pockmarks, 07.01. – 06.02.2013 / Auckland – Lyttleton & 07.02. – 01.03.2013 / Lyttleton – Wellington, Eds.: Jörg Bialas / Ingo Klaucke / Jasmin Mögeltönder, 126 pp, DOI: 10.3289/GEOMAR_REP_NS_7_2013
8	The SUGAR Toolbox - A library of numerical algorithms and data for modelling of gas hydrate systems and marine environments, Eds.: Elke Kossel, Nikolaus Bigalke, Elena Piñero, Matthias Haeckel, 168 pp, DOI: 10.3289/GEOMAR_REP_NS_8_2013
9	RV ALKOR Fahrtbericht / Cruise Report AL412, 22.03.-08.04.2013, Kiel – Kiel. Eds: Peter Linke and the shipboard scientific party, 38 pp, DOI: 10.3289/GEOMAR_REP_NS_9_2013
10	Literaturrecherche, Aus- und Bewertung der Datenbasis zur Meerforelle (Salmo trutta trutta L.) Grundlage für ein Projekt zur Optimierung des Meerforellenmanagements in Schleswig-Holstein. Eds.: Christoph Petereit, Thorsten Reusch, Jan Dierking, Albrecht Hahn, 158 pp, DOI: 10.3289/GEOMAR_REP_NS_10_2013
11	RV SONNE Fahrtbericht / Cruise Report SO227 TAIFLUX, 02.04. – 02.05.2013, Kaohsiung – Kaohsiung (Taiwan), Christian Berndt, 105 pp, DOI: 10.3289/GEOMAR_REP_NS_11_2013
12	RV SONNE Fahrtbericht / Cruise Report SO218 SHIVA (Stratospheric Ozone: Halogens in a Varying Atmosphere), 15.-29.11.2011, Singapore - Manila, Philippines, Part 1: SO218- SHIVA Summary Report (in German), Part 2: SO218- SHIVA English reports of participating groups, Eds.: Birgit Quack & Kirstin Krüger, 119 pp, DOI: 10.3289/GEOMAR_REP_NS_12_2013
13	KIEL276 Time Series Data from Moored Current Meters. Madeira Abyssal Plain, 33°N, 22°W, 5285 m water depth, March 1980 – April 2011. Background Information and Data Compilation. Eds.: Thomas J. Müller and Joanna J. Waniek, 239 pp, DOI: 10.3289/GEOMAR_REP_NS_13_2013

GEOMAR Reports

No.	Title
14	RV POSEIDON Fahrtbericht / Cruise Report POS457: ICELAND HAZARDS Volcanic Risks from Iceland and Climate Change: The Late Quaternary to Anthropogenic Development Reykjavík / Iceland – Galway / Ireland, 7.-22. August 2013. Eds.: Reinhard Werner, Dirk Nürnberg and the shipboard scientific party, 88 pp, DOI: 10.3289/GEOMAR_REP_NS_14_2014
15	RV MARIA S. MERIAN Fahrtbericht / Cruise Report MSM-34 / 1 & 2, SUGAR Site, Varna – Varna, 06.12.13 – 16.01.14. Eds: Jörg Bialas, Ingo Klauke, Matthias Haeckel, 111 pp, DOI: 10.3289/GEOMAR_REP_NS_15_2014
16	RV POSEIDON Fahrtbericht / Cruise Report POS 442, "AUVinTYS" High-resolution geological investigations of hydrothermal sites in the Tyrrhenian Sea using the AUV "Abyss", 31.10. – 09.11.12, Messina – Messina, Ed.: Sven Petersen, 32 pp, DOI: 10.3289/GEOMAR_REP_NS_16_2014
17	RV SONNE, Fahrtbericht / Cruise Report, SO 234/1, "SPACES": Science or the Assessment of Complex Earth System Processes, 22.06. – 06.07.2014, Walvis Bay / Namibia - Durban / South Africa, Eds.: Reinhard Werner and Hans-Joachim Wagner and the shipboard scientific party, 44 pp, DOI: 10.3289/GEOMAR_REP_NS_17_2014
18	RV POSEIDON Fahrtbericht / Cruise Report POS 453 & 458, "COMM3D", Crustal Structure and Ocean Mixing observed with 3D Seismic Measurements, 20.05. – 12.06.2013 (POS453), Galway, Ireland – Vigo, Portugal, 24.09. – 17.10.2013 (POS458), Vigo, Portugal – Vigo, Portugal, Eds.: Cord Papenberg and Dirk Klaeschen, 66 pp, DOI: 10.3289/GEOMAR_REP_NS_18_2014
19	RV POSEIDON, Fahrtbericht / Cruise Report, POS469, "PANAREA", 02. – 22.05.2014, (Bari, Italy – Malaga, Spain) & Panarea shallow-water diving campaign, 10. – 19.05.2014, Ed.: Peter Linke, 55 pp, DOI: 10.3289/GEOMAR_REP_NS_19_2014
20	RV SONNE Fahrtbericht / Cruise Report SO234-2, 08.-20.07.2014, Durban, -South Africa - Port Louis, Mauritius, Eds.: Kirstin Krüger, Birgit Quack and Christa Marandino, 95 pp, DOI: 10.3289/GEOMAR_REP_NS_20_2014
21	RV SONNE Fahrtbericht / Cruise Report SO235, 23.07.-07.08.2014, Port Louis, Mauritius to Malé, Maldives, Eds.: Kirstin Krüger, Birgit Quack and Christa Marandino, 76 pp, DOI: 10.3289/GEOMAR_REP_NS_21_2014
22	RV SONNE Fahrtbericht / Cruise Report SO233 WALVIS II, 14.05-21.06.2014, Cape Town, South Africa - Walvis Bay, Namibia, Eds.: Kaj Hoernle, Reinhard Werner, and Carsten Lüter, 153 pp, DOI: 10.3289/GEOMAR_REP_NS_22_2014
23	RV SONNE Fahrtbericht / Cruise Report SO237 Vema-TRANSIT Bathymetry of the Vema-Fracture Zone and Puerto Rico Trench and Abyssal Atlantic Biodiversity Study, Las Palmas (Spain) - Santo Domingo (Dom. Rep.) 14.12.14 - 26.01.15, Ed.: Colin W. Devey, 130 pp, DOI: 10.3289/GEOMAR_REP_NS_23_2015
24	RV POSEIDON Fahrtbericht / Cruise Report POS430, POS440, POS460 & POS467 Seismic Hazards to the Southwest of Portugal; POS430 - La-Seyne-sur-Mer - Portimao (7.4. - 14.4.2012), POS440 - Lisbon - Faro (12.10. - 19.10.2012), POS460 - Funchal - Portimao (5.10. - 14.10.2013), POS467 - Funchal - Portimao (21.3. - 27.3.2014), Ed.: Ingo Grevemeyer, 43 pp, DOI: 10.3289/GEOMAR_REP_NS_24_2015
25	RV SONNE Fahrtbericht / Cruise Report SO239, EcoResponse Assessing the Ecology, Connectivity and Resilience of Polymetallic Nodule Field Systems, Balboa (Panama) – Manzanillo (Mexico), 11.03. -30.04.2015, Eds.: Pedro Martínez Arbizu and Matthias Haeckel, 204 pp, DOI: 10.3289/GEOMAR_REP_NS_25_2015

GEOMAR Reports

No.	Title
26	RV SONNE Fahrtbericht / Cruise Report SO242-1, JPI OCEANS Ecological Aspects of Deep-Sea Mining, DISCOL Revisited, Guayaquil - Guayaquil (Ecuador), 29.07.-25.08.2015, Ed.: Jens Greinert, 290 pp, DOI: 10.3289/GEOMAR_REP_NS_26_2015
27	RV SONNE Fahrtbericht / Cruise Report SO242-2, JPI OCEANS Ecological Aspects of Deep-Sea Mining DISCOL Revisited, Guayaquil - Guayaquil (Ecuador), 28.08.-01.10.2015, Ed.: Antje Boetius, 552 pp, DOI: 10.3289/GEOMAR_REP_NS_27_2015
28	RV POSEIDON Fahrtbericht / Cruise Report POS493, AUV DEDAVE Test Cruise, Las Palmas - Las Palmas (Spain), 26.01.-01.02.2016, Ed.: Klas Lackschewitz, 17 pp, DOI: 10.3289/GEOMAR_REP_NS_28_2016
29	Integrated German Indian Ocean Study (IGIOS) - From the seafloor to the atmosphere - A possible German contribution to the International Indian Ocean Expedition 2 (IIOE-2) programme - A Science Prospectus, Eds.: Bange, H.W. , E.P. Achterberg, W. Bach, C. Beier, C. Berndt, A. Biastoch, G. Bohrmann, R. Czeschel, M. Dengler, B. Gaye, K. Haase, H. Herrmann, J. Lelieveld, M. Mohtadi, T. Rixen, R. Schneider, U. Schwarz-Schampera, J. Segsneider, M. Visbeck, M. Voß, and J. Williams, 77pp, DOI: 10.3289/GEOMAR_REP_NS_29_2016
30	RV SONNE Fahrtbericht / Cruise Report SO249, BERING – Origin and Evolution of the Bering Sea: An Integrated Geochronological, Volcanological, Petrological and Geochemical Approach, Leg 1: Dutch Harbor (U.S.A.) - Petropavlovsk-Kamchatsky (Russia), 05.06.2016-15.07.2016, Leg 2: Petropavlovsk-Kamchatsky (Russia) - Tomakomai (Japan), 16.07.2016-14.08.2016, Eds.: Reinhard Werner, et al., DOI: 10.3289/GEOMAR_REP_NS_30_2016
31	RV POSEIDON Fahrtbericht/ Cruise Report POS494/2, HIERROSEIS Leg 2: Assessment of the Ongoing Magmatic-Hydrothermal Discharge of the El Hierro Submarine Volcano, Canary Islands by the Submersible JAGO, Valverde – Las Palmas (Spain), 07.02.-15.02.2016, Eds.: Hannington, M.D. and Shipboard Scientific Party, DOI: 10.3289/GEOMAR_REP_NS_31_2016
32	RV METEOR Fahrtbericht/ Cruise Report M127, Extended Version, Metal fluxes and Resource Potential at the Slow-spreading TAG Mid-ocean Ridge Segment (26°N, MAR) – Blue Mining@Sea, Bridgetown (Barbados) – Ponta Delgada (Portugal) 25.05.-28.06.2016, Eds.: Petersen, S. and Shipboard Scientific Party, DOI: 10.3289/GEOMAR_REP_NS_32_2016
33	RV SONNE Fahrtbericht/Cruise Report SO244/1, GeoSEA: Geodetic Earthquake Observatory on the Seafloor, Antofagasta (Chile) – Antofagasta (Chile), 31.10.-24.11.2015, Eds.: Jan Behrmann, Ingo Klaucke, Michal Stipp, Jacob Geersen and Scientific Crew SO244/1, DOI: 10.3289/GEOMAR_REP_NS_33_2016
34	RV SONNE Fahrtbericht/Cruise Report SO244/2, GeoSEA: Geodetic Earthquake Observatory on the Seafloor, Antofagasta (Chile) – Antofagasta (Chile), 27.11.-13.12.2015, Eds.: Heidrun Kopp, Dietrich Lange, Katrin Hannemann, Anne Krabbenhoeft, Florian Petersen, Anina Timmermann and Scientific Crew SO244/2, DOI: 10.3289/GEOMAR_REP_NS_34_2016
35	RV SONNE Fahrtbericht/Cruise Report SO255, VITIAZ – The Life Cycle of the Vitiaz-Kermadec Arc / Backarc System: from Arc Initiation to Splitting and Backarc Basin Formation, Auckland (New Zealand) - Auckland (New Zealand), 02.03.-14.04.2017, Eds.: Kaj Hoernle, Folkmar Hauff, and Reinhard Werner with contributions from cruise participants, DOI: 10.3289/GEOMAR_REP_NS_35_2017

GEOMAR Reports

No.	Title
36	RV POSEIDON Fahrtbericht/Cruise Report POS515, CALVADOS - CALabrian arc mud VolcAnoes: Deep Origin and internal Structure, Dubrovnik (Croatia) – Catania (Italy), 18.06.-13.07.2017, Eds.: M. Riedel, J. Bialas, A. Krabbenhoef, V. Bähre, F. Beeck, O. Candoni, M. Kühn, S. Muff, J. Rindfleisch, N. Stange, DOI: 10.3289/GEOMAR_REP_NS_36_2017
37	RV MARIA S. MERIAN Fahrtbericht/Cruise Report MSM63, PERMO, Southampton – Southampton (U.K.), 29.04.-25.05.2017, Eds.: Christian Berndt and Judith Elger with contributions from cruise participants C. Böttner, R. Gehrman, J. Karstens, S. Muff, B. Pitcairn, B. Schramm, A. Lichtschlag, A.-M. Völsch, DOI: 10.3289/GEOMAR_REP_NS_37_2017
38	RV SONNE Fahrtbericht/Cruise Report SO258/1, INCON: The Indian - Antarctic Break-up Engima, Fremantle (Australia) - Colombo (Sri Lanka), 07.06.-09.07.2017, 29.04.-25.05.2017, Eds.: Reinhard Werner, Hans-Joachim Wagner, and Folkmar Hauff with contributions from cruise participants, DOI: 10.3289/GEOMAR_REP_NS_38_2017
39	RV POSEIDON Fahrtbericht/Cruise Report POS509, ElectroPal 2: Geophysical investigations of sediment hosted massive sulfide deposits on the Palinuro Volcanic Complex in the Tyrrhenian Sea, Malaga (Spain) – Catania (Italy), 15.02.-03.03.2017, Ed.: Sebastian Hölz, DOI: 10.3289/GEOMAR_REP_NS_39_2017
40	RV POSEIDON Fahrtbericht/Cruise Report POS518, Baseline Study for the Environmental Monitoring of Subseafloor CO ₂ Storage Operations, Leg 1: Bremerhaven – Bremerhaven (Germany), 25.09.-11.10.2017, Leg 2: Bremerhaven – Kiel (Germany), 12.10.-28.10.2017, Eds.: Peter Linke and Matthias Haeckel, DOI: 10.3289/GEOMAR_REP_NS_40_2018
41	RV MARIA S. MERIAN Fahrtbericht/Cruise Report MSM71, LOBSTER: Ligurian Ocean Bottom Seismology and Tectonics Research, Las Palmas (Spain) – Heraklion (Greece), 07.02.-27.02.2018, Eds.: H. Kopp, D. Lange, M. Thorwart, A. Paul, A. Dannowski, F. Petersen, C. Aubert, F. Beek, A. Beniest, S. Besançon, A. Brotzer, G. Caielli, W. Crawford, M. Deen, C. Lehmann, K. Marquardt, M. Neckel, L. Papanagnou, B. Schramm, P. Schröder, K.-P. Steffen, F. Wolf, Y. Xia, DOI: 10.3289/GEOMAR_REP_NS_41_2018
42	RV METEOR Fahrtbericht/Cruise Report M143, SLOGARO: Slope failures and active gas expulsion along the Romanian margin – investigating relations to gas hydrate distribution, Varna (Romania) – Heraklion (Greece), 12.12.-22.12.2017, Eds.: M. Riedel, F. Gausepohl, I. Gazis, L. Hähnel, M. Kampmeier, P. Urban, J. Bialas, DOI: 10.3289/GEOMAR_REP_NS_42_2018
43	RV POSEIDON Fahrtbericht/Cruise Report POS510, ANYDROS: Rifting and Hydrothermal Activity in the Cyclades Back-arc Basin, Catania (Italy) – Heraklion (Greece), 06.03.-29.03.2017, Ed.: M.D. Hannington, DOI: 10.3289/GEOMAR_REP_NS_43_2018
44	RV POSEIDON Fahrtbericht/Cruise Report POS524, GrimseyEM: Geophysical and geological investigations in the vicinity of the Grimsey Hydrothermal Field offshore Northern Iceland for the assessment of the geothermal potential and the exploration for potential mineralizations within the seafloor, Reykjavik (Iceland) – Bergen (Norway), 7.6 - 26.6.2018, Eds.: Sebastian Hölz and Sofia Martins, DOI: 10.3289/GEOMAR_REP_NS_44_2018
45	RV POSEIDON Fahrtbericht/Cruise Report POS527, Baseline Study for the Environmental Monitoring of Subseafloor CO ₂ Storage Operations, Kiel – Kiel (Germany), 15.8. - 3.9.2018, Eds.: Eric Achterberg and Mario Esposito, DOI: 10.3289/GEOMAR_REP_NS_45_2018

GEOMAR Reports

No.	Title
46	RV SONNE Fahrtbericht/Cruise Report SO264, SONNE-EMPEROR: The Plio/Pleistocene to Holocene development of the pelagic North Pacific from surface to depth – assessing its role for the global carbon budget and Earth's climate, Suva (Fiji) – Yokohama (Japan), 30.6. – 24.8.2018 Ed.: Dirk Nürnberg, DOI: 10.3289/GEOMAR_REP_NS_46_2018

For GEOMAR Reports, please visit:
https://oceanrep.geomar.de/view/series/GEOMAR_Report.html

Reports of the former IFM-GEOMAR series can be found under:
https://oceanrep.geomar.de/view/series/IFM-GEOMAR_Report.html



Das GEOMAR Helmholtz-Zentrum für Ozeanforschung Kiel
ist Mitglied der Helmholtz-Gemeinschaft
Deutscher Forschungszentren e.V.

The GEOMAR Helmholtz Centre for Ocean Research Kiel
is a member of the Helmholtz Association of
German Research Centres

Helmholtz-Zentrum für Ozeanforschung Kiel / Helmholtz Centre for Ocean Research Kiel

GEOMAR
Dienstgebäude Westufer / West Shore Building
Düsternbrooker Weg 20
D-24105 Kiel
Germany

Helmholtz-Zentrum für Ozeanforschung Kiel / Helmholtz Centre for Ocean Research Kiel

GEOMAR
Dienstgebäude Ostufer / East Shore Building
Wischhofstr. 1-3
D-24148 Kiel
Germany

Tel.: +49 431 600-0
Fax: +49 431 600-2805
www.geomar.de